# Wave Glider fisheries acoustics: Environmental drivers of North Sea zooplankton patchiness

A thesis submitted to the School of Environmental Sciences at the University of East Anglia in partial fulfilment of the requirements for the degree of Doctor of Philosophy

Martina Juliette Bristow

April 2023

# Abstract

Zooplankton are a key component of marine ecosystems across the world's oceans, playing an important role in the biological carbon pump and serving as a trophic link between primary production and higher predators. Monitoring zooplankton is difficult as they form patchy aggregations of varying scales. Understanding how variability in the pelagic environment influences patchiness of zooplankton distributions is crucial to improve monitoring and predict how environmental change might affect their role in the ecosystem.

Advances in autonomous technologies have opened up new possibilities for ocean observations. Autonomous surface vehicles (ASVs) have shown promise as mobile sensor platforms capable of conducting acoustic surveys of fish and zooplankton at small spatio-temporal resolutions. We deployed an echosounder-equipped Wave Glider ASV in the North Sea to collect in-situ measurements of the environment and acoustic measurements of pelagic animal distributions. By combining and analysing these measurements, I investigate environmental drivers of zooplankton patchiness at sub-mesoscale and sub-seasonal scales.

In this thesis, I reveal diel vertical migration behaviour of physonect siphonophores and the critical importance of bathymetry in structuring spatial distributions of zooplankton and schooling fish. I evaluate the Wave Glider's capacity as an acoustic platform, finding that, as with other surface vessels, data quality is affected by the wind. At wind speeds above $10\,\mathrm{m\,s^{-1}}$ attenuation and transient noise resulted in significant data loss, however below this speed acoustic data of high quality were obtained. Poor integration of the echosounder onto the Wave Glider also resulted in significant data loss; means to optimise integration are discussed. Further, I present a novel technique to semi-quantitively assess acoustic data

quality and efficacy of data cleaning, which I call the ‘two-layer comparison technique’. Overall, I conclude that an acoustically-equipped Wave Glider has the potential to make a significant contribution to our understanding of the environmental drivers of zooplankton patchiness.

# Contents

**Abstract** ii

**List of Figures** ix

**List of Tables** xiv

**List of Abbreviations** xvii

**Acknowledgements** xviii

**Dedication** xx

**1 Introduction** 1

1.1 The North Sea . . . 1

1.1.1 Pelagic food webs . . . 2

1.1.2 Monitoring zooplankton . . . 3

1.1.3 Oceanography . . . 4

1.1.4 Study region: the central North Sea . . . 6

1.1.5 Climatic drivers of ecosystem change . . . 6

1.2 Diurnal movement patterns of fish and zooplankton . . . 10

1.2.1 Impacts of DVM on the biological carbon pump . . . 12

1.3 Fisheries acoustics . . . 13

1.3.1 Instruments and data visualisation . . . 14

1.3.2 Acoustic backscatter . . . 15

1.3.3 TVG compensation of signal losses . . . 17

1.3.4 Classifying acoustic data . . . 19

1.3.5 Echo integration . . . 23

1.3.6 Acoustic data quality . . . . . 24
1.4 Autonomous vehicles as acoustic survey platforms . . . . . 29
1.4.1 The Wave Glider . . . . . 32
1.4.2 Deployment of *Lyra*, an acoustically-equipped Wave Glider, in the central North Sea . . . . . 33
1.5 Observing diel vertical migrations of fish and zooplankton . . . . . 36
1.6 Research aims and thesis structure . . . . . 38

**2 Impacts of the wind on acoustic data collected by the Wave Glider 42**
2.1 Introduction . . . . . 42
2.1.1 Impacts of transient noise and attenuation on acoustic data quality . 44
2.1.2 Detecting transient noise and attenuation in acoustic data . . . . . 45
2.1.3 Platform-dependence of adverse weather impacts . . . . . 50
2.1.4 Aims of this study . . . . . 51
2.2 Methods . . . . . 52
2.2.1 Acoustic and ancillary data collection . . . . . 52
2.2.2 Echosounder calibration . . . . . 52
2.2.3 Data processing . . . . . 53
2.2.4 Detecting attenuation and transient noise . . . . . 59
2.2.5 Analysing the effects of wind speed on data quality . . . . . 63
2.2.6 Two-layer comparison technique to measure bias and filter efficacy 64
2.3 Results . . . . . 65
2.3.1 Platform motion . . . . . 65
2.3.2 Preliminary visual assessment of acoustic data quality . . . . . 68
2.3.3 Effect of wind speed on data degradation near the surface . . . . . 69
2.3.4 Data degradation caused by attenuation and transient noise . . . . . 74
2.3.5 Two-layer comparisons: increased bias in data from windy periods . 88
2.3.6 False positive and false negative detections . . . . . 91
2.4 Discussion . . . . . 93
2.4.1 Effects of the wind on acoustic data quality . . . . . 93
2.4.2 Data cleaning filters and the two-layer comparison technique . . . . 99

2.4.3 Operational recommendations . . . . . 106

**3 Characterising daily vertical movement patterns of fish and zooplankton 110**

3.1 Introduction . . . . . 110

3.1.1 Plasticity of DVM behaviour . . . . . 110

3.1.2 Aims of this study . . . . . 114

3.2 Methods . . . . . 115

3.2.1 Acoustic classification scheme . . . . . 115

3.2.2 Analysis of diel patterns . . . . . 121

3.2.3 Determining the taxonomical composition of acoustic groups . . . . 124

3.3 Results . . . . . 127

3.3.1 Classification of backscatter into acoustic groups . . . . . 127

3.3.2 Composition of acoustic groups . . . . . 131

3.3.3 Diel patterns of each acoustic group . . . . . 139

3.4 Discussion . . . . . 147

3.4.1 DVM of North Sea physonect siphonophores . . . . . 148

3.4.2 Evaluation of the classification scheme . . . . . 154

3.4.3 North Sea schooling fish . . . . . 156

**4 Environmental drivers of zooplankton and fish school patchiness 160**

4.1 Introduction . . . . . 160

4.1.1 Influence of environmental conditions on pelagic animal distributions in the central North Sea . . . . . 160

4.1.2 Aims of this study . . . . . 165

4.2 Methods . . . . . 166

4.2.1 Overview of GAMMs . . . . . 166

4.2.2 Response variables . . . . . 167

4.2.3 Predictor variables . . . . . 167

4.2.4 Modelling . . . . . 174

4.2.5 Seaglider subsurface measurements . . . . . 176

4.3 Results . . . . . 179

4.3.1 Spatial patterns in backscatter . . . . . 179

4.3.2 Oceanography of the transect region . . . . . 182
4.3.3 Models for each acoustic group . . . . . 189
4.4 Discussion . . . . . 208
4.4.1 Summary of model results . . . . . 208
4.4.2 Importance of bottom depth to pelagic animals in a shallow ecosystem 210
4.4.3 Light and the time of day . . . . . 213
4.4.4 Seasonal stratification . . . . . 215
4.4.5 Environmental drivers of fish school distributions . . . . . 216
4.4.6 Reverse DVM behaviour of calanoid copepods? . . . . . 217
4.4.7 The importance of considering spatial and temporal scales . . . . . 219
4.4.8 The utility of incorporating oceanographic data from gliders . . . . 223

**5 Conclusions 224**

5.1 Suitability of the Wave Glider as a platform for fisheries acoustic surveys . 225
5.1.1 Quality of acoustic data collected by the Wave Glider . . . . . 225
5.1.2 Observing DVM behaviour and the influence of the environment on zooplankton and fish distributions . . . . . 228
5.1.3 Considerations for biomass and abundance acoustic surveys . . . . 235
5.2 Looking to the future . . . . . 236

**Appendices 303**

**A Effect of calibration temperature and salinity settings on range and TVG 303**

A.1 Purpose . . . . . 303
A.2 Methods . . . . . 304
A.3 Results . . . . . 306
A.3.1 Temperature and salinity profiles . . . . . 306
A.3.2 Range offset . . . . . 307
A.3.3 Absorption and TVG . . . . . 308
A.4 Discussion . . . . . 308

**B Unfiltered 70 kHz backscatter echograms 310**

**C LCAS and LCTN sensitivity analyses 313**

C.1 Introduction . . . . . 313

C.2 Methods . . . . . 315

C.3 Results . . . . . 316

C.4 Discussion . . . . . 318

**D Seabed and Water Column layer Sv-difference correlations 320**

**E Cleaning the 200 kHz data 327**

**F Threshold sensitivity analysis for fish school detections 328**

F.1 Purpose . . . . . 328

F.2 Methods . . . . . 331

F.3 Results . . . . . 333

F.4 Discussion . . . . . 338

**G Zooplankton net samples 345**

**H Variability in the vertical distribution of the gas-filled scattering layer 351**

# List of Figures


1.1.1 General water properties and circulation pattern of the North Sea . . . . . 2

1.1.2 Long-term trends in North Sea SST and various components of the plankton community from 1960 to 1995 . . . . . 10

1.3.1 Time-varied-gain functions to compensate for losses of 70 kHz and 200 kHz signals, to 100 m range . . . . . 18

1.3.2 Frequency response patterns modelled for a range of different scatterers . 21

1.3.3 Conceptual diagram of data quality and bias in raw and cleaned acoustic data and suitability for different purposes . . . . . 24

1.3.4 Echograms illustrating the time-varied-gain applied to 70 kHz and 200 kHz data, to 100 m range . . . . . 26

1.3.5 Frequency response of typical sources of ambient noise in the ocean . . . 27

1.4.1 Schematic of Wave Glider propulsion . . . . . 32

1.4.2 Schematic of *Lyra*, the Cefas-owned Wave Glider SV3, adapted with echosounder system . . . . . 34

1.4.3 Custom-built foam mount attached aft of *Lyra's* surface float by a metal strut 34

1.4.4 *Lyra's* path between 9th May and 17th June 2018 . . . . . 35

2.1.1 Echograms showing examples of acoustic data degradation, adapted from Figure 2.1 in Jech et al. (2021) . . . . . 46

2.1.2 Photographs of the Wave Glider *Lyra* in different sea conditions . . . . . 51

2.2.1 Autocorrelation plots for wind speed data averaged over various time periods. 54

2.2.2 Processing steps used to detect transient noise and attenuation . . . . . 56

2.2.3 Echogram of 70 kHz backscatter data from Transect 1 depicting various extracted layers . . . . . 59

2.2.4 Examples of suspected degraded data . . . . . 60

2.2.5 Patterns in seabed (SB) layer backscatter used to inform the SRAS filter . 61
2.3.1 Time series of wind speed, bubble plume depth, backscatter in the NS, WC, and SB layers, and vessel roll . . . . . 66
2.3.2 Platform motion and its relationship to wind speed . . . . . 67
2.3.3 Empirical cumulative distribution probabilities of distances to the transect 68
2.3.4 Echograms of 70 kHz backscatter from Transects 1 and 5 depicting degraded data . . . . . 69
2.3.5 Density of wind speed observations during periods when a bubble layer was present or absent . . . . . 70
2.3.6 Relationships between wind speed and water column backscatter at different depths . . . . . 71
2.3.7 Boxplots of daytime and nighttime NS layer backscatter, by wind speed category . . . . . 71
2.3.8 Echogram showing the depth of bubble plumes and the distortion of subunit echoes during windier weather . . . . . 72
2.3.9 Relationships between wind speed and water column backscatter at depths near the subunit . . . . . 73
2.3.10 Proportions of data degraded by attenuation or transient noise, plotted against wind speed . . . . . 75
2.3.11 Draftsman plot showing relationships between wind speed, vessel roll, proxy bubble metrics, and rates of data degradation . . . . . 76
2.3.12 Correlations between lagged wind speed and attenuation, bubble plume depth, and transient noise . . . . . 77
2.3.13 Relative wind direction against vessel speed, roll, and bubble plume depth, grouped by wind speed category . . . . . 79
2.3.14 Relative wind direction against rates of attenuation (AS %) and transient noise (TN %), by wind speed category . . . . . 80
2.3.15 Boxplots of mean backscatter of degraded data, by wind speed category . 82
2.3.16 Water column layer Sv-differences against wind speed, coloured by filter results . . . . . 83

2.3.17 Sv-differences of clean and degraded data in the seabed (SB) and water column (WC) layers, grouped by wind speed category . . . . . 83
2.3.18 Examples of unfiltered and clean data from two contrasting transects . . . 85
2.3.19 Boxplots of backscatter and Sv-differences of the cleaned data in the SB and WC layers, by wind speed category . . . . . 87
2.3.20 Effect of data cleaning filters on Sv-difference of the SB and WC layers, by wind speed . . . . . 88
2.3.21 Effects of data cleaning filters on two-layer comparison correlation coefficients, by wind speed . . . . . 90
2.3.22 Sv-differences of filtered (cleaned) data in the seabed (SB) and water column (WC) layers, grouped by wind speed category . . . . . 92

3.2.1 Transit time across each bin, categorised by the time of day . . . . . 123
3.2.2 Ring net sample stations on cruise CEND 07-18 and concurrent location of *Lyra* . . . . . 125
3.2.3 Paired ring nets used to sample zooplankton at the beginning of the mission 126
3.3.1 Echograms depicting the classification process within the analysis layer, Transect 8 . . . . . 127
3.3.2 Histogram of unaveraged dB-difference cell values ($\Delta\text{MVBS}_{200-70}$) from which the GF and FL groups were determined . . . . . 128
3.3.3 Time series of energetic and positional properties of each group: fish schools, gas-filled and fluid-like zooplankton . . . . . 129
3.3.4 Histograms of group energetic properties . . . . . 130
3.3.5 Histograms of fish school positional and morphometric properties . . . . 133
3.3.6 Examples of fish school shapes, as viewed in echograms, from Transect 1 and Transect 7 . . . . . 134
3.3.7 Fish school positional, energetic and morphometric properties . . . . . 135
3.3.8 Fish school detection bias due to wind speed . . . . . 138
3.3.9 Diel variation in energetic and positional descriptors for each acoustic group 139
3.3.10 70 kHz echograms depicting possible dispersed gas-bladdered fish . . . . 141

3.3.11 Boxplots of hourly averaged energetic and positional properties for the gas-filled group . . . 143
3.3.12 Differences between average 70 kHz daytime and nighttime backscatter of the gas-filled group . . . 145
3.3.13 Boxplots of energetic and positional metrics for the gas-filled group, averaged by 2° solar altitude intervals and separated into pre- and post-noon periods . . . 146

4.2.1 SST time series with high and low frequency butterworth filtered components 169
4.2.2 Draftsman plot exploring collinearity between environmental predictor variables . . . 171
4.2.3 Draftsman plot of relationships between environmental predictor variables 172
4.2.4 Surface fluorescence measurements (arbitrary units), grouped by time of day 173
4.2.5 Position of Seaglider 510 in relation to the transect waypoints and *Lyra* . . 178
4.3.1 Bathymetry along the transect and in the surrounding region . . . 179
4.3.2 Position of the GF layer and fish schools along each transect . . . 180
4.3.3 Bottom depth and mean daytime and nighttime GF and FL NASS along the transect . . . 181
4.3.4 Depths of the upper and lower thermoclines . . . 182
4.3.5 Longitudinal sections of Seaglider 510 temperature, salinity, optical backscatter, fluorescence, and saturated oxygen data . . . 183
4.3.6 Correlation between salinity and optical backscattering at 470 nm and salinity and temperature in the BML . . . 186
4.3.7 Salinity in the BML by transect, with GAM smooth (blue line) . . . 187
4.3.8 Hovmüller plots of surface water properties . . . 188
4.3.9 Partial effects of predictor variables in the Gas-Filled group energetic GAMMs . . . 191
4.3.10 Partial effects of predictor variables in the Gas-Filled group positional GAMMs . . . 192
4.3.11 Partial effects of predictor variables in Fish School positional GAMMs . . 197
4.3.12 Partial effects of predictor variables in Fish School energetic GAMMs . . 198

4.3.13 Partial effects of predictor variables in Fluid-Like group energetic GAMMs 202

4.3.14 Partial effects of predictor variables in Fluid-like group positional GAMMs 203

4.4.1 Echogram of raw acoustic backscatter, showing vertical heterogeneity (patchiness) in acoustic backscatter within the main sound scattering layer 222

A.2.1 Position, temperature, and practical salinity measured by Seaglider SG510 together with Lyra's concurrent position . . . . . 305

A.3.1 Mean temperature and salinity depth profiles from cases 1 (calibration constants), 2 (start of mission), and 3 (end of mission) . . . . . 306

A.3.2 Depth profiles of acoustic-relevant parameters for cases 1 (calibration constants), 2 (start of mission); and 3 (end of mission) . . . . . 307

B.0.1 Raw $70\,\mathrm{kHz}$ volume backscatter echograms of Transects 1 to 5 . . . . . 310

B.0.2 Raw $70\,\mathrm{kHz}$ volume backscatter echograms of Transects 6 to 10 . . . . . 311

B.0.3 Raw $70\,\mathrm{kHz}$ volume backscatter echograms of Transects 11 to 15 . . . . . 312

C.3.1 Effects of different kernel-threshold combinations on average backscatter across the mission . . . . . 318

F.3.1 Boxplots of positional, energetic, and morphometric cluster descriptors, for thresholds coloured from red, $-55\,\mathrm{dB}$, to yellow, $-60\ \mathrm{dB}$ . . . . . 335

F.3.2 Number of clusters detected at each threshold and relationships between cluster depth and: dB-difference; and time of day, coloured by threshold . 337

F.3.3 Examples of clusters with perimeters exceeding $10\,\mathrm{km}$ . . . . . 338

H.0.1 Variability in altitude and centre of mass of the GF layer . . . . . 351

H.0.2 Pre- and post-noon observations of extremes in centre of mass and altitude 352

# List of Tables


2.1 Wind and vessel movement measurements made by sensors onboard *Lyra* . 52

2.2 Key echosounder calibration parameters . . . . . 53

2.3 Horizontal layers of the backscatter data, used to assess the impact of wind on acoustic data quality . . . . . 58

2.4 Estimated proportions of false positive detections made by the attenuation and transient noise filters, grouped by wind speed category . . . . . 92

3.1 Acoustic energetic, positional, and morphological descriptors . . . . . 122

4.1 Predictor variables tested in the GAMMs . . . . . 168

4.2 Final GAMM specifications . . . . . 177

4.3 Maximum effect sizes of environmental drivers in GAMMs . . . . . 209

4.4 Differences in NASS and altitude of GF and FL backscatter east and west of the ridge at $2.4°\mathrm{E}$ . . . . . 213

C.1 Decibel span of impacts on mean and median backscatter in the SB and WC layers after appying the LCAS and LCTN filters with thresholds of $1\,\mathrm{dB}$ . . 317

D.1 Spearman's correlation coefficients for SB and WC Sv-differences of unfiltered data, per $1\,\mathrm{m\,s^{-1}}$ wind speed interval . . . . . 321

D.2 Spearman's correlation coefficients for SB and WC Sv-differences after application of the SRAS filter, per $1\,\mathrm{m\,s^{-1}}$ wind speed interval . . . . . 322

D.3 Spearman's correlation coefficients for SB and WC Sv-differences after application of the LCAS filter, per $1\,\mathrm{m\,s^{-1}}$ wind speed interval . . . . . 323

D.4 Spearman's correlation coefficients of SB and WC Sv-differences after application of the SRAS and LCAS filters, per $1\,\mathrm{m\,s^{-1}}$ wind speed interval 324

D.5 Spearman's correlation coefficients for SB and WC Sv-differences after application of the LCTN filter, per $1\,\mathrm{m\,s^{-1}}$ wind speed interval . . . . . 325

D.6 Spearman's correlation coefficients for SB and WC Sv-differences after application of the SRAS, LCAS, and LCTN filters, per $1\,\mathrm{m\,s^{-1}}$ wind speed interval . . . . . 326

F.1 Transects used for threshold analysis . . . . . 331

F.2 Detection parameters used for SHAPES algorithm detection of potential fish school clusters . . . . . 332

G.1 Net sample stations . . . . . 346

G.2 Number and proportion of fluid-like and gas-filled acoustic scattering organisms sampled by nets . . . . . 347

G.3 Total count of each zooplankton taxon sampled by net . . . . . 348

G.4 Mesozooplankton $< 2\,\mathrm{mm}$ fraction of net subsamples . . . . . 349

G.5 Macrozooplankton $\geq 2\,\mathrm{mm}$ fraction of net subsamples . . . . . 350

# List of Abbreviations

**AS** Attenuated signal. 59, 60, 62, 63, 65, 74, 75, 77, 78, 82, 83, 89, 91, 313, 315

**ASE** Above subunit echo layer (see Table 2.3). 57, 63, 72, 73

**BML** Bottom mixed layer. 182, 184, 185, 186, 189, 195, 207, 215, 216, 221, 222, 230, 237

**BSE** Below subunit echo layer (see Table 2.3). 57, 63, 72, 73

**DCM** Deep chlorophyll maximum. 12, 182, 184, 185, 189, 193, 207, 221, 230

**DVM** Diel vertical migration. 10, 11, 12, 23, 35, 36, 37, 38, 39, 63, 84, 101, 110, 111, 112, 113, 114, 115, 123, 128, 138, 139, 140, 142, 145, 146, 147, 149, 150, 151, 152, 153, 154, 162, 164, 165, 174, 180, 190, 194, 204, 206, 211, 214, 217, 218, 224, 227, 228, 229, 230, 231, 232, 237, 238, 351

**FL** Fluid-like (acoustic group). 114, 115, 119, 120, 121, 122, 124, 126, 127, 128, 130, 131, 132, 138, 140, 144, 153, 154, 165, 167, 174, 175, 180, 181, 200, 201, 204, 205, 206, 207, 210, 211, 212, 215, 217, 218, 220, 345

**FS** Fish school (acoustic group). 114, 115, 117, 119, 120, 121, 122, 123, 124, 126, 127, 128, 130, 138, 153, 158, 165, 167, 174, 175, 195, 196, 199, 210, 216

**GF** Gas-filled (acoustic group). 114, 115, 119, 120, 121, 122, 123, 124, 126, 127, 128, 130, 131, 138, 140, 142, 143, 144, 147, 149, 150, 153, 154, 155, 165, 167, 174, 179, 180, 181, 189, 190, 193, 194, 195, 200, 201, 204, 205, 206, 210, 211, 212, 213, 215, 217, 218, 221, 345, 351

**LCAS** Local Convolution Attenuated Signal filter (see Subsection 2.2.4). 55, 59, 62, 64, 87, 88, 89, 99, 101, 313, 315, 316, 317, 318, 320

**LCTN** Local Convolution Transient Noise filter (see Subsection 2.2.4). 55, 59, 62, 64, 84, 86, 88, 89, 99, 101, 313, 314, 315, 316, 317, 318, 320

**LTOC** Low threshold only clusters (see Appendix F). 334, 335, 337, 339, 343

**MML** Middle mixed layer. 182, 184, 185, 230

**MW1** Mid-water 1 layer (see Table 2.3). 57, 69, 70

**MW2** Mid-water 2 layer (see Table 2.3). 57, 69, 70

**NNS** Northern North Sea. 4, 5

**NS** Near surface layer (see Table 2.3). 57, 59, 63, 65, 69, 70, 72, 75

**SB** Seabed layer (see Table 2.3). 57, 59, 60, 62, 64, 65, 81, 82, 83, 84, 87, 88, 92, 313, 316, 317, 320

**SE** Subunit echo layer (see Table 2.3). 57, 63, 72, 73, 74

**SML** Surface mixed layer. 182, 184, 185, 189, 230

**SNS** Southern North Sea. 4, 5

**SRAS** Seabed Reference Attenuated Signal filter (see Subsection 2.2.4). 55, 59, 60, 61, 87, 88, 89, 99, 100, 101, 315, 318, 320

**SSL** Sound scattering layer. 55, 68, 70, 75, 84, 85, 94, 101, 117, 119, 127, 145, 149, 150, 152, 155, 157, 193, 194, 222, 227, 230, 231, 314, 331, 336, 337, 338, 339

**TN** Transient noise. 59, 62, 63, 65, 74, 75, 77, 78, 82, 83, 89, 91, 313, 315

**TVG** Time-varied-gain. 17, 18, 25, 26, 27, 28, 52, 86, 105, 303, 304, 306, 307, 308, 327

**WC** Water column layer (see Table 2.3). 57, 59, 62, 64, 65, 81, 82, 83, 84, 86, 87, 88, 92, 316, 317, 320

# Acknowledgements

I am truly grateful for the supervision that I received from Bastien Queste, Karen Heywood, Jeroen van der Kooij, and Sophie Fielding. You made a wonderful team and each brought unique insights to this project. Thank you for the time and effort that you have put in and for the thought-provoking discussions which have helped me to grow as a research scientist. Bastien, you have always succeeded to cut to the core of what I needed to understand and focus on, and explain things to me in a simple, elegant way. Jeroen, you brought the North Sea to life for me and enabled me to go on many enjoyable adventures at sea. Sophie, you have been a huge support and I have enjoyed our discussions about acoustics and animal behaviour tremendously.

Olav Rune Godø inspired me to undertake research in the field of fisheries acoustics, and Rokas Kubilius gave me the confidence to begin working with acoustic data. The ICES WG-FAST community, too, has been so encouraging, and folks at Echoview and Simrad were very kind answering my many questions.

My thanks to those involved in the AlterEco project. Particularly Fabio Campanella for showing me the ropes at sea. Also, Dave Pearce and other scientists and crew onboard the RV Cefas Endeavour on cruises CEND 07-18 and CEND 15-18 who made the deployment of *Lyra* possible, kept us safe, and worked tirelessly through the night and driving rain to assist with the collection of samples. Thank you to scientists at Plymouth Marine Laboratory, in particular Andrea McEvoy and Elaine Fileman who taught me many fascinating things about tiny sea creatures, and Angus Atkinson.

The ever-changing student community at British Antarctic Survey has made my working environment a friendly, happy place to be. Friends at the University of East Anglia, too, who I have met with for coffee and chats on my many visits have made such a difference to my PhD experience. Several people stand out: Robert Blackwell, Lianne Harrison, Rachael Sanders, Tracey Dornan, Tom Hull, and Arlie McCarthy.

I am also indebted to the unwavering support and kindness of my friends and family throughout these years. My heartfelt thanks goes to my father, Peter, for his tireless efforts to support me with seeing the thesis through to completion. Also, my mother, Zuzana Bristow, for believing in me and listening through all my ups and downs, moc děkuji. My sisters Christina and Hana Bristow, and many friends including Natalie Lambert, Suzanne Makki, Chris Hoad, Callum Lawson, Fliss Purchase, Stephanie DeWhalley, Stephen Rowley, Gareth Thomas, Jeanette Hawkes, and Sarah Walsh to name a few - each of you have lifted me up and spurred me on. Thanks to my fellow badminton players for letting me blow off steam and giving me perspective on life as a researcher. Gabriel Tun, you were there for me during a tough few months writing up. This meant a great deal to me.

I would also like to acknowledge the sense of purpose, comfort, and joy that my cats Tuppence and Nancy brought me, as well as my dearest Rascal and Fluffy and other feline friends, especially Purdey, Ula, Freya, and Sammy. Stripes are on my soul and stars are in the night sky.

Finally, I acknowledge my hot water bottle which has been by my side day in, day out.

# Dedication

Dedicated to *The Sea*

> *From depths of living waters we arise,*
> *When thou dost call;*
> *Up from the caverns of an ancient sea,*
> *Bound in thy thrall;*
> *We grasp our many-chording harps of nacrèd shell,*
> *Lean on a heaving surge's rounded swell,*
> *From brows sweep back the tendril-twining locks,*
> *And sing:*
>
> *Du Sterblicher, was machst Du hier?*
> *Geh heim! zurück!*
> *Für Dich zu salzig ist das "Meerall" Bier,*
> *Der Wallfischschnitt zu dick.*
> *Wir alle sind zwei hundert tausend tausend Jahre alt,*
> *Du Neues noch ....*
> *Potz tausend! dort steht Neptun zornig brausend.*
> *Ihr Schwestern, sinkt!*
> *Erdbub', 's ist Schade doch.*

Percy William Shedd and Henrik Ibsen, *The Oceanides*, 1902

# 1

# Introduction

## 1.1 The North Sea

The North Sea is a semi-enclosed continental shelf sea that lies between mainland northwestern continental Europe, Great Britain, and Scandinavia (Figure 1.1.1, A). This marine region is of particular economic importance to many maritime industries in the bordering countries, in particular to fisheries and energy industries (Halsnæs et al., 2016; Pinnegar et al., 2016). These industries, however, and other human activities such as coastal development, have placed considerable pressure on North Sea ecosystems (Walday and Kroglund, 2002). Consequently, activities that heavily impact the North Sea are regulated in an attempt to maintain the health of its marine ecosystems.

For effective ecosystem-based management of the North Sea, the monitoring of key biological ecosystem indicators across the North Sea and the wider Northeast Atlantic has been identified as critically important (EU, 2008; McQuatters-Gollop et al., 2022). Ecosystem indicators consider elements of the ecosystem that are not the traditional focus of biological monitoring efforts (e.g. fish stock surveys) such as ecosystem functioning and plankton abundance, distribution, and community composition (OSPAR, 2017). Fundamental to the utility of biological monitoring efforts is understanding how variability in the environment shapes species distributions, community structure, and ecological relationships. This thesis investigates sub-mesoscale ($< 10\,\mathrm{km}$) environmental drivers of zooplankton distributions in the central North Sea, observed using acoustic data collected by an autonomous surface vehicle (ASV), the Wave Glider, during Spring 2018.

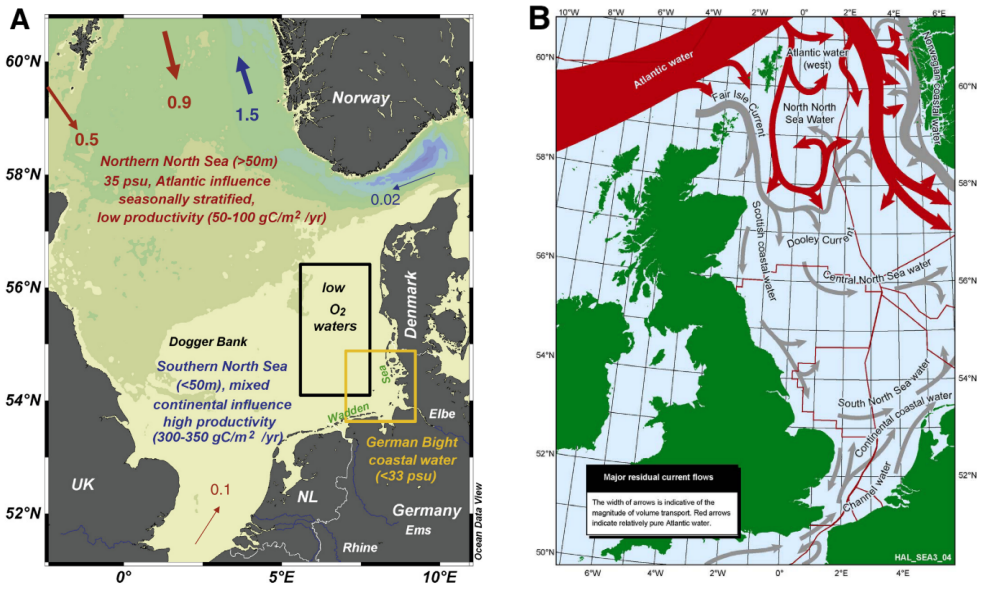


Figure 1.1.1: **General water properties and circulation pattern of the North Sea.** A) Differences between Northern North Sea and Southern North Sea water properties, and the division between regions at Dogger Bank. Average water mass transports indicated by arrows and numbers (Sverdrup units). Image reproduced from Figure 1 in Emeis et al. (2015). B) General circulation, showing inflow of Atlantic water into the North Sea. Image reproduced from Figure A3d.1 in Appendix 3 of UK Government (2009).

### 1.1.1 Pelagic food webs

Zooplankton are a polyphyletic group that encompass a huge variety of taxa, some of which are planktonic for only part of their life cycle, usually during larval stages. The majority of zooplankton are heterotrophs, deriving energy from grazing on phytoplankton or consuming other, usually smaller, zooplankton. They form key components of marine food webs, serving as the link between primary production and higher trophic levels such as marine mammals, seabirds, and piscivorous fishes. This trophic linkage is mediated by the consumption of zooplankton by larval fish, themselves planktonic during this life stage, and by so-called 'forage' fish which are small, fast-growing and short-lived planktivorous pelagic fish species that are consumed by larger fish and other top marine predators (Pikitch et al., 2014; Ratnarajah et al., 2023; Steinberg and Landry, 2017).

The North Sea sustains a wide variety of fish species including a diverse assemblage of forage fishes, many of which are commercially important and support large-scale industrial

fisheries. Of particular economic importance are fisheries for herring (*Clupea harengus*), sprat (*Sprattus sprattus*), Norway pout (*Trisopterus esmarkii*), and lesser sandeel (*Ammodytes marinus*) (Engelhard et al., 2014). These forage fish species and others, such as European anchovy (*Engraulis encrasicolus*), rely on a diet primarily consisting of zooplankton both in their larval and adult stages (Lindegren et al., 2018; Raab et al., 2012; Mehl and Westgård, 1983; Bromley, 1997). These fishes form the prey-base for many larger, piscivorous fish such as cod (*Gadus morhua*), haddock (*Gadus aeglefinus*), whiting (*Gadus merlangus*), saithe (*Pollachius virens*) and horse mackerel (*Trachurus trachurus*), which themselves can be the subject of commercially important fisheries, as well as seabirds and marine mammals in the North Sea (Cury et al., 2011; Engelhard et al., 2014).

### 1.1.2 Monitoring zooplankton

Given the central role of zooplankton in North Sea food webs as the direct or indirect prey-base for many commercially important fish species and other animals, monitoring zooplankton distributions is recognised as fundamental to an ecosystem-based approach to its management (Mackinson and Daskalov, 2007; McQuatters-Gollop et al., 2022; Lindegren et al., 2009; Ressler et al., 2012). However, zooplankton can be difficult to monitor due to their propensity to form patchy, ephemeral distributions (Klais et al., 2016; Hjøllo et al., 2021).

By their very nature, zooplankton have limited capacity to swim against currents and so physical forcings, such as currents, upwelling and downwelling, and strong density gradients (for example, horizontal gradients across fronts and vertical gradients across thermoclines), can exert a powerful influence on shaping their distribution in the water column (Denman et al., 2001; McGillicuddy, Jr, 2001). But patchiness is also the product of active mechanisms which aggregate or disperse animals. For example, directed movements (i.e. swimming) to gain access to better foraging conditions, reduce predation risk, and seek environments associated with lower metabolic costs can increase spatial heterogeneity in zooplankton distributions (Folt and Burns, 1999; Prairie et al., 2012; Robinson et al., 2021).

Physical and biological processes that affect patchiness act over different scales. At large scales ($> 10\,\mathrm{km}$), mesoscale physical processes dominate, whereas at very small scales ($< 10\,\mathrm{m}$), biological processes dominate (Folt and Burns, 1999; Prairie et al., 2012). At sub-mesoscales (1-10 $\mathrm{km}$), both physical and biological processes are expected to exert significant control on zooplankton patch dynamics. The study of drivers of zooplankton patchiness at the sub-mesoscale level therefore makes for a challenging but fascinating problem to address, since both behavioural mechanisms and physical forcings play a role in shaping their distributions both horizontally and vertically within the water column.

Monitoring surveys typically analyse data at sub-mesoscale or smaller resolution, and therefore a better understanding of the drivers of patch dynamics at these scales may lead to improvements in survey design and the accuracy and precision of survey-derived estimates. Furthermore, understanding the relationships between zooplankton distributions, including their utilisation of different regions of the water column, and their environment is crucial to a better understanding of ecosystem function and the prediction of future change. This is of particular importance since ocean ecosystems in the North Sea and worldwide are undergoing rapid transitions due to climate change (Otto et al., 2014; Klais et al., 2016; Pershing et al., 2010; Ratnarajah et al., 2023).

### 1.1.3 Oceanography

The North Sea has two main oceanographic regimes, that of the Northern North Sea (NNS) region and the Southern North Sea (SNS) region. These regions are divided by a shallow bathymetric feature: Dogger Bank, which lies at approximately $54.45°$N, $1.55°$E (Figure 1.1.1, A). Like many other continental shelf seas, the North Sea is relatively shallow with an average mean depth of $90\,\mathrm{m}$ (Ducrotoy et al., 2000). However, depths range from 0-$500\,\mathrm{m}$ in the NNS, contrasting with the much shallower depths south of Dogger Bank in the SNS, which typically only reach $50\,\mathrm{m}$ (Van Leeuwen et al., 2015).

North Sea waters are comprised mostly of inflow from the North Atlantic and fresher water originating from coastal runoff and riverine output, with general circulation that follows a counter-clockwise direction (Figure 1.1.1, B). Water properties in the NNS are dominated

by colder, saltier oceanic waters entering from the North Atlantic into the northern basin, whereas fresher input coming from the English Channel has a greater influence on water properties in the SNS (Emeis et al., 2015). The varying mixture of different waters flowing through the North Sea, including those of oceanic and coastal origin, are a key driver of variation in physical water properties over small temporal and spatial scales (Sheehan et al., 2020; Salt et al., 2013; Mathis et al., 2015). These water masses of differing origins are associated with the transport of different zooplankton communities across the region (Turrell, 1992; Lindley and Batten, 2010; Edwards et al., 1999). Consequently, the different oceanographic regimes of the NNS and SNS are reflected by the differing ecosystems, including different zooplankton communities, within these regions (Otto et al., 1990; Emeis et al., 2015; Fransz et al., 1991; Krause et al., 1995).

Situated in the mid-latitudes, the vertical structure of the water column in the North Sea undergoes rapid change over seasonal timescales, exhibiting spatial heterogeneity across the region (Van Leeuwen et al., 2015). Owing to its shallowness, the SNS is typically warmer than the NNS and remains well-mixed throughout the year. The NNS, on the other hand, undergoes seasonal stratification during late Spring, forming a two-, or sometimes three-layer system with warmer water above the pycnocline(s) and cooler water nearer the bottom. This system persists until stratification in the upper water column breaks down in late autumn and winter (Van Leeuwen et al., 2015; Sharples et al., 2006).

Stratification provides the necessary stability to promote vast blooms of phytoplankton in spring, the timing of which affects the abundance and composition of zooplankton populations (Melle and Skjoldal, 1998; Sharples et al., 2006). The timing of phytoplankton and zooplankton growth periods in turn affects juvenile fish recruitment (Platt et al., 2003). Springtime therefore represents a critical time of year when oceanographic changes associated with the onset of stratification exert significant control over biological growth rates and consequently lead to pronounced shifts in zooplankton dynamics.

### 1.1.4 Study region: the central North Sea

The central North Sea region, which lies north of Dogger Bank, follows the oceanographic regime of the NNS and undergoes seasonal stratification (Figure 1.1.1, A). The region is relatively shallow; typical depths rarely exceed $100\,\mathrm{m}$. Consequently, even the deepest water near the seabed is situated within the epipelagic, with steep vertical gradients in sunlight pervading the water column during the day. A relatively shallow mixed layer depth in this seasonally stratified region also allows for the formation of deep chlorophyll maxima during spring (Weston et al., 2005; Fernand et al., 2013).

Stratification acts to stabilise the water column and limit vertical exchange of nutrients, leading to seasonal oxygen depletion below the thermocline (Queste et al., 2016). Vertical gradients in light, temperature, oxygen, and phytoplankton distributions create a highly structured pelagic environment during Spring in the central North Sea. However, it is also a highly dynamic environment at this time of year, influenced by variable inflow of North Atlantic waters (Sheehan et al., 2020), which the prevailing current transports eastwards across the region (Figure 1.1.1, B), rapid changes in temperature near the surface, and rapid population growth across a diversity of taxa (Van Leeuwen et al., 2015; Krause et al., 1995; Sharples et al., 2006). Stratification in the North Sea is predominantly thermally-driven, and can result in average differences in water temperature between near the seabed and at the surface of more than $10\,^{\circ}\mathrm{C}$ during the summer months (Van Leeuwen et al., 2015). This creates a highly heterogeneous environment for zooplankton and fish, where conditions in some parts of the water column are changing more rapidly than elsewhere and both foraging conditions and the abundance and distribution of predators can fluctuate over short timescales.

### 1.1.5 Climatic drivers of ecosystem change

The North Atlantic Oscillation (NAO), an alternation between air pressure differences between the Azores High and Iceland Low, is the dominant mode of climate variability across the North Atlantic and North Sea (Wanner et al., 2001; Becker and Pauly, 1996).

A positive NAO index defines a state of greater pressure difference associated with strong westerly winds, whereas a negative NAO index is associated with weak westerlies. Stronger westerlies bring warmer air to the North Sea but also enhance the strength of the Atlantic subpolar gyre. This leads to increased shelf exchange and hence increased inflow of Atlantic waters into the North Sea (van der Molen and Pätsch, 2022a). Consequently, the NAO is correlated with several important atmospheric and oceanographic variables in the North Sea. These include precipitation, sea surface temperature (SST), salinity anomalies, sea surface pressure, surface pH and $CO_2$ uptake, wave-height and sea-level (Becker and Pauly, 1996; Salt et al., 2013; Chen et al., 2014; Mariotti and Arkin, 2007; van der Molen and Pätsch, 2022a; Mathis et al., 2015). The strengths of correlations between oceanographic variables are spatially heterogeneous across the region and also vary seasonally, being typically stronger during the winter when wind speed anomalies are higher, and also vary over longer annual and multi-annual timescales. Stronger and more variable winds in winter also result in a less stable circulation pattern compared to summer, as well as inducing vertical mixing that breaks down stratification (Mathis et al., 2015; van der Molen and Pätsch, 2022a).

The state of the NAO also influences advection of Atlantic waters into the North Sea through the English Channel in the southwest and the Fair Isle Passage near the Orkney Islands in the northwest (Turrell, 1992). Advection of North Atlantic water transports salt, nutrients, and colder temperatures to the North Sea, together with oceanic plankton (van der Molen and Pätsch, 2022a; Ottersen et al., 2001; Heath et al., 1999). Several episodic inflow events, attributed mainly to wind forcing, have been observed over recent decades (Winther and Johannessen, 2006). However, in regions of the North Sea where advection is weaker, such as central regions, changes in surface temperatures are mainly driven by air-sea exchange processes (Becker and Pauly, 1996; Hjøllo et al., 2009). Whilst the NAO explains some of the variability in the strength of North Atlantic inflow into the North Sea, it does not account for it entirely. Other factors, such as the strength of the North Atlantic Current and shelf edge current, also influence North Sea water properties, particularly in peripheral regions near inflow passages across the northern North Sea and English Channel (Mathis et al., 2015; van der Molen and Pätsch, 2022a).

Episodic inflows of oceanic water have had a considerable impact on North Sea ecosystems and led to pronounced shifts in plankton community structure (Edwards et al., 2001; Planque and Fromentin, 1996; Alvarez-Fernandez et al., 2012). Notable hydro-climatic events in the late 20$^{th}$ century include: the Great Salinity Anomaly of the 1970s when a pulse of cold, fresher water advected through the North Sea and inflow of Atlantic water was reduced, delaying the onset of the spring bloom (Edwards et al., 2002); an inflow of warmer, southerly-derived oceanic water associated with a reversal in the NAO index to a strongly positive state in the late 1980s, that triggered a series of stepwise changes that ultimately led to an ecosystem 'regime shift' after 1987 (Reid et al., 2001; Beaugrand, 2004); and a similar reversal to a strong positive NAO index in 1997 when anomalously warm water advecting northwards brought more temperate species to the southern North Sea, increasing the abundance of neritic plankton such as echinoderm and decapod larvae (Edwards et al., 1999).

The regime shift of 1987 initiated profound changes in the seasonal dynamics, community structure, and distributional ranges of North Sea plankton (Reid et al., 2001; Beaugrand et al., 2003). This had far-reaching consequences that impacted higher trophic levels and fisheries (Beaugrand, 2003; Kirby et al., 2009; Reid et al., 2001), altered synchrony between geographically distant plankton populations (Defriez et al., 2016), and caused abrupt changes in the benthos (Kröncke and Knust, 1995; Kirby et al., 2008). In fact, a cascade of regime shifts was revealed to have occurred during the 1980s, forced by rapid changes in temperature that impacted both marine and terrestrial ecosystems worldwide (Reid et al., 2016).

Many changes were observed during the North Sea regime shift. Of relevance here are those that describe how zooplankton distributions and communities were restructured as a consequence of environmental changes. Through a process of trophic amplification (Kirby and Beaugrand, 2009), higher temperatures led to changes in phytoplankton composition and elevated biomass (Edwards et al., 2001; Reid et al., 2001; Alheit et al., 2005), although primary production since declined (Capuzzo et al., 2018); an insurgence of warm-water decapods linked with the decline in bivalves and poor flatfish recruitment (Lindley et al., 2010; Kirby et al., 2008); and reduced abundance and range of the boreal *Calanus finmarchicus* copepod concomitant with increased abundance and northwards range expansion of the

congeneric temperate *Calanus helgolandicus* (Beaugrand, 2003; Alheit et al., 2005; Reid et al., 2003).

Enhanced inflow associated with positive NAO indices is also thought to have brought more jellyfish to the region, with higher temperatures and associated changes in pH creating more favourable conditions for their proliferation (Attrill et al., 2007; Kirby et al., 2009). Species richness of zooplankton was estimated to have increased despite resident cold-water holoplankton having declined (Lindley and Batten, 2010). Particularly near inflow regions, a rise in the number of meroplankton and temperate species generally drove transient increases in species richness; however Lindley and Batten (2010) argue that overall the increase in species richness is indicative of a long-term trend associated with the rising trend in sea surface temperature (Beaugrand, 2003).

Temperature plays a pivotal role in the physiology and life history traits of many zooplankton, which in part explains its effects on their ecology and spatiotemporal distributions (Richardson, 2008; Horne et al., 2016; Evans et al., 2020). Thermal tolerances and preferences differ between species, but, being poikilotherms, zooplankton physiology and activity are strongly temperature-dependent (Hirche, 1987; Halsband-Lenk, 2001). Metabolic, ingestion, reproductive, and respiration rates of many zooplankton species found in the North Sea are tightly coupled to water temperature (Heine et al., 2019; Lee et al., 2003; Ward and Hirst, 2007; Widmer et al., 2016; Gambill et al., 2018). Through both its direct and indirect influences, temperature is arguably the oceanographic variable of foremost significance in structuring marine ecosystems (Richardson, 2008).

Clearly, temperature has been an important driver of changes in the North Sea ecosystem over recent decades (Figure 1.1.2), with plankton community dynamics heavily influenced by variable inflow of colder oceanic water (Reid et al., 2003). However, whilst atmospheric and oceanographic properties are known to be strongly associated with changes in zooplankton distributions over seasonal, annual and multi-annual timescales and across regional spatial scales in the North Sea, it is less well known whether these properties drive distribution patterns over shorter, sub-seasonal timescales and sub-mesoscale spatial scales.

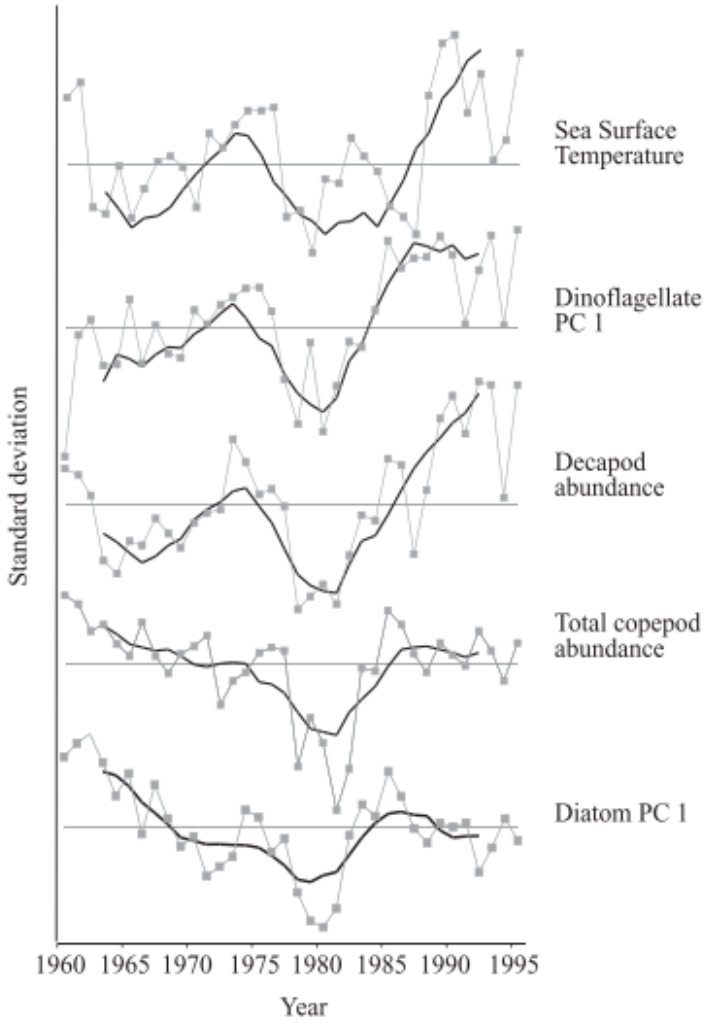


Figure 1.1.2: **Long-term trends in North Sea sea surface temperature (SST) and various components of the plankton community from 1960 to 1995.** Figure 1 from Edwards et al. (2002). Annual (grey squares, lines) and 3 year running means (bold line) of SST, first principal component (PC 1) of phytoplankton biomass (dinoflagellates, diatoms), and abundance of zooplankton (decapods, copepods), with data standardised to zero mean (horizontal line) and unit variance.

## 1.2 Diurnal movement patterns of fish and zooplankton

Diel vertical migration (DVM) is a ubiquitous behaviour across the world's oceans and lakes undertaken by numerous zooplankton and fish species (Hays, 2003). It describes the daily phenomenon of organisms migrating to and from deeper waters associated with varying light levels over the diel period. DVM is considered to be foremost a strategy to balance the trade-off between foraging in near-surface waters, associated with higher quality and quantity

of phytoplankton prey, and reducing the risk of visual detection by predators (Lampert, 1989). Classic, or nocturnal, DVM is the most commonly documented migration pattern; organisms migrate towards the surface at dusk and spend the nighttime in shallower waters, returning to deeper waters around the onset of dawn (Bandara et al., 2021). Spending daylight hours in deeper water reduces exposure to light levels that increase the risk of detection by visual predators (Giske et al., 1994; Aarflot et al., 2020). At dusk organisms migrate upwards to spend the night in shallower waters with more favourable foraging conditions. Other theories have been proposed to explain the adaptive significance of DVM (reviewed in Lampert, 1989). These include: metabolic advantages to intermittent feeding that allow for algal recovery during the day; and feeding in warmer waters at night but resting in colder water during the day in order to reduce metabolic demands (Enright, 1977; McAllister, 1969; McLaren, 1963). However, reducing light-mediated predation risk, which varies according to the diel cycle, provides the most straightforward, unifying explanation of disparate vertical migration patterns.

Variations of the classic DVM patterns include: reverse DVM, whereby organisms reside in shallower waters during the day and migrate to depth at night (Ohman et al., 1983; Zwolinski et al., 2007); and twilight or double DVM, whereby organisms ascend at dusk and descend at dawn as per classic DVM, but also perform a second migration (often termed 'midnight sinking') by returning to depth during the middle of the night and reascending prior to dawn (Cohen and Forward, 2005a; Tarling et al., 2002). Both alternative variations in DVM pattern can be explained by the same need to balance the trade-off between foraging and predator-avoidance. Reverse DVM behaviour may be driven primarily by the need to avoid predators that perform classic DVM, rather than by the need to avoid visual predators (Ohman et al., 1983; Irigoien et al., 2004). Several, sometimes contested, explanations for the midnight sinking behaviour that defines twilight DVM have been put forward. These include: that it is a response to the arrival of classic DVM-performing predators; that organisms are passively sinking due to low activity rates; and that organisms are retreating to safer depths once satiated, with ascent later in the night to commence foraging once again (Tarling et al., 2002; Pearre, 2003a,b; Cohen and Forward, 2005b). Hereon, use of the term DVM refers to the classic DVM pattern, unless otherwise stated.

Many forage fish species display diurnal patterns of movement behaviour that impact the patchiness of their distribution in the water column. Forage fish are typically obligate schoolers, aggregating in schools that remain at depth during the daytime (although see Zwolinski et al., 2007) to reduce their predation risk, and disperse at night to forage, mainly on zooplankton (Magurran, 1990; Fernandes et al., 2001; Cardinale et al., 2003). Schools are shoals or aggregations of fish that exhibit co-ordinated movement behaviour (Pitcher, 1978). They may be monospecific or comprised of a mixture of species (Stanton et al., 2012). Schooling serves to increase detection of, and reduce response times to, predators, thus providing substantial fitness benefits (Magurran, 1990). However, schooling may come at the cost of increased local resource depletion particularly within central regions of the school (Killen et al., 2012). Typical diurnal patterns in schooling fish behaviour therefore influence both the heterogeneity of fish distributions in the water column, and their average position in the water column.

### 1.2.1 Impacts of DVM on the biological carbon pump

Zooplankton occupy a central position in pelagic ecosystems by mediating energy transfer between primary producers and higher trophic level predators. As such they are an important component of the biological carbon pump (BCP) (Boyd et al., 2019; Steinberg and Landry, 2017). DVM by zooplankton actively transports carbon and nitrogen across a range of depths each day (Iversen, 2023; Darnis et al., 2017). Boyd et al. (2019) estimated that the mesopelagic-migrant pump, i.e. active transport to depth by vertical migrations, stores the equivalent of $60\,\%$ of the carbon accounted for by the biological gravitational pump (the component of the BCP that accounts for passive sinking under gravity). Archibald et al. (2019) estimated that more than $12\,\%$ of global carbon export from the euphotic zone can be attributed to DVM. Bianchi et al. (2013b) modelled the contribution of DVM to carbon export at three study sites across a range of latitudes with distinct ecosystems and DVM dynamics, producing estimates that ranged between 10-20 $\%$ of total export. In a high-arctic fjord in winter, Darnis et al. (2017) estimated that export due to DVM exceeded $40\,\%$ of wintertime particulate organic carbon (POC) sinking.

Estimates of the contribution of zooplankton DVM to carbon export are wide-ranging owing in part to the complexity of interaction-processes that control export efficiency, variability in biological productivity, and the variability in DVM behaviour itself. Zooplankton interact with aggregates of POC in a multitude of ways that can result in either further aggregation which increases BCP efficiency, for example by ingesting small aggregates and producing larger, faster-sinking faecal pellets (Belcher et al., 2017; Pauli et al., 2021), or the fragmentation of aggregates, for example by swimming activity (Dilling and Alldredge, 2000; Goldthwait et al., 2004), which can decrease BCP efficiency. DVM behaviours vary seasonally, regionally, and according to species and life-history stages of migrators, affecting in turn the active transport of carbon (Isla et al., 2015; Takahashi et al., 2009; Dypvik et al., 2012; Klevjer et al., 2016; Darnis et al., 2017; Gorgues et al., 2019). The amplitude of migrations (vertical distance covered), depth distributions of the migrations (where in the water column they take place), and proportion of migrators within a population, are key aspects of DVM behaviour that impact the efficiency of the migrant-pump (Gorgues et al., 2019; Takahashi et al., 2009). Even shallow migrations have the potential to influence carbon export in shelf seas by transporting carbon across pycnoclines where organic matter may otherwise accumulate, for example at the deep chlorophyll maximum (DCM).

## 1.3 Fisheries acoustics

Fisheries acoustic methods are increasingly used to study the abundance, distribution, ecology and behaviour of fish and zooplankton, particularly in relation to the ecosystems in which they live (e.g. Greenlaw, 1979; Maclennan and Holliday, 1996; Godø et al., 2014; Handegard et al., 2013). Acoustic methods are a powerful tool with widespread applications that include the study of: inter- and intra-specific interactions; behavioural responses to anthropogenic structures and stressors; associations with physical features of pelagic and benthic environments; aggregation and social behaviour; migration, movement and habitat use; and geographic range distributions (reviewed in Benoit-Bird and Lawson, 2016). Acoustics can even be used to shed light on the physiology of animals, for example by remotely sizing fish (Kubilius et al., 2020). Quantitative estimates of animal biomass,

abundance and distributions can be produced from acoustic survey data. These biomass and abundance estimates are routinely used to inform fisheries stock assessments and contribute to ecosystem-based management Doray et al. (2018); Reiss et al. (2021); ICES (2023); Trenkel et al. (2011); Fernandes et al. (2002). These applications are largely possible due to the ability of acoustic tools to rapidly survey vast expanses of the underwater environment, providing a synoptic overview of animal distributions. In addition, acoustic sampling can produce measurements at high spatial and temporal resolutions, and is non-invasive. However, as an indirect sampling method, acoustic measurements can often only provide a coarse taxonomic resolution and they benefit from auxiliary data, such as net or optical samples, for ground-truthing (Benoit-Bird and Lawson, 2016).

### 1.3.1 Instruments and data visualisation

Acoustic surveys utilise a variety of instruments, including side-scan and multi-beam sonar, acoustic current doppler profilers (ADCPs), and acoustic cameras (Simmonds and MacLennan, 2005). However, by far the most common instrument used in fisheries acoustics is the scientific echosounder. Scientific echosounders are highly precise and accurate transceivers which convert between electrical signals (voltage) and sound pressure waves. The echosounder sends a transmit signal of known frequency, power and duration to the transducer which converts the signal to a short pulse of sound, known as a *ping*. This pulse of sound is emitted as a focused acoustic beam with a known strength and pattern of directivity. The echosounder then listens for echoes returning from scatterers encountered by the acoustic signal in the water column, mapping their range (and hence depth) by calculating the time it takes for the echoes to return. Scattering occurs when a sound wave encounters a change in density along its propagation path. Both solid objects and fluids can scatter sound. Generally, a greater density difference between the scatterer and the medium results in proportionally more acoustic energy being reflected, and hence a greater backscattering strength. Conventional fisheries acoustic surveys use a combination of narrowband frequencies at 18, 38, 70, 120, 200, and 333 kHz, and - less common, but sometimes used for studying very small targets such as zooplankton - 1 MHz. The term *ping* is used to refer both to the transmitted signal and the signal received during the listening

period from returning echoes (backscatter), and can be referenced by the time and location that the transmit and receive cycle occurred.

Scientific echosounders are most commonly installed on research vessels with the transducers located on the bottom of the hull or drop keel, oriented to point the acoustic beam vertically downward (Simmonds and MacLennan, 2005). Each ping samples the water column directly below the ship, mapping the acoustic environment as the ship travels along. However, echosounders can be installed on a variety of platforms and oriented in different ways according to the platform type. For example, they have been installed on underwater gliders such that the acoustic beam is downward-facing during downcasts of the glider, downward-facing on towed bodies and ASVs, and upward-facing on bottom-mounted stationary moorings (e.g. Benoit-Bird et al., 2018; Reiss et al., 2021; Meyer-Gutbrod et al., 2012; Trevorrow, 2003; Kloser, 1996).

Each ping records returning echoes as an array of power values. These arrays can be visualised in echograms which depict data from each ping as consecutive vertical lines. Commonly, power is converted to an acoustic quantity known as volume backscattering strength for echogram visualisation, with variations in backscattering strength depicted using a colour scale. Samples from the listening period of each ping are converted to an estimate of range or depth (y-axis). Pings are plotted along the horizontal axis to represent either time, along-track distance, or geographical coordinates. Visual interpretation of echograms has historically been fundamental to the analysis of fisheries acoustics data (Simmonds and MacLennan, 2005; Peña, 2021; Blackwell et al., 2019b), although analyses that incorporate non-graphical means of interpreting data, such as machine learning techniques for classification, are becoming increasingly common (Malde et al., 2020; Handegard et al., 2021).

### 1.3.2 Acoustic backscatter

Volume backscattering strength is an acoustic quantity derived from received power, one of the fundamental metrics recorded by the echosounder, in units of decibels ($\mathrm{dB}$) relative to $1\,\mathrm{W}$ reference power. Volume backscattering strength is more useful for measuring

acoustic reflections from organisms in the water column than power since it describes the reflected sound energy normalised by the volume of water sampled, and accounts for known attenuation losses due to beam spreading and absorption. As range from the transducer increases, so too does the width of the acoustic beam and hence the sampling volume. Normalising by the size of the sampling volume allows for meaningful comparisons to be made between measurements at different depths of the water column, and is therefore essential for quantitative analyses. However, as a consequence of the increasing acoustic beam width with depth (range), samples are averaged over a larger volume with increasing depth, resulting in more horizontal smearing of echoes.

Formally, volume backscattering strength, symbolised $S_v$, describes the mean strength of acoustic backscattering in $\mathrm{dB\ m^{-1}}$ (Maclennan et al., 2002). It is a decibel quantity in the logarithmic domain, related to its linear counterpart the volume backscattering coefficient, $s_v$, by the relationship $S_v = 10log_{10}(s_v)$. When averaged over a finite sampling volume, defined by the cross-section of the main acoustic beam and a finite sampling period, this quantity can also be termed Mean Volume Backscattering Strength (MVBS). Unless otherwise noted, all arithmetic operations using volume backscattering strength in this thesis were conducted in the linear ($s_v$) domain, and acoustic symbols and quantities follow the conventions adopted by the wider fisheries acoustics community as set out in Maclennan et al. (2002).

### Derivation of backscattering strength from power

Volume backscattering strength can be derived from received power using a form of the sonar equation given by Equation 1.3.1, where $R$ is the corrected range ($\mathrm{m}$), $P_r$ is the received power ($\mathrm{dB\ re\ 1\ W}$), $P_t$ is the transmitted power ($\mathrm{W}$), $\alpha$ is the acoustic absorption coefficient ($\mathrm{dB\ m^{-1}}$) which describes the energy loss of sound pressure waves in seawater, $c$ is the speed of sound in seawater ($\mathrm{m\ s^{-1}}$), $\tau$ is the pulse duration ($\mathrm{s}$), $\psi$ is the equivalent two-way beam angle (steradians), $G_0$ is the transducer peak gain (non-dimensional), $\lambda$ is the wavelength of the acoustic signal equivalent to $c/f$ ($\mathrm{m}$) where $f$ is the central frequency ($\mathrm{Hz}$), and $corr$ is a correction factor ($\mathrm{dB\ re\ 1\ m^{-1}}$).

$$S_v(R, P_r) = P_r + 20log_{10}R + 2\alpha R - 10log_{10}\left(\frac{c\tau\psi}{2}\right) - 10log_{10}\left(\frac{P_t G_0^2 \lambda^2}{16\pi^2}\right) - 2corr \tag{1.3.1}$$

The $10log_{10}(c\tau\psi/2)$ term in Equation 1.3.1 scales backscattering by the sampling volume approximated by a spherical shell of thickness $c\tau/2$ (half the pulse length) intersected by the equivalent beam angle, $\psi$, to account for transducer directivity. The final two terms of Equation 1.3.1 are both correction factors determined during calibration of the echosounder. The penultimate term applies an on-axis gain which accounts for the difference between a mathematically idealised lossless transmit intensity and the intensity actually achieved by the transducer (Demer et al., 2015). The $corr$ correction factor, if used, aims to account for differences between the theoretically estimated pulse duration and the actual (effective) pulse duration achieved by the transducer. The $20log_{10}R + 2\alpha R$ terms in Equation 1.3.1 are collectively known as the time-varied-gain function (TVG). This function applies gain to compensate for some forms of predictable signal losses during propagation.

### 1.3.3 TVG compensation of signal losses

Absorption of sound waves by seawater and geometric spreading of the acoustic beam causes signal loss, otherwise known as attenuation, with range. With knowledge of the water properties, such as temperature, salinity, pH, and the wavelength or frequency of the transmitted signal, it is possible to predict the effects of beam spreading and absorption fairly precisely such that the TVG function can be applied to compensate for these signal losses when converting from power to volume backscatter.

A fundamental physical principle of the conservation of energy holds that the sum of the sound intensity integrated over the travelling wavefront is, at most, equal to the intensity of the transmitted signal. This redistribution of intensity over a larger area is referred to as beam spreading, which describes both the physical spreading of the beam with range and the consequent decrease in energy at the wavefront. From a point source, spherical

geometric spreading of a sound wave in an isotropic medium reduces the intensity of the sound wave at any one point at the wavefront according to the inverse square law, where the loss is equal to $1/4\pi R^2$ at distance $R$ (range) along the propagation path. For a single transmit-receive cycle of an echosounder signal, geometric spreading has "acted twice" to reduce the sound intensity: first when the signal is transmitted from the transducer, and a second time when the signal is backscattered from the acoustic target and travels back towards the transducer. Thus, spherical geometric spreading rapidly reduces the intensity of an active acoustic signal proportionally to $R^{-4}$ for a target detected at range $R$.

The nominal TVG function for volume backscatter calculations is $TVG(R) = 20log_{10}R + 2\alpha R$, where $R$ is the range to the acoustic target, defined as $R = ct/2$, i.e. the distance from the transducer is half the time ($t$) taken for the signal to travel to the target and back again multiplied by the speed of sound underwater ($c$). At short range, signal loss is dominated by geometric spreading rather than absorption (Figure 1.3.1), however at greater depths absorption losses can dominate.

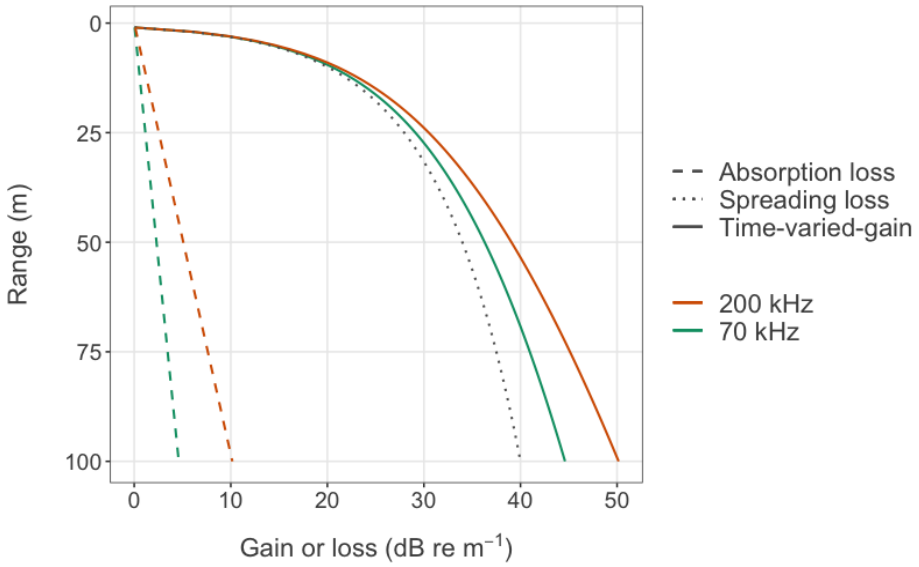


Figure 1.3.1: **Time-varied-gain functions (solid lines) to compensate for losses (broken lines) of 70 kHz (green) and 200 kHz (orange) signals, to 100 m range.** Absorption (dashed) and geometric spreading losses (dotted) cause increasing, but largely predictable, signal loss with range. TVG increasingly amplifies the signal with range to normalise backscatter of acoustically identical targets at different ranges. Geometric spreading is frequency-independent.

Energy loss from absorption in seawater occurs due to viscosity and the relaxation of certain compounds present in the water, converting sound energy to heat. The absorption coefficient, $\alpha$, is measured in $\mathrm{dB}$ per unit distance and depends on pH, frequency, water temperature and salinity (Foote, 1981). The reduction of sound intensity of the signal at point $R$ along the propagation path is given by: $I(R) = I_0 10^{-\frac{\alpha R}{10}}$, where $I_0$ is the transmit intensity. For an acoustic signal transmitted and received by a transducer, absorption acts along a path twice the length of the range.

### 1.3.4 Classifying acoustic data

Acoustics can provide information on a wide variety of animals that cohabit the water column, enabling studies of interactions between different components of the ecosystem (Benoit-Bird and Lawson, 2016; Godø et al., 2014). This ability to sample a wide variety of animals, however, means that backscatter data must first be partitioned and apportioned to meaningful scattering groups in order to distinguish taxa and interpret biological patterns within the data (Korneliussen, 2018). This process is known as classification. This is usually achieved by grouping data according to its acoustic properties, incorporating ecological knowledge of known scatterers in the ecosystem to identify which animals may be responsible for each group, and verifying independently using one or more ground-truthing techniques. Ground-truthing is most commonly carried out by comparing acoustic data to complementary net or optical samples taken in the same place and time as the acoustic sampling was carried out (Simmonds and MacLennan, 2005; Korneliussen, 2018; McClatchie et al., 2000). Net and optical samples often provide taxonomic and size-class information that are not available through acoustic analyses alone. Ground-truthing using an independent methodology is important not only to determine which organisms may be responsible for the observed patterns in backscatter but also to assess the likelihood of acoustic masking which may obscure the presence of weaker scatterers (McClatchie et al., 2000; Kloser et al., 2016).

Frequency response describes the relationship between backscattering strength of a scatterer and frequency. The strength of backscattering from an animal is frequency dependent, the relationship being principally a function of the material properties of the animal, its size,

and its orientation in the acoustic beam (Simmonds and MacLennan, 2005; Stanton et al., 1996). Gelatinous and small, larval zooplankton tend to be very weak scatterers, whereas animals that are large, or contain gas-inclusions, hard carapaces or shells, tend to be stronger scatterers.

Scattering by different kinds of fish and zooplankton can be distinguished by the frequency response pattern (Trenkel and Berger, 2013; Stanton et al., 1996; Martin et al., 1996). Whilst not a unique taxonomical identifier, frequency response can be indicative of different acoustic scattering groups. Figure 1.3.2 illustrates common frequency response patterns characteristic of different kinds of scatterers. Fish with swimbladders, which contain gas, and zooplankton with gas-inclusions typically resonate strongly at frequencies lower than those used for fisheries acoustics which normally range from $18$ to $333\,\mathrm{kHz}$. Above the resonance frequency, target strength of these gas-bearing animals either remains relatively constant or declines gradually (Scoulding et al., 2015; Proud et al., 2019). In contrast, zooplankton that do not contain gas are typically weak scatterers, classed as either fluid-like or elastic-shelled scatterers depending on whether the boundary of the body can support a shear wave (Stanton et al., 1998). Elastic-shelled scatterers typically have stronger target strengths than fluid-like scatterers, however both exhibit a similar frequency response pattern. This pattern is characterised by a steep rise is target strength over the Rayleigh scattering region at frequencies below the resonant frequency (which is related to the ratio between acoustic wavelength and cross-sectional area of the scatterer in the acoustic beam), and above the resonant frequency target strength oscillates with decreasing amplitude in what is known as the geometric scattering region (Stanton et al., 1996; Martin et al., 1996; Lavery et al., 2007).

Zooplankton such as copepods, euphausiids, medusae, chaetognaths and larval crustaceans are usually modelled as fluid-like scatterers, whereas zooplankton with hard elastic shells, such as thecosome pteropods, are modelled as elastic-shelled scatterers (Lavery et al., 2007; Stanton et al., 1994). Fish that do not have gas-filled swimbladders, such as Atlantic mackerel (*Scomber scombrus*), still tend to scatter more strongly than most fluid-like scatterers, however their frequency response pattern does not exhibit the strong resonance spike characteristic of fish which have gas-filled swimbladders; the pattern may be more

variable, depending more heavily on orientation of the fish in the acoustic beam (Gorska et al., 2007; Foote, 1980; Scoulding et al., 2017).

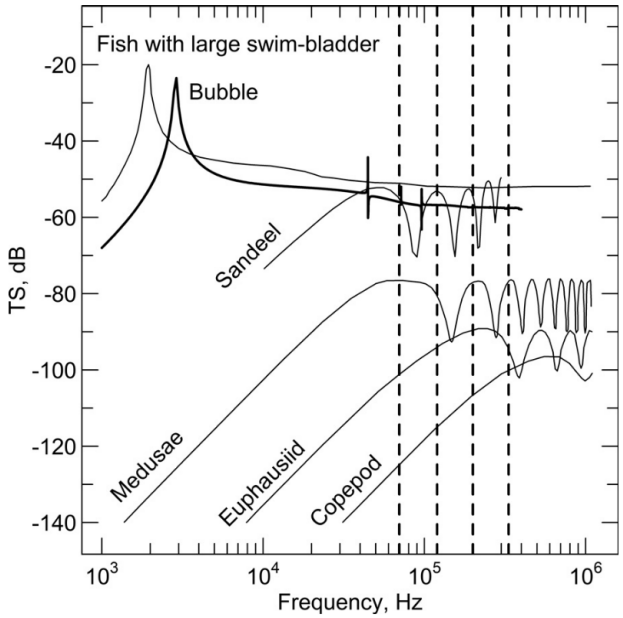


Figure 1.3.2: **Frequency response patterns modelled for a range of different scatterers**; Reproduced from Figure 1 in Kubilius and Pedersen (2016). These types of scatterers and their frequency response patterns are representative of animals commonly found in the North Sea. Target strength (TS, derived from backscatter strength) is plotted against frequency. Vertical dashed lines demarcate 70, 120, 200 and 333 kHz.

Both scattering strengths and characteristics of the frequency response pattern can be used to classify backscatter, often achieved by thresholding or using multiple frequencies, or a combination of both techniques (Fernandes, 2009; Korneliussen, 2018). Thresholding separates backscatter dominated by strong scatterers from backscatter from weaker scatterers only. Since backscatter is assumed to be mostly representative of the dominant scatterers within the sampling volume, information about weaker scatterers may be lost (Uumati, 2013). Thresholds must be chosen carefully, taking into consideration the expected densities of scatterers in the water column, since higher densities of scatterers produce stronger backscatter than more sparsely distributed scatterers.

Multi-frequency techniques exploit the relative difference between scattering at different frequencies to classify backscatter (Korneliussen et al., 2016). One such multi-frequency technique is dB-differencing, which describes the ratio between target strength or volume backscatter at two frequencies, obtained by subtracting the strength at one frequency from another in the decibel (logarithmic) domain. If the dB-difference falls within a specified dB-window (i.e. a range of accepted dB-difference values), then the backscatter can be attributed particular groups, such as fish or zooplankton (Sato et al., 2015; Ballón et al., 2011; Fielding et al., 2012), or used to classify monospecific aggregations (e.g. Watkins and Brierley, 2002). The dB-difference ratio is unaffected by the density of scatterers, providing a relatively robust technique to separate scatterers in backscatter data when animal densities are unknown or highly variable.

Sound scattering layers (SSLs) typically contain diverse assemblages of zooplankton and small fish. As a consequence, backscatter from within SSLs often contains a mixture of signals from scatterers with different frequency response patterns. Acoustically dominant scatterers can mask signals from weaker scatterers, and backscatter can be comprised of a superposition of signals from scatterers with contrasting frequency response patterns. Multi-frequency classification techniques rely on comparing against known frequency response patterns of single species or scattering types (Korneliussen et al., 2016), and so the mixture of signals in SSLs can make classifying them and determining relative acoustic contributions from different organisms contained within them particularly challenging.

Recent work applying Bayesian methods to inverse modelling of mixed assemblages has proved tentatively successful for separating the contributions of different scatterers, however this requires input about which scatterers are expected to be present in the water column (Urmy and De Robertis, 2021). Despite the challenges of classifying backscatter from mixed assemblages, characteristic features of backscatter data such as morphology, position in the water column, and energetic properties (e.g. backscattering strength and dB-difference) have been used successfully to classify mixed assemblages in some ecosystems, (e.g. mixed aggregations of coral reef fish in Campanella and Taylor, 2016).

### 1.3.5 Echo integration

Echo integration is a common method used to average backscatter data, and is an integral step in deriving useful biomass, density, and abundance estimates of acoustic targets. Data is integrated horizontally by either distance or time and vertically by depth. Echo integration is possible owing to the principle of echo linearity. This principle states that the mean echo energy from $n$ targets within a sampled volume is equal to the sum of echo energy contributions from each of the $n$ targets insonified individually, i.e. echoes are additive, which holds for the majority of cases (Foote, 1983). This means that, regardless of how much data is integrated (i.e. over what distances and depths), proportionality remains between the mean volume backscattering (in the linear domain) and the mean density of scatterers.

Acoustic surveys typically produce measurements at high spatial and temporal resolutions, which result in large datasets. Echo integration is a useful way to reduce the storage size of data and memory-intensive processing. It also provides benefits such as reducing the influence of spatial and temporal autocorrelation which is prevalent in acoustic survey data, smoothing over some forms of noise, and enabling statistics to be produced at appropriate scales, for example at scales suitable for capturing relationships with the behavioural or physical processes being investigated. Echo integration reduces the resolution of the data, which can be beneficial since it reduces the size of datasets, but it can also lose information. However, fine-scale details about animal distribution are often superfluous to the needs of fisheries abundance and biomass surveys. Large-scale averaging is usually preferred for these surveys since survey transects often span many nautical miles and data may be recorded to hundreds of metres depth, resulting in large, autocorrelated datasets. By contrast, studies that require accurate measurements of small-scale changes in the distribution of organisms, such as studies on DVM behaviour over short distances (tens of metres) and timescales (minutes or hours), should not be averaged over very large distances (Daase et al., 2016; Ludvigsen et al., 2018). The size of integration bins must be carefully chosen in order to preserve information content. However, it is still prudent to perform echo integration, since acoustic measurements are susceptible to white and speckle noise due to the extreme sensitivity of echosounder hardware to various acoustic, electrical, mechanical and thermal interferences

(Peña, 2016). Echo integration, at an appropriate scale, can therefore help to reduce the impact of this kind of noise.

### 1.3.6 Acoustic data quality

Biomass and abundance estimates from acoustic surveys are relied upon to inform fisheries and ecosystem research and management in the North Sea and elsewhere across the globe (Simmonds and MacLennan, 2005; Fernandes et al., 2002). The accuracy and comparability of these estimates are crucial for understanding how populations respond to stressors such as climate change and fisheries pressure (Zimmermann and Werner, 2019). Besides monitoring, acoustic surveys can also provide insights into the behaviour of organisms, and, together with environmental data, can be used to understand drivers of distributional patterns that structure ecosystems (for example, Benoit-Bird and Lawson, 2016; Benoit-Bird et al., 2016; Ludvigsen et al., 2018; Lezama-Ochoa et al., 2014). Ecologically-focused research also requires data that are relatively accurate and consistent, although the stringency of these requirements depends on the intended use of the data (Figure 1.3.3).

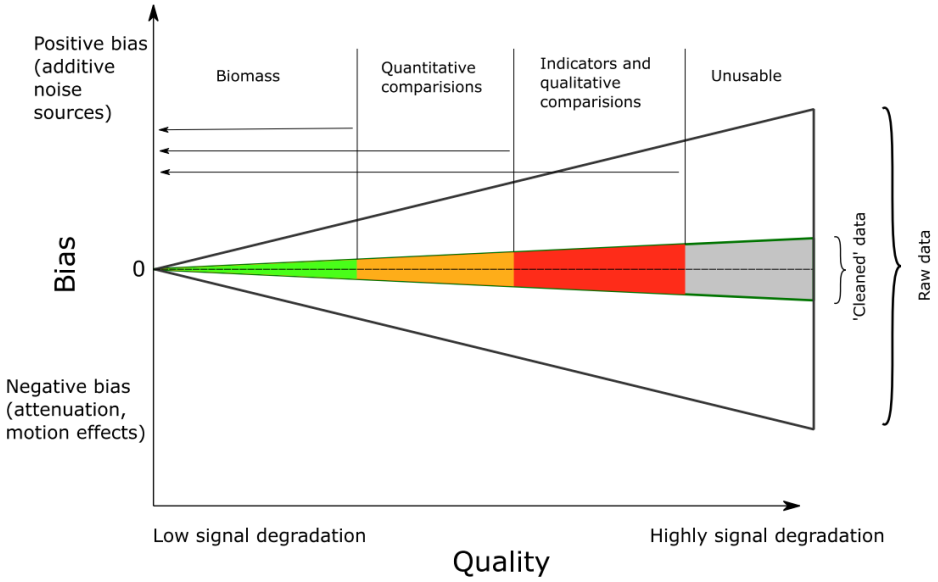


Figure 1.3.3: **Conceptual diagram of data quality and bias in raw and cleaned acoustic data and suitability for different purposes**. Reproduced from Figure 7.1 from Jech et al. (2021). Biomass and abundance surveys require high quality data (low signal degradation, minimal bias), whereas other studies may not have such stringent requirements.

The term *data quality* can embody a multitude of concepts, but broadly speaking it is defined as how fit data are for their intended use. In the field of fisheries acoustics, the intended uses of data are primarily the detection, classification, and estimation of abundance and distribution of organisms in the water column. Poor quality data, that is, data where the signal is degraded, may include a high degree of false information (inaccuracy and imprecision), incomplete or missing information (poor coverage), or superfluous information which may obscure patterns of interest. These three characteristics of poor quality acoustic data manifest as: noise (false information) - external signals are added to the backscattered echoes, potentially resulting in overestimation if not removed or corrected, or underestimation if removal results in loss of target signal; attenuation (incomplete information) - signal is dampened resulting in underestimation and potentially also preventing detection of targets; and masking (superfluous information) - non-target scatterers dominate the signal reducing the ability to detect and classify targets and potentially resulting in either over- or underestimation.

Degraded data can introduce two kinds of error: bias and random error. Bias describes systematic error, often caused by noise or attenuation, which results in over- or under-estimation of quantities and thus primarily affects accuracy, whereas random error increases variability in the data and hence affects precision of estimated quantities. Bias associated with particular environmental conditions, time of day, or depth ranges, can skew results and potentially lead to type I or type II errors and is often the most problematic kind of error in acoustic data used for either marine resource management or ecological research.

### Noise

Noise is defined as any positive contribution to the received signal in addition to that from backscatter (returning echoes). TVG not only amplifies the desired component of the signal, but also amplifies any noise as well. Since noise is range-independent, but the gain applied by TVG increases exponentially with range, the signal-to-noise ratio rapidly deteriorates with range. Absorption losses increase with frequency, and so TVG amplifies higher frequencies more than lower frequencies (Foote, 1981). This typically results in a shallower noise floor for higher frequency signals, limiting the range of usable data (Figure 1.3.4).

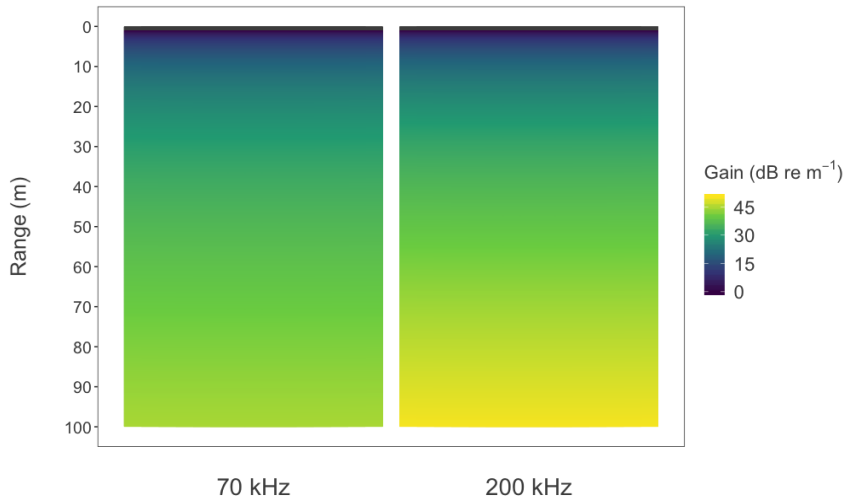


Figure 1.3.4: **Echograms illustrating the time-varied-gain applied to 70 kHz (left) and 200 kHz (right) data, up to 100 m range.** More gain is applied to higher frequencies to compensate for increased absorption losses, resulting in a shallower noise floor and less usable data.

Noise corrupts backscattered signals, adding positive bias to backscatter measurements. Low signal-to-noise ratios can mask target signal and alter the characteristic properties of the acoustic data, such as the frequency response, as well as increasing the perceived backscattering strength. Both effects have implications for the ability to classify the data correctly. If noise-affected data is misclassified as target backscatter, then noise can lead to overestimations of targets. Noise could also lead to a negative bias of target estimates if target signal is masked to such a degree that the target is not identified and is subsequently excluded from derivation of the estimate.

Noise in fisheries acoustic data is usually categorised into one of four types: transient noise, background noise, impulse noise, and speckle noise. This categorisation scheme is based on the source of the noise, its duration, its intensity, and its presentation in echograms. Transient noise is a type of noise that is sporadic and lasts for a short duration (in the order of seconds or minutes), whereas background (or ambient) noise is fairly constant over periods of hours, days and weeks (De Robertis and Higginbottom, 2007; Ryan et al., 2015). The source of noise is range-independent; therefore generally the intensity of the noise signal increases with range due to TVG. This effect can most easily be seen in the case of background noise as a ramping up of backscattering strength at range, as illustrated in

Figure 1.3.4. Both transient and background noise can be caused by waves, however there are also many other possible sources of background noise (Hildebrand, 2009) (Figure 1.3.5).

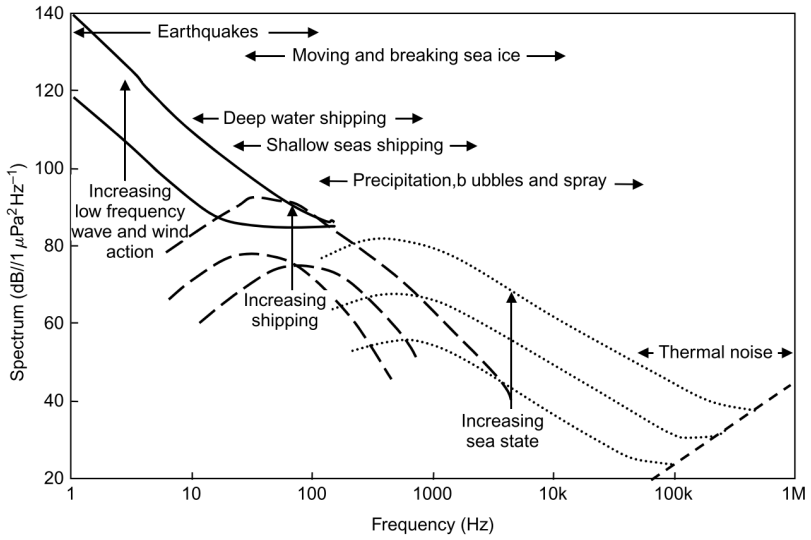


Figure 1.3.5: **Frequency response of typical sources of ambient noise in the ocean.** Figure 2.26 from Simmonds and MacLennan (2005).

Impulse noise can be caused by interference from other instruments on the acoustic platform, and typically presents as spikes of strong backscatter in the echograms (Ryan et al., 2015). Speckle noise occurs due to the extreme sensitivity of the echosounder which results in stochastic fluctuations of the voltage measured by the transducer (Peña, 2016).

## Attenuation

Attenuation is a reduction in signal strength. Scatterers along the propagation path of an acoustic signal can both scatter and absorb some of the energy from the signal, thereby reducing the strength of the signal that continues along the propagation path. Here, the term attenuation describes a reduction in signal strength that occurs in addition to absorption and scattering caused by seawater (which is accounted for by TVG). Echosounder signals are attenuated through two main mechanisms: transducer motion, and shadowing or extinction of the signal by strong scatterers.

Transducer motion describes a situation where the transducer face is not oriented in the same way during transmit and receive of the signal (Stanton, 1982). Echosounder software assumes alignment of the acoustic axes for the transmit and receive signal. Because the acoustic beam of most transducers is highly directive, misalignment in the acoustic axes can result in inaccurate amplification by TVG which typically negatively biases backscatter measurements. The signal may be lost entirely if the transducer face is turned completely away from returning echoes, resulting in a *ping drop-out*.

Forward movement and heave of a vessel can cause misalignment of the acoustic axis, however it is primarily angular motion (i.e. pitch and roll) that causes the most significant attenuation. Attenuation due to transducer motion worsens with range and is most problematic for transducers with small beam angles as they typically have higher directivity. The most common cause of transducer motion on surface vessels is rough seas with surface waves that pitch and roll the vessel.

Attenuation by weak, sparsely distributed scatterers is negligible as they remove proportionally very little energy from the signal. However, when scatterers occur in dense aggregations shadowing may occur, whereby scatterers farther in range appear comparatively weaker than those closer to the transducer. Complete attenuation of the signal by shadowing results in acoustic extinction. This phenomenon has been reported to occur under dense Norwegian spring-spawning herring aggregations, evidenced in echograms by the temporary 'disappearance' of the seabed echo underneath the herring (Foote, 1990; Toresen, 1991). Shadowing and extinction may be caused by various types of scatterers, whether biotic, such as fish schools, krill swarms, or particularly dense zooplankton aggregations, or abiotic, such as clouds of bubbles.

Bubbles directly below the transducer present a major impediment to the collection of good quality fisheries acoustics data (Dalen and Løvik, 1981; Shabangu et al., 2014). Bubbles are generated at the surface by interactions at the air-sea interface, and can be entrained deeper into the water column by wind-driven surface waves or swept under the transducer by wave-vessel interactions, forming layers beneath the surface (Trevorrow, 2003; Delacroix et al., 2016). Gas bubbles are strong, resonant scatterers across the frequency range used for

fisheries acoustics (Novarini and Bruno, 1982). As such, bubble layers beneath the transducer have the capacity to mask biological signal and can also cause shadowing by absorbing and scattering sound in other directions, attenuating signal beyond the bubble layer.

### Impacts of adverse weather on acoustic data quality

The quality of acoustic data collected by surface vessels typically worsens in windier, wavier conditions, principally due to increased transducer motion, the generation of more extensive and dense bubble layers beneath the surface, and an increase in background and transient noise associated with breaking waves, wave impacts, and collapsing bubbles. The impacts of adverse weather on acoustic data quality have been the subject of recent attention by members of the fisheries acoustics research community. The specialist ICES WG-FAST Topic Group for the Quality of Acoustic Data in Inclement Weather sought to address the lack of coherent guidelines and recommendations for collection and post-processing of acoustics acquired during adverse weather by producing a collaborative report in 2021 (Jech et al., 2021). The report defines issues of data degradation due to noise and attenuation that are worsened by adverse weather and presents available techniques to assess and mitigate their impacts, with a primary focus on acoustics collected by downwards-facing transducers mounted on surface vessels. Case studies illustrate a range of impacts across various datasets. They highlight that, whilst many deployments show similar associations between wind speed and data degradation, the specific impacts are highly platform-, dataset-, instrumentation-, environment-, and study-dependent. Given the idiosyncratic nature of acoustic data quality issues, it will be prudent to assess how new acoustic platforms may perform under a range of environmental conditions.

## 1.4 Autonomous vehicles as acoustic survey platforms

Organisations involved in marine research, resource management and ocean observing systems are increasingly looking for cost-effective solutions to monitor fish and zooplankton populations, particularly in the face of rising ship fuel costs. Many organisations are

considering the use of autonomous vehicles as a means to augment or replace traditional ship-based acoustic monitoring surveys (Reiss et al., 2021; Levine et al., 2021; De Robertis et al., 2021; Guihen et al., 2014; Meyer-Gutbrod et al., 2012; Sepp et al., 2022; Camus et al., 2021; Swart et al., 2016).

Autonomous vehicles can be powered by a variety of energy sources. Non propeller-driven autonomous vehicles are typically wave- or wind-powered, or buoyancy-driven. This primary reliance on renewable energy sources for their propulsion reduces the environmental footprint associated with data collection at sea, which may help enable organisations to meet carbon net-zero goals (Turrell, 2019; Siddorn et al., 2022).

Autonomous vehicles can potentially access regions that are not easily accessed by ship (Fernandes et al., 2003; Brierley et al., 2002). Safety at sea is paramount, and so it may be advantageous for autonomous vehicles, rather than manned ships, to carry out research in hazardous regions. They can be used for focused, persistent monitoring of a region, being less hampered by the need to coordinate multiple activities as is often the case for ship-based surveys (Pedersen et al., 2019). This kind of usage also frees up ship time for other activities.

The integration of autonomous echosounders on to autonomous vehicles has opened up new possibilities in bioacoustic ocean observations, such as under ice cover (Brierley et al., 2002) and in the deep sea (Dunlop et al., 2018). Acoustic data collected by a variety of ASVs and autonomous underwater vehicles have shown the breadth of biological research questions that can be addressed using these vehicles (for examples, see Swart et al., 2016; De Robertis et al., 2019; Brierley et al., 2003; Suberg et al., 2014; Guihen et al., 2014; Moline et al., 2015; Geoffroy et al., 2017; Gastauer et al., 2022; Ohman et al., 2019; Benoit-Bird et al., 2018; Ludvigsen et al., 2018; Pedersen et al., 2019).

Most autonomous vehicles come with standard sensor packages that do not include acoustic systems. Echosounders used on autonomous vehicles often need to be operable in an autonomous mode, and be suitably compact to fit on the platform and light enough not to adversely affect its buoyancy (Chave et al., 2018). The integration of echosounder systems is still at an early experimental stage for many autonomous vehicles. There remain questions regarding the ability of these platforms to collect acoustic data accurate enough to produce

quantitative estimates comparable to those produced by ship-based acoustic data in order for the use of autonomous vehicles to be integrated into pre-existing surveys (Greene et al., 2014; Chu et al., 2019; Guihen et al., 2014).

Transducer placement is one of several factors that affect a platform's ability to collect good quality acoustic data. For autonomous vehicles in particular, there are considerations of both where and how the transducers are attached, and which kinds of transducers can be integrated. ASVs typically have much shallower drafts than research vessels ($< 0.5\,\mathrm{m}$, versus research vessels $1.5$ to $7.5\,\mathrm{m}$), allowing for the integration of transducers under the hull at much shallower depths. This has the potential to reveal new insights into animal distributions in near-surface regions that may be missed by ship-based acoustics due to the surface blind zone. However, this may come at an increased risk of data degradation since the density of bubbles increases closer to the surface. For this reason, acoustic transducers are often positioned under the deepest part of the hull or on a skeg or keel (e.g. Meinig et al., 2015; Pedersen et al., 2019).

Space is at a premium on autonomous vehicles since they are typically much smaller than ships but they need to host a variety of sensors as well as house processors, battery packs and navigation systems. Frequency largely determines the size of acoustic transducers; lower frequencies require larger transducer faces. This places limitations on how many, and which frequency, transducers can be installed on smaller platforms. Recent advances in the design of piezoelectric arrays on transducer faces have led to the development of compact transducers that can be installed on autonomous vehicles. However, most applications on autonomous vehicles still opt for transducers with frequencies at or above $70\,\mathrm{kHz}$, except for larger ASVs such as the Saildrone which can more easily accommodate larger, lower frequency transducers (Meinig et al., 2015; Chu et al., 2019).

Despite space, power and weight limitations of sensor integration on to autonomous vehicles, there are still numerous ways that echosounders and acoustic transducers can be integrated on to these vehicles (Chave et al., 2018; Verfuss et al., 2019). The available options are mostly dependent on vehicle design, choice of acoustic system components, and requirements of the study. However, due to the trade-offs involved, different ways to integrate acoustic

systems require testing and optimisation for different applications, and it is not uncommon for modifications to have to be made following initial testing in order to improve data quality (e.g. Meyer-Gutbrod et al., 2012; Swart et al., 2016; Pedersen et al., 2019).

### 1.4.1 The Wave Glider

The Wave Glider SV3 is an ASV developed by Liquid Robotics that harnesses wave action for its propulsion (Liquid Robotics, Inc., 2018). It has a two-part design consisting of a surface float and a submarine unit (subunit) connected by an $8\,\mathrm{m}$ umbilical cable (Figure 1.4.1). As waves move the surface float up and down, the subunit wings adjust their angle to lift and fall, propelling the vehicle forward. In general, the greater the differential between lift at the float and the subunit - i.e. the taller the waves - the faster the Wave Glider will travel, up to an average maximum speed of $1.54\,\mathrm{m\,s^{-1}}$ by wave power alone (Liquid Robotics, Inc., 2015).

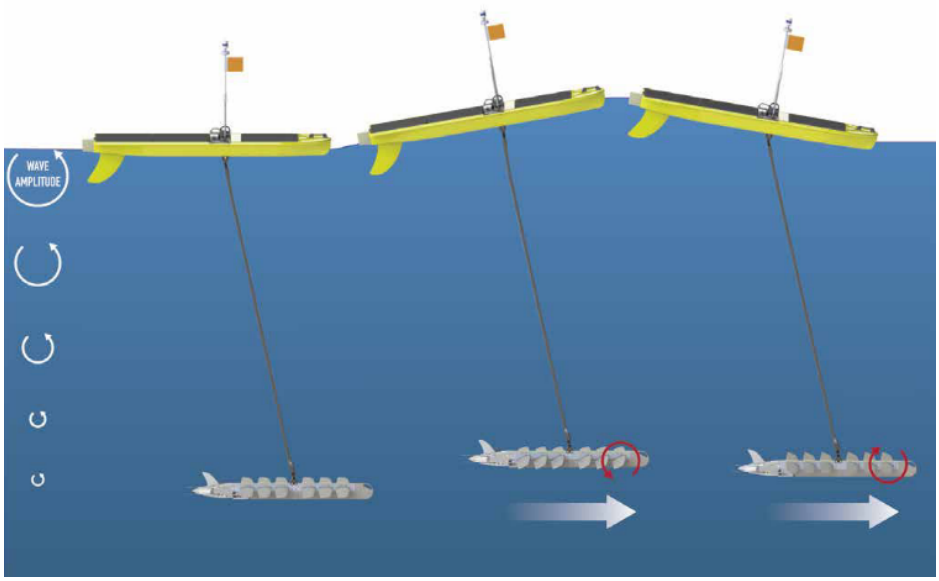


Figure 1.4.1: **Schematic of Wave Glider propulsion.** As the waves move the float up, the angle of the subunit fins changes to convert tension through the umbilical into forward motion. As the waves move the float downwards, the subunit sinks under gravity. Figure 2 from Greene et al. (2014).

The surface float houses the majority of the electronics, communications systems and sensors and the subunit converts wave energy to forward propulsion. Its modular design allows it to be easily adapted to carry additional sensors that fit within size, weight and power limitations. On-board sensors and communications systems are powered by battery. Supplemental solar modules can also be used to power additional thrusters, if needed, and recharge the battery. By virtue of its position at the surface, the Wave Glider can take measurements from both above and below the surface in a similar manner to ships, and the standard sensor package includes sensors for taking both oceanographic and meteorological measurements (Liquid Robotics, Inc., 2023).

### 1.4.2 Deployment of *Lyra*, an acoustically-equipped Wave Glider, in the central North Sea

The Cefas-owned model SV3 Wave Glider, named *Lyra*, was equipped with standard sensor packages for meteorological observations and adapted to accommodate a Simrad Wideband Transceiver mini (WBT-mini) echosounder system (Kongsberg Maritime, 2023) (Figure 1.4.2). The echosounder was housed in the science payload bay of the surface float with its own dedicated battery pack.

Two split-beam transducers were connected to the WBT mini with acoustic beams oriented vertically downwards: the ES70-18CD and ES200-7CD operating at nominal frequencies of 70 kHz and 200 kHz respectively (see 'Acoustic transducers' label in Figure 1.4.2). The transducers were situated half a metre aft and half a metre below the float in a custom-built foam mount attached via a strut to the rear of the float (Figure 1.4.3).

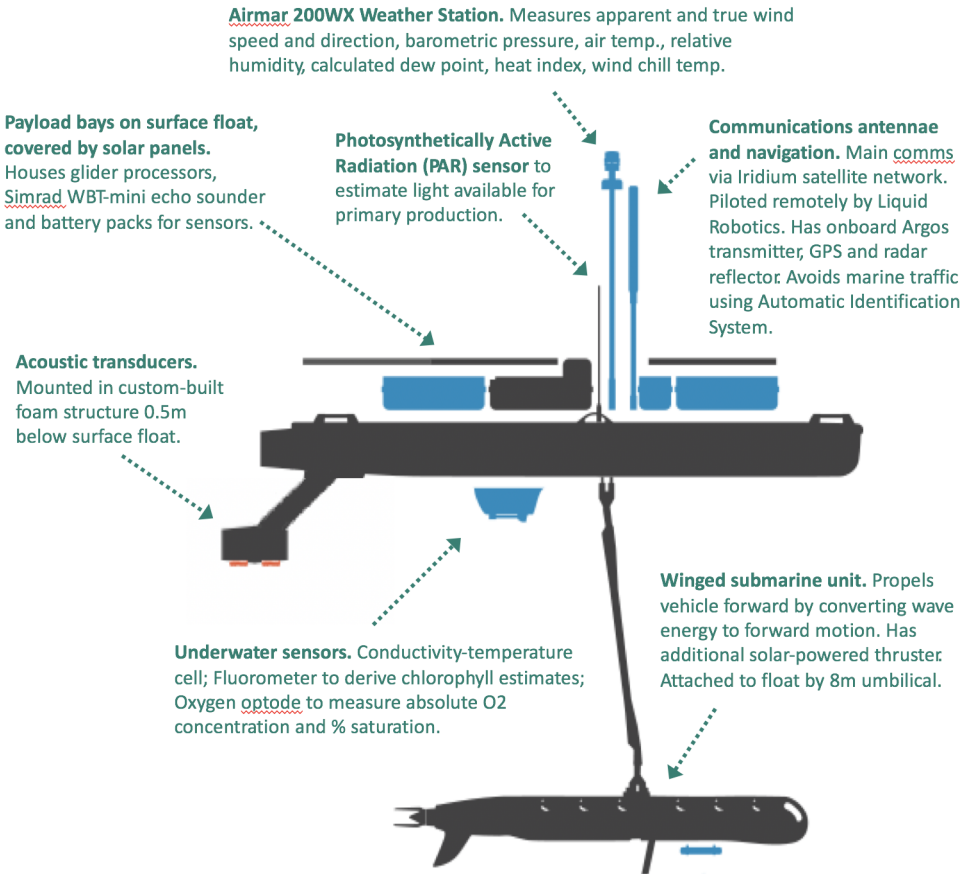


Figure 1.4.2: **Schematic of *Lyra*, the Cefas-owned Wave Glider SV3, adapted with echosounder system.** Image not to scale. Adapted from Liquid Robotics, Inc. (2023).

Figure 1.4.3: **Custom-built foam mount attached aft of *Lyra's* surface float by a metal strut.** The foam mount was designed to securely accommodate the acoustic transducers which were connected to the WBT-mini in the float via cables running along the strut.

*Lyra* was deployed in the central North Sea to collect acoustic, positional, and environmental (sea surface water properties and meteorological) data (Figure 1.4.4). Measurements were taken across fifteen repeat zonal transects between $1.5°$E and $2.5°$E at $56.2°$N, a nominal distance of $64\,\mathrm{km}$ between transect waypoints (red triangles in Figure 1.4.4), over the course of twenty-one days from the $10^{\mathrm{th}}$ to the $31^{\mathrm{st}}$ of May 2018.

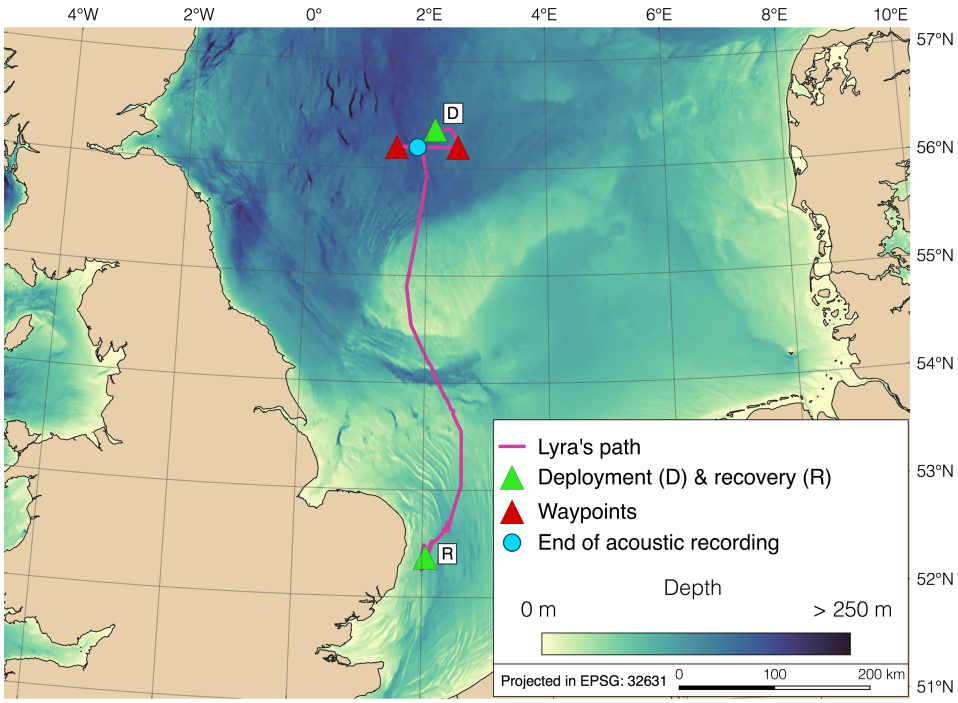


Figure 1.4.4: ***Lyra's* path between $9^{\mathrm{th}}$ May and $17^{\mathrm{th}}$ June 2018.** *Lyra* carried out acoustic and environmental sampling over repeat transects between waypoints (red triangles) in the central North Sea, after which she travelled south to meet the recovery vessel.

The WBT-mini echosounder collected both $70$ and $200\,\mathrm{kHz}$ narrowband backscatter data. There was a delay of approximately two and a half seconds after sampling at $200\,\mathrm{kHz}$ before sampling at $70\,\mathrm{kHz}$, and a delay of approximately seven and a half seconds after sampling at $70\,\mathrm{kHz}$ before sampling at $200\,\mathrm{kHz}$. This meant that the effective ping rate of each frequency was one ping every ten seconds ($0.1\,\mathrm{Hz}$). Acoustic data were recorded to a maximum range of $100\,\mathrm{m}$.

## 1.5 Observing diel vertical migrations of fish and zooplankton

Most in-situ studies of DVM measure the net effects of population-level migration by comparing vertical distributions or abundance of organisms at different times of the 24-hour cycle, usually contrasting measurements from night and day (Pearre, 1979; Bandara et al., 2021). Two types of sampling gear are commonly used to do this and, more generally, measure vertical and horizontal distributions of animals in the water column: nets and acoustics.

Nets have long been the traditional tool to study DVM and distributions of marine and freshwater animals (Bandara et al., 2021). Their main advantage over acoustics is that taxonomic resolution and size-distributions of animals are more readily available. Such information is crucial for determining which components of the ecosystem are migrating, how far, and when, and untangling mixed vertical migration patterns. Continuous Plankton Recorder (CPR) surveys have provided records of plankton in surface waters that have been used for marine monitoring for over 70 years (Henderson and Marshall, 1944). CPR observations of day-night differences in relative zooplankton abundance have contributed greatly to our knowledge about DVM, including DVM of species in the North Sea (Hays et al., 1996; Henderson and Marshall, 1944; Batten and Burkill, 2010). However, whilst CPR surveys record continuously across time and space, they only capture animals from near-surface waters and thus may not observe critical components of the ecosystem - particularly if some species perform migrations entirely above or below the sampling depth (usually $8$ to $10\,\mathrm{m}$) (Dippner and Krause, 2013).

Nets that sample more of the water column can provide some of the information that CPR surveys miss; however, because most nets cannot be operated near the seabed, they are unable to sample the entire water column. Oblique or vertical hauls of open nets through the water column are of limited use for studies of DVM since they cannot resolve samples by depth, but can be used to identify species present that are not sampled by the CPR. In contrast, depth-stratified closing nets can track shifting relative abundances through the water column and have proven useful for tracking large shifts in zooplankton vertical distributions (i.e. movements that extend beyond the vertical resolution achievable by the nets, which can

in some cases be 10s of metres of water depth) (Ohman and Romagnan, 2016; Aarflot et al., 2019; Klevjer et al., 2016).

Zooplankton often form horizontal layers in the water column, some of which can be exceedingly thin but stretch for kilometres and persist for days despite changes to their structure caused by physical processes and predation pressure (McManus et al., 2005; Cheriton et al., 2007; Benoit-Bird, 2009). Using high resolution acoustics from an autonomous underwater vehicle operated within close range of targets, Benoit-Bird et al. (2017) revealed that squid, fish, and zooplankton in scattering layers tended to group according to species and size within the layers. Both horizontal and vertical patchiness may not be well-accounted for by net sampling; even specialised equipment such as the Multiple Opening/Closing Net and Environmental Sensing System (MOCNESS) may be unable to resolve such fine-scale features (Whitmore et al., 2019). Depth-stratified nets sample discrete points in time and space, usually at fairly low resolution. In contrast, acoustics can sample at comparatively high resolution. Temporal resolution is typically one ping per second, providing horizontal resolution in the order of metres for most mobile platforms and an almost instantaneous sampling of all available depths. This means that acoustics can provide a near-synoptic image of animal distributions in the water column and so may be better suited to assessing patchy distributions of zooplankton.

Like all sampling gears, both nets and acoustics are selective and their samples will represent some animals better than others. Nets selectively sample animals according to their anatomy, swimming ability, and avoidance behaviour (Hamner et al., 1975; Kankaala, 1984; Wiebe et al., 1982). In principle, mesh size dictates what size individuals will be retained within the net, however the orientation of elongate animals, such as chaetognaths, may affect their retention in nets (Dippner and Krause, 2013). Gelatinous animals may be extruded through the mesh by the force of water flowing through (Whitmore et al., 2019). Enhanced swimming ability, increased perception distance and vision can result in many zooplankton escaping capture by nets. The relationship between avoidance and net aperture size is complex, however, with some species seemingly better able to escape capture from larger nets (Wiebe et al., 1982). For these reasons, net type and size are usually chosen to suit the sampling of taxa with specific traits, notably body size and swimming capacity.

Acoustic measurements, on the other hand, bias samples in a different way by representing stronger backscattering targets better than weaker scatterers (Lavery et al., 2007). Acoustic sampling is density-dependent: an echosounder may fail to register signal from weak scatterers at low densities, and conversely strong targets at very high densities may produce acoustic extinction and shadowing beyond the range of the targets (Foote et al., 1992). Nevertheless, for most targets sampled at appropriate frequencies, the relationship between acoustic backscatter and density of animals is approximately linear (Foote, 1983). Studies of DVM that incorporate both acoustic and net observations benefit from the complementary nature of these differing sampling methods.

In recent years, acoustically-equipped autonomous vehicles have proven capable of detecting DVM (Benoit-Bird et al., 2018; Pedersen et al., 2019; Bandara et al., 2022) and elucidating patterns in vertical migration timing related to animal size and their capacity to evade predators (Benoit-Bird and Moline, 2021). Since transducers on ASVs can often be positioned nearer the surface than those on the hulls of ships, ASVs may be particularly well suited to observing migrations that take place close to the surface. ASVs that are not propellor-propelled are also typically very quiet and dimly lit, if at all, and so are potentially less likely to induce avoidance or attraction behaviours that could skew observations of DVM behaviour.

## 1.6 Research aims and thesis structure

Oceanographic properties are known to influence the vertical and horizontal patchiness of zooplankton distributions over large temporal and spatial scales, i.e. changes that span tens of kilometres or occur over months, years, or decades. However, over smaller scales, such as sub-mesoscale spatial scales and hours or days, there is less knowledge of how environmental variation influences patchiness of zooplankton distributions. In this thesis, I analyse acoustic and environmental data that were collected simultaneously by the Wave Glider *'Lyra'* during a deployment in the central North Sea in Spring 2018 for the purpose of addressing this knowledge gap. In addition, because the Wave Glider is a relatively recent invention and its use as a fisheries acoustics platform is in its infancy, I assess the suitability of the Wave

Glider as an acoustic platform for studying fish and zooplankton distributions and DVM behaviour and provide recommendations for its future use.

Wind is one of the primary environmental factors influencing the quality of acoustic data collected by surface vessels (Jech et al., 2021). In Chapter 2, I evaluate the quality of acoustic data collected by *Lyra*, paying particular attention to the mechanisms through which increasing wind speeds might deteriorate acoustic data quality. This is achieved by analysing relationships between wind speed, vessel motion, and the presence of bubble layers near the surface, and exploring correlations between these factors and the rates and severity of attenuation and transient noise in the acoustic data. As part of this analysis, I demonstrate a novel technique, the 'two-layer comparison technique', that I developed which can be used to semi-quantitatively assess the efficacy of data cleaning on the degree of bias caused by noise and attenuation in a dataset. This technique which can be used to compare the quality of acoustic data between disparate datasets. The chapter provides a quantitative evaluation of the platform's susceptibility to transient noise and attenuation under a range of wind speeds. It also brings to light acoustic data quality considerations that are unique to wave- and wind-powered ASVs, as well as those that are unique to the Wave Glider and to *Lyra* in particular. Finally, I provide recommendations for improving the quality of acoustic data acquired by Wave Gliders during adverse weather, and discuss operational considerations during deployment.

A study on patchiness would not be complete without exploring the DVM behaviour of different animal groups, since this ubiquitous behaviour is arguably one of the most significant factors influencing variability in vertical distributions of zooplankton and fish. Chapter 3 presents an analysis of diurnal vertical movement behaviour of animals based on acoustic backscatter distributions. In this chapter, I classify the acoustic data into three scattering groups which broadly represent three biological groups: schooling swimbladdered fish, fluid-like zooplankton, and gas-bearing zooplankton. As no direct validation data for the acoustic classification are available, I use net samples, knowledge of North Sea pelagic marine ecology, and, in the case of fish schools, an analysis of the morphology of the acoustic backscatter aggregations to support my hypotheses about the taxonomic composition of these groups. Finally, I analyse summary metrics derived from the backscatter distributions that

describe proxy biomass and average vertical position in the water column to reveal diurnal movement and aggregation patterns of each group, including DVM behaviour of gas-bearing zooplankton.

Chapter 4 investigates environmental drivers of zooplankton and fish school patchiness at sub-mesoscales using Generalised Additive Mixed Models. These models elucidate the relative importance and effects of environmental factors such as light levels, time of day, wind speed, bottom depth, and various surface water properties, such as temperature, salinity, turbidity, and fluorescence, on both horizontal and vertical backscatter distributions of each group (fish schools, gas-bearing zooplankton, and fluid-like zooplankton). I interpret the model results in the context of the known behaviour and ecology of the animals represented by the three acoustic groups. This underlines that, regardless of which group is considered, bottom depth plays a critical role in structuring pelagic animal distributions in the shallow central North Sea. I use water column environmental data from a co-located underwater glider to contextualise the oceanography of the region during the deployment period. This reveals the progression of seasonal stratification with the formation of a three-layer system defined by two thermoclines. The glider data also reveals the presence of an oceanographic front, associated with a ridge along the seabed, which correlates with shifts in vertical distributions of zooplankton and an increase in horizontal aggregation at the position of the fronts, further underlining the influence of bathymetry on pelagic animal distributions in this region.

In the final chapter, I draw together conclusions from the previous three chapters to provide a summary assessment of the suitability of the Wave Glider as an acoustic platform, its utility for the study of environmental drivers of fish and zooplankton patchiness in shallow environments such as the central North Sea and ecological insights into drivers of fish and zooplankton distributions at sub-mesoscale spatial scales and temporal scales of hours and days. This chapter identifies key environmental and operational considerations for successful acoustic surveys using a Wave Glider and highlights lessons learnt from *Lyra's* pioneering deployment. Finally, I discuss the role of acoustic surveys by autonomous surface vehicles, such as the Wave Glider, to complement, augment, or replace traditional ship-based acoustic surveys, particularly given the likelihood of their increasing use in the future, as marine

monitoring and research organisations aim towards carbon net-zero operations at sea.

# 2

# Impacts of the wind on acoustic data collected by the Wave Glider

## 2.1 Introduction

Adverse weather increases the likelihood of surface vessels collecting poor quality acoustic data, particularly that which has been degraded by transient noise, background noise, and attenuation (Jech et al., 2021). Acoustically-equipped ASVs have the potential to provide cost-effective, low carbon-footprint alternatives to traditional ship-based acoustic surveys (Swart et al., 2016). However, new platforms must be able to demonstrate that they can reliably collect data of adequate quality in order to provide value to scientific research and monitoring (Centurioni et al., 2019; Greene et al., 2014). Although there exist performance evaluations which assess the capability of ASVs to carry out acoustic surveys (Chu et al., 2019; De Robertis et al., 2021), there is a paucity of studies that assess the impacts of weather on the acoustic data that they collect. The exceptions include studies by De Robertis et al. (2019) and associated analyses by Jech et al. (2021), which provide detailed accounts of the effect of wind on attenuation in acoustic data collected by Saildrones.

Fisheries acoustics systems have been integrated onto Wave Gliders at least twice in recent years. Swart et al. (2016) and Pedersen et al. (2019) present acoustic studies using Wave Gliders with transducers mounted aft of the float in a similar fashion to *Lyra*. Although the effects of adverse weather on acoustic data quality were not the main focus of these works, both touched on aspects relevant to this topic. Swart et al. (2016) described the relationship

between Wave Glider instantaneous wind speed and bubble layers formed underneath the surface, finding that stronger winds led to deepening of the bubble layer and an increase in total backscatter of the bubble layer and hence its propensity to attenuate the acoustic signal. Pedersen et al. (2019) noted that the Wave Glider experienced increased bubble-related attenuation during periods of higher wind speeds and intuited that it underwent more extreme pitch and roll in windier conditions, judged by discontinuities visible in the echograms. However, neither study quantified the impact of data degradation under variable environmental conditions.

A quantitative assessment of the quality of acoustic data collected by Wave Gliders that evaluates the impact of adverse weather is therefore needed. This chapter addresses this need by quantifying the effects of data degradation in the $70\,\mathrm{kHz}$ acoustic data collected by *Lyra*, investigating the role that wind played in increasing the severity and frequency of transient noise and attenuation, increasing rotational and forward motion of *Lyra* and the formation and persistence of bubble layers beneath the surface, as well as improving our understanding of the mechanisms through which higher wind speeds reduce the quality of acoustic data collected by the Wave Glider.

Wind-driven sea surface waves play an important role in developing higher sea-states. At negligible wind speeds less than $3\,\mathrm{m\,s^{-1}}$ (Beaufort scale 0-1), the sea surface is calm and may have a mirror-like quality to it. Seas subject to wind speeds of 3 to $5\,\mathrm{m\,s^{-1}}$ (Beaufort scale 2-3) see small waves begin to break, infrequently forming white horses (Dahl and Jessup, 1995; Dahl, 2003). As wind speeds increase further, whitecaps become more frequent and wave heights increase. Above $10\,\mathrm{m\,s^{-1}}$ (Beaufort scale 6) large waves begin to form, and during gale force winds above $17\,\mathrm{m\,s^{-1}}$ (Beaufort scale 8) breaking waves are ubiquitous across the sea surface.

There are numerous mechanisms through which higher wind speeds and sea states could increase transient noise and attenuation. These include: increased pitch and roll which lead to transducer motion (Dunford, 2005; Furusawa and Sawada, 1991); more frequent and impactful collisions between waves and the acoustic platform (Ryan et al., 2015); and crashing waves and collapsing bubbles which generate noise (Wenz, 1962; Brekhovskikh and

Lysanov, 2003). In addition, enhanced air-sea interactions in windy weather can generate a layer of bubbles under the sea surface.

Wind stress at the surface can drive the surface mixed layer deeper, entraining bubbles deeper into the water column and developing plumes that extend tens of metres below the surface (Novarini and Bruno, 1982; Trevorrow, 2003). The backscattering strength of bubbles in plumes decays exponentially downwards from the surface as a general consequence of the fact that both the size of bubbles and their numerical density within plumes typically reduce with depth (Trevorrow, 2003). These changes are consistent with the notion of bubbles breaking up, dissolving, and being diluted due to mixing the longer they persist in the water column. Despite their propensity to rise and diminish over time, bubble plumes at strengths of $\geq 50\,\mathrm{dB}$ (at $200\,\mathrm{kHz}$) have been recorded to depths of $25\,\mathrm{m}$ (Trevorrow, 2003), illustrating that atmospheric phenomena at the surface have the potential to introduce strong abiotic scatterers to substantial depths. Bubbles may also be driven deeper by vessel hydrodynamics. Bubble sweep-down occurs when air is forced below the hull of a vessel where the transducers are located (Delacroix et al., 2016), and may be exacerbated by increased relative speeds between the vessel and wavefronts.

### 2.1.1 Impacts of transient noise and attenuation on acoustic data quality

Effects of transient noise and attenuation on data quality are case-dependent, and both types of degradation have the potential to lead to significant over- and under-estimates of acoustic backscattering strengths and hence acoustically-derived biomass and abundance estimates.

Transient noise introduces positive bias to backscatter measurements. This type of noise describes short-lived spikes in backscattering strength that occur at irregular intervals, usually lasting for between one to several pings. As such, Ryan et al. (2015) postulate that waves hitting the platform may be the most common cause of transient noise in acoustic data collected by surface vessels, and therefore the impacts of transient noise may worsen in rougher seas. Transient noise can have a substantial effect on data quality. For example, Ryan et al. (2015) calculated a $32\,\%$ reduction in area backscattering strength after removing samples affected by transient noise in one dataset, despite removing only $1.4\,\%$ of the data.

This demonstrates how only a few affected samples have the potential to bias biomass estimates substantially.

Attenuation dampens returning echoes, negatively biasing backscatter measurements. Rougher seas are expected to increase attenuation through two main mechanisms: increased vessel pitch and roll which leads to transducer motion, and the formation of more dense and extensive bubble layers below the surface. Attenuation due to bubbles varies according to bubble size distributions and density, and frequency of the acoustic signal, amongst other factors (Dalen and Løvik, 1981; Novarini et al., 1998). citeSimmonds2005 suggested that attenuation due to bubbles may cause up to $90\,\%$ signal loss. Even if some signal remains, if it is weaker than the echosounder detection threshold then it will register as a ping dropout. Various factors influence how transducer motion reduces echosounder sensitivity, including the range of targets, beam directivity and beamwidth, and the timing, rate, and amplitude of motion experienced (Saavedra et al., 2012; Simmonds and MacLennan, 2005).The effects of transducer motion on backscatter measurements are highly dependent on the design of the acoustic transducer, however Stanton (1982) provided an example for a circular transducer with a $5^\circ$ beamwidth. This work showed that an angular displacement of transducer position by $4^\circ$ between signal transmission and reception can introduce an integration error of $64\,\%$ for targets detected at $400\,\mathrm{m}$.

In addition to their effects on backscatter measurements, both noise and bubbles under the transducer can result in loss of information about targets by acoustically masking weaker biological backscatter signals. Masking reduces the detectability of targets and noise can alter frequency response, which may affect multi-frequency classifications. Typically, data in regions affected by bubbles and transient noise are removed from further analyses. Thus, the more data is affected, the more information is potentially lost.

### 2.1.2 Detecting transient noise and attenuation in acoustic data

In echograms, transient noise and attenuation typically present as pings of stronger or weaker backscatter relative to neighbouring pings (previous or subsequent pings), persisting across one or several pings (Figure 2.1.1). Methods to detect data affected by transient noise or

attenuation are therefore commonly based on detecting steep gradients in backscatter across a small selections of pings to pick out those pings with comparatively much stronger or weaker backscatter (Ryan et al., 2015; De Robertis et al., 2019; Honkalehto et al., 2011; Irigoien et al., 2014). These methods often employ the following approach: identify cells where backscatter is stronger (weaker) than the surrounding neighbourhood, exceeding (below) these values by a chosen threshold; pings with affected cells are marked as affected by transient noise (attenuation).

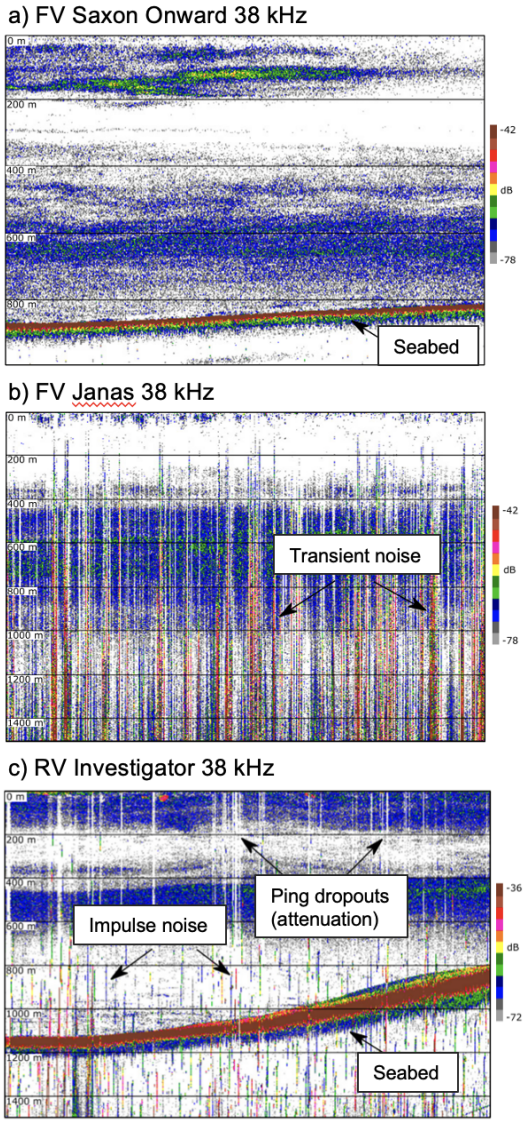


Figure 2.1.1: **Echograms showing examples of acoustic data degradation, adapted from Figure 2.1 in Jech et al. (2021).** Panel a) is an example of high quality data; b) shows data heavily impacted by transient noise; and c) shows data affected by impulse noise (non weather-related) and attenuation. Colour scale depicts strongest backscatter in red/brown, weakest in blue/grey, and missing data/empty water as white).

Detection of affected data can be carried out using a semi-automated filter or by visually scrutinising echograms and marking affected cells manually. The magnitude of signals affected by transient noise and attenuation fluctuates, as does the strength of underlying biological backscatter. Therefore, an optimal threshold to distinguish affected data from natural variability in biological signals must be established. Various other parameter settings must also be applied, for example the size of the neighbourhood to which cell values are compared (number of other cells or pings) needs to be selected.

Visual scrutiny of echograms is an important preliminary step in the data cleaning process. It allows the analyst to get a sense of the ubiquity and presentation of noise and attenuation in the dataset. However, using visual scrutiny alone to identify degraded data can be unreliable. Graphical representations of backscatter data vary with plotting software, and zoom level and colour-bar threshold settings impact a person's ability to discern patterns in backscatter (Peña, 2021; Blackwell et al., 2019b). Even controlling for these factors, scrutinising data at a suitably high zoom level may make manual detections and checks unfeasible given the high volume of data typically collected (e.g. 179,229 pings in this study). This underlines the need to find robust and time-effective methods to clean data.

Semi-automated methods to detect degraded data are arguably more systematic, repeatable, and consistent than manual approaches that rely on visual scrutiny, but they may struggle to distinguish between fluctuations caused by noise or attenuation or those due to natural variability in biotic backscatter. Manual detection methods can suffer from appreciable subjectivity due to intra- and inter-operator variability, but, importantly, the human brain can rapidly assess a vast amount of information, arriving at judgements that take into account multitudes of features with relative ease. Such complex decision-making cannot easily be replicated in filter design; filters are not typically able to capture the multiple characteristic features of degraded data and instead only focus on one or two characteristics. Each approach has its merits. Ideally, the combination of both approaches can capitalise on fast-processing speed and consistency of semi-automated filters, using manual oversight to double-check and adjust results as necessary.

Common approaches to detect bubbles beneath the surface are also either based on visual scrutiny or semi-automated filters, for example see Swart et al. (2016). Bubble layers can usually be seen in echograms as regions of strong backscatter beneath the surface that may extend into v-shaped plumes at irregular intervals (Crawford and Farmer, 1987). Semi-automated approaches to defining bubble layers and plumes usually apply a threshold which distinguishes bubbles from weaker biotic scattering and then employ an algorithm to identify regions of vertically contiguous backscatter which exceeds the threshold, so as to demarcate how far the layer extends below the surface (e.g. see Jech et al., 2021).

Data cleaning procedures seek to correct or remove poor quality data in post-processing. However, the efficacy of these techniques is difficult to establish, and remaining data may still be compromised by undetected bias. Ryan et al. (2015) reported that despite applying data cleaning procedures to one of their datasets, a significant degree of attenuation remained, warranting exclusion of its use in biomass estimations. Despite the 'cleaned' data appearing normal in the echogram, i.e. without the tell-tale sign of stripes of attenuated pings (see Figure 2.1.1), the seabed echo was reduced by 3-6 $\mathrm{dB}$ when the ship changed orientation and speed. This points to the problem of persistent attenuation, which is usually caused by a layer of bubbles remaining under the transducers for a prolonged period (Ryan et al., 2015). Analogous to an increase in background noise, this kind of attenuation may persist for a long period of time, making it difficult to detect using filters that identify only short-lived fluctuations in backscattering strength.

Persistent attenuation can sometimes be detected by comparing measurements of a reference scatterer. In some cases, it can even be remedied by applying a correction factor established from these measurements, allowing degraded data that otherwise may have had to have been discarded to be kept. Detecting persistent attenuation from a reference scatterer (and, in particular, determining a correction factor) is most reliable when using reference scatterers that have low variability in backscattering strength (Ryan et al., 2015). For this reason, and because it exists everywhere and is often shallow enough to be easily recorded by echosounders, the seabed is the most common reference scatterer used to detect persistent attenuation (Dalen and Løvik, 1981; Honkalehto et al., 2011).

Repeated measurements of a reference scatterer can be compared under different hydrodynamic conditions, for example to compare effects of transducer depth, travel direction relative to wind and waves, or travel speeds, or even to approximately calibrate an echosounder when the standard reference sphere method is not practical (Egil Ona, personal comment, December 2018). Shabangu et al. (2014) compared seabed backscatter measurements taken by transducers mounted either on the keel and hull of a ship, at $8\,\mathrm{m}$ and $5.5\,\mathrm{m}$ depth respectively, to determine that data from the hull-mounted transducer required a variable multiplicative correction factor of up to 2.3 in order to produce comparable survey results to those from the keel-mounted transducer (deemed less affected by near-surface bubble attenuation). However, data that have been badly degraded are still likely to be compromised even after removal or correction of transient noise or attenuation; it should be carefully considered whether regions of badly degraded data should be cleaned and retained or discarded (Jech et al., 2021).

No gold standard exists against which the efficacy of data cleaning procedures can be measured since each currently available method to detect noise or attenuation has inherent biases that may result in false negatives (fail to detect degraded data) and false positives (misattribute noise or attenuation to natural fluctuations in biotic backscatter). Diagnostic measures of data cleaning efficacy are often qualitative and subjective, based on visual scrutiny of echograms. More quantitative measures of the degree of data degradation rely on comparison to a presumed 'cleaner' reference dataset, as exemplified by Shabangu et al. (2014) and Ryan et al. (2015). Detections are unlikely to be comprehensive and so it is worth attempting to assess the efficacy of detection methods and consider potential bias remaining in supposedly clean data before using data for ecological analyses or stock assessment.

The percentage of degraded pings can provide a rough indication of the likelihood that data quality is still compromised despite the application of data cleaning procedures (Jech et al., 2021). Often, when the percentage exceeds a chosen threshold the data are discarded (Honkalehto et al., 2011). However, the percentage of degraded pings does not provide a comparable metric among datasets, since detections are dataset- and threshold-specific. There is a need for a diagnostic metric that can evaluate the degree of degradation which is comparable across different datasets, and quantify the removal of bias associated with noise

and attenuation throughout the data cleaning process.

### 2.1.3 Platform-dependence of adverse weather impacts

The impacts of adverse weather on acoustic data quality are platform-dependent. Transducer depth is perhaps the single most important factor that determines how bubbles generated at the surface affect the acoustic signal. Locating transducers as deep as possible on surface vessels can help to reduce the effects of bubble-attenuation (Shabangu et al., 2014; Ona and Traynor, 1990), albeit at the expense of not being able to acquire data as close to the surface. One potential advantage of ASVs such as the Wave Glider is that transducers can be mounted relatively shallow - in the case of *Lyra*, at $0.5\,\mathrm{m}$ below the surface - and therefore have the potential to obtain acoustic measurements from regions close to the surface that are typically missed by ship-based acoustic surveys (Fernandes et al., 2003). On the other hand, locating the transducers this close to the surface comes at an increased risk of bubble-attenuation.

The size of a platform and its design influences the way that the platform pitches and rolls in the waves, which largely determines the impact of attenuation due to transducer motion as well as hydrodynamics that can influence bubble sweep-down (Delacroix et al., 2016; Mallat et al., 2018). Many ASVs are small and travel at comparatively slow speeds, and so may not generate as much bubble sweep-down as larger, faster ships (Guo et al., 2021). However, at $3.05\,\mathrm{m}$ long and $0.81\,\mathrm{m}$ wide, the Wave Glider float is smaller than wavelengths of typical surface waves from sea states dominated by swell and wind seas (Toffoli and Bitner-Gregersen, 2017), which could make it more susceptible to roll (Chu et al., 2019).

Transient noise caused by waves hitting the acoustic platform will also be dependent on platform size and shape. Unlike research vessels which typically have a draft of several metres, the Wave Glider's draft is only around $23\,\mathrm{cm}$ and the surface float sits almost flush with the sea surface during calm weather (Figure 2.1.2). Consequently, the Wave Glider may experience impacts from surface waves in a different way to ships; waves may more easily break over the float but there is less surface area exposed on the hull both above and below water than compared to that on the hull of a ship.

Figure 2.1.2: **Photographs of the Wave Glider *Lyra* in different sea conditions.** In both calm (left) and mildly wavy (right) seas the platform sits fairly flush with the surface, although some tilt from the horizontal, indicative of roll, can be seen when in the waves.

### 2.1.4 Aims of this study

This chapter explores ways in which stronger winds led to worsening quality of the acoustic data collected by the Wave Glider, *Lyra*, during her mission in the central North Sea during May 2018. To do this, I determine rates and severity of transient noise and attenuation using semi-automated detection filters and also derive estimates for the depth and acoustic intensity of bubble plumes beneath the surface. I then analyse how these variables correlate with wind speed and direction, and vessel forward and rotational motion. To detect transient noise and attenuation, I adapt semi-automated filtering techniques for application to *Lyra's* acoustic dataset, and develop a newly described filter to detect persistent attenuation using the seabed as a reference scatterer. Finally, I semi-quantitatively assess the degree of bias in the acoustic dataset, tracking changes associated with data cleaning and the relationship between bias and wind speed. This study aims to provide a comprehensive description of acoustic data quality issues experienced by *Lyra* that are associated with adverse weather, and provide recommendations for future studies that might use acoustically-equipped Wave Gliders on how to mitigate against the collection of poor quality acoustic data.

## 2.2 Methods

### 2.2.1 Acoustic and ancillary data collection

Analyses in this chapter use narrowband 70 kHz backscatter data collected by *Lyra* in May 2018 (see Subsection 1.4.2) together with vessel position, vessel rotational motion, and wind speed measurements as listed in Table 2.1.

Table 2.1: **Wind and vessel measurements made by sensors onboard *Lyra***.

| **Sensor** | **Location** | **Measurements (units)** | **Sampling frequency** |
|---|---|---|---|
| Airmar WeatherStation 200WX | 1 m above centre of float | True wind speed ($\mathrm{m\,s^{-1}}$) | 1 Hz |
| | | True wind direction (°) | |
| | | GPS coordinates (decimal degrees) | |
| Motion Reference Unit | Centre of float | Roll (° from horizontal) | 1 Hz, burst 1 in 5 mins |
| Transducer linked to WBT-mini echosounder | 0.5 m depth, aft of float | 70 kHz $S_v$ (dB re $1\,\mathrm{m^{-1}}$) | 0.1 Hz |

### 2.2.2 Echosounder calibration

The WBT-mini echosounder was calibrated at Hamilton Dock, Lowestoft, UK on the 28$^{\text{th}}$ of June 2018 using the standard sphere method first described by Foote et al. (1987). Calibrations were conducted using a 20 mm diameter tungsten carbide sphere (with 6% cobalt) of known acoustic reflectivity, appropriate for calibrating the frequency bands of both the 70 and 200 kHz transducers according to ICES guidelines (Demer et al., 2015). Values of the absorption coefficient ($\alpha$) used in the calibrations were calculated according to Francois and Garrison (1982). Key calibration parameters are provided in Table 2.2.

Table 2.2: **Key echosounder calibration parameters.**

| | |
|---|---|
| Temperature at calibration site (°C) | 18 |
| Temperature value applied to data (°C) | 8 |
| Salinity at calibration site (*ppt*) | 33 |
| Salinity value applied to data (*ppt*) | 35 |
| ES70-18CD Gain (dB) | 19.6 |
| ES200-7CD Gain (dB) | 27.4 |

An investigation into the effect of applying default depth-constant temperature and salinity values to calibrate the acoustic data determined that these parameter choices had little impact on range offset and amplification by TVG (Appendix A).

### 2.2.3 Data processing

Vessel speed and direction estimates were derived from GPS coordinates using R package 'geosphere' (Hijmans, 2021). Transect turning-points were determined from the GPS coordinates and checked visually in QGIS (QGIS Development Team, 2018). Coordinates were minute-averaged, retaining the original transect turning points, to smooth a small number of spurious points, and reconstructed to a resolution of $1\,\mathrm{Hz}$ by imputation. Quality-controlled GPS coordinates differed from the raw values by a maximum of $29\,\mathrm{m}$ latitudinally (mean $0.004\,\mathrm{m}$) and $25\,\mathrm{m}$ longitudinally (mean $0.003\,\mathrm{m}$).

#### 2.2.3.1 Reducing autocorrelation in the wind speed data

Autocorrelation is prevalent in many time series. Wind speeds were temporally autocorrelated, shown by correlated lagged values in Figure 2.2.1. This is unsurprising given that they were collected at $1\,\mathrm{Hz}$ resolution; wind speeds at one moment in time are likely to be similar to wind speeds within the previous few minutes or hours. Regression models assume that residuals are independent; non-independence of samples due to temporal or spatial autocorrelation can bias parameter estimates and reduce the reliability of model

results. To reduce the degree of autocorrelation and improve the reliability of regression analyses, data were averaged across nine-hour intervals. Wind speed measurements binned over nine-hour intervals were still significantly positively autocorrelated at the first lag, with a moderate correlation of $0.64$, however lags beyond this were not (Figure 2.2.1, E). Wind speeds were categorised as either calm, moderate or windy: *Calm* $< 5\,\mathrm{m\,s^{-1}} \leq$ *Moderate* $< 7.5\,\mathrm{m\,s^{-1}} \leq$ *Windy*. All other variables used for regression analyses were similarly averaged over nine-hour intervals.

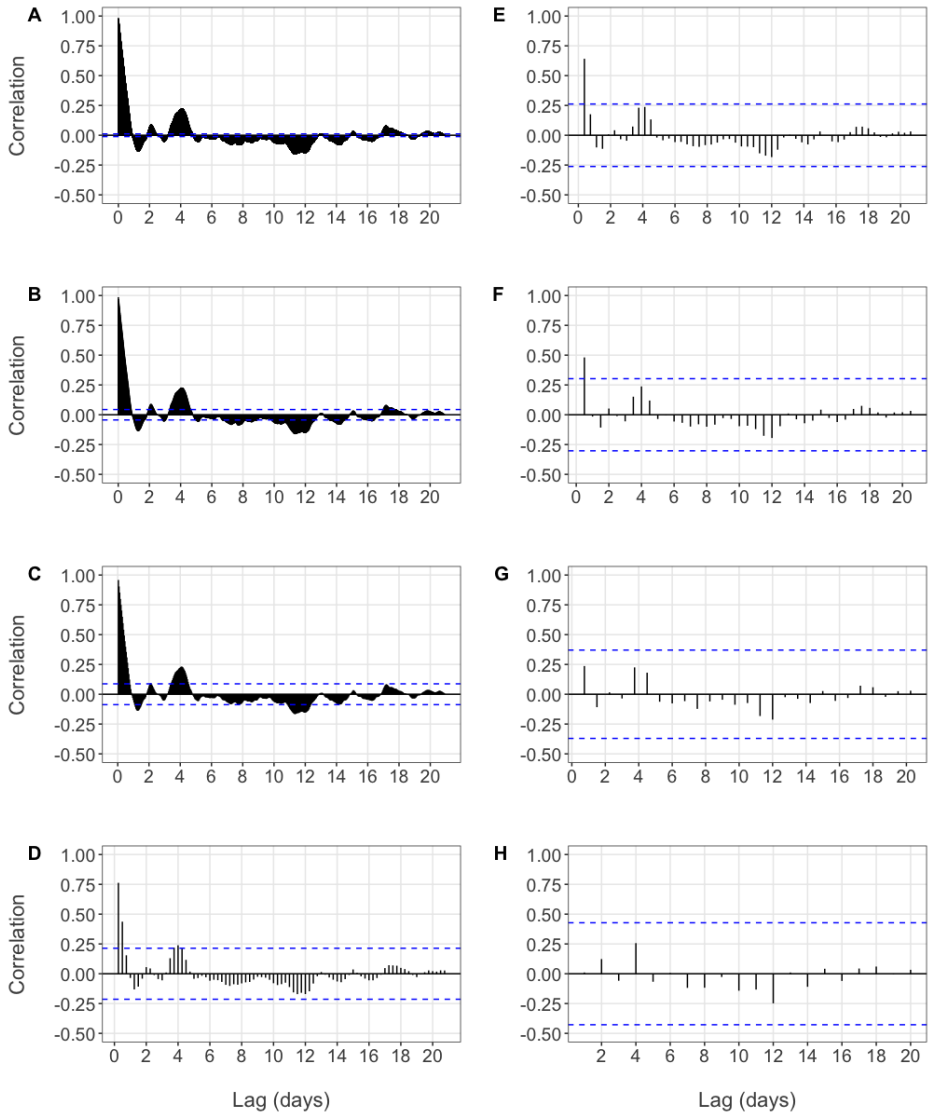


Figure 2.2.1: **Autocorrelation plots for wind speed data averaged over various time periods.** Averaging over A) 1 minute B) 15 minute C) 1 hour D) 6 hour E) 9 hour F) 12 hour G) 18 hour and H) 1 day. Dashed blue lines indicate $95\,\%$ confidence intervals outside of which values were considered significantly autocorrelated.

Averaging reduced the likelihood of dependence between consecutive samples, but also reduced the temporal and spatial resolution of the data. Binning by nine-hour intervals was a compromise between reducing the effects of autocorrelation whilst still retaining reasonable sample sizes for statistical testing ($n = 56$). For analyses which required a finer resolution, one-minute averaged data were used. Averaging over either one-minute or nine-hour intervals also helped to reduce the effects of random error, and smoothed over periodic timescales of platform motion (i.e. pitch and roll cycles, in the order of seconds). Unless otherwise stated, all results show nine-hour averaged data.

#### 2.2.3.2 Acoustic data processing

Figure 2.2.2 describes the order of acoustic data processing steps, including the application of filters to detect data degraded by attenuation and transient noise.

The $70\,\mathrm{kHz}$ backscatter data were imported into Echoview Software Pty Ltd (2021) together with the calibration files, and temporally aligned with the GPS coordinates. Backscatter data within the first $2\,\mathrm{m}$ were affected by ring-down and hence excluded. A bottom line was defined using the Echoview 'best bottom detection algorithm' and manually edited where necessary to ensure horizontal continuity.

A threshold offset line set to $-65\,\mathrm{dB}$ was applied, acting downwards from the $2\,\mathrm{m}$ exclusion limit, to delineate the depth of the bubble layer. The $-65\,\mathrm{dB}$ threshold was chosen following visual assessment of a range of threshold offset lines between $-75\,\mathrm{dB}$ and $-60\,\mathrm{dB}$. The main sound scattering layer (SSL) typically had backscattering strengths that were weaker than $-65\,\mathrm{dB}$, and thresholds below $-65\,\mathrm{dB}$ often led to the line extending deeper into the SSL when night came as the SSL rose towards the surface. Thresholds greater than $-65\,\mathrm{dB}$ failed to capture some instances where vertical continuity of backscatter suggested that bubble plumes extended deeper. Therefore, the $-65\,\mathrm{dB}$ threshold was deemed a good compromise to describe depth of the bubble layer without inadvertently confusing biological signal with bubbles.

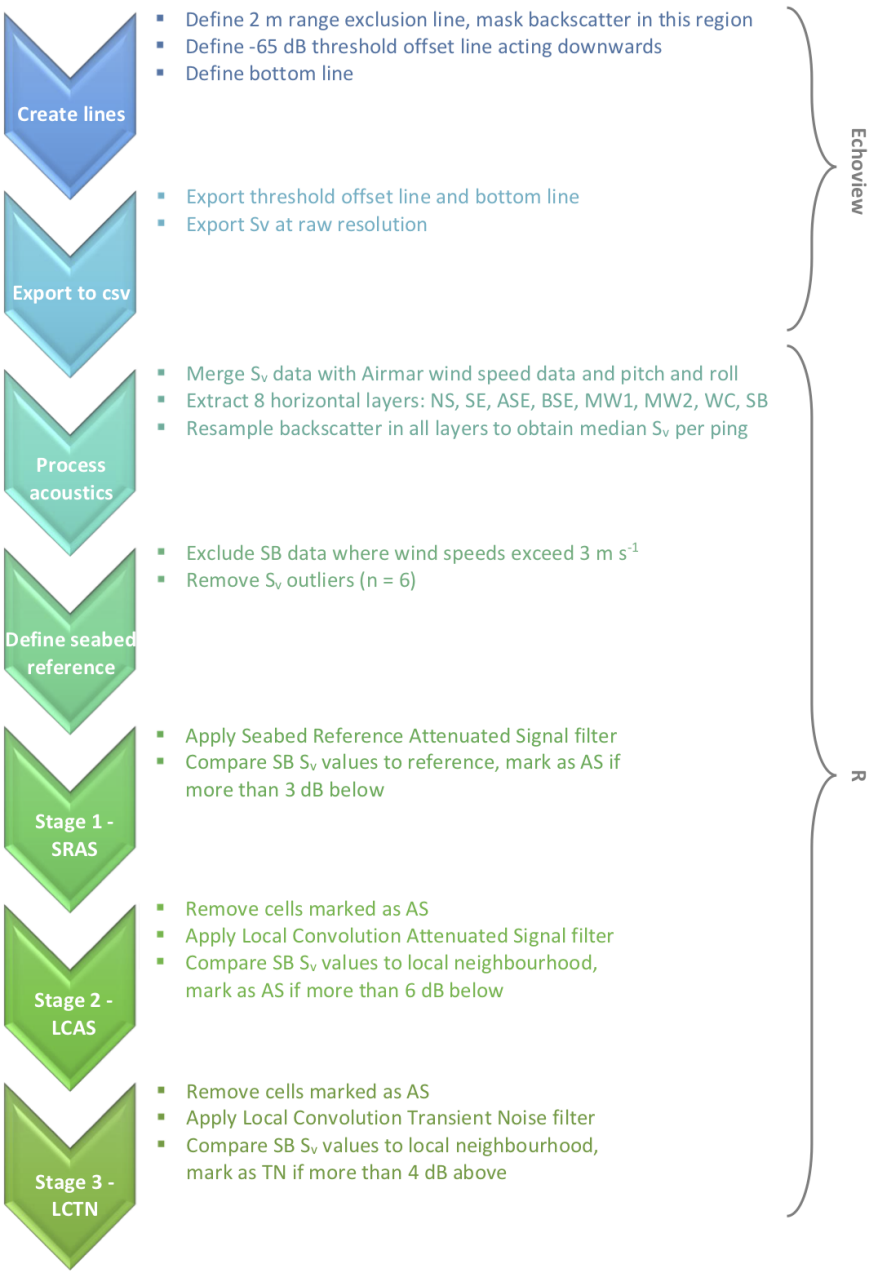


Figure 2.2.2: **Processing steps used to detect transient noise and attenuation.** Initial processing was carried out in the Echoview software, followed by implementation of detection filters (SRAS, LCAS and LCTN) in R Core Team (2022). See text for further explanations of terms and details of the process.

Narrowband $70\,\mathrm{kHz}$ volume backscatter data ($S_v$) at the original resolution, and bottom and threshold offset (bubble plume depth) lines were exported as comma separated variable files and imported into RStudio Team (2022) for further analysis using R Core Team (2022).

Eight horizontal layers of backscatter data were extracted and each resampled vertically to obtain median backscatter values per layer, per ping (Table 2.3). Visual examples of three of these layers, the Near-Surface (NS), Water Column (WC), and Seabed (SB) layers, are shown in Figure 2.2.3. The NS layer was used to provide a proxy measure of the backscattering strength of bubbles under the surface. The Mid-water 1 (MW1) and Mid-water 2 (MW2) layers were defined to compare the impact of bubbles in the NS layer with backscatter deeper in the water column. The subunit created strong echoes and phantom echoes in the upper $36\,\mathrm{m}$ of the water column (see horizontal yellow bands in Figure 2.2.3). The Subunit Echo (SE), Above Subunit Echo (ASE), and Below Subunit Echo (BSE) layers were used to investigate the impact of wind speed on backscatter caused by the subunit interference. The WC and SB layers were defined for the purpose of applying data cleaning filters to detect transient noise and attenuation and remove affected pings, and were also used to estimate the degree of bias introduced by windier weather.

Table 2.3: **Horizontal layers of the backscatter data, used to assess the impact of wind on acoustic data quality.** For explanations of their purpose, see main text.

| **Layer** | **Thickness (m)** | **Range (m)** | **Description** |
|---|---|---|---|
| Near-surface (NS) | 5 | 2 - 7 | Fixed depth layer above the subunit echo |
| Above Subunit Echo (ASE) | 0.2 | 7.4 - 7.6 | Fixed depth layer in close proximity to the subunit echo |
| Subunit Echo (SE) | 0.2 | 8.4 - 8.6 | Fixed depth layer within the subunit echo |
| Below Subunit Echo (BSE) | 0.2 | 10.4 - 10.6 | Fixed depth layer in close proximity to the subunit echo |
| Mid-water 1 (MW1) | 2 | 29 - 31 | Fixed depth layer between third and fourth phantom subunit echoes |
| Mid-water 2 (MW2) | 5 | 40 - 45 | Fixed depth layer below the last phantom subunit echo |
| Water Column (WC) | 15 | Variable | Bottom-referenced, $10\,\mathrm{m}$ to $25\,\mathrm{m}$ above bottom<br>Depths ranged from $46\,\mathrm{m}$ to $89\,\mathrm{m}$ |
| Seabed (SB) | 2 | Variable | Bottom-referenced, $1\,\mathrm{m}$ to $3\,\mathrm{m}$ below bottom<br>Depths ranged from $71\,\mathrm{m}$ to $100\,\mathrm{m}$ |

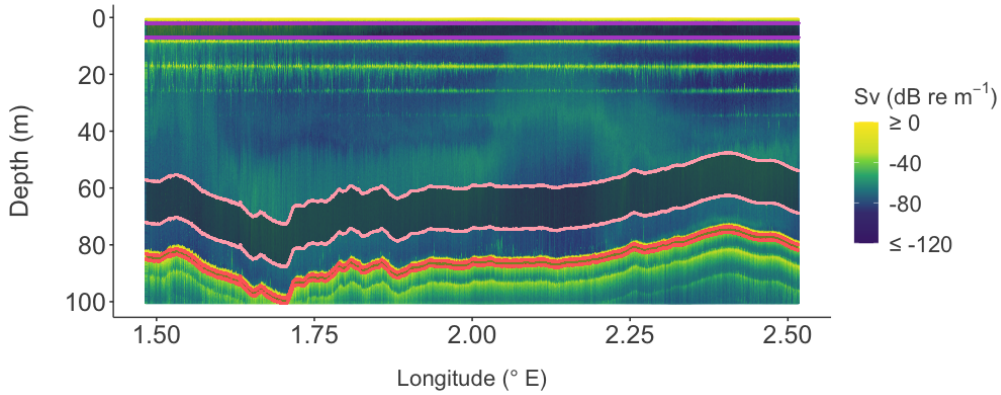


Figure 2.2.3: **Echogram of 70 kHz backscatter data from Transect 1 depicting various extracted layers.** Shaded regions within outlined layers depict the near-surface (NS, purple), water column (WC, pink) and seabed (SB, red) layers. Strong backscatter (yellow) due to ring-down and the near-field effect can be seen at the top of the echogram. Horizontal bands of strong backscatter at regular $8\,\mathrm{m}$ depth intervals in the top $36\,\mathrm{m}$ were caused by interference in the acoustic beam by the subunit.

### 2.2.4 Detecting attenuation and transient noise

Attenuation and transient noise were apparent in echograms of unprocessed backscatter, typically presenting as single pings (stripes) with distinctly stronger or weaker backscatter than neighbouring pings (Figure 2.2.4). Two complementary filters were developed to detect pings affected by attenuation - the Seabed Reference Attenuated Signal (SRAS) filter and the Local Convolution Attenuated Signal (LCAS); and one filter was developed to detect pings affected by transient noise - the Local Convolution Transient Noise (LCTN) filter.

The SRAS filter compared backscatter in the SB layer against reference values in the SB layer determined for $0.1^{\circ}$ longitudinal bins of the transect (approximately $620\,\mathrm{m}$) during periods where wind speeds did not exceed $3\,\mathrm{m\,s^{-1}}$. The SRAS filter was designed to detect pings most severely affected by attenuation, including those within a regime of persistent attenuation. Local convolution filters were developed for automated detection of short-lived attenuation and transient noise (LCAS and LCTN), which were also applied to the SB layer. These filters were based on the impulse noise filters described by Anderson et al. (2005) and Ryan et al. (2015), and the transient noise filter described by Ryan et al. (2015), containing elements from each but tailored for this dataset and application to a select region of the acoustic data (the SB layer). These filters compared ping median backscatter values against

reference values derived from the mean of spatially and temporally local pings. Pings identified by either the SRAS or LCAS filter were marked as 'AS', denoting that the ping was affected by attenuation (Attenuated Signal). Pings identified by the LCTN filter were marked as 'TN', denoting that the ping was affected by Transient Noise. Marked pings were removed following the order in Figure 2.2.2 before subsequent filters were applied.

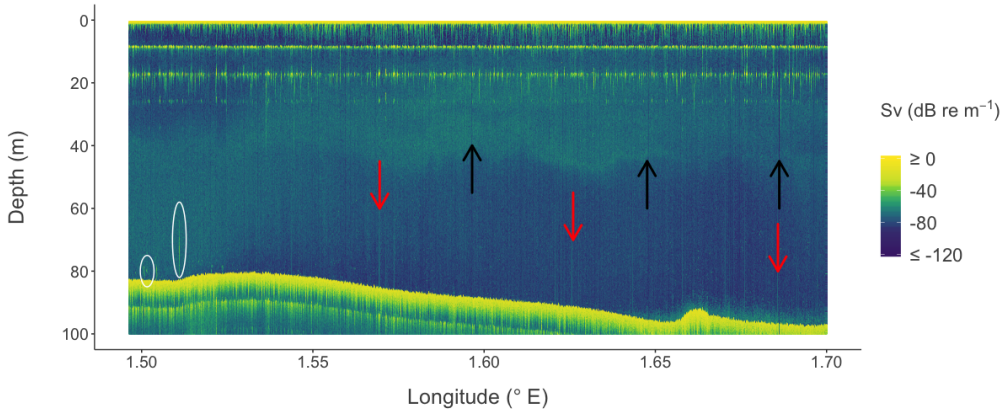


Figure 2.2.4: **Examples of suspected degraded data.** Pings affected by attenuation (black arrows) and transient noise (red arrows), as well as strongly scattering biological aggregations (white circles) which could be confused for noise indicated in 70 kHz echogram. Stronger backscatter ($S_v$) shown in yellow, weaker backscatter in dark blue.

### The Seabed Reference Attenuated Signal (SRAS) filter

Plotting seabed backscatter (ping median values from the SB layer) against longitude (position across the transect) grouped by wind speed category revealed stark differences in the minimum backscatter values recorded for the same regions depending on the wind speed (Figure 2.2.5, A). During calm weather, seabed backscatter measurements rarely dipped below $-35\,\mathrm{dB}$ (only $0.01\,\%$ of data collected during calm weather), regardless of *Lyra's* position along the transect. In contrast, when wind speeds exceeded $7.5\,\mathrm{m\,s^{-1}}$, the minimum backscattering value was $-96\,\mathrm{dB}$ and there were numerous instances where seabed backscatter was below $-35\,\mathrm{dB}$ ($2.9\,\%$ of data collected during windy weather).

The SRAS filtering procedure was as follows: extract SB backscatter values when wind speeds were less than $3\,\mathrm{m\,s^{-1}}$; visually inspect backscatter distribution and remove outliers ($n = 6$) (red circles in Figure 2.2.5, B); select the minimum backscatter value as a reference

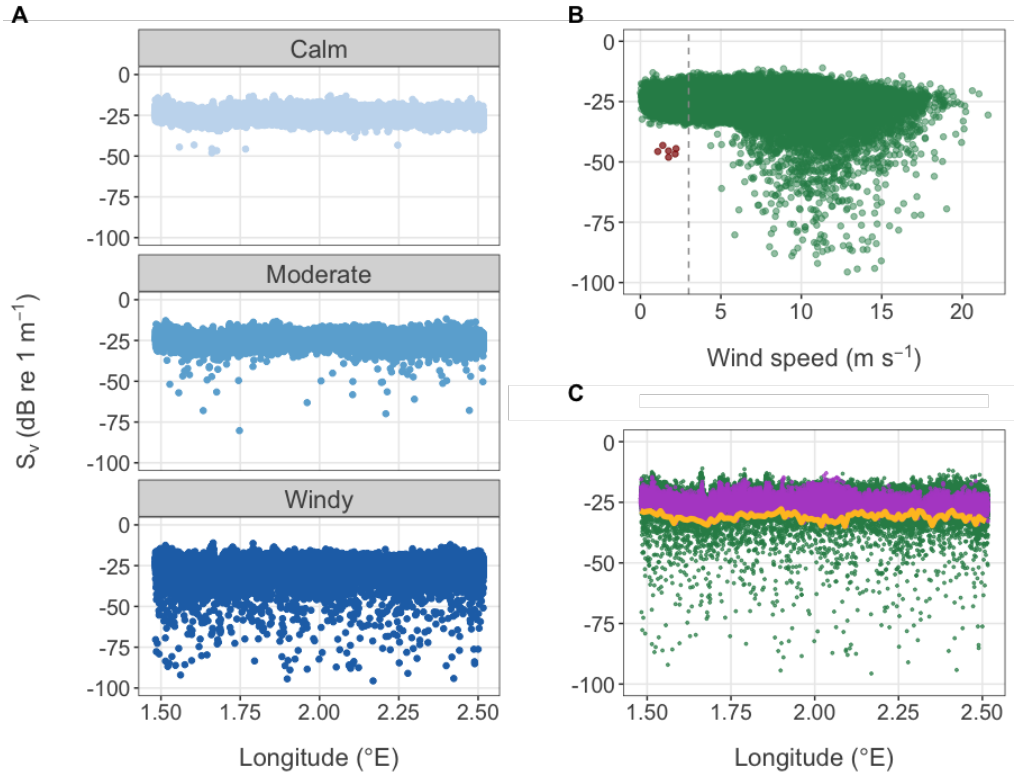


Figure 2.2.5: **Patterns in seabed (SB) layer backscatter ($S_v$) used to inform the SRAS filter.** A) SB $S_v$ against longitude, by wind speed category. B) SB $S_v$ against wind speed, dashed grey line demarcates datapoints used as SRAS reference values (winds $< 3\,\mathrm{m\,s^{-1}}$) excluding outliers in red. C) SB $S_v$ coloured according to wind speed: green $\geq 3\,\mathrm{m\,s^{-1}}$, purple $< 3\,\mathrm{m\,s^{-1}}$. Gold line depicts reference values used for the SRAS filter.

for each $0.01°$ longitudinal bin along the transect (gold line in Figure 2.2.5, C); compare all SB backscatter values against the appropriate reference according to its longitudinal position along the transect; mark pings with SB $S_v$ that fall below the reference minus a threshold ($\delta$) as AS. Following a sensitivity analysis, a threshold of $\delta = 3\,\mathrm{dB}$ was chosen.

The SRAS filter defined reference values from backscatter measurements made during very calm weather (wind speeds below $3\,\mathrm{m\,s^{-1}}$) because these were assumed to be most representative of the seabed echo, i.e. least degraded by attenuation or transient noise. To capture spatial variation in the seabed, reference values were defined for one hundred and four $0.01°$ longitudinal bins along the transect, each covering a distance of approximately $620\,\mathrm{m}$ across the transect and containing between 16 and 599 pings per bin (mean $209 \pm 113$) when wind speeds were less than $3\,\mathrm{m\,s^{-1}}$. Latitudinal variation across the transect line was small; $69\,\%$ of pings were within $100\,\mathrm{m}$ of the transect line. Reference backscatter values

spanned a range of 7 dB, from −28 dB to −35 dB (gold line in Figure 2.2.5, C).

**Local convolution filters: LCAS and LCTN**

The LCAS and LCTN filters were designed to differentiate pings with respectively stronger and weaker backscatter in the seabed compared to neighbouring pings. First, SB layer backscatter values (cells) were convolved using a 9x1 kernel, equally-weighted by a factor of one for all cells except the central cell which was set to zero (Equation 2.2.1), applied centrally to each cell to obtain the mean of the 4-ping neighbourhood either side of the cell.

$$K_{9\text{x}1} = \begin{bmatrix} 1 & 1 & 1 & 1 & 0 & 1 & 1 & 1 & 1 \end{bmatrix} \tag{2.2.1}$$

Next, the convolved backscatter values were subtracted in the linear domain from the paired (by ping) original SB layer backscatter values. These resulting values describe the difference in backscatter between those of the cell (ping median backscatter in the layer) and the mean, in the linear domain, of the neighbouring cells, and are hereafter referred to as 'Sv-difference' values with units of dB re $1\,\mathrm{m}^{-1}$ (or simply, dB). Cells with Sv-difference values that exceeded chosen thresholds, i.e. satisfied Equation 2.2.2 or Equation 2.2.3, were respectively marked as either AS (attenuated) or TN (affected by transient noise).

$$S_{vi} < 10log_{10}\left(\frac{\left(\sum_{j=-k}^{k} s_{vi+j}\right) - s_{vi}}{2k}\right) + \delta \tag{2.2.2}$$

$$S_{vi} > 10log_{10}\left(\frac{\left(\sum_{j=-k}^{k} s_{vi+j}\right) - s_{vi}}{2k}\right) + \delta \tag{2.2.3}$$

where $s_{vi} = 10^{\frac{S_{vi}}{10}}$ is the linear volume backscattering coefficient of cell $i$, $\delta$ is the threshold in dB, and $k$ is such that $n = 2k + 1$ denotes a kernel of size $n$x1.

The LCAS filter was applied to mark pings with SB Sv-difference values that exceeded a threshold of $\delta = -6\,\mathrm{dB}$ as AS. Following this, the LCTN filter was applied and marked pings with SB Sv-difference values that exceeded a threshold of $\delta = 4\,\mathrm{dB}$ as TN. The thresholds ($-6\,\mathrm{dB}$ and $4\,\mathrm{dB}$) and the kernel width (9, the number of neighbouring pings in each comparison) were chosen following sensitivity analyses (Appendix C) which showed that, of the sizes tested, kernel size made little difference to mean and median backscattering strengths in either the WC or SB layers.

### 2.2.5 Analysing the effects of wind speed on data quality

Relationships between rates of attenuation and transient noise, wind speed, roll, and bubble layer metrics (plume depth and NS layer backscatter) were investigated using scatter plots, Spearman's rank correlation coefficients, and linear regression models where appropriate. Rates of attenuation and transient noise were defined as the proportion of AS or TN marked pings per minute or per nine-hour interval respectively. The severity of attenuation or transient noise was calculated for each wind speed category. Severity was defined as the increase or decrease in backscattering strength of AS or TN marked pings compared to backscattering strength of the cleaned data where AS and/or TN pings had been removed. Rose diagrams, grouped by wind speed category, were plotted to explore relationships between the relative direction of the wind to *Lyra* and rates of attenuation and transient noise, vessel speed, roll, and bubble plume depth. Wind speeds were compared between periods when bubble layers were detected (plume depths greater than $2\,\mathrm{m}$, the default depth of the threshold offset line) and when they were not. Average night and day NS layer backscatter was compared, grouped by wind speed category, to establish whether there was a diel signal indicative of DVM performing organisms which affected the utility of NS layer backscatter to act as a proxy for density of the bubble layer. The effect of wind speed on contributions of the subunit on water column backscatter measurements was investigated by comparing relationships between backscatter from the ASE, SE, and BSE layers, and visual scrutiny of echograms.

To assess whether past wind activity or instantaneous wind speeds were more strongly correlated with rates of attenuation and transient noise, and with bubble plume depths, Spearman's rank correlation coefficients were calculated for rolling-average past wind speeds lagged by periods of one minute, five minutes, ten minutes, half an hour, an hour, an hour and a half, two hours, and two and a half hours. Kendall's tau statistics were calculated to evaluate whether coherence between wind speeds and bubble metrics differed before, during, and after a two and a half day period of strong sustained winds.

### 2.2.6 Two-layer comparison technique to measure bias and filter efficacy

For this chapter I developed a technique to semi-quantitatively assess the degree of bias associated with short-lived attenuation or transient noise in acoustic datasets. I have called this technique the *'two-layer comparison technique'*, as it compares the correlation strengths between pairs of Sv-differences in two distinct horizontal layers of the data. In this study, I applied the two-layer comparison technique to the SB and WC layers. The technique involves calculating Sv-differences by applying the same local convolution kernel as used for the LCAS and LCTN filters. Spearman's rank correlation coefficients are then calculated to determine the degree of synchronicity between fluctuations in backscattering strengths of the two layers.

The principle underlying the technique's ability to identify bias due to transient noise or attenuation is that, although backscatter is expected to vary on a ping-by-ping basis in both layers, because these forms of data degradation affect the entire ping, backscatter is more likely to increase or decrease synchronously across both the water column and seabed if it has been affected by transient noise or attenuation. By contrast, natural variation in seabed and water column backscatter would not be expected to cause synchronous changes across the layers because backscattering strengths in these layers would be expected to vary independently on a ping-by-ping basis. That is, there is no reason why an increase or decrease in backscattering strength in the seabed that is caused by natural variation would be correlated with a similar increase or decrease in backscattering strength in the water column, at least not on a ping-by-ping basis.

For this study on the impacts of wind on acoustic data quality, I subsetted the data into $1\,\mathrm{m\,s^{-1}}$ wind speed intervals to reveal whether there was any pattern of increasing bias (I.e. increasing correlation strength) with windier weather. I also used the technique to compare correlation coefficients before and after each filter was applied to track the removal of bias through the data cleaning process.

In addition to using the two-layer comparison technique to measure the reduction of bias after data cleaning, various other means were used to assess the effects that the data cleaning filters had on the acoustic data. These included: visual inspection of echograms of unprocessed and cleaned data, calculating the proportion of data removed $(\mathrm{percent})$ for different wind speed categories, calculating the effect of removing degraded data (AS and TN marked pings) on average seabed and water column backscatter, comparing average backscattering strengths of degraded and 'clean' data in the seabed and water column, and calculating differences to along-track resolution following the removal of degraded pings.

## 2.3 Results

### 2.3.1 Platform motion

*Lyra* encountered a variety of weather conditions during the mission. Wind speeds ranged from perfectly still, recorded at $0\,\mathrm{m\,s^{-1}}$, to gusts of $22\,\mathrm{m\,s^{-1}}$ (level 9 on the Beaufort wind force scale, indicative of strong gales) (Figure 2.3.1, A). Wind speeds were variable across a range of different timescales. There were periods of several hours where wind speeds were fairly constant and similar periods of highly changeable wind speeds. Midway through the mission there was a period of sustained strong winds which lasted for two and a half days, from approximately 11pm on 15$^{\mathrm{th}}$ May to midday on 18$^{\mathrm{th}}$ May. Wind speeds exceeded $7.5\,\mathrm{m\,s^{-1}}$, reaching a maximum minute-averaged wind speed of over $16\,\mathrm{m\,s^{-1}}$ (Figure 2.3.1, A). During this period the vessel experienced substantial roll (Figure 2.3.1, D), bubble plumes extended more than $10\,\mathrm{m}$ below the surface (Figure 2.3.1, B) and backscattered strongly near the surface (Figure 2.3.1, C), and rates of AS and TN peaked (Figure 2.3.1, rug plots in A-F).

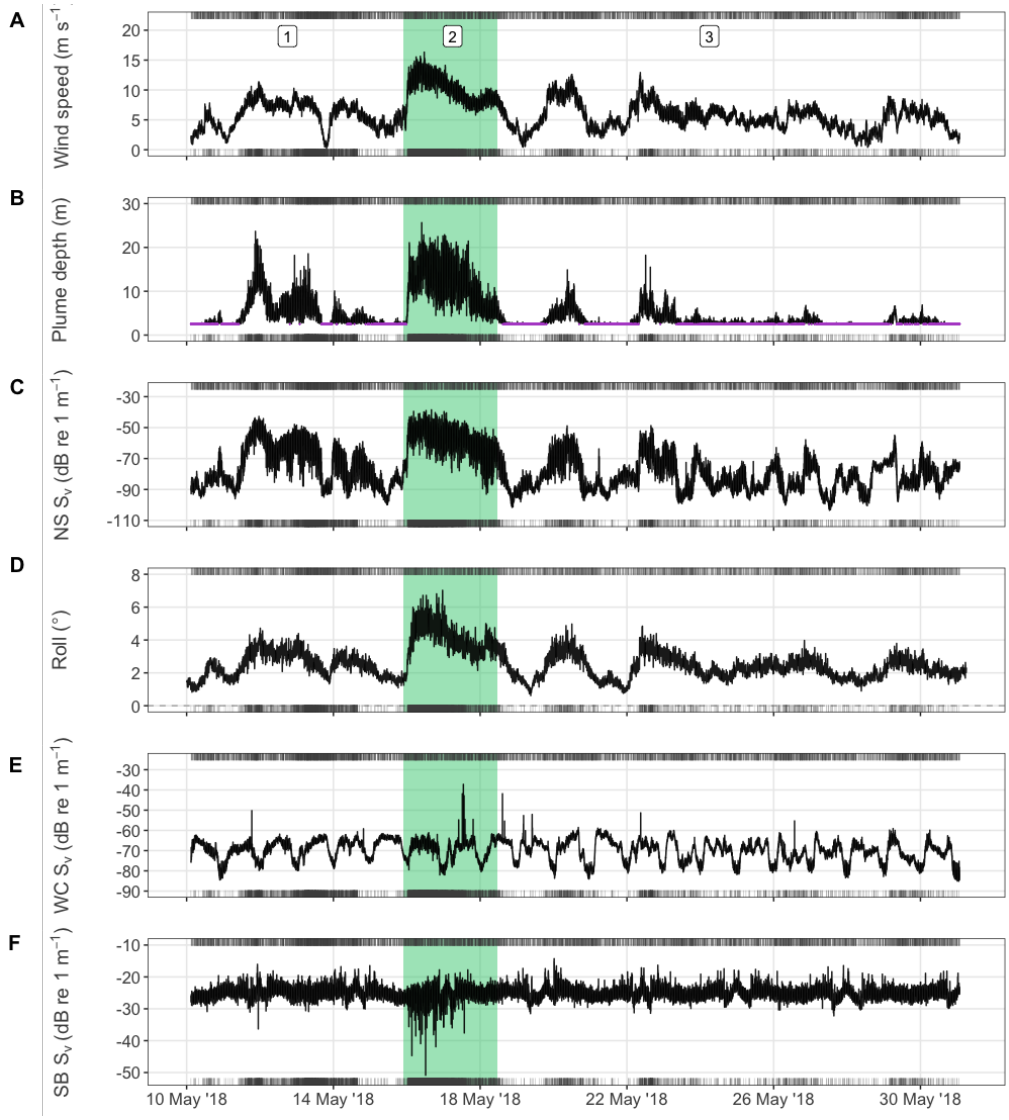


Figure 2.3.1: **Time series of wind speed (A), bubble plume depth (B), backscatter in the NS (C), WC (E), and SB (F) layers, and vessel roll (D).** Three time periods enumerated to show before (1), during (2, shaded green) and after (3) the period of sustained strong winds. All data minute averaged except TN (top rug) and AS pings (bottom rug) shown on each subplot. Purple points in (B) indicate that no bubble layer was detected.

*Lyra* travelled at an average speed of $0.53 \pm 0.15\,\mathrm{m\,s^{-1}}$ (range $0.08$ to $0.99\,\mathrm{m\,s^{-1}}$) (Figure 2.3.2, A). Vessel speed increased as wind speed increased, however the relationship was not linear. Vessel speed increased by more than $40\,\%$ as wind speeds doubled from $5$ to $10\,\mathrm{m\,s^{-1}}$, but above wind speeds of $10\,\mathrm{m\,s^{-1}}$ vessel speed stayed relatively constant (Figure 2.3.2, B). Mean roll amplitude was $2.3 \pm 1.0°$, ranging from $0.01$ to $7.5°$ (Figure 2.3.2, C). Roll was strongly correlated with wind speed (linear model: adjusted $R^2 = 0.70$, $p < 0.001$) (Figure 2.3.2, D). Roll amplitude approximately doubled from 2 to

4° as wind speeds increased from 5 to 10 $\mathrm{m\,s^{-1}}$.

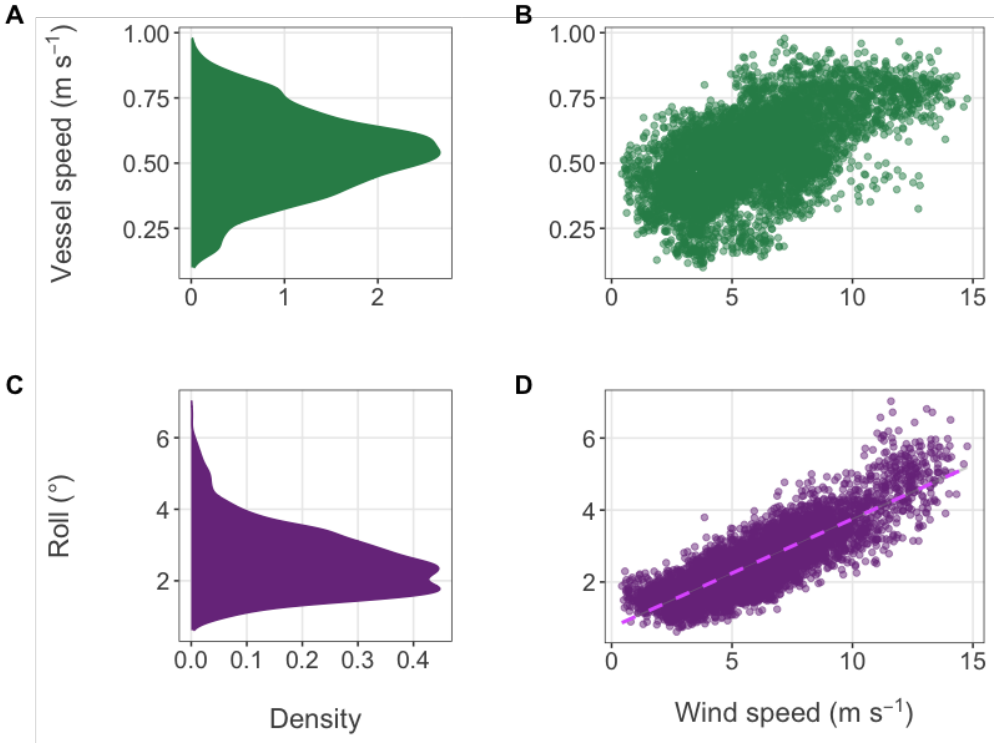


Figure 2.3.2: **Platform motion and its relationship to wind speed**. Density of vessel speed (A) and roll (C) observations. Relationships between wind speed and vessel speed (B) and roll (D). Linear model between roll and wind speed (lilac dashed line, D): $R^2_{adj} = 0.7$, gradient = 0.3, $P < 0.001$. Plots use minute-averaged vessel speed data and five-minute averaged roll data.

*Lyra* stayed within 100 m of the transect line 65 % of the time (Figure 2.3.3). Latitudinal deviations of more than 250 m beyond the transect line were uncommon, lasting only 1.1 % of the time. Large excursions from the transect line were deliberate piloting manoeuvres to avoid marine traffic (personal comment, D. Pearce, email April 2019). Only one deviation further than 1 km occurred, and this lasted for forty-eight minutes. The average transect path length was 64.6± 0.3 km (ranging from 64.3 to 65.0 km), with transect crossings taking an average duration of 1.4 ± 0.3 days to complete (ranging from 1 to 1.8 days).

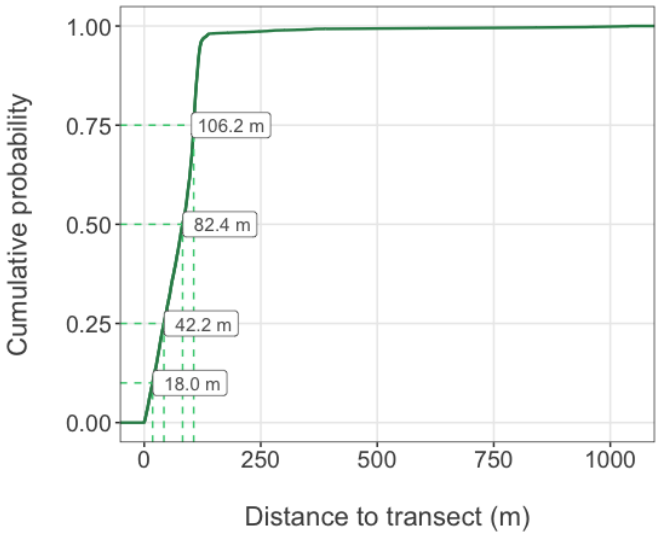


Figure 2.3.3: **Empirical cumulative distribution probabilities of distances to the transect.** Distances to transect within which *Lyra* stayed are highlighted for 25 %, 50 % and 75 % of the time by dashed lines. For example, *Lyra* stayed within 18 m of the transect line for 10 % of the mission.

### 2.3.2 Preliminary visual assessment of acoustic data quality

Several features were apparent in echograms of the 70 kHz volume backscatter data. Water column biota and the seabed were sampled throughout the mission, near-surface bubble plumes were evident intermittently through the mission, and there was evidence of degraded data and unwanted signal (Figure 2.3.4). All 70 kHz echograms are shown in Appendix B. Attenuation and transient noise were visible in the echograms, appearing as vertical stripes, typically a single ping wide, of weaker and stronger backscatter respectively (Figure 2.3.4). The echograms showed evidence of extensive attenuation during *Lyra's* fifth transect crossing which took place between early morning of the 16$^{th}$ May and early morning of the 17$^{th}$ May, a time when wind speeds peaked (Figure 2.3.1, rug plots in A).

An unusual feature was observed in the acoustic data throughout the mission: the Wave Glider's subunit interfered with the acoustic beam causing multiple horizontal bands of strong backscatter at regular 8 m depth intervals below the surface (Figure 2.3.4). This repeated banding was caused by the initial echo rebounding between the surface and the subunit, creating 'phantom' echoes that decayed in strength to negligible levels by approximately 36 m. The subunit and phantom echoes were stronger than typical biological

signal in the SSL, resulting in substantial acoustic masking of biota in the upper $36\,\mathrm{m}$.

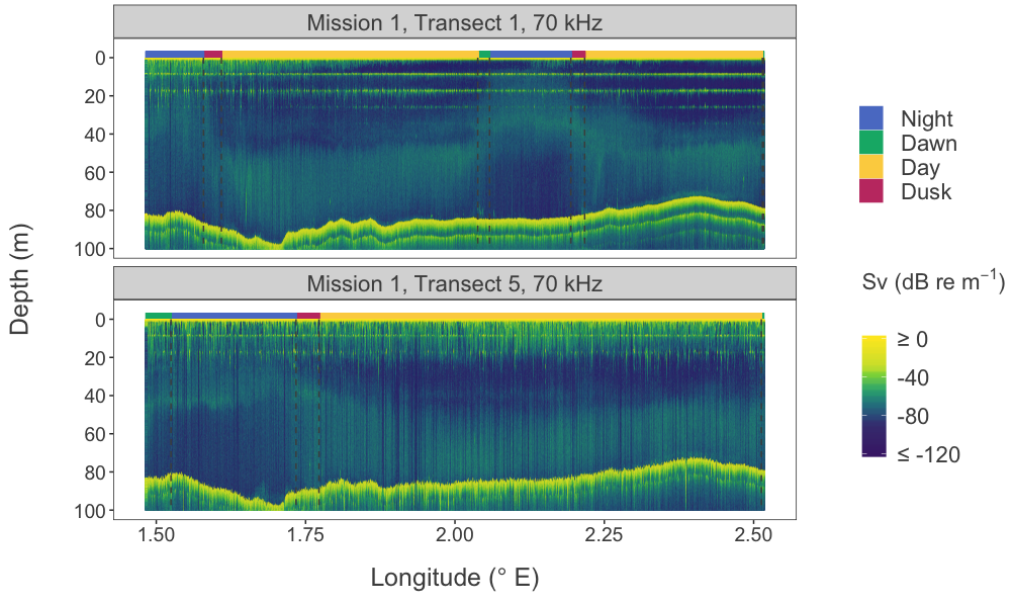


Figure 2.3.4: **Echograms of 70 kHz backscatter from Transects 1 and 5 depicting degraded data.** Numerous vertical stripes of weak backscatter, indicative of attenuation, were recorded during Transect 5. Stripes of stronger backscatter, possibly indicating transient noise, are visible in the deeper part of the water column at night but more easily seen in the seabed echo (yellow stripes), extending to the maximum recorded range.

### 2.3.3 Effect of wind speed on data degradation near the surface

Bubble plumes were often observed during periods when wind speeds exceeded $5\,\mathrm{m\,s^{-1}}$ (Figure 2.3.1, B). During periods of strong winds plumes extended several metres below the surface, reaching a maximum depth of $25.7\,\mathrm{m}$ on 16$^{\text{th}}$ May. A layer of bubbles persisted for seventy-nine hours during *Lyra's* fifth and sixth transect crossings, coinciding with the period of strong sustained wind speeds (Figure 2.3.1, A & B). The bubble layer was detected during $67\,\%$ of the mission. When the bubble layer was absent, the average wind speed was $3.7 \pm 1.6\,\mathrm{m\,s^{-1}}$, ranging from $0.2$ to $8.4\,\mathrm{m\,s^{-1}}$. When the bubble layer was present, the average wind speed was greater at $7.2 \pm 2.2\,\mathrm{m\,s^{-1}}$, ranging from $0.7$ to $16.3\,\mathrm{m\,s^{-1}}$ (Figure 2.3.5). Bubble layers were recorded as both present and absent for wind speeds between 2.2-$8.4\,\mathrm{m\,s^{-1}}$, suggesting that instantaneous wind speed alone cannot predict the presence of the bubble layer within this wind speed range.

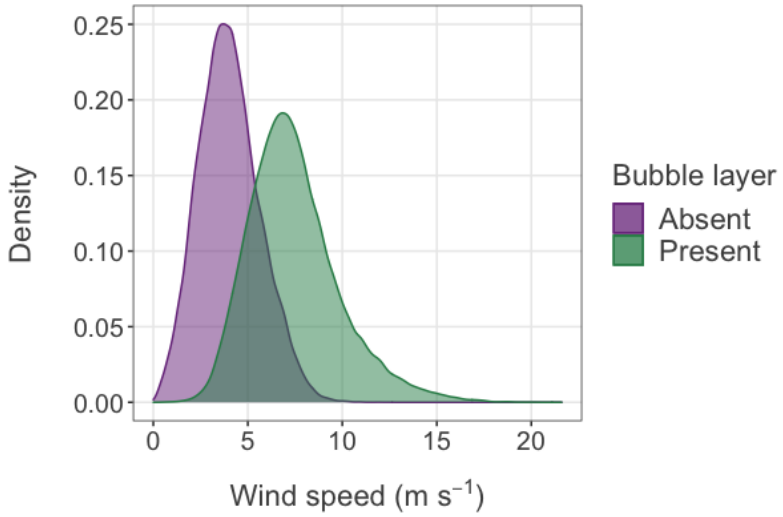


Figure 2.3.5: **Density of wind speed observations during periods when a bubble layer was present (green) or absent (purple).**

Wind speed explained much of the variance in NS layer backscatter (linear model, $R^2 = 0.69, p < 0.01$). Average wind speeds of $12\,\mathrm{m\,s^{-1}}$ coincided with an almost 10,000-fold ($40\,\mathrm{dB}$) increase in sound intensity of the NS layer backscatter, compared to backscatter during $2\,\mathrm{m\,s^{-1}}$ winds. Whilst higher wind speeds were associated with stronger backscatter at depths between 2 to $7\,\mathrm{m}$ (NS layer), no trend was apparent deeper in the water column at the depths of the MW1 layer (29 to $31\,\mathrm{m}$) or the MW2 layer ($40$ to $45\,\mathrm{m}$) (Figure 2.3.6). Average backscatter in these layers did not vary with wind speed and remained below $-67\,\mathrm{dB}$, in contrast to backscatter in the NS layer which reached levels of $-51\,\mathrm{dB}$ during Transect 5 when wind speeds exceeded $12\,\mathrm{m\,s^{-1}}$ (Figure 2.3.1, C). Therefore, even if bubble plumes did extend beyond a depth of $29\,\mathrm{m}$ but were not detected by the method used here, they did not noticeably impact the $70\,\mathrm{kHz}$ backscatter data.

Mean backscatter in the NS layer was stronger during the night when the SSL ascended towards the surface than during the daytime when the SSL descended to depth. Daytime measurements were between $0.5\,\mathrm{dB}$ to $4\,\mathrm{dB}$ lower than those made during nighttimes. Day-night differences were less pronounced during windier weather because NS $S_v$ was dominated by signal from bubbles (Figure 2.3.7). When the weather was calm at night, mean backscatter rarely exceeded $-65\,\mathrm{dB}$, the threshold used to delineate bubble plume depth, suggesting that the SSL was unlikely to have interfered with bubble plume detection.

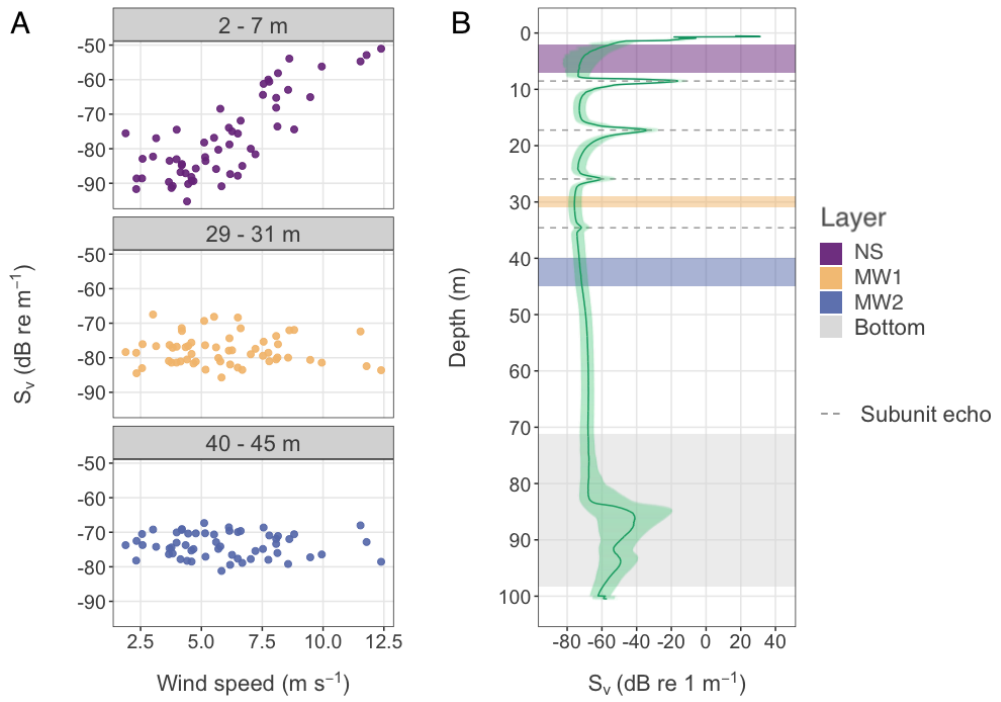


Figure 2.3.6: **Relationships between wind speed and water column backscatter at different depths.** A) Wind speed against average backscatter in near-surface (NS, purple, 2-7 m), mid-water 1 (MW1, yellow, 29-31 m) and mid-water 2 (MW2, blue, 40-45 m) layers. B) Mission averaged backscatter depth profile (green line, IQR shaded green) and location of layers, subunit and phantom echoes (dashed grey lines) and bottom range (shaded grey).

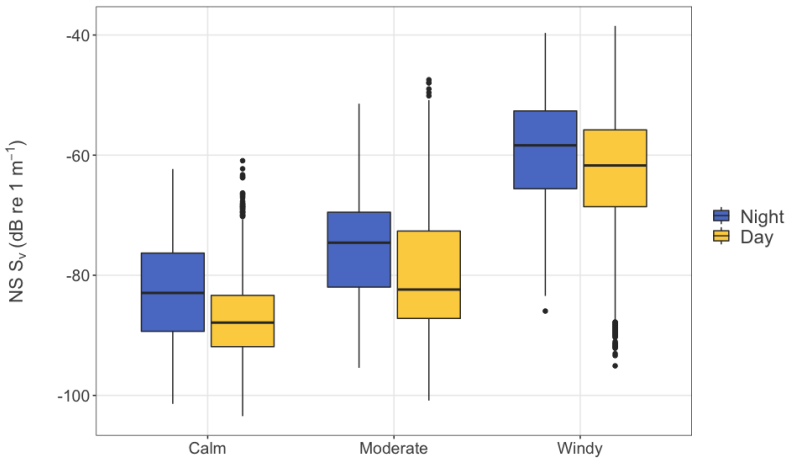


Figure 2.3.7: **Boxplots of daytime and nighttime NS layer backscatter, by wind speed category.** Night is defined as periods when the sun was more than 12° below the horizon. Day is defined as periods when the sun was above the horizon.

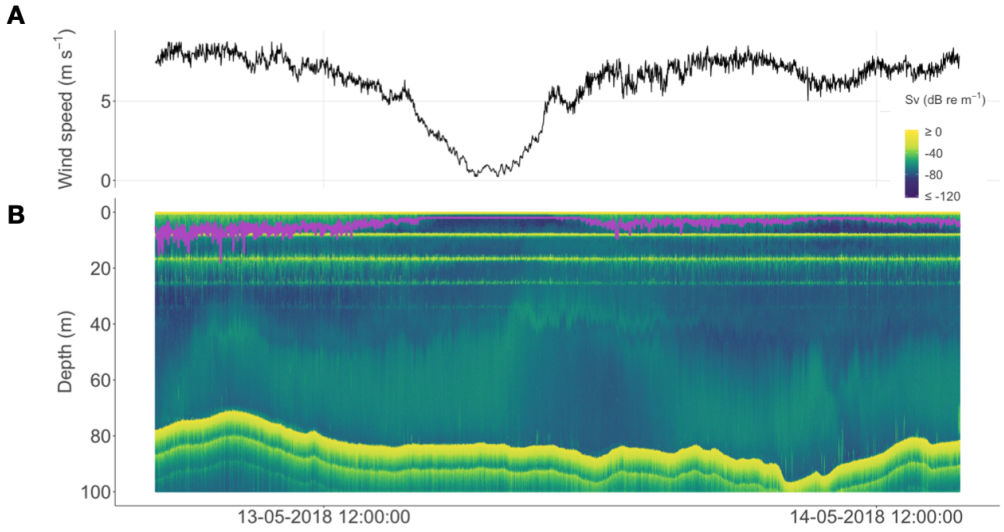


Figure 2.3.8: **Echogram showing the depth of bubble plumes and the distortion of subunit echoes during windier weather.** A) Wind speed time series. B) Bubble plume depth (purple line) superimposed on 70 kHz Transect 3 backscatter echogram. Stronger backscatter ($S_v$) shown in yellow, weaker in blue.

Higher wind speeds were accompanied by both deeper bubble plumes and visible changes to the continuity and vertical spread of the subunit echo and its phantom echoes (Figure 2.3.8). During periods of calm, the subunit echoes formed fairly coherent horizontal bands. However, as wind speeds increased the echoes became more fragmented and vertically stretched. This complicated matters, since it was difficult to define horizontal exclusion layers to mask the unwanted signal from the subunit. As a result, statistical analyses in subsequent chapters exclude all acoustic data shallower than $36\,\mathrm{m}$. Distortion of the subunit echoes primarily affected the phantom echoes, i.e. the echoes which had been reflected back from the sea surface and were observed as horizontal bands at depths below $16\,\mathrm{m}$ (Figure 2.3.8). During windy weather the sea surface is more wavy and less flat. This could have caused the signal to be scattered in different directions, resulting in fragmentation of the echo. A wavy surface would also have reflected the signal at slightly different times, which could explain the appearance of vertical stretching in the echograms. The subunit echoes did not seem to affect the detection of bubble plumes (judged visually). This is probably because the $-65\,\mathrm{dB}$ threshold offset line identified contiguous regions of backscatter above the threshold that extended from the surface, and although the subunit echoes were often stronger than $-65\,\mathrm{dB}$, they were fragmented at times when the bubble layer deepened.

Linear models were fitted to backscatter data from the SE, ASE, and BSE layers to explore whether wind speed was correlated with changes to the subunit echo. Unlike the positive monotonic relationship between backscatter in the NS layer and wind speed, mean backscatter in the SE layer decreased as wind speed increased (Figure 2.3.9, A). The effect size was small, described by a linear model with gradient of $-0.7$ ($R^2 = 0.6, p < 0.001$). This contrasted with the positive gradients of linear models fitted to the ASE (gradient $2.6, R^2 = 0.5, p < 0.001$) and BSE layers (gradient $1.5, R^2 = 0.7, p < 0.001$) (Figure 2.3.9, A). These positive gradients are probably the result of increased bubble backscatter. However, the subunit echo was much stronger than bubble backscatter (typically $-25\,\mathrm{dB}$) and so any contribution of bubble backscatter would have been masked by the subunit in the SE layer (Figure 2.3.9, B).

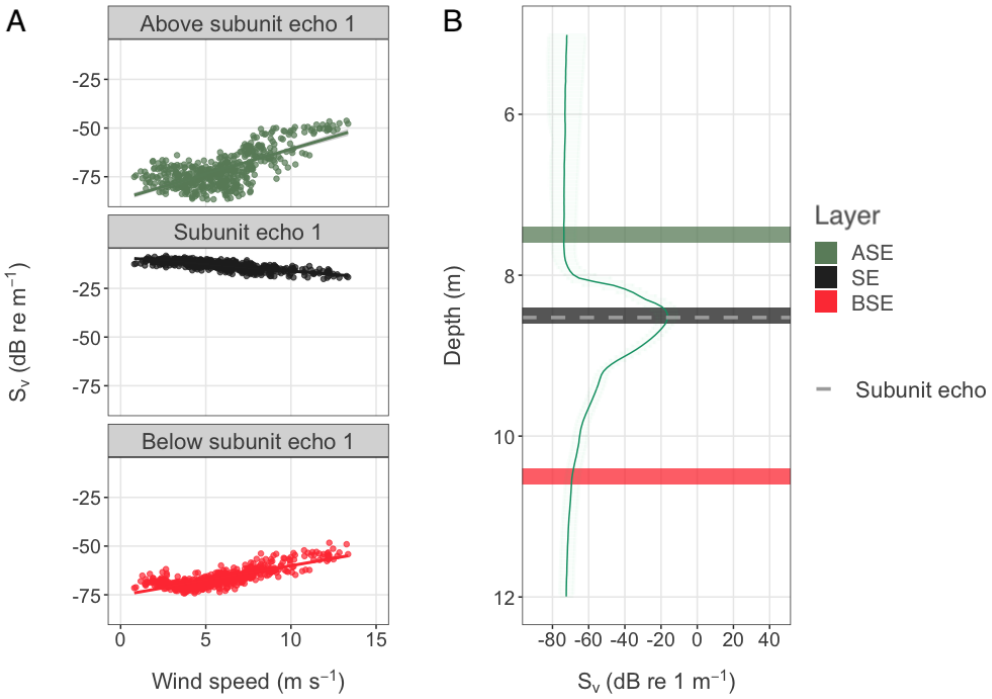


Figure 2.3.9: **Relationships between wind speed and water column backscatter at depths near the subunit.** A) Wind speed against backscattering strength in the layer above the subunit (ASE, green, 7.4-7.6 m), at the depth of the subunit (SE, black, 8.4-8.6 m) and a layer below the subunit (BSE, red, 10.4-10.6 m), with linear models fitted (see main text). B) Mission averaged backscatter depth profile (blue-green line) and location of layers, including the position of the strongest average subunit echo (dashed grey line).

The steeper gradients in linear models that described the relationships between wind speed and backscatter at shallower depths suggest that bubble backscattering strengths decayed with depth (Figure 2.3.6). This is in agreement with Trevorrow (2003) who found that backscattering strengths of surface bubble plumes decayed exponentially with depth. The contrasting decrease in SE layer backscatter with increasing wind speed could have been caused by a difference in the relative motion of the subunit to the float (and hence transducers) during wavier conditions, resulting in less interference in the acoustic beam.

### 2.3.4 Data degradation caused by attenuation and transient noise

#### 2.3.4.1 Proportions of degraded data and patterns with wind speed

In total, $5.5\,\%$ of pings were identified by the data cleaning filters as suffering from data degradation due to either attenuation or transient noise. During calm conditions when wind speeds were less than $5\,\mathrm{m\,s^{-1}}$, the proportion of degraded pings was extremely low (overall $< 3\,\%$). Above winds of $5\,\mathrm{m\,s^{-1}}$, the proportion of AS and TN marked pings both increased. Rates of attenuation increased exponentially as wind speeds rose above $5\,\mathrm{m\,s^{-1}}$ up to $17\,\mathrm{m\,s^{-1}}$, above which the number of data points was very low ($n < 20$) and the proportion of pings affected did not show a clear trend with wind speed (Figure 2.3.10, green in B). Rates of attenuation increased with wind speed much faster than rates of transient noise, which only increased marginally (Figure 2.3.10, purple in B). On average, attenuation was more than ten times as frequent during windy conditions (wind speeds $> 7.5\,\mathrm{m\,s^{-1}}$) than during calm weather (wind speeds $< 5\,\mathrm{m\,s^{-1}}$). The proportion of pings affected by transient noise increased by a factor of 1.4 as wind speeds increased from calm ($< 5\,\mathrm{m\,s^{-1}}$) to windy ($\geq 7.5\,\mathrm{m\,s^{-1}}$). At low wind speeds, transient noise was the dominant source of data degradation, however during windy weather attenuation affected more than twice as many pings as transient noise.

The proportion of degraded pings remained below $10\,\%$ for wind speeds up to $10\,\mathrm{m\,s^{-1}}$ (Figure 2.3.10, B). However, above $10\,\mathrm{m\,s^{-1}}$ the proportion increased by up to $40\,\%$, primarily driven by the increase in rates of attenuation. The vast majority of acoustic data

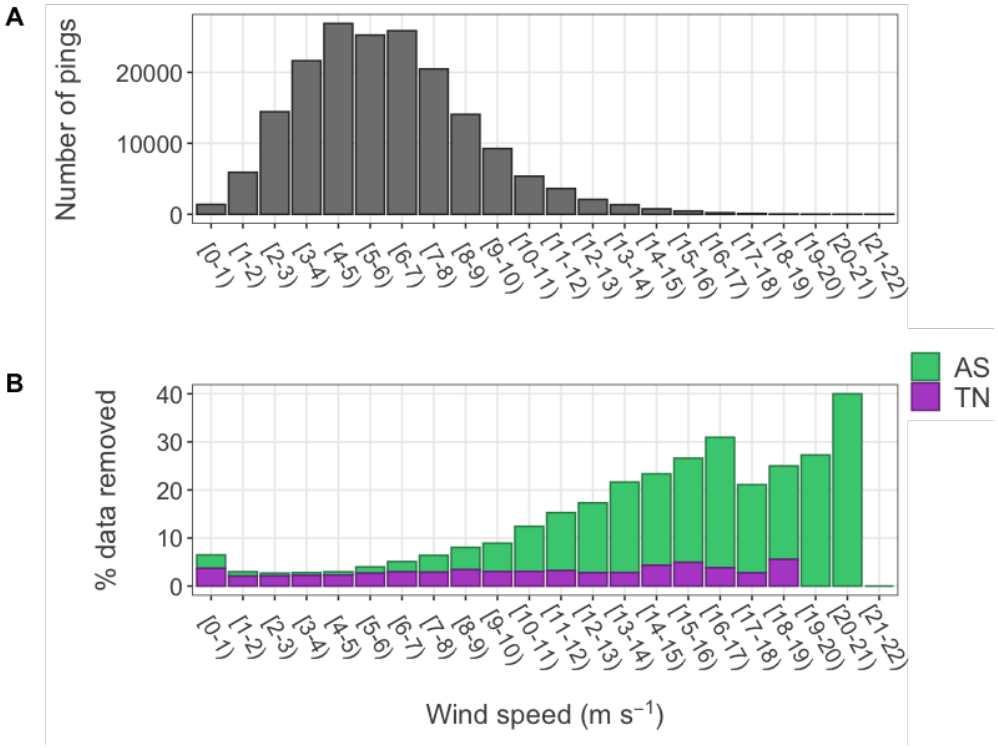


Figure 2.3.10: **Proportions of data degraded by attenuation or transient noise, plotted against wind speed.** A) Number of degraded pings and B) percentage of pings affected by attenuation (AS, green) and transient noise (TN, purple) that were identified and removed by filters.

was collected during periods when average wind speeds were below $10\,\mathrm{m\,s^{-1}}$ (Figure 2.3.10, A). This means that most of the acoustic data were of adequate or good quality, and data degradation caused by attenuation and transient noise only impacted data during a small proportion of the total mission time.

### 2.3.4.2 Relationships with vessel roll, wind, and the bubble layer

Higher rates of attenuation and transient noise were associated with increased wind speeds, stronger backscatter in the NS layer, increased amplitude of vessel roll, and deeper bubble plumes. The correlation between the rates of these two forms of data degradation was strongly positively monotonic ($\rho(56) = 0.86, p < 0.01$), indicating that if attenuation frequently occurred then transient noise did also (Figure 2.3.11). This is unsurprising given that impacts of both forms of data degradation are known to be weather-dependent and increase with windier and wavier conditions (Jech et al., 2021).

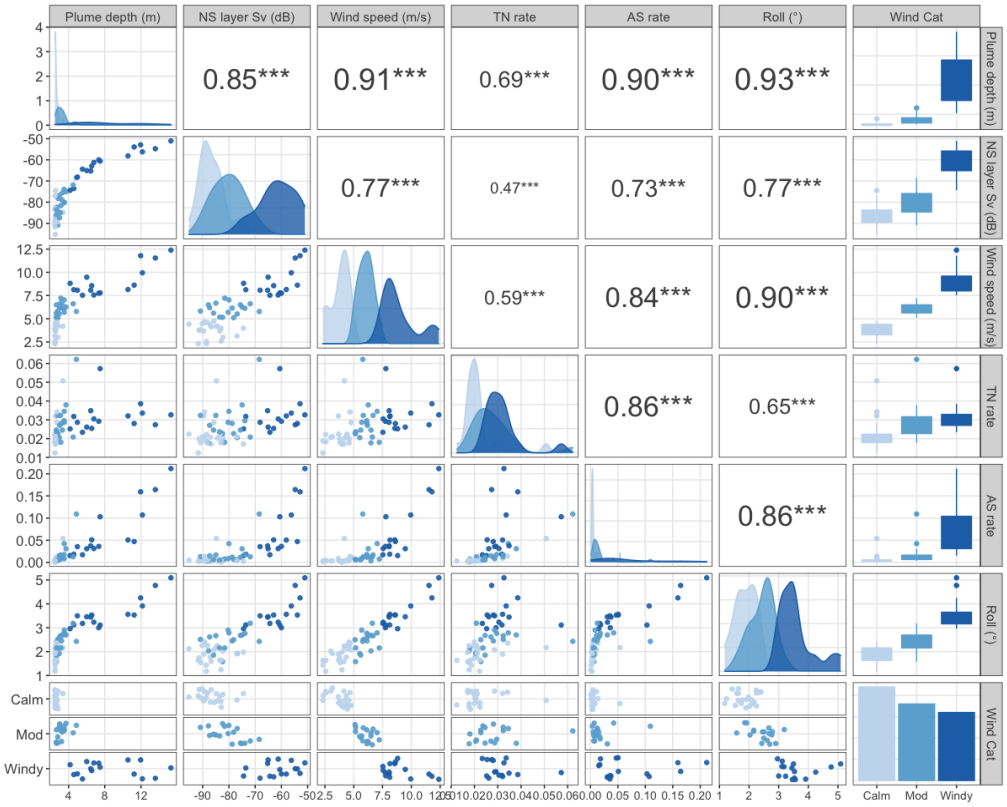


Figure 2.3.11: **Draftsman plot showing relationships between wind speed, vessel roll, proxy bubble metrics, and rates of data degradation.** Plots in upper triangle show Spearman's correlation coefficients where '***' denotes $p < 0.001$. Diagonals are density plots. Scatter plots in lower triangle. 'Wind Cat' denotes wind speed category (Calm $<$ $5\,\mathrm{m\,s^{-1}} \leq$ Moderate (Mod) $\leq 7.5\,\mathrm{m\,s^{-1}}$ Windy), which colours the plots. All plots use nine-hour averaged data.

Strong positive monotonic relationships ($0.73 < \rho(56) < 0.90, p < 0.001$) were found between rates of attenuation and roll, wind speed, and bubble layer variables (plume depth and NS layer backscatter) ('AS rate' in Figure 2.3.11). Similar, but more moderate, positive monotonic relationships ($0.47 < \rho(56) < 0.69, p < 0.01$) were found between rates of transient noise and the aforementioned variables ('TN rate' in Figure 2.3.11). Of the variables tested, backscatter in the NS layer was least correlated with rates of data degradation ('NS layer Sv' in Figure 2.3.11). As discussed earlier, backscatter from biota in the SSL contributed to measurements made near the surface, explaining why this variable was only a weak proxy for the acoustic intensity of bubbles and conditions at the near-surface.

Data degradation rates were more correlated with roll and bubble plume depth than with wind speed (Figure 2.3.11). This is probably because roll and bubble plume depth acts as a better proxies for wave conditions at the surface than instantaneous wind speed; wind stress at the surface takes time to build waves and entrain bubbles into the water column. Indeed it was found that correlations between wind speed and bubble plume depth, and wind speed and data degradation rates, were higher when tested using lagged average rolling wind speeds, rather than the instantaneous wind speed (tested with lags up to two and a half hours). Correlations peaked when tested with 30- to 60-minute lagged wind speeds (Figure 2.3.12). This suggests that instantaneous wind speeds are not as important as average recent conditions in building up sea-surface waves, and explains some of the heteroskedasticity in relationships of minute-averaged variables with wind speed; short-lived fluctuations during windy periods (e.g. gusts and temporary lulls) do not necessarily translate to changes in surface wave expressions, as it takes time for changes to wind stress at the surface to alter the sea-state.

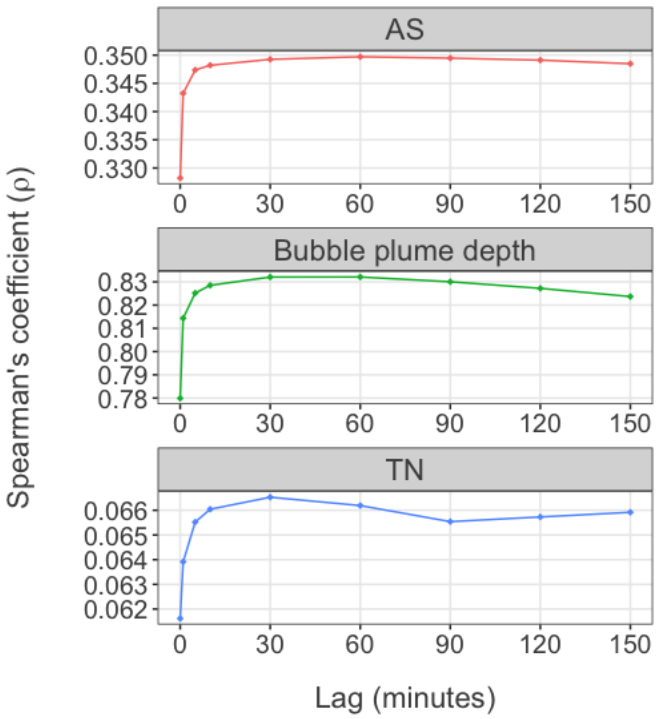


Figure 2.3.12: **Correlations between lagged wind speed and attenuation (AS, top), bubble plume depth (middle), and transient noise (TN, bottom).** All $P$ values were $< 0.001$.

The importance of recent wind activity was further exemplified by differences in correlation strengths between bubble metrics and wind speed before, during and after the period of sustained strong winds (periods [1], [2] and [3] in A of Figure 2.3.1). Kendal's correlation coefficients were highest during the period of strong winds ($\tau_{plume,2} = 0.81, \tau_{NS,2} = 1.00$), and lower prior to and after that period ($\tau_{plume,1} = 0.72, \tau_{NS,1} = 0.75, \tau_{plume,3} = 0.77, \tau_{NS,3} = 0.35$, all $p < 0.001$). This suggests that there was greater coherence during the period of prolonged, sustained strong wind speeds than during periods of more changeable, but overall calmer, weather conditions. This lends further support to the hypothesis that instantaneous conditions are less important to data quality than average recent conditions.

Wind direction had little impact on vessel speed (Figure 2.3.13, A). The strongest winds came from starboard and port directions, and consequently the vessel was slightly faster when strong winds came from these directions. Roll amplitudes and bubble plume depths were also greatest during cross-winds, which may have similarly been a consequence of the strength of the winds rather than the direction (Figure 2.3.13, B & C).

**Possible effects of wind direction**

Rates of both attenuation and transient noise were higher when the wind came from aft of the vessel (Figure 2.3.14). This pattern was more apparent the higher the wind speed. Both head winds and tail winds were associated with higher rates of transient noise in windier weather, despite the fact that the strongest wind speeds in these wind speed categories were from cross-winds. Lower rates of attenuation and transient noise were observed when winds came from port-bow or starboard-quarter directions ($315^\circ$ and $135^\circ$). These relative wind directions coincide with lower bubble plume depths and less roll, which may explain the lower rates of data degradation.

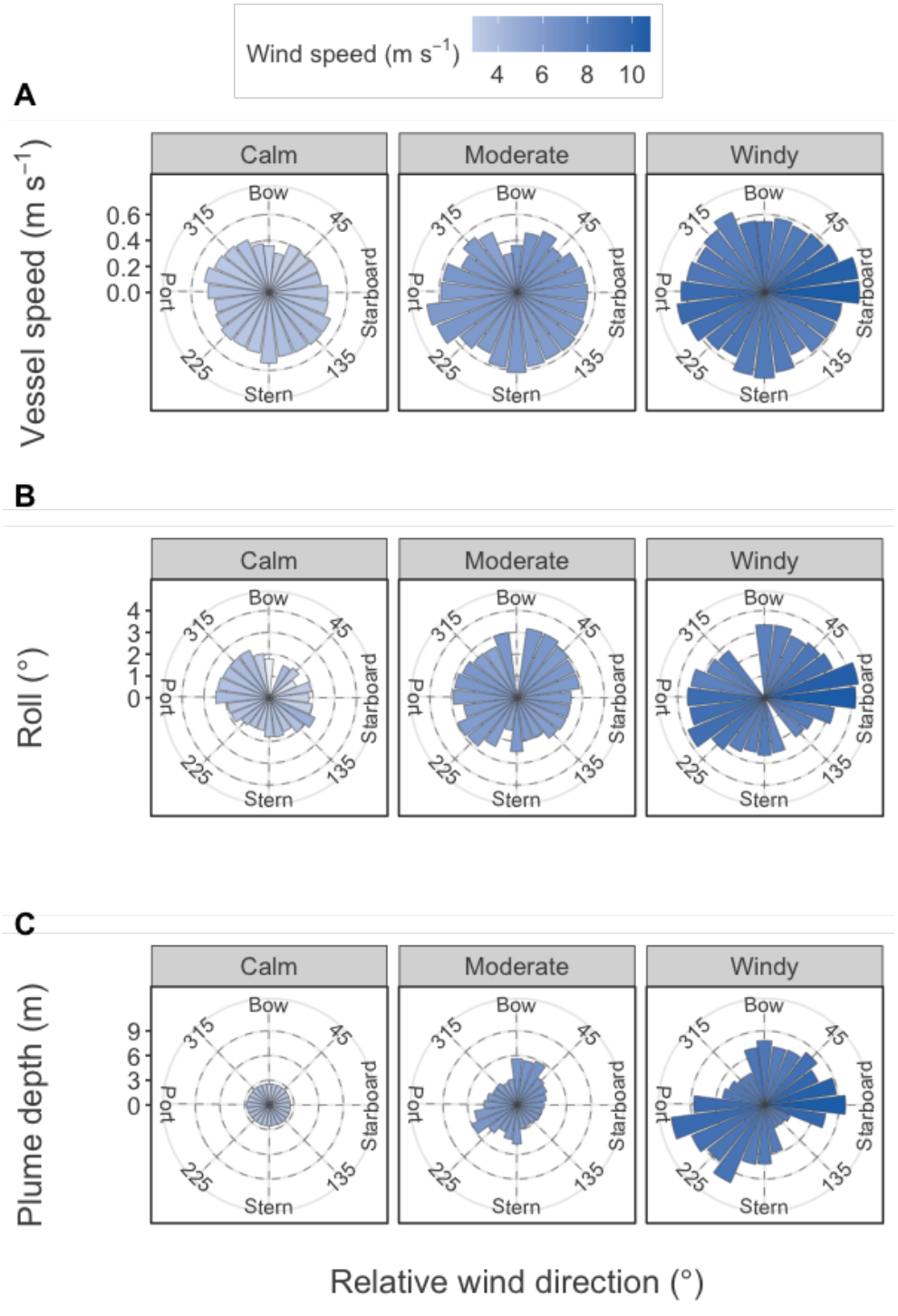


Figure 2.3.13: **Relative wind direction against A) vessel speed, B) roll, and C) bubble plume depth, grouped by wind speed category.** Relative wind direction shown as circular coordinates. Segments coloured by wind speed. Bow indicates a head wind, stern indicates a tail wind (wind coming from behind). Note: roll amplitudes were not recorded for some wind direction and speed combinations because roll was sampled at a lower resolution than the other variables shown, and these combinations were rarely encountered.

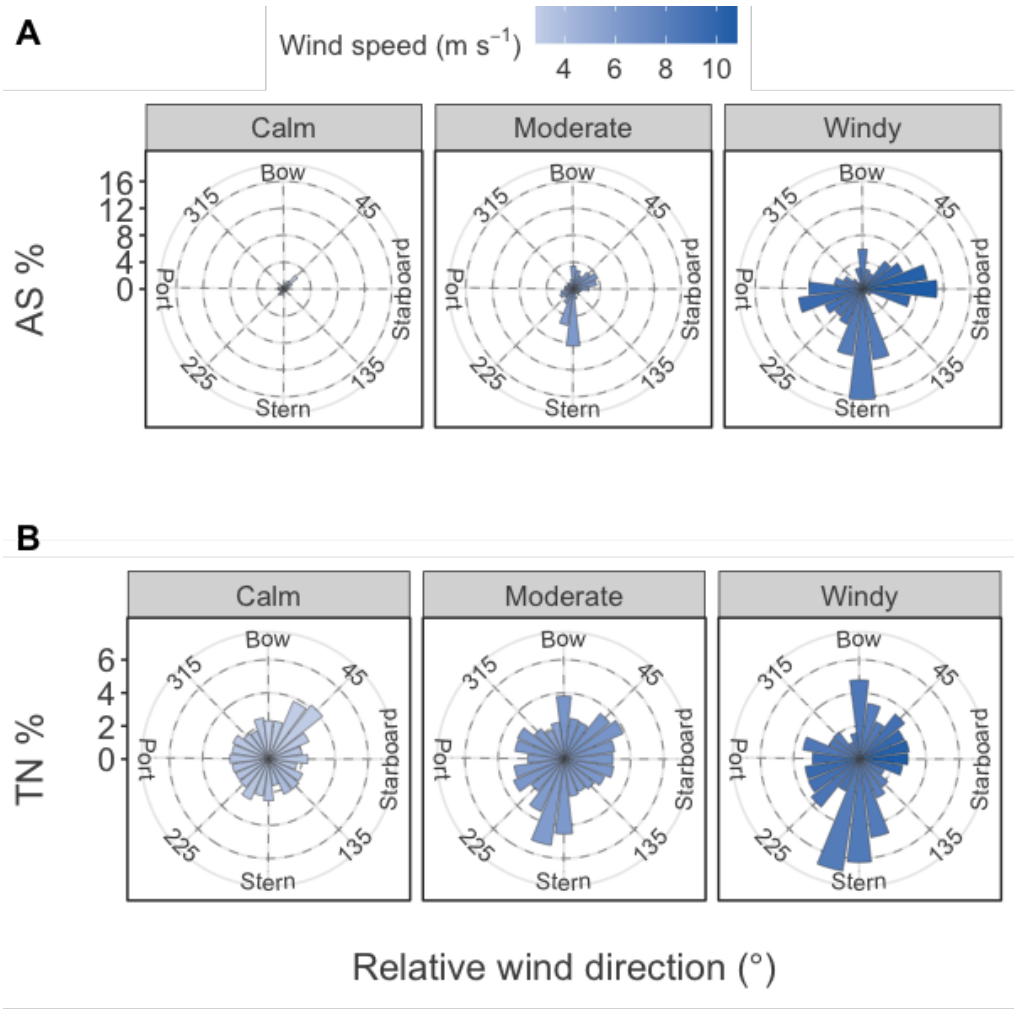


Figure 2.3.14: **Relative wind direction against rates of A) attenuation (AS %) and B) transient noise (TN %), by wind speed category.** Relative wind direction shown as circular coordinates. Segments coloured by wind speed. Bow indicates a head wind, stern indicates a tail wind (wind coming from behind).

#### 2.3.4.3 Effects of data degradation on along-track resolution

Windy weather had two compounding effects that reduced the along-track (horizontal) resolution of the data and coverage of transects. Firstly, faster transit speeds but a fixed ping rate meant greater distances between successive pings. Using average transect transit speeds, average along-track resolution with a ten-second ping interval ranged from $4.0\,\mathrm{m}$ during the calmest transect to $7.6\,\mathrm{m}$ during the windiest transect. Secondly, the proportion of pings identified as degraded and hence removed increased during windy weather. The proportion of pings removed ranged from $3\,\%$ in Transect 9 (average wind speed $5\,\mathrm{m\,s^{-1}}$) to $22\,\%$ in Transect 5 (average wind speed $12\,\mathrm{m\,s^{-1}}$). This meant that whilst some of the calmest

transects had coverage from more than 10,000 pings which were of good quality, the windiest transect had coverage from less than 7,000 pings, and this data showed signs of wind-related bias even after applying the cleaning filters. The combined effects resulted in an average 2.5-fold reduction in along-track spatial resolution since pings during the windiest transects were sampling on average every $10\,\mathrm{m}$, compared to every $4\,\mathrm{m}$ during the calmest transects. Note that this is an average estimate only, however, and the spatio-temporal resolution is likely to have been much more variable than during calm weather.

#### 2.3.4.4 Relationships between wind speed and the severity of data degradation

As wind speeds increased, not only did the incidence of data degradation increase, but the severity of its impact on backscatter measurements did as well. Mean backscattering strength of attenuated pings in the water column was $1.9\,\mathrm{dB}$ lower than in water column data that excluded the attenuated pings. Conversely, mean backscattering strength of water column pings affected by transient noise was $0.12\,\mathrm{dB}$ higher than data where pings affected by transient noise had been excluded. This suggests that the attenuation and transient noise filters generally removed pings that had lower and higher water column backscatter respectively than the filtered, cleaned data, as would be expected if the filters were effective. This is not trivial, since the filters were applied to data from the seabed but still had the expected effects on water column data.

Average backscatter of attenuated pings decreased as wind speeds increased in both the WC and SB layers (Figure 2.3.15), indicating that the severity of attenuation (i.e. its impact on reducing backscattering strengths) increased in windier weather. Average backscatter of transient noise affected pings increased marginally as wind speeds increased in both the WC and SB layers (Figure 2.3.15), indicating that the severity of transient noise also increased in windier weather, but the effect was smaller. During calm conditions, mean backscatter of attenuated data in the WC layer was $-66.8\,\mathrm{dB}$, whereas during windy conditions it decreased to $-70.2\,\mathrm{dB}$, thus the severity of attenuation increased by $3.4\,\mathrm{dB}$, representing more than a 2-fold increase. In contrast, the severity of transient noise increased in water column backscatter by only $1.00\,\mathrm{dB}$ between these wind speed categories. A similar pattern

was observed in the SB data; attenuation worsened by $2.3\,\mathrm{dB}$ but the severity of transient noise increased by only $0.67\,\mathrm{dB}$.

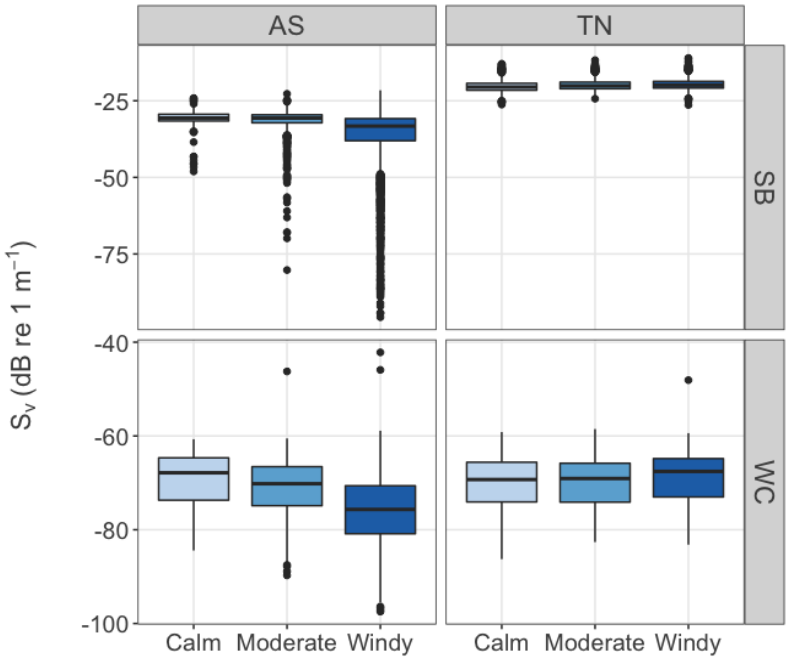


Figure 2.3.15: **Boxplots of mean backscatter of degraded data, by wind speed category.** Attenuated (AS) and transient noise affected (TN) backscatter in the seabed (SB) and water column (WC) layers shown.

The increase in severity of data degradation, particularly attenuation, with increasing wind speed is further exemplified by the relationships between water column Sv-differences and wind speed for attenuated pings, transient noise affected pings, and cleaned data. As wind speeds increased, the Sv-differences of AS marked pings decreased, indicating that attenuation increased in severity (linear model: $R^2_{adj} = 0.24$, gradient $= -0.86, p < 0.001$) (Figure 2.3.16, A). Similarly, as wind speeds increased, Sv-differences of TN marked pings in the water column layer increased, i.e. transient noise increased in severity (linear model: $R^2_{adj} = 0.12$, gradient $= 0.17, p < 0.001$) (Figure 2.3.16, B). This contrasts with water column Sv-differences of the cleaned data (AS and TN pings removed), which hardly varied with wind speed at all (linear model: $R^2_{adj} = 0.002$, gradient $= 0.02, p = 0.002$) (black points and black line in A and B of Figure 2.3.16). Wind speed had a greater effect on the severity of attenuation than it did on transient noise (linear model gradients: $|0.86|_{AS} > |0.17|_{TN}$).

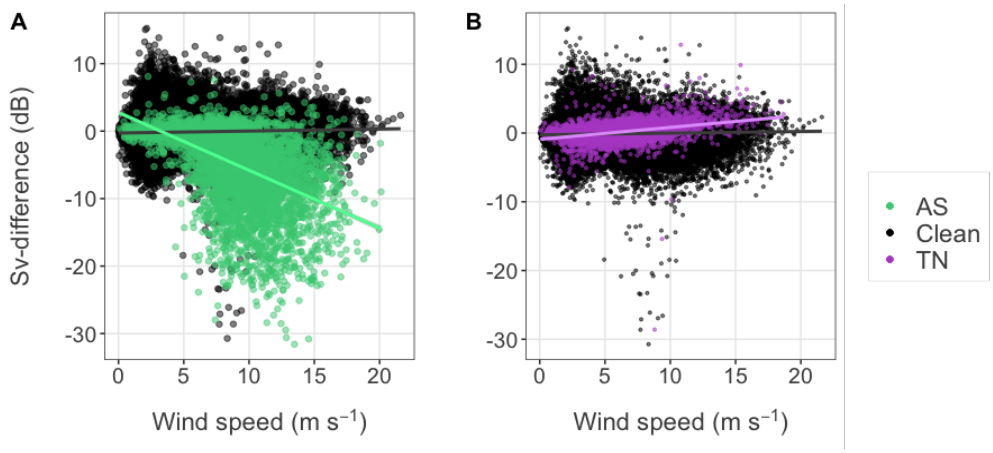


Figure 2.3.16: **Water column layer Sv-differences against wind speed, coloured by filter results.** A) Clean (black) and attenuated (AS, green) data; B) Clean (black) and transient noise affected (TN, purple) data. Linear models fitted to attenuated (green line), transient noise affected (purple line) and clean data (black lines), see text for details.

In calm weather, ping-paired Sv-differences of the SB and WC layers were more or less randomly distributed around zero in both layers. However as wind speeds, increased the relationship became more linear with a positive correlation between the two variables, particularly in the negative direction (Figure 2.3.17). Correlated deviations from zero are indicative of attenuation (negative direction) or transient noise (positive direction). Extension further into the third quadrant of the plot than the first quadrant in Figure 2.3.17 shows, in an alternative way, that within this particular dataset the effects of attenuation were more severe than those of transient noise.

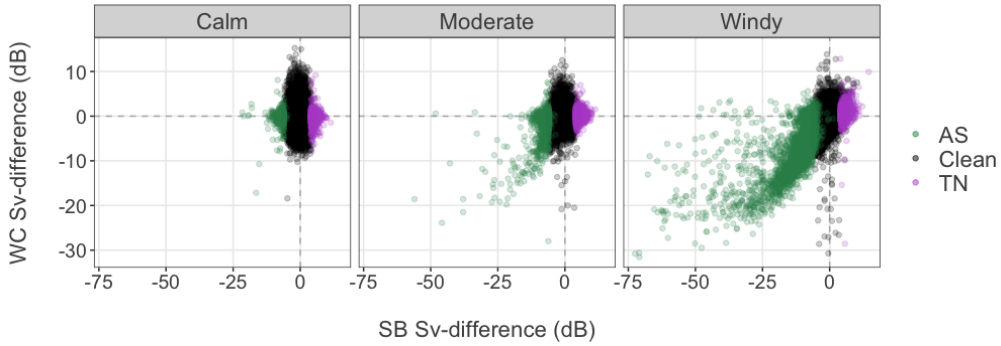


Figure 2.3.17: **Sv-differences of clean and degraded data in the seabed (SB) and water column (WC) layers, grouped by wind speed category.** Data affected by attenuation (AS) shown in green and transient noise (TN) shown in purple. Clean data shown in black. Horizontal nad vertical dashed grey lines indicate where values do not differ from median of neighbouring eight pings in WC and SB layers respectively.

Interestingly, there were two groups of datapoints with WC Sv-difference values below $-10\,\mathrm{dB}$. One group had a corresponding reduction in backscatter in the SB layer, and consequently was identified by the attenuation filters (bottom-left quadrant in Figure 2.3.17, green points). The other group had a marked decrease in backscatter in the WC layer but no corresponding reduction in backscatter in the SB layer, and therefore was not identified by the attenuation filters (black points close to vertical dashed line in Figure 2.3.17). Water column backscattering strengths of these pings ranged from $-80\,\mathrm{dB}$ to $-59\,\mathrm{dB}$ which falls within the range of water column backscatter for all clean pings ($-87\,\mathrm{dB}$ to $-31\,\mathrm{dB}$). This tells us that the water column was not empty of scatterers, and thin regions of empty water contrasted against patchy biotic scatterers did not produce these extreme water column Sv-differences. These outlying datapoints all occurred during daytime when backscattering strengths at the position of the WC layer were generally high due to DVM of the main SSL. It is therefore possible that natural biotic patchiness in the SSL was responsible for the apparent sudden decreases in backscatter. Although plausible, further exploration of the data and echograms is required to establish whether this scenario explains the observed pattern.

#### 2.3.4.5 Visual impact of data cleaning on echograms

Echograms showing 24-hour periods during Transects 1 and 5 demonstrate the effect of applying the data cleaning filters on visual representation of the backscatter data (Figure 2.3.18). Winds were fairly calm during Transect 1 with average speeds of $4.8\,\mathrm{m\,s^{-1}}$. Only $4\,\%$ of pings were identified as degraded by either attenuation or transient noise during Transect 1. In contrast, Transect 5 was very windy with average speeds of $12.1\,\mathrm{m\,s^{-1}}$ and consequently a much higher proportion ($22\,\%$) of pings were identified as degraded by the filters. Barely any visual difference can be seen between echograms of cleaned and unfiltered Transect 1 data because rates of attenuation and transient noise were very low during this time (Figure 2.3.18, A & B).

Transient noise is difficult to see in the echograms during daytime because the upper part of the water column was dominated by echoes from the subunit and bubble layer, and the lower part of the water column contained relatively strong, patchy echoes from biota in the

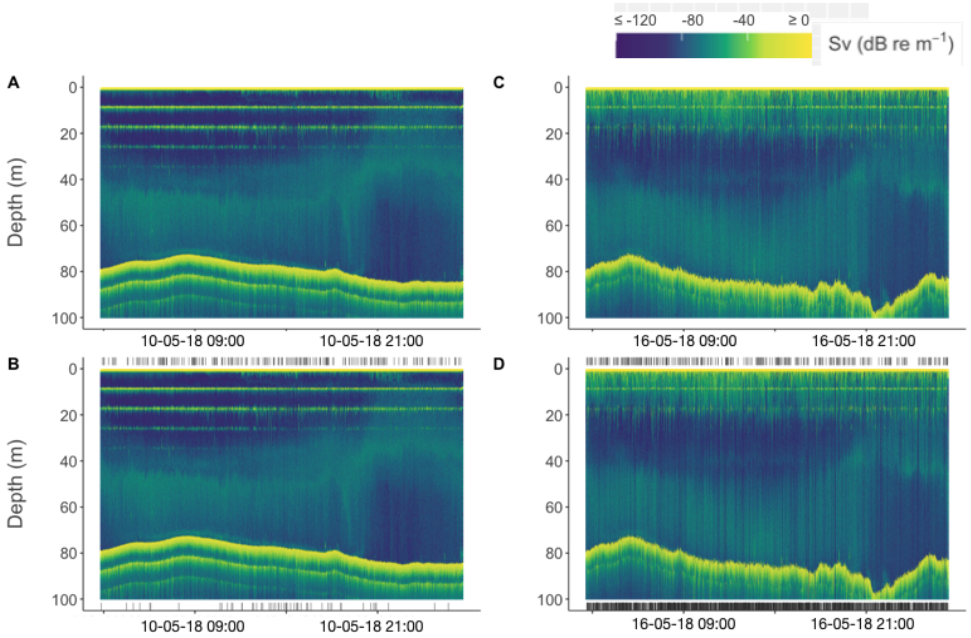


Figure 2.3.18: **Examples of unfiltered and clean data from two contrasting transects.** Clean and unfiltered 70 kHz backscatter data from Transect 1 (A, B) and Transect 5 (C, D). Lower and upper rug plots in B) and D) show pings identified as attenuated or affected by transient noise respectively. Stronger backscatter ($S_v$) in yellow, weaker in dark blue.

SSL. However, at night when the SSL moved up towards the surface, instances of suspected transient noise are easier to see. For example, not long after 21:00 on 10$^{th}$ May 2018 a vertical stripe of strong backscatter can be seen. This ping was not identified by the LCTN filter, presumably because either any increase in SB backscatter, if it occurred, was below the threshold used by the filter (Figure 2.3.18, A & B). Visual scrutiny of the echograms suggests that although the filters removed most of the apparent degraded data, some instances of both transient noise and attenuation remained in the cleaned Transect 5 data which can be seen as vertical striping through the bubble layer, main SSL and seabed in Figure 2.3.18 (C). Although the appearance of Transect 5 improved dramatically after data cleaning, it is evident that the data quality is still poorer than both clean and unfiltered data collected during Transect 1.

Poor delineation of acoustic features is another symptom of poor data quality associated with inclement weather. In contrast to Transect 1, the seabed echo in Transect 5 appears jagged (Figure 2.3.18, B & D). Other acoustic features also appear more jagged, such as the bubble layer, the edges of the SSL, and subunit echoes; however changes to the boundaries

of these features are harder to discern visually. This jagged appearance is the result of differences in range which could have been caused by either heave (the vessel moving up and down in the waves), which would have a constant effect with depth, or pitch, roll or yaw changing the angle of the acoustic beam, which would have a worsening impact with depth. It could also have resulted from changes to the sound speed due to the entrainment of bubbles below the surface, since bubbles alter the compressibility of the acoustic medium (Medwin, 1976). It is also possible that the jagged seabed echo was caused by jerkier motion during faster transit speeds since the subunit acts as a tug to pull the float along with each passing wave (Manley and Willcox, 2010). Meyer-Gutbrod et al. (2012) described imprecise depth estimates resulting in a jagged seabed appearance which were attributed to a jerking motion between the acoustic transducers, which were located on a tow body attached to the subunit, and the subunit.

#### 2.3.4.6 Effects of the filters on backscattering strength

Removing attenuated pings increased the mean backscattering strength of the water column layer by $0.044\,\mathrm{dB}$, and removing pings affected by transient noise decreased mean backscatter by $0.003\,\mathrm{dB}$. The removal of both kinds of degraded data increased mean backscatter by $0.042\,\mathrm{dB}$ over the course of the mission. This suggests that attenuation had the dominant impact on water column backscatter and introduced the most bias, but note that the relative dominance of attenuation or transient noise may vary according to depth because transient noise is amplified by TVG and hence is range-dependent, however attenuation can be independent of range (Ryan et al., 2015).

There was barely any difference to overall WC backscattering strengths between cleaned data collected during calm and moderate wind conditions, however there was a slight observable increase in cleaned backscatter data collected during windy weather (Figure 2.3.19, A, bottom). This might indicate that much of the weather-related bias had been removed by the filters at lower wind speeds, but some remained at higher wind speeds. Cleaned seabed data also showed a slight increase in backscattering strength of data collected during windy weather (Figure 2.3.19, A, top). This could indicate that some

transient noise remains in data collected during windy weather that has not been identified by the LCTN filter. There was a slightly larger range of Sv-differences of cleaned seabed data during windy weather as compared to calm or moderate wind conditions, which might suggest that some transient noise remained in data collected during windy weather, however there was no observable corresponding pattern in water column Sv-differences (Figure 2.3.19, B). Judging the efficacy of filters on removing bias using simple summary statistics such as average backscattering strengths is problematic, however, particularly when the overall effect on mean backscatter and Sv-difference is small compared to the variance. It is the effects on target backscatter that are most important to consider.

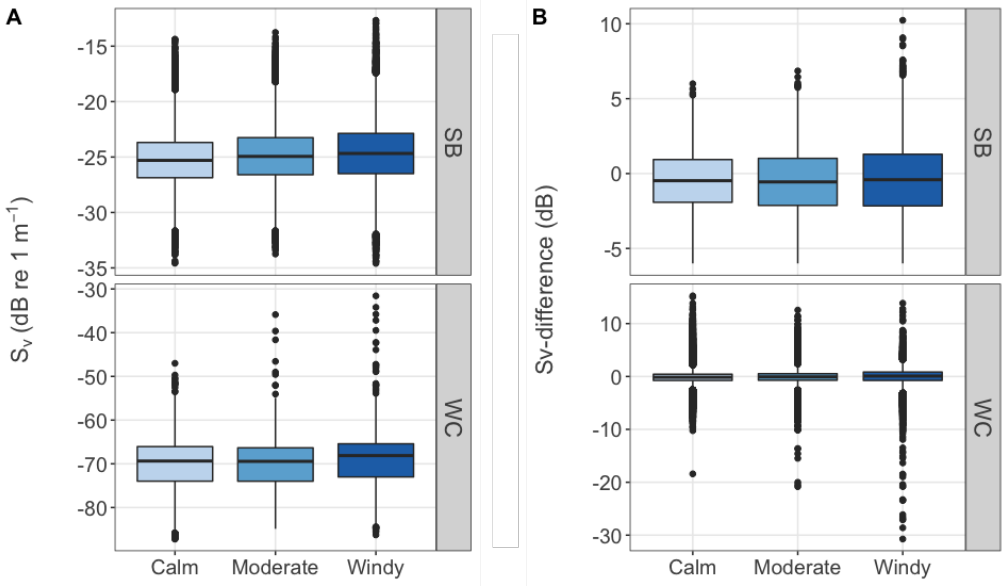


Figure 2.3.19: **Boxplots of A) backscatter and B) Sv-differences of the cleaned data in the SB and WC layers, by wind speed category.**

To assess the component effects of each filter, their effect on mean backscattering strengths was plotted for $1\,\mathrm{m\,s^{-1}}$ wind speed intervals (Figure 2.3.20). The attenuation filters had the largest impact on mean water column backscatter during periods when wind speeds exceeded $10\,\mathrm{m\,s^{-1}}$, and the SRAS filter consistently had a greater impact on backscattering strengths than the LCAS. This is unsurprising given that the SRAS filter was applied first and was designed to detect the most severely impacted pings. Despite the apparent efficacy of the SRAS filter, the LCAS filter still removed data that would have caused a negative bias in backscatter, indicating that it removed attenuated pings that were not detected by the SRAS

filter (Figure 2.3.20, brown points). When wind speeds were their highest, the combination of these filters removed data that would have led to a decrease in average backscattering strength of more than a decibel (Figure 2.3.20, green points in bottom panel). A similar pattern was observed in seabed backscatter data (Figure 2.3.20, brown, yellow and green points in top panel).

The transient noise filter reduced mean water column backscattering strengths of data collected during all weather conditions. The effect was negligible when wind speeds were below $10\,\mathrm{m\,s^{-1}}$ but increased during periods when wind speeds exceeded $10\,\mathrm{m\,s^{-1}}$ (Figure 2.3.20, purple points in bottom panel). The effect on seabed backscatter data was similar to that for water column data, although more pronounced (Figure 2.3.20, purple points in top panel).

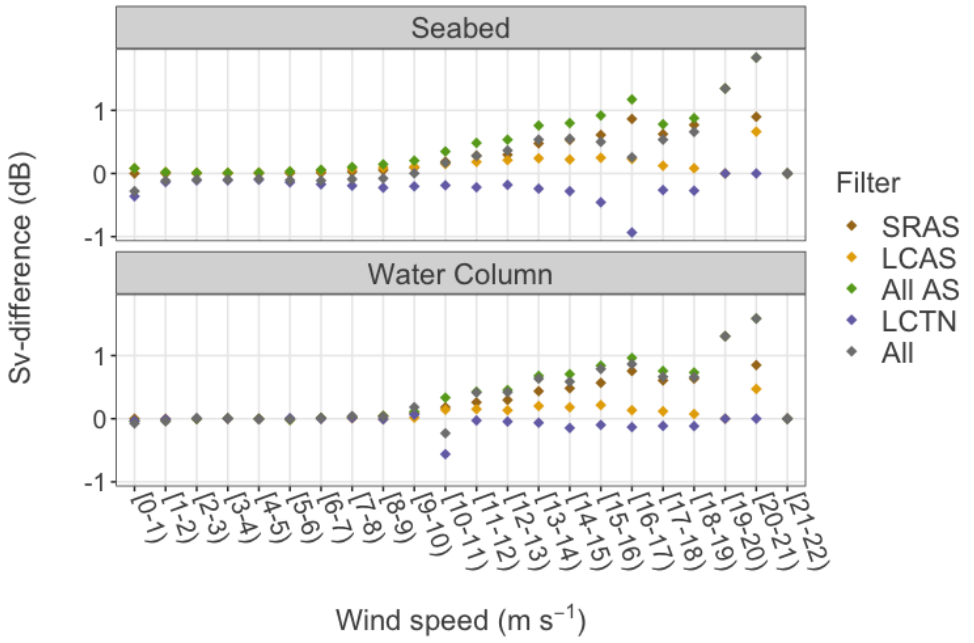


Figure 2.3.20: **Effect of data cleaning filters on Sv-difference of the SB and WC layers, by wind speed.** All AS = both SRAS and LCAS. All = SRAS, LCAS and LCTN.

### 2.3.5 Two-layer comparisons: increased bias in data from windy periods

Results of applying the two-layer comparison technique successively throughout the data cleaning procedure provided support that the filters had indeed reduced bias in the dataset, and

that windier weather had introduced increasing bias into the data (Figure 2.3.21). The removal of pings identified by the filters as degraded reduced the two-layer comparison correlation coefficients of data collected during windy weather by a third, bringing them closer to baseline levels ($\rho \approx 0$) observed during calm weather (Figure 2.3.21, C). Correlations were not significant before or after applying any filter for data collected when wind speeds were calm, between $1$ to $5\,\mathrm{m\,s^{-1}}$. This can be explained by the fact that the data quality was good during these periods and thus there was no relationship between fluctuations in seabed and water column backscatter; there was almost no bias and hence no correlation. Correlation coefficients for each wind speed interval can be found in Appendix D.

The attenuation filters reduced coefficients for all wind speeds where correlations were significant ($p < 0.01$) (Figure 2.3.21, A). The SRAS filter had a greater impact on reducing correlation coefficients than the LCAS, and its impact generally increased with higher wind speeds. The attenuation filters reduced the two-layer comparison correlation coefficients of the whole dataset by $0.041$, from $\rho = 0.144$ (unfiltered, $p < 0.001$) to $\rho = 0.103$ (all AS marked pings removed, $p < 0.001$). This suggests that whilst these filters reduced the amount of bias in the dataset, a considerable proportion remained even after data cleaning.

Application of the LCTN filter had little impact on two-layer comparison correlation coefficients of data collected during windy weather. Although it did reduce coefficients for some wind speed intervals, the difference it made was barely perceptible in plots showing its effects by wind speed (Figure 2.3.21, B). Consequently, this filter did not contribute much to the overall reduction in bias. It reduced correlations by $0.004$ over the whole mission, from $\rho = 0.144$ (unfiltered, $p < 0.001$) to $\rho = 0.140$ (TN pings removed, $p < 0.001$), a comparatively small change compared to the impact that the attenuation filters had which were an order of magnitude larger.

Overall, the combined effect of the filters, applied in order, reduced the two-layer comparison correlation coefficient of the whole mission by $0.047$, from $\rho = 0.144$ (unfiltered, $p < 0.001$) to $\rho = 0.097$ (both AS and TN pings removed, $p < 0.001$). This constitutes a reduction of almost a third.

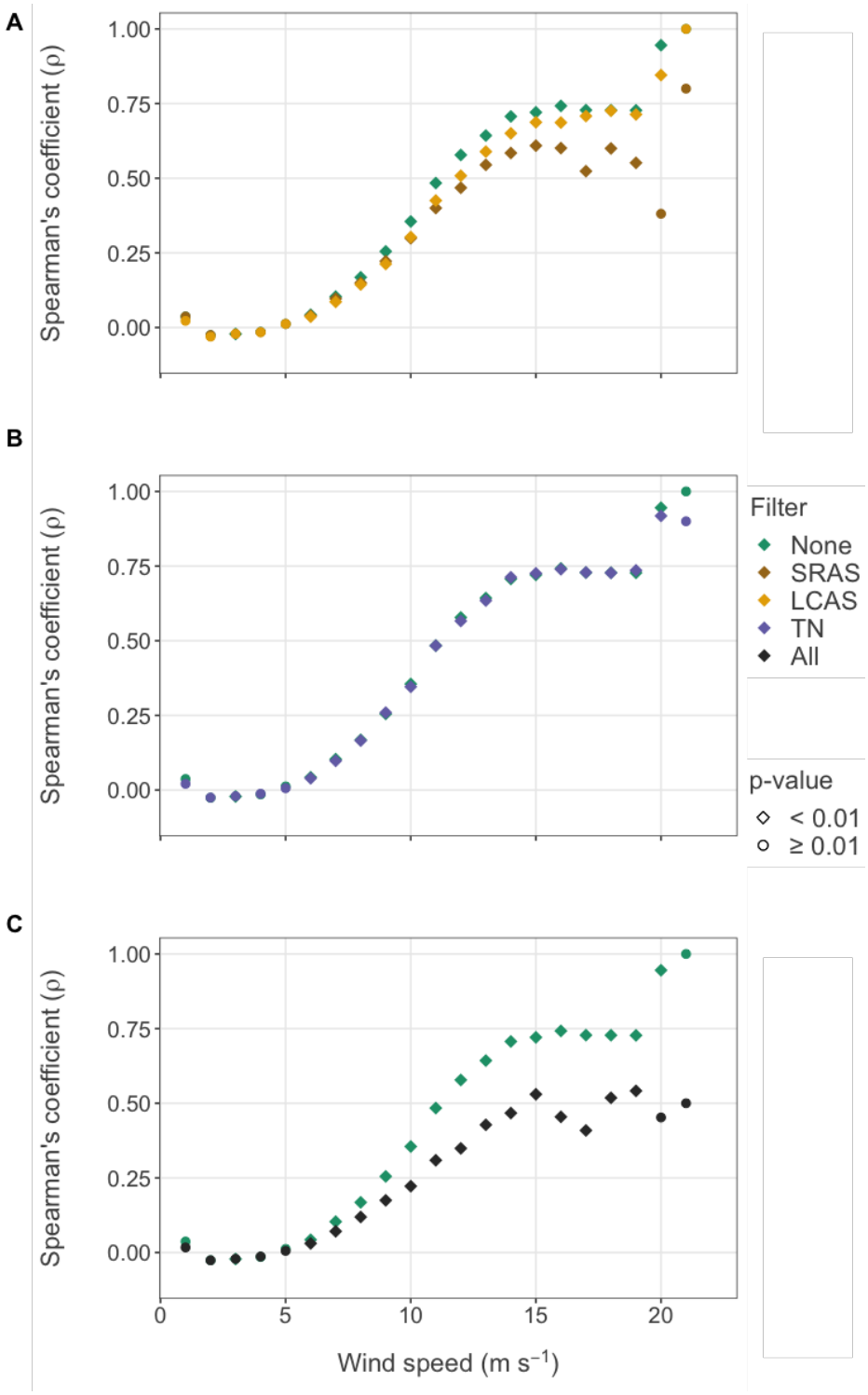


Figure 2.3.21: **Effects of data cleaning filters on two-layer comparison correlation coefficients, by wind speed.** Spearman's rank correlation coefficients between Seabed and Water Column layer local Sv-differences after application of A) Seabed Reference Attenuated Signal (SRAS) and Local Convolution Attenuated Signal (LCAS) filters B) Local Convolution Transient Noise (LCTN) filter and C) all filters. Statistical significance indicated by diamond ($p < 0.01$) or circle ($p \geq 0.01$) shape. The LCTN filter had barely any effect on correlation coefficients; purple points in B) generally overlap the green points.

### 2.3.6 False positive and false negative detections

To derive an estimate of false positive detections the percentages of detections where fluctuations in the seabed and water column backscatter occurred in opposing directions were calculated (Table 2.4). For example, cases where seabed backscatter increases, but water column backscatter decreases, could indicate that any transient noise detection was a false positive. However, false positive estimates using this method are only very approximate. Fluctuations in water column backscatter are common, often caused by patchy biota in SSLs, and could have counteracted the influence of attenuation or transient noise, resulting in overestimating the number of false positives. Conversely, fluctuations between seabed and water column backscatter could have occurred in the same direction and similar magnitude by chance; correlations are not proof of data degradation and the number of false positives may have been underestimated. Nevertheless, these figures provide a rough proxy for false positives.

The estimated number of false positive detections decreased as wind speed increased, suggesting that the proportion of true detections of degraded data by the filters increased during windy weather. According to this metric, the attenuation filters had a better success rate than the transient noise filter in all weather conditions, possibly because attenuation could be more easily discerned by the filters as it had a more severe impact on backscatter, i.e. it caused a greater contrast to background (seabed) backscatter.

Overall, the attenuation filters were estimated to have removed just over $0.5\,\%$ of data unnecessarily, with the filter having an average false positive rate of $18\,\%$ over the course of the mission. The transient noise filter was estimated to have removed approximately $1.2\,\%$ of data unnecessarily, and had an average false positive rate of $44\,\%$ over the course of the mission which is more than twice as much as the attenuation filters. Even in calm weather, there was a baseline of false positive detections estimated by this method which was higher for the transient noise filter than the attenuation filters (Table 2.4). From these results, and the negligible impact that the transient noise filter appeared to have on bias and water column backscattering strengths, I conclude that the transient noise filter was not very effective on this dataset.

Table 2.4: **Estimated proportions of false positive detections made by the attenuation and transient noise filters, grouped by wind speed category.** AS denotes detections made by the attenuation filters, TN denotes detections made by the transient noise filter.

| | **AS (%)** | **TN (%)** |
|---|---|---|
| Calm | 42 | 57 |
| Moderate | 31 | 47 |
| Windy | 10 | 28 |

False negatives are also likely to have occurred. Two-layer comparison correlation coefficients of cleaned data were still higher than baseline levels found during calm weather, suggesting a failure of the filters to detect some instances of degraded data and bias remaining in the dataset (Figure 2.3.21). The tendency towards a positive correlation between Sv-differences of cleaned data in the SB and WC layers with increasing wind speed can be seen best in Figure 2.3.22. This figure suggests that there may be instances of both transient noise and attenuation remaining in the cleaned dataset during windy periods. However, whether these have a substantial impact on water column or target backscattering is open to question.

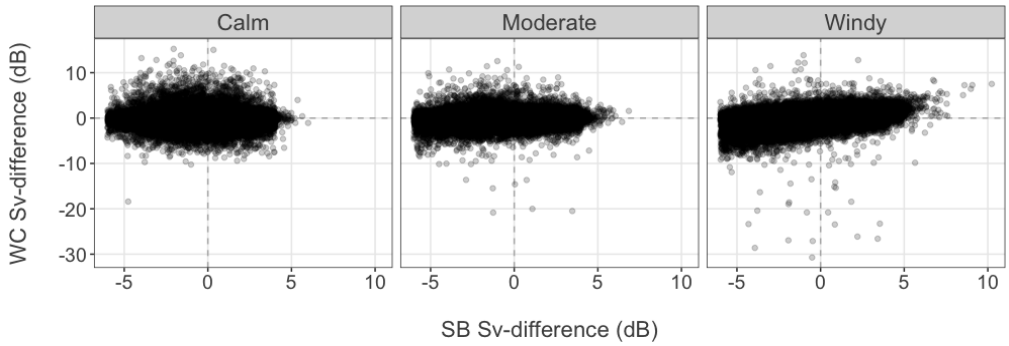


Figure 2.3.22: **Sv-differences of filtered (cleaned) data in the seabed (SB) and water column (WC) layers, grouped by wind speed category.** Dashed grey lines indicate where values do not differ from median of neighbouring eight pings in WC (horizontal) and SB (vertical) layers.

## 2.4 Discussion

### 2.4.1 Effects of the wind on acoustic data quality

*Lyra* successfully demonstrated that the Wave Glider has the potential to collect good quality acoustic data. A small proportion of the acoustic data collected by *Lyra* was degraded by attenuation and transient noise, however a relatively large proportion of the acoustic data was degraded due to masking caused by the subunit. Neither background noise nor impulse noise was visually apparent in echograms. Overall, less than $6\,\%$ of the data was identified as affected by transient noise or attenuation; a proportion similar to that found by De Robertis et al. (2019) ($5.5\,\%$) using a Saildrone ASV to collect acoustic data under similar weather conditions (mean wind speed during the Saildrone survey was $5.9 \pm 2.8\,\mathrm{m\,s^{-1}}$; mean wind speed during this Wave Glider survey was $6.0 \pm 2.3\,\mathrm{m\,s^{-1}}$; both surveys collected $95\,\%$ of data during periods when wind speeds were less than $11\,\mathrm{m\,s^{-1}}$). All three forms of data degradation worsened when wind speeds increased.

Attenuation imparted more bias than transient noise, affecting more pings and having a greater impact on backscatter in the water column. Rates and severity of attenuation also increased more rapidly than transient noise as wind speeds increased. Windier weather led to the formation and deepening of bubble plumes. Denser and deeper plumes which formed during periods of windy weather resulted in stronger scattering by bubbles under the transducers, increasing attenuation by bubble-shadowing. These layers persisted for some time after wind speeds decreased, introducing a lag between changes in wind speed and changes in acoustic data quality. Windier weather also led to increased vessel motion; both forward transit speed and roll. Both bubble-shadowing and transducer motion could explain the increase in rate and severity of attenuation during windier weather.

The Wave Glider demonstrated good track-keeping ability regardless of changes in the weather, staying within $115\,\mathrm{m}$ of the transect line for $90\,\%$ of the mission. This is an important consideration for acoustic surveys as mobile platforms are often required to sample along pre-defined transects. This ability to keep to track and travel forwards regardless of the relative wind and surface wave directions gives it an advantage over some wind-powered

ASVs, such as the Saildrone and Sailbuoy, since they tack back and forth in order to sail upwind (De Robertis et al., 2021; Offshore Sensing - Sailbuoy, 2023). Another advantage of the Wave Glider is that, whilst wind-powered unmanned sailing vessels will drift if the wind dies, the Wave Glider will continue moving forwards so long as there are surface waves. Aside from the degradation of near-surface data caused by the subunit, the Wave Glider proved a suitable platform for the collection of acoustic data, obtaining excellent quality acoustic data during calm weather conditions.

Subunit interference persisted throughout the mission and severely compromised data in the upper part of the water column. Stronger winds led to the increased fragmentation and vertical stretching of the subunit echoes, making it difficult to find an appropriate method to remove affected data that was reliable under a range of wind speed conditions. The problem of subunit interference is specific to the way that acoustic transducers are attached to the Wave Glider's float. Swart et al. (2016) and Pedersen et al. (2019), who also integrated transducers aft of the surface floats of their Wave Gliders, both reported similar issues with subunit interference. However, in the study by Swart et al. (2016), the majority of subunit echoes were weaker than target backscatter: $93\,\%$ of echoes were weaker than $-65\,\mathrm{dB}$ at $38\,\mathrm{kHz}$. *Lyra* suffered much worse subunit interference in the $70\,\mathrm{kHz}$ data: the average subunit echo was $>-20\,\mathrm{dB}$, and the first two phantom echoes were on average above $-60\,\mathrm{dB}$ and $-40\,\mathrm{dB}$ respectively - much stronger than typical backscattering strengths of the SSL which were estimated to range from $-90$ to $-75\,\mathrm{dB}$ in this region of the water column.

Maximum bubble plume depths were concordant with those reported by Trevorrow (2003) who made measurements using an inverted echosounder operating at $200\,\mathrm{kHz}$ on a mooring (i.e. in the absence of bubble sweep-down) and employed a $50\,\mathrm{dB}$ threshold to separate bubble and biotic backscatter. During *Lyra's* deployment, plumes reached depths of $26\,\mathrm{m}$ that were associated with periods when wind speeds exceeded $10\,\mathrm{m\,s^{-1}}$; Trevorrow (2003) reported maximum plume depths of $25\,\mathrm{m}$ associated with wind speeds of up to $20\,\mathrm{m\,s^{-1}}$. The incidence of bubble layer presence rose sharply when wind speeds exceeded $2.5\,\mathrm{m\,s^{-1}}$, concordant with observations that sea-surface waves begin to break at average wind speeds of $3\,\mathrm{m\,s^{-1}}$, producing bubbles near the surface which can be detected acoustically at typical fisheries acoustics frequencies (Thorpe, 1992; Crawford and Farmer, 1987; Dahl and Jessup,

1995; Dahl, 2003). These similarities suggest that the bubbles beneath the surface could have been primarily induced by ocean-atmosphere interactions rather than by bubble sweep-down. This is supported by the analysis in Swart et al. (2016) which showed that wind direction relative to the Wave Glider did not influence the depth of the bubble layer underneath, which might have been expected if vessel hydrodynamics led to bubble sweep-down. Independent measurements of near-surface bubbles, such as those from an inverted echosounder on a mooring, would be necessary to infer the extent to which bubble sweep-down from the Wave Glider contributes to the bubble plumes below the transducer, if at all.

Acoustic data collected by the Wave Glider *Lyra* suffered from attenuation associated with windy weather and near-surface bubbles in a similar, non-linear way to data collected by ships and other ASVs (Shabangu et al., 2014; De Robertis et al., 2019; Delacroix et al., 2016). The incidence of attenuation was negligible below wind speeds of $5\,\mathrm{m\,s^{-1}}$, affecting less than $1\,\%$ of data, and showed only a weak correlation with wind speed. But the incidence of attenuation increased much more rapidly above wind speeds of $7.5\,\mathrm{m\,s^{-1}}$ - by a factor of six for wind speeds of $10\,\mathrm{m\,s^{-1}}$ - and affected as much as $27\,\%$ of data during periods where wind speeds were in excess of $17\,\mathrm{m\,s^{-1}}$. This was mirrored by the relationship between attenuation and the bubble layer. Both the depth of plumes and strength of bubble backscatter increased sharply as wind speeds rose above $7.5\,\mathrm{m\,s^{-1}}$.

De Robertis et al. (2019) described a very similar non-linear relationship between wind speeds and attenuation, whereby there was comparatively little attenuation when wind speeds were below $5\,\mathrm{m\,s^{-1}}$, but above this the rate of attenuation doubled for every $5\,\mathrm{m\,s^{-1}}$ increase in wind speed. De Robertis et al. (2019) noted that when wind speeds rose above $8\,\mathrm{m\,s^{-1}}$, attenuation due to near-surface bubbles affected almost $22\,\%$ of pings during one of their Saildrone deployments. At wind speeds in excess of $10\,\mathrm{m\,s^{-1}}$, the severity of attenuation increased rapidly. In a study comparing the effects of bubble-attenuation on acoustic data collected by hull-mounted and a deeper keel-mounted transducer on a ship, Shabangu et al. (2014) observed that backscattering ratios between the transducers increased as wind speed increased in a similar non-linear fashion. Ratios did not differ much for wind speeds under $10\,\mathrm{m\,s^{-1}}$, but above this speed the ratio began to change more rapidly, and above wind speeds of $15\,\mathrm{m\,s^{-1}}$ a correction factor of $2.3$ was necessary for backscattering strengths to

be comparable between the two transducers. In an acoustic Wave Glider study, Swart et al. (2016) found that bubble layer depth and total backscatter within this layer increased rapidly as wind speeds rose above 12 knots (approximately $6\,\mathrm{m\,s^{-1}}$), however the effect that this had on attenuation of the acoustic signal was not explored.

Transducer depth is a major factor contributing to the impact of near-surface bubble masking and attenuation of acoustic data collected by surface vehicles. A common solution put forward to mitigate the impact is to position the transducer deeper in the water column (Shabangu et al., 2014; Ona and Traynor, 1990). Backscattering strengths from bubble plumes decrease exponentially from the surface (Trevorrow, 2003)), therefore positioning transducers deeper avoids regions where the strongest bubble backscatter can mask and attenuate signal or can even avoid the bubble layer entirely. Depth of the keel-mounted transducers on the Saildrone was not explicitly stated in De Robertis et al. (2019), however it is inferred from Mordy et al. (2017) to have been approximately $2\,\mathrm{m}$ below the surface, $1.5\,\mathrm{m}$ deeper than *Lyra's* transducers. It is therefore reassuring that despite *Lyra's* transducers being particularly close to the surface, good quality acoustic data could be collected throughout much of the deployment.

Coherence between bubble plume depth and bubble backscatter reduced following an extended period of persistently strong winds (a stormy period). This could be due to a looser coupling between wind speed and the expression of sea surface waves during the period of changeable weather that followed the stormy period. The mechanisms through which wind speed translates to changes in sea surface wave expression are dependent on fetch, duration of winds, variability of wind direction, and existing sea state, amongst many other factors. Therefore, surface wave expression is affected by factors that can build up over time, and instantaneous wind speeds may be associated with a variety of sea surface waves. This in turn means that distributions of bubbles below the surface are also in part dependent on these factors and not solely on the instantaneous wind speed. Past wind activity was shown to influence the relationship between bubble plume depth and wind speed, and also the relationships between data degradation rates and wind speed, with average wind speeds from the previous half an hour to an hour slightly more correlated than instantaneous wind speeds. However, bubble plume depth and roll were perhaps better indicators of average data quality

than wind speed, since they are a more direct proxy for wave conditions at the sea surface.

It was not possible to determine whether bubble-shadowing or transducer motion was the dominant cause of attenuation. There was a high degree of multicollinearity between bubble layer metrics, roll, and wind speed, which confounded analyses, and no independent validation data. In some datasets, the Dunford correction can be used to estimate and correct for transducer motion (Dunford, 2005), however this correction factor could not be reliably determined because roll sampling frequency ($1\,\mathrm{Hz}$) was not known to be sufficiently fast to preclude aliasing. I am thus prevented from making targeted recommendations to reduce the impact of attenuation, however it is likely that both transducer motion and bubble-shadowing are responsible for attenuation of *Lyra's* acoustic data, and repositioning the acoustic transducers (necessary to reduce subunit interference) may affect the balance between these two sources of atttenuation.

Forward propulsion of the Wave Glider relies on differential motion between the surface float and subunit (Smith et al., 2011; Daniel et al., 2011). This differential is dependent on wave height, which increases in higher sea states. Therefore, Wave Glider transit speeds are inherently linked to wind speed due to the formation of waves at the sea surface by wind stress. Although there was a linear relationship between 9-hour average vessel speeds and wind speeds, this relationship should not be extrapolated to higher wind speeds; Wave Glider speed is fundamentally limited by the ratio between float length and wave height (Kessel, 2019). The maximum achievable speed through water by the SV3 Wave Glider is estimated to be $1.54\,\mathrm{m\,s^{-1}}$ (Liquid Robotics, Inc., 2015), and is not expected to increase further with wind and wave conditions above sea state 4 which is associated with wind speeds of up to $10\,\mathrm{m\,s^{-1}}$ (Kessel, 2019; Met Office, 2023). In the minute-averaged data, the increase in vessel speed levelled off above wind speeds of approximately $10\,\mathrm{m\,s^{-1}}$. The fastest transit speeds of the Wave Glider may therefore be associated with a range of poor acoustic data quality scenarios since higher sea states are expected to increase the impacts of attenuation and transient noise, as well as ambient noise levels, despite the vessel's speed remaining fairly constant.

This chapter focused primarily on the effects of wind speed on acoustic data quality. However, relative wind direction, i.e. the orientation of the vessel to the wind, as well as the orientation of the vessel to surface waves, are known to impact the performance of ASVs and the quality of acoustic data they collect (Jech et al., 2021). Following winds have often been associated with the lower impacts of attenuation in acoustic data collected by ships, in contrast to head winds which typically have larger impacts (Dalen and Løvik, 1981; Shabangu et al., 2014; Saavedra et al., 2012). However, the influence of relative wind direction on attenuation is platform-dependent and there is no simple rule to determine the optimal orientation of a vessel to the wind or waves to minimise the effects of attenuation. For example, the RRS Discovery is said to suffer worse attenuation when oriented beam-on to oncoming wavefronts, but this is the opposite in the case of the similarly-sized RRS James Clark Ross (S. Fielding personal comment, December 2021). Seabed backscatter measurements taken from a Saildrone were reportedly most affected by attenuation when the vessel was on a beam reach (perpendicular to the wind), thought to be related to vessel instability causing transducer motion, and least affected on a broad reach (sailing in a similar direction to the wind) (Jech et al., 2021). In extreme cases, instability associated with a platform's orientation to the wind and waves can lead to capsize events, for example Grare et al. (2021) reported several capsize events of a SV2 Wave Glider associated with travel in cross-winds. There were a few instances in *Lyra's* deployment where minute-averaged maximum roll amplitudes exceeded $20°$. These instances occurred when wind speeds were in excess of $10\,\mathrm{m\,s^{-1}}$. In general, maximum roll amplitudes were more moderate, ranging between $5$ and $8°$ and there was no indication that *Lyra* suffered a capsize event.

It is reasonable to expect that Wave Glider transit speeds are affected by relative wind direction. Swart et al. (2016) reported faster vessel speed during stronger winds ($15$ to $22$ knots, i.e. 'windy' wind speed category in this study) when the wind came from the starboard quarter direction, however, at lower wind speeds ($< 15$ knots, i.e. wind speed categories 'calm' and 'moderate' in this study) transit speeds were faster when the wind came from the port side. This study found little evidence of a relationship between vessel speed and relative wind direction, however a full statistical analysis to account for the effect of wind speed on vessel speed was not conducted.

Relative wind direction did appear to influence rates of data degradation by attenuation and transient noise. During this deployment, winds were strongest when the Wave Glider was oriented perpendicular to the wind, particularly when wind came from the starboard side. Roll amplitude and bubble depths were greatest under cross-wind conditions, but this could be coincidental and related to the fact that wind speeds were highest during periods when the vessel was oriented perpendicular to the wind. However, it was following winds that were associated with the highest rates of attenuation and transient noise. This makes some intuitive sense: the transducers were located aft of the stern of the float, and could therefore be more susceptible to rotational instabilities, crashing waves, or bubbles being pushed under the transducer when the wind comes from behind the vessel. The overriding influence of wind speed on data degradation made it challenging to identify likely mechanisms through which following winds led to increased rates of attenuation and transient noise. However, given that there is good evidence that relative wind direction does affect rates of data degradation, a future in-depth statistical analysis on acoustic data collected by a Wave Glider under a variety of wind speeds and directions is warranted.

### 2.4.2 Data cleaning filters and the two-layer comparison technique

Three filters were used to clean the acoustic data: the SRAS and LCAS filters were used to detect attenuation, and the LCTN was used to detect transient noise. The SRAS filter provided a first-order correction by removing attenuated data that had the most severe impact on water column backscatter, detecting much of the persistent attenuation that occurred during sustained windy periods. The ability of the SRAS filter to detect attenuation is limited by the natural variability of reference scatterer (the seabed). This means that is not well suited to detect instances of mild attenuation, whether short-lived or persistent. The LCAS filter complemented the SRAS filter by detecting short-lived reductions in backscattering strength. It was not limited by the natural variability of seabed backscatter, allowing it to detect instances of attenuation where the reduction in signal strength was relatively small and therefore to detect some instances of attenuation missed by the SRAS filter.

Data cleaning improved the appearance of echograms and reduced two-layer comparison correlation coefficients, indicating that the filters were effective in removing much of the data affected by attenuation and transient noise. However, all three filters likely made both false positive (misidentifying good quality data) and false negative (not identifying all the degraded data) detections. Despite applying three filters to remove degraded data, two-layer comparison correlation coefficients were still moderately correlated above wind speeds of $13\,\mathrm{m\,s^{-1}}$, and were still weakly correlated during less windy weather, suggesting that not all instances of transient noise and short-lived attenuation were detected and there may have been a substantial number of false negative detections.

All local convolution filters have a limited ability to distinguish between natural variation in genuine echoes from scatterers (background backscatter) and transient noise or attenuation. The ability to distinguish between these two sources of variability is determined by the contrast between the two. When background backscatter is relatively uniform, smaller (stricter) thresholds can be used to detect affected data, thus reducing false negatives, without substantially increasing the risk of making false positive detections. When background backscatter is patchy, the contrast is reduced and smaller thresholds can substantially increase the rate of false positive detections. For this reason, it is often inevitable that some affected data are retained after cleaning using these kinds of filters, because thresholds that are strict enough to remove all instances of attenuation or transient may remove an unacceptable amount of data.

The SRAS filter took advantage of four features of the acoustic dataset: areas were revisited on repeat transects; the seabed was always within range; backscatter from the seabed varied minimally at small spatial scales during calm weather; and there was reasonable spatial coverage across the whole transect during calm weather. It relied upon two key assumptions: that seabed backscattering strengths were constant in time (the seabed's acoustic characteristics did not change), and measurements made during calm weather were the most unbiased available. The first of these assumptions is supported by the observation that average seabed backscatter and its variability during calm weather were relatively constant when sampled during different periods of the mission. The second assumption is supported by the fact that correlations between fluctuations in the seabed and water column

during calm weather were close to zero. Therefore, seabed backscatter measurements taken during calm weather provided a robust baseline against which measurements could be compared to determine bias introduced by windy weather.

It is important to ensure that bias is not accidentally introduced by the data cleaning procedure itself. In preliminary testing, application of the LCAS and LCTN filters to water column data revealed a time of day bias associated with DVM of the main SSL, which altered background backscattering strengths and patchiness. Instead, filters were applied to seabed backscatter, reducing the risk of imparting bias to water column data. No time of day bias was observed when the filters were applied to seabed backscatter, and because two-layer comparison correlations between water column and seabed fluctuations were negligible in calm conditions, any false positive detections made by application of the filter on seabed backscatter would probably have had a random effect on backscatter in the water column and not introduced systematic bias.

The LCAS and LCTN filters were based on filters designed to identify short-lived fluctuations that persist across several pings in ship-based open ocean acoustic data (Ryan et al., 2015). Ryan et al. (2015) emphasised that these kinds of filters rely on spatial autocorrelation from overlapping sampling volumes to minimise the proportion of false positive detections. Spatial autocorrelation increases with depth because of beam spreading which increases overlap by successive pings. It also increases with faster ping rates, but decreases if vessel transit speeds increase. In this study, acoustic data were only recorded to $100\,\mathrm{m}$ with a ping rate of $0.1\,\mathrm{Hz}$. This is a shallower range and slower ping rate compared to the typical values used in ship-based surveys that were considered by Ryan et al. (2015) (ping rates of $1\,\mathrm{Hz}$ and recording ranges that spanned several hundreds metres). However, the slow transit speeds of the Wave Glider meant that, despite this, sampling volumes of consecutive pings overlapped at typical seabed depths. At speeds of $0.5$, $1$ and $1.5$ knots respectively, the percentage of areal beam overlap (calculated as an idealised cone) between successive pings was estimated to be $57\,\%$ at $70\,\mathrm{m}$ depth and $68\,\%$ at $80\,\mathrm{m}$ depth for the $70\,\mathrm{kHz}$ transducer. The efficacy of local convolution filters therefore depends on transit speeds of the platform, the ping rate that the echosounder system can achieve, and the depth of recordings. Here, I have shown that these kinds of filters can be used effectively on acoustic data collected by a Wave Glider.

'Non-local means' filters could provide an alternative to local convolution filters for the detection of short-lived attenuation and transient noise. These types of filter are widely used for image denoising, often in conjunction with other kinds of filters (Buades et al., 2011; Manjón et al., 2008; Shreyamsha Kumar, 2013; Rousselle et al., 2012; Dutta et al., 2013), but are not routinely applied to fisheries acoustics data. In the context of image processing, non-local means filters compare pixels within a window to the mean of every pixel in the whole image, where the mean of each pixel is weighted by its similarity within a same-sized window. Similarity metrics can be based on any prescribed feature. Seabed backscatter could be weighted according to characteristics of seabed backscatter distribution, such as variance or gradients of change. In this way, subsets of the data which have similar backscattering properties can be weighted more heavily, regardless of whether pings were sampled close by in time or space (so they need not be local). This kind of filter could prove useful in instances where local convolution filters do not perform well, for example where seabed backscatter gradients change suddenly at boundaries where the substrate changes, in effect adapting to each different situation by changing the filter threshold according to instances where other references for that situation exist in the dataset. Non-local means filters are typically based entirely on data-driven similarities, however the SRAS filter developed here is, in a sense, a hybrid of non-local means and local convolution filters: non-local weightings were based on both assumptions of temporal invariance in the seabed echo (non-local) and spatial similarities within longitudinal bins (local).

There are a multitude of image processing filters which could be adapted for the field of fisheries acoustics but have yet to be fully exploited (for an example, see Peña, 2016). Other potential avenues for further work to improve data cleaning include using ancillary echosounder output, such as impedance and phase angle data, to evaluate data quality under different wind conditions. These data are typically not used for detecting attenuation or transient noise, although their potential utility has been suggested for these purposes (e.g. in Jech et al., 2021) and for the detection of other data quality issues, such as aliased seabed echoes (Blackwell et al., 2019a).

Ryan et al. (2015) advocated the need for further work to quantify bias remaining in seemingly clean data, particularly since poor data quality is not always apparent by visual scrutiny of

echograms. I addressed this need by developing the two-layer comparison technique. This technique is a unique and novel aspect of this work which advances on current techniques to evaluate the degree of bias in acoustic datasets. It provides a semi-quantitative diagnostic tool to assess the degree of bias within a dataset, and can therefore be used to evaluate the efficacy of data cleaning procedures. The technique can identify bias imparted by short-lived attenuation or transient noise by using the fact that these types of data degradation cause fluctuations in backscattering strengths that persist over one or a few pings (although the technique can be modified by adjusting the size of the convolution kernel to detect noise or attenuation that persists for longer) and affect entire pings. Bias caused by background noise or persistent attenuation is not reliably identified by this technique since these degrade many consecutive pings, and alternative methods to diagnose these types of data degradation should be used where possible. Bias caused by impulse noise is also not reliably identified since this kind of noise persists for extremely short durations, typically less than the amount of time it takes to record one ping, and thus fluctuations would not necessarily occur in tandem across different layers within the ping.

Following application of the cleaning filters, correlation coefficients produced by the two-layer comparison technique reduced towards baseline levels established during calm weather, indicating that the filters had removed pings affected by attenuation and transient noise. However, even after data cleaning, there was still a pattern of increasing bias with increasing wind speed, indicating that the quality of data collected during windy weather was still not of the same quality as data collected during calm weather. Data collected during windy periods may be too compromised for use in studies that require acoustic backscatter measurements with a high degree of precision and accuracy, even after cleaning (Jech et al., 2021). Filter thresholds that remain constant throughout application across the dataset may not be appropriate for data collected under a range of weather conditions.

Stricter thresholds may be more effective for cleaning data collected during windy periods in order to bring the level of bias to a similar level throughout the dataset. However, strict thresholds could result in the removal of an unacceptable amount of good data during calm periods, when more relaxed threshold may be more appropriate. The effects of wind speed on data degradation are variable, and this variability may contribute to variability in the efficacy

of the filters in identifying poor quality data. Filter efficacy undoubtedly depends on the severity and rate of data degradation, which varies with wind speed, as well as the patchiness of the underlying data (here, the seabed backscatter), since all of the filters used rely on detecting a pattern that contrasts against the underlying data. The two-layer comparison technique lends itself to sensitivity analyses to establish potentially suitable thresholds for detection filters, as one of a suite of metrics that could include effects on target or water column backscatter following the removal of affected data and changes to spatiotemporal resolution or survey coverage. If imposing stricter thresholds removes a substantial amount of data but has a negligible effect on reducing bias, then an optimal threshold may have been surpassed.

The two-layer comparison technique that I describe in this chapter could be used for a variety of applications besides assessing filter efficacy, and need not be applied across a range of wind-speed intervals. For example, the technique could be applied to investigate the role that other factors known to influence noise and attenuation, for example changes in transducer depth for keel-mounted transducers, play and to assess their impacts. Alternatively, a running average of the correlation coefficient could be calculated to provide a near real-time metric of data quality as surveys proceed.

Whilst the two-layer comparison technique shows promise, it has several potential shortcomings. Firstly, the technique is unable to identify the sources of bias, although systematically tracking changes in bias after applying data cleaning filters in turn can help to identify which types of data degradation are present and which was most problematic, as was done in this study. This process could help to narrow down the mitigation measures which may be most effective for future deployments.

Secondly, the metric produced is only semi-quantitative. Correlation strengths are dependent on factors other than just the rate and severity of noise or attenuation. For example, whilst the correlation strength ($\rho$) is influenced by the severity of data degradation it is also influenced by the variability of underlying data in the layers considered. Furthermore, correlation values are not necessarily indicative of the impact of data degradation on water column data or the impact on target estimates themselves.

Thirdly, the correlation coefficient is an estimate of bias, but not a measure of how this bias affects acoustically-derived estimates of biological targets - the principal concern driving data cleaning of fisheries acoustic datasets. The relationship between these two metrics will vary amongst datasets and study aims, however the relationships can be explored by sensitivity analyses that look at how target estimates are affected by data cleaning procedures with a range of different thresholds (levels of stringency).

Finally, not every acoustic study is able to sample the seabed. This is particularly common for open-ocean surveys where the seabed may be hundreds of metres below the surface and either beyond the recording range or seabed backscatter may be unusable due to high levels of TVG-amplified background noise, a particular concern for higher frequency data. In theory, the two-layer comparison technique could be applied to two layers of water column backscatter data. If the layers are sufficiently vertically separated then the application of this technique could be extended to include open-ocean datasets. The technique may be less effective when there is an underlying correlation between backscatter in the two layers but such instances are extremely unlikely to occur in practice. Whilst biological coupling between the seabed and biota in the water column, or biota at different depths of the water column, may exist, it is unlikely that backscatter would consistently vary synchronously at the resolution of single pings. Future studies to evaluate the application of the two-layer comparison technique to water column data only would be invaluable, since if the technique proves robust it could enable the assessment of bias and data cleaning efficacy across a much wider array of acoustic datasets.

Establishing the source of transient noise in acoustic data can pose a considerable challenge. This is particularly true for data collected by autonomous vehicles since acousticians are not available onboard to investigate the source of the noise or monitor interventions that aim to reduce the noise. In *Lyra's* acoustic data, transient noise generally only lasted across single pings. This is consistent with the description of transient noise in Ryan et al. (2015), which describes it as occurring irregularly and lasting for several pings, after accounting for the differences in ping rate. There was a modest increase in both the rate and severity of transient noise as wind speeds increased, and an inverse relationship between the estimated proportion of false positive transient noise detections and wind speed. These two relationships lend

support to the idea that transient noise is generally caused by wave-platform collisions, since the temporal frequency and force of impacts from waves hitting the platform, and hence noise, are anticipated to increase as stronger winds induce wavier conditions at the sea surface (Ryan et al., 2015). Video systems could be attached to the Wave Glider to record either subsurface or above the surface (Galgani et al., 2003; Cervino and Douglas, 2017). These could provide footage to help determine whether wave-platform collisions coincide with transient noise detections in the acoustic data and to identify the source of the noise.

Other possible sources of transient noise during *Lyra's* deployment include nearby breaking waves, variable electrical noise, and cavitation. Noise from nearby breaking waves is also expected to increase in both severity and temporal frequency during windier conditions. However, given the ubiquity of nearby breaking waves, they are collectively more likely to contribute to overall ambient noise levels and variability, rather than presenting as well-defined, short-lived fluctuations in noise. Pedersen et al. (2019) suspected that the source of variable intensity noise present in their Wave Glider-collected acoustic data could have been electrical in nature, but the elevated noise levels persisted for several minutes at a time. Transient noise in *Lyra's* data was therefore unlikely to have been generated by the same mechanism. Cavitation, which describes explosive sounds induced by high power sound waves, are another possible source of sharp noise spikes in the acoustic signal. However, cavitation was unlikely to have been produced by the low-power transmissions of the WBT-mini (set to 150 W and 200 W respectively for the ES200-7CD and ES70-18CD transducers). Wave-platform collisions remain the most plausible explanation for the transient noise experienced.

### 2.4.3 Operational recommendations

Most interventions that could potentially improve the quality of acoustic data collected by the Wave Glider involve re-engineering the way that transducers are mounted onto the platform. Moving the transducers is crucial for reducing or eliminating subunit interference, potentially allowing for acoustic observation of biota near the surface. For most ASVs, the options for transducer location are limited to areas underneath or extensions behind the hull. The Wave

Glider's unique two-part design offers opportunities to attach the transducers either to the float, at shallow depths compared to transducers on ships and some other ASVs, or to attach them to the subunit, situated several metres below the surface, as proposed by Greene et al. (2014).

Reasonable actions to mitigate data degradation include: increasing the transducer depth either by extending the strut or attaching the transducer to the subunit to reduce both bubble-shadowing and subunit interference; steadying the transducer mount, for example by putting the transducers on a gimbal, to reduce transducer motion; or using alternative materials between the float and transducer mount to dampen vibrations, reducing the impact of wave-platform collisions. Whilst these changes could help improve acoustic data quality, it is important to note that they could also have unintended consequences. For example, extending the strut increases the risk of breakage under heavy impacts or severance of the electrical connection between the echosounder and transducer. The risk of losing acoustic equipment may increase if the transducer is housed in a tow body attached to the subunit; the umbilical that tethers the subunit to the float can become entangled and break (J. Horne, personal comment, April 2019), and risk of entanglement may increase with a tow body attached. Attaching the transducer to the subunit may provide several benefits: bubble-shadowing is expected to be less of a problem at depth and self-radiated noise of the Wave Glider may be quieter at the subunit compared to the float (Bingham et al., 2012). However, placing transducers deeper also necessarily limits coverage of near-surface regions and can introduce unwanted movement. Meyer-Gutbrod et al. (2012) reported that transducers mounted on a tow-body attached to the subunit experienced jerky motion, although this could be partially remedied by installing an S-shaped cable to connect the tow-body and subunit, the subunit's rudder radiated noticeable noise when turning, and attaching the tow-body resulted in slower transit speeds by up to $10\,\%$. There are therefore several considerations that must be taken into account when re-engineering the position of transducers on the Wave Glider.

Transducers are best integrated in such a way as to optimise the trade-off between data quality and coverage according to the intended use of the data. If studies require near-surface data on weak scatterers, then transducers should be mounted at a shallow depth (i.e. from the float) and subunit interference must be entirely eliminated. However, if the study's targets

are relatively strong scatterers, then minimal subunit interference may not hamper the aims of the study (Swart et al., 2016). If studies do not require the analysis of biota near the surface, then mounting transducers deeper (whether extended from the float or attached to the subunit) is perhaps the best way to improve the quality of acoustic data. It is worth appreciating that although the Wave Glider has the potential to take acoustic measurements closer to the surface than ships, the quality of this data is subject to weather-related impacts, such as bubble-shadowing, and may only be of adequate quality during calm weather. A more extensive analysis of the effects of weather impacts on acoustic data quality in the first few tens of metres underneath the surface is needed, however this kind of analysis will only be reliable if it uses data unaffected by subunit interference.

Transducer motion can also be mitigated by re-engineering the mounting of the transducers. They could be mounted on a gimbal to reduce angular motion (Pedersen et al., 2019; Chu et al., 2019), although note that there are currently no studies that assess whether this intervention leads to improved acoustic data quality. Pedersen et al. (2019) reported variable electrical noise that could conceivably have been related to the operation of the gimbal on their Wave Glider. Despite having the transducers mounted on a gimbal, echograms showed evidence that roll still affected the acoustic data. I therefore caution against potentially costly interventions unless it can be reasonably demonstrated that there is a particular need for those actions and that they will improve the overall acoustic data quality.

Alternatively, transducers could be attached to a tow-body from the subunit, in an attempt to reduce the propensity for the transducer to be subject to the motions of surface waves (Greene et al., 2014). Meyer-Gutbrod et al. (2012) reported that transducers attached to the subunit experienced higher rates of pitch than roll due to the undulating movement of the subunit. Using a gimbal, roll amplitudes averaged $\pm$ 2°, and pitch amplitude averaged $\pm$ 7°. This followed modification of the tow cable to prevent jerky motion of the subunit transferring to the tow body. *Lyra's* float experienced only slightly higher average roll, averaging 2.3°. Therefore it is not clear whether relocating *Lyra's* transducers would impart a significant improvement to data quality by reducing transducer motion, and it may be worth focusing efforts on reducing the impacts of near-surface bubbles instead.

The association between transit speeds and the proportion of degraded data compounds effects on the spatio-temporal resolution of cleaned data. Decreased horizontal resolution and the removal of poor quality data associated with higher wind speeds has implications for the spatial coverage of regions, and both lower resolution and coverage add to uncertainties of biomass, abundance, and other acoustically-derived estimates. Acoustic survey data are ideally collected at a consistent spatial and temporal resolutions. To mitigate the decrease in resolution at higher wind speeds, the acoustic sampling rate could be adjusted in near-real time, either by programming autonomous control in mission planning or by making adjustments remotely.

In windy weather, acoustic sampling rates could be adjusted according to two contrary strategies. Sampling could be paused to extend the mission's longevity and obtain more consistent quality acoustic data over the course of the mission. For example, De Robertis et al. (2021) paused Saildrone acoustic surveys when wind speeds exceeded $12\,\mathrm{m\,s^{-1}}$. This action preserves battery life, a salient concern for autonomous vehicle operations, and reduces the amount of poor quality acoustic data collected, thus reducing the amount of data that requires storage and processing. Alternatively, the acoustic sampling rate can be increased during periods of strong winds. This may counteract the anticipated reduced spatial resolution of the data by increasing the likelihood of obtaining sufficient spatial and temporal coverage from unaffected samples following data cleaning. It is advisable to assess the efficacy of cleaning, however, to determine whether retained data is still compromised beyond a tolerable degree. Although instantaneous wind speeds were found to correlate strongly with metrics of poor acoustic data quality, our lag analysis suggests that data quality is more strongly correlated with average conditions within the previous half an hour to an hour. Therefore, changes to sampling strategies within an hour of strong, persistent winds would be worthwhile.

# 3

# Characterising daily vertical movement patterns of fish and zooplankton

## 3.1 Introduction

### 3.1.1 Plasticity of DVM behaviour

Vertical gradients in perceived predation pressure and food availability are fundamental to the expression of vertical migration behaviour, with cyclic variation on diel timescales driving the synchronised movements of individuals. However, DVM behaviour of an individual organism is not fixed. Instead, individuals respond dynamically to the changing trade-off between their need to forage and the need to reduce their risk of predation, which varies according to changes in their internal state and their external environment. This can result in a variety of DVM behaviours occurring within a single population.

Echosounders can measure net (i.e. population-level) changes in DVM behaviour. Common metrics to describe DVM behaviour include migration rates, amplitude, timing, and proportion of migrators. Migration amplitude describes the vertical distance between minimum and maximum depths. Timing refers to the time at which ascents and descents are initiated and cease. Migration rates describe the speed at which migratory organisms or layers move from minimum to maximum depths. Nuances in these metrics can reveal trait-based and environmentally-driven variation in DVM behaviour patterns (Ohman and Romagnan, 2016; De Robertis et al., 2000; Benoit-Bird and Moline, 2021; Bos et al., 2021).

If changes to the DVM trade-off are approximately similar amongst a population, then resulting behavioural changes would be expected to be similar. However, if changes to the DVM trade-off differ amongst individuals within the population, this may result in less synchronised behaviour. A change in the synchronicity of DVM may be observed acoustically by changes to the migration rate, timing, and amplitude of net migration, as well as the proportion of migrators.

Cottier et al. (2006) provided intriguing evidence that Calanus copepods can switch between synchronised and unsynchronised migrations depending on the seasonal light regime. Under constant illumination during the Arctic's midnight sun there ceased to be an optimal time of day for copepods to migrate into the riskier surface waters to feed. ADCP data revealed that although synchronised migrations did not occur on diel timescales, copepods still made vertical migrations by conducting individual forays towards the surface, presumably timed according to individual needs. These populations began to perform synchronised DVM as autumn approached and light levels once again varied throughout the day. Migratory animals may therefore be capable of adapting their migration timing according to the relative importance of dynamic external and internal stimuli. The more important individual needs are, the less synchronised migrations may be.

The hunger-satiation hypothesis maintains that an individual's propensity to migrate will vary according to their satiation state: a migratory animal is more likely to remain in relative safety at depth when satiated whereas a hungry animal may risk migrating in order to find food (Pearre, 2003a). Hunger has been shown to affect decision-making and modulate risk-taking behaviour across the animal kingdom, with hungrier individuals more likely to expose themselves to predation risk (Moran et al., 2021). This presumably confers an adaptive advantage whereby individuals in areas of prolonged low food concentrations alter their normal behaviour in order to seek much-needed nourishment, otherwise they may starve.

The hunger-satiation hypothesis has been proposed to explain some of the intra-population variability in migratory behaviour that results in a reduction of DVM synchrony, since individuals are expected to act according to their individual needs (Pearre, 2003a). Empirical

evidence to support the hunger-satiation hypothesis is not always consistent, robust, or easy to obtain (reviewed in Pearre (2003a)), particularly since measuring internal states, such as whether an animal is hungry or not, is notoriously difficult to achieve even in laboratory settings (Marques et al., 2020). By analysing stomach fullness of migrants and non-migrants at different depths during midnight and midday, Bos et al. (2021) demonstrated that some species are less likely to migrate if they are sufficiently fed, however not all species tested followed this pattern. Ichii et al. (2020) described an unexpectedly shallow distribution of krill that occurred when prey concentrations were very low, postulating that the importance of meeting physiological demands outweighed the increased risk of predation.

Many endogenous factors are known to influence migration behaviour. Body size can alter migration amplitude, mean night and day depths, and whether or not DVM takes place at all for certain size-classes (Ichii et al., 2020; De Robertis et al., 2000; Gastauer et al., 2022; Ohman and Romagnan, 2016). De Robertis et al. (2000) found that larger euphausiids had shorter residence times near the surface during the night as they ascended later and descended earlier than smaller individuals, with swimming ability unlikely to explain this difference. Several other studies have also found size-dependent migration timing and depth distributions. As a general rule, smaller organisms are found in shallower water than larger organisms, and will ascend sooner than, and descend later than, larger organisms. DVM of smaller organisms therefore tends to have smaller migration amplitudes than those of larger organisms (Aarflot et al., 2019; Ohman and Romagnan, 2016; De Robertis et al., 2000; Andersen and Sardou, 1994).

Body condition can also influence an individual's decision to perform DVM. Hays et al. (2001) found that non-migrant *Metridia pacifica* copepods had substantially higher lipid content than migrants. This supports the hypothesis that vertical migrations might only occur when energy requirements necessitate that an individual exposes itself to increased predation risk near the surface in order to feed, expending what may be a substantial amount of energy to swim upwards against gravity over relatively large distances. Similarly, body size and ontogenetic development can affect an organism's propensity to migrate and thus the proportion of migrators within a population. For example, the smallest and largest copepods studied by Ohman and Romagnan (2016) were found to remain at similar depths throughout

the diel period and it was only intermediate-sized copepods that exhibited size-dependent depth distributions and migration behaviour.

DVM may be a facultative, rather than obligate, behaviour for some species. Within species that are known to perform DVM, some components of the population may be non-migratory and remain at depths associated with daytime residence (Bos et al., 2021; Pearre, 2003a; Ohman and Romagnan, 2016; Kaartvedt et al., 2009; Dypvik et al., 2012). Non-migration may be a permanent trait or may only occur during particular life-history stages or physiological states.

Adjusting vertical position in the water column is not the only strategy employed by zooplankton to reduce predation risk. Many epipelagic zooplankton are translucent; reducing their contrast to surrounding water reduces their conspicuousness to visual predators (Johnsen, 2001). Some zooplankton such as the copepod *Pareuchaeta norvegica* even alter their pigmentation on diel timescales to reduce their contrast during the most illuminated parts of the day (Vestheim and Kaartvedt, 2006). Some non-migratory copepods alternate between feeding and non-feeding behaviours with a diel rhythm. Increased mobility associated with feeding and enhanced contrast due to visibility of food in the gut may increase vulnerability to visual predators, and therefore cessation of feeding activity during the day has been proposed as a means to reduce predation risk (Durbin et al., 1990). However, Torgersen (2003) argues that an assumed increase in vulnerability to predation due to movement may be less applicable in the pelagic environment since many fish predators typically hunt whilst swimming at speed and so relatively small motions of zooplankton prey may be insignificant. Foraging success has been shown to be independent of prey motility for some adult planktivores, including herring and euphausiids (Torgersen, 2001; Janssen, 1982), however weak swimmers such as fish larvae may still gain an advantage in the detection of motile prey (Torgersen, 2003). Some species may cease to migrate as they develop, owing to an improved capability to detect and capture prey at depth. Migrating to surface waters to feed, even at night when waters are less illuminated, may not outweigh the increased predation risk associated with being larger and more conspicuous (Dypvik et al., 2012; Ohman and Romagnan, 2016). Limited vertical resolution in some studies may result in a failure to detect subtle shifts in position. For example, the copepod *Arcatia hudsonica*,

once thought to be non-migratory, was shown to undergo shallow DVM over a few metres under experimental conditions where predators were introduced, but cease migrations in manipulations where predators were absent (Bollens and Frost, 1991). This illustrates plasticity in behavioural responses that determine whether migratory behaviour is undertaken or not.

### 3.1.2 Aims of this study

Despite extensive CPR records of zooplankton in the North Sea, few studies have explicitly investigated DVM behaviour of those species sampled (Colebrook, 1966; Hays, 1995). Studies in the North Atlantic of zooplankton taxa also common in the North Sea have documented DVM of many species (Hays, 1996; Angel and Pugh, 2000), however few studies of DVM in the North Sea exist (although see Hays et al., 1996, 2001). There is also a paucity of acoustic studies of North Sea zooplankton; the focus of most North Sea acoustic surveys tends to be on commercially important fish species (ICES, 2023) where backscatter from zooplankton is typically excluded as 'noise' (although see Fässler et al., 2012; Mair et al., 2004, 2005; Machairopoulou et al., 2013). No literature was found that details DVM behaviour (timing, migration rates and amplitude etc.) of North Sea zooplankton determined acoustically, beyond reporting that DVM has been observed (e.g. Mair et al., 2005). An updated account of zooplankton DVM behaviour in the North Sea, or its absence, is therefore needed.

The North Sea is a mid-latitude temperate shelf sea. Consequently, I anticipate that daily variation in light levels will influence the vertical distribution of some zooplankton, and result in observable synchronised DVM behaviour. This study aims to describe the diel behaviour, with specific reference to vertical position, of three broad biological groups using acoustic data collected by a Wave Glider. I employ an acoustically-derived classification scheme based on theoretical scattering properties to partition water column backscatter data into the following groups: gas-filled zooplankton (GF), fluid-like zooplankton (FL), and schools of fish with swimbladders (FS). Temporal patterns of backscatter in each group are described over diel timescales, and descriptors of average DVM behaviour (amplitude, timing,

proportion of migrators in population, migration rates) are provided where appropriate.

Various environmental factors are known to influence DVM behaviour, including: food availability (Ichii et al., 2020); circadian rhythms (Häfker et al., 2017); lunar cycles (Last et al., 2016) and other light sources, such as artificial light (Moore et al., 2000; Ludvigsen et al., 2018); water clarity (Ohman and Romagnan, 2016; Aarflot et al., 2020), and the presence and abundance of predators (Urmy and Benoit-Bird, 2021; Hahn et al., 2019; Hays et al., 1996). The influence of environmental gradients on vertical distribution patterns will be investigated in Chapter 4; here I consider theory pertaining to endogenous controls on DVM behaviour to explain observed differences in synchronicity of DVM.

## 3.2 Methods

### 3.2.1 Acoustic classification scheme

Narrowband 70 kHz and 200 kHz backscatter data were processed in Echoview (Echoview Software Pty Ltd, 2021) to classify three groups: 'Fish Schools' (FS), 'Fluid-Like' (FL), and 'Gas-Filled' (GF). Classified backscatter data for each group were then exported to R (R Core Team, 2022) for further processing and analysis. The main processing steps were ordered as follows:

i Define the analysis layer
ii Smooth backscatter data
iii Detect fish schools (FS group)
iv Separate remaining data by dB-difference into FL and GF groups
v Export vertically integrated data for each group
vi Derive additional energetic, positional and morphological metrics
vii Horizontally average (bin) data

#### Analysis layer

Narrowband 70 kHz and 200 kHz $S_v$ data were cleaned of transient noise and attenuation as per Section 2.2. An analysis layer was created which constituted a horizontal layer of

the water column. A $36\,\mathrm{m}$ upper limit was defined to exclude backscatter contaminated by subunit phantom echoes and the surface bubble layer. To define the lower limit, a bottom detection algorithm was implemented in Echoview to identify the seabed. However, during windy weather, attenuation of the acoustic signal caused the seabed echo to fluctuate from ping to ping, resulting in poor performance of the algorithm. To improve horizontal contiguity, a back step of $2\,\mathrm{m}$ was applied to the bottom line and further manual scrutiny and editing carried out. The resulting analysis layer had a vertical thickness that varied between 33 and $62\,\mathrm{m}$ (mean $46 \pm 6\,\mathrm{m}$), depending on bathymetry.

**Data smoothing**

Multifrequency techniques such as dB-differencing are sensitive to mismatches between transmission delays and volumes sampled by different transducers, necessitating a degree of smoothing (Korneliussen, 2018; Korneliussen and Ona, 2002). The $70$ and $200\,\mathrm{kHz}$ transducers pinged sequentially with an approximate $2.5\,\mathrm{s}$ interval between each closest ping-pair. For typical vehicle speeds of $0.6\,\mathrm{m\,s^{-1}}$, acoustic axes of each ping-pair were $1.5\,\mathrm{m}$ apart, with consequent mismatches between the volumes of water sampled further exacerbated by differing transducer beam widths. At greater ranges, the proportion of volume mismatch reduces at depth due to beam spreading. At relatively close range ($<$ $100\,\mathrm{m}$) and with sequential pinging, our data required smoothing. A median 3x3 pixel filter was applied to reduce natural stochastic variability in acoustic backscatter and improve spatial comparability (Korneliussen et al., 2008). This filter smoothed across $30\,\mathrm{s}$ time intervals (approximately $7.5\,\mathrm{m}$ to $45\,\mathrm{m}$ along-track) and $0.14\,\mathrm{m}$ vertically, thus reducing effects of mismatch even near the surface as well as reducing the effect of any short-lived noise and attenuation still apparent in the data.

**Detecting fish schools**

Schools of swimbladdered fish typically present in echograms as well-defined, compact, oblong-shaped hotspots of strong backscatter relative to their surroundings (Petitgas and Levenez, 1996). However, some aggregations that do not strictly conform to the definition

of schooling (i.e. synchronised movement behaviour), such as shoals, look similar when observed acoustically. Although not all aggregations exhibit schooling behaviour, for this study the term 'fish school' was used to describe any hotspot of strong backscatter at $70\,\mathrm{kHz}$ with the characteristics described above, and thus could include shoals that do not exhibit synchronised schooling behaviour.

In acoustic surveys, fish schools are often detected by applying a variant of the SHAPES algorithm to backscatter data (Coetzee, 2000). SHAPES detects clusters of backscatter above a chosen threshold which meet certain morphological criteria. Detection parameters are set to limit minimum school lengths and heights, as well as distances between schools (known as the minimum linking distance) that determine whether proximate candidate schools are considered part of a single, larger school. Output from the SHAPES algorithm applied to $70\,\mathrm{kHz}$ backscatter data, implemented in Echoview's Fish Detection Module, formed the basis for the 'Fish School' (FS) acoustic group. Minimum total school length and height were set to at least double the horizontal and range resolution of the data respectively (following Tarling et al., 2009). Variable vehicle speeds, and hence along-track resolution, necessitated careful choice of a single representative value upon which to base school length parameters. On the basis that a typical speed of $0.6\,\mathrm{m\,s^{-1}}$ resulted in $6\,\mathrm{m}$ between acoustic axes of sequential pings, minimum horizontal school length was set to $12\,\mathrm{m}$, i.e. two adjoining pixels. At speeds of $0.88\,\mathrm{m\,s^{-1}}$ (99th percentile) and $0.17\,\mathrm{m\,s^{-1}}$ (1st percentile), the minimum length of $12\,\mathrm{m}$ required contiguity of backscatter over 2 and 8 pixels respectively. The minimum distance required to resolve targets vertically was $19.2\,\mathrm{cm}$ according to the formula $\frac{c\tau}{2}$ where $c = 1482\,\mathrm{m\,s^{-1}}$ is the speed of sound in seawater, and $\tau = 256\,\mu\mathrm{s}$ is the ping duration (Parker-Stretton et al., 2009). With 2249 pixels per ping over $100\,\mathrm{m}$ range, vertical resolution of targets required at least five pixels. On this basis, minimum total school height was set to $1\,\mathrm{m}$, i.e. vertical contiguity over at least twenty-two pixels. Maximum vertical and horizontal linking distances were set to $15\,\mathrm{m}$ (three hundred and thirty-seven pixels) and $36\,\mathrm{m}$ (six pixels wide at typical speed) respectively.

A minimum threshold is usually applied prior to fish school detection algorithms in order to limit detections to regions of the echogram where backscattering strengths are relatively high (Korneliussen et al., 2009; Campanella and Taylor, 2016; Gastauer et al., 2017). The

background against which detection takes place impacts the performance of SHAPES, since poor contrast with surrounding backscatter may blur school boundaries. During spring, backscattering strengths in the densest regions of the main SSL were comparable to those observed in fish schools distinct from the SSL. This complicated detections as preliminary analyses revealed that very high thresholds excluded most of the SSL at the expense of failing to detect some schools. Conversely, low thresholds resulted in vast swathes of the SSL being selected, despite morphological and energetic characteristics differing markedly from fish school candidates which, in contrast, had well-defined boundaries. In order to optimise fish school detection, morphometric, positional and energetic properties of clusters detected with six different thresholds were evaluated in a sensitivity analysis (Appendix F). This identified a threshold of $-57\,\mathrm{dB}$ as optimal for detecting clusters with properties suggestive of fish schools.

Pixels in the 3x3 smoothed data whose majority volume fell within the clusters output by SHAPES were classed as belonging to a fish school. These were scrutinised and fish school regions buffered where necessary to prevent contamination of the zooplankton groups by strong fish school echoes. A series of filters were applied prior to running SHAPES to improve detections: i) the $-57\,\mathrm{dB}$ minimum threshold, ii) 3x3 erosion, iii) 3x3 dilation and lastly iv) 5x5 dilation filter. These filters reduced background backscatter, better defined cluster boundaries and reduced stochastic variability by limiting the influence from outliers (i); reduced the likelihood of diffuse clusters from being selected (ii); and expanded cluster boundaries (iii - iv) (Korneliussen et al., 2009). Erosion filters shrink features and remove small connecting artefacts such as bridges and branches thereby reducing fragmented or diffusely distributed clusters of strong backscatter into smaller, more isolated pockets less likely to be selected. Larger, strong, well-connected clusters are retained. Dilation filters expand features and enhance connections by filling in small gaps, accentuating remaining clusters. A dilation filter (5x5 pixels) larger than the erosion filter (3x3 pixels) meant that eroded edges were somewhat compensated for by expanding fish school boundaries outward.

Misattribution of zooplankton backscatter in the FS group is preferential to misattribution of FS backscatter in the zooplankton groups. This is because contamination of zooplankton groups with fish school backscatter could substantially bias results as fish school echoes are typically much stronger than those from the SSL. In contrast, contamination of the FS group with zooplankton backscatter would probably have a negligible effect on FS backscatter patterns. Dilation therefore ensured that all fish school backscatter was included within the FS group (Ballón et al., 2011; Korneliussen et al., 2009).

**Separation of the gas-filled and fluid-like acoustic groups**

To classify regions of backscatter that were not identified as fish schools, FS regions were masked as 'no data' and remaining backscatter partitioned into the acoustic groups 'fluid-like' (FL) and 'gas-filled' (GF) zooplankton according to dB-difference in mean volume backscattering strength between $200$ and $70\,\mathrm{kHz}$, denoted $\Delta\mathrm{MVBS}_{200-70}$. This quantity defines the ratio between backscattering strengths at $200\,\mathrm{kHz}$ and $70\,\mathrm{kHz}$, calculated by subtracting in the logarithmic (decibel) domain.

For most small fluid-like scatterers found in the North Sea, $70\,\mathrm{kHz}$ is expected to sample the lower part of the Rayleigh scattering region in their frequency response pattern, and $200\,\mathrm{kHz}$ is expected to sample either the upper part of the Rayleigh region or the geometric region, resulting in a positive dB-difference ($\Delta\mathrm{MVBS}_{200-70} > 0$). In contrast, North Sea zooplankton with gas inclusions are expected to backscatter more strongly at $70\,\mathrm{kHz}$ than $200\,\mathrm{kHz}$, and so produce a negative dB-difference. Frequency response of gas bubbles declines above a resonance frequency, which is usually lower than $70\,\mathrm{kHz}$ for bubbles approximating $1\,\mathrm{mm}$ in diameter (Kubilius and Pedersen, 2016). Gas-filled scatterers, such as physonect siphonophores with pneumatophore gas-inclusions approximating $1\,\mathrm{mm}$ (Warren et al., 2001), are therefore expected to have a negative dB-difference ($\Delta\mathrm{MVBS}_{200-70} < 0$).

Accordingly, pixels with negative dB-difference were categorised as belonging to the GF group and those with a positive dB-difference as belonging to the FL group. Since elastic-shelled scatterers exhibit a similar frequency response pattern to fluid-like scatterers, albeit with stronger target strength due to hard pieces of their anatomy such as carapaces and

shells, they are anticipated to produce a positive dB-difference and hence would fall into the FL group. No pixels had a dB-difference of zero ($\Delta\text{MVBS}_{200-70} = 0$), which might have indicated either a level response at both frequencies or empty water within the volumes sampled. However, there were many pixels with near-zero dB-difference values. Of those pixels with a dB-difference between $-0.01$ and $0.01\,\text{dB}$, backscattering strengths at $70\,\text{kHz}$ ranged from $-110$ to $-49\,\text{dB}$ re $1\,\text{m}^{-1}$ (IQR from $-76$ to $-67\,\text{dB}$ re $1\,\text{m}^{-1}$). For comparison, pixels with a dB-difference greater than $|2|\text{dB}$ ranged from $-126$ to $-36\,\text{dB}$ re $1\,\text{m}^{-1}$ (IQR from $-73$ to $-64\,\text{dB}$ re $1\,\text{m}^{-1}$). It is therefore plausible that pixels with dB-difference values close to zero did not represent empty water, even considering that there may have been some background noise recorded, since these values lie within the range of expected backscattering strength values for volumes of water that likely contained biological scatterers. The separation by dB-difference at $0\,\text{dB}$ was therefore chosen such that the GF and FL groups represented two broad biological groups of zooplankton, separated according to their scattering type.

**Separation of backscatter into the three acoustic groups**

Backscatter from each group were separated as follows. FS: pixels where fish schools were not detected were marked as $-999\,\text{dB}$, i.e. devoid of fish schools. GF: pixels where fish schools were detected were marked as 'no data' since it was unknown whether gas-filled organisms were present within those sampling volumes; their signal could have been dominated by the fish school. Pixels not classed as either fish schools or gas-filled were set to $-999\,\text{dB}$, i.e. devoid of gas-bearing zooplankton. FL: pixels assigned to the FS and GF groups were set to 'no data' since fluid-like zooplankton organisms that belong to this group may have been present but their presence masked by the stronger backscatter of the other groups.

### 3.2.2 Analysis of diel patterns

#### Acoustic descriptors of DVM

Backscatter data for each group were integrated in Echoview (Echoview Software Pty Ltd, 2021) and acoustic descriptors exported to R (R Core Team, 2022) where additional descriptors (dB-difference, altitude, and elongation) were derived (Table 3.1). Fish schools were treated as whole entities by integrating each fish school region. For the GF and FL groups, data were vertically integrated over each ping. Three categories of acoustic descriptors were considered: those that described energetic properties (describing the strengths of echoes), positional properties (describing where the weighted mean depth of backscatter was in relation to the surface and to the bottom) and morphological properties (describing the shape of the backscatter, used for fish schools only).

Solar altitude ($\alpha$) - the angle of elevation of the sun above the horizon - was derived from time and coordinates according to the R package 'oce' using function Sunangles (Kelley and Richards, 2022). Each ping (GF and FL) or region (FS) was assigned a time of day category according to solar altitude in the following manner:

- Night, between nautical dusk and dawn ($\alpha < -12°$)
- Nautical dawn, after minimum solar altitude ($-12° \leq \alpha < -6°$)
- Civil dawn, following nautical dawn ($-6° \leq \alpha < 0°$)
- Day, between civil dawn and dusk ($\alpha \geq 0°$)
- Civil dusk, after maximum solar altitude ($-6° \leq \alpha < 0°$)
- Nautical dusk, following civil dusk ($-12° \leq \alpha < -6°$)

Table 3.1: **Acoustic energetic, positional, and morphological descriptors.** Morphological descriptors were only derived for the FS group.

| **Type** | **Descriptor (units)** | **Symbol** | **Description** |
|---|---|---|---|
| Energetic | Volume backscattering strength (dB re $1\,\mathrm{m}^{-1}$) | $S_v$ or MVBS | Proxy for numerical density of organisms within group. |
| | Nautical area scattering strength (dB re $1(\mathrm{m}^2\mathrm{nmi}^{-2})$) | NASS | Derived using $S_A = 10\log_{10}(s_A)$ (Maclennan et al., 2002), normalised by water column thickness for GF and FL groups. Proxy for biomass of group. |
| | dB-difference (dB re $1\,\mathrm{m}^{-1}$) | $\Delta\mathrm{MVBS}_{200-70}$ | Difference (in decibel domain) between $S_v$ at 200 kHz and $S_v$ at 70 kHz. |
| Positional | Centre of mass (m) | COM | Weighted mean depth of backscatter, given by: $\mathrm{COM} = \frac{\int_{z_1}^{z_2} z\, s_v(z)\, dz}{\int_{z_1}^{z_2} s_v(z)\, dz}$ where $z$ is depth, $s_v = 10^{\frac{S_v}{10}}$, and $z_1$ and $z_2$ define the lower and upper depth limits of the analysis layer respectively (Bez and Rivoirard, 2001). |
| | Altitude (m) | ALT | Height of centre of mass above the seabed. |
| Morphological | Thickness (m) | T | Mean vertical extent or height. |
| | Length (m) | L | Along-track length. |
| | Area ($\mathrm{m}^2$) | A | Thickness multiplied by length ($TL$). |
| | Perimeter (m) | P | Region boundary length in the plane of the echogram. |
| | Elongation (dimensionless) | E | Ratio between length and thickness ($L/T$) (Weill et al., 1993). |

### Horizontal averaging

Data were averaged in equally-sized longitudinal bins each covering $600\,\mathrm{m}$ along-transect with mean values obtained for all variables in order to reduce effects of spatial autocorrelation. This produced uniquely labelled bins by bin number (1-108) and transect (1-15). Studies of DVM require gradients to be observed at a high-enough temporal resolution to observe movements that occur over relatively short timescales; ascents and descents can take place over a matter of minutes to hours during twilight when light levels change rapidly. As such, data should ideally retain a sufficiently high temporal resolution to resolve these processes. Bin durations ranged from $4$ to $76$ minutes, however most bins covered less than an hour (IQR $15$ to $21$ minutes, mean $18$ minutes $\pm 6$ minutes). Weighted average solar altitude angles were used to categorise the time of day for each bin. The longest duration bins occurred during daytime thus limiting integration over crucial periods (generally during twilight) when organisms performing DVM actively migrated *en masse* (Figure 3.2.1). The longest duration bin occurring in twilight averaged data over a time period of less than $54$ minutes. The shortest duration bins still maintained adequate sampling representation, typically averaging across at least thirty pings.

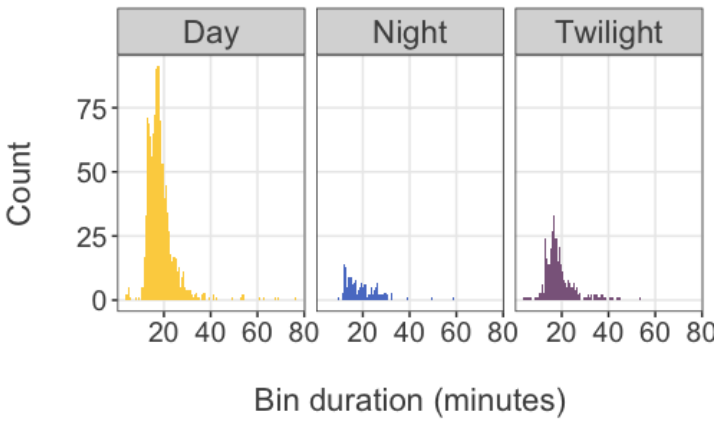


Figure 3.2.1: **Transit time across each bin, categorised by the time of day.** Each longitudinal bin covered $600\,\mathrm{m}$ of the transect line.

**Statistical and visual analyses**

For each group, time series and boxplots were plotted to explore how positional and energetic descriptors varied according to the time of day. For the FS group, relationships between positional, energetic and morphological descriptors were explored with scatter plots; schools with anomalous properties were examined in further detail. For the GF group, a detailed analysis of DVM patterns was conducted; energetic and positional metrics were plotted according to hour of the day and solar altitude. Intensity of DVM, here defined as the relative change in backscatter strength between night and day within a particular depth strata, can be used to infer the proportion of migratory scatterers. The intensity of DVM was estimated by calculating the difference in median backscatter between daytime and the following nighttime using GF classified backscatter data that was vertically averaged per ping but not horizontally averaged (i.e. unbinned). Boxplots of GF backscatter for each day and night period were plotted and the difference between each day-night period (night following day) and the overall average difference in each day-night period was calculated to produce an overall estimate of intensity.

Synthetic echograms depicting each group were produced by combining echograms of backscatter for each individual group, excluding regions that were masked. These were visually scrutinised to provide context for and aid interpretation of the statistical patterns observed for each group.

### 3.2.3 Determining the taxonomical composition of acoustic groups

Net samples provided examples of zooplankton that were present in the water column which might have comprised the GF and FL acoustic groups. For the FS acoustic group, acoustic descriptors and literature examples of swimbladdered schooling fish in the North Sea were used to infer possible species and group composition. Morphological, positional, and energetic properties of fish schools were analysed, with attention paid to schools exhibiting potentially outlying characteristics that might indicate differing taxonomical composition.

### Zooplankton net samples

Ring net samples were taken by the RV Endeavour to characterise zooplankton present in the water column just prior to the start of the mission (between 8th and 10th of May 2018) (Figure 3.2.2). It is recommended that validation samples are taken at the same time as and in as close proximity as possible to the acoustic sampling in order to achieve the most synoptic validation of the acoustics possibleMcClatchie et al. (2000). However, the Endeavour was required to maintain a distance of at least $100\,\mathrm{m}$ from *Lyra* in order to avoid triggering the Wave Glider's collision avoidance system. In practice, the Endeavour kept a distance that ranged between $360\,\mathrm{m}$ and $1.3\,\mathrm{km}$ (mean $655\,\mathrm{m}$) whilst carrying out net sampling.

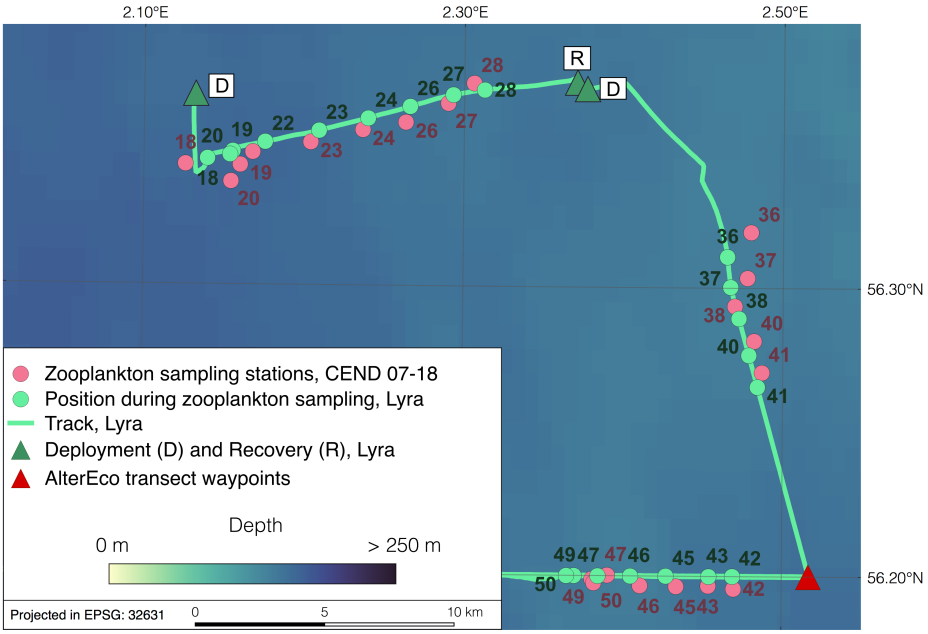


Figure 3.2.2: **Ring net sample stations on cruise CEND 07-18 and concurrent location of *Lyra*.** Fourteen of the twenty-one stations were located off-transect, the remaining six stations were sampled as *Lyra* undertook Transect 1. *Lyra* was recovered and redeployed to adjust fixtures between stations 28 and 36.

Two ring nets were deployed simultaneously, however only samples from the $270\,\mu\mathrm{m}$ mesh net ($0.95\,\mathrm{cm}$ diameter, $0.71\,\mathrm{m}^2$ opening area) were analysed (Figure 3.2.3). The net was configured with a flowmeter to estimate volume of water sampled and a mini-CTD to determine maximum net depth. Samples were taken whilst the vessel was stationary. Vertical hauls were taken from approximately $7\,\mathrm{m}$ above the seabed to the surface. Sampling took place almost every hour where possible, $n = 20$ (Table G.1).

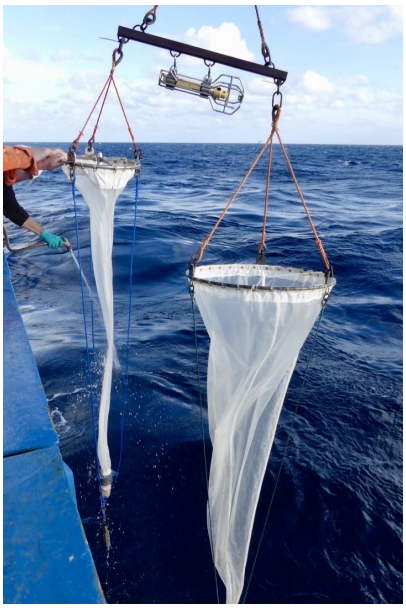

Figure 3.2.3: **Paired ring nets used to sample zooplankton at the beginning of the mission.** $80\,\mu m$ mesh (left) and $270\,\mu m$ mesh (right) nets were attached via a crossbar with mini-CTD. Photograph courtesy of Tobias Ehmen.

Samples were stored in $4\,\%$ formaldehyde and processed via microscopy by the author and by project partners at Plymouth Marine Laboratory. Samples were split into two fractions by passing through a $2\,mm$ mesh: animals retained constituted the $2\,mm+$ 'macrozooplankton' fraction, and animals that passed through but were retained on a $63\,\mu m$ sieve constituted the $63\,\mu m$ 'mesozooplankton' fraction. Mesozooplankton were sub-sampled to achieve a count of between 100-150 individuals. Large macrozooplankton fauna were extracted, identified, and lengths measured and categorised by size: 2-6 mm, 6-10 mm, 10-14 mm, >14 mm.

Animals were categorised according to their scattering type - fluid-like, gas-filled, or elastic-shelled - based on examples in the literature (Stanton et al., 1996; Martin et al., 1996; Lavery et al., 2007). These categories were translated to expected acoustic group for our classification scheme, based on whether the dB-difference would likely be positive or negative. Abundance estimates were not calculated because flowmeter measurements were found to be unreliable and variability in the angle of the net from vertical meant that samples were not always comparable. Instead, numerical abundance of subsampled taxa and the proportion of individuals within each acoustic group were considered per station and totalled across all stations to characterise the zooplankton community.

## 3.3 Results

### 3.3.1 Classification of backscatter into acoustic groups

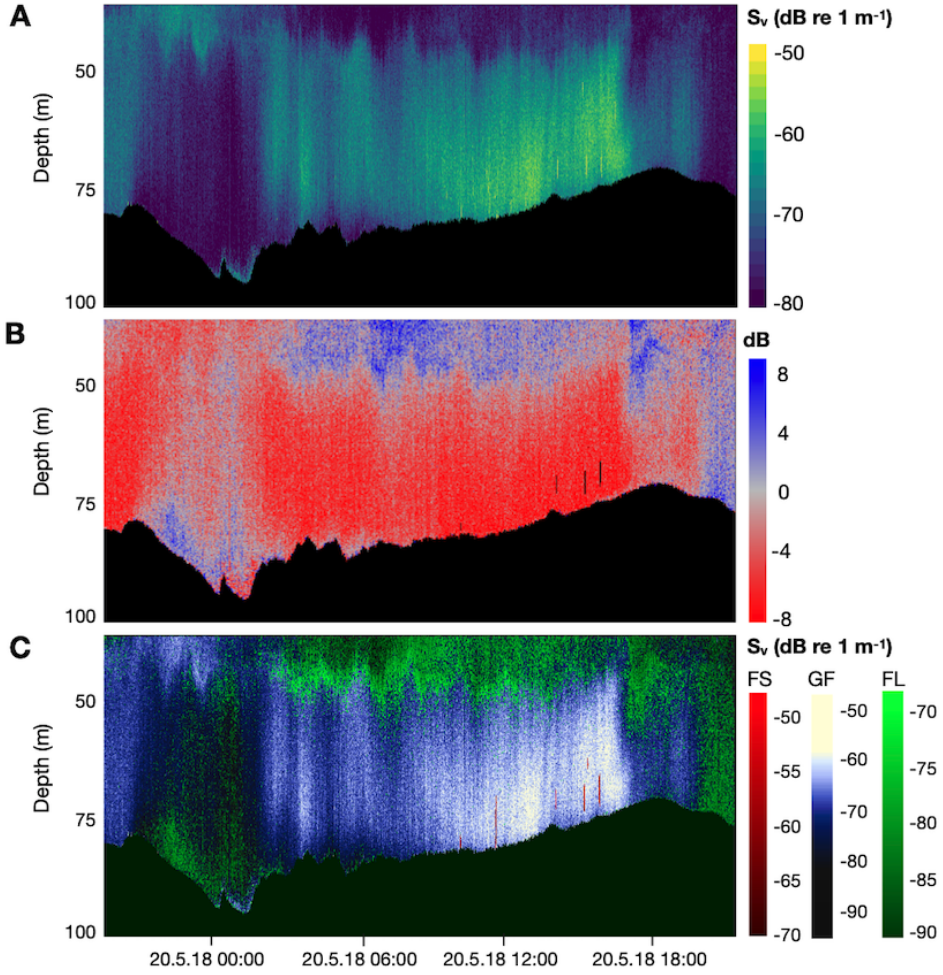


Figure 3.3.1: **Echograms depicting the classification process within the analysis layer, Transect 8.** Panels show: A) MVBS at 70 kHz; B) $\Delta$MVBS$_{200-70}$ for differentiating gas-filled and fluid-like groups; and C) synthetic echogram depicting MVBS$_{70}$ for each group with corresponding colour scales. Regions acoustically dominated by fish schools (FS) are shown in red, gas-filled organisms (GF) in blue to white, and fluid-like scatterers (FL) in green. Regions outside the analysis layer are black.

Classification of the backscatter data into three groups corresponded to partitioning echograms into three distinct regions: FS, 'hotspots' of strong backscatter generally found close to the bottom during daytime; the main SSL, primarily comprised of GF backscatter, which was stronger towards the (vertical) middle of the layer and which displayed a clear diel vertical movement pattern; and more diffuse FL backscatter apparent in regions where

the GF layer was absent. Regions of FL backscatter were interspersed throughout the echograms, separated by the main GF layer. These regions were usually found above the GF layer during daytime and below it during the night. This is exemplified in the synthetic echogram shown in Figure 3.3.1, where FL backscatter (visualised in green) is only apparent in the deeper part of the analysis layer for a few hours around midnight on the 20$^{th}$ and 21$^{st}$ of May, and only apparent in the shallower part of the analysis layer during the intervening daytime.

Fluid-like organisms may well have been present where gas-filled organisms dominated the acoustic backscatter; strong signals from gas-filled organisms mask those of weaker fluid-like scatterers, even when the latter occur in higher densities (Lavery et al., 2007). In the echograms, unaveraged cell dB-differences transitioned across $0\,\mathrm{dB}$ with a fairly smooth gradient; this smooth transition is also reflected by the unimodal distribution of cell values in the dB-difference histogram of combined GF and FL backscatter (Figure 3.3.2). Sampling volumes are likely to contain a mixture of fluid-like and gas-filled organisms. The smooth transition across $0\,\mathrm{dB}$ could have been due to density ratios of FL:GF gradually changing to the point where one signal type dominated the other. This fits with the observation that the GF backscatter was strongest near the vertical centre of the layer, gradually reducing above and below. Although inconclusive, this hints that there could have been a ubiquitous backdrop of fluid-like scatterers against which a conspicuous gas-filled layer displayed classic nocturnal DVM behaviour.

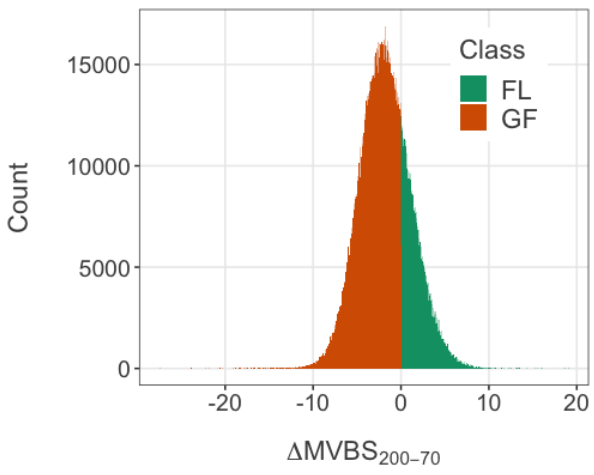


Figure 3.3.2: **Histogram of unaveraged dB-difference cell values ($\Delta$MVBS$_{200-70}$) from which the GF and FL groups were determined.** Data from only one transect shown due to computational demands.

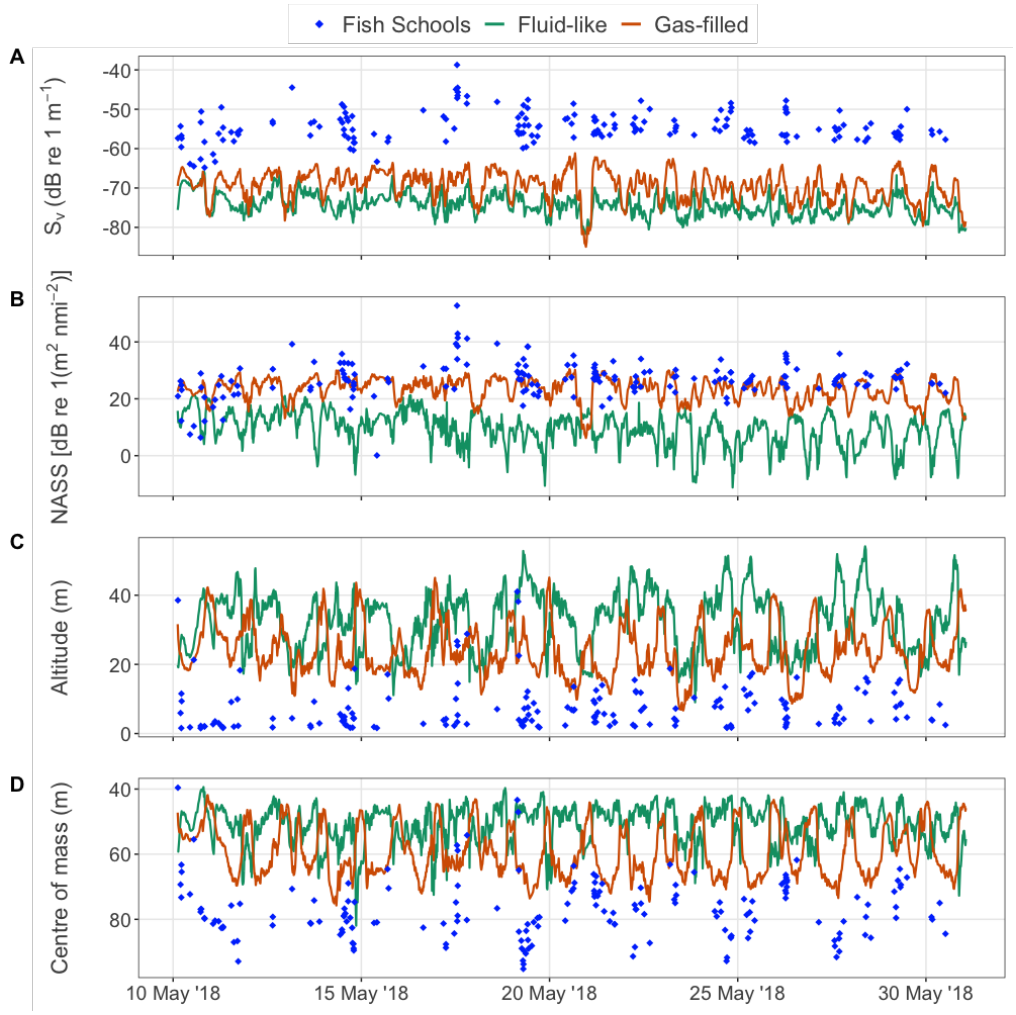


Figure 3.3.3: **Time series of energetic and positional properties of each group: fish schools (blue), gas-filled (orange) and fluid-like (green) zooplankton.** A) Mean backscatter ($S_v$), a proxy for density, B) nautical area scattering strength (NASS), a proxy for biomass, C) altitude, height above the bottom, and D) depth of the centre of mass.

The patterns that each group exhibited were fairly consistent throughout the time series (Figure 3.3.3). There was no obvious temporal trend in fish school energetic or positional properties, however there was a pattern whereby detections were clustered during daytime periods and fish schools were generally not detected at night. FS energetic and positional properties were variable, however the degree of variability remained fairly constant throughout the time series. Similarly, there was no obvious trend in GF and FL energetic and positional properties. Properties of these groups exhibited greater variation within 24-hour periods than across the time series. GF and FL backscatter appeared positively correlated in the time series (Figure 3.3.3, A), however both NASS and positional metrics appeared inversely correlated, such that peaks in GF backscatter generally coincided with troughs in

backscatter (and vice versa) (Figure 3.3.3, B-D). This could be due to acoustic masking of FL signals by GF scatterers.

Energetic properties of the three groups followed the expected hierarchy, with fish schools having the largest NASS and strongest backscatter at 70 kHz, fluid-like regions having low NASS and weakest backscatter, and the gas-filled layer having middling values (Figure 3.3.4, left and middle columns). FS had the widest range of dB-difference values, ranging from $-28$ to 2 dB, which entirely overlapped the dB-difference range of the GF group and partially overlapped the dB-difference range of the FL group (Figure 3.3.4, right column). Fish schools and gas-filled organisms were both predicted to resonate at low frequencies and thus produce a negative dB-difference, with resonance of fish schools predicted to be strongest. The strongly negative dB-differences of some schools fits with expectations, however the few schools with positive dB-difference do not.

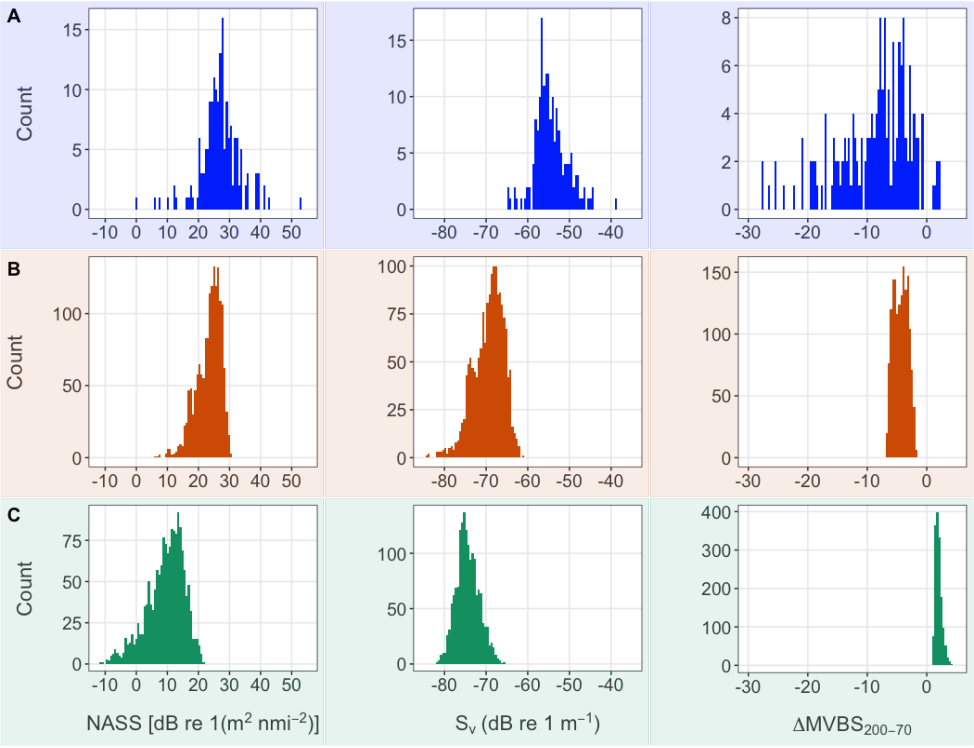


Figure 3.3.4: **Histograms of group energetic properties.** Nautical area scattering strength (NASS), mean volume backscatter ($S_v$) and dB-difference ($\Delta\text{MVBS}_{200-70}$) binned values shown for A) fish school, B) gas-filled, and C) fluid-like groups.

The apparent lack of GF dB-difference values close to $0\,\mathrm{dB}$ was an artefact of averaging (primarily the vertical averaging, but also across the $600\,\mathrm{m}$ bins) and not an indication that the GF and FL groups were energetically distinct at the resolution of cells (Figure 3.3.4, right column in B). Positive dB-difference of the binned FL group was centred around values just below $2\,\mathrm{dB}$, however the positive shift in mode compared to Figure 3.3.2 (where the FL mode was close to $0\,\mathrm{dB}$) is due to effects of averaging.

### 3.3.2 Composition of acoustic groups

#### Fluid-like and gas-filled groups

Net samples contained a diversity of invertebrate zooplankton and some icthyoplankton. Hydrozoa, echinoderm larvae, and chaetognaths were prevalent. However, samples were numerically dominated by small crustaceans, notably calanoid copepods. In sufficient numbers, chaetognaths have the potential to contribute significantly to backscatter (Mair et al., 2005). However, net samples suggest that the abundance of calanoid copepods outnumbered chaetognaths by a factor of twenty-eight. Thus, their contribution to the backscatter of the FL group was likely negligible, assuming they occurred within the same acoustic sampling volumes as other zooplankton such as copepods and euphausiids (Fielding et al., 2004; Benfield et al., 1998). Calanoid copepods were considered to be the dominant acoustic scatterers at $70\,\mathrm{kHz}$ in the FL group, and the distribution of FL backscatter was therefore considered to be largely representative of their distribution in the water column. *Calanus helgolandicus* (as opposed to *Calanus finmarchicus*) dominated the subsamples of CVI Calanus sp identified from the net samples (average $80\,\%$). Total numerical abundances of counted individuals from subsamples and their acoustic-group assignations can be found in Appendix G. At every station, more than $99.5\,\%$ of identified organisms were categorised as fluid-like or elastic-shelled scatterers, placing them within the FL group.

There were a few organisms sampled that could potentially have been gas-filled scattering types. These were fish larvae of sufficient size to potentially contain an inflated swimbladder, and gas-bearing siphonophores. Larval swimbladdered fish typically inflate their

swimbladders when they reach a critical length. Cod inflate their swimbladders when they have grown to at least $5\,\mathrm{mm}$ in length (Yin and Blaxter, 1986); for anchovy when larvae reach $10\,\mathrm{mm}$, although inflation may occur in individuals as small as $6\,\mathrm{mm}$ (Hunter and Sanchez, 1976); and for herring when larvae reach at least $22\,\mathrm{mm}$ (Blaxter et al., 1981; Folkvord et al., 2020). Based on this, fish larvae larger than $6\,\mathrm{mm}$ were assigned to the gas-filled group; smaller fish larvae were assigned to the fluid-like group. Physonect siphonophores such as *Nanomia cara* and *Agalma elegans* contain a gas-filled pneumatophore (one per individual) used to alter buoyancy and are known to occur in the North Sea (Conway, 2012). The sampling of *Nanomia* nectophores at several stations and the sampling of at least thirty gas-bearing individuals in a single sample (inferred from pneumatophore count) suggests that physonect siphonophores were not uncommon in this region.

The overwhelming dominance of organisms assigned to the FL group in net samples likely reflects the inability of nets to adequately sample gas-filled organisms. Larger fish larvae and juvenile or adult fish with gas swimbladders may have sufficient swimming capability to avoid net capture (Skjoldal et al., 2013). Gelatinous organisms are notoriously difficult to sample using nets as their fragile bodies are easily damaged, with fragments easily passing through the mesh (Proud et al., 2019; Frost et al., 2012). Even accounting for the variable catchability of organisms, it could still have been the case that fewer gas-filled than fluid-like scatterers were present (or that there was lower biomass of gas-filled scatterers), since even at lower densities their strong acoustic response can dominate backscatter of fluid-like scatterers (Warren et al., 2001).

**Fish schools**

In total $175$ fish schools were detected in the analysis layer. The vast majority ($n = 167$) were observed during daytime; only seven were observed during twilight and only one during nighttime. Fish schools were typically found close to the bottom, between $60$ and $80\,\mathrm{m}$, with only three schools having a centre of mass shallower than $50\,\mathrm{m}$ (Figure 3.3.5, A & B). Elongation, the ratio between length and thickness of a school, was generally lower

than 200 (Figure 3.3.5, C). Horizontal lengths ranged from several tens to hundreds of metres, however most schools were detected over less than $250\,\mathrm{m}$ along-track (Figure 3.3.5, D). Distributions of fish school properties were continuous, with a few notable outliers in size, energetics and position in the water column, demarcated by the dashed lines in Figure 3.3.5. These schools had otherwise unremarkable characteristics, leaving little reason to conclude that particular parameters could distinguish schools into disparate groups. The majority of schools had a strongly negative dB-difference, indicating the presence of gas bubbles within these scatterers (i.e. swimbladders).

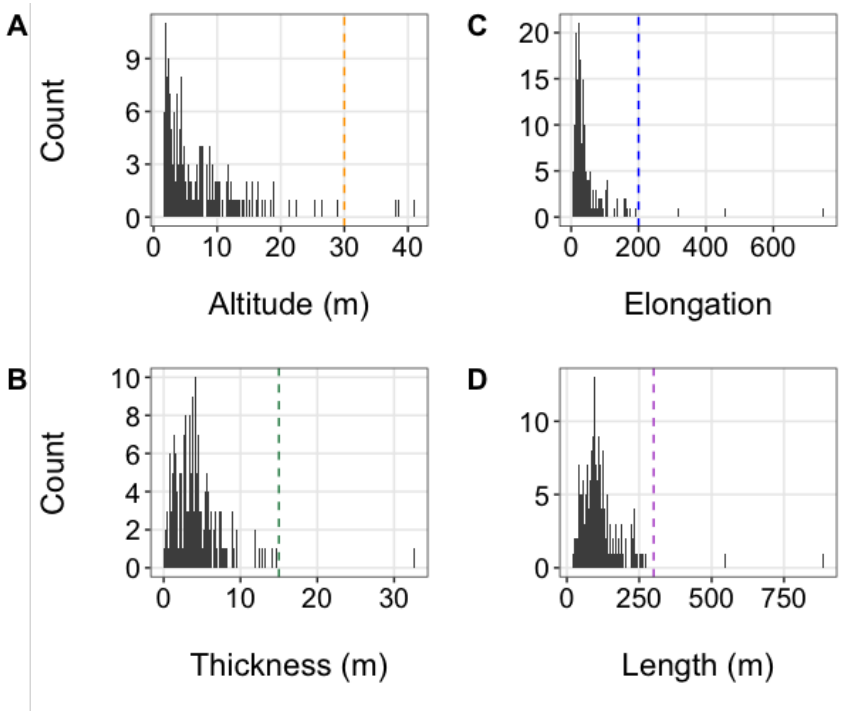


Figure 3.3.5: **Histograms of fish school positional and morphometric properties.** Distributions of A) altitude, B) thickness, C) elongation, and D) length are unimodal and positively-skewed. Outliers were defined according to the coloured dashed lines (outliers to the right). The fish schools with altitudes above $30\,\mathrm{m}$ had centres of mass above $50\,\mathrm{m}$. The single school with thickness $> 15\,\mathrm{m}$ had a NASS value far exceeding those of other schools. Two school lengths exceeded $250\,\mathrm{m}$ and three schools exceeded elongation ratios of $200$.

Fish school composition, dimensions, movement, formation and disaggregation are dynamic; schooling often reflects functional dependencies rather than direct associations with the diel cycle or typified behaviour for species (Bertrand et al., 2006; Laurel et al., 2004; Kaltenberg and Benoit-Bird, 2009). Nevertheless, morphometric properties, position (e.g. depth in the water column), and diel behaviour of acoustically-detected schools can help to discriminate between species (D'Elia et al., 2014; Gastauer et al., 2017; Scalabrin and Massé, 1993) and even between schools, *sensu stricto*, and other aggregations of fish (Benoit-Bird and Waluk, 2021). Overall, schools had broadly similar properties and may therefore have been comprised of the same species; a likely candidate being Atlantic herring (*Clupea harengus*). This conclusion is based on several known facts: herring are widespread in the North Sea during spring and summer; they have a propensity to school near the bottom during daytime (Beare et al., 2002b), forming schools of variable dimensions (Misund, 1993) that disperse at night, which could render them less detectable using the SHAPES fish school detection algorithm after applying the fixed $-57\,\mathrm{dB}$ threshold; and they have a high target strength resulting in estimates of school backscatter that range between $-40$ to $-45\,\mathrm{dB}$ re $1\,\mathrm{m}^{-1}$ at $38\,\mathrm{kHz}$ (Beare et al., 2002b).

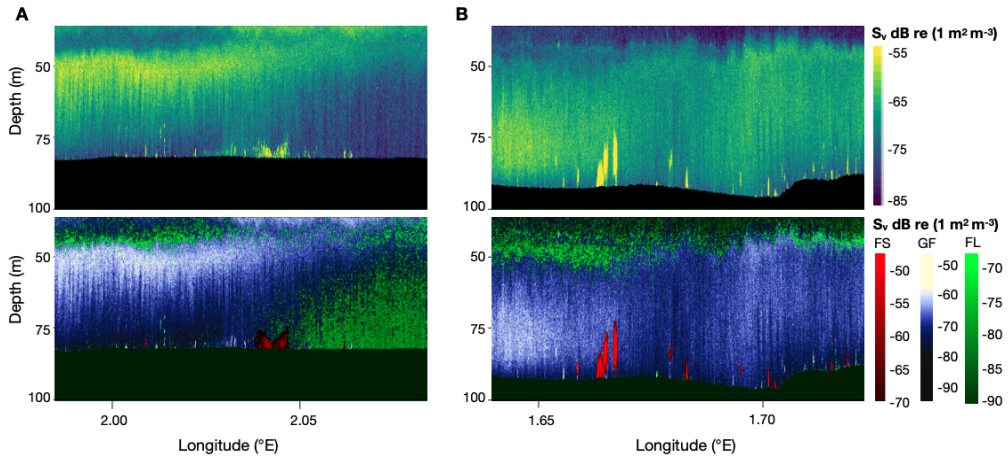


Figure 3.3.6: **Examples of fish school shapes, as viewed in echograms, from A) Transect 1 and B) Transect 7.** Top panels show backscatter at $70\,\mathrm{kHz}$, lower panels show classified backscatter. A) shows a diffuse, elongated school that stretched more than $900\,\mathrm{m}$ horizontally. B) shows the typical fish school shapes observed, which present as compact pole-like structures (although all schools were in reality longer than they were tall).

Fish schools appeared as pole-like structures in the echograms except for a single, more diffuse school, better described as a tower-shaped school, sensu Petitgas and Levenez (1996) (Figure 3.3.6). However, the appearance of schools in echograms can be somewhat misleading, as horizontal and vertical scalings differ greatly in typical echogram presentation. In actuality, all schools were longer horizontally than they were tall, with elongation values greater than 1 (dashed line in Figure 3.3.7, A).

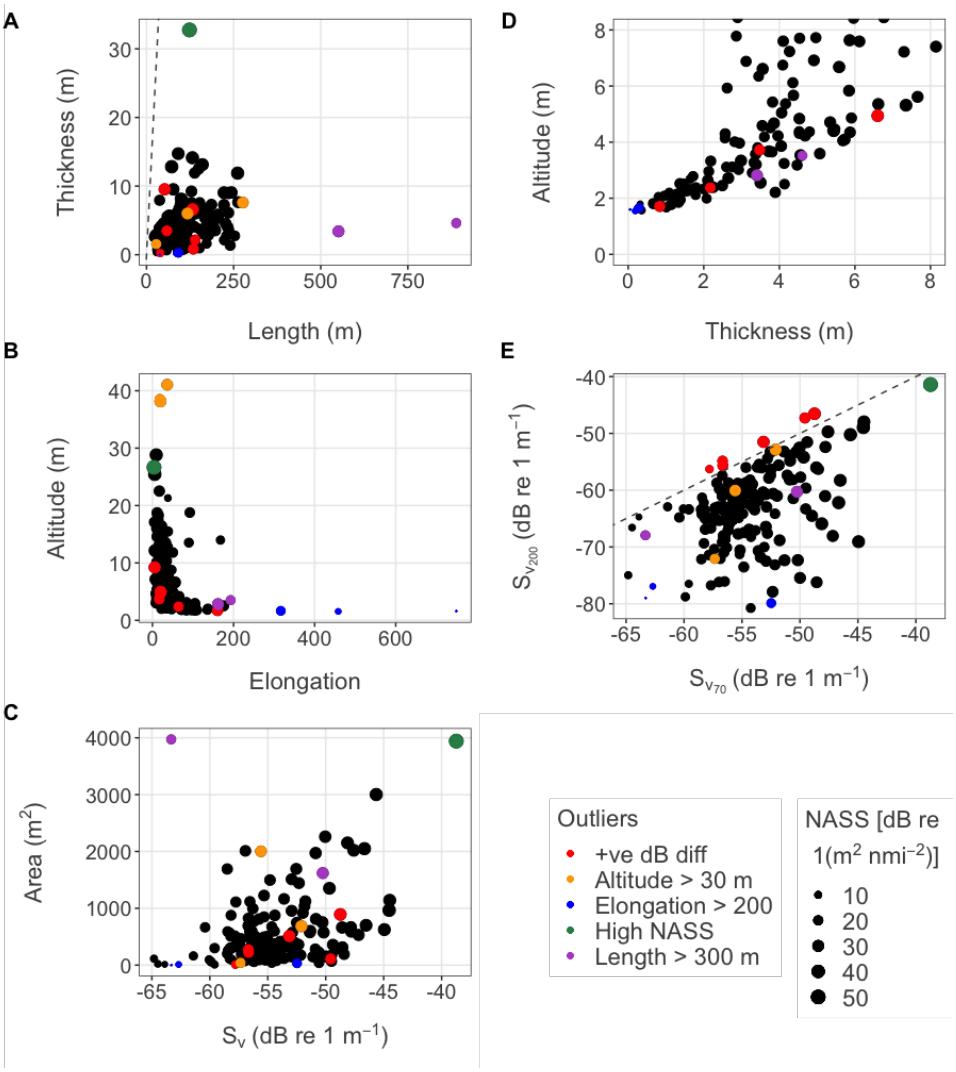


Figure 3.3.7: **Fish school positional, energetic and morphometric properties.** Coloured points indicate outliers. Dashed lines in A) marks 1:1 ratio of thickness to length and E) $\Delta\text{MVBS}_{200-70} = 0$. All fish schools are shown except in D) which is constrained to maximum $8\,\text{m}$ thickness and $8\,\text{m}$ altitude to highlight effect of near-bottom cut-off.

Schools travelling at speed are known to elongate along their direction of travel and thin out cross-ways (Kent et al., 2019). This provides hydrodynamic benefits and enhances information transfer within schools. Variability in elongation and length is therefore expected even when sampling similar sized schools, since schools may be encountered at different angles relative to their direction of travel and at different relative speeds. Two schools had particularly extreme elongation ratios (Figure 3.3.7, blue points), seemingly driven by low thickness values. Panel B in Figure 3.3.7 suggests that these schools were very close to the bottom, situated across the lower boundary of the analysis layer (approximately $2\,\mathrm{m}$ above the bottom), extending below it and thus may have been taller than reported. These schools did not show any remarkable distinguishing energetic characteristics: NASS values were characteristic of small schools, being between $0.1$ and $18.5\,\mathrm{dB}$ re $1(\mathrm{m}^2\ \mathrm{nmi}^{-2})$; with $\Delta\mathrm{MVBS}_{200-70}$ ranging between $-27$ and $-14\,\mathrm{dB}$.

Larger schools had greater NASS and $S_v$ than smaller schools (Figure 3.3.7, C). Assuming similar species-composition amongst schools, greater NASS may indicate higher biomass due to larger body sizes or increased abundance and fish packing densities, both of which would be reflected by stronger average backscattering (Misund, 1993). NASS mostly ranged between $0.1$ to $41.2\,\mathrm{dB}$ re $1(\mathrm{m}^2\ \mathrm{nmi}^{-2})$ (mean $26.8 \pm 6.3$), although one very large and strong outlier had a NASS value of almost $53\,\mathrm{dB}$ re $1(\mathrm{m}^2\ \mathrm{nmi}^{-2})$. This particular school was anomalously thick, extending more than $32\,\mathrm{m}$ vertically, and had the lowest elongation value ($E = 3.8$) found (Figure 3.3.7, green points in A-C) and its large NASS value resulted from both its size and strong backscatter ($-39\,\mathrm{dB}$ re $1\,\mathrm{m}^{-1}$ at $70\,\mathrm{kHz}$).

Thicker schools remained close to the bottom at their deepest extent. Their extension vertically upwards had the effect of decreasing the depth of their centre of mass. However, this apparent shallowing should not necessarily be interpreted as evidence that larger schools preferred shallower habitat. Rather, larger schools spread out in all available directions (horizontally and vertically upwards), maintaining their tendency towards close proximity to the bottom (Figure 3.3.7, D).

The schools that extended farthest horizontally (long schools, purple points in Figure 3.3.7) were detected over distances of more than $300\,\mathrm{m}$ but otherwise had unremarkable positional

and energetic properties. In the echograms, one school appeared as a well-defined pole-like structure and was detected across more than $500\,\mathrm{m}$ along-track during a period of high winds where speeds reached over $14\,\mathrm{m\,s^{-1}}$. This school was represented by only ten pings after eight intervening pings had been removed in data cleaning. It is possible that excessive ping removal during poor weather resulted in schools in close proximity appearing as a single entity. The longest school, detected over almost $900\,\mathrm{m}$ along-track, had patchy and diffuse backscattering in both vertical and horizontal directions, quite unlike all other pole- or globular-like school structures (Figure 3.3.6, A). This school was detected during a period of calm weather where wind speeds were slower than $2\,\mathrm{m\,s^{-1}}$, thus horizontal resolution was high. It may represent an aggregation of a different fish species, possible candidates being cod or whiting since gadoids are known to form looser aggregations than most pelagic forage fish and their shoals often stretch out for hundreds of metres along the bottom (Mello and Rose, 2005; Burgos et al., 2008).

Schools with a positive dB-difference (Figure 3.3.7, red points) had similar morphometric, positional and energetic properties to those with negative dB-difference expected of swimbladdered fish. Plot E in Figure 3.3.7 suggests that MVBS of positive dB-difference schools were not remarkable at either 70 or $200\,\mathrm{kHz}$, and many fish schools had dB-difference values close to zero (dashed line). Inspection of echograms ruled out the possibility of accidental bottom contamination in the $200\,\mathrm{kHz}$ data within these schools, a possibility since the bottom line was defined using $70\,\mathrm{kHz}$, and transducers were operated asynchronously. Positive dB-difference may reflect contamination by other scatterers within the sampling volume or variation in acoustic reflectivity due to, for example, behaviour such as a change in net orientation. Alternatively, positive dB-difference may have resulted from sampling volume mismatches due to ping asynchrony and differing transducer beam-widths.

### Windspeed-related bias in fish school detections

Fewer schools were detected during windier weather, and those that were appeared to have stronger backscatter, greater NASS, and were longer horizontally (Figure 3.3.8). The rate of detections, standardised by daytime hours, during wind speeds greater than $5\,\mathrm{m\,s^{-1}}$ was less

than half the rate during calmer weather. Median school lengths differed by $30\,\mathrm{m}$ when detected during calm ($< 5\,\mathrm{m\,s^{-1}}$) versus windy ($> 7.5\,\mathrm{m\,s^{-1}}$) conditions. Kolmogorov-Smirnoff tests comparing NASS, $S_v$ and length in calm and windy conditions were significant ($p < 0.01$). No biological reason could be found in the literature to explain why there would be fewer schools during windy weather. Horizontal sampling resolution was reduced during windy weather due to two compounding effects: reduced data quality meant that a higher proportion of pings had to be removed, and higher winds resulted in faster transit speeds due to increased surface wave activity (Chapter 2). Lower horizontal sampling resolution may have decreased the probability of detecting schools, particularly small schools, and those that were detected may have contained a lower ratio of pings that sampled the edge of schools versus the centre of schools. Sampling volumes at the edge of schools contain both fish and non-fish backscatter, and therefore pings that sample the edge of schools may have lower backscattering strength. With fewer edge detections during windy weather, NASS and MVBS could therefore appear higher.

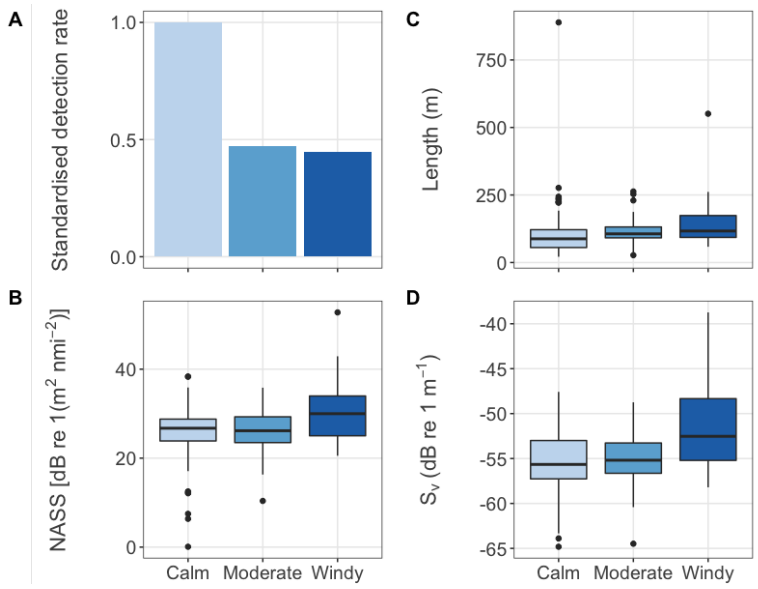


Figure 3.3.8: **Fish school detection bias due to wind speed.** Detection rates were standardised by hours of daytime. Wind speed categories are: calm $< 5\,\mathrm{m\,s^{-1}}$, moderate 5 to $7.5\,\mathrm{m\,s^{-1}}$, and windy $> 7.5\,\mathrm{m\,s^{-1}}$.

### 3.3.3 Diel patterns of each acoustic group

The GF layer exhibited a clear DVM signal, visible by eye in the echograms. Figure 3.3.9 shows variation in position and energetics according to time of day for the GF class. Echogram regions classified as FL or FS showed no visible signs of DVM; however, regular changes in energetic and positional properties were observed each day.

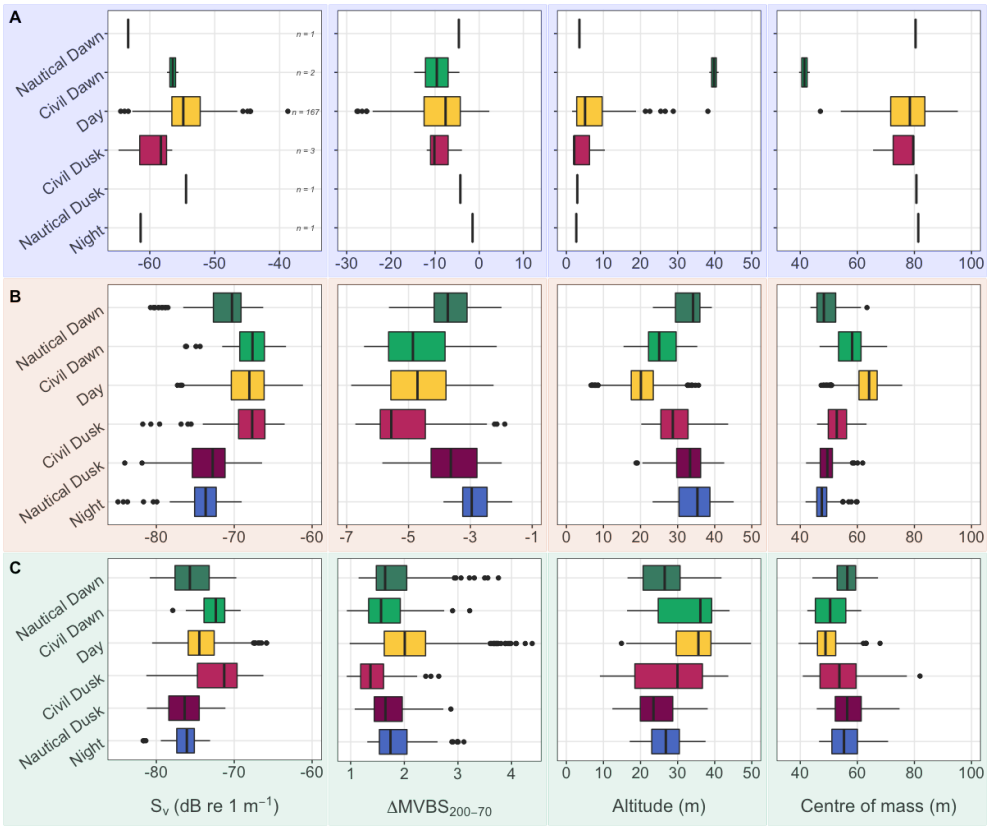


Figure 3.3.9: **Diel variation in energetic and positional descriptors for each acoustic group.** Boxplots show energetic descriptors (backscattering strength, $S_v$; dB-difference, $\Delta\text{MVBS}_{200-70}$) and positional descriptors (altitude and centre of mass) for A) fish schools (blue background); B) gas-filled (orange background); and C) fluid-like (green background) groups. Fish school detections outside of daytime were rare (n=1).

#### 3.3.3.1 Fish schools

There was a clear diel rhythm in fish school presence and absence, however no evidence of DVM was apparent from school properties (Figure 3.3.9). Although positional and energetic properties varied throughout each day, these variations lacked an obvious cyclical pattern.

Pelagic schooling fish are known to disperse into loose aggregations at nightfall or disperse individually, often moving to shallower regions of the water column to forage. In lower numerical densities, these fish may not reflect the acoustic signal sufficiently to exceed the detection threshold that I used. Even if they do, the reduction in contiguity of sufficiently strong backscatter may have precluded their detection by the SHAPES algorithm. The lack of fish school detections during nighttime was therefore most probably a consequence of the disaggregation of schools at dusk. Alternatively, schools may have moved out of the analysis layer, either below (within $2\,\mathrm{m}$ of the bottom) or above $36\,\mathrm{m}$ depth. However, I did not observe any tendency for schools to move towards these depths during twilight.

The low number of fish school observations outside of daytime prevented statistical analysis of schools detected during twilight when vertical migration, if exhibited, was expected to occur. Properties of the seven schools observed outside of daytime were within typical ranges observed for schools observed during daytime. Intriguingly, inspection of backscatter prior to smoothing for classification revealed specks of high backscatter during the night throughout the analysis layer (Figure 3.3.10). These specks were often $> -55\,\mathrm{dB}$, and spanned across a single ping in width and between $20$ to $30\,\mathrm{cm}$ vertically. Similar distributions of these specks were not evident during the daytime. This raises the possibility that these specks were fish that had dispersed from their daytime schools.

#### 3.3.3.2 Fluid-like scatterers

Diel changes in vertical position of the FL group suggest a reverse DVM pattern because the centre of mass shallows during the day and deepens at night. However, these apparent movements could be an artefact of acoustic masking by the GF group. During the day, the GF layer was pervasive through much of the analysis layer but generally stayed below $45\,\mathrm{m}$. This left a shallow region at the top of the analysis layer where FL signals could be observed. At night, the GF layer moved up revealing FL signal in the deepest regions of the analysis layer. Consequently FL vertical movements appeared as the inverse of the GF classic DVM pattern. Statistical plots obscure detail traces of FL regions switching above and below the GF layer at twilight, however echograms depict this transition well (Figure 3.3.1).

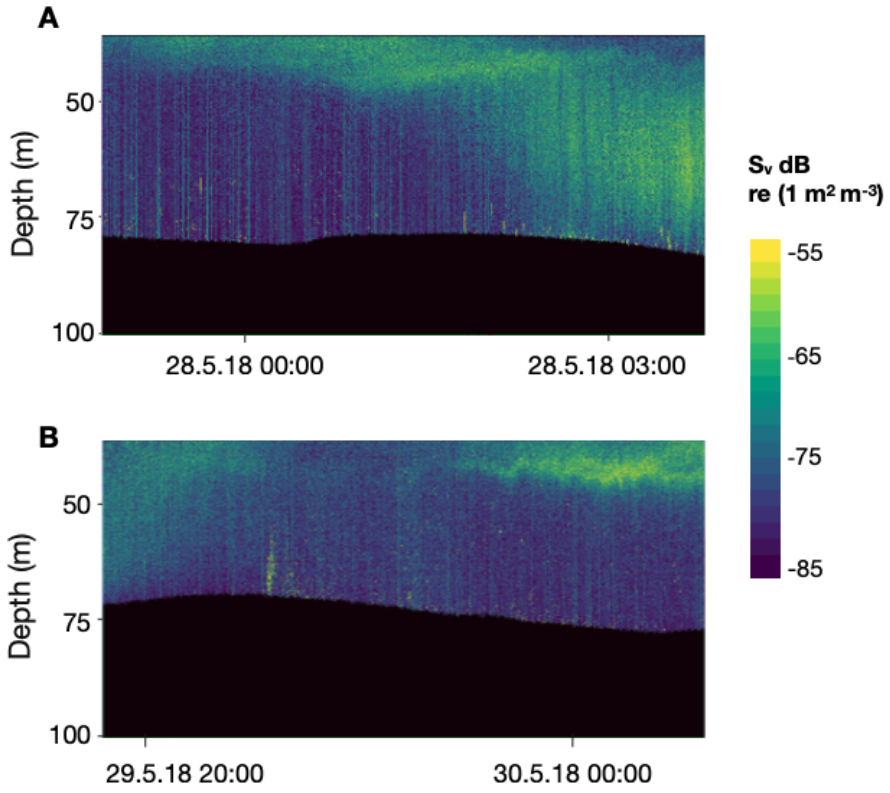


Figure 3.3.10: **70 kHz echograms depicting possible dispersed gas-bladdered fish.** Speckles of strong backscatter (yellow) observed during twilight and night could be dispersed gas-bladdered fish. Examples are taken from Transect 14 (A) and 15 (B), although this phenomenon was observed during numerous nighttimes throughout the mission. MVBS shown prior to application of 3x3 median filter, after which most of the speckled backscatter were filtered out.

Copepod vertical distributions and migration amplitudes may be structured according to body size (Aarflot et al., 2019; Ohman and Romagnan, 2016). Larger individuals tend to occupy deeper regions of the water column, with those that perform classic DVM ascending towards the surface later than smaller individuals that occupy shallower regions of the water column. Time of day and depth were confounded in FL measurements as data from deeper regions were only available during the night, and data from shallower regions only available during the day. Consequently the FL communities observed acoustically at night and day are likely to have differed. Diel changes in FL dB-difference (Figure 3.3.9, C) could reflect shifting ratios of GF and FL scatterers as well as changes in scatterer orientation, but also could be due to sampling different populations at different depths. Without additional data from, for example, depth stratified net samples it was not possible to determine whether

the FL group undertook DVM of any kind. However, literature suggests that many of the zooplankton species abundant in our net samples do perform vertical migrations (Angel and Pugh, 2000; Hays et al., 1996).

#### 3.3.3.3 Gas-filled scatterers

The gas-filled scattering layer was deepest during daytime with a centre of mass typically below $60\,\mathrm{m}$ (around $20\,\mathrm{m}$ above the bottom) and shallowest at night with centre of mass typically above $50\,\mathrm{m}$ (about $35\,\mathrm{m}$ above the bottom). The layer remained at depth from early morning until the late afternoon when it began to rise towards the surface (Figure 3.3.11). During daytime, the GF layer was contained within the analysis layer. Backscatter was heterogeneously distributed such that the (vertically) central region of the layer was strongest. Consequently both MVBS and NASS were lowest at night when the bulk of the layer, including the strong central region, ascended above the $36\,\mathrm{m}$ upper limit of the analysis layer.

Twilight marks the period when light levels dramatically change. This transition was mirrored by rapid change in both vertical position and energetic properties. An asymmetry between upwards and downwards movements of the layer was apparent; evening ascents were more gradual than the comparatively rapid morning descents. The difference between average day and night acoustic centres of mass produced an estimate of DVM amplitude over $15.5\,\mathrm{m}$. Although this does not sound particularly large, this constitutes almost $20\,\%$ of the average water depth. Foraging success rate of visual fish predators in epipelagic waters - and hence mortality risk of their zooplankton prey - is considerably impacted by only small depth variations due to the exponential decay of light with depth (Aarflot et al., 2020).

Daily amplitude and migration timing were difficult to ascertain on a day-to-day basis due to high intra-diel variability in the centre of mass and altitude, which meant that the daytime 'resting' depths were rarely static (Appendix H). In shallow systems such as the North Sea, both bathymetry and light exert a strong influence on vertical distributions of zooplankton (Aarflot et al., 2019). This created difficulties in distinguishing whether changes in depth were transient, resulting from modulations to the competing influences of light and available water column depth, or demarcated the 'beginning' of synchronised migrations. Average

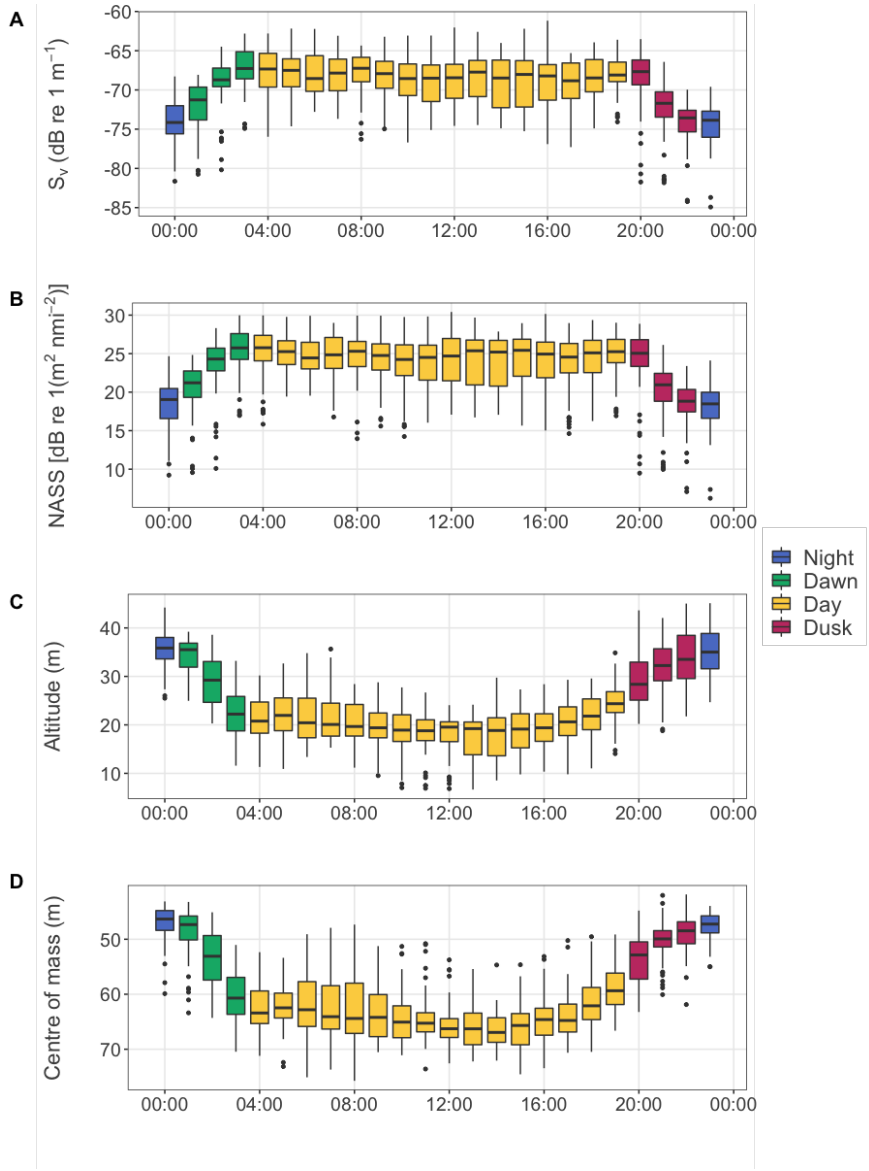


Figure 3.3.11: **Boxplots of hourly averaged energetic and positional properties for the gas-filled group.** Upper panels show energetic properties; A) mean volume backscattering strength ($S_v$, a proxy for animal density), and B) nautical area scattering strength (NASS, a proxy for biomass). Lower panels show position of the centre of mass in relation to C) the bottom and D) the surface.

migration timing was determined based on the combination of sustained movements of both centre of mass and altitude in grouped data. Descents took place over approximately 3 hours between 1am and 4am, whereas ascents began around 5pm and continued through the evening and even after midnight (Figure 3.3.11, C & D). These figures produced conservative descent and ascent rate estimates of $1.4\,\mathrm{mm\,s^{-1}}$ and $0.7\,\mathrm{mm\,s^{-1}}$ respectively (average amplitude of $15\,\mathrm{m}$, occurring over three and six hour time-windows) for the GF layer.

Echograms revealed that the lower part of the GF layer tended to rise from the near-bottom at around 8pm and descended back to the near-bottom around 3am. This pattern was consistent throughout the mission. The descent coincided with the mass downward movement of the layer; in this respect the layer appeared to move synchronously with changes in energetic properties coinciding with changes in positional metrics. In contrast, organisms near the bottom of the layer began to ascend a couple of hours after the centre of mass of the layer began to ascend, suggesting that some scatterers remained at depth for longer. The upper part of the layer appeared to ascend and descend more gradually, often with upwards movement initiated before 6pm. These seemingly differential rates of vertical motion throughout the layer suggest that, rather than the whole layer moving in concert, organisms occupying different regions of the water column migrated upwards at different times and rates. This may explain why the reductions in energetics around dusk do not follow the same gradient as the upwards movement of the layer (Figure 3.3.11), which could be explained by the fact that different species and size-classes likely occupy different vertical strata within the layer. The differential movement, seen only in the latter part of the day, may reflect behavioural decision-making by organisms rather than physical constraints on distribution alone (Aarflot et al., 2020; Cerbin et al., 2003; De Robertis et al., 2000).

The dB-difference of the GF group shows a diel pattern of lower values during the day (median $3.0\,\mathrm{dB}$) than the night (median $4.7\,\mathrm{dB}$) (Figure 3.3.9). Lower dB-difference at night could reflect a reduced ratio of GF to FL scatterers caused by the migration of the GF layer outside the analysis layer.

At civil dusk, scatterers in the deepest regions of the layer began to ascend. On several occasions, a diffuse layer was seen joining the GF layer by moving upwards from the near-bottom during the later stages of the ascent of the deepest regions of the GF layer. Curiously, dB-difference was most negative during civil dusk, which generally occurred between 7-9pm during that time of year. These diffuse layers were probably comprised of bentho-pelagic fish. Bentho-pelagic fish in the North Sea, such as cod, plaice, and some flatfish, are often demersal during the day, taking refuge in habitat on the seafloor, but move into the water column at night (Beamish, 1966). These fish do not always ascend to near-surface waters; instead their daily movement pattern can be better described as

bottom-dwelling during the day, and off-bottom at night. This behaviour provides an alternative strategy to reduce the risk from pelagic, visual predators. Bentho-pelagic fish are generally larger and more opaque than siphonophores. This makes them relatively conspicuous, necessitating their occupation of darker (deeper) habitat to reduce their vulnerability to predation (Giske et al., 1994), which may manifest as a delayed ascent in comparison to smaller or more translucent organisms. The upwards migration of these fish could have contributed to the observed changes in dB-difference, particularly those fish with swimbladders. Changes in orientation associated with upward swimming during dusk are another factor that may have contributed to the changes to dB-difference observed at dusk.

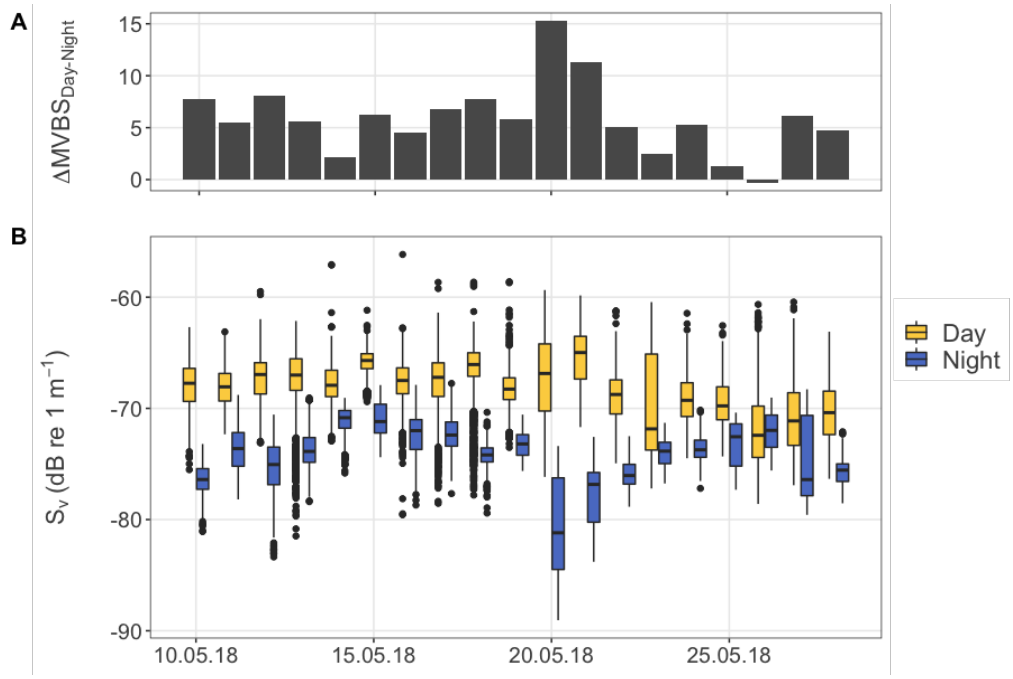


Figure 3.3.12: **Differences between average 70 kHz daytime and nighttime backscatter of the gas-filled group.** A) dB-difference between median backscatter during daytime and the following night. B) backscatter distributions during each day and night period.

Median daytime backscatter was usually stronger than the previous and following nighttime periods (Figure 3.3.12). An exception occurred on the 26$^{th}$ of May where median daytime backscattering was lower than backscatter the following night. This apparent reversal was caused by particularly low daytime backscatter sampled over the eastern edge of the transect. Here, backscatter tended to be weaker and the SSL appeared depressed despite shallower bathymetry. DVM intensity varied on a daily basis by an average of $5.6\,\mathrm{dB} \pm 3.5\,\mathrm{dB}$,

representing an almost fourfold increase in backscatter during day compared to night.

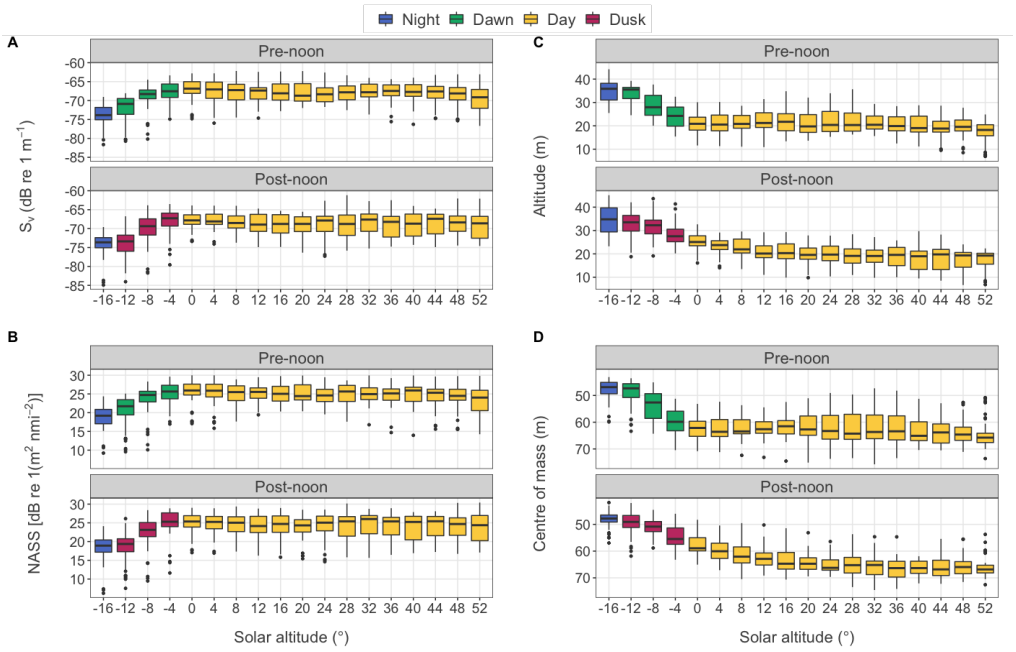


Figure 3.3.13: **Boxplots of energetic and positional metrics for the gas-filled group, averaged by $2°$ solar altitude intervals and separated into pre- and post-noon periods.** Panels on the left show energetic properties; A) mean volume backscattering strength ($S_v$, a proxy for animal density), and B) nautical area scattering strength (NASS, a proxy for biomass). Panels on the right show position of the centre of mass in relation to C) the bottom and D) the surface.

To investigate whether ascent and descent cues were related to light levels, positional and energetic metrics were plotted as a function of solar altitude, split by noon to reveal differences between dusk and dawn (Figure 3.3.13). The layer descended prior to sunrise with movements initiated around the point when the sun was $-12°$ below the horizon, and it ceased descent by the time the sun reached the horizon at $0°$. By contrast, the layer began to ascend when the sun was still above the horizon, with movements initiated when solar elevation angles were as high as $12°$. This means that afternoon ascents were probably initiated when light levels were higher than those at the point when the layer ceased its descent. Whilst positional metrics exhibited clear asymmetry during transitional periods, changes in energetic metrics occurred only during nautical twilight, and the gradient of change was symmetrical between dawn and dusk. This could have been caused by symmetrical movements of the layer into and out of the analysis layer ($36\,\mathrm{m}$) about the time of the solar zenith. Although ascents appeared more gradual than descents, earlier initiation may have resulted in the centre of mass reaching similar depths by nautical dusk and dawn (Figure 3.3.13, C & D).

## 3.4 Discussion

DVM of zooplankton and fish has been studied for over 200 years in aquatic systems across the globe (Bandara et al., 2021; Conroy et al., 2020; Hobbs et al., 2018; Fischer et al., 2015; Liu et al., 2022). Consequently, there exists a huge volume of studies on DVM behaviours, particularly for copepods, fish, daphnia, and euphausiid species in marine and freshwater environments. However, there are markedly few studies that describe DVM behaviour of North Sea physonect siphonophores. These organisms have been invoked numerous times to explain acoustic patterns that do not fit with those inferred from net sampling (Blanluet et al., 2019; Mair et al., 2004, 2005; Lavery et al., 2007). Reports of DVM by *Nanomia sp.* can be found in the literature but are often limited to documenting the occurence of DVM, rather than providing a description of how these siphonophores migrate (e.g. migration amplitude, timing) (Warren et al., 2001; Benfield et al., 2003).

This chapter presented acoustic observations of synchronised nocturnal DVM behaviour of gas-filled organisms, likely physonect siphonophores, in the North Sea. It detailed aspects of their DVM behaviour, including migration amplitude, the proportion of migratory backscatter, and migration rates and timing. If it is assumed that average $6\,\mathrm{dB}$ reductions in backscatter at night relate to proportional decreases in the numerical density of scatterers, then approximately $75\,\%$ of the population is estimated to have migrated out of the analysis layer at night, and animals were four times more densely packed during the day than at night. But this assumption is almost undoubtedly invalid given the complex, nonlinear relationships between acoustic properties and biological abundance, and the likelihood of diel changes in orientation and composition of scatterers (Simmonds and MacLennan, 2005; Simard and Sourisseau, 2009). Nevertheless, our estimate is similar to estimates of the proportion of migratory biomass in other ecosystems (Escribano et al., 2009; Postel et al., 2007), such as in the Northern Humboldt Current system where almost $80\,\%$ of epipelagic macrozooplankton biomass was estimated to undertake DVM (Ballón et al., 2011). Migrations of approximately $75\,\%$ of the organisms in the GF layer, with average amplitudes of $15\,\mathrm{m}$, highlight the ecological importance of even relatively shallow DVM.

### 3.4.1 DVM of North Sea physonect siphonophores

#### Differences between dawn and dusk migrations

The asymmetry between upwards and downwards migration timing and rates was indicative of less synchronised ascents compared to descents. This asymmetry could be explained in terms of differential risk tolerance of individuals. Individual differences in physiology and internal state can modulate DVM behaviour, resulting in variability in the synchronicity of migrations or propensity to migrate (Ichii et al., 2020; Bos et al., 2021; Hays et al., 2001). Just as Pearre (2003b) commented that *"Satiation-cued descent . . . would generally only be observed as a vertical dispersal and a gradual increase of the mean depth of the population"*, here I posit that individual variation in hunger-levels could have caused the vertical dispersion and more gradual ascent observed at dusk. This contrasts with dawn when descent appeared to be reliably cued by light or circadian rhythm, with the layer reaching its average daytime residence depth by the time the sun reached the horizon every morning.

The asymmetry I observed mirrors differences in dawn and dusk schooling behaviour seen in some fish. Rapid aggregation at dawn is believed to be the result of active processes to reduce predation risk, whereas slower dispersal at dusk is the result of more passive processes led by individual foraging decision (Fréon et al., 1996; Cardinale et al., 2003). The onset of dawn signals to animals simultaneously that predation risk may increase rapidly. Presumably after a night spent in waters with favourable feeding conditions many animals are more satiated than when they arrived, and so the importance of avoiding predators prevails. Towards dusk, individuals with higher and more immediate energy requirements may be more likely to forgo the safety of darkness earlier in order to access food sooner. It is doubtful that other physiological variations such as body size could explain the observed asymmetry, since an individual's risk due to variable physiology alone is likely to be similar at dusk and dawn. However, metabolic demands are size-dependent. Hunger-induced changes in risk tolerance may act differentially according to size. Studies have found that smaller organisms tend to reside in shallower regions than larger organisms, and migrate towards the surface prior to larger counterparts (Gastauer et al., 2022; De Robertis et al., 2000; Ohman and Romagnan,

2016; Benoit-Bird and Moline, 2021). A combination of vertical separation in the water column according to body size, differential size-related risks, and size-related metabolic demands could explain the vertical dispersion observed whereby the upper regions of the layer ascended earlier than the lower regions.

**Taxonomic composition of the gas-filled acoustic group**

The net samples characterised the zooplankton as consisting almost entirely of fluid-like scatterers. Yet, our acoustic study found that the water column was acoustically dominated by scatterers with a frequency response stronger at $70\,\mathrm{kHz}$ than $200\,\mathrm{kHz}$, indicative of gas-bearing animals. Gas-bearing organisms, such as physonect siphonophores, can dominate acoustic backscatter of fluid-like scatterers such as copepods, even when the latter are numerous (Blanluet et al., 2019; Lavery et al., 2007; Proud et al., 2019). Furthermore, gelatinous zooplankton are notoriously difficult to sample with commonly used nets, such as the $270\,\mu\mathrm{m}$ ring net used for this study, and so are likely to have been underrepresented in the net samples. Even equipment specifically adapted to better sample these organisms, such as Reeve nets (Reeve, 1981), can damage their fragile bodies and result in abundance underestimations (Warren et al., 2001).

Our understanding of siphonophore depth distributions and ecology have been advanced considerably by the use of optical sensors (Blanluet et al., 2019; Benfield et al., 2003; Proud et al., 2019; Kloser et al., 2016; Hosia and Båmstedt, 2008; Trevorrow et al., 2005), since imaging and video systems are not invasive. Using a complement of sampling techniques including broadband acoustics, net sampling, video and optical imaging, Blanluet et al. (2019) determined that siphonophores were largely responsible for strongly resonant SSLs observed during spring in the Bay of Biscay. Here, I similarly propose that DVM patterns of the main SSL observed in our North Sea study region may be largely representative of physonect siphonophore behaviour, but additional validation data are required to verify this hypothesis.

Larval fish are unlikely to account for patterns in the GF group. Most North Sea fish spawn at specific times of the year. Gadoids spawn in winter, and North Sea herring spawn in

the autumn (ICES, 2005). By the end of spring, herring larvae will have developed into juveniles and begun to school. Only eleven fish larvae large enough to potentially have an inflated swimbladder were found in our net samples, although this size-class may be underrepresented due to their increased capacity to see and swim away from nets as the larvae mature. Fish larvae can perform DVM, however this usually occurs in near-surface waters above the thermocline (Ferreira et al., 2012; Sabatés, 2004), which in our study would place them above the analysis layer.

Peak abundance of adult *Nanomia cara* in western Norwegian fjords was found to occur in late May and early June (Hosia and Båmstedt, 2008). *Nanomia cara* are strong scatterers, with target strengths estimated at $-75\,\mathrm{dB}$ at $420\,\mathrm{kHz}$ by Greene et al. (1998) in the Gulf of Maine, and backscatter of dense patches of SSLs near Massachusetts Bay reaching over $-50\,\mathrm{dB}$ at $120\,\mathrm{kHz}$ (Warren et al., 2001). The GF layer had backscatter strengths that, in some particularly strong patches, exceeded $-60\,\mathrm{dB}$ at $70\,\mathrm{kHz}$. The presence, migration behaviour, and scattering properties of the main SSL are therefore consistent with its scattering source being attributed to gas-bearing siphonophores such as *Nanomia cara*. Other physonect siphonophores, such as *Agalma elegans*, may also have contributed to the GF group backscatter as this species is known to inhabit the North Sea, however net samples were unable to confirm or rule out their presence.

Since, for many species, DVM is considered a predator-avoidance strategy and modification of this behaviour the result of behavioural plasticity rather than selective pressure (De Robertis et al., 2000), we might expect predators of physonect siphonophores to be present within the North Sea. Very little is known about which organisms prey on siphonophores, but leatherback turtles (*Dermochelys coriacea*) and ocean sunfish (*Mola mola*) are two species known to consume siphonophores (Den Hartog and Van Nierop, 1984; Nakamura et al., 2015; Hetherington et al., 2022). Both species are present in UK waters, however no reports of leatherback turtles in the North Sea were found and reports of ocean sunfish in the North Sea were exceedingly rare and limited to anecdotal evidence.

Unlike larval fish, siphonophores are non-visual predators. This means that siphonophore feeding is not necessarily inhibited by low light levels and they may be able to feed at any time

of day, depending on prey availability. Physonect siphonophores consume a variety of prey, including copepods, decapods, euphausiids, chaetognaths, and fish larvae (Purcell, 1981; Hetherington et al., 2022), many of which may perform DVM themselves to avoid visual predators such as planktivorous fish. Therefore, DVM by siphonophores may allow them to follow prey throughout the day and night. This poses the question of whether siphonophores in these waters are likely to be more driven by hunger towards the late afternoon than at other times of day.

**Diel variation in dB-difference**

Numerous factors may have contributed to the diel changes in frequency response that were observed, the two most significant being orientation and composition. Species-composition of the gas-filled group likely changed as day transitioned to night. Bentho-pelagic fish swam upwards into the water column, swimbladdered fish schools dispersed, and the mixture of gas-filled and fluid-like scatterers altered as migrators moved at different rates. In addition, target strength, and hence frequency response, is a function of incidence angle, usually described in terms of orientation or tilt angle of the organism (Simmonds and MacLennan, 2005). Changes in organism associated with upwards and downwards swimming are known to affect target strengths of many fish and other organisms (Blaxter and Batty, 1990; Kubilius and Ona, 2012; McQuinn and Winger, 2003). For this reason, comparisons of backscatter to detect DVM usually focus solely on differences between daytime and nighttime observations. However, orientations may change due to behaviours correlated with time of day also. Parra et al. (2019) found that chaetognaths and shrimp were more likely to be randomly oriented at night but vertically oriented upwards during the day. Based on scattering models, they considered that differences in relative backscatter anomaly between night and day (used as evidence for DVM) could be accounted for solely by changes in orientation.

Frequency response may also have been affected by changes in fish swimbladder morphology with depth. The volume of the swimbladder in physostomous fish changes during extensive vertical migrations (Zwolinski et al., 2007; Fässler et al., 2009; Ganias et al., 2015). These fish cannot increase gas concentrations in the swimbladder unless at the

surface (Ona, 1990). According to Boyle's law, swimbladder volume decreases as pressure increases with depth. Disregarding the complexities of changes in shape as the volume decreases, depth has an overall effect of increasing the resonant frequency and reducing the target strength of physostomous Atlantic herring (*Clupea harengus*) (Blaxter and Batty, 1990; Løvik and Hovem, 1979; Gorska and Ona, 2003). Whether physonect siphonophores maintain pneumatophore volume with changing hydrostatic pressure remains to be determined conclusively. Our study region was relatively shallow (at less than $100\,\mathrm{m}$), so effects of depth on the volume of gas-inclusions in this group are unlikely to have been substantial. The diel pattern in dB-difference is intriguing and warrants further investigation to understand what factors underlie the cyclical changes that were observed.

**Migration rates**

Our migration rate estimates ($0.7\,\mathrm{mm\,s^{-1}}$ ascent and $1.4\,\mathrm{mm\,s^{-1}}$ descent) are substantially slower than estimates for vertical migration rates from other studies. Global estimates of downward migration speeds of SSLs, also derived from acoustic data, are more than fifty times faster at $76.6 \pm 36\,\mathrm{mm/s}$, and upwards migration estimates are almost two orders of magnitudes larger at $65.6\,\mathrm{mm\,s^{-1}}$ (Bianchi and Mislan, 2016). Shallower migrations tended to be slower than deeper migrations; compiled data came from a variety of ocean basins to derive the global estimates, with average migration depths of $411 \pm 87\,\mathrm{m}$ (Bianchi and Mislan, 2016). Cade and Benoit-Bird (2015) reported average SSL ascent rates of $47\,\mathrm{mm\,s^{-1}}$ and descent rates of $50\,\mathrm{mm\,s^{-1}}$ but relative ascent and descent speeds varied across cruises. Our migration rates were much slower than the 2 to $6\,\mathrm{cm\,s^{-1}}$ ADCP-derived vertical swimming speeds for individual animals performing DVM in the Northeast Atlantic estimated by Heywood (1996). Notably, the aforementioned studies and others, such as Parra et al. (2019), also report average descent rates that are faster than ascent.

Discrepancies between our migration rates estimates and those from other studies might have occurred due to differing taxonomic composition of the SSLs, differences in methodology to derive the estimates, available water column depth, and probable underestimation of DVM amplitude in our case. Bianchi and Mislan (2016) noted that mesopelagic fish were

likely dominant contributors to the backscatter in many of the SSLs that they considered. Cade and Benoit-Bird (2015) did not provide information on the taxonomic composition within the layers they considered. Composition was similarly not known for (Heywood, 1996, 's) study, although dominant scatterers were thought to be copepods, notably *Calanus finmarchicus*, euphausiids, and amphipods. There is a paucity of information regarding vertical swimming speeds of *Nanomia cara* and *Agalma elegans*, however Sutherland et al. (2019) reported forward and reverse swimming speeds of the related *Nanomia bijuga* to reach up to $134\,\mathrm{mm\,s^{-1}}$, two orders of magnitude faster than our layer descent rate. First feeding $10\,\mathrm{mm}$ long herring larvae can swim at speeds of $5$ to $20\,\mathrm{mm\,s^{-1}}$ (Batty, 1984). Our migration rates are therefore probably within the swimming capabilities of *Nanomia* siphonophores and larval fish big enough to have inflated their swimbladders.

Synchronised movement at the population level is expected to be slower than individual swimming speeds, particularly as individuals at the leading edge of a migrating layer may retreat backwards towards the centre (Heywood, 1996). How rates are measured is also important: our study loosely defined the initiation of migration by concomitant and sustained movement of the centre of mass of the layer with reference to both the surface and bottom, however this was judged subjectively by eye, based on grouped data. By contrast, Cade and Benoit-Bird (2015) define the period of migration used to calculate migration rates by noting the times when the bottom of the layer began and ceased sustained movement each day. Accuracy of our estimates was likely affected by the upper limit of our analysis layer since most of the GF layer moved above $36\,\mathrm{m}$ at night. This made estimating the initiation of descent in the morning and cessation of ascent in the evening particularly challenging. Our figures are likely to be conservative. Average amplitude was probably greater than $15\,\mathrm{m}$ since the true centre of mass for the GF layer at night was undoubtedly shallower than our calculation which was based on backscatter only within the analysis layer. This probable underestimation has a knock-on effect on the accuracy of migration rates, resulting in slower rates than in actuality. The proportion of migratory backscatter may also have been underestimated since the vertical range of the analysis layer encompassed between $47\,\%$ to $63\,\%$ of the total water column depth. By vertically integrating over the whole analysis layer finer detail of vertical movements within the analysis layer may have been lost.

### 3.4.2 Evaluation of the classification scheme

There are two main aspects of our classification approach that introduced uncertainty and potential error. Firstly, taxonomic compositions of the GF and FS groups were unverified due to insufficient ground-truthing. Candidate taxa were proposed based mostly on knowledge of North Sea species and their scattering properties. Thus, I cannot discount the possibility that DVM patterns of the GF layer do not accurately represent behaviour of either siphonophores or larval swimbladdered fish, but instead they might represent combined signals of disparate behavioural patterns. However, given that there is a clear, coherent DVM pattern observed, it seems probable that scatterers responsible for the GF backscatter exhibit similar DVM behaviour. Secondly, the classification is hierarchical according to dominance of backscatter at the measured narrowband frequencies within each cell; consequently misclassification is highly probable as only one category can be assigned to each cell. Furthermore, the correspondence between averaged volume backscatter with positive (negative) dB-difference and individual FL (GF) scatterers is undoubtedly an oversimplification. Acoustic dominance of gas-filled organisms and their prevalence during the mission presented such a major source of bias that apparent reverse DVM by the FL group could well have been an artefact of the hierarchical classification rather than a biological reality.

#### Misclassification

As with similar multifrequency classification schemes, misclassification of cells is highly plausible (Ballón et al., 2011; Sato et al., 2015). Sampling volumes (or cells) may have contained mixtures of organisms from different groups; our designation reflects acoustic dominance rather than organisms with the highest numerical abundance or biomass. Furthermore, dividing scatterers based on whether dB-difference is above or below $0\,\mathrm{dB}$ belies the reality that some gas-filled animals can produce a positive dB-difference and some fluid-like scatterers can produce a negative dB-difference. Net samples revealed that copepods, chaetognaths, euphausiids, amphipods, decapods and pteropods likely dominated the FL group, however animals with very small gas inclusions could have also contributed to backscatter in this group.

Siphonulae are the small larval stages of siphonophores. They begin to fill their pneumatophores with carbon monoxide gas from 3-5 days old (Sherlock and Robison, 2000; Pickwell et al., 1964). In the Gulf of Maine, Benfield et al. (2003) found that siphonulae tended to occur in SSLs at mid-depths ($50$ to $150\,\mathrm{m}$), vertically separated from regions with higher densities of adult siphonophores and other targets with similar scattering properties. Mid-depths were characterised by relatively strong backscatter, and here high densities of siphonulae were sampled by the MOCNESS net. As with adult siphonophores, siphonulae are thought to be capable of modifying their depth to maintain their position within favourable temperature distributions and capable of performing DVM (Benfield et al., 2003; Warren et al., 2001). Benfield et al. (2003) modelled target strengths of siphonulae with pneumatophores sized between $0.1$ to $0.3\,\mathrm{mm}$ at various depths up to $100\,\mathrm{m}$, predicting resonance across a range of frequencies stretching from below $70\,\mathrm{kHz}$ to over $200\,\mathrm{kHz}$. Siphonulae were not found in our $270\,\mu\mathrm{m}$ net samples, however this does not rule out their presence since these small, gelatinous organisms are particularly difficult to capture (Benfield et al., 2003). If present, siphonulae could have contributed to either the GF and FL groups, depending on how depth and size of their pneumatophore influenced resonance. With relatively strong target strengths, siphonulae have the potential to bias patterns of the FL group.

Group composition may have varied according to time of day, possibly leading to misclassification of some cells. For example, backscatter from individual fish dispersing from schools at dusk may have reduced the dB-difference of cells, leading to more cells being classified as GF. The likelihood of diel changes in composition means that producing a robust estimate of the migratory proportion of the GF group using acoustics alone may be problematic, and perhaps best achieved with data from depth-stratified net samples. Clearly the problem of classifying mixed assemblages of zooplankton in a diverse ecosystem such as the North Sea is challenging. Gear are biased towards sampling particular types of organisms, as demonstrated by the acoustic detections of strongly reflective gas-filled scatterers, contrasting with the almost exclusive capture of fluid-like scatterers by net. Our classification scheme would clearly benefit from a complement of different sampling gears to characterise the SSL and fish schools that were observed (McClatchie et al., 2000).

### 3.4.3 North Sea schooling fish

In the North Sea, several species of fish with swimbladders cohabit. These include: gadoids such as whiting (*Merlangius merlangus*), haddock (*Melanogrammus aeglefinus*), Norwegian pout (*Trisopterus esmarkii*) and cod (*Gadus morhua*); clupeids such as European sardines (*Sardina pilchardus*), anchovies (*Engraulis encrasicolus*), Atlantic herring (*Clupea harengus*), and sprat (*Sprattus sprattus*); and Osmeridae such as capelin (*Mallotus villosus*) and European smelt (*Osmerus eperlanus*). Norway pout have a similar acoustic signature to herring, however in the North Sea they are generally found in deeper waters (Fässler et al., 2007; Sparholt et al., 2002). Juvenile Atlantic cod are known to aggregate but tend to settle near the seabed in areas with complex bottom habitats and form diffuse aggregations (Laurel et al., 2004). Large adult cod tend to be solitary but form large spawning aggregations near the coast at certain times of the year (González-Irusta and Wright, 2016). Characteristic acoustic marks of individual cod single targets were not observed; however a single large school with unusually diffuse backscatter was sampled at the beginning of the mission that could have been comprised of juvenile cod. Even if present, individual predators such as cod may not have been sampled in the beam simply due to low probability of encounter.

Other schooling fish occur in the North Sea, such as mackerel (*Scomber scombrus*) and lesser sandeels (*Ammodytus marinus*) (van der Kooij et al., 2016; Van Der Kooij et al., 2008). However, lacking swimbladders they are comparatively weak scatterers, and schools would have to contain a high density of fish in order to exceed the threshold of $-57\,\mathrm{dB}$ which was applied for fish school detections (Foote, 1980; Gorska et al., 2007). Mackerel schools are thought to backscatter more strongly at $200\,\mathrm{kHz}$ than $70\,\mathrm{kHz}$ by between $2$ to $4\,\mathrm{dB}$, owing to stronger backscatter reflected from the backbone at higher frequencies (Gorska et al., 2007). I detected six schools that had average dB-difference above $0\,\mathrm{dB}$, up to a maximum of $2.2\,\mathrm{dB}$. These schools had mean backscatter values at $70\,\mathrm{kHz}$, ranging between $-58$ to $-47\,\mathrm{dB}$, and so could conceivably have been mackerel (Korneliussen and Ona, 2004). Sandeels are associated with specific habitats and exhibit strong site fidelity (Jensen et al., 2011; Van Der Kooij et al., 2008). In spring and summer they bury themselves in muddy substrate during the night and emerge in the daytime to shoal and feed (Van Der Kooij

et al., 2008). In the central North Sea, sandeel populations are confined to areas of suitable nighttime habitat around Dogger Bank, which lies considerably further south from our study region, thus ruling out the possibility that I detected sandeel schools.

Atlantic herring are known to form large, monospecific schools which exhibit a strong scattering response with the dominant contribution of backscatter arising from the swimbladder (Toresen, 1991). Resonance of adult fish is usually below $70\,\mathrm{kHz}$, which means that they are expected to produce a negative dB-difference at $\Delta\mathrm{MVBS}_{200-70}$ (Nero et al., 2004), although frequency response can be highly variable (Fernandes, 2009). Despite the lack of conventional narrowband frequencies for fish species identification (i.e. $18\,\mathrm{kHz}$, $38\,\mathrm{kHz}$) and the lack of trawl or optical data for ground-truthing, the position of the fish schools in the water column, their diel patterns, and their morphology are consistent with the assumption that the schools were comprised of Atlantic herring (Cardinale et al., 2003).

Non-fish sources of backscatter attributed to the fish school group were considered, including: dense aggregations of gas-bearing zooplankton such as siphonophores, noise, and bubbles. Abiotic sources were ruled out based on morphology. Bubbles may be associated with diving seabirds, layers of gas-producing phytoplankton, or plumes extending downwards from the surface, none of which would present as pole-like or globular clusters located near the bottom during daytime only (Brierley and Fernandes, 2001; Chu et al., 2021; Trevorrow, 2003; Godø et al., 2013). Increases in ambient noise (background or transient noise) typically affect entire pings, and corruption by other instrumentation (impulse noise) results in short, regular vertical spikes throughout the echogram (Ryan et al., 2015). Neither of these noise sources tends to produce well-defined hotspots of backscatter. Biotic sources could conceivably be responsible for some of the detections that occurred amongst dense regions of the SSL. For example, dense patches of siphonophores have been recorded as reaching backscattering strengths of more than $-50\,\mathrm{dB}$ at $120\,\mathrm{kHz}$ in some instances (Warren et al., 2001). Techniques that consider the gradient of backscatter at 'school' edges and contrast edges against the background scattering such as that developed by (Benoit-Bird and Moline, 2021) could improve separation of dense zooplankton patches within SSLs and bona fide fish schools.

Schools were generally located in close proximity to the bottom. Larger schools expanded in all available directions being both longer horizontally and thicker. Given that individuals occupying peripheral positions in schools may be subject to increased predation risk (Magurran, 1990; Larsson, 2012), it is unclear why individuals at the top of thick schools would forgo positions in deeper, darker regions where presumably risk from visual predators during the daytime is lower. Access to positions further down may be limited, particularly for fish with reduced aerobic capacities; such fish are known to occupy peripheral positions in an attempt to avoid low oxygen conditions within central regions of large schools (Domenici et al., 2007). Also, reorganisation may be disruptive to school dynamics (Romey, 1996). Occupation of frontal positions within schools are known to enhance foraging success, albeit associated with increased energetic swimming costs needed to maintain lead positions (Krause et al., 1992; McLean et al., 2018). It is conceivable that, for fish that are visual predators themselves, being at the top of schools positions them for both more favourable light conditions for foraging and proximity to higher prey densities within the SSL. These fish may therefore experience greater foraging success than those towards the bottom of the school. Furthermore, membership of much larger schools may confer greater advantages in predator perception, information sharing, and reduced energetic costs associated with swimming regardless of position that outweigh the disadvantages of occupying positions associated with higher mortality risk from visual predators (Marras et al., 2015; Larsson, 2012; Krause et al., 1992).

Speeds of swimming fish schools and speeds of the sampling platform have implications for the detectability of fish schools. Detection probability decreases when fish schools swim fast in a horizontal direction or when the platform travels at high speed. The Wave Glider is relatively slow compared to ships but its speed is variable depending on wind speed (Chapter 2). Schools of North Sea herring have been recorded swimming at speeds of up to $4.8\,\mathrm{m\,s^{-1}}$ (Misund and Aglen, 1992) - almost five times as fast as *Lyra's* maximum recorded speed - making them a relatively fast-moving target. There was considerable decline in the rate of FS detections during windy weather which was probably in part due to reduced horizontal sampling resolution caused by increased vessel speed and removal of bad data. Future analyses using the Wave Glider may benefit from adjustment of school detection

parameters according to vessel speed and also careful manual scrutiny of fish schools in acoustic data collected during windy weather.

# 4

# Environmental drivers of zooplankton and fish school patchiness

## 4.1 Introduction

### 4.1.1 Influence of environmental conditions on pelagic animal distributions in the central North Sea

The upper pelagic is structured by several vertical environmental gradients that are of great significance to marine life. Sunlight is perhaps the most significant variable, providing energy near the surface during the day for autotrophic organisms at the base of the marine food web, and influencing behaviour that structures trophic dynamics between pelagic predators and prey throughout the water column. Vertical temperature gradients also play a significant role in structuring the water column and influencing metabolic rates of organisms that live in the epipelagic. In the central North Sea, the persistence of a near-permanent thermocline retains winter-temperature water close to the bottom throughout the year. This permits cold-adapted zooplankton such as the ecologically important copepod *Calanus finmarchicus* to remain reproductively active at depth in the North Sea for an extended period, despite an increase in SST over recent decades (Jónasdóttir and Koski, 2011).

Through the spring a second, seasonal thermocline develops in the central North Sea due to surface warming by the sun, extending deeper below the surface as the season progresses (Fernand et al., 2013). This solar warming at the surface produces a thermally stratified

water column where temperatures between the surface and bottom may vary by more than 10 °C (Van Leeuwen et al., 2015). The conditions at this time of year also bring about vast blooms of phytoplankton, providing a rich energy source for many zooplankton in the surface mixed layer and at the deep chlorophyll maximum, the latter typically forming at the lower thermocline (Weston et al., 2005; Fernand et al., 2013). Wind-driven mixing alters vertical temperature and salinity gradients by generating turbulence near the surface that can penetrate deeper layers to bring nutrients and colder water towards the surface. Vertical gradients in turbulence also influence zooplankton feeding, reproduction and mortality; a degree of turbulence can enhance encounter rates for many species, however excessive amounts can have detrimental effects (Gilbert and Buskey, 2005; Visser et al., 2001; Visser and Stips, 2002; MacKenzie et al., 1994). Turbulence generated by surface wind stress can drive copepod distributions deeper in the water column in an apparent avoidance behaviour (Incze et al., 2001; Tanaka, 2019; Maar et al., 2006). In regions where depths are too shallow for copepods to descend to relative safety, turbulence due to extreme weather events can result in high levels of mortality (Maud et al., 2018).

The underwater light environment fundamentally varies according to latitude, time of year, and time of day, but also varies according to regional and temporal fluctuations in hydrographic conditions that affect water clarity and shading (Capuzzo et al., 2013). Shading describes a reduction in the intensity of light that penetrates to depth. Shading can also change the composition of the light since only select wavelengths of light may be attenuated. Many fish and zooplankton that vertically migrate over diel timescales also adjust their vertical position in accordance with sub-diel temporal variations in underwater light levels (Omand et al., 2021). Scattering layers comprised of vertically migrating fish and zooplankton often stay below isolumes; a strategy that allows these animals to access shallower regions of the water column when light intensity is temporarily reduced due to shading whilst maintaining an approximately constant light-mediated predation risk (Hays, 2003; Hobbs et al., 2021). However, scattering layers do not always track isolume movements precisely. In many cases, scattering layers remain deeper than the isolume itself and exhibit a lagged response to rapid fluctuations (Omand et al., 2021; Kaartvedt et al., 2017), the latter possibly having evolved as a strategy to minimise unnecessary energy

expenditure that might otherwise occur should animals move in response to short-lived fluctuations in light levels.

Both atmospheric and underwater conditions can influence shading and hence the position of isolumes. Cloud-cover and wildfire smoke alter the optical properties of light that reaches the ocean surface by selectively attenuating light intensity at different wavelengths. Such atmospheric changes have been shown to induce changes in the vertical positioning of fish and zooplankton (Omand et al., 2021; Urmy et al., 2016). For example, Kaartvedt et al. (2017) observed that scattering layers in the mesopelagic zone (depths between 200-1000 $\mathrm{m}$) responded rapidly to the darkening of ambient light levels due to a passing storm by moving upwards in the water column. Variability in surface and underwater conditions also affect fish and zooplankton movements. Both the timing and amplitude of DVM can be modified by shading due to sea ice and snow cover, and, if enough light is prevented from penetrating through the ice, synchronised DVM behaviour may even cease (Hobbs et al., 2018; Wallace et al., 2010). Shading can also occur due to a reduction in water clarity caused by increased concentrations of sediments, phytoplankton and other particulates, which can in turn influence the vertical distributions of fish and zooplankton (Kaartvedt et al., 2012, 1996; Hobbs et al., 2021). The distributions of particulates are affected by many processes, including the formation and persistence of pycnoclines which enhance vertical structure (e.g. leading to high concentrations of chlorophyll at the thermocline) and mixing forces such as wind stress which can act to homogenise particles within the surface mixed layer and, if strong enough, overcome density gradients to redistribute material across pycnoclines. Therefore, the attenuation of light beneath the surface is not simply a function of depth, but also the depth-dependent optical properties of the water column during any given time.

Static features of the environment, such as bathymetry and persistent current flow, may play an important role in structuring zooplankton spatial distributions. The shallow bathymetry of the North Sea constrains the potential distributions of animals vertically, limiting the extent of diel vertical migrations for many animals and forcing them to reside in a shallower, and thus lighter, environment than they otherwise might in the open ocean (Longhurst and Williams, 1979). DVM behaviour itself can result in spatial patchiness, particularly when amplitudes vary within the migratory population (Chen et al., 2021). Topographic features,

including bathymetric gradients, influence currents and can act to accumulate zooplankton, which in turn may lead to the formation of hotspots of higher trophic level activity (Hazen et al., 2013; Genin, 2004). In shallow systems where optimal depth of daytime refuge is limited by the seabed, uneven bathymetry can induce horizontal patchiness as zooplankton that encounter the seabed move horizontally along the slope towards deeper regions (Chen et al., 2021).

Certain topographic features and flow regimes can lead to intermittent depletion of zooplankton. For example, *topographic blockage* describes a mechanism whereby zooplankton are advected over a region of shallower bathymetry that prevents them from accessing safer, darker depths during daytime, which can result in increased mortality due to exposure to visual predators (Genin et al., 1994; Genin, 2004; Aarflot et al., 2019). Topographic blockage can cause diel fluctuations in abundance when zooplankton are replenished overnight by advection but depleted each day as a consequence of their inability to find refuge at depth. For oceanic species such as *C. finmarchicus* which regularly descend to depths of hundreds of metres in the North Atlantic (Longhurst and Williams, 1979), advection from deeper waters into the shallow North Sea ($< 100\,\mathrm{m}$) may constitute topographic constraint (Aarflot et al., 2019).

SST emerges from the literature as one of the most important water properties associated with changes in the North Sea ecosystem (Reid et al., 2016; Edwards et al., 2001; Beare et al., 2002a). Episodic incursions of warm, more saline, oceanic water have been linked to unusual occurrences of more southerly distributed species across a diverse range of taxa (Lindley et al., 2010; Edwards et al., 1999; Beare et al., 2002a, 2004). An overall trend of increasing SSTs over recent decades has been linked with biogeographic shifts and reductions in abundance and diversity of cold water species (Beare et al., 2004; Lindley et al., 2010). This shift is best documented for the two most dominant calanoid copepod species in the North Sea: *Calanus helgolandicus* and *C. finmarchicus*, the latter species identified as particularly important for cod recruitment (Beaugrand, 2003; Beaugrand and Kirby, 2010). Geographic range of the temperate *C. helgolandicus* has expanded northwards through the North Sea, whilst the geographic range of the boreal *C. finmarchicus* has contracted to the northernmost regions of the North Sea, and these range expansions and contractions were

concomitant with increasing and decreasing abundances of the respective species (Beare et al., 2002a; Montero et al., 2021).

Relationships between SST and North Sea fish and plankton abundances and distributions have been studied extensively, although studies typically focus on patterns that emerge over seasonal, annual, and multi-annual timescales (Beaugrand, 2003; Lindley et al., 2010; Beaugrand and Kirby, 2010; Colebrook, 1985; Alvarez-Fernandez et al., 2012; Richardson and Schoeman, 2004). Synergistic effects of wind speed and temperature were identified by Alvarez-Fernandez et al. (2012) as the most important abiotic drivers of seasonal phytoplankton biomass in the North Sea between 1970-2008, as weaker winds and higher temperatures promoted stronger and more stable stratification that prevented mixing of nutrients from below the photic zone. The strength, or intensity, of stratification has been shown to affect vertical positioning of zooplankton and their horizontal patchiness (Beare et al., 2002a; Lezama-Ochoa et al., 2014; Chen et al., 2021). For example, stratification leads to enhanced separation in the vertical distributions of *C. finmarchicus* and *C. helgolandicus* in the North Sea, thought to be primarily related to these species' different temperature preferences (Jónasdóttir and Koski, 2011). Stratification also induces internal waves which enhance vertical gradients in current velocities, and stratified layers may have different horizontal current speeds and directions. Since synchronised DVM acts to synchronise depth-dependent horizontal velocities of zooplankton, stratification can enhance horizontal patchiness (Chen et al., 2021).

Alongside temperature and stratification strength, other properties such as oxygen levels, salinity and water clarity can influence zooplankton and fish distributions. These properties can influence DVM behaviour of migratory animals by altering the energetic costs and benefits of migration through changes to plankton food webs and the distribution of food resources (Ichii et al., 2020; Beare et al., 2002a; Hall and Lewandowska, 2022), metabolism and physiological tolerance (Wishner et al., 2013, 2018; Ekau et al., 2010), or perceived predation pressure (Ohman and Romagnan, 2016; Aarflot et al., 2019). Besides oceanographic influences on zooplankton distributions, the social environment including predator and prey distributions can induce or reduce movement and aggregative behaviour that serve as defence or escape mechanisms. Predator presence has been shown to influence

DVM behaviour and spatial patchiness of zooplankton at both short timescales, oftentimes by an almost instantaneous reaction, as well as longer, multi-generational timescales (Urmy and Benoit-Bird, 2021; Bollens and Frost, 1991; Hays et al., 1996; Gliwicz, 1986).

Clearly, there exist a multitude of environmental factors that influence the abundance and distribution of pelagic life in the North Sea. Chapter 3 described the DVM behaviour of gas-filled (GF) zooplankton, diel patterns in fish school (FS) observations, and separated backscatter of fluid-like (FL) zooplankton. *Lyra's* mission was timed to coincide with the onset of stratification in the central North Sea, taking environmental measurements alongside acoustic data in order to investigate relationships between the changing water properties and the spatial distributions of animals. *Lyra* sampled repeatedly across a transect which covered a $64\,\mathrm{km}$ longitudinal section of the central North Sea. The bathymetry of this transect line varies with bottom depths ranging between $71$ and $98\,\mathrm{m}$. This creates peaks and troughs, and rugged and flat regions which provide diverse habitats for both demersal and pelagic organisms.

### 4.1.2 Aims of this study

This chapter investigates relationships between environmental parameters and zooplankton and fish distributions at sub-seasonal timescales during the spring stratification period in 2018. My question is: which environmental variables drove the horizontal and vertical backscatter distributions of the pelagic animal groups that were observed acoustically in the central North Sea during spring?

To address this question, I use Generalised Additive Mixed Models (GAMMs) to analyse relationships between environmental variables and spatial distributions of classified backscatter. Seaglider data from the vicinity is used in order to contextualise the results of the GAMMs, providing subsurface measurements of many of the environmental variables tested. I hypothesise that light levels and bottom depth would be key determinants of vertical position of GF backscatter, given that this group exhibited DVM behaviour. For both planktonic groups (GF and FL), I anticipate that circulation patterns and frontal features may influence horizontal distributions, since planktonic animals are often unable to swim against

strong currents and therefore more subject to physical forcing. I hypothesise that associations between water properties and fish school spatial distributions would be weaker than those with zooplankton, as fish are highly mobile and schools dynamically respond to many social as well as physical cues. However, persistent oceanographic features that result in areas of locally enhanced production might act to aggregate fish and form hotspots of biological activity (Hazen et al., 2013).

## 4.2 Methods

### 4.2.1 Overview of GAMMs

GAMMs are a statistical method which can model complex non-linear dependence of a response on predictor variables. GAMMs use smoothing splines ('smooths') to model relationships between continuous predictor variables and response variables, and use 'factors' to define discrete predictor variables, and can include geographic coordinates and time-points to account for spatial and temporal dependencies in the data. Response variables can be fitted with a choice of distributions besides Gaussian, extending options available in similar regression analyses. GAMMs are an extension of Generalised Additive Models (GAMs) that allow for the inclusion of random effect arguments and can be fitted with correlation structures to account for spatial or temporal autocorrelation. This makes them particularly well-suited to modelling ecological relationships from observational time series where data have been collected across various repeat locations. GAMs have proven informative for understanding drivers of ecosystem variability (Swartzman et al., 1992; Boswell et al., 2020; Van Der Kooij et al., 2008; Lindegren et al., 2020; Denis et al., 2002) and also detecting the influence of changes in methodology, for example in fisheries abundance estimates (Moriarty et al., 2020). Interested readers may wish to consult Wood (2017) and Zuur et al. (2009) for detailed explanations of how GAMs function, the kinds of research questions they are best suited to address, and examples of their utility in ecological research.

In recent years GAMMs have been applied to fisheries and zooplankton acoustic data, for example elucidating environmental drivers of vertical backscatter distribution patterns in

the Scotia Sea (Dornan, 2019), habitat preference of sandeels at Dogger Bank in the North Sea (Van Der Kooij et al., 2008), and vertical distribution patterns of micronekton across different oceanographic features in the Gulf of Mexico (Boswell et al., 2020). Here, I used GAMMs to explore relationships between acoustic descriptors of biological distributions derived from backscatter measurements and a suite of environmental variables collected by the Wave Glider, *Lyra*, in a small-scale study of environmental drivers of zooplankton patchiness in the North Sea.

### 4.2.2 Response variables

Positional and energetic descriptors of backscatter from the gas-filled (GF), fluid-like (FL), and fish school (FS) groups described in Chapter 3 were input as response variables for the GAMMs. These included: centre of mass of backscatter (COM); altitude (ALT); nautical area scattering strength (NASS); and mean backscatter ($S_v$) - see descriptions in Table 3.1.

### 4.2.3 Predictor variables

Concurrent with the acoustic measurements, measurements of surface water properties were taken from approximately $0.5\,\mathrm{m}$ below the surface and wind speed measurements were taken from approximately $1\,\mathrm{m}$ above the surface by sensors onboard *Lyra*. Following quality control, these environmental measurements were input as predictor variables in the GAMMs, along with four acoustically-derived proxy biological variables which were also input as predictors: NASS of the FS group (FSNASS), backscattering strength of the FS group (FSSv), NASS of the GF group (GFNASS), and backscattering strength of the GF group (GFSv), see Table 4.1. These acoustically-derived variables were included to explore whether the presence of fish schools had an observable effect on vertical distributions of the GF backscatter, and whether the presence of the GF layer influenced observed patterns in FL backscatter.

Table 4.1: **Predictor variables tested in the GAMMs.**

| **Variable** | **Abbreviation** | **Units** | **Data source** |
|---|---|---|---|
| Sea surface temperature | SST | °C | Aanderaa 4319 CT |
| SST, low frequency component | temp_lfc | | |
| SST, high frequency component | temp_hfc | | |
| Practical salinity | sal | Practical salinity units (PSU) | |
| Optical backscatter at 700 nm | turbidity | Formazin turbidity units (FTU) | Seapoint Turbidity Meter |
| Chlorophyll fluorescence at 470 nm | fluor | Arbitrary units | Seapoint Chlorophyll Fluorometer |
| Photosynthetically Active Radiation | PAR | $\mu\text{mol}\,\text{m}^{-2}\,\text{s}^{-1}$ | LI-COR LI-192 with Cefas log amplifier |
| Bottom depth | bottom | m | WBT-mini echosounder, 70 kHz |
| Surface bubble plume depth | bub_depth | | |
| Fish school thickness | thickness | | |
| Gas-filled NASS | GFNASS | dB re $1(\text{m}^2\text{nmi}^{-2})$ | |
| Fish school NASS | FSNASS | | |
| Gas-filled backscatter | GFSv | $\text{dB}\,\text{m}^{-1}$ | |
| Fish school backscatter | FSSv | | |
| True wind speed | wind_speed | $\text{m}\,\text{s}^{-1}$ | Airmar WeatherStation 200WX |
| Longitude | lon | °E | |
| Solar altitude | solar_alt | ° above horizon | |

### Temperature signals

SST showed an increasing trend over the course of the mission with daily fluctuations related to solar warming in the daytime and cooling at night. To separate effects of diel cycles from longer-term trends in the time series, a butterworth filter of order 5 with a period of 1.1 days was applied in both directions. This split the signal to produce a high frequency component (temp-hfc) where fluctuations that occurred on timescales of a day or shorter were retained, and a low frequency component (temp-lfc) where fluctuations due to seasonal warming and longer-acting wind mixing events were retained (Figure 4.2.1). The amplitude of the temp-hfc signal suggests that day-night variation in surface water temperature recorded by *Lyra* was much smaller than 0.5 °C (red line in Figure 4.2.1), whereas gradual warming over several weeks in May led to an increase in temperature of approximately 5 °C (blue line in Figure 4.2.1). Both frequency components, as well as the unfiltered temperature data, were tested in the GAMMs.


Figure 4.2.1: **SST time series (black solid line, coincident with the blue line) with high (red) and low (blue) frequency butterworth filtered components.** Vertical dashed lines indicate acoustic data collection period.

### Collinearity amongst predictor variables

Prior to modelling, collinearity among predictor variables was assessed visually using scatter plots and by calculating Spearman's correlation coefficient in order to assess the strength of monotonicity. Including collinear variables in GAMMs can decrease the statistical power and

increase the likelihood of type II errors, therefore only one of each pair of strongly collinear variables was selected for the final models (Zuur et al., 2009). Variables with significant ($p < 0.01$) values above a magnitude of $\rho = 0.5$ were considered for removal.

Surface photosynthetically active radiation (PAR) and solar altitude were highly collinear during daytime periods ($\rho = 0.88$, $p < 0.01$) (Figure 4.2.2, A). PAR presumably provided a more accurate proxy for subsurface light levels during daytime as it reflected the intensity of ambient light modulated by factors such as cloud cover. However, the PAR sensor is limited by its lack of sensitivity in low light conditions and recorded no values throughout the night and much of twilight. Solar altitude, on the other hand, varies throughout the 24-hour period, acting as a proxy for both light levels during all times of day and biological diurnal clock timing. Both variables were therefore retained for initial testing. PAR measurements were tested both as recorded and log-transformed to down-weight extreme values. PAR was slightly correlated with the temp-hfc signal, likely because the butterworth filter was designed to capture daily fluctuations in temperature, and so correlation between temperature changes due to solar warming each day and the daily light cycle is unsurprising. Since the correlation coefficient was less than 0.5, temp-hfc was retained for use in the GAMMs.

During non-daytime periods, turbidity was collinear with wind speed and bubble plume depth ($\rho = 0.66$, $p < 0.01$ for both variable pairs) but had no discernible relationship with fluorescence ($\rho =$ -0.06, $p > 0.1$), suggesting that surface measurements of turbidity were dominated by the detection of air bubbles ubiquitous in windy weather (Figure 4.2.2, B). Turbidity and bubble plume depth were consequently not used in the GAMMs; however wind speed was retained.

Water properties are often associated with certain water masses, and changes in one property can influence another (for example, changes in primary production may influence oxygen levels), thus variables were not anticipated to be completely independent. GAMMs aim to establish the relative contribution of each predictor variable supplied, however robust interpretations of models rely on understanding the possible links between environmental variables. To assist with interpretations, collinearity between retained predictor variables was evaluated quantitatively in a similar fashion by calculating Spearman's rank correlation

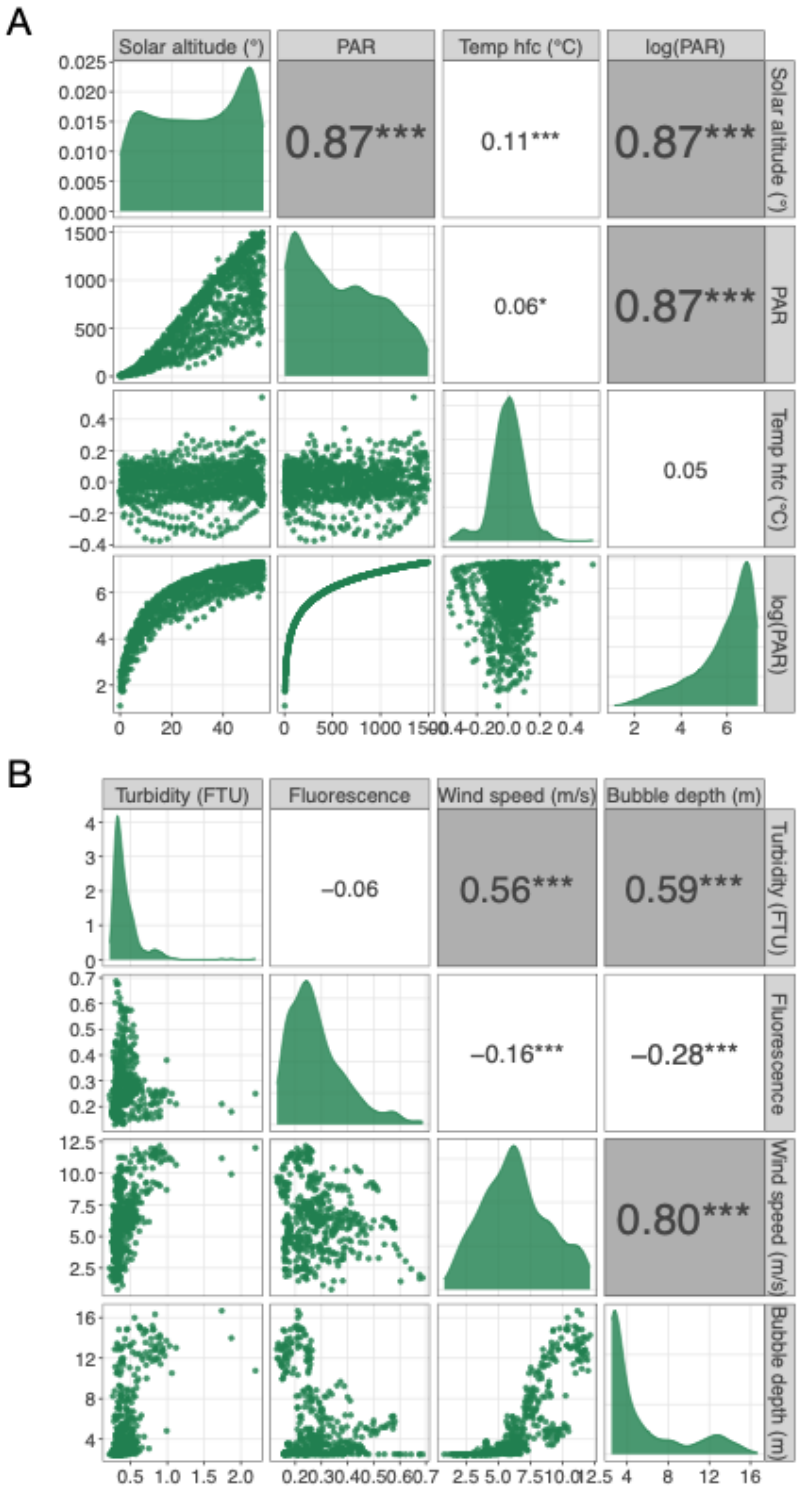


Figure 4.2.2: **Draftsman plot exploring collinearity between environmental predictor variables.** A) Daytime relationships between solar altitude, PAR, and the high frequency component of SST. B) Non-daytime relationships between turbidity, fluorescence, wind speed, and bubble plume depth. Scatter plots in the lower left triangle of subplots. Spearman's rank correlation coefficients in the upper right triangle of subplots, with significance value indicated by asterisks (' ' $p \geq 0.1$; '$*$' $p < 0.1$; '$**$' $p < 0.05$; '$***$' $p < 0.01$), and shaded grey where coefficients exceed 0.5. Density plots in diagonal subplots.

coefficients and scatter plots (Figure 4.2.3). Although retained predictor variables did not exceed the arbitrary threshold of $|\rho| \geq 0.5, p < 0.01$, some were significantly collinear, albeit with weaker correlation strengths. For example, higher surface salinities tended to be recorded alongside higher SSTs. High wind speeds were associated with low SSTs whereas low wind speeds were associated with a wider range of SSTs encompassing both low and high values, resulting in a negative correlation ($\rho = -0.45$). Fluorescence and salinity were slightly positively correlated ($\rho = 0.29, p < 0.01$), whereas fluorescence and wind speed were slightly negatively correlated ($\rho = -0.16, p < 0.01$).

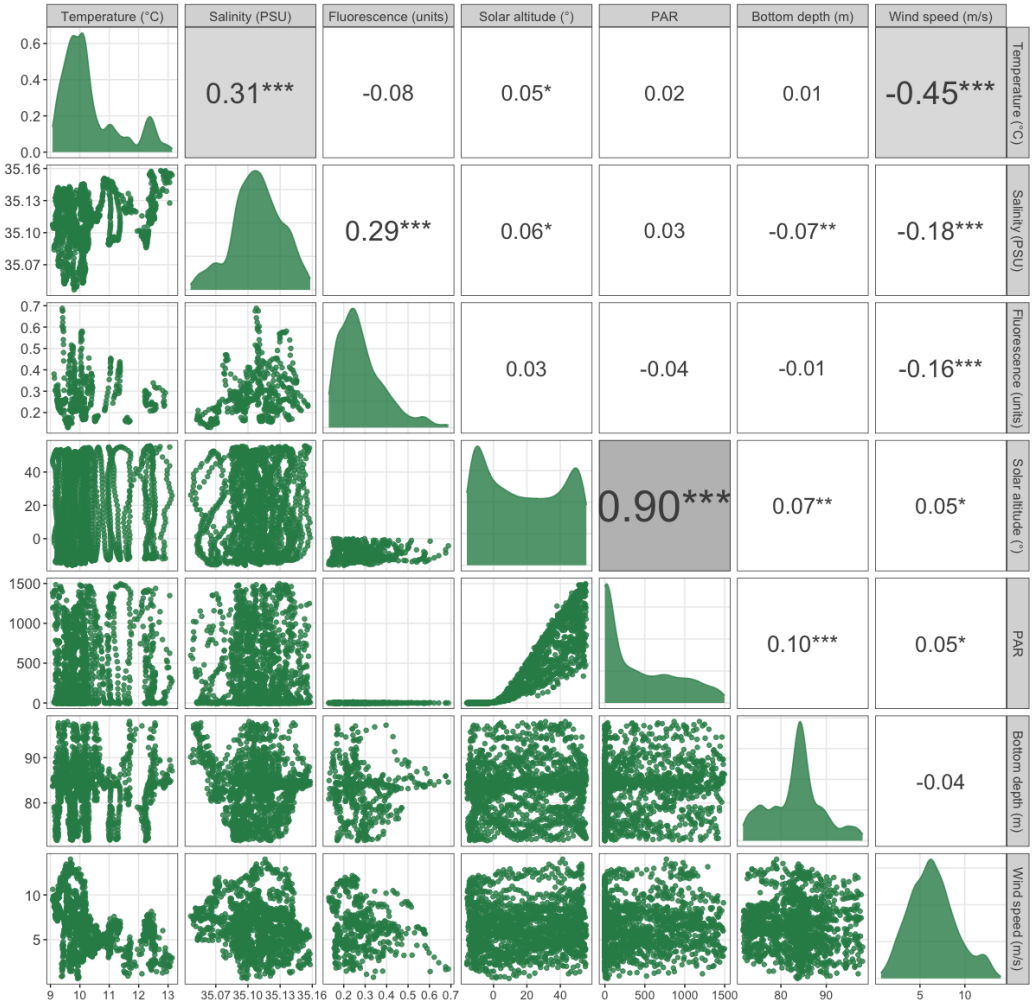


Figure 4.2.3: **Draftsman plot of relationships between environmental predictor variables.** For brevity, high and low frequency SST components are omitted. Scatter plots in the lower left triangle of subplots. Spearman's rank correlation coefficients in the upper right triangle of subplots, with significance value indicated by asterisks (' ' $p \geq 0.1$; '$*$' $p < 0.1$; '$**$' $p < 0.05$; '$***$' $p < 0.01$), and shaded grey where coefficients exceed 0.5. Density plots in diagonal subplots.

**Fluorescence quenching**

Fluorescence values were depressed when irradiance levels were high, suggesting that non-photochemical quenching occurred during the day (Figure 4.2.4). Two-sample Kolmogorov-Smirnoff tests confirmed that twilight and nighttime distributions were similar (twilight-night $D = 0.09, p = 0.33$), but both comparisons of day and nighttime and day and twilight distributions differed substantially (day-night $D = 0.58, p < 0.01$, day-twilight $D = 0.62, p < 0.01$).

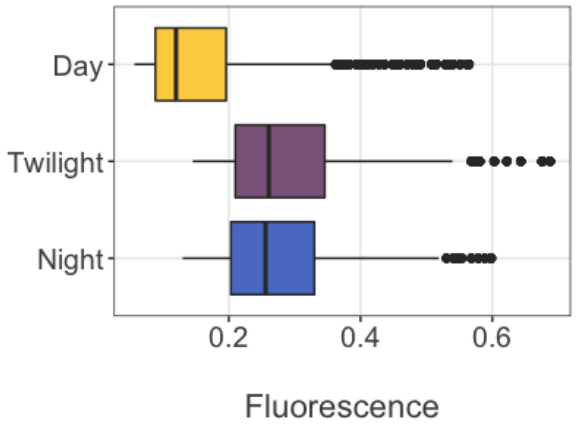


Figure 4.2.4: **Surface fluorescence measurements (arbitrary units), grouped by time of day.** Quenching resulted in lower daytime fluorescence readings.

Two often-used methods to correct for chlorophyll quenching include interpolating between time periods with valid data (i.e. non-daytime values) or using the ratio of optical backscatter to fluorescence measurements from valid data during twilight and night to reconstruct fluorescence using daytime optical backscatter measurements (Hemsley et al., 2015; Sackmann et al., 2008). However, neither of these methods was appropriate for this dataset. *Lyra's* nighttime fluorescence and Seaglider fluorescence data in the euphotic zone both showed spatio-temporal variability at scales much smaller than those required to be interpolated across, rendering the first method unreliable. Daytime intervals lasted for around sixteen consecutive hours during which time *Lyra* would often have traversed across more than $30\,\mathrm{km}$. The ratio of optical backscatter to fluorescence must remain fairly constant in order to use the second method described above to correct for quenching. Two problems precluded correction by the second method: 1) turbidity was highly correlated

with wind speed and bubble plume depth, indicating that air bubbles dominated detections during windy weather, and the correlation between optical backscatter and fluorescence was low and non-significant (Figure 4.2.2, B) and 2) turbidity measurements are not directly comparable to optical backscatter measurements. Therefore, daytime measurements were discarded and only twilight and nighttime measurements were retained.

### 4.2.4 Modelling

GAMMs were fitted to model response variables for different time of day categories, using predictor variables according to data availability. For the FL group, only nighttime data were used since acoustic masking by the GF group dominated the signal during daytime and twilight. Preliminary testing using gaussian and scaled-t families to model residuals found that a gaussian distribution performed well in terms of test statistics, visual assessment of residual plots, and processing speed, and was consequently used for all models.

Models for the GF group included all data and a subset of only daytime data, in order to establish whether relationships between predictors were mostly the result of transitional periods during twilight where DVM behaviour was expected to exert the main control on distributions, or whether these variables still influenced vertical position and geographic position during daytime when the layer remained relatively static at depth. FS response variables were modelled both with and without a fish school outlier identified in Chapter 3 (large size with high NASS detected on 17$^{\text{th}}$ May 2018). GF and FS models in each of their respective cases produced similar relationships using the same set of predictor variables. For brevity, only results of models using all data are presented.

Spatial and temporal autocorrelation is common in environmental time series, particularly in acoustic data where sampled water volumes and echoes from the organisms within them may overlap in successive pings (Zuur et al., 2009; Zhi et al., 2021). Autocorrelation can skew results of statistical analyses, including GAMMs, and lead to overestimation of the relative importance of variables. *Lyra* made repeat measurements along a zonal transect, and so in addition to along-track spatial autocorrelation within each transect, areas were revisited at differing time intervals throughout the mission. Despite averaging over $600\,\mathrm{m}$ horizontal

bins, there is a reasonable likelihood that spatial or temporal autocorrelation remained in some of the data.

In an attempt to account for spatial and temporal autocorrelation, two correlation structures were fitted to preliminary GAMMs. An auto-regressive (AR1) temporal correlation structure, here named 'bindex', provided an index of each longitudinal bin as encountered chronologically (1-1618). Another structure tested, named 'bin-trans', indexed bin numbers (1-108, west to east) for each transect (1-15), where applicable. These structures primarily accounted for either temporal (bindex) or within-transect spatial (bin-trans) autocorrelation, so longitude was also included as a predictor variable to test whether any geographic spatial dependencies were present. Evidence of autocorrelation remaining in model residuals was discerned by comparing $p$ values of Moran's I statistics for models with and without correlation structures fitted using the R package 'ape' (Paradis and Schliep, 2019; Zhi et al., 2021). Moran's I determines whether neighbouring data (in time or space) are more similar than would be expected under the null hypothesis that the data are randomly distributed. Therefore, a $p$ value of $p < 0.05$ was taken as evidence that autocorrelation remained in the model tested. Preliminary testing indicated that the bindex correlation structure performed best and this structure was subsequently fitted to all final models.

GAMMs were created and tested using the 'mgcv' package in R (Wood, 2011). Model residuals were plotted using the 'gam.check' function and visually inspected. Models were selected based on: explanatory power, where higher adjusted $R^2$ values explain more deviance; model parsimony, where lower Akaike Information Criterion (AIC) and Bayesian Information Criterion (BIC) values indicate a more optimally informative model, accounting for the cost of increased model complexity; and effect size, where larger F statistic values indicates an improved model fit. All models included smooth terms with five knots, and were fitted with the bindex correlation structure.

Single predictor models informed the choice of predictor variables to include in so-called full models. Full models were formed by combinations of statistically significant predictor variables, however the statistically significant single predictors for FL GAMMs were not always found to be statistically significant in full models. Instead, full models were created

by testing combinations of various predictors to determine a set of better performing models with interpretable results. Although unquenched fluorescence was a significant predictor in the single FS models for NASS, with a seemingly strong explanatory power ($R^2 = 0.73, p < 0.01$), there were only seven fish schools detected during non-daytime hours when fluorescence measurements were unquenched. On the grounds of low statistical power and exclusion of the majority of the data, fluorescence was therefore not used in full FS models. Final models for each acoustic group-response-time variable combination were selected from the sets of full models (Table 4.2).

### 4.2.5 Seaglider subsurface measurements

Subsurface measurements of various water properties were made by the University of East Anglia's *Seaglider 510* along the same transect line (Figure 4.2.5 between red triangles in A). These were also analysed to provide oceanographic context for interpreting GAMM results. The Seaglider experienced some latitudinal deviation from the transect line during its first crossing in this time period, and, due to the difference in horizontal travel speeds between the Seaglider and *Lyra*, the two vessels were only geographically co-located within one kilometre during six timeperiods in May: morning of the 11$^{\text{th}}$, late morning of the 18$^{\text{th}}$, late morning to mid afternoon on the 20$^{\text{th}}$, evening of the 24$^{\text{th}}$, evening of the 29$^{\text{th}}$ extending overnight into the 30$^{\text{th}}$, and finally during late morning of the 30$^{\text{th}}$ (Figure 4.2.5, B).

Temperature, salinity, optical backscatter at $470\,\mathrm{nm}$, fluorescence, and oxygen measurements were made by a Seabird unpumped glider CTD, Seabird Scientific ECO-puck, and Aanderaa 4330F with fast foils over four transects that overlapped the acoustic data collection period from 11$^{\text{th}}$ May until 1$^{\text{st}}$ June 2018. Data were processed using the UEA Seaglider Toolbox (Hull and Kaiser, 2023). Temperature, salinity, oxygen and fluorescence data were plotted as zonal sections for each transect. Salinity and fluorescence data were gridded in $2\,\mathrm{m}$ depth by $2$ hour bins to improve graphical visualisation. Two thermoclines were defined using a threshold method. Salinity, temperature, and twilight- and nighttime-only fluorescence data in the upper $5\,\mathrm{m}$ were averaged over $0.02°$ bins for comparisons with *Lyra's* surface measurements.

Table 4.2: **Final GAMM specifications.** Smooth (s()) terms were allowed five knots. All models used the 'bindex' correlation structure.

| Group | Period | Response | Model terms | AIC | BIC | $R^2$ adj | F |
|---|---|---|---|---|---|---|---|
| Gas-filled | All | NASS | s(solar_alt) + s(bottom) + s(lon) + s(time) | 4318 | 4377 | 0.69 | 3.81 |
| | | Sv | s(solar_alt) + s(bottom) + s(lon) + s(time) | 4310 | 4369 | 0.63 | 3.81 |
| | | COM | s(solar_alt) + s(bottom) + s(lon) + s(time) | 5620 | 5679 | 0.83 | 3.74 |
| | | ALT | s(solar_alt) + s(bottom) + s(lon) + s(time) | 5620 | 5679 | 0.82 | 3.74 |
| | Day | NASS | s(solar_alt) + s(bottom) + s(lon) + s(time) | 2924 | 2980 | 0.60 | 3.94 |
| | | Sv | s(solar_alt) + s(bottom) + s(lon) + s(time) | 2917 | 2972 | 0.52 | 3.95 |
| | | COM | s(solar_alt) + s(bottom) + s(lon) + s(time) | 3839 | 3894 | 0.63 | 3.86 |
| | | ALT | s(solar_alt) + s(bottom) + s(lon) + s(time) | 3848 | 3893 | 0.55 | 3.87 |
| Fish school | All | NASS | s(thickness) + s(wind) | 827 | 848 | 0.65 | 3.77 |
| | | Sv | s(thickness) + s(wind) | 769 | 790 | 0.26 | 1.00 |
| | | COM | s(thickness) + s(wind) + s(bottom) | 904 | 930 | 0.64 | 3.62 |
| | | ALT | s(thickness) + s(wind) | 900 | 921 | 0.38 | 1.14 |
| Fish school, no outlier | All | NASS | s(thickness) + s(wind) | 814 | 835 | 0.65 | 3.81 |
| | | Sv | s(thickness) + s(wind) | 766 | 787 | 0.18 | 2.09 |
| | | COM | s(thickness) + s(wind) + s(bottom) | 918 | 944 | 0.63 | 3.63 |
| | | ALT | s(thickness) + s(wind) | 914 | 935 | 0.35 | 1.00 |
| Fluid-like | Night | NASS | s(lon) + s(time) + s(GFNASS) + s(wind) | 584 | 616 | 0.71 | 1.47 |
| | | Sv | s(salinity) + s(lon) + s(time) + s(GFSv) + s(wind) + s(bottom) | 388 | 433 | 0.72 | 1.00 |
| | | COM | s(salinity) + s(lon) + s(GFNASS) + s(wind) + s(bottom) | 719 | 757 | 0.70 | 2.86 |
| | | ALT | s(salinity) + s(lon) + s(GFNASS) + s(wind) + s(bottom) | 717 | 749 | 0.67 | 1.96 |

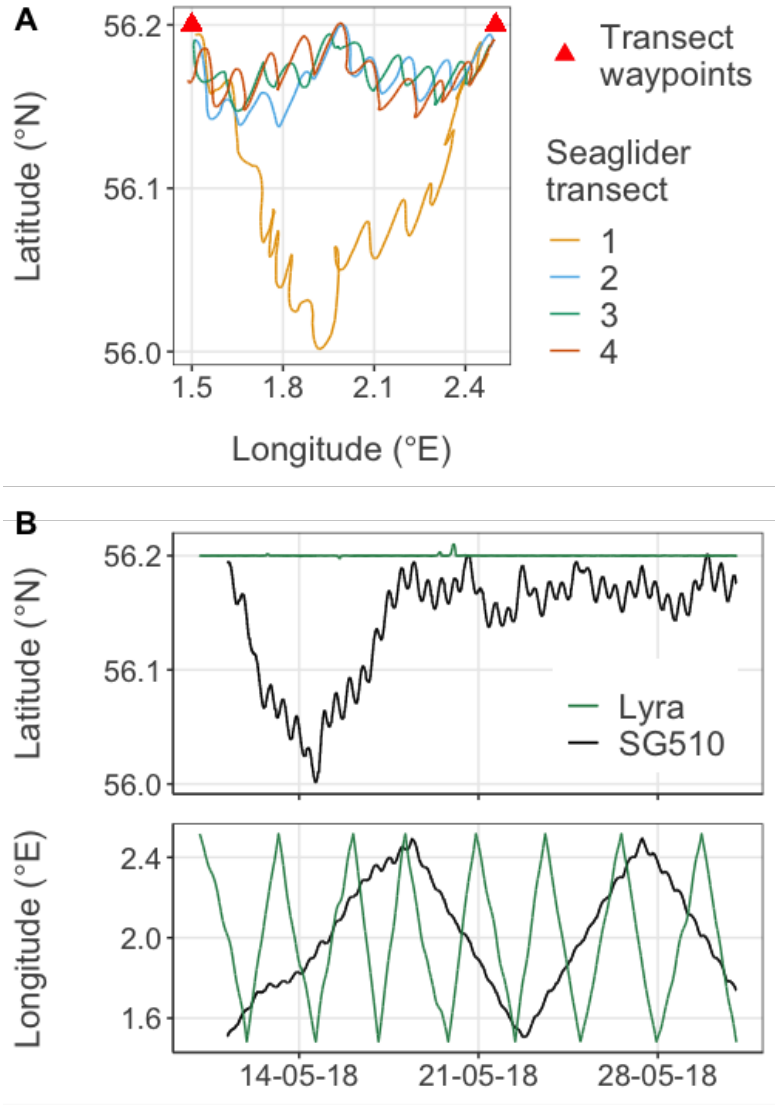


Figure 4.2.5: **Position of Seaglider 510 in relation to A) the transect waypoints and B) *Lyra*.** Seaglider transect crossings were much slower than *Lyra's* transit, and took approximately seven, four, five, and four days respectively for the chronologically numbered transects shown in panel A). During its first transect crossing, the Seaglider deviated south from the transect line.

## 4.3 Results

### 4.3.1 Spatial patterns in backscatter

The bathymetry of the region in which the transect is situated has two notable features. There is a trough that runs northwest to southeast at approximately $1.7°$E, descending to almost $100\,\mathrm{m}$ at its deepest point. There is also a crossover of ridge peaks above $75\,\mathrm{m}$ near $2.4°$E (Figure 4.3.1). *Lyra's* passage back and forth across the transect recorded average depths per longitudinal bin that varied by less than $0.5\,\mathrm{m}$ as *Lyra* followed a relatively consistent path with minimal latitudinal variation. Any minor latitudinal variation did not affect bottom measurements made by the echosounder much, since meridional bathymetric gradients in this region are generally fairly flat.

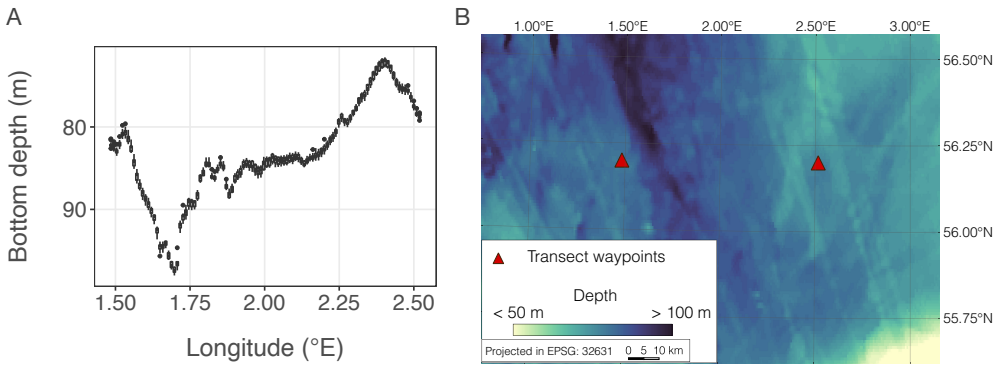


Figure 4.3.1: **Bathymetry along the transect and in the surrounding region.** A) Boxplots (boxes indicating interquartile range) of bottom depth along transect during acoustic data collection and B) map of bathymetry (General Bathymetric Chart of the Oceans, 2014) in the region of the transect.

Fish schools were detected across the transect, generally remaining in close proximity to the bottom (Figure 4.3.2). Where they appeared in clusters, they tended to be situated over the trough at $1.7°$E or along the western slope of the ridge at $2.4°$E (from hereon, termed 'trough' and 'ridge' respectively). With the exception of a handful of schools, there was an absence of fish schools over the ridge peak itself and the eastern slope.

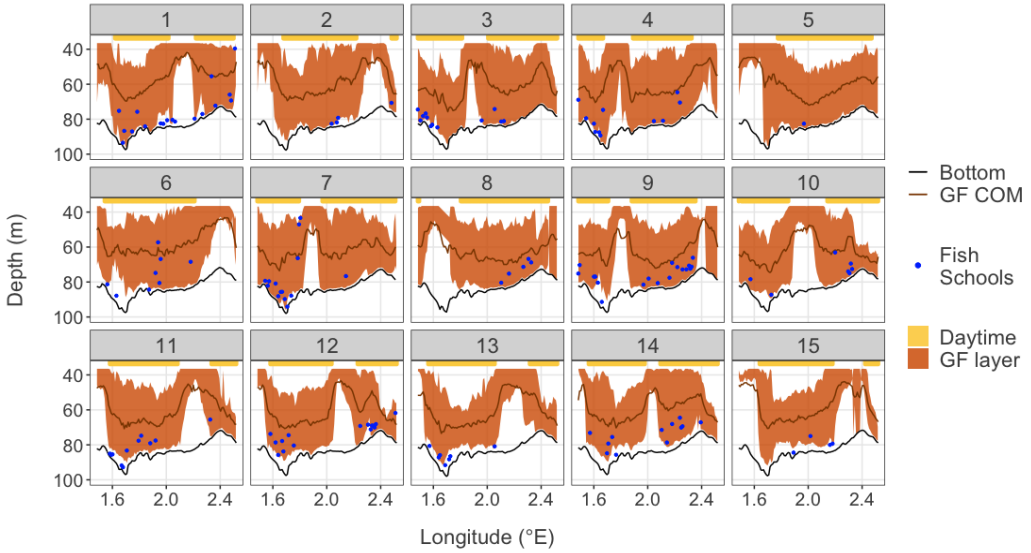


Figure 4.3.2: **Position of the GF layer and fish schools along each transect.** Centre of mass of the gas-filled group (GF COM) shown by dark orange line. GF layer bounds (orange shading) defined by $-73\,\mathrm{dB}$ threshold offset lines. Blue dots indicate the detection of a fish school. Black line indicates bottom bathymetry. Yellow strip at top of each subplot indicates daytime hours.

GF backscatter was present across the transect at all times of day (Figure 4.3.2). During daytime, there was considerable horizontal variation in the depth of the upper bound of the layer, defined by a $-73\,\mathrm{dB}$ threshold offset line. Also, the upper bound typically deepened as bathymetry deepened, but also fluctuated at smaller-scales, which may have been related to variation in thermocline depth and internal waves. By contrast, the lower bound typically followed the contour of the bottom. The GF layer did not appear to respond to the presence of fish schools, as the lower bound often extended to similar depths as the fish schools and the layer was not absent from regions where high densities of fish schools were detected. This is not unsurprising since North Sea forage fish are not known to predate on siphonophores, the organisms suspected of comprising the GF group (Den Hartog and Van Nierop, 1984; Nakamura et al., 2015; Hetherington et al., 2022). This observation was supported by the lack of significance of FSNASS or FSSv predictors in the single GF GAMMs.

GF backscattering strengths were often depressed and the upper bound of the layer was often deeper over the ridge peak and along the eastern slope, despite the shallow bathymetry in this region (see Transects 2-3, 7, 10-15 in Figure 4.3.2). West of the ridge, daytime upper bound tended to sit at around $40\,\mathrm{m}$ depth, i.e. near the lower thermocline depth. However,

over the ridge and east of it, the upper bound depth was often deeper than $60\,\mathrm{m}$. This region had lower NASS when comparing either daytime or nighttime distributions (Figure 4.3.3). GF organisms that preferred depths shallower than $60\,\mathrm{m}$ may have been absent or dispersed horizontally east of the ridge due to the flow regime over the ridge. The distribution of FL NASS across the transect during daytime showed an inverse relationship with GFNASS, likely due to acoustic masking. However, nighttime FL NASS was highest near the ridge and tended to be greater at night, possibly indicating reverse DVM behaviour or the relative absence of GF organisms during the night in this region (Figure 4.3.3).

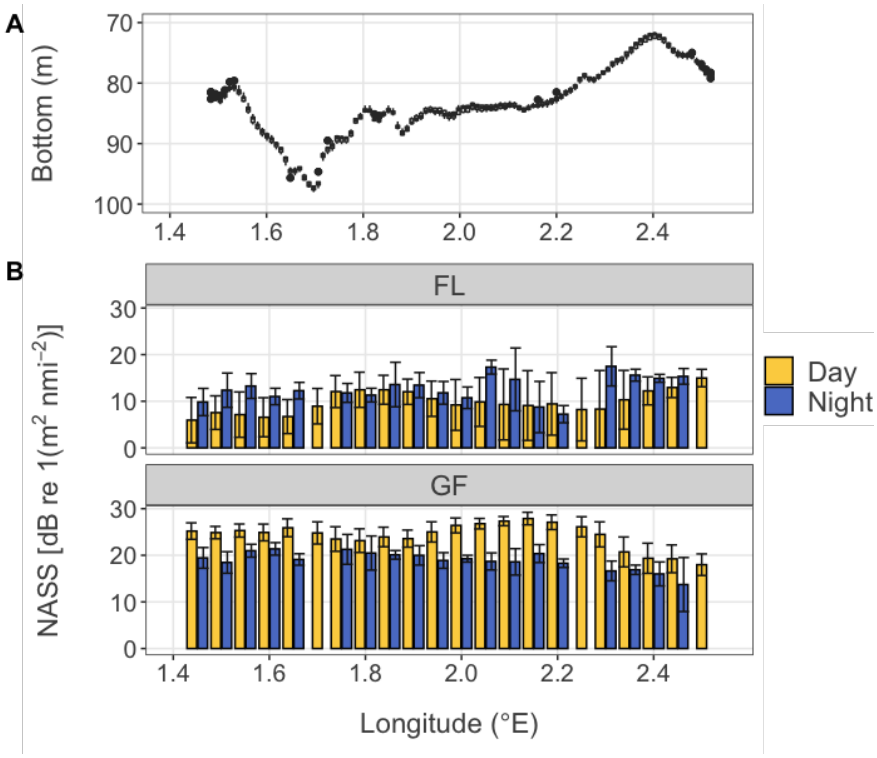


Figure 4.3.3: **Bottom depth and mean daytime and nighttime GF and FL NASS along the transect.** A) Boxplots of bottom depth as measured by echosounder, grouped by $0.01°$ longitudinal bin. B) Distributions of mean NASS grouped by $0.05°$ bins, error bars show $\pm$ standard deviation.

### 4.3.2 Oceanography of the transect region

Seaglider observations provided insight into the physical and biogeochemical structure of the water column in the vicinity of the transect, information that was unobtainable by *Lyra* whose non-acoustic measurements were restricted to the surface. Timing of the mission coincided with the development of stratification into a three-layer system defined by two thermoclines: a weaker upper thermocline of variable depth (mean $18.6 \pm 6.8\,\mathrm{m}$) and a stronger lower thermocline that remained at a more constant depth (mean $42.5 \pm 2.3\,\mathrm{m}$) but that gradually deepened over the course of the time series (Figure 4.3.4).

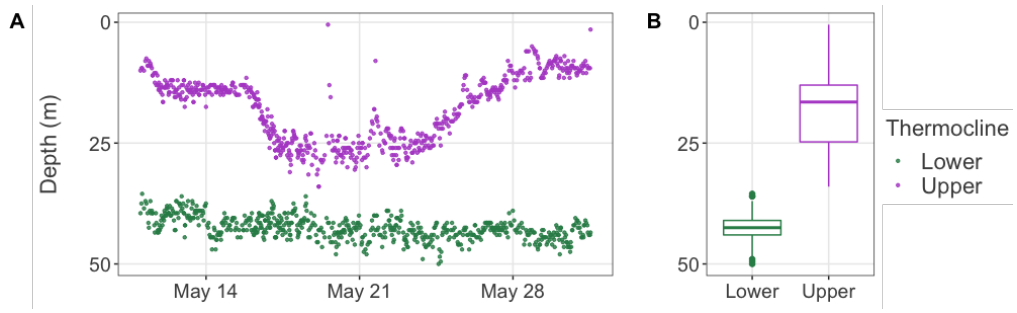


Figure 4.3.4: **Depths of the upper (purple) and lower (green) thermoclines.** Panel A shows change in thermocline positions over time. Panel B shows boxplots of grouped data.

Temperature measurements tracked the development of the upper thermocline (Figure 4.3.5, A), and the thermoclines induced density gradients that separated the water column into a surface mixed layer (SML), a middle mixed layer (MML), and a bottom mixed layer (BML), visible as orange and pink, purple, and dark blue layers in Figure 4.3.5 (A). Fluorescence measurements show the persistence of a deep chlorophyll maximum (DCM) (Figure 4.3.5, D), and other variables revealed features such as fronts delineating a transient column of higher salinity and lower oxygen water (Figure 4.3.5, A, B & E) and a region of persistently colder, fresher and less oxygenated water with comparatively higher optical backscatter and fluorescence readings in the deeper part of the water column that gradually diminished over time (Figure 4.3.5, A-E).

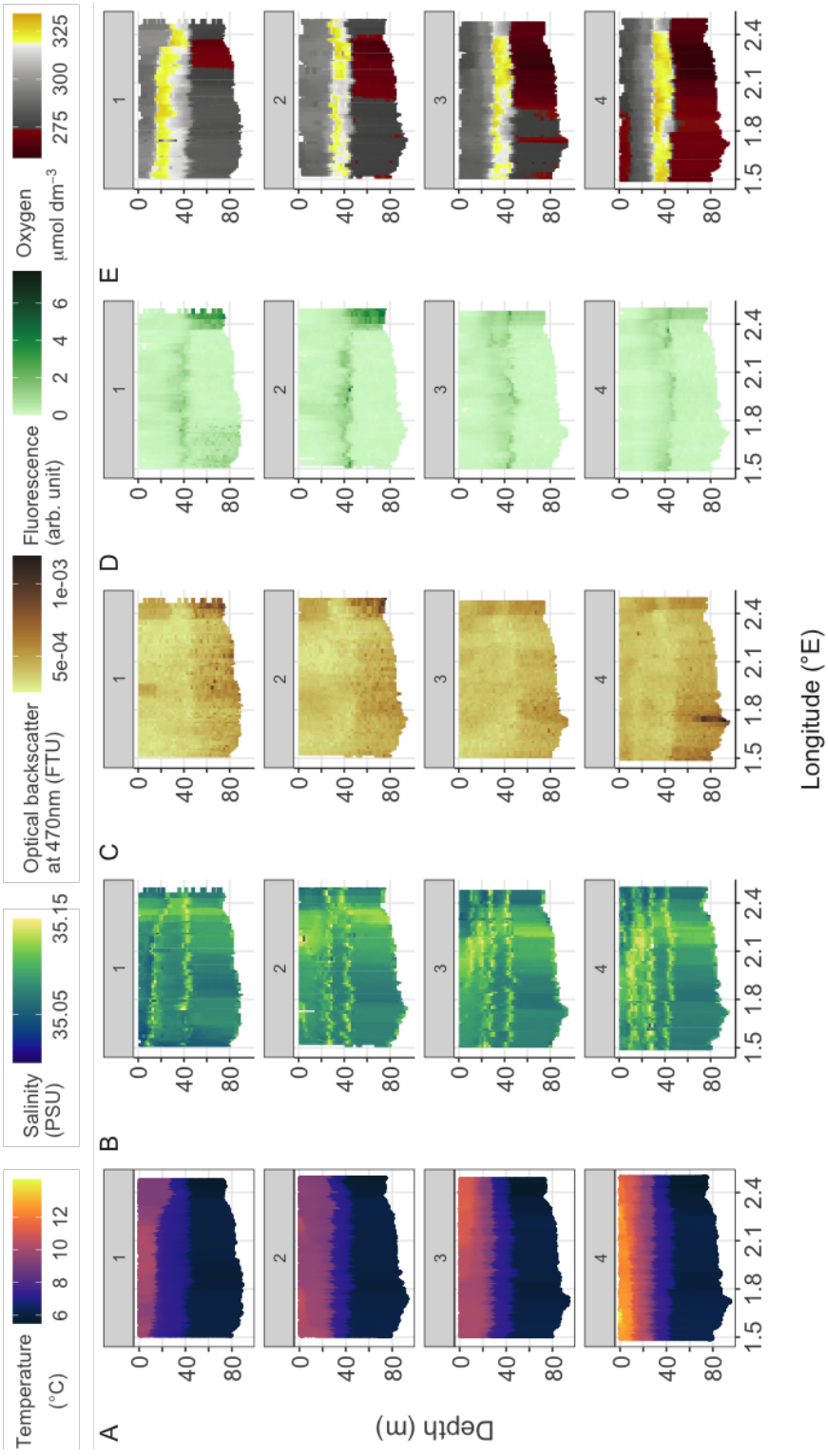


Figure 4.3.5: **Longitudinal sections of Seaglider 510 temperature, salinity, optical backscatter, fluorescence, and saturated oxygen data.** Sections from top to bottom show glider transects 1-4. The glider travelled west to east on odd numbered transects and east to west on even numbered transects. Some erroneous high salinity values are evident at the thermoclines due to thermal lag in the CTD sensor (a common problem for gliders).

In general, oxygen levels in the water declined over the course of the mission, possibly due to slowing of primary production following the spring bloom and an increase in respiratory activity of growing heterotrophic populations. Figure 4.3.5 (E) shows a marked difference between oxygenation of layers separated by the thermoclines. Water column stability imposed by stratification prevents vertical mixing, leading to the formation of oxyclines, which can have both significant ramifications for and be further modified by biological distributions (Slater et al., 2020; Miller and Graham, 2012; Perry et al., 2008; Pischedda et al., 2008; Binetti et al., 2020; Breitburg et al., 2018). In line with other studies in the North Sea (Greenwood et al., 2010; Queste et al., 2016), oxygen levels were lowest in the BML, likely due to oxygen consumption by respiring organisms at the seabed, reduced primary production due to the limitation of light, and limited resupply of oxygen via vertical mixing due to stratification. Whilst oxygen levels in the BML were low (minima of $260\,\mu\mathrm{mol\,dm^{-3}}$), they were not as depleted as those recorded by Queste et al. (2013) who reported measurements as low as $180\,\mu\mathrm{mol\,dm^{-3}}$ in 2010, and were not indicative of hypoxic conditions (Painting et al., 2005). The MML had the highest oxygen levels. Whilst warmer than the BML, water in the MML is less subject to solubility changes due to surface warming than the SML, and increased productivity at the DCM probably explains the higher oxygenation in this layer.

The majority of the acoustic analysis layer was comprised of the BML since the analysis layer considered regions below $36\,\mathrm{m}$ depth, thus the main focus here is on patterns in the BML itself and associations between water properties in the BML and the SML, from where measurements from *Lyra* were input as predictor variables in the GAMMs.

The upper thermocline deepened abruptly following the period of persistent strong winds that began on 16$^{\text{th}}$ May 2018 (Figure 4.3.5, A), mixing colder water from the MML into the SML and causing temporary cooling of the SML. Temperatures generally increased in the SML due to solar warming as spring advanced towards summer, whereas temperatures in the MML and BML remained fairly constant. The only noticeable temperature variations in the BML appeared to be associated with spatial features along the transect, with a patch of colder water ($5.95\,^{\circ}\mathrm{C}$, compared to BML average of $6.02\,^{\circ}\mathrm{C}$ observed near $1.8^{\circ}\mathrm{E}$ and another region of colder water (minimum $5.65\,^{\circ}\mathrm{C}$ east of the ridge at $2.4^{\circ}\mathrm{E}$. These regions of colder BML water were also fresher than neighbouring waters (Figure 4.3.5, B).

Fluorescence was both vertically and horizontally heterogeneous. The DCM was clearly visible at the position of the lower thermocline, varying in fluorescent intensity throughout the time series (Figure 4.3.5, D). In the North Sea, the DCM often forms as a thin layer near the thermocline, and can account for almost two-thirds of production in the central North Sea (Fernand et al., 2013; Weston et al., 2005). Fernand et al. (2013) similarly observed a three-layer system defined by a double thermocline, and also observed higher levels of chlorophyll fluorescence in the MML than the SML as also seen from the glider observations in this study.

Within the BML, there was a region of patchy high fluorescence at the western edge of the transect during the start of the time series (Figure 4.3.5, D), however the highest fluorescence was observed at the eastern edge of the transect over the ridge. Here a patch of intense fluorescence persisted over repeated transects, decaying in intensity towards the latter half of the mission. The accumulation of fluorescing material at depths usually associated with light-limiting growth is unusual and could represent subduction of chlorophyll from a highly productive region of the DCM, perhaps due to hydrodynamic flow over the ridge combined with wind-driven mixing. Observations of this patch during Transect 1 coincided with the period of strong winds which began whilst the glider was sampling at $2.20°$E during Transect 1 and ceased when the glider was sampling at $2.48°$E during Transect 2. Storms are capable of injecting nutrients, oxygen and particles from upper layers into the BML (Rabalais et al., 2009). Therefore, the higher oxygen and fluorescence values seen in this region could be the result of wind-driven mixing bringing oxygen from the MML and chlorophyll from the DCM into the BML. Increased fluorescence in the BML following the strong wind event was not seen across the west of the transect, and it is unlikely that water column compression due to the shallower bathymetry could account for the increased values seen over the eastern slope of the ridge, indicating that this region was likely more productive than elsewhere.

Salinity exhibited steep horizontal gradients but was comparatively uniform with depth; higher values at the surface often coincided with higher values within the MML and BML (Figure 4.3.5, B). Note that extreme salinity values and sharp vertical gradients across the thermoclines shown in Figure 4.3.5 (B) are a result of thermal lag of the CTD sail on the glider, and should be considered erroneous. A column of saltier water was apparent along the

western slope of the ridge, forming fronts either side. The fronts gradually moved westwards as the time series progressed, but at a slightly faster rate in the SML than the BML. The column of saltier water in the BML was also less turbid and warmer than water to the east or west (Figure 4.3.5, C). These distinct properties, demarcated by sharp horizontal gradients, point to a conclusion that water in this region originated from oceanic inflow (Winther and Johannessen, 2006).

North Atlantic inflow water is typically less turbid than water of riverine or estuarine origins, more saline, and often also warmer (Winther and Johannessen, 2006). Preliminary tests of correlation between salinity and optical backscatter, and between salinity and temperature in the BML ($2\,\mathrm{m}$ by $2\,\mathrm{m}$ gridded data below $50\,\mathrm{m}$ depth) show that there was an overall very weak negative correlation between salinity and optical backscatter ($\rho = -0.16, p < 0.001$), and a very weak correlation between salinity and temperature ($\rho = 0.14, p < 0.001$). When analysed by transect, all correlations were significant and showed that correlation strengths were similarly either very weak or weak ($p < 0.001$), except for the correlation between temperature and salinity in transect 1 when the Seaglider deviated from $56.2°$ latitude and thus was not co-located with *Lyra's* transect for its duration (Figure 4.3.6). These results provide some support, albeit weak, for the view that the fronts observed near the ridge delineated water of a different, more oceanic origin.

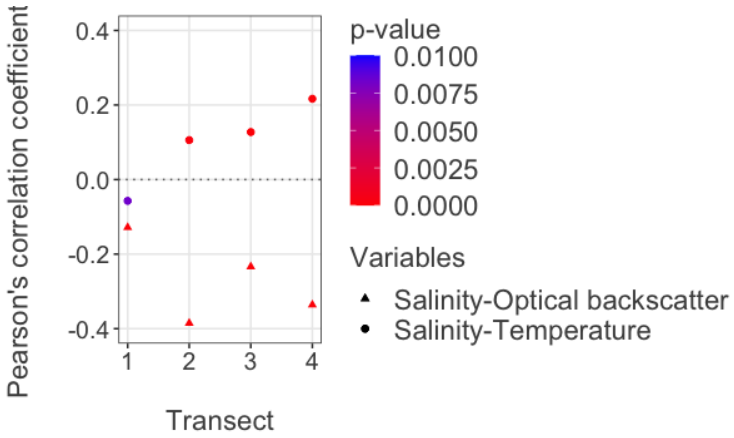


Figure 4.3.6: **Correlation between salinity and optical backscattering at 470 nm (triangles) and salinity and temperature (°C, circles) in the BML.** Pearson's correlation coefficient calculated per transect using $2\,\mathrm{m}$ by $2\,\mathrm{m}$ gridded Seaglider data from below $50\,\mathrm{m}$ depth, coloured by $p$ value of correlation test.

This column of distinct water appeared as a narrow band of high salinity values several kilometres across (zonal width), gradually extending in the zonal direction as it transited westwards and presumably mixed with the less saline water in the region, given that the frontal gradients became less steep. This can be seen in Figure 4.3.7, where the GAM smooth fitted to salinity values shows a gradual flattening of the curve above 35.1 PSU and movement westwards. Although the glider was south of the nominal transect line (at 56.1°N) when it sampled near the ridge at 2.25°E during Transect 1, it was travelling northeastwards towards the transect line when over the ridge (Figure 4.2.5). This pulse of warm, saline water spreading through the region could be related to the variability of North Atlantic inflow over short (weekly) timescales (Sheehan et al., 2020).

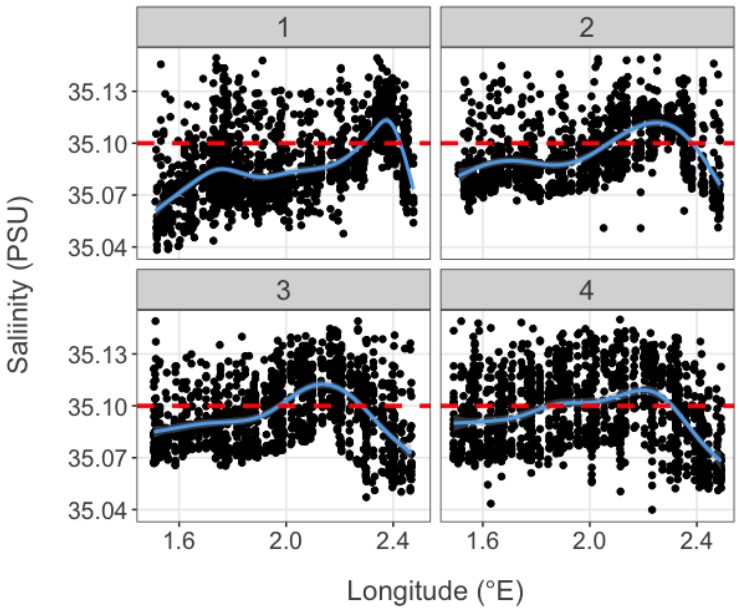


Figure 4.3.7: **Salinity in the BML by transect, with GAM smooth (blue line).** Gridded (2 m by 2 m) salinity values within the BML below 50 m, dashed red line indicating 35.1 PSU for visual reference.

Across slopes of a ridge, it is common to find fronts emerging due to differing current speeds and/or direction either side. The western slope was characterised by warmer, saltier and less turbid water that had lower fluorescence values, whereas the eastern slope was characterised by colder, fresher water and high fluorescence values. Glider data can be used to estimate tidal current strengths (Sheehan et al., 2018) and having this information could prove useful to understand how local changes in flow influence zooplankton distributions across the front.

However, due to time constraints I did not pursue this analysis.

Surface measurements of temperature and fluorescence made by *Lyra* reflect those from the upper $5\,\mathrm{m}$ made by the Seaglider (Figure 4.3.8). Figure 4.3.8 (A) tracks the development of stratification by solar warming at the surface, up to a maximum recorded temperature of $13\,^{\circ}\mathrm{C}$. Cooling of the surface waters due to mixing by strong winds between the $16^{\mathrm{th}}$ to $18^{\mathrm{th}}$ May 2018 is evident in the temperature data collected by both vehicles.

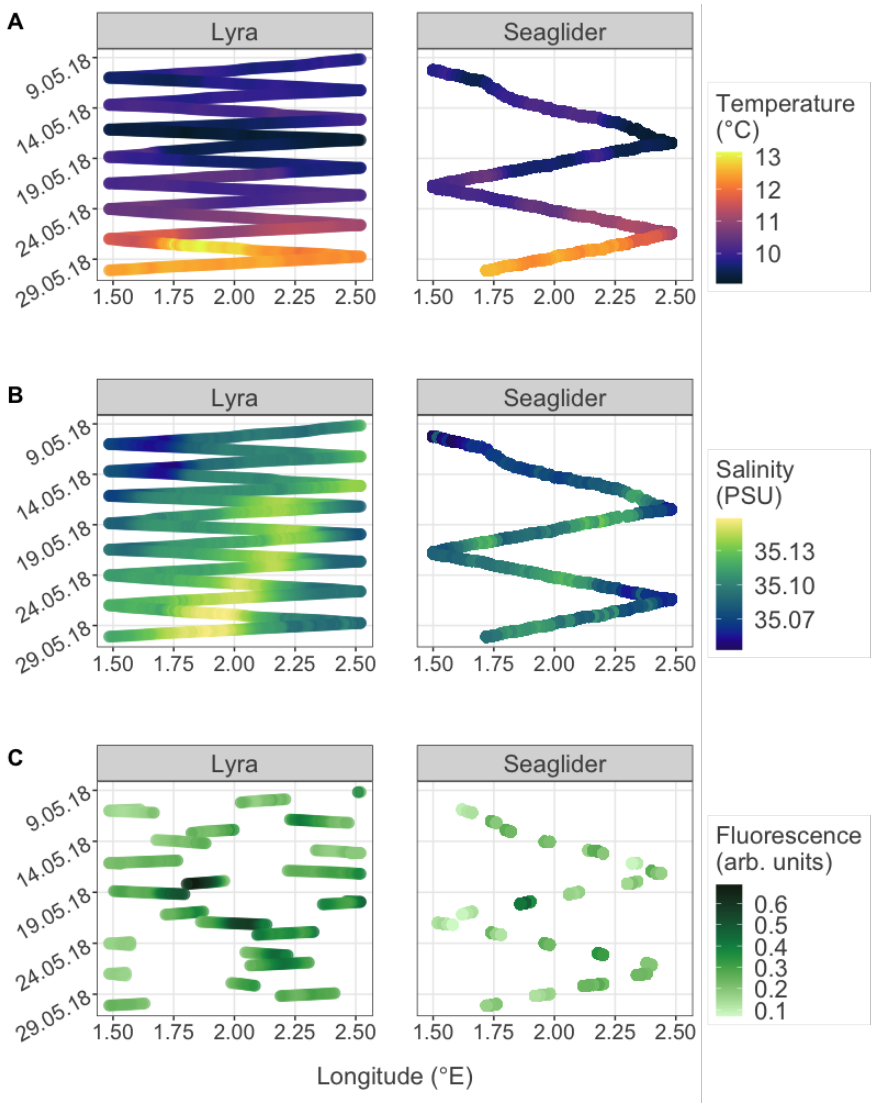


Figure 4.3.8: **Hovmüller plots of surface water properties.** A) Temperature, B) salinity, and C) fluorescence measurements collected by *Lyra* (left), and Seaglider 510 (right) averaged over the upper $5\,\mathrm{m}$.

*Lyra's* salinity measurements track the movement of the higher salinity front travelling westwards seen by the glider (Figure 4.3.8, B). Seaglider salinity measurements from the near-surface show some resemblance to *Lyra's* measurements but the front is less distinct and there is more variability at short timescales, however this disparity could be due to the comparison of measurements taken from different depths and geographic locations; there was a particularly notable departure from the transect line at $56.2°$N during the Seaglider's first transect. It is also possible that the Seaglider salinity data was affected by thermal lag of the CTD sail when crossing density gradients in the upper $5\,\mathrm{m}$ as stratification intensified, however little evidence of this is visible in the Seaglider sections (Figure 4.3.5, B).

Patterns of surface fluorescence collected by *Lyra* and the Seaglider were similar (Figure 4.3.8, C). The highest values recorded by *Lyra* at approximately $1.8$ to $1.9°$E on the $18^{\text{th}}$ of May were mirrored by those recorded by the Seaglider in the same region the following night. This occurred after the period of persistent strong winds, where wind speeds exceeded $7\,\mathrm{m\,s^{-1}}$ for more than two and half days. The strong winds resulted in increased mixing in the surface waters, and could well have mixed chlorophyll accumulated at the DCM throughout the water column including into the SML, increasing surface fluorescence over the following hours and days. Fluorescence at the surface, whether measured by *Lyra* or the Seaglider, was not well correlated with fluorescence at the DCM or within the BML. Thus, it is unsurprising that fluorescence was not found to be a significant predictor in any of the GAMMs developed to explain fish or zooplankton distributions in depths below $36\,\mathrm{m}$ (i.e. primarily the BML).

### 4.3.3 Models for each acoustic group

#### 4.3.3.1 Gas-Filled group models

All GAMMs for GF group included the predictor variables solar altitude, longitude, time, and bottom depth. This suggests that variables which correspond to non-varying geographic features across the transect, the diel cycle, and change through the spring season were most important in determining the distribution of gas-filled scatterers in the analysis layer. The 'time' variable may act as a proxy for a correlated hidden variable, such as stratification

strength or population changes during the season. These results emphasise that the main drivers of gas-filled zooplankton distributions for the spatio-temporal scales analysed were limited to those that varied within fixed spatial, diel, or sub-seasonal structures.

**Changes in GF distributions over time**

Progression of time was associated with a decrease in backscatter and NASS (Figure 4.3.9, A and E). This could have had several causes, including: a decrease in abundance or biomass, perhaps associated with mortality due to predation; a reduction in backscattering strength, perhaps due to a change in the size of gas-inclusions within the organisms coincident with their physiological development; or a change in group composition, for example juvenile fish with gas-filled swimbladders leaving the GF group and beginning to form schools as they mature. The latter possibility, however, was not supported by a coincident change in fish school backscatter during the mission.

Curiously, time had a parabolic influence on vertical position, with the period during the middle of the mission coinciding with a deepening of the layer and movement towards the bottom (Figure 4.3.10, A & E). The parabola was asymmetric, with the shallowest centre of mass (highest altitude) at the start of the mission. One explanation considered was that the layer was moving in response to changes in the lunar cycle, since changes in the brightness of the moon associated with lunar phase are known to alter depth distributions of DVM-performing zooplankton (Last et al., 2016). However, the full moon occurred on the 30$^{th}$ April 2018 and 29$^{th}$ May 2018, with the new moon on the 15$^{th}$ May 2018. This runs counter to the expectation that, given the GF layer exhibited classic DVM behaviour, the layer would shallow during the new moon and deepen at full moon. It is further unlikely to explain the observed trend since lunar brightness is only expected to influence zooplankton at night when the dominant influence of sunlight had diminished. During the night the (acoustic) bulk of the layer had ascended above the analysis layer, and night was the time of day category with the shortest duration. Thus any influence of the moon during these periods may not have been sufficient to drive the observed trend. Indeed, for daytime-only models, the smooth for time displayed the same parabolic pattern.

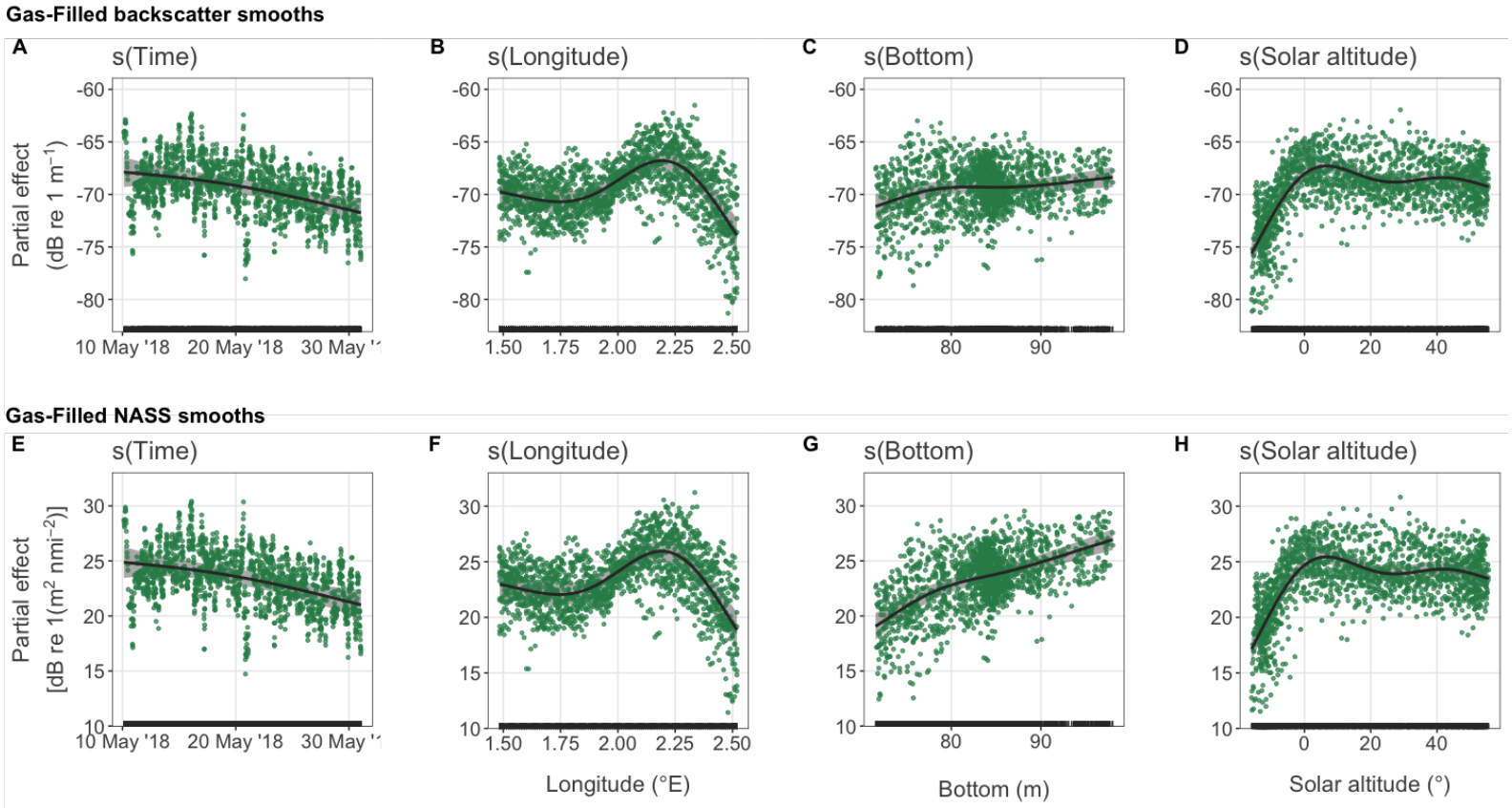


Figure 4.3.9: **Partial effects of predictor variables in the Gas-Filled group energetic GAMMs.** Partial effect plots show the modelled effect on the response variable of each predictor as a smooth, assuming all other modelled predictor variables are held constant at their mean. Smooths (black line) and model residuals (green points) shown for backscatter (A-D) and NASS (E-H) models. Shaded grey area shows 95 % confidence intervals for each smooth. Y-axes of the partial effects plots have been shifted to show the likely result of varying the predictor variable on response variable values.

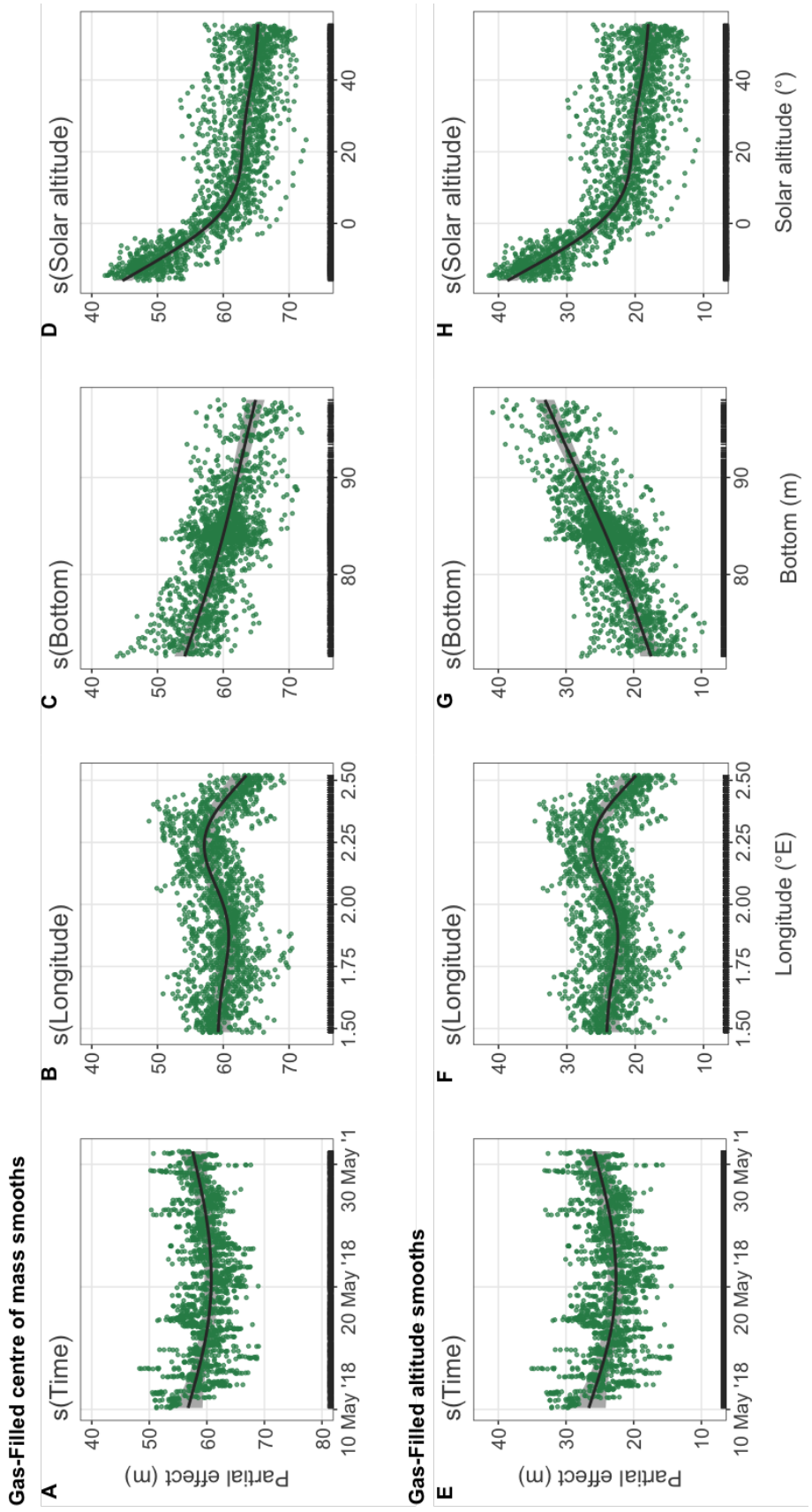


Figure 4.3.10: **Partial effects of predictor variables in the Gas-Filled group positional GAMMs.** Smooths (black line) and model residuals (green points) shown for centre of mass (A-D) and altitude (E-H) models. See Figure 4.3.9 for the description of partial effects plots.

Change in upper thermocline depth, correlating with the passage of time, was considered. The upper thermocline deepened during the middle part of the mission in response to strong winds on the 16$^{\text{th}}$ May, then gradually shallowed after the 22$^{\text{nd}}$ May towards its original position around $13\,\mathrm{m}$ (Figure 4.3.4, A). However, this movement does not mirror the pattern modelled for the GF centre of mass well, since deepening of the thermocline occurred much more abruptly than the deepening of the centre of mass. In addition, any mechanism for driving the distribution of GF layer deeper would likely have had an impact on $S_v$ and NASS as well, but this was not seen. The inclusion of time as a predictor in the centre of mass model had only a small effect on the amount of variance explained by the model ($R^2$ increased from $0.81$ to $0.83$) and time was not found significant in single predictor models ($p = 0.014$), which raises some doubt as to the validity of including this variable in the model.

**Bathymetry: bottom depth and position across the transect**

Model smooths for bottom depth showed linear relationships (C & G in both Figure 4.3.9 and Figure 4.3.10). Backscattering strength and NASS increased in deeper regions and the layer descended into deeper water where possible. However, the centre of mass did not deepen at the same rate as the bottom, partly owing to the non-uniform vertical distribution of scatterers in the water column, which could have contributed to the increase in altitude in deeper regions (Figure 4.3.10, C & G). Over the depth range of the bottom ($26\,\mathrm{m}$, from $72$ to $98\,\mathrm{m}$), the centre of mass smooth varied by $11\,\mathrm{m}$ (Figure 4.3.10, C). This is a substantial depth difference owing to changes in bottom bathymetry alone, representing a difference of up to $11\,\%$ of the available water column depth. The overall distribution of gas-filled organisms descended where deeper bathymetry allowed, however the centre of mass did not deepen at the same rate as the bottom. If a shallower bottom depth merely acted to compress the SSL, then backscattering strength would be expected to increase but NASS remain fairly constant. However, NASS decreased as the bottom shallowed, suggesting that some of the GF scatterers may have moved above the upper limit of the analysis layer (Figure 4.3.9, G). This could be related to hydrographic conditions, for example if the SSL was tracking a shift in the thermocline above shallower regions, however no association between bathymetry and lower thermocline depth was observed in the Seaglider data which might be expected if

this were the case. This implies that over shallow bathymetry some organisms that would otherwise reside at depths located within the analysis layer (below$36\,\mathrm{m}$) - where the DCM lay and prey likely aggregated - instead remained above it, even during daytime. In other words, depth preferences may vary according to the available vertical extent, but also according to the depth distributions of other organisms within the SSL. Many zooplankton communities in SSLs have been shown to be vertically structured, often according to size or life-history stage, including siphonophores, which may explain this phenomenon (Benfield et al., 2003; Ohman and Romagnan, 2016; Aarflot et al., 2019).

Longitude had a similar effect on all response variables (B & F in both Figure 4.3.9 and Figure 4.3.10). The most prominent pattern was an increase in backscatter and NASS with concurrent shallowing of the layer away from the bottom at $2.25°$E (Figure 4.3.9, B & F). At this location a small but relatively abrupt peak in bathymetry (approximately $1\,\mathrm{m}$ in the vertical) exists along the western slope of the ridge (Figure 4.3.1). Further east of the ridge, backscatter and NASS rapidly declined and the centre of mass of the layer deepened towards the bottom, despite the relatively shallower bathymetry. Westwards of $2.25°$E, backscatter and NASS remained relatively constant. A similar pattern was modelled for positional metrics. A slight reduction in energetic properties and deepening of the layer occurred near $1.9°$E where the bathymetry deepened abruptly by around $4\,\mathrm{m}$, however no such response was observed over the larger trough at $1.7°$E which extended down to a maximal depth of $98\,\mathrm{m}$.

**Solar altitude and the diel cycle**

Chapter 3 described how the main SSL, comprised of the GF group, performed classic DVM every day. It is unsurprising then that solar altitude was an important predictor for all GF models. Within the diel period, centre of mass was shallowest during the minimal solar altitude (night), deeper during twilight as the GF layer migrated ($-12° <$ solar altitude $< 0°$), and deepest during maximal solar altitude angles (daytime) when the sun reached its zenith (Figure 4.3.10, D). Altitude followed a similar pattern: the layer reached its closest proximity to the bottom when the sun was highest in the sky (Figure 4.3.10, H). Backscatter

and NASS were reduced at night (solar altitude $< -6°$) as the layer moved above the upper limit of the analysis layer, but remained relatively high during the daytime. According to the model, differences in solar altitude resulted in average depth changes of $21\,\mathrm{m}$ by the GF layer, representing $48\,\%$ of the average thickness of the analysis layer. This figure is likely to be an underestimate, since the GF layer was only measured below $36\,\mathrm{m}$.

Curiously, there was a slight fluctuation and reduction in backscatter and NASS as solar altitude increased towards its zenith (Figure 4.3.9, D & H). This could occur if part of the GF layer had descended below the lower limit of the analysis layer (situated approximately $2\,\mathrm{m}$ above the bottom) - a likely possibility since positional metrics showed that the layer continued to deepen until the sun reached its highest point in the sky. Alternatively, organisms may have adjusted their orientation depending on solar altitude during the daytime, possibly because the position of the sun on the sky influences both the polarisation of light and light levels (Cronin and Marshall, 2011). Diel changes in the orientation of many zooplankton species have been observed, however studies tend to compare night and daytime orientations rather than investigating whether variability during the daytime period is evident (Parra et al., 2019).

#### 4.3.3.2 Fish School group models

Only three predictor variables were useful for modelling FS backscatter distributions. Wind speed and thickness were common predictor variables to all FS GAMMs. The model for centre of mass also included bottom depth as a predictor.

**Wind speed, an artefact of fish school detection methods?**

Wind speed was significant in positional models that included three fish schools shallower than $50\,\mathrm{m}$ that were situated far away from the bottom ($> 30\,\mathrm{m}$ altitude) and were detected during particularly calm winds ($< 1.5\,\mathrm{m\,s^{-1}}$) (Figure 4.3.11, points circled in red in A and D). Without these three datapoints, wind speed was not significant ($p = 0.33$), and thickness alone explained approximately a third of the variance in altitude ($R^2 = 0.36, p < 0.001$).

Between wind speeds of 3 to $10\,\mathrm{m\,s^{-1}}$, fish school altitudes remained a few metres above the bottom; this flat profile would ordinarily not result in a predictor being found significant in explaining variance of a response variable. The non-linear smooths for wind speed both showed increasingly large confidence intervals at the extremes of the ranges, where smooths deviated from a flat profile. Taken together, it seems unlikely that wind speed is in fact a true driver of fish school vertical distributions in the BML. This underlines the importance of careful interpretation of GAMM smooths and evaluating whether modelled patterns are likely to be indicative of real biological or physical patterns, or driven by artefacts of the data.

Wind speed may only have been a significant predictor variable in the backscatter and NASS models because of the detection bias discussed in Chapter 3, where increasing wind speeds and associated changes in along-track resolution led to increased measurements of backscatter and NASS, as well as a lower rate of detections. This is mirrored by the wind speed smooths in the partial effects plots, which show increasing backscatter and NASS with wind speed (Figure 4.3.12, A & C). However, it was not possible to conclusively determine whether the inclusion of wind speed in the FS models was due to the aforementioned methodological bias or whether it represented a real biological response in fish schooling behaviour to changes associated with increasing wind stress at the surface.

**Thickness (size) of fish schools**

Larger (thicker) schools appeared to have been positioned in shallower water than smaller schools (Figure 4.3.11, B & E). However, this was most likely the result of the asymmetrical vertical expansion of schools as they increased in size rather than variation in depth preference of fish. As schools increased in size they could only extend upwards; the lowest parts of the vast majority of schools were situated in close proximity to the seabed regardless of their size. Effect sizes on centre of mass and altitude across the span of school thicknesses ($32.5\,\mathrm{m}$) was modelled to be $27\,\mathrm{m}$ in both instances, suggesting that they varied synchronously (Figure 4.3.11, B & E). This supports the interpretation that thickness only impacted altitude due to the asymmetrical extension upwards as schools increased in size.

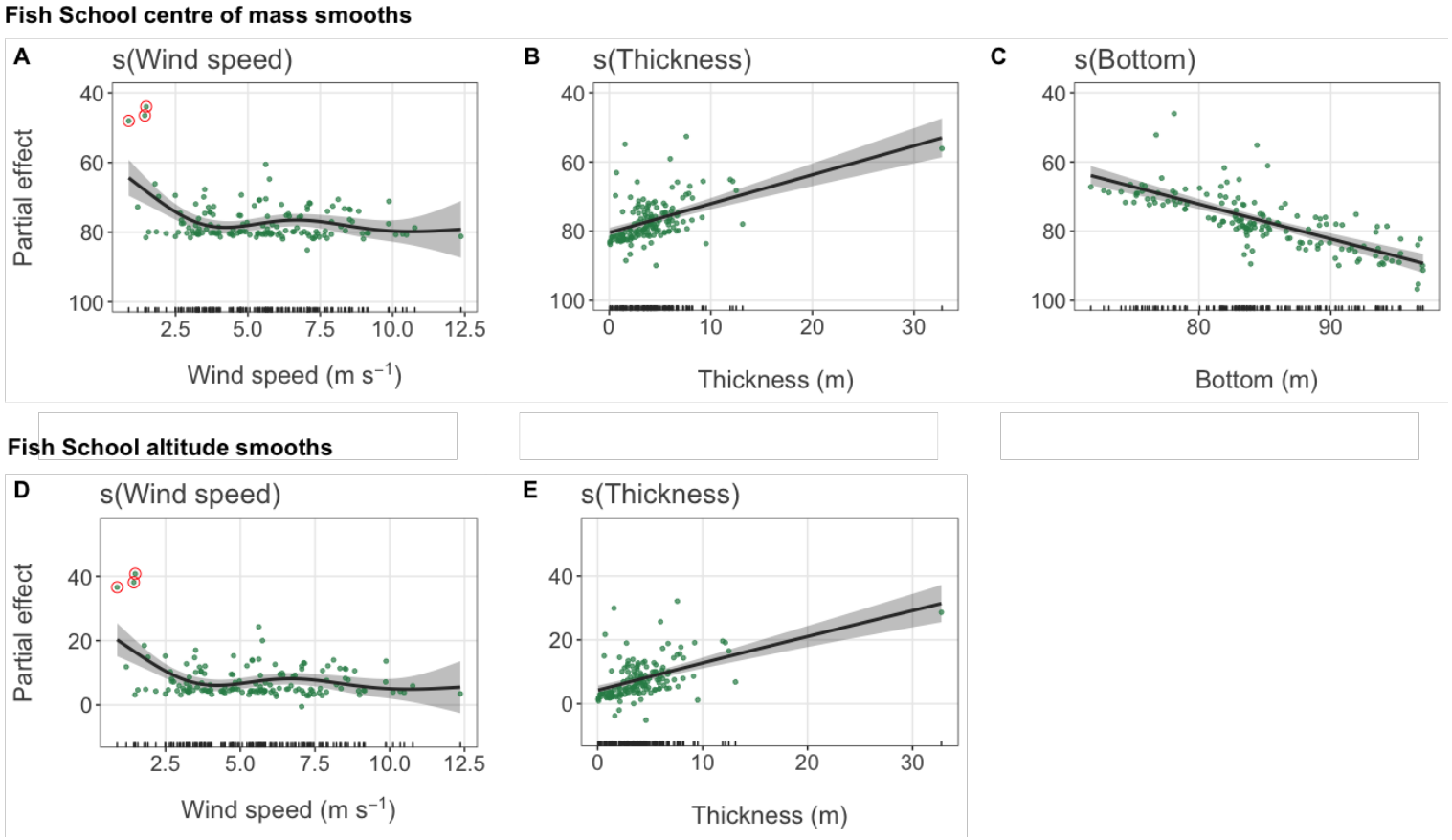


Figure 4.3.11: **Partial effects of predictor variables in Fish School positional GAMMs.** Smooths (black line) and model residuals (green points) shown for centre of mass (A-C) and altitude (D, E) models. Points circled in red highlight fish schools found far from the bottom (altitude $> 30\,\mathrm{m}$) in a shallow region of the analysis layer ($< 50\,\mathrm{m}$) which were responsible for driving the increase in the smooths at low wind speeds and apparent statistical significance of this variable in the models. See Figure 4.3.9 for the description of partial effects plots.

Of the variables tested, thickness of fish schools was the largest determinant of their energetic properties; thicker schools had greater NASS and backscatter (Figure 4.3.12, B & D). Subsection 3.3.2 showed that thicker schools tended to be larger overall and have stronger average backscatter, making the increase in NASS with size unsurprising. Larger schools typically contain more fish, and this alone may explain this pattern. Thickness explained less of the variance in $S_v$ than in NASS ($R^2 = 0.16$ and $R^2 = 0.62$ respectively in single predictor models). The comparatively low level of backscatter variance explained by thickness may reflect the importance of other, unmeasured variables such as species composition, orientation, and packing density on acoustic intensity - the last of which can dynamically respond to biotic factors such as average fish size, food availability and foraging behaviour, and predation pressure (Hager and Helfman, 1991; Rieucau et al., 2015; Romenskyy et al., 2020).

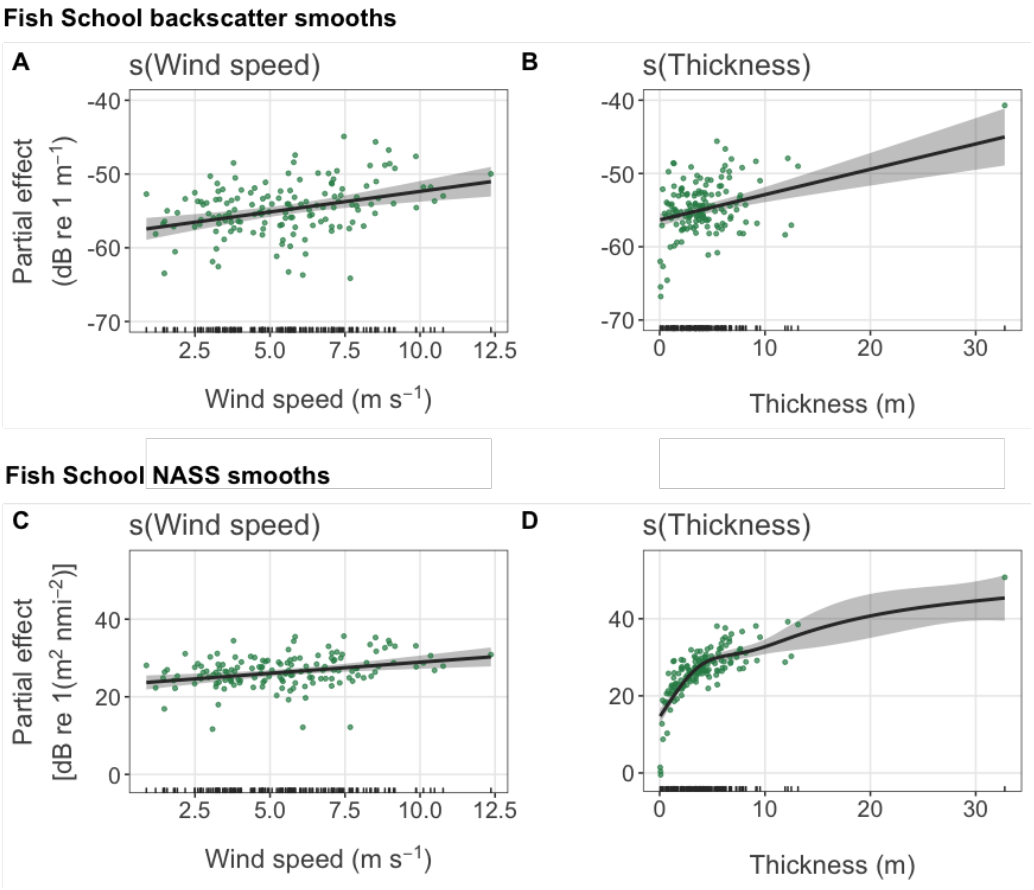


Figure 4.3.12: **Partial effects of predictor variables in Fish School energetic GAMMs.** Smooths (black line) and model residuals (green points) shown for backscatter (A, B) and NASS (C, D) models. See Figure 4.3.9 for the description of partial effects plots.

Whilst the relationship between thickness and backscatter was linear, that with NASS was not, although uncertainty around the smooth grew rapidly above $10\,\mathrm{m}$ thickness. The increase in NASS was most pronounced for relatively short schools ($< 4\,\mathrm{m}$), becoming more gradual above this value (Figure 4.3.12, D). Thicknesses ranged from half a metre to $33\,\mathrm{m}$, which was estimated to impact NASS by up to $31\,\mathrm{dB}$ re $1(\mathrm{m}^2\ \mathrm{nmi}^{-2})$ and $S_v$ by $11\,\mathrm{dB}$. However, the partial effect smooth estimated that the difference in thickness from very small schools ($< 1\,\mathrm{m}$ tall) to larger schools of around $10\,\mathrm{m}$ tall influenced NASS by almost $15\,\mathrm{dB}$ re $1(\mathrm{m}^2\ \mathrm{nmi}^{-2})$, which represented most of the modelled variance, disregarding the outlying large school (thickness $> 30\,\mathrm{m}$). By contrast, wind speed, which ranged from $0.7$ to $14.0\,\mathrm{m\,s}^{-1}$ was estimated to impact NASS by $6.6\,\mathrm{dB}$ re $1(\mathrm{m}^2\ \mathrm{nmi}^{-2})$, and $S_v$ by $11\,\mathrm{dB}$. Clearly, the effects of wind speed, whether due to methodological bias or a genuine biological response, can have a substantial impact on acoustic measurements of fish schools, particularly backscatter.

Given the importance of thickness as an explanatory variable in the FS models, additional GAMMs were constructed to try to identify whether environmental variables influenced thickness. Single and full models were tested (results not shown), and it was determined that the best model for thickness included only the low frequency component of SST, but this only had low explanatory capacity ($R^2 = 0.128, p < 0.001$). It was further found that the inclusion of SST was in part driven by a singular outlying school with thickness above $30\,\mathrm{m}$ (the large NASS outlier identified in Subsection 3.3.2), without which the significance of the low frequency component of SST variable dropped to $p = 0.067$, and explanatory capacity to $R^2 = 0.054$. Therefore, it seems that thickness of schools was independent of the environmental variables tested.

**Bathymetry: topographical constraint on fish school distributions**

Bottom depth was perhaps the most important determinant of the depth of fish schools in the water column since without this variable the centre of mass model $R^2$ dropped from $0.64$ to $0.18$, whereas without wind speed or thickness the model $R^2$ values remained above $0.53$. Together, bottom depth and thickness explained almost three quarters of the variance in

centre of mass ($R^2 = 0.71, p < 0.001$). Changes of $26\,\mathrm{m}$ in bottom depth, ranging from 72 to $98\,\mathrm{m}$, were estimated to impact centre of mass measurements by $25\,\mathrm{m}$ in a linear manner (Figure 4.3.11, C). Bottom depth was not a significant predictor of altitude, in line with the notion that schools tended to stay as deep as possible in order to reduce detection by visual predators. This suggests that fish schools tended to maintain a similar altitude regardless of bottom depth, maintaining a close proximity to the bottom but avoiding being very close to it, indicating that bottom depth exerted a strong control on fish school daytime depth distributions. This highlights the fact that in the shallow environment of the North Sea, schooling forage fish often reside in shallower habitat than they might elsewhere where the waters are deeper.

#### 4.3.3.3 Fluid-Like group models

Energetic and positional metrics of fluid-like scatterers during the night were modelled using combinations of the following predictor variables: salinity, longitude, bottom, wind speed, time, and an energetic property of the GF group.

**Changes over the course of the mission**

The passage of time was modelled to have the effect of decreasing both NASS and $S_v$ by $10.6\,\mathrm{dB}$ re $1(\mathrm{m}^2\ \mathrm{nmi}^{-2})$ and $4.2\,\mathrm{dB}$ respectively over the 20 night mission (Figure 4.3.13, A & E). The time smooth trends were linear although there was substantial variation within each nighttime period, shown by vertical spread of points at each date in Figure 4.3.13 (A, E), and uncertainty grew in the smooth estimates after the first two weeks. No effect of time was found in models of GF NASS during the night (results not shown), although time decreased overall levels of GF NASS (Figure 4.3.9, E), suggesting that the trends in FL NASS and $S_v$ with time are likely to be real and not an artefact caused by reduced acoustic masking by gas-filled scatterers. The decreasing trends in FL NASS and $S_v$ with time might indicate a reduction in biomass and abundance, or that acoustic properties of fluid-like scatterers changed and these animals became weaker scatterers over time, whether due to physiological development or a change in community composition perhaps. That

distributions of fluid-like and gas-filled scatterers overlapped more over time is another possibility, however the decreasing trends in both FL and GF NASS over time suggest that this was unlikely.

**Relationships between gas-filled and fluid-like backscatter distributions**

There was a negative linear relationship between GF and FL NASS, and an apparent deepening of the distribution as GF NASS increased, both of which lend support to the argument of acoustic masking by GF backscatter (C in Figure 4.3.13 and G in Figure 4.3.14). During the night, FL backscatter was only visible below the GF layer which was situated at the top of the analysis layer (see Figure 3.3.1), contrasting with daylight hours when the GF layer descended and FL backscatter tended only to be visible at the top of the analysis layer. If the gas-filled layer descended further into the analysis layer during the night, this would compress the observable distribution of fluid-like scatterers below, which fits with the modelled responses described above.

In contrast to NASS, backscattering strength had a positive linear relationship with GF backscatter (Figure 4.3.13, G) indicating that in regions where there were higher densities of gas-filled scatterers there were also higher densities of fluid-like scatterers. Given that both GF and FL groups were thought to be primarily comprised of zooplankton (as opposed to nekton), physical mechanisms may have led to the passive accumulation of zooplankton biomass in particular areas, or may have actively aggregated where favourable feeding or environmental conditions occurred for both groups (Franks, 1992). Alternatively, regions where copepod and chaetognath (FL) aggregations were more dense may have attracted their siphonophore predators (GF).

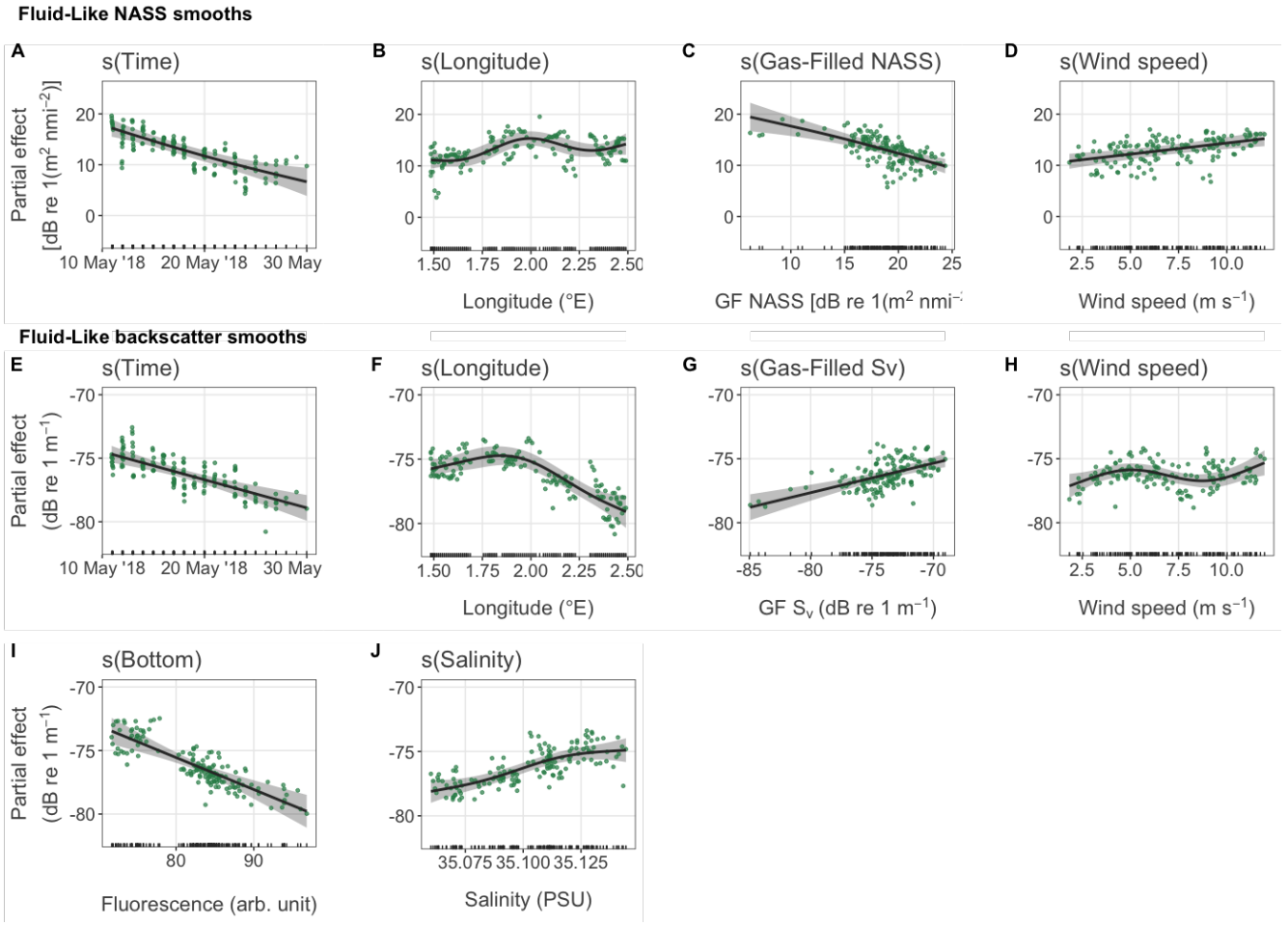


Figure 4.3.13: **Partial effects of predictor variables in Fluid-Like group energetic GAMMs.** Smooths (black line) and model residuals (green points) shown for NASS (A-D) and backscatter (E-J) models. See Figure 4.3.9 for the description of partial effects plots.

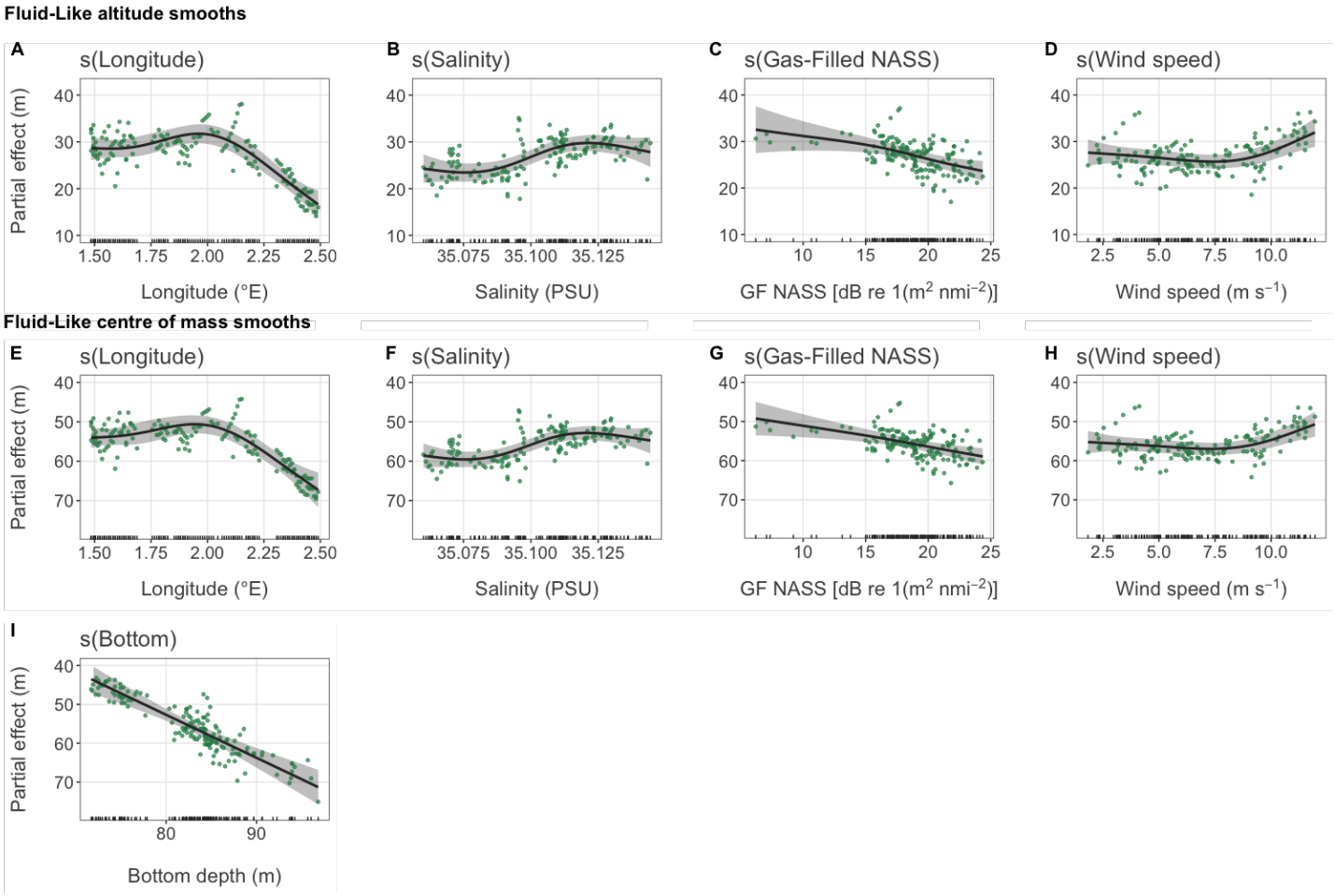


Figure 4.3.14: **Partial effects of predictor variables in Fluid-like group positional GAMMs.** Smooths (black line) and model residuals (green points) shown for altitude (A-D) and centre of mass (E-I) models. See Figure 4.3.9 for the description of partial effects plots.

**Longitude: position across the transect**

All longitude smooths were non-linear with an inflection point near to $2.0°$E; NASS peaked at $2.0°$E and backscatter around $1.85°$E (B & F in Figure 4.3.13 and A & E in Figure 4.3.14). Further east, longitude had the effect of decreasing backscatter by $4.7\,\mathrm{dB}$. NASS decreased slightly either side but began to increase again east of $2.25\,\mathrm{m}$. Peaks in GF NASS and GF backscattering strengths coincided with the smaller seabed peak at $2.25°$E, east of which levels dropped dramatically and the GF layer reduced in thickness (Figure 4.3.9, B & F). The decrease in altitude of the FL group east of $2.0°$E appeared to be due to a reduction or absence of scatterers in the shallower regions of the analysis layer rather than contraction of the layer or masking by the GF layer, since there was no increase in backscatter (A in Figure 4.3.14 and F in Figure 4.3.13).

This deepening and reduction in backscattering strength is akin to that observed in the GF layer during daytime. Lower biomass of GF organisms and the reduction in volume attributed to the GF group in this region could have led to proportionally more of the FL distribution becoming 'visible' (unmasked). Thus, whilst density of fluid-like scattering organisms may have also decreased in this region, the increased 'visibility' of FL backscatter could explain the measured increase shown in NASS (Figure 4.3.3). The longitude smooth for positional metrics followed a similar pattern to that for the backscatter model, peaking at $2.0°$E and decreasing further east but remaining at a similar level westwards. This mirroring of the GF layer depression over the ridge supports an argument that aggregations of gas-filled and fluid-like scattering zooplankton had similar horizontal distribution patterns. This could be caused by physical mechanisms passively aggregating all planktonic organisms, or aggregations may have been actively maintained in specific locations, perhaps those with favourable conditions, by swimming and prey-following behaviour.

**Salinity: changes in distributions associated with an oceanic front**

There was a non-linear relationship between positional metrics and salinity (Figure 4.3.14, B & F). Sea surface salinities above $35.1\,\mathrm{PSU}$ were associated with a shallower centre

of mass situated further from the seabed. The value of $35.1\,\mathrm{PSU}$ demarcates the front of warmer, saltier, less turbid, less oxygenated oceanic water spreading westwards over the ridge. This water mass may have brought with it organisms that had shallower nighttime depth distributions, or organisms may have responded to correlated changes in water properties. It is possible that FL organisms responded to the increase in water clarity by moving upwards, an explanation that fits with a hypothesis of reverse DVM behaviour.

Sea surface salinity had a positive correlation with backscatter, but was not relevant to the model for NASS (Figure 4.3.13, J). The linear increase in backscatter with salinity suggests that rather than organisms with different acoustic properties being brought in by oceanic water, which would probably have resulted in a discontinuity around $35.1\,\mathrm{PSU}$, instead FL organisms responded to the changes in water properties by gradually increasing their density, whether through active or passive mechanisms. It is unlikely that organisms from shallower regions descended into the analysis layer to induce the apparent shallowing of distribution, as this would have caused a relative increase in NASS (proxy biomass) but no such increase was observed. Instead, FL organisms in the analysis layer distributed themselves closer towards the surface, and in doing so increased their average density. No relationship was found between GF NASS and salinity, which could have indicated that the reduction in NASS in higher salinity regions was due to acoustic masking.

**Bathymetry: Interplay with other environmental conditions, topographic constraint and possible reverse DVM behaviour**

Deeper water was associated with weaker backscatter, however no relationship between bottom depth and NASS was evident (Figure 4.3.13, I), suggesting that the increased availability of space allowed FL organisms to spread out vertically. Bottom depth was not relevant to altitude, however longitude was. FL organisms were distributed closer to the bottom near the ridge at the east of the transect where the salinity front passed through (A in Figure 4.3.14 and B in Figure 4.3.5). Here, the seabed shallowed above $85\,\mathrm{m}$ but the distribution did not respond by moving closer to the bottom (decreasing altitude) in the same way over similar depths elsewhere along the transect. This suggests that it was not solely

bathymetry that influenced vertical position of scatterers; environmental conditions at particular geographic locations were also important.

Zooplankton often avoid being in close proximity to the seabed as benthic filter-feeding and motile predators increase the risk of mortality in this zone. In addition, turbulence due to shear stress of flow along a rough bottom can reduce the ability of some copepods to detect predators, resulting in increased feeding rates of zooplanktivorous benthic fish (Robinson et al., 2013). Some benthic animals produce jets to bring food within reach, creating an even more turbulent environment near the seabed (Lassen et al., 2006). However, in shallow regions, the increased risk due to increased ambient light levels and spatial overlap with classic DVM performing predators may have altered the trade-off between avoidance of benthic predators and avoidance of pelagic predators, resulting in some fluid-like scattering organisms positioning themselves closer to the bottom than they might otherwise. The longitudinal smooth suggests that the relationship between FL distributions and the bottom (indicated by altitude), differed according to geographic proximity to the ridge (Figure 4.3.14, A). Given that bottom depth was not a relevant predictor in the model, it is plausible that longitude is acting as a proxy for different hydrographic or hydrodynamic regimes induced by the bathymetry, as opposed to the bathymetry itself.

The linear relationship between bottom depth and centre of mass is consistent with a hypothesis of reverse DVM, where distributions would move to deeper water at night (Figure 4.3.14, I). This is intriguing because the distribution of GF scatterers moved upwards at dusk and was thought to remain in shallower water during the night, lessening the likelihood that this apparent deepening was due to increased acoustic masking in deeper regions. There was no relationship between solar altitude (a proxy for time of day) and the depth of the FL distributions as might be expected if organisms were travelling to depth during the night, however this does not entirely rule out the possibility of reverse DVM, as organisms may have already moved to depth by the time that nighttime commenced and may have only moved upwards during dawn or later in the day. On the other hand, the deeper distribution of organisms in deeper water could merely be the result of the depth preferences of non-migratory organisms. Regardless of whether reverse DVM behaviour did or did not occur, the movement to deeper regions of the water column where bathymetry permits

suggests that fluid-like scattering organisms are topographically constrained in this region of the North Sea.

**Shallowing of distributions in response to strong winds, or misclassification of backscatter?**

Wind speed was significant in all FL models. This variable may act as a proxy for the strength of wind-driven vertical turbulence gradients extending below the surface (Hunt and Sajjadi, 2018), or backscatter from particulates or bubbles entrained into the BML due to strong winds. Wind speed was not relevant to any of the GF models, ruling out the possibility of the relevance to FL distributions as a consequence of acoustic masking.

Wind speed had little influence on vertical position until speeds exceeded $7.5\,\mathrm{m\,s^{-1}}$, at which point the centre of mass shallowed by several metres (Figure 4.3.14, D & H). This speed corresponded with the development of bubble plumes that extended more than $10\,\mathrm{m}$ beneath the surface (Figure 2.3.11). Bubble plume depth measurements did not exceed $30\,\mathrm{m}$, however these measurements were derived using a threshold offset line with a threshold of $-65\,\mathrm{dB}$ at $70\,\mathrm{kHz}$ that detected regions of contiguous backscatter extending beneath the surface, and was not designed to detect sparsely distributed bubbles, or those bubbles which backscattered more weakly. Misclassified backscatter originating from either bubbles or particulates entrained into the BML due to wind-driven mixing could feasibly explain the shallowing of the centre of mass and increases in NASS and Sv (D & H in Figure 4.3.13 and H in Figure 4.3.14). It was observed that chlorophyll was injected from the DCM into the BML at the east of the transect on the 17$^{\text{th}}$ May (Figure 4.3.5, D), coinciding with a period of prolonged wind speeds in excess of $7.5\,\mathrm{m\,s^{-1}}$. Therefore, it is plausible that other types of particulates or gas bubbles were also mixed into the BML during this period. Small bubbles are generally weaker scatterers and have higher resonant frequencies. Should they backscatter more strongly at $200\,\mathrm{kHz}$ than $70\,\mathrm{kHz}$, they may have been misclassified as FL backscatter.

Strong winds can also be associated with storms that bring clouds and rainfall, reducing ambient light levels. Zooplankton and mesopelagic fish have been shown to respond to

passing rain storms and cloudy weather events by temporarily adjusting their vertical position in the water column (Kaartvedt et al., 2017; Omand et al., 2021). However, the relationship between wind and vertical position of fluid-like scatterer distributions was only observed at night when PAR readings were zero due to a lack of instrument sensitivity. During the daytime, higher wind speeds did not correspond to darker ambient atmospheric conditions: there was only a very weak correlation between wind speeds and PAR but this indicated that, if anything, light levels *increased* with wind speed (Spearman's $\rho = 0.05, p < 0.01$). However, it is possible that wind-driven mixing could have increased shading in the water column, thereby reducing underwater light levels, since mixing can entrain and resuspend particulates and lead to a decrease in water clarity. Although the period of strong, sustained winds coincided with increased optical backscatter measurements, this appears to have occurred only in a particular region of the transect (Figure 4.3.5, C). Alternatively, zooplankton may have responded to, or been disturbed by, increased turbulence during windy weather (Tiselius, 1998). Turbulence propagating downwards from wind-driven mixing is usually associated with deepening of copepod distributions, even below the pycnocline (Incze et al., 2001; Maar et al., 2006). If mixing had brought more FL zooplankton from upper layers down into the BML this could have led to the observed increase in NASS and potentially also the shallowing of the centre of mass. Without additional data, such as in-situ light or turbidity measurements, to input into the models, it is difficult to determine the causal mechanisms underlying the observed dependencies on wind speed.

## 4.4 Discussion

### 4.4.1 Summary of model results

Table 4.3 summarises the influential drivers of zooplankton and fish school patchiness as measured by descriptors of acoustic backscatter distributions. Bottom depth had a substantial effect on the vertical position of all three groups in the water column, underlining that the shallow central North Sea can limit zooplankton and fish school vertical distributions.

Table 4.3: **Maximum effect sizes of environmental drivers in GAMMs.** Units as per response variable.

| Group | Response | Longitude | Bottom depth | Time | Wind Speed | Solar altitude | Gas-filled NASS/Sv | Thickness | Salinity |
|---|---|---|---|---|---|---|---|---|---|
| Fluid-Like | NASS | 4 | | **11** | 4 | | 10 | | |
| | Sv | 4 | **6** | 4 | 2 | | 4 | | 3 |
| | Altitude | **15** | | | 6 | | 9 | | 6 |
| | Centre of mass | 17 | **28** | | 6 | | 10 | | 7 |
| Gas-Filled | NASS | 7 | **8** | 4 | | **8** | | | |
| | Sv | 7 | 3 | 4 | | **8** | | | |
| | Altitude | 6 | 16 | 4 | | **21** | | | |
| | Centre of mass | 6 | 11 | 4 | | **21** | | | |
| Fish Schools | NASS | | | | 6 | | | **31** | |
| | Sv | | | | 6 | | | **11** | |
| | Altitude | | | | 15 | | | **27** | |
| | Centre of mass | | 25 | | 15 | | | **27** | |

Thickness emerged as the most important driver explaining variation in fish school distributions. Bottom depth was the only environmental driver found to influence the distribution of fish schools in the water column (disregarding wind speed). In contrast, FL patchiness was associated with changes in salinity across a sub-mesoscale front. Changes in FL backscatter distributions were driven by a variety of environmental variables, as well as some variables that may have acted as proxies for other environmental parameters (e.g. time, longitude, salinity), and the presence of the GF backscatter. Unfortunately, it was not possible to establish whether the relationship between GF and FL backscatter distributions represented a behavioural response of copepod prey to the presence of siphonophore predators since the analysis was confounded by acoustic masking inherent in the hierarchical classification scheme.

Wind speed smooths in the FS and FL models could have represented behavioural responses of animals to increased turbulence caused by wind-mixing, however the observed patterns also fit with explanations of altered backscatter distributions due to methodological artefacts (FS) and bubble scattering (FL). Therefore, the interpretation of wind speed as a significant environmental driver of fish and zooplankton distributions should be treated with caution.

According to the models, variability in water properties and wind speed did not influence GF backscatter distributions, although some environmental dependence was found. Geographic position along the transect, a possible proxy for the hydrodynamic regime, bottom depth, time, and solar altitude, which may have acted as a combined proxy for both time of day and light levels, influenced all aspects of GF backscatter distributions considered. Solar altitude had the strongest effect on both horizontal and vertical GF patchiness, mediating vertical migration behaviour and thus movement into and out of the analysis layer.

### 4.4.2 Importance of bottom depth to pelagic animals in a shallow ecosystem

All three groups responded to the increased availability of vertical space over regions with deeper seabeds by deepening their distributions, indicating that the shallowness of the central North Sea imposes a substantial constraint on vertical movements of zooplankton and fish. The seabed not only constrains vertical distributions of pelagic animals, but also influences

hydrodynamic flow and provides habitat for many benthic species. Turbulent dissipation rates are typically higher closer to boundaries such as the surface, the seabed, and between water masses. Dissipation rates can be particularly high near the seabed due to the reduction in orthogonal current velocity to zero at the fluid-solid interface. Simulated turbulent dissipation rates for the northern North Sea have been shown to vary by several orders of magnitude over a few tens of metres above the seabed (Burchard et al., 2002). Strong vertical gradients in turbulence may facilitate zooplankton in orienting themselves in relation to the seabed.

Although deeper, darker pelagic habitats may be safer from visual predators, dwelling near the bottom poses its own risks: planktivorous benthic fish and tactile invertebrates can capture zooplankton that stray within reach. Vertically migrating organisms do not simply opt to descend as deep as possible: predation risk varies for different size-classes and species, whose tolerance of turbulence may also vary (Prairie et al., 2012; Ohman and Romagnan, 2016). Whilst zooplankton distributions deepened where bathymetry allowed, they did not congregate near the bottom in shallower areas. During daytime, vertical distributions of GF backscatter were unimodal, with peak acoustic density several metres above the bottom. GF and FL centres of mass in areas shallower than $85\,\mathrm{m}$ were on average $22 \pm 8\,\mathrm{m}$ and $26 \pm 5\,\mathrm{m}$ above the bottom during the day and night respectively.

De Robertis et al. (2000) postulated that behavioural decision-making plays a role in size-dependent timing of euphausiid DVM, after observing differences between vertical migration behaviour in depth-limited and open-ocean environments. The distribution of backscatter above shallow bathymetry and its comparison to distributions over deeper regions similarly point to the role of behavioural decision-making in migration amplitude and vertical positioning of zooplankton in the North Sea. Smaller copepods are prey for some larger individuals, and active behavioural mechanisms which maintain size segregation may therefore play a role in vertically structuring the distribution of copepod biomass, even over shallow topography where many individuals are forced to occupy less favourable depths (Aarflot et al., 2019). My results highlight that, in the relatively shallow North Sea, bottom depth can impact the vertical spread of zooplankton in sound scattering layers, affecting the structure of distributions much higher up in the water column.

Zooplankton backscatter was heterogeneously distributed across the transect, but this patchiness was not solely explained by variation in bottom depth or water properties. There were regions of increased backscatter along the transect which represented regions where zooplankton were more accumulated, even after accounting for increases due to other environmental variables. This was evident by the dependence of all the zooplankton models (GF and FL) on longitude. Longitude could have acted as a proxy for a hidden variable which had (relatively) fixed geographic variation, such as time-invariant current flow associated with bottom topography.

The most notable difference across the transect was the marked reduction in backscatter and vertical distributions east of the comparatively shallow ($71\,\mathrm{m}$ depth) ridge at $2.4°$E. The ridge slopes had a fairly gradual gradient with an average incline at the western ridge slope of only $0.0012°$, and an even more gradual incline of $0.0007°$ along the eastern slope. However, this moderate bathymetric feature was associated with a marked change in the apparent biomass and vertical distribution of backscatter either side. Average daytime NASS and altitude of the GF layer were lower east of the ridge peak than westwards across the transect by $24\,\%$ ($6\,\mathrm{dB}$ re $1(\mathrm{m}^2\ \mathrm{nmi}^{-2})$ and $36\,\%$ ($7.5\,\mathrm{m}$) respectively (Table 4.4). Average FL altitude was also lower east of the ridge peak by a similar proportion of $31\,\%$ ($8.6\,\mathrm{m}$), however NASS was increased by $21\,\%$ ($2.6\,\mathrm{dB}$ re $1(\mathrm{m}^2\ \mathrm{nmi}^{-2})$, possibly due to reduced masking by the GF group. The Seaglider sections make clear that these seemingly small changes in bathymetry around the ridge were associated with variable conditions in the water column (Figure 4.3.5), likely mediated by differing current flows over and across different sides of the ridge. Without further information it is not possible to infer the extent to which currents may have passively aggregated zooplankton along the western slope of the ridge, or whether zooplankton actively aggregated in particular regions which had favourable oceanographic or foraging conditions.

Table 4.4: **Differences in NASS and altitude of GF and FL backscatter east and west of the ridge at 2.4°E.**

| | | NASS [dB re 1($m^2$ $nmi^{-2}$)] | | | Altitude (m) | | |
|---|---|---|---|---|---|---|---|
| | | **Mean ± sd** | **Min** | **Max** | **Mean ± sd** | **Min** | **Max** |
| **GF** | **West of 2.4 °E** | 25.1 ± 2.6 | 14.7 | 30.4 | 21.1 ± 4.3 | 7.0 | 35.6 |
| **(day)** | **East of 2.4 °E** | 19.1 ± 3.0 | 14.0 | 36.5 | 13.6 ± 4.3 | 6.7 | 24.3 |
| **FL** | **West of 2.4 °E** | 12.6 ± 4.1 | 3.8 | 21.0 | 28.1 ± 4.5 | 17.1 | 37.5 |
| **(night)** | **East of 2.4 °E** | 15.2 ± 1.3 | 13.5 | 17.9 | 19.5 ± 1.7 | 17.1 | 22.6 |

### 4.4.3 Light and the time of day

Counter to expectations, the models suggested that solar altitude was a stronger driver of GF vertical distributions than PAR measurements made at the surface. Many zooplankton are sensitive to subtle shifts in low ambient light environments and adjust their vertical position accordingly, even during the relatively dark polar night (Hobbs et al., 2021). The PAR sensor lacked sensitivity and was unable to register very low light levels. Consequently, it recorded a value of zero at night. In contrast, solar altitude continued to vary throughout the 24-hour period, and may have been a better proxy metric to track subtle changes in light through the night than the PAR measurements. However, if variation in light levels alone were responsible for variation in the position and backscattering strength of organisms then PAR measurements were expected to have a greater explanatory power than solar altitude in daytime models, but this was not the case. In daytime models, solar altitude still explained more variation in vertical position than PAR ($R^2_{solaralt} = 0.63$ versus $R^2_{PAR} = 0.60$ in centre of mass models that included longitude, time and bottom depth; and $R^2_{solaralt} = 0.09$ versus $R^2_{PAR} = 0.07$ in centre of mass single predictor models). This is surprising since zooplankton have been shown to modulate their vertical position according to short-lived fluctuations in ambient light levels and incident ultraviolet (UV) radiation during the day, for example due to passing cloud-cover and wildfire smoke (Balino and Aksnes, 1993; Omand et al., 2021; Urmy et al., 2016) and it suggests that solar altitude might act as a proxy for more than light levels alone.

Solar altitude may represent other, hidden variables which exhibit a diel cycle. For example, solar altitude is correlated with endogenous diurnal clock timing, known to be an important driver of vertical migration behaviour, and changes in polarisation of sunlight. Little is known about how changes in the polarisation of sunlight throughout the day might affect zooplankton DVM behaviour, however it is known that some marine animals have visual systems that can detect and respond to polarisation in the contexts of prey detection, communication, and navigation (Marshall et al., 2019; Wehner, 2001). Whilst sunlight exhibits a distinct diel cycle in polarisation in air, patterns of polarised light underwater can be distorted by turbidity and surface waves, as well as multiple-path scattering at depth (Zhou et al., 2017; Cronin and Marshall, 2011). Whether this renders polarisation of sunlight underwater an unreliable cue for migration by zooplankton situated anywhere but the uppermost few metres is not clear (Shashar et al., 2004; Cronin and Shashar, 2001). Future investigation into behavioural responses of zooplankton to changes in the polarisation of sunlight underwater at depth is needed to provide empirical evidence on this interesting but complex topic.

The PAR sensor measured wavelengths within a range relevant to photosynthesis, i.e. between $400$-$700\,\mathrm{nm}$, which is not necessarily the most biologically-relevant range of wavelengths for zooplankton. Since exposure to UV radiation can be potentially harmful, many zooplankton are capable of detecting this kind of light and exhibit different feeding and vertical migration behavioural responses to different wavelengths within the visible and UV spectra (Martynova and Gordeeva, 2010). The UV spectrum ranges from $100$-$400\,\mathrm{nm}$, i.e. wavelengths are shorter than those detected by the PAR sensor. Cohen et al. (2015) found that the visual sensitivity of krill (*Thysanoessa inermis*) declined to negligible levels at wavelengths above $600\,\mathrm{nm}$, thus changes in light at longer wavelengths within the range of PAR would be poorly detected by these animals. In summary, the spectrum measured by the PAR sensor may fail to capture wavelengths of light that can be detected by zooplankton, and some of the wavelengths in PAR may not have been detected well by zooplankton.

### 4.4.4 Seasonal stratification

Stratification plays an important role in the life histories and distributions of North Sea copepods. The onset of annual population increase in *Calanus helgolandicus* is triggered by strengthening stratification during spring (Irigoien and Harris, 2003). As stratification proceeds, so too does vertical separation of the ecologically similar congeneric copepods *Oithona atlanticus* and *O. similis*, and *Calanus helgolandicus* and *C. finmarchicus* in the water column (Lindegren et al., 2020), which may be observed as changes in relative presence of certain copepod stages at particular depths (Reygondeau and Beaugrand, 2011). Population changes and changes in depth preferences associated with stratification could result in changes to acoustic properties over time.

Time had the largest effect on FL NASS of all modelled variables. It was estimated to decrease NASS by $11\,\mathrm{dB}$ re $1(\mathrm{m}^2\ \mathrm{nmi}^{-2})$ over the 21-day mission (Table 4.3). The decrease in NASS could have been caused by a reduction in biomass, changes in acoustic properties of GF organisms, or change in vertical distribution of FL backscatter. Time may have acted as a proxy for stratification strength since both had an overall increasing linear trend during May. However, SST - in particular the low frequency component of SST - was expected to follow the index of stratification strength more faithfully than time, since SST would have responded to wind mixing that cooled surface water and delayed the process of stratification. Notably, mixing occurred during the period of strong winds between the 16$^{\text{th}}$ to the 18$^{\text{th}}$ of May 2018 and this was reflected in the low frequency component of SST (Figure 4.2.1). Yet, neither SST nor either of its filtered components were significant predictors of FL distributions.

The difference in average surface to BML temperature increased by around $2.5\,^{\circ}\mathrm{C}$ over the 21-day mission, representing only the preliminary stages of stratification in the seasonally stratified central North Sea. Therefore, although this crucial early stage in the development of stratification led to changes in the vertical structure of the water column in the upper $40\,\mathrm{m}$, the mission may have been too short for changes to acoustic properties in response to increased stratification (if they occurred) to have been detected in the analysis layer using the methods employed.

### 4.4.5 Environmental drivers of fish school distributions

Fish school distributions were not associated with water properties. This is unsurprising as fish schools are highly mobile, dynamic entities whose sizes and structures may largely depend on immediate conditions such as proximity, number and density of conspecifics as well as predation pressure, and these conditions likely vary over short ($<$ day) timescales. Fish schools typically form at the onset of dawn and break up at dusk; this was the pattern that observed acoustically in Chapter 3. Yet solar altitude and PAR did not explain fish school vertical distributions or energetic properties (proxies for school size and possibly packing density) in the GAMMs. Whilst formation is likely cued by changing light levels, other factors may drive distribution and movement behaviour once formed.

Bottom depth was found to exert significant control on the vertical position of schools. Regardless of the depth of the water column, during hours of daylight the fish schools generally stayed close to the bottom at a constant altitude. Almost $75\,\%$ of fish schools had a centre of mass within $10\,\mathrm{m}$ of the bottom, and more than $96\,\%$ were found within $20\,\mathrm{m}$ of the bottom. It is unlikely that this proximity to the bottom can be explained by improved foraging in this region, since the main prey of forage fish are zooplankton, such as copepods, which tend to avoid the bottom due to the risk of predation by benthic organisms (Motro et al., 2005; Holzman et al., 2005). Therefore, this bottom-hugging behaviour suggests that the shallow bathymetry in the central North Sea acts to constrain fish school vertical distributions and fish schools may be forced to reside in shallower depths than they would otherwise.

Temperature and salinity, particularly associated with variability in Atlantic inflow, are thought to exert important controls on population sizes, timing of spawning, and growth rates of North Sea fish (Beaugrand and Kirby, 2010; Baudron et al., 2014; Fincham et al., 2013; Corten, 1990). However, these relationships are often observed over much longer timescales, typically years or decades, rather than the sub-seasonal timescales studied here. It is therefore unsurprising that horizontal gradients of water properties in the BML, such as temperature and salinity, were not found to be important drivers of fish school distributions in this study. Whilst longitude was a critical driver of zooplankton patchiness, it was not a

predictor in the FS models, possibly because fish schools are highly mobile and ephemeral, forming and disbanding in daily cycles, with aggregations that may be comprised of different individuals each day.

### 4.4.6 Reverse DVM behaviour of calanoid copepods?

The FL models provide tentative support for a hypothesis of reverse DVM behaviour by calanoid copepods. Reverse DVM is typically a strategy used to minimise spatial overlap with classic DVM performing predators, and thus might have been used by copepods to avoid siphonophores present in the study region. This pattern of DVM differs from the classic DVM behaviour of calanoid copepods in the North Sea reported by Hays et al. (1996). However, calanoid copepods, along with other zooplankton, are known to exhibit an array of different DVM patterns and can modify migration behaviour to suit different habitats (Burt and Tortell, 2018; Berge et al., 2014). Across stations in the Irish Sea, Irigoien et al. (2004) found that *Calanus finmarchicus*, *C. helgolandicus*, and Pseudocalanus spp. performed both classic and reverse DVM, with direction of migration dependent on location. They appeared to flexibly adapt their behaviour according to the DVM behaviour of chaetognaths in different regions, reversing the direction of DVM as a strategy to minimise spatial overlap with these predators. In the Skagerrak, Tiselius (1998) reported classic DVM of *C. finmarchicus*, whereas in the Clyde Sea Tarling et al. (2002) described midnight sinking of this species as a response to the arrival of euphausiid predators in surface waters at night. In Dabob Bay in Washington, Pseudocalanus sp. were also found to perform reverse DVM as a response to DVM behaviour of chaetognaths (Ohman et al., 1983). Clearly, the literature supports evidence for a variety of DVM strategies utilised by calanoid copepods, showing that behaviours are not fixed but can respond flexibly to the biotic and abiotic environment, as well as endogenous factors such as lipid state and ontogeny that modify DVM amplitude, timing, and even direction (Ohman and Romagnan, 2016; Hays et al., 2001; Dale and Kaartvedt, 2000; Hays et al., 1996).

Both chaetognaths and physonect siphonophores are predators of calanoid copepods, but physonects also predate on chaetognaths (Hetherington et al., 2022; Frid et al., 1994). It is

possible that FL backscatter patterns were confounded by contrasting DVM signals from different taxa in the group, or that the DVM pattern of acoustically dominant scatterers masked those of other taxa. Calanoid copepods were thought to dominate the acoustic backscatter in the FL group, and therefore migration behaviour of chaetognaths, if exhibited, could not be reliably determined from the acoustic data alone. Thus, if there was a pattern of copepod reverse DVM, it is not clear whether this might have occurred in response to the classic DVM of siphonophores in the GF group or to any undetected migration behaviour of chaetognaths.

If the FL group did indeed conduct reverse DVM, this raises the question of why the GF group performed classic DVM given that some of their prey actively avoided shallower waters at night. Siphonophores are tactile, rather than visual, predators, so they do not necessarily need to seek lighter ambient conditions in order to improve foraging success. In fact, lighter environments may provide prey with a detection advantage. Thus, since siphonophores ascended at night, it would make adaptive sense if either better foraging conditions occurred in shallower water or they gained a metabolic advantage by accessing warmer or more oxygenated water near the surface at night. Better foraging conditions might occur if there is improved availability or concentrations of suitable prey - such as small copepods, non gas-bearing gelatinous animals, chaetognaths, or fish larvae - in shallower water (Hetherington et al., 2022). It is highly plausible that fluid-like scattering organisms observed acoustically in the analysis layer do not represent the totality of prey biomass available for physonect siphonophores. Correlations between proxy abundance or biomass (NASS and $S_v$) of the GF and FL groups could not be used to determine whether they both peaked in the analysis layer during the daytime because of the issue of acoustic masking. However, Uribe-Palomino et al. (2019) found positive correlations between DVM-performing siphonophore and copepod abundances in surface waters (0-3 $\mathrm{m}$) of the Colombian Pacific Ocean, although in this study the siphonophore community was dominated by Calycophorans, and only a few Physonects were sampled.

### 4.4.7 The importance of considering spatial and temporal scales

Spatial and temporal scales of behavioural and physical processes affect the scales of zooplankton patchiness (McGillicuddy, Jr, 2001; Prairie et al., 2012). At very small spatial scales ($1\,\mathrm{mm}$ to $10\,\mathrm{m}$) individual behaviours can dominate physical processes, whereas mesoscale ($10\,\mathrm{km}$ to $200\,\mathrm{km}$) patchiness is primarily driven by physical processes (Prairie et al., 2012). This study addressed sub-mesoscale ($1\,\mathrm{km}$ to $10\,\mathrm{km}$) relationships between biological distributions and their environment, where influences of both behavioural and physical processes were expected to drive distribution patterns.

Studies of long-term trends have long been important for understanding how fish and zooplankton distributions may shift in the face of climatic and oceanographic changes (Reid et al., 2016; Beaugrand, 2003; Beaugrand and Kirby, 2010; Beaugrand, 2004). However, the importance of smaller scale processes in influencing patch dynamics and how these processes feed into larger patterns in biological distributions has been increasingly recognised in recent decades (Luo et al., 2014; Keerthi et al., 2022; Greer et al., 2013, 2020; Nayak et al., 2021; Maldonado-Aguilar et al., 2023). For example, Keerthi et al. (2022) described how small-scale ($<$ 3 months, $< 50\,\mathrm{km}$) fluctuations in surface chlorophyll contribute to, and can set, conditions for following years, and how the influence of these small-scale changes may accumulate over subsequent years. Studies of small-scale zooplankton patchiness can reveal previously unknown behaviour, for example the vertical migration behaviour of copepods and other zooplankton over short distances ($< 100\,\mathrm{m}$) under ice-cover (Daase et al., 2016).

Sampling resolution and the resolution of analyses can greatly impact the nature, strength, and statistical significance of relationships between biological distributions and environmental parameters, as patchiness may be nested over a range of scales (Urmy and Warren, 2019; Prairie et al., 2012; Denis et al., 2002). Scott et al. (2023) recently demonstrated that decreasing the spatial resolution of copepod biomass and chlorophyll data could lead to more variable and lower statistical significance of correlations between these two variables, emphasising that sampling resolution must be matched to the scales of ecological processes in order to capture relationships effectively. Mismatches between sampling resolution and those of ecological processes can lead to a failure to capture relationships consistently, or at

all (Cade and Benoit-Bird, 2015).

Relationships between biological distributions and their environment may also not be evident if only instantaneous correlations are analysed. In many cases, it is reasonable to expect a lag between environmental change and biological responses to that change (Denman et al., 2001). For example, Maud et al. (2018) found that copepod mortality due to major storm events was correlated with peak wind speeds within the three days prior. Wind-driven mixing and across-shelf flow are important processes that redistribute heat, salt, and nutrients, can increase turbulence that breaks down stratification, and mediate the transport of zooplankton from different origins throughout the North Sea. Many of these processes require time for changes to propagate through the region and through the water column in order to affect biological distributions (Jones et al., 2020; Winther and Johannessen, 2006; Kröncke et al., 1998; Reid et al., 2016; Guadayol et al., 2009; Francis et al., 2012). This study could therefore be extended by analysing time-lagged cross-correlations of parameters.

Zooplankton distributions often exhibit patchiness over scales that are finer than those of physical variables that describe water properties, which tend to follow gradual spatial and temporal gradients (discounting sharp discontinuities such as thermoclines and fronts) (Prairie et al., 2012). In studies that considered variation over longer temporal scales (seasons, years, or decades), temperature emerged as one of most important abiotic parameters associated with zooplankton distributions in the North Sea (Beaugrand, 2003; Beaugrand and Kirby, 2010). Yet SST did not explain vertical or horizontal distribution patterns in any of the three acoustic groups in this study, which may be a consequence of the disparate scales considered (for example Denis et al., 2002). However, an association between a mesoscale oceanographic feature and copepod distributions was apparent in this study, indicated by the relationship between FL distribution and SSS which acted as a tracer for different water masses. Boswell et al. (2020) employed GAMMs to study environmental drivers of zooplankton and micronekton in the Gulf of Mexico using acoustic data aggregated over similar spatial scales ($500\,\mathrm{m}$ along-track bins), and found similar correlations between distributions and mesoscale oceanographic features.

Klais et al. (2016) investigated patterns of zooplankton patchiness in the Baltic Sea at spatiotemporal scales similar to those considered in this study, by modelling abundance over spatial distances less than $100\,\mathrm{km}$ and timescales less than $90$ days. Small zooplankton with short reproductive timescales (small copepods and cladocerans) exhibited greater temporal than spatial variability at these scales. In contrast, larger zooplankton which had longer reproductive timescales, such as *Pseudocalanus* spp. and *Limnocalanus macrurus*, exhibited greater spatial than temporal variability at these scales. This was thought to be because their reproductive timescales (typically one generation per year) exceeded the temporal scale of the study but spatial gradients in salinity and temperature over mesoscale distances ($10\,\mathrm{m}$-$1\,\mathrm{km}$) exerted significant stress on these organisms (Klais et al., 2016). In this study, proxy abundance and biomass ($S_v$ and NASS) of fluid-like scatterers, which represent copepods of various sizes, was mostly driven by time, although variables that influenced spatial variability across the transect were also relevant (Table 4.3). In contrast, variables that described spatial variability across the transect had a greater modelled effect on proxy abundance and biomass of gas-filled scatterers. Knowledge about the reproductive cycles and life spans of *Nanomia cara*, the physonect siphonophore species thought to be responsible for the GF group backscatter, is extremely limited. However, descriptions in Carré (1969) suggest that the related species *Nanomia bijuga* is still in its larval stage as a siphonula at twenty days old. Temporal drivers of the GF group might then become more prominent over longer timescales.

Data on rare events, such as storms which can influence zooplankton and fish distributions over short time-scales (Maud et al., 2018; Kaartvedt et al., 2017; Jones et al., 2020), can be lost in coarse resolution data and analyses, as can fine-scale details. Glider profiles showed that chlorophyll at the DCM fluctuated over small spatio-temporal scales, and the relationship between surface, BML and DCM chlorophyll was complex, exhibiting greater coherence following the period of sustained strong winds. This underlines the need to collect high-resolution ancillary data from co-located vehicles in order to be able to capture relevant ecological relationships and understand how particular events may change the nature of these relationships.

Although acoustic data were collected at high resolution, vertical integration and averaging across 600 m horizontal bins caused the loss of fine-scale details in the backscatter distributions. Echograms of unaveraged data revealed the intermittent presence of thin, undulating bands of backscatter near the lower thermocline (Figure 4.4.1). Thin, persistent layers of phytoplankton often form in this region and can extend across many kilometres, maintained by the vertical stability imposed by stratification (Dekshenieks et al., 2001; McManus et al., 2005; Cowles et al., 1998). These patches of concentrated food can increase the vertical heterogeneity of zooplankton which aggregate to forage, and can also provide alternative functions such as refuge above and within the layers that contribute to the vertical structuring of zooplankton communities (Greer et al., 2013). However, the centre of mass metric described only the central vertical tendency of backscatter. It cannot differentiate between compact and vertically dispersed distributions, nor between those that are unimodal and multimodal. Methods to identify and enumerate distinct layers have revealed more complex vertical distributions and migration behaviours than the traditional assumption of a single, coherent SSL (Berge et al., 2014; Klevjer et al., 2012; Urmy et al., 2012). Detail such as this could provide further insight into how different trophic levels are vertically structured in the relatively depth-constrained environment of the North Sea.

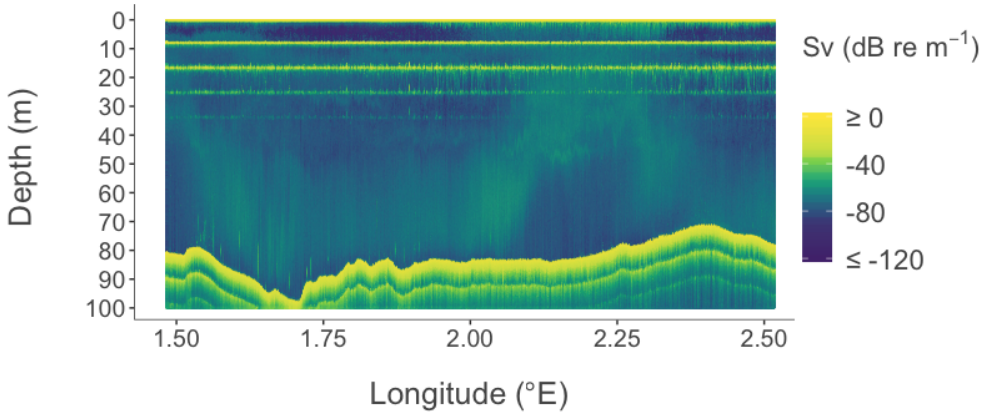


Figure 4.4.1: **Echogram of raw acoustic backscatter, showing vertical heterogeneity (patchiness) in acoustic backscatter within the main sound scattering layer.** Backscatter measurements at 70 kHz from Transect 13.

### 4.4.8 The utility of incorporating oceanographic data from gliders

Oceanographic parameters are often highly correlated, hence available metrics may act as proxies for other parameters, and patterns may be obscured by contrasting effects. Correlated oceanographic parameters are not merely a statistical phenomenon, but tell us something about the reality of life in the pelagic, and the trade-offs that animals face (Cade and Benoit-Bird, 2015). Ascertaining evidence of causal mechanisms would be invaluable to understand how variation in environmental drivers translate to shifts in zooplankton distributions. This was beyond the scope of this study, however water column measurements of oceanographic variables made by the co-located Seaglider greatly helped in interpreting the relationships identified by the models. These measurements allowed spatiotemporal variation in the BML to be observed, crucial for understanding the conditions zooplankton may have experienced in the analysis layer, as well as how variation in surface properties (used as input in the GAMMs) related to variation at depth.

Subsurface measurements made by the glider could be further exploited by extending this study to testing environmental measurements made within the analysis layer in the GAMMs, particularly those that do not correlate well with surface measurements, such as fluorescence. Furthermore, measurements of tidal current directions and speeds can be derived from glider data (Sheehan et al., 2018), which could enhance our understanding of circulation in regions where distinct changes in zooplankton distributions were observed, such as over the ridge (described in Subsection 4.3.1). Gliders can host a suite of sensors that could benefit similar future studies. In-situ PAR measurements account for changes in water clarity and absorption that are lacking from the surface measurements made by *Lyra*, and measurements of microstructure could help to disentangle the possible mechanisms through which wind speed appears to influence distributions. Density profiles can reveal the locations of thermoclines, and stratification strength can be derived from water column temperature data. Whilst surface environmental measurements from *Lyra* alone were sufficient to discern some associations with the acoustic data, high resolution subsurface measurements made by gliders could offer a unique opportunity to improve our understanding of environmental drivers of biological patchiness at the sub-mesoscale and smaller spatial scales.

# 5

# Conclusions

*Lyra's* deployment in May 2018 was the first demonstration of a fisheries acoustic survey conducted by an ASV in UK waters of the North Sea, sampling across repeat transects for a combined distance of almost $1000\,\mathrm{km}$ over the course of a 21 day mission. *Lyra* autonomously sampled the surface and sub-surface environment using a variety of sensors, enabling the study of environmental drivers of sub-mesoscale zooplankton and fish school patchiness over sub-seasonal timescales. This revealed DVM behaviour of gas-bearing zooplankton and diel patterns of swimbladdered forage fish school formation and disaggregation. *Lyra* demonstrated the Wave Glider's capabilities to collect good quality acoustic data, as well as highlighting some of the challenges faced when using ASVs as acoustic platforms, and the Wave Glider in particular. Similar to other surface vessels, stronger winds negatively impacted the quality of the acoustic data, primarily by causing attenuation of the acoustic signal. The multicollinearity between wind speed, acoustic masking and attenuation caused by sub-surface bubbles, and vessel forward and rotational motion is common to other wind- and wave-powered ASVs. This multicollinearity has implications both for along-track resolution and spatial coverage of acoustic data. The Wave Glider's subunit, a strong scatterer, was detected in the acoustic beams. Subunit interference persisted throughout the dataset, resulting in a significant loss of data and precluding subsequent analyses of biota from the surface to $36\,\mathrm{m}$ depth. One of the most significant challenges faced by ASVs used for acoustic surveys is that there is currently no reliable, direct way to validate acoustic classifications. This and other challenges and benefits of using ASVs for acoustic surveys will be discussed in this chapter, together with a synthesis of my findings about drivers of zooplankton and fish distributions in the central North Sea.

## 5.1 Suitability of the Wave Glider as a platform for fisheries acoustic surveys

### 5.1.1 Quality of acoustic data collected by the Wave Glider

Greene et al. (2014) outlined the need for an analysis of data quality to be included in future work to assess the technical and economical viability of using a fleet of acoustically-equipped Wave Gliders to contribute to fish stock surveys in the United States. More recently, Jech et al. (2021) identified a pressing need for assessments of how adverse weather affects acoustic data collected by different kinds of autonomous vehicles. This is particularly important since they look set to replace or augment the use of research vessels for routine acoustic surveys (for example, see Reiss et al., 2021; De Robertis et al., 2021). To meet this need, I conducted an in-depth evaluation of the impact of wind on acoustic data quality collected by the Wave Glider *'Lyra'*.

I found that strong winds introduced substantial bias in *Lyra's* acoustic data, primarily through attenuation of the signal. The relationship between wind speed and attenuation was similar to that observed in acoustic data collected by other types of ASVs and ships (Shabangu et al., 2014; De Robertis et al., 2019). However, there is at least one factor affecting data quality that is unique to wave- and wind-powered ASVs such as the Wave Glider: transit speeds are positively correlated to wind speed. This means that, in windy weather, along-track resolution might decrease not only due to the removal of more bad data, but, if the ping rate is constant, it is further compounded by the vehicle covering larger distances between successive pings. Changeable and lower spatial resolution may not be problematic for surveys in which the acoustic data will be echo integrated over large spatial scales. However, consistent and comprehensive coverage of an area is important for biomass and abundance surveys, and the detail provided by finer spatio-temporal resolution acoustic data is often needed for studies of behavioural processes.

The configuration of the echosounder system, particularly transducer placement, plays a major role in determining the suitability of the Wave Glider as an acoustic platform. It was

hoped that the acoustic measurements made by *Lyra* would reveal patterns in near-surface distributions of zooplankton, a feat not often achieved by traditional ship-based acoustics due to the depths where transducers are usually mounted. Whilst *Lyra* did acquire some usable data close to the surface, much of the water column above $36\,\mathrm{m}$ was unusable due to subunit interference which masked biological signals. Whilst *Lyra's* data shows that the Wave Glider has the ability to take acoustic measurements from closer to the surface than ships typically can, this ability is critically dependent on finding a suitable way to mount transducers so that the subunit does not interfere with the acoustic beam.

Subunit interference, which was perhaps the most problematic form of degradation in *Lyra's* acoustic data, was not a weather-related issue but a consequence of the location where the acoustic transducers were mounted. However, to mitigate this problem by relocating the acoustic transducers, it is first necessary to consider how wind and wave conditions might affect data quality. Attaching transducers deeper could alleviate some of the weather-related data quality issues, such as wave impacts and bubble-shadowing (Trevorrow, 2003). Bingham et al. (2012) reported overall low levels of platform noise for the Wave Glider, with lower self-noise at the subunit compared to the float. Therefore, attaching the transducers to a tow-body from the subunit itself, pointing downwards, could both eliminate subunit interference and reduce weather-related impacts, without necessarily increasing platform noise. However, this option would mean that targets within approximately $10\,\mathrm{m}$ of the surface could not be observed acoustically by a downwards facing transducer. Alternatively, to retain the option of observing targets close to the surface, the transducers could still be attached to the float using a strut behind the vehicle, but the strut could be extended farther aft. The addition of a gimbal on the transducer mount may further help to prevent the acoustic beam from pointing towards the subunit during rough conditions.

Acoustic surveys collect data at an impressive rate. For example, Pedersen et al. (2019) reported that their six-month Wave Glider and Sailbuoy deployments generated $224$ and $716\ GB$ of acoustic data respectively. This precludes transmission of data to shore in real-time due to time and cost constraints, and full acoustic datasets can only be retrieved from autonomous vehicles upon their recovery. Consequently, there has been recent interest in developing processing methods to derive summary metrics small enough to be relayed

to shore in near real-time and that are suitable for running on the on-board processors of autonomous vehicles, i.e. that are not memory-demanding, do not require fast processing speeds, and are not power-hungry (Blackwell, 2020). Transmission of summary metrics from autonomous vehicles to shore could allow on-shore pilots to adapt vessel navigation and sampling regimes remotely in order to take advantage of presenting opportunities. A non-acoustic example of this is sampling rare events such as harmful algal blooms (Beckler et al., 2019). Summary metrics are usually discussed in the context of characterising the ecosystem, identifying hotspots of acoustic targets (for example, using ASVs as scouts for fisheries), or to identify events and enable adaptive sampling (Urmy et al., 2012; Blackwell et al., 2019b). However summary metrics could also be used to inform pilots on-shore about acoustic data quality, alerting them to the need to mitigate problems with data collection or alter sampling strategies to reduce unnecessary power consumption and storage of poor quality data during adverse weather. Alternatively, if transmission to shore is not possible, echosounder programs could be designed to incorporate updates from summary metrics in order to autonomously adapt acoustic sampling regimes in a similar manner.

The two-layer comparison technique has the potential to be adapted to provide a useful summary metric to characterise the quality of acoustic data collected by any kind of platform, particularly autonomous platforms such as the Wave Glider since they lack crew onboard to oversee data quality. Development and assessment of the technique for this purpose is beyond the scope of this work. However, should a computationally inexpensive method for producing this summary metric be attainable then this technique could be adapted for use on autonomous platforms, either to adjust sampling regimes autonomously or informing onshore pilots of the estimated quality of the acoustic data. In its current format, the technique derives two values per ping using a pair of two-metre deep layers which are then tested for correlation, producing a single value for a set of pings. This demonstrates that a relatively small proportion of the acoustic data can be used to derive a useful metric to evaluate bias associated with attenuation and transient noise.

### 5.1.2 Observing DVM behaviour and the influence of the environment on zooplankton and fish distributions

*Lyra's* mission illustrates the capability of an acoustically-equipped Wave Glider to detect DVM of zooplankton in a shallow shelf sea, potentially obtaining new insights into the vertical migration behaviour of gas-bearing siphonophores in the central North Sea. Chapter 3 provided a first description of net migration amplitudes and rates observed during late spring when there was an apparent abundance of gas-bearing zooplankton in the water column. Analysing the difference between net movement of the SSL at dawn and dusk revealed an intriguing asymmetry between ascent and descent behaviour. This asymmetry could be evidence of intra-population variation in endogenous drivers of DVM behaviour which lead to less synchronised shifts in the individual trade-offs between foraging and predator avoidance at dusk (Pearre, 2003a). That is to say, after a night of feeding, most or all of the animals will prioritise predator avoidance at dawn, whereas in the afternoon, some animals may prioritise foraging to meet their energy demands over predator avoidance, and the differences in the balance of trade-offs that individuals face will vary according to their internal state.

To reliably study DVM behaviour, the normal movement behaviours of animals must be unperturbed by the presence of the observation platform. Avoidance or attraction behaviour induced by observation platforms can alter perceived net vertical migration behaviours, and since behavioural responses to stimuli are often species-specific, attraction or avoidance could also confuse signals from different kinds of migrators. In the relatively shallow North Sea, mass vertical movements take place over a matter of hours and migrations extend over only a few tens of metres in depth, i.e. the spatial and temporal scales of this behaviour are relatively small. Studies of DVM in the North Sea and similar shallow environments may therefore be particularly sensitive to platform-induced avoidance or attraction. ASVs could offer several advantages over ships for acoustic observations of DVM by virtue of their typically quieter operation, reduced lighting and minimal areal footprint.

Since light is the predominant cue mediating vertical position in the water column, changes to underwater light levels caused by the platform could confound observations of DVM.

Artificial light can cause avoidance or attraction whereby animals swim either towards or away from the light source. Artificial light emanating from a ship has been shown to affect zooplankton and fish behaviour down to $200\,\mathrm{m}$ in the Arctic (Berge et al., 2020). On deck lighting can not only induce vertical and horizontal movement of animals, but can also affect their orientation which in turn affects acoustic backscatter measurements (Trevorrow et al., 2005). However, deck lighting is necessary on manned vessels for safety reasons. Light from some sensors may induce avoidance behaviour; Benoit-Bird et al. (2010) found that light from an open path fluorometer was responsible for avoidance of a profiling instrument, with reactions observed up to $13\,\mathrm{m}$ from the sensor. In contrast, the Wave Glider possesses only one small light above the surface, used to make the platform visible to other vessels at sea, and, in the case of *Lyra*, the only underwater light source was a small, dim, intermittent flash of green light produced by the WetLabs Ecopuk to measure fluorescence, which was unlikely to have been perceived by organisms at depths of the analysis layer (i.e. below $36\,\mathrm{m}$).

Platforms can also change the underwater light environment by creating shadows. Ocean gliders have been shown to induce an avoidance reaction in krill below the platform as it travels downwards (Guihen et al., 2014, 2022). The reaction may be due to a sudden shadowing effect as the glider passes overhead, since glider upcasts do not seem to elicit similar reactions, and so neither sensor lights nor water perturbation were likely to explain the behaviour. Shadows cast by the Wave Glider and the perturbation of water by the surface float and the subunit (at $8\,\mathrm{m}$ depth) could potentially induce avoidance behaviour in the upper water column, though the impacts are unlikely to be as severe as those caused by larger vessels such as ships.

Sound, too, has the potential to influence the swimming behaviour of animals. Studies on behavioural responses of animals, in particular fish, to vessel noise have proved variable and contradictory; however if a reaction is observed it usually indicates avoidance (De Robertis and Handegard, 2013; De Robertis et al., 2008; Misund, 1997; Mitson, 1995; Fernandes et al., 2000). The relatively quiet operation of the Wave Glider compared to screw propelled ships provides a potential advantage for observing animals that are sensitive to vessel noise (Bingham et al., 2012). In summary, the Wave Glider has a much smaller areal footprint than ships, it travels much more slowly, it has less onboard lighting, and it is quieter. It is therefore

far less likely to elicit a strong behavioural avoidance or attraction response from fish or zooplankton than ships, making it particularly well suited to the study of DVM behaviour and animal distributions near the surface.

Unfortunately, the lack of usable data above $36\,\mathrm{m}$ prevented a thorough analysis of how animals distributed themselves in the upper water column and how distributions may have shifted in response to strengthening stratification during the spring season. Without classification of backscatter in the MML and SML, the vertical distributions of gas-bearing zooplankton at night could not be confidently described. Fortunately, echograms helped to interpret the patterns found in the classified backscatter. The echograms indicated that the main SSL, which was acoustically dominated by gas-bearing zooplankton, moved above the analysis layer at night and remained near the surface until just before dawn, as expected for classic DVM behaviour.

*Lyra's* deployment was timed to coincide with spring stratification in the central North Sea when dramatic physical changes occur in the epipelagic, driven by enhanced solar warming at the surface. Vertical density gradients, such as those associated with thermal stratification, acted to aggregate food for zooplankton at the DCM and prevented mixing between different water masses. Given that planktonic organisms have a limited ability to swim against ocean currents, which are typically near-horizontal, the presence of vertical density gradients provide zooplankton with a means to gain access to food or different environmental conditions better suited for metabolism or reproduction (Harris, 1988; Lindegren et al., 2020). Although GAMM analyses did not reveal any obvious association between the progression of stratification and shifts in backscatter distributions in the BML, enhanced vertical structuring of the physical environment due to stratification was mirrored by enhanced vertical structuring of the SSL in the MML and SML; echograms showed the formation and increasing prominence over time of thin, undulating scattering layers near the upper thermocline. Reliable and good quality acoustic observations from the upper part of the water column may be crucial to understanding how stratification affects biological distributions in the water column in the shallow North Sea.

In order for the Wave Glider to get closer to its full potential as an acoustic platform, the

issue of subunit interference must be resolved. This issue is idiosyncratic to the method of transducer integration and so does not necessarily preclude the Wave Glider from being a useful platform for the acoustic study of biological distributions near the surface. Mounting transducers at the rear of the surface float clearly risks subunit interference that could result in substantial data loss near the surface (Pedersen et al., 2019; Swart et al., 2016).

Acoustics have the ability to simultaneously sample different components of the ecosystem. Classified acoustic data have the potential to reveal the interplay of distinct migration behaviours by different animals. However, without a robust classification scheme, DVM signals from disparate biological groups could be confounded and movement patterns obscured or misattributed to the wrong types of organisms. I partitioned backscatter data into three acoustic groups that represented three biological groups, providing only a somewhat coarse biological resolution. Nevertheless, distinct patterns in diel movement behaviour were observed in two of the three groups. Schools of swimbladdered fish were observed forming at dawn and disbanding at dusk, remaining close to the bottom throughout daylight hours. The main SSL, which primarily represented gas-bearing zooplankton, exhibited a classic DVM pattern throughout the time series. However, the acoustic classification was only ground-truthed using net samples taken by a nearby ship during the early part of the mission, and these net samples poorly represented fish and gelatinous zooplankton due to gear selectivity. This method of ground-truthing is not as robust as other direct, synoptic ground-truthing methods which are recommended for validating acoustic classifications (McClatchie et al., 2000).

The problem of remote species identification has been identified as one of the great challenges facing fisheries acoustics (Horne, 2000). It is of particular relevance to acoustic studies that use ASVs, since options to collect validation data are limited by significant logistical constraints. Ideally, independent physical or optical samples would be taken by the vehicle itself to directly validate acoustic data classified as target or non-target species. Although validating acoustic classifications using samples taken by another platform cannot provide direct targeted validation of acoustic regions of interest, there is still value in integrating data from different platforms to validate acoustic data. For example, Reiss et al. (2021) used krill length data obtained from diet analysis of penguins to validate glider-based acoustic

abundance estimates of krill. The workaround this study used, to take net samples from a nearby ship to characterise the zooplankton community present in the vicinity of *Lyra*, is a method that has been used before to verify classifications of acoustic measurements taken by both autonomous vehicle acoustics (Pedersen et al., 2019) and other ships (Sato et al., 2015). The ship-based approach to validation places a requirement on the ship to be co-located with the ASV. For short-term missions, such as *Lyra's*, this may be relatively straightforward to achieve by sampling immediately after deploying the vehicle and upon recovery. Taking samples at these times from a nearby location would increase the likelihood of sampling similar organisms to those observed acoustically and better represent any changes in zooplankton community composition over time. For longer missions, when ground-truthing may be needed several times to represent the changing composition of SSLs, having to repeatedly navigate a ship to the vehicle's location somewhat negates the benefits of using an autonomous vehicle.

Validation using only data collected by the autonomous vehicle itself is preferable. One feasible option is to integrate an optical system that can process images of zooplankton (Ohman et al., 2019). Ongoing development of in-situ plankton imaging systems have recently focused on semi-automated methods to collate high-speed plankton data in near real-time from onboard ships (Scott et al., 2021). Novel applications of similar systems integrated on to autonomous platforms are beginning to show promise and could potentially lead to near-realtime classification of acoustics in the future (Wang et al., 2022). However, all optical systems are confined to sampling over a short range underwater because of the rapid attenuation of light, so autonomous surface vehicles can only obtain images or video of animals present in the near-surface environment.

Environmental DNA (eDNA) sampling may be better suited to surface vehicles as they only require small volumes of water to be collected and can provide information on the recent presence of organisms throughout the water column (Garlapati et al., 2019). Work is underway to develop eDNA methods that can produce quantitative estimates of marine organisms (Lacoursière-Roussel et al., 2016; Hansen et al., 2018). Automated samplers are being tested on autonomous vehicles with good results (Truelove et al., 2022), and elsewhere the use of eDNA profiles to complement and ground-truth acoustic data is being

evaluated, with results showing that eDNA can reveal shifts in taxonomic composition over DVM-relevant timescales (Easson et al., 2020; Shelton et al., 2022). Ideally, any technique to ground-truth acoustics collected by an autonomous vehicle will need to provide targeted validation of aggregations and layers, as well as depth-resolved samples, both of which pose a substantial challenge for surface vehicles without means to lower equipment to depth.

For autonomous campaigns, the combination of complementary autonomous technologies may prove the most effective way to validate acoustic data (Moline and Benoit-Bird, 2016). Similar future acoustic studies using Wave Gliders would benefit from concurrent depth-resolved net or optical samples obtained from other vehicles to validate acoustic classifications. Ideally, this would incorporate gear and methods better suited to sample gelatinous organisms (Knutsen et al., 2018). This is of particular relevance to monitoring zooplankton in the North Sea because future warming scenarios give rise to environmental conditions that will likely favour gelatinous organisms and lead to their dominance in temperate pelagic food webs (Heneghan et al., 2023; Attrill et al., 2007). Ground-truth samples would ideally take place at representative time points throughout the data collection period. This would improve upon the net sampling method used in this study, which was limited to a 24-hour period and used vertical hauls using open nets that provided no depth resolution and which were poorly suited to sampling all components of the zooplankton. Depth-resolved zooplankton data could help to answer unresolved questions from this study, such as whether distributions of fluid-like and gas-bearing scatterers overlap in space, and whether fluid-like scatterers, such as Calanus copepods, vertically migrate on diel timescales in situations where their siphonophore predators are prevalent in the water column. Underwater buoyancy gliders could prove a viable option for collecting depth-resolved optical samples (Ohman et al., 2019; Wang et al., 2022). Gliders already transit through the water column, allowing them to target layers of interest. However, there is preliminary evidence that gliders can induce avoidance behaviour, thought to occur because zooplankton perceive the glider as predators, although more work is needed in this area to evaluate avoidance effects and their potential utility (Guihen et al., 2014; Benoit-Bird and Lawson, 2016). Currently, the routine collection of depth-resolved net samples requires manned vessels from which to deploy the nets as ASVs such as the Wave Glider cannot feasibly

collect these (Pedersen et al., 2019), and neither can underwater gliders, although innovation in autonomous deep-sea sampling systems may change this over the coming years (Billings et al., 2017).

The discrepancy between the prevalence of fluid-like zooplankton scatterers inferred from net samples and acoustic dominance of gas-bearing zooplankton highlights the differences in selectivity and biases associated with net and acoustic sampling methods (Wiebe et al., 1982; Lavery et al., 2007). Acoustic dominance by stronger, gas-bearing scatterers resulted in significant acoustic masking of fluid-like scatterers, such as copepods, other crustaceans and crustacean larvae, chaetognaths, and hydrozoa. This precluded the study of diel shifts in fluid-like scatterer distributions. The combination of complementary methods that better sample different components of the plankton helps to unpick biases associated with acoustic sampling (Blanluet et al., 2019; Gastauer et al., 2022; Whitmore et al., 2019). In situations where strong scatterers, such as gas-bearing zooplankton and fish, are prevalent in SSLs, it is advisable to conduct additional, non-acoustic sampling to observe distributions of weak scatterers (Knutsen et al., 2018; Blanluet et al., 2019).

Acoustic masking by dominant scatterers is not an uncommon occurrence in acoustic studies. Many hierarchical multi-frequency classification schemes note similar discrepancies between inferred abundance or biomass of fluid-like and gas-bearing scatterers derived from net samples and acoustics, and also identify that backscatter might easily be misclassified, particularly since sampling volumes may contain backscatter from more than one group (Mair et al., 2005; Ballón et al., 2011; Sato et al., 2015). Sato et al. (2015) succeeded in achieving a high level of classification accuracy ($95$ to $100\,\%$) of fish school species by using several dB-difference windows to partition the data. However, these windows were derived using a subset of acoustic data for which directed trawl samples for validation had been obtained. Without direct ground-truthing samples to validate *Lyra's* acoustics, the separation of zooplankton groups by dB-difference at $\Delta\mathrm{MVBS}_{200-70} = 0$ rested on the theory of scattering properties for fluid-like and gas-bearing scatterers, taking into consideration which species might be present in the North Sea and their typical sizes. This was not straightforward, however, as there is a lack of information about the frequency responses of these kinds of organisms at $70$ and $200\,\mathrm{kHz}$, since these frequencies are not commonly used for acoustic

surveys. With the growing application of broadband acoustics and expansion of frequency response reference libraries, the robustness of remote classifications such as this may improve in the future (Korneliussen et al., 2016; Blanluet et al., 2019; Stanton et al., 2012). The development of reliable remote classification methods would have a substantial impact on the utility of ASVs for acoustic studies.

### 5.1.3 Considerations for biomass and abundance acoustic surveys

Data from acoustic surveys are routinely used to produce biomass and abundance estimates used for fisheries stock monitoring. Rising ship fuel costs and the environmental footprint of ship-based surveys look set to promote the increased use of acoustically-equipped ASVs as alternatives to ships for this kind of work (Simmonds and MacLennan, 2005; Reiss et al., 2021; De Robertis et al., 2021). This thesis does not directly evaluate the contributions that an acoustically-equipped Wave Glider could make to fisheries stock assessment surveys or ecosystem-based marine resource management; however there are issues relevant to this topic that warrant discussion.

Biomass and abundance estimates can only be reliably derived from data of excellent quality (Jech et al., 2021). This requires accurate measurements of backscatter from target species which can be discriminated from other sources, and confidence in the acoustic classification. These requirements are not easily achieved using Wave Gliders or other ASVs. Firstly, echosounders must be accurately calibrated to ensure acoustic measurements are accurate and estimates are comparable across surveys; however logistical constraints make accurate calibrations of ASV mounted echosounders difficult to achieve in practice. Secondly, as discussed earlier, acoustic classifications must be validated using independent samples that have adequate taxonomic resolution in order to ensure that estimates are derived from target backscatter only.

Calibrations typically require that a calibration sphere is positioned underneath the transducers where the sphere is carefully moved around (Foote et al., 1987; Demer et al., 2015). In order to ensure that measurements of the sphere are obtained from various positions under the transducer, it is common to monitor calibrations live using the

echosounder software. However, these actions are made more difficult to perform on an ASV since it is unmanned. The logistical challenges posed by calibrating an echosounder integrated on an unmanned vessel at sea meant that the echosounder system used on *Lyra* had to be calibrated elsewhere, in this case in a harbour which had markedly different water properties from those experienced during the mission. Additionally, because the Wave Glider can only be deployed in water deeper than $15\,\mathrm{m}$ (due to operational risk of umbilical and subunit damage in shallow water), the echosounder system had to be calibrated prior to its integration onto *Lyra*. Calibrating in different environments to those where sampling takes place can introduce errors in the accuracy of acoustic measurements (Demer et al., 2015), and calibrating an echosounder that is not integrated onto the platform means that platform noise cannot be accounted for by the calibration, again potentially introducing error. Ideally, calibrations are conducted in-situ where the echosounder is integrated on to the platform. This option might require the use of manned small boats and a means to tether the Wave Glider in order to stop it moving because even small waves can cause the vehicle to move forward. However, this might prove too unsafe and time-consuming to be a realistic option. Consequently, whilst the Wave Glider may be a suitable acoustic platform for many ecological studies, care should be taken to address potential issues affecting accuracy of acoustic data intended for monitoring efforts.

## 5.2 Looking to the future

Zooplankton that inhabit shelf seas contend with a range of environmental conditions which fluctuate over various spatio-temporal scales (Klais et al., 2016). This is particularly true of the North Sea where hydrographical conditions can vary over both short (weekly) and longer (annual and decadal) timescales due to varying inflow of Atlantic and coastal waters (Sheehan et al., 2020; Beaugrand, 2003). The shallow depths typical of many shelf seas can prevent zooplankton and forage fish accessing deeper habitats to seek refuge from visual predators; prey must find effective strategies to share the limited vertical space with predators. It is precisely this shallowness and dynamism that contribute to making shelf seas disproportionately productive and host to a diverse assemblage of species. It is no wonder

then that, historically, the North Sea has been one of the most productive fisheries regions in the world (Quante and Colijin, 2016).

However, the North Sea is experiencing increasingly rapid environmental change. Shifts in large scale weather patterns are driving trends in hydrographic conditions - in particular increasing sea surface temperature, earlier onset and increased strength of stratification, and declines in water clarity - that are having significant impacts on present and predicted future North Sea ecosystem dynamics (Defriez et al., 2016; Reygondeau and Beaugrand, 2011; Capuzzo et al., 2018; Lindegren et al., 2018; Montero et al., 2021; van der Molen and Pätsch, 2022b; Opdal et al., 2019). Globally, zooplankton biomass is predicted to decline and gelatinous organisms are predicted to increasingly dominate zooplankton community composition, reducing the availability and nutritional content of food for small pelagic fish (Heneghan et al., 2023). These projections also hold for the North Sea, albeit with regional differences, and evidence of climate-induced shifts of this nature have already been observed (Attrill et al., 2007; Capuzzo et al., 2018; Lynam et al., 2010, 2005).

Future warming scenarios are likely to affect many biological processes linked with stratification of the North Sea. Changes to the timing of seasonal warming, including earlier onset and later breakdown of seasonal stratification, is anticipated to lead to mismatches in phenological development of predator and prey species, altering trophic dynamics (Richardson and Schoeman, 2004; Edwards and Richardson, 2004; Quante and Colijin, 2016; Mackas et al., 2012). Predicted future declines in water clarity in the North Sea, combined with enhanced stratification which limits vertical nutrient mixing, are predicted to affect timing of phytoplankton blooms as well as influencing DVM behaviour, affecting trophic interactions between visual predators and their prey (Capuzzo et al., 2015, 2018; Opdal et al., 2019; Aarflot et al., 2020). Steep density gradients associated with strong stratification can act to isolate the BML, leading to a potential decline in oxygen levels under more stable and prolonged stratification scenarios (Queste et al., 2016). Oxygen depletion could add an additional constraint on the vertical use of space by pelagic animals. For example, low oxygen levels in the BML could have a limiting effect on the extent of vertical migrations (Bianchi et al., 2013a). However, there is considerable uncertainty over predicted changes to oxygen levels in the North Sea and elsewhere, partly because oxygen production

and consumption by biological activity, which plays a relatively large role in determining oxygen concentrations, are complex to model under future warming scenarios (Queste et al., 2016; Emeis et al., 2015; Mahaffey et al., 2020).

This thesis considered environmental drivers of pelagic animal distributions using data from an acoustic survey that spanned a relatively small region of the central North Sea (less than $64\,\mathrm{km}$) and took place over twenty-one days in spring. Such a small-scale survey provides only a brief snapshot of seasonal ecosystem dynamics, and relationships found here between animal distributions and their environment may not be relevant to other contexts. Survey timing and duration can exert a significant influence on the observability of patterns, and small-scale surveys may fail to adequately capture important processes (Huret et al., 2018). Both environmental gradients and behavioural strategies that influence patchiness vary seasonally and spatially, and species respond in diverse ways to environmental change (Klais et al., 2016; Irigoien et al., 2004; Otto et al., 2014). Mean background conditions, variability, and the strengths of covariance among ocean variables will very likely shift under future warming scenarios (Trifonova et al., 2021). This will impact trade-offs governing behavioural strategies that influence patchiness, such as DVM. Consequently, the relative importance of particular environmental drivers identified in this thesis is unlikely to remain fixed in time or necessarily be applicable to animal distributions in other regions of the North Sea (Trifonova et al., 2021).

Large-scale changes in the climate and oceanography of the North Sea would mediate background conditions relevant for the small-scale processes, and could alter available ecological niches. Understanding how the associations between physical and biological variation over different scales are connected to each other is important in order to be able to predict how climate change might impact zooplankton community composition, population sizes, geographic range and the patchiness of their distributions (Folt and Burns, 1999; Prairie et al., 2012; Keerthi et al., 2022). Indeed, the patchiness of zooplankton spatial distributions could influence how they respond to climate-induced changes in the environment (Otto et al., 2014). The effects that multiple interacting stressors due to climate change, fishing, and other anthropogenic activities will have on the North Sea ecosystem are unclear, in part because biological distributions may become decoupled from their current environmental

drivers (van der Molen and Pätsch, 2022b; Trifonova et al., 2021). This underlines the need for ongoing, persistent monitoring of a diverse range of ecosystem components, both biotic and abiotic, to understand how environmental change over both small and large scales is impacting biological distributions (Ratnarajah et al., 2023).

Long time series are crucial for understanding how environmental change impacts pelagic animal distributions (Edwards et al., 2010; Ratnarajah et al., 2023). Persistent acoustic and environmental monitoring by ASVs, such as the Wave Glider, provides a means to achieve this without many of the constraints of ship-based surveys (Pedersen et al., 2019; De Robertis et al., 2019). One of the major advantages of using autonomous vehicles for routine monitoring is that they can be deployed for extended periods of time to conduct single-focus research. In contrast, research ships typically have to juggle many competing usage demands, restrictions on schedules, and other constraints associated with having crew on board such as the need to dock regularly and adhere to strict safety requirements (Verfuss et al., 2019).

Another key benefit of using ASVs to conduct sampling instead of ships is the lower carbon cost of data capture and reduced environmental impact of ASVs on the marine environment (Siddorn et al., 2022). In a world where societies are striving to reach carbon net-zero goals, the use of autonomous vehicles for ocean science looks set to increase (Turrell, 2019). ASVs are less energy demanding than ships, and many vehicles harvest a significant proportion of their energy from renewable sources and consequently do not produce harmful emissions at sea. In recognition of their capacity to provide a greener and more sustainable alternative to ship-based sampling, the Net Zero Oceanographic Capability, a project which scoped ways to transition ocean science in the UK to net zero by 2040, emphasised the importance of incorporating autonomous technologies, including data collection platforms, into strategies for delivering scientific excellence in a net-zero carbon future (NOC, 2021).

Acoustically-equipped ASVs are unlikely to directly replace ships, nor should they. The inherent differences in ASV capabilities and logistics provide both advantages and disadvantages to their use in ocean science (Verfuss et al., 2019; Sepp et al., 2022). Manned research vessels are still recognised as the linchpin of marine observation systems in a net-zero carbon future, albeit with modifications - particularly in relation to their reliance on

hydrocarbon fuels. The multidisciplinary capabilities of research vessels should be leveraged to maximise opportunities for collaboration amongst scientists (Turrell, 2019; NOC, 2021). Where ASVs do replace or augment ship-based monitoring efforts, challenges will need to be addressed surrounding the integration of ASV-collected data with pre-existing datasets (Révelard et al., 2022).

The real power of ASVs to transform fisheries acoustic surveys will be seen when data from numerous vehicles can be combined, whether this takes the form of combining complementary data from different vehicles that each undertake a different function, or combining data from fleets of the same vehicle to improve synoptic coverage of an area (Greene et al., 2014). Multi-platform ocean observing systems in which autonomous platforms are a significant component are becoming increasingly common (Heslop et al., 2019). It has already been recognised that the Wave Glider has the potential to contribute to multi-platform observing systems, provided their integration follows recommendations to optimise networks of autonomous platforms (e.g. in Whitt et al., 2020; Révelard et al., 2022). Greene et al. (2014) advocated the use of fleets of Wave Gliders to conduct acoustic surveys, citing that costs involved, even with multiple vehicles, could be substantially lower than those of traditional ship-based acoustic surveys. Temporal fluctuations in zooplankton patchiness, especially for smaller zooplankton that have shorter reproductive cycles, are particularly acute during springtime in northern, temperate shelf seas (Klais et al., 2016). It is therefore crucial to consider the timing and duration of zooplankton monitoring surveys (Huret et al., 2018). Uncertainty surrounding shifts in phenological timing, associated with changes in the onset and development of seasonal stratification, make predicting optimal survey timing during spring difficult. Instead, persistent monitoring over periods longer than typically possible using ship-based acoustic surveys may be a better way to ensure that temporal variation is captured. *Lyra's* successful deployment indicates the potential that fleets of ASVs have to monitor zooplankton over extended periods (weeks or months) and to capture data on important temporal and spatial processes that influence variation in zooplankton patchiness. ASVs could therefore meet the need to conduct persistent acoustic zooplankton monitoring in shelf seas where it would be unrealistic for ships to do the same, due to cost and time constraints.

In order for acoustically-equipped Wave Gliders to reach their full potential, priority should be given to solving the logistical challenges that the Wave Glider faces and developing statistical techniques to improve acoustic accuracy and precision. In particular, we must find innovative ways to calibrate echosounders in-situ, to obtain robust validation data to support acoustic classifications or to improve remote classification methods, and to re-engineer the way that acoustic transducers are integrated onto the platform such that subunit interference does not degrade the quality of acoustic data. Broadband acoustics offer a potential way forward in remote species classification, with novel applications of Bayesian inversion methods to disentangle contributions of different scatterers in mixed assemblages of particular relevance to classifying mixtures of zooplankton within SSLs (Urmy and De Robertis, 2021; Benoit-Bird and Waluk, 2020). Advances in the applications of machine learning to large fisheries acoustic datasets, too, should be used to improve the efficiency and accuracy of the classification of taxonomic groups and acoustic features (such as the seabed and fish schools) (Sarr et al., 2021; Yassir et al., 2023). Additionally, to fully exploit Wave Glider data, it may be necessary to combine it with disparate datasets obtained from various types of observational platform. Statistical techniques such as Bayesian modelling can help to improve the precision of estimates derived from combined datasets (Nnanatu et al., 2020), enabling information obtained by Wave Gliders to contribute to much broader studies of marine ecosystems.

Autonomous vehicles are likely to become a mainstay of ocean observing in the future due to their ability to sample in remote and hazardous regions, their cost-effectiveness, and their reduced environmental footprint (Whitt et al., 2020; NOC, 2021). Although Wave Glider acoustic surveys do not currently present a viable option for acoustic abundance and biomass estimation, this thesis demonstrates that they still have the capacity to contribute to ecosystem-based management. Understanding environmental drivers of pelagic fish and zooplankton distributions is crucial to North Sea marine ecosystem management, and to achieve this scientists require good quality, high-resolution, in-situ data from persistent monitoring campaigns, which the Wave Glider can deliver. Consequently, I envisage that combined acoustic surveys and environmental monitoring by Wave Gliders will play a crucial part in the future of ocean science.

# Bibliography


Aarflot, J. M., Aksnes, D. L., Opdal, A. F., Skjoldal, H. R., and Fiksen, Ø. (2019). Caught in broad daylight: Topographic constraints of zooplankton depth distributions. *Limnology and Oceanography*, 64(3):849–859.

Aarflot, J. M., Dalpadado, P., and Fiksen, Y. (2020). Foraging success in planktivorous fish increases with topographic blockage of prey distributions. *Marine Ecology Progress Series*, 644:129–142.

Alheit, J., Möllmann, C., Dutz, J., Kornilovs, G., Loewe, P., Mohrholz, V., and Wasmund, N. (2005). Synchronous ecological regime shifts in the central Baltic and the North Sea in the late 1980s. In *ICES Journal of Marine Science*, volume 62, pages 1205–1215.

Alvarez-Fernandez, S., Lindeboom, H., and Meesters, E. (2012). Temporal changes in plankton of the North Sea: Community shifts and environmental drivers. *Marine Ecology Progress Series*, 462(2):21–38.

Andersen, V. and Sardou, J. (1994). Pyrosoma atlanticum (Tunicata, Thaliacea): Diel migration and vertical distribution as a function of colony size. *Journal of Plankton Research*, 16(4):337–349.

Anderson, C. I., Brierley, A. S., and Armstrong, F. (2005). Spatio-temporal variability in the distribution of epi- and meso-pelagic acoustic backscatter in the Irminger Sea, North Atlantic, with implications for predation on Calanus finmarchicus. *Marine Biology*, 146(6):1177–1188.

Angel, M. V. and Pugh, P. R. (2000). Quantification of diel vertical migration by

micronektonic taxa in the northeast Atlantic. In *Hydrobiologia*, volume 440, pages 161–179. Kluwer Academic Publishers.

Archibald, K. M., Siegel, D. A., and Doney, S. C. (2019). Modeling the Impact of Zooplankton Diel Vertical Migration on the Carbon Export Flux of the Biological Pump. *Global Biogeochemical Cycles*, 33(2):181–199.

Attrill, M. J., Wright, J., and Edwards, M. (2007). Climate-related increases in jellyfish frequency suggest a more gelatinous future for the North Sea. *Limnology and Oceanography*, 52(1):480–485.

Bailey, R. S. (1975). Observations on diel behaviour patterns of North Sea gadoids in the pelagic phase. *Journal of the Marine Biological Association of the United Kingdom*, 55(1):133–142.

Balino, B. M. and Aksnes, D. L. (1993). Winter distribution and migration of the sound scattering layers, zooplankton and micronekton in Masfjorden, western Norway. *Marine Ecology Progress Series*, 102(1-2):35–50.

Ballón, M., Bertrand, A., Lebourges-Dhaussy, A., Gutiérrez, M., Ayón, P., Grados, D., and Gerlotto, F. (2011). Is there enough zooplankton to feed forage fish populations off Peru? An acoustic (positive) answer. *Progress in Oceanography*, 91(4):360–381.

Bandara, K., Basedow, S. L., Pedersen, G., and Tverberg, V. (2022). Mid-summer vertical behavior of a high-latitude oceanic zooplankton community. *Journal of Marine Systems*, 230(March):103733.

Bandara, K., Varpe, Ø., Wijewardene, L., Tverberg, V., and Eiane, K. (2021). Two hundred years of zooplankton vertical migration research. *Biological Reviews*, 96(4):1547–1589.

Batten, S. D. and Burkill, P. H. (2010). The Continuous Plankton Recorder: towards a global perspective. *Journal of Plankton Research*, 32(12):1619–1621.

Batty, R. S. (1984). Development of swimming movements and musculature of larval herring (Clupea harengus). *Journal of Experimental Biology*, 110:217–229.

Baudron, A. R., Needle, C. L., Rijnsdorp, A. D., and Tara Marshall, C. (2014). Warming temperatures and smaller body sizes: Synchronous changes in growth of North Sea fishes. *Global Change Biology*, 20(4):1023–1031.

Beamish, F. W. H. (1966). Vertical Migration by Demersal Fish in the Northwest Atlantic. *Journal of the Fisheries Research Board of Canada*, 23(1):109–139.

Beare, D. J., Batten, S., Edwards, M., and Reid, D. G. (2002a). Prevalence of boreal Atlantic, temperate Atlantic and neritic zooplankton in the North Sea between 1958 and 1998 in relation to temperature, salinity, stratification intensity and atlantic inflow. *Journal of Sea Research*, 48(1):29–49.

Beare, D. J., Burns, F., Greig, A., Jones, E. G., Peach, K., Kienzle, M., McKenzie, E., and Reid, D. G. (2004). Long-term increases in prevalence of North Sea fishes having southern biogeographic affinities. *Marine Ecology Progress Series*, 284(1998):269–278.

Beare, D. J., Reid, D. G., and Petitgas, P. (2002b). Spatio-temporal patterns in herring (Clupea harengus L.) school abundance and size in the northwest North Sea: Modelling space-time dependencies to allow examination of the impact of local school abundance on school size. *ICES Journal of Marine Science*, 59(3):469–479.

Beaugrand, G. (2003). Long-term changes in copepod abundance and diversity in the north-east Atlantic in relation to fluctuations in the hydroclimatic environment. In *Fisheries Oceanography*, volume 12, pages 270–283.

Beaugrand, G. (2004). The North Sea regime shift: Evidence, causes, mechanisms and consequences. *Progress in Oceanography*, 60(2-4):245–262.

Beaugrand, G., Brander, K. M., Lindley, J. A., Souissi, S., and Reid, P. C. (2003). Plankton effect on cod recruitment in the North Sea. *Nature*, 426(6967):661–664.

Beaugrand, G. and Kirby, R. R. (2010). Climate, plankton and cod. *Global Change Biology*, 16(4):1268–1280.

Becker, G. A. and Pauly, M. (1996). Sea surface temperature changes in the North Sea and their causes. *ICES Journal of Marine Science*, 53(6):887–898.

Beckler, J. S., Arutunian, E., Moore, T., Currier, B., Milbrandt, E., and Duncan, S. (2019). Coastal Harmful Algae Bloom Monitoring via a Sustainable, Sail-Powered Mobile Platform. *Frontiers in Marine Science*, 6(October):1–14.

Belcher, A., Tarling, G. A., Manno, C., Atkinson, A., Ward, P., Skaret, G., Fielding, S., Henson, S. A., and Sanders, R. (2017). The potential role of Antarctic krill faecal pellets in efficient carbon export at the marginal ice zone of the South Orkney Islands in spring. *Polar Biology*, 40(10):2001–2013.

Benfield, M., Wiebe, P., Stanton, T., Davis, C. S., Gallager, S. M., and Greene, C. H. (1998). Estimating the spatial distribution of zooplankton biomass by combining Video Plankton Recorder and single-frequency acoustic data. *Deep-Sea Research Part II*, 45:1175–1199.

Benfield, M. C., Lavery, A. C., Wiebe, P. H., Greene, C. H., Stanton, T. K., and Copley, N. J. (2003). Distributions of physonect siphonulae in the Gulf of Maine and their potential as important sources of acoustic scattering. *Canadian Journal of Fisheries and Aquatic Sciences*, 60(7):759–772.

Benoit-Bird, K. (2009). Dynamic 3-dimensional structure of thin zooplankton layers is impacted by foraging fish. *Marine Ecology Progress Series*, 396:61–76.

Benoit-Bird, K. J. and Lawson, G. L. (2016). Ecological Insights from Pelagic Habitats Acquired Using Active Acoustic Techniques. *Annual Review of Marine Science*, 8(1):463–490.

Benoit-Bird, K. J. and Moline, M. A. (2021). Vertical migration timing illuminates the importance of visual and nonvisual predation pressure in the mesopelagic zone. *Limnology and Oceanography*, 66(8):3010–3019.

Benoit-Bird, K. J., Moline, M. A., Schofield, O. M., Robbins, I. C., and Waluk, C. M. (2010). Zooplankton avoidance of a profiled open-path fluorometer. *Journal of Plankton Research*, 32(10):1413–1419.

Benoit-Bird, K. J., Moline, M. A., and Southall, B. L. (2017). Prey in oceanic sound scattering layers organize to get a little help from their friends. *Limnology and Oceanography*, 62(6):2788–2798.

Benoit-Bird, K. J., Patrick Welch, T., Waluk, C. M., Barth, J. A., Wangen, I., McGill, P., Okuda, C., Hollinger, G. A., Sato, M., and McCammon, S. (2018). Equipping an underwater glider with a new echosounder to explore ocean ecosystems. *Limnology and Oceanography: Methods*, 16(11):734–749.

Benoit-Bird, K. J., Southall, B. L., and Moline, M. A. (2016). Predator-guided sampling reveals biotic structure in the bathypelagic. *Proceedings of the Royal Society B: Biological Sciences*, 283(1825):20152457.

Benoit-Bird, K. J. and Waluk, C. M. (2020). Exploring the promise of broadband fisheries echosounders for species discrimination with quantitative assessment of data processing effects. *The Journal of the Acoustical Society of America*, 147(1):411–427.

Benoit-Bird, K. J. and Waluk, C. M. (2021). Remote acoustic detection and characterization of fish schooling behavior. *The Journal of the Acoustical Society of America*, 150(6):4329–4342.

Berge, J., Cottier, F., Varpe, Ø., Renaud, P. E., Falk-Petersen, S., Kwasniewski, S., Griffiths, C., SØreide, J. E., Johnsen, G., Aubert, A., Bjærke, O., Hovinen, J., Jung-Madsen, S., Tveit, M., and Majaneva, S. (2014). Arctic complexity: A case study on diel vertical migration of zooplankton. *Journal of Plankton Research*, 36(5):1279–1297.

Berge, J., Geoffroy, M., Daase, M., Cottier, F., Priou, P., Cohen, J. H., Johnsen, G., McKee, D., Kostakis, I., Renaud, P. E., Vogedes, D., Anderson, P., Last, K. S., and Gauthier, S. (2020). Artificial light during the polar night disrupts Arctic fish and zooplankton behaviour down to 200 m depth. *Communications Biology*, 3(1):102.

Bertrand, A., Barbieri, M. A., Gerlotto, F., Leiva, F., and Córdova, J. (2006). Determinism and plasticity of fish schooling behaviour as exemplified by the South Pacific jack mackerel Trachurus murphyi. *Marine Ecology Progress Series*, 311:145–156.

Bez, N. and Rivoirard, J. (2001). Transitive geostatistics to characterise spatial aggregations with diffuse limits: An application on mackerel ichtyoplankton. *Fisheries Research*, 50(1-2):41–58.

Bianchi, D., Galbraith, E. D., Carozza, D. A., Mislan, K. A., and Stock, C. A. (2013a). Intensification of open-ocean oxygen depletion by vertically migrating animals. *Nature Geoscience*, 6(7):545–548.

Bianchi, D. and Mislan, K. A. S. (2016). Global patterns of diel vertical migration times and velocities from acoustic data. *Limnology and Oceanography*, 61(1):353–364.

Bianchi, D., Stock, C., Galbraith, E. D., and Sarmiento, J. L. (2013b). Diel vertical migration: Ecological controls and impacts on the biological pump in a one-dimensional ocean model. *Global Biogeochemical Cycles*, 27(2):478–491.

Billings, A., Kaiser, C., Young, C. M., Hiebert, L. S., Cole, E., Wagner, J. K., and Van Dover, C. L. (2017). SyPRID sampler: A large-volume, high-resolution, autonomous, deep-ocean precision plankton sampling system. *Deep Sea Research Part II: Topical Studies in Oceanography*, 137:297–306.

Binetti, U., Kaiser, J., Damerell, G., Rumyantseva, A., Martin, A., Henson, S., and Heywood, K. (2020). Net community oxygen production derived from Seaglider deployments at the Porcupine Abyssal Plain site (PAP; northeast Atlantic) in 2012–13. *Progress in Oceanography*, 183.

Bingham, B., Kraus, N., Howe, B., Freitag, L., Ball, K., Koski, P., and Gallimore, E. (2012). Passive and Active Acoustics Using an Autonomous Wave Glider. *Journal of Field Robotics*, 29(6):911–923.

Blackwell, R., Harvey, R., Queste, B., and Fielding, S. (2019a). Aliased seabed detection in fisheries acoustic data. *arXiv preprint*. http://arxiv.org/abs/1904.10736.

Blackwell, R. E. (2020). *Real-time reporting of marine ecosystem metrics from active acoustic sensors*. Doctoral dissertation, University of East Anglia.

Blackwell, R. E., Harvey, R., Queste, B. Y., and Fielding, S. (2019b). Colour maps for fisheries acoustic echograms. *ICES Journal of Marine Science*, 1:1–9.

Blanluet, A., Doray, M., Berger, L., Romagnan, J. B., Le Bouffant, N., Lehuta, S., and Petitgas, P. (2019). Characterization of sound scattering layers in the Bay of Biscay using broadband acoustics, nets and video. *PloS one*, 14(10):e0223618.

Blaxter, J. H., Denton, E. J., and Gray, J. A. (1981). The auditory bullae-swimbladder system in late stage herring larvae. *Journal of the Marine Biological Association of the United Kingdom*, 61(2):315–326.

Blaxter, J. H. S. and Batty, R. S. (1990). Swimbladder "behaviour" and target strength. *Rapp. P.-v. Réun. Cons. int. Explor. Mer*, 189:233–244.

Bollens, S. M. and Frost, B. W. (1991). Diel vertical migration in zooplankton: Rapid individual response to predators. *Journal of Plankton Research*, 13(6):1359–1365.

Bos, R. P., Sutton, T. T., and Frank, T. M. (2021). State of Satiation Partially Regulates the Dynamics of Vertical Migration. *Frontiers in Marine Science*, 8.

Boswell, K. M., D'Elia, M., Johnston, M. W., Mohan, J. A., Warren, J. D., Wells, R. J. D., and Sutton, T. T. (2020). Oceanographic Structure and Light Levels Drive Patterns of Sound Scattering Layers in a Low-Latitude Oceanic System. *Frontiers in Marine Science*, 7(51):1–15.

Boyd, P. W., Claustre, H., Levy, M., Siegel, D. A., and Weber, T. (2019). Multi-faceted particle pumps drive carbon sequestration in the ocean. *Nature*, 568(7752):327–335.

Brautaset, O., Waldeland, A. U., Johnsen, E., Malde, K., Eikvil, L., Salberg, A. B., and Handegard, N. O. (2020). Acoustic classification in multifrequency echosounder data using deep convolutional neural networks. *ICES Journal of Marine Science*, 77(4):1391–1400.

Breitburg, D., Levin, L. A., Oschlies, A., Grégoire, M., Chavez, F. P., Conley, D. J., Garçon, V., Gilbert, D., Gutiérrez, D., Isensee, K., Jacinto, G. S., Limburg, K. E., Montes, I., Naqvi, S. W. A., Pitcher, G. C., Rabalais, N. N., Roman, M. R., Rose, K. A., Seibel, B. A., Telszewski, M., Yasuhara, M., and Zhang, J. (2018). Declining oxygen in the global ocean and coastal waters. *Science*, 359(46):1–11.

Brekhovskikh, L. M. and Lysanov, Y. (2003). *Fundamentals of Ocean Acoustics*. Modern Acoustics and Signal Processing. Springer-Verlag, New York.

Brierley, A. S. and Fernandes, P. G. (2001). Diving depths of northern gannets: acoustic observations of Sula bassana from an autonomous underwater vehicle. *The Auk*, 118(April):529–534.

Brierley, A. S., Fernandes, P. G., Brandon, M. A., Armstrong, F., Millard, N. W., McPhail, S. D., Stevenson, P., Pebody, M., Perrett, J., Squires, M., Bone, D. G., and Griffiths, G. (2002). Antarctic krill under sea ice: Elevated abundance in a narrow band just south of ice edge. *Science*, 295(5561):1890–1892.

Brierley, A. S., Fernandes, P. G., Brandon, M. A., Armstrong, F., Millard, N. W., McPhail, S. D., Stevenson, P., Pebody, M., Perrett, J., Squires, M., Bone, D. G., and Griffiths, G. (2003). An investigation of avoidance by Antarctic krill of RRS James Clark Ross using the Autosub-2 autonomous underwater vehicle. *Fisheries Research*, 60(2-3):569–576.

Bromley, P. (1997). Diel feeding patterns and the development of food webs in pelagic 0-group cod (Gadus morhuaL.), haddock (Melanogrammus aeglefinusL.), whiting (MerlangiusmerlangusL.), saithe (Pollachius virensL.), and Norway pout (Trisopterus esmarkiiNilsson) in the north. *ICES Journal of Marine Science*, 54(5):846–853.

Buades, A., Coll, B., and Morel, J.-M. (2011). Non-Local Means Denoising. *Image Processing On Line*, 1:208–212.

Burchard, H., Bolding, K., Rippeth, T. P., Stips, A., Simpson, J. H., and Sündermann, J. (2002). Microstructure of turbulence in the northern North Sea: A comparative study of observations and model simulations. *Journal of Sea Research*, 47(3-4):223–238.

Burgos, J. M., Horne Burgos, J. K., Burgos, J. M., and Horne, J. K. (2008). Characterization and classification of acoustically detected fish spatial distributions. *ICES Journal of Marine Science*, 65(7):1235–1247.

Burt, W. J. and Tortell, P. D. (2018). Observations of Zooplankton Diel Vertical Migration From High-Resolution Surface Ocean Optical Measurements. *Geophysical Research Letters*, 45(24):13,396–13,404.

Cade, D. E. and Benoit-Bird, K. J. (2015). Depths, migration rates and environmental associations of acoustic scattering layers in the Gulf of California. *Deep-Sea Research Part I: Oceanographic Research Papers*, 102:78–89.

Campanella, F. and Taylor, J. C. (2016). Investigating acoustic diversity of fish aggregations

in coral reef ecosystems from multifrequency fishery sonar surveys. *Fisheries Research*, 181:63–76.

Camus, L., Andrade, H., Aniceto, A. S., Aune, M., Bandara, K., Linn, S., Christensen, K. H., Cook, J., Daase, M., Dunlop, K., Falk-petersen, S., Fietzek, P., Fonnes, G., Ghaffari, P., Gramvik, G., Graves, I., Pederick, J., Pedersen, G., Sperrevik, A. K., Sørensen, K., Tassara, L., and Tjøstheim, S. (2021). Ecosystem Monitoring and Research Platforms in the Arctic — The Glider Project †. *Sensors*, 21:6752.

Capuzzo, E., Lynam, C. P., Barry, J., Stephens, D., Forster, R. M., Greenwood, N., McQuatters-Gollop, A., Silva, T., van Leeuwen, S. M., and Engelhard, G. H. (2018). A decline in primary production in the North Sea over 25 years, associated with reductions in zooplankton abundance and fish stock recruitment. *Global Change Biology*, 24(1):e352–e364.

Capuzzo, E., Painting, S. J., Forster, R. M., Greenwood, N., Stephens, D. T., and Mikkelsen, O. A. (2013). Variability in the sub-surface light climate at ecohydrodynamically distinct sites in the North Sea. *Biogeochemistry*, 113(1-3):85–103.

Capuzzo, E., Stephens, D., Silva, T., Barry, J., and Forster, R. M. (2015). Decrease in water clarity of the southern and central North Sea during the 20th century. *Global Change Biology*, 21(6):2206–2214.

Cardinale, M., Casini, M., Arrhenius, F., and Håkansson, N. (2003). Diel spatial distribution and feeding activity of herring (Clupea harengus) and sprat (Sprattus sprattus) in the Baltic Sea. In *Aquatic Living Resources*, volume 16, pages 283–292.

Carré, D. (1969). Étude Histologique du développement de Nanomia bijuga (Chiaje, 1841), siphonophore physonecte, Agalmidae. *Cahiers de Biologie Marine*, 10:325–341.

Centurioni, L. R., Turton, J. D., Lumpkin, R., Braasch, L., Brassington, G., Chao, Y., Charpentier, E., Chen, Z., Corlett, G., Dohan, K., Donlon, C., Gallage, C., Hormann, V., Ignatov, A., Ingleby, B., Jensen, R., Kelly-Gerreyn, B. A., Koszalka, I. M., Lin, X., Lindstrom, E., Maximenko, N., Merchant, C. J., Minnett, P., O'Carroll, A. G., Paluszkiewicz, T., Poli, P., Poulain, P., Reverdin, G., Sun, X., Swail, V., Thurston, S.,

Wu, L., Yu, L., Wang, B., and Zhang, D. (2019). Global in-situ observations of essential climate and ocean variables at the air-sea interface. *Frontiers in Marine Science*, 6(JUL).

Cerbin, S., Balayla, D. J., and Van De Bund, W. J. (2003). Small-scale distribution and diel vertical migration of zooplankton in a shallow lake (lake Naardermeer, the Netherlands). *Hydrobiologia*, 491(1994):111–117.

Cervino, N. P. and Douglas, A. M. (2017). Wave glider system for real-time range tracking. *Johns Hopkins APL Technical Digest (Applied Physics Laboratory)*, 33(4):250–255.

Chave, R., Buermans, J., Lemon, D., Taylor, J. C., Lembke, C., DeCollibus, C., Saba, G. K., and Reiss, C. S. (2018). Adapting Multi-Frequency Echo-sounders for Operation on Autonomous Vehicles. In *OCEANS 2018 MTS/IEEE Charleston*, pages 1–6. IEEE.

Chen, B., Masunaga, E., Smith, S. L., and Yamazaki, H. (2021). Diel vertical migration promotes zooplankton horizontal patchiness. *Journal of Oceanography*, 77(1):123–135.

Chen, X., Dangendorf, S., Narayan, N., O'Driscoll, K., Tsimplis, M. N., Su, J., Mayer, B., and Pohlmann, T. (2014). On sea level change in the North Sea influenced by the North Atlantic Oscillation: Local and remote steric effects. *Estuarine, Coastal and Shelf Science*, 151:186–195.

Cheriton, O. M., McManus, M. A., Holliday, D. V., Greenlaw, C. F., Donaghay, P. L., and Cowles, T. J. (2007). Effects of mesoscale physical processes on thin zooplankton layers at four sites along the west coast of the U.S. *Estuaries and Coasts*, 30(4):575–590.

Chu, D., Ostrovsky, I., and Homma, H. (2021). Acoustic scattering by gas-bearing cyanobacterium Microcystis: Modeling and in situ biomass assessment. *Science of The Total Environment*, 794:148573.

Chu, D., Parker-Stetter, S., Hufnagle, L. C., Thomas, R., Getsiv-Clemons, J., Gauthier, S., and Stanley, C. (2019). 2018 unmanned surface vehicle (saildrone) acoustic survey off the west coasts of the united states and canada. In *OCEANS 2019 MTS/IEEE SEATTLE*, pages 1–7. IEEE.

Coetzee, J. (2000). Use of a shoal analysis and patch estimation system (SHAPES) to characterise sardine schools. *Aquatic Living Resources*, 13(1):1–10.

Cohen, J. H., Berge, J., Moline, M. A., Sørensen, A. J., Last, K., Falk-Petersen, S., Renaud, P. E., Leu, E. S., Grenvald, J., Cottier, F., Cronin, H., Menze, S., Norgren, P., Varpe, Ø., Daase, M., Darnis, G., and Johnsen, G. (2015). Is ambient light during the high Arctic polar night sufficient to act as a visual cue for zooplankton? *PLoS ONE*, 10(6):1–12.

Cohen, J. H. and Forward, R. B. (2005a). Diel vertical migration of the marine copepod Calanopia americana. I. Twilight DVM and its relationship to the diel light cycle. *Marine Biology*, 147(2):387–398.

Cohen, J. H. and Forward, R. B. (2005b). Diel vertical migration of the marine copepod Calanopia americana. II. Proximate role of exogenous light cues and endogenous rhythms. *Marine Biology*, 147(2):399–410.

Colebrook, J. M. (1966). Continuous plankton records: seasonal cycles of phytoplankton and copepods in the northeastern North Atlantic and the North Sea. *Deep Sea Research and Oceanographic Abstracts*, 13(4):772.

Colebrook, J. M. (1985). Sea surface temperature and zooplankton, North Sea, 1948 to 1983. *ICES Journal of Marine Science*, 42(2):179–185.

Conroy, J. A., Steinberg, D. K., Thibodeau, P. S., and Schofield, O. (2020). Zooplankton diel vertical migration during Antarctic summer. *Deep-Sea Research Part I: Oceanographic Research Papers*, 162(June):103324.

Conway, D. V. P. (2012). Marine Zooplankton of Southern Britain - Part 1: Radiolaria, Heliozoa, Foraminifera, Ciliophora, Cnidaria, Ctenophora, Platyhelminthes, Nemertea, Rotifera and Mollusca. Occasional publication of the Marine Biological Association 25.

Corten, A. (1990). Long-term trends in pelagic fish stocks of the North Sea and adjacent waters and their possible connection to hydrographic changes. *Netherlands Journal of Sea Research*, 25(1-2):227–235.

Cottier, F. R., Tarling, G. A., Wold, A., and Falk-Petersen, S. (2006). Unsynchronized and synchronized vertical migration of zooplankton in a high arctic fjord. *Limnology and Oceanography*, 51(6):2586–2599.

Cowles, T. J., Desiderio, R. A., and Carr, M. E. (1998). Small-scale planktonic structure: persistence and trophic consequences. *Oceanography*, 11(1):4–9.

Crawford, G. B. and Farmer, D. M. (1987). On The Spatial Distribution of Ocean Bubbles. *Journal of Geophysical Research*, 92(8):8231–8243.

Cronin, T. W. and Marshall, J. (2011). Patterns and properties of polarized light in air and water. *Philosophical Transactions of the Royal Society B: Biological Sciences*, 366(1565):619–626.

Cronin, T. W. and Shashar, N. (2001). The linearly polarized light field in clear, tropical marine waters: Spatial and temporal variation of light intensity, degree of polarization and e-vector angle. *Journal of Experimental Biology*, 204(14):2461–2467.

Cury, P. M., Boyd, I. L., Bonhommeau, S., Anker-Nilssen, T., Crawford, R. J. M., Furness, R. W., Mills, J. A., Murphy, E. J., Österblom, H., Paleczny, M., Piatt, J. F., Roux, J.-P., Shannon, L., and Sydeman, W. J. (2011). Global Seabird Response to Forage Fish Depletion—One-Third for the Birds. *Science*, 334(6063):1703–1706.

Daase, M., Hop, H., and Falk-Petersen, S. (2016). Small-scale diel vertical migration of zooplankton in the High Arctic. *Polar Biology*, 39(7):1213–1223.

Dahl, P. H. (2003). The contribution of bubbles to high-frequency sea surface backscatter: A 24-h time series of field measurements. *The Journal of the Acoustical Society of America*, 113(2):769–780.

Dahl, P. H. and Jessup, A. T. (1995). On bubble clouds produced by breaking waves: an event analysis of ocean acoustic measurements. *Journal of Geophysical Research*, 100(C3):5007–5020.

Dahlgren, C. P. and Eggleston, D. B. (2000). Ecological processes underlying ontogenetic habitat shifts in a coral reef fish. *Ecology*, 81(8):2227–2240.

Dale, T. and Kaartvedt, S. (2000). Diel patterns in stage-specific vertical migration of Calanus finmarchicus in habitats with midnight sun. *ICES Journal of Marine Science*, 57(6):1800–1818.

Dalen, J. and Løvik, A. (1981). The influence of wind-induced bubbles on echo integration surveys. *Journal of the Acoustical Society of America*, 69(6):1653–1659.

Daniel, T., Manley, J., and Trenaman, N. (2011). The Wave Glider: Enabling a new approach to persistent ocean observation and research. *Ocean Dynamics*, 61(10):1509–1520.

Darnis, G., Hobbs, L., Geoffroy, M., Grenvald, J. C., Renaud, P. E., Berge, J., Cottier, F., Kristiansen, S., Daase, M., E. Søreide, J., Wold, A., Morata, N., and Gabrielsen, T. (2017). From polar night to midnight sun: Diel vertical migration, metabolism and biogeochemical role of zooplankton in a high Arctic fjord (Kongsfjorden, Svalbard). *Limnology and Oceanography*, 62(4):1586–1605.

De Robertis, A. and Handegard, N. (2013). Fish avoidance of research vessels and the efficacy of noise-reduced vessels: a review. *ICES Journal of Marine Science*, 70(1):34–45.

De Robertis, A. and Higginbottom, I. (2007). A post-processing technique to estimate the signal-to-noise ratio and remove echosounder background noise. *ICES Journal of Marine Science*, 64(6):1282–1291.

De Robertis, A., Hjellvik, V., Williamson, N. J., and Wilson, C. D. (2008). Silent ships do not always encounter more fish: comparison of acoustic backscatter recorded by a noise-reduced and a conventional research vessel. *ICES Journal of Marine Science*, 65:623–635.

De Robertis, A., Jaffe, J., and Ohman, M. (2000). Size-dependent visual predation risk and the timing of vertical migration: An optimization model. *Limnology and Oceanography*, 45(8):1838–1844.

De Robertis, A., Lawrence-Slavas, N., Jenkins, R., Wangen, I., Mordy, C. W., Meinig, C., Levine, M., Peacock, D., and Tabisola, H. (2019). Long-term measurements of fish backscatter from Saildrone unmanned surface vehicles and comparison with observations from a noise-reduced research vessel. *ICES Journal of Marine Science*, 76(7):2459–2470.

De Robertis, A., Levine, M., Lauffenburger, N., Honkalehto, T., Ianelli, J., Monnahan, C. C., Towler, R., Jones, D., Stienessen, S., and McKelvey, D. (2021). Uncrewed surface vehicle

(USV) survey of walleye pollock, Gadus chalcogrammus, in response to the cancellation of ship-based surveys. *ICES Journal of Marine Science*, 78(8):2797–2808.

Deblois, E. M. and Rose, G. A. (1996). Cross-shoal variability in the feeding habits of migrating Atlantic cod ( Gadus morhua). *Oecologia*, 108:192–196.

Defriez, E. J., Sheppard, L. W., Reid, P. C., and Reuman, D. C. (2016). Climate change-related regime shifts have altered spatial synchrony of plankton dynamics in the North Sea. *Global Change Biology*, 22(6):2069–2080.

Dekshenieks, M. M., Donaghay, P. L., Sullivan, J. M., Rines, J. E., Osborn, T. R., and Twardowski, M. S. (2001). Temporal and spatial occurrence of thin phytoplankton layers in relation to physical processes. *Marine Ecology Progress Series*, 223:61–71.

Delacroix, S., Germain, G., Berger, L., and Billard, J. Y. (2016). Bubble sweep-down occurrence characterization on Research Vessels. *Ocean Engineering*, 111(January):34–42.

D'Elia, M., Patti, B., Bonanno, A., Fontana, I., Giacalone, G., Basilone, G., and Fernandes, P. G. (2014). Analysis of backscatter properties and application of classification procedures for the identification of small pelagic fish species in the Central Mediterranean. *Fisheries Research*, 149:33–42.

Demer, D. A., Berger, L., Bernasconi, M., Bethke, E., Boswell, K. M., Chu, D., Domokos, R., Dunford, A., Fassler, S., Gauthier, S., Hufnagle, L. T., Jech, J. M., Bouffant, N., Lebourges-Dhaussy, A., Lurton, X., Macaulay, G. J., Perrot, Y., Ryan, T., Parker-Stetter, S., Stienessen, S., Weber, T., and Williamson, N. (2015). Calibration of acoustic instruments. Technical Report 32.

Den Hartog, J. C. and Van Nierop, M. M. (1984). A study on the Gut contents of six Leathery Turtles Dermochelys Coriacea (Linnaeus) (Reptilia: Testudines: Dermochelyidae) from British waters and from the Netherlands. *Zoologische Verhandelingen*, 209(1):1–36.

Denis, V., Lejeune, J., and Robin, J. P. (2002). Spatio-temporal analysis of commercial trawler data using General Additive models: Patterns of Loliginid squid abundance in the north-east Atlantic. *ICES Journal of Marine Science*, 59(3):633–648.

Denman, K. L., Dower, J. F., and He, X. (2001). Patch dynamics. *Encyclopedia of Ocean Sciences*, 4:2107–2114.

Dilling, L. and Alldredge, A. L. (2000). Fragmentation of marine snow by swimming macrozooplankton: A new process impacting carbon cycling in the sea. *Deep-Sea Research Part I: Oceanographic Research Papers*, 47(7):1227–1245.

Dippner, J. W. and Krause, M. (2013). Continuous plankton recorder underestimates zooplankton abundance. *Journal of Marine Systems*, 111-112:263–268.

Domenici, P., Lefrançois, C., and Shingles, A. (2007). Hypoxia and the antipredator behaviours of fishes. *Philosophical Transactions of the Royal Society B: Biological Sciences*, 362(1487):2105–2121.

Doray, M., Petitgas, P., Romagnan, J. B., Huret, M., Duhamel, E., Dupuy, C., Spitz, J., Authier, M., Sanchez, F., Berger, L., Dorémus, G., Bourriau, P., Grellier, P., and Massé, J. (2018). The PELGAS survey: Ship-based integrated monitoring of the Bay of Biscay pelagic ecosystem. *Progress in Oceanography*, 166:15–29.

Dornan, T. (2019). *Southern Ocean mesopelagic fish Scales, drivers and the effects of environmental variability*. PhD thesis, University of Bristol.

Ducrotoy, J. P., Elliott, M., and de Jonge, V. N. (2000). The north sea. *Marine pollution bulletin,*, 41(1-6):5–23.

Dunford, A. J. (2005). Correcting echo-integration data for transducer motion. *The Journal of the Acoustical Society of America*, 118(4):2121–2123.

Dunlop, K. M., Jarvis, T., Benoit-Bird, K. J., Waluk, C. M., Caress, D. W., Thomas, H., and Smith, K. L. (2018). Detection and characterisation of deep-sea benthopelagic animals from an autonomous underwater vehicle with a multibeam echosounder: A proof of concept and description of data-processing methods. *Deep Sea Research Part I: Oceanographic Research Papers*, 134:64–79.

Durbin, A. G., Durbin, E. G., and Wlodarczyk, E. (1990). Diel feeding behavior in the marine copepod Acartia tonsa in relation to food availability. *Marine Ecology Progress Series*, 68(1-2):23–45.

Dutta, J., Leahy, R. M., and Li, Q. (2013). Non-Local Means Denoising of Dynamic PET Images. *PLoS ONE*, 8(12):e81390.

Dypvik, E., Røstad, A., and Kaartvedt, S. (2012). Seasonal variations in vertical migration of glacier lanternfish, Benthosema glaciale. *Marine Biology*, 159(8):1673–1683.

Easson, C. G., Boswell, K. M., Tucker, N., Warren, J. D., and Lopez, J. V. (2020). Combined eDNA and Acoustic Analysis Reflects Diel Vertical Migration of Mixed Consortia in the Gulf of Mexico. *Frontiers in Marine Science*, 7(July):1–13.

Echoview Software Pty Ltd (2021). Echoview software. Echoview Software Pty Ltd, Hobart, Australia.

Edwards, M., Beaugrand, G., Hays, G. C., Koslow, J. A., and Richardson, A. J. (2010). Multi-decadal oceanic ecological datasets and their application in marine policy and management. *Trends in Ecology and Evolution*, 25(10):602–610.

Edwards, M., Beaugrand, G., Reid, P., Rowden, A., and Jones, M. (2002). Ocean climate anomalies and the ecology of the North Sea. *Marine Ecology Progress Series*, 239:1–10.

Edwards, M., John, A. W., Hunt, H. G., and Lindley, J. A. (1999). Exceptional influx of oceanic species into the North Sea late 1997. *Journal of the Marine Biological Association of the United Kingdom*, 79(4):737–739.

Edwards, M., Reid, P., and Planque, B. (2001). Long-term and regional variability of phytoplankton biomass in the Northeast Atlantic (1960-1995). *ICES Journal of Marine Science*, 58(1):39–49.

Edwards, M. and Richardson, A. J. (2004). Impact of climate change on marine pelagic phenology and trophic mismatch. *Nature*, 430(7002):881–884.

Ekau, W., Auel, H., Portner, H. O., and Gilbert, D. (2010). Impacts of hypoxia on the structure and processes in pelagic communities (zooplankton, macro-invertebrates and fish). *Biogeosciences*, 7(5):1669–1699.

Emeis, K.-C., van Beusekom, J., Callies, U., Ebinghaus, R., Kannen, A., Kraus, G., Kröncke, I., Lenhart, H., Lorkowski, I., Matthias, V., Möllmann, C., Pätsch, J., Scharfe, M., Thomas,

H., Weisse, R., and Zorita, E. (2015). The North Sea — A shelf sea in the Anthropocene. *Journal of Marine Systems*, 141:18–33.

Engelhard, G. H., Peck, M. A., Rindorf, A., C. Smout, S., van Deurs, M., Raab, K., Andersen, K. H., Garthe, S., Lauerburg, R. A., Scott, F., Brunel, T., Aarts, G., van Kooten, T., and Dickey-Collas, M. (2014). Forage fish, their fisheries, and their predators: who drives whom? *ICES Journal of Marine Science*, 71(1):90–104.

Enright, J. T. (1977). Diurnal vertical migration: Adaptive significance and timing. Part 1. Selective advantage: A metabolic model1. *Limnology and Oceanography*, 22(5):856–872.

Escribano, R., Hidalgo, P., and Krautz, C. (2009). Zooplankton associated with the oxygen minimum zone system in the northern upwelling region of Chile during March 2000. *Deep-Sea Research Part II: Topical Studies in Oceanography*, 56(16):1083–1094.

EU (2008). Directive 2008/56/EC of the European Parliament and of the Council. *Official Journal of the European Union*.

Evans, L. E., Hirst, A. G., Kratina, P., and Beaugrand, G. (2020). Temperature-mediated changes in zooplankton body size: large scale temporal and spatial analysis. *Ecography*, 43(4):581–590.

Fässler, S. M., Fernandes, P. G., Semple, S. I., and Brierley, A. S. (2009). Depth-dependent swimbladder compression in herring Clupea harengus observed using magnetic resonance imaging. *Journal of Fish Biology*, 74(1):296–303.

Fässler, S. M., Santos, R., García-Núñez, N., and Fernandes, P. G. (2007). Multifrequency backscattering properties of Atlantic herring (Clupea harengus) and Norway pout (Trisopterus esmarkii). *Canadian Journal of Fisheries and Aquatic Sciences*, 64(2):362–374.

Fässler, S. M. M., Teal, L. R., Lusseau, S. M., and Ruardij, P. (2012). Determining herring habitat quality from acoustically derived zooplankton abundance in the northern North Sea. *ICES CM*.

Fernand, L., Weston, K., Morris, T., Greenwood, N., Brown, J., and Jickells, T. (2013).

The contribution of the deep chlorophyll maximum to primary production in a seasonally stratified shelf sea, the North Sea. *Biogeochemistry*, 113(1-3):153–166.

Fernandes, P., Macdonald, L., Aukland, R., Reid, D., Simmonds, E. J., and Shanks, A. (2001). Changes in the availability of herring to the North Sea acoustic survey; the impact of diurnal migration. *ICES CM*.

Fernandes, P. G. (2009). Classification trees for species identification of fish-school echotraces. In *ICES Journal of Marine Science*, volume 66, pages 1073–1080. Oxford Academic.

Fernandes, P. G., Brierley, A. S., Simmonds, E. J., Millard, N. W., Mcphail, S. D., Armstrong, F., Stevenson, P., and Squires, M. (2000). Fish do not avoid survey vessels. *Nature*, 404(6773):35–36.

Fernandes, P. G., Gerlotto, F., Holliday, D. V., Nakken, O., and Simmonds, E. J. (2002). Acoustic applications in fisheries science: the ICES contribution. *ICES Marine Science Symposia*, 215:483–492.

Fernandes, P. G., Stevenson, P., Brierley, A. S., Armstrong, F., and Simmonds, E. J. (2003). Autonomous underwater vehicles: Future platforms for fisheries acoustics. In *ICES Journal of Marine Science*, volume 60, pages 684–691.

Ferreira, A. S. d. A., Stenevik, E. K., Vollset, K. W., Korneliussen, R., and Folkvord, A. (2012). Vertical migration of Norwegian spring-spawning herring larvae in relation to predator and prey distribution. *Marine Biology Research*, 8(7):605–614.

Fielding, S., Griffiths, G., and Roe, H. S. (2004). The biological validation of ADCP acoustic backscatter through direct comparison with net samples and model predictions based on acoustic-scattering models. *ICES Journal of Marine Science*, 61(2):184–200.

Fielding, S., Watkins, J. L., Collins, M. A., Enderlein, P., and Venables, H. J. (2012). Acoustic determination of the distribution of fish and krill across the Scotia Sea in spring 2006, summer 2008 and autumn 2009. *Deep Sea Research Part II: Topical Studies in Oceanography*, 59-60:173–188.

Fincham, J. I., Rijnsdorp, A. D., and Engelhard, G. H. (2013). Shifts in the timing of spawning in sole linked to warming sea temperatures. *Journal of Sea Research*, 75:69–76.

Fischer, J. M., Olson, M. H., Theodore, N., Williamson, C. E., Rose, K. C., and Hwang, J. (2015). Diel vertical migration of copepods in mountain lakes: The changing role of ultraviolet radiation across a transparency gradient. *Limnology and Oceanography*, 60(1):252–262.

Folkvord, A., Lakso, E., Laupsa, M., Meier, S., Musialak, L. A., and Sundby, S. (2020). Swimbladder filling in herring larvae: effects of food oil on the water surface. *Marine Biology Research*, 16(6-7):446–457.

Folt, C. L. and Burns, C. (1999). Biological drivers of zooplancton patchiness. *Trends in Ecology and Evolution*, 14(8):300–305.

Foote, K., Knudsen, H., Vestnes, G., MacLennan, D., and Simmonds, E. (1987). Technical Report: "Calibration of acoustic instruments for fish density estimation: A practical guide". *ICES Cooperative Research Reports (CRR)*, 83(2):831–832.

Foote, K. G. (1980). Importance of the swimbladder in acoustic scattering by fish: A comparison of gadoid and mackerel target strengths. *Journal of the Acoustical Society of America*, 67(6):2084–2089.

Foote, K. G. (1981). Absorption term in time-varied gain functions. Technical report.

Foote, K. G. (1983). Linearity of fisheries acoustics, with addition theorems. *The Journal of the Acoustical Society of America*, 73(6):1932.

Foote, K. G. (1990). Correcting acoustic measurements of scatterer density for extinction. *The Journal of the Acoustical Society of America*, 88(3):1543–1546.

Foote, K. G., Ona, E., and Toresen, R. (1992). Determining the extinction cross section of aggregating fish. *The Journal of the Acoustical Society of America*, 91(4):1983–1989.

Francis, T. B., Scheuerell, M. D., Brodeur, R. D., Levin, P. S., Ruzicka, J. J., Tolimieri, N., and Peterson, W. T. (2012). Climate shifts the interaction web of a marine plankton community. *Global Change Biology*, 18(8):2498–2508.

Francois, R. E. and Garrison, G. R. (1982). Sound absorption based on ocean measurements. Part II: Boric acid contribution and equation for total absorption. *The Journal of the Acoustical Society of America*, 72(6):879–1890.

Franks, P. J. (1992). Sink or swim: Accumulation of biomass at fronts. *Marine Ecology Progress Series*, 82:1–12.

Fransz, H. G., Colebrook, J. M., Gamble, J. C., and Krause, M. (1991). The zooplankton of the north sea. *Netherlands Journal of Sea Research*, 28(1-2):1–52.

Fréon, P., Gerlotto, F., and Soria, M. (1996). Diel variability of school structure with special reference to transition periods. *ICES Journal of Marine Science*, 53(2):459–464.

Frid, C. L., Newton, L. C., and Williams, J. A. (1994). The feeding rates of Pleurobrachia (ctenophora) and Sagitta (chaetognatha), with notes on the potential seasonal role of planktonic predators in the dynamics of north sea zooplankton communities. *Netherlands Journal of Aquatic Ecology*, 28(2):181–191.

Frost, J. R., Denda, A., Fox, C. J., Jacoby, C. A., Koppelmann, R., Nielsen, M. H., and Youngbluth, M. J. (2012). Distribution and trophic links of gelatinous zooplankton on Dogger Bank, North Sea. *Marine Biology*, 159(2):239–253.

Furusawa, M. and Sawada, K. (1991). Effects of Transducer Motion on Quantifying Single Fish Echoes. *Nippon Suisan Gakkaishi (Japanese Edition)*, 57(5):857–864.

Galgani, F., Hervé, G., and Carlon, R. (2003). Wavegliding for marine litter. *Comm. int. Mer Médit*, 46(2):1142–1149.

Gama, J. (2016). *sonar: Fundamental Formulas for Sonar*. R package version 1.0.2.

Gambill, M., McNaughton, S. L., Kreus, M., and Peck, M. A. (2018). Temperature-dependent settlement of planula larvae of two scyphozoan jellyfish from the North Sea. *Estuarine, Coastal and Shelf Science*, 201:64–71.

Ganias, K., Michou, S., and Nunes, C. (2015). A field based study of swimbladder adjustment in a physostomous teleost fish. *PeerJ*, 3(4):e892.

Garlapati, D., Charankumar, B., Ramu, K., Madeswaran, P., and Ramana Murthy, M. V. (2019). A review on the applications and recent advances in environmental DNA (eDNA) metagenomics. *Reviews in Environmental Science and Bio/Technology*, 18(3):389–411.

Gastauer, S., Nickels, C. F., and Ohman, M. D. (2022). Body size- and season-dependent diel vertical migration of mesozooplankton resolved acoustically in the San Diego Trough. *Limnology and Oceanography*, 67(2):300–313.

Gastauer, S., Scoulding, B., and Parsons, M. (2017). An Unsupervised Acoustic Description of Fish Schools and the Seabed in Three Fishing Regions Within the Northern Demersal Scalefish Fishery (NDSF, Western Australia). *Acoustics Australia*, 45(2):363–380.

General Bathymetric Chart of the Oceans (2014). The GEBCO 2014 Grid. http://www.gebco.net.

Genin, A. (2004). Bio-physical coupling in the formation of zooplankton and fish aggregations over abrupt topographies. *Journal of Marine Systems*, 50(1-2):3–20.

Genin, A., Greene, C., Haury, L., Wiebe, P., Gal, G., Kaartvedt, S., Meir, E., Fey, C., and Dawson, J. (1994). Zooplankton patch dynamics: daily gap formation over abrupt topography. *Deep-Sea Research Part I*, 41(5-6):941–951.

Geoffroy, M., Cottier, F. R., Berge, J., and Inall, M. E. (2017). AUV-based acoustic observations of the distribution and patchiness of pelagic scattering layers during midnight sun†. *ICES Journal of Marine Science*, 74(9):2342–2353.

Gilbert, O. M. and Buskey, E. J. (2005). Turbulence decreases the hydrodynamic predator sensing ability of the calanoid copepod acartia tonsa. *Journal of Plankton Research*, 27(10):1067–1071.

Giske, J., Aksnes, D., and Fiksen, O. (1994). Visual predators, environmental variables and zooplankton mortality risk. *Vie et Milieu/Life & Environment*, pages 1–9.

Gliwicz, M. Z. (1986). Predation and the evolution of vertical migration in zooplankton. *Nature*, 320(24):746–748.

Godø, O. R., Handegard, N. O., Browman, H. I., Macaulay, G. J., Kaartvedt, S., Giske, J., Ona, E., Huse, G., and Johnsen, E. (2014). Marine ecosystem acoustics (MEA): quantifying processes in the sea at the spatio-temporal scales on which they occur. *ICES Journal of Marine Science*, 71(8):2357–2369.

Godø, O. R., Sivle, L. D., Patel, R., and Torkelsen, T. (2013). Synchronous behaviour of cetaceans observed with active acoustics. *Deep Sea Research Part II: Topical Studies in Oceanography*, 98:445–451.

Goldthwait, S., Yen, J., Brown, J., and Alldredge, A. (2004). Quantification of marine snow fragmentation by swimming euphausiids. *Limnology and Oceanography*, 49(4 I):940–952.

González-Irusta, J. M. and Wright, P. J. (2016). Spawning grounds of Atlantic cod (Gadus morhua) in the North Sea. *ICES Journal of Marine Science*, 73(2):304–315.

Gorgues, T., Aumont, O., and Memery, L. (2019). Simulated Changes in the Particulate Carbon Export Efficiency due to Diel Vertical Migration of Zooplankton in the North Atlantic. *Geophysical Research Letters*, 46(10):5387–5395.

Gorska, N., Korneliussen, R. J., and Ona, E. (2007). Acoustic backscatter by schools of adult Atlantic mackerel. *ICES Journal of Marine Science*, 64(6):1145–1151.

Gorska, N. and Ona, E. (2003). Modelling the acoustic effect of swimbladder compression in herring. *ICES Journal of Marine Science*, 60(3):548–554.

Grare, L., Statom, N. M., Pizzo, N., and Lenain, L. (2021). Instrumented Wave Gliders for Air-Sea Interaction and Upper Ocean Research. *Frontiers in Marine Science*, 8(August):1–21.

Greene, C. H., Meyer-Gutbrod, E. L., McGarry, L. P., Hufnagle Jr., L. C., Chu, D., McClatchie, S., Packer, A., Jung, J.-B., Acker, T., Dorn, H., and Pelkie, C. (2014). A Wave Glider Approach to Fisheries Acoustics Transforming How We Monitor the Nation's Commercial Fisheries in the 21st Century. *Oceanography*, 27(4, SI):168–174.

Greene, C. H., Wiebe, P. H., Pershing, A. J., Gal, G., Popp, J. M., Copley, N. J., Austin, T. C., Bradley, A. M., Goldsborough, R. G., Dawson, J., Hendershott, R., and Kaartvedt,

S. (1998). Assessing the distribution and abundance of zooplankton: A comparison of acoustic and netsampling methods with D-BAD MOCNESS. *Deep-Sea Research Part II: Topical Studies in Oceanography*, 45(7):1219–1237.

Greenlaw, C. (1979). Acoustical of zooplankton. *Limnological Oceanography*, 24(2):226–242.

Greenwood, N., Parker, E. R., Fernand, L., Sivyer, D. B., Weston, K., Painting, S. J., Kröger, S., Forster, R. M., Lees, H. E., Mills, D. K., and Laane, R. W. (2010). Detection of low bottom water oxygen concentrations in the North Sea; Implications for monitoring and assessment of ecosystem health. *Biogeosciences*, 7(4):1357–1373.

Greer, A. T., Cowen, R. K., Guigand, C. M., Mcmanus, M. A., Sevadjian, J. C., and Timmerman, A. H. (2013). Relationships between phytoplankton thin layers and the fine-scale vertical distributions of two trophic levels of zooplankton. *Journal of Plankton Research*, 35(5):939–956.

Greer, A. T., Lehrter, J. C., Binder, B. M., Nayak, A. R., Barua, R., Rice, A. E., Cohen, J. H., McFarland, M. N., Hagemeyer, A., Stockley, N. D., Boswell, K. M., Shulman, I., DeRada, S., and Penta, B. (2020). High-Resolution Sampling of a Broad Marine Life Size Spectrum Reveals Differing Size- and Composition-Based Associations With Physical Oceanographic Structure. *Frontiers in Marine Science*, 7.

Guadayol, Ò., Peters, F., Marrasé, C., Gasol, J. M., Roldán, C., Berdalet, E., Massana, R., and Sabata, A. (2009). Episodic meteorological and nutrient-load events as drivers of coastal planktonic ecosystem dynamics: A time-series analysis. *Marine Ecology Progress Series*, 381:139–155.

Guihen, D., Brearley, J. A., and Fielding, S. (2022). Antarctic krill likely avoid underwater gliders. *Deep-Sea Research Part I: Oceanographic Research Papers*, 179(October 2021):103680.

Guihen, D., Fielding, S., Murphy, E. J., Heywood, K. J., and Griffiths, G. (2014). An assessment of the use of ocean gliders to undertake acoustic measurements of zooplankton:

the distribution and density of Antarctic krill ( Euphausia superba ) in the Weddell Sea. *Limnology and Oceanography: Methods*, 12(6):373–389.

Guo, C., Xu, P., Wang, W., Han, Y., fei Kuai, Y., and wei Fan, Y. (2021). Experimental study on bubble sweep-down characteristics of research vessels. *Ocean Engineering*, 228(April):108963.

Häfker, N. S., Meyer, B., Last, K. S., Pond, D. W., Hüppe, L., and Teschke, M. (2017). Circadian Clock Involvement in Zooplankton Diel Vertical Migration. *Current Biology*, 27(14):2194–2201.e3.

Hager, M. C. and Helfman, G. S. (1991). Safety in numbers: shoal size choice by minnows under predatory threat. *Behavioral Ecology and Sociobiology*, 29(4):271–276.

Hahn, M. A., Effertz, C., Bigler, L., and von Elert, E. (2019). 5$\alpha$-cyprinol sulfate, a bile salt from fish, induces diel vertical migration in Daphnia. *eLife*, 8.

Hall, C. A. and Lewandowska, A. M. (2022). Zooplankton Dominance Shift in Response to Climate-Driven Salinity Change: A Mesocosm Study. *Frontiers in Marine Science*, 9(June):1–10.

Halsband-Lenk, C. (2001). *Temperature impact on reproduction and development of congener marine copepods : a key to distribution patterns?* PhD thesis.

Halsnæs, K., Drews, M., and Clausen, N.-E. (2016). Socio-economic Impacts—Offshore Activities/Energy. In *North Sea Region Climate Change Assessment*, pages 409–415. Springer.

Hamner, W. M., Madin, L. P., Alldredge, A. L., Gilmer, R. W., and Hamner, P. P. (1975). Underwater observations of gelatinous zooplankton: Sampling problems, feeding biology, and behavior1. *Limnology and Oceanography*, 20(6):907–917.

Handegard, N. O., Andersen, L. N., Brautaset, O., Choi, C., Eliassen, I. K., Heggelund, Y., Hestnes, A. J., Malde, K., Osland, H., Ordonez, A., Patel, R., Gei, T. V. E., and Vatnehol, S. (2021). Fisheries acoustics and Acoustic Target Classification. Report from the COGMAR/CRIMAC workshop on machine learning methods in fisheries acoustics. Technical report, Rapport fra havforskningen.

Handegard, N. O., Buisson, L. D., Brehmer, P., Chalmers, S. J., De Robertis, A., Huse, G., Kloser, R., Macaulay, G., Maury, O., Ressler, P. H., Stenseth, N. C., and Godø, O. R. (2013). Towards an acoustic-based coupled observation and modelling system for monitoring and predicting ecosystem dynamics of the open ocean. *Fish and Fisheries*, 14(4):605–615.

Hansen, B. K., Bekkevold, D., Clausen, L. W., and Nielsen, E. E. (2018). The sceptical optimist: challenges and perspectives for the application of environmental DNA in marine fisheries. *Fish and Fisheries*, 19(5):751–768.

Haralabous, J. and Georgakarakos, S. (1996). Artificial neural networks as a tool for species identification of fish schools. *ICES Journal of Marine Science*, 53(2):173–180.

Harris, R. P. (1988). Interactions between diel vertical migratory behavior of marine zooplankton and the subsurface chlorophyll maximum. *Bulletin of Marine Science*, 43(3):663–674.

Hays, G. C. (1995). Ontogenetic and seasonal variation in the diel vertical migration of the copepods Metridia lucens and Metridia longa. *Limnology and Oceanography*, 40(8):1461–1465.

Hays, G. C. (1996). Large-scale patterns of diel vertical migration in the North Atlantic. *Deep-Sea Research Part I: Oceanographic Research Papers*, 43(10):1601–1615.

Hays, G. C. (2003). A review of the adaptive significance and ecosystem consequences of zooplankton diel vertical migrations. In *Hydrobiologia*, volume 503, pages 163–170.

Hays, G. C., Kennedy, H., and Frost, B. W. (2001). Individual variability in diel vertical migration of a marine copepod: Why some individuals remain at depth when others migrate. *Limnology and Oceanography*, 46(8):2050–2054.

Hays, G. C., Warner, A. J., and Lefevre, D. (1996). Long-term changes in the diel vertical migration behaviour of zooplankton. *Marine Ecology Progress Series*, 141(1-3):149–159.

Hazen, E. L., Suryan, R. M., Santora, J. A., Bograd, S. J., Watanuki, Y., and Wilson, R. P. (2013). Scales and mechanisms of marine hotspot formation. *Marine Ecology Progress Series*, 487:177–183.

Heath, M., Backhaus, J., Richardson, K., McKenzie, E., Slagstad, D., Beare, D., Dunn, J., Fraser, J., Gallego, A., Hainbucher, D., Hay, S., Jónasdóttir, S., Madden, H., Mardaljevic, J., and Schacht, A. (1999). Climate fluctuations and the spring invasion of the North Sea by Calanus finmarchicus. *Fisheries Oceanography*, 8(SUPPL. 1):163–176.

Heine, K. B., Abebe, A., Wilson, A. E., and Hood, W. R. (2019). Copepod respiration increases by 7A meta-analysis. *Limnology And Oceanography Letters*, 4(3):53–61.

Hemsley, V. S., Smyth, T. J., Martin, A. P., Frajka-Williams, E., Thompson, A. F., Damerell, G., and Painter, S. C. (2015). Estimating Oceanic Primary Production Using Vertical Irradiance and Chlorophyll Profiles from Ocean Gliders in the North Atlantic. *Environmental Science and Technology*, 49(19):11612–11621.

Henderson, G. T. D. and Marshall, N. B. (1944). Ecological investigations with the Continuous Plankton Recorder: the zooplankton (other than Copepoda and young fish) in the southern North Sea, 1932-1937. *Hull Bulletins of Marine Ecology*, 1(6):255–275.

Heneghan, R. F., Everett, J. D., Blanchard, J. L., Sykes, P., and Richardson, A. J. (2023). Climate-driven zooplankton shifts cause large-scale declines in food quality for fish. *Nature Climate Change*, 13(5):470–477.

Heslop, E., Tintoré, J., Rotllan, P., Álvarez-Berastegui, D., Fontera, B., Mourre, B., Gómez-Pujol, L., March, D., Casas, B., Nolan, G., and Durand, D. (2019). SOCIB integrated multi-platform ocean observing and forecasting: from ocean data to sector-focused delivery of products and services. *Journal of Operational Oceanography*, 12(sup2):S67–S79.

Hetherington, E. D., Damian-Serrano, A., Haddock, S. H., Dunn, C. W., and Choy, C. A. (2022). Integrating siphonophores into marine food-web ecology. *Limnology And Oceanography Letters*, 7(2):81–95.

Heywood, K. J. (1996). Diel vertical migration of zooplankton in the northeast Atlantic. *Journal of Plankton Research*, 18(2):163–184.

Hijmans, R. J. (2021). geosphere: Spherical trigonometry. R package version 1.5-14. https://CRAN.R-project.org/package=geosphere.

Hildebrand, J. A. (2009). Anthropogenic and natural sources of ambient noise in the ocean. *Marine Ecology Progress Series*, 395:5–20.

Hinrichsen, H. H., von Dewitz, B., Lehmann, A., Bergström, U., and Hüssy, K. (2017). Spatio-temporal dynamics of cod nursery areas in the Baltic Sea. *Progress in Oceanography*, 155:28–40.

Hirche, H.-J. (1987). Temperature and plankton II. Effect on respiration and swimming activity in copepods from the Greenland Sea. *Marine Biology*, 94:347–356.

Hjøllo, S. S., Hansen, C., and Skogen, M. D. (2021). Assessing the importance of zooplankton sampling patterns with an ecosystem model. *Marine Ecology Progress Series*, 680:163–176.

Hjøllo, S. S., Skogen, M. D., and Svendsen, E. (2009). Exploring currents and heat within the North Sea using a numerical model. *Journal of Marine Systems*, 78(1):180–192.

Hobbs, L., Banas, N. S., Cohen, J. H., Cottier, F. R., Berge, J., and Varpe, A. (2021). A marine zooplankton community vertically structured by light across diel to interannual timescales. *Biology Letters*, 17(2).

Hobbs, L., Cottier, F., Last, K., and Berge, J. (2018). Pan-Arctic diel vertical migration during the polar night. *Marine Ecology Progress Series*, 605:61–72.

Holzman, R., Reidenbach, M. A., Monismith, S. G., Koseff, J. R., and Genin, A. (2005). Near-bottom depletion of zooplankton over a coral reef II: Relationships with zooplankton swimming ability. *Coral Reefs*, 24(1):87–94.

Honkalehto, T., Ressler, P. H., Towler, R. H., and Wilson, C. D. (2011). Using acoustic data from fishing vessels to estimate walleye pollock (Theragra chalcogramma) abundance in the eastern Bering Sea. *Canadian Journal of Fisheries and Aquatic Sciences*, 68(7):1231–1242.

Horne, C. R., Hirst, A. G., Atkinson, D., Neves, A., and Kiørboe, T. (2016). A global synthesis of seasonal temperature–size responses in copepods. *Global Ecology and Biogeography*, 25(8):988–999.

Horne, J. K. (2000). Acoustic approaches to remote species identification: A review.

Hosia, A. and Båmstedt, U. (2008). Seasonal abundance and vertical distribution of siphonophores in western Norwegian fjords. *Journal of Plankton Research*, 30(8):951–962.

Huijbers, C. M., Nagelkerken, I., and Layman, C. A. (2015). Fish movement from nursery bays to coral reefs: a matter of size? *Hydrobiologia*, 750(1):89–101.

Hull, T. and Kaiser, J. (2023). Post-recovery ocean glider data from Seagliders deployed in the North Sea during the AlterEco project, November 2017-April 2019 (version 2). doi:10.5285/f15f9c60-f2aa-5f4c-e053-6c86abc01a81.

Hunt, J. and Sajjadi, S. (2018). Mechanisms And Modelling of Wind Driven Waves. *Procedia IUTAM*, 26:3–13.

Hunter, J. R. and Sanchez, C. (1976). Diel changes in swim bladder inflation of the larvae of the northern anchovy, Engraulis mordax. *Fishery Bulletin*, 74:847–855.

Huret, M., Bourriau, P., Doray, M., Gohin, F., and Petitgas, P. (2018). Survey timing vs. ecosystem scheduling: Degree-days to underpin observed interannual variability in marine ecosystems. *Progress in Oceanography*, 166:30–40.

Huse, I. and Korneliussen, R. (2000). Diel variation in acoustic density measurements of overwintering herring (Clupea harengus L.). *ICES Journal of Marine Science*, 57(4):903–910.

ICES (2005). ICES FishMap: Herring. International Council for the Exploration of the Sea (ICES). https://www.ices.dk/about-ICES/projects/EU-RFP/EU Repository/ICESFIshMap/ICES FishMap species factsheet-herring.pdf.

ICES (2023). Acoustic trawl surveys. International Council for the Exploration of the Sea (ICES). https://www.ices.dk/data/data-portals/Pages/acoustic.aspx.

Ichii, T., Mori, Y., Mahapatra, K., Trathan, P. N., Okazaki, M., Hayashi, T., and Okuda, T. (2020). Body length-dependent diel vertical migration of Antarctic krill in relation to food

availability and predator avoidance in winter at South Georgia. *Marine Ecology Progress Series*, 654:53–66.

Incze, L., Hebert, D., Wolff, N., Oakey, N., and Dye, D. (2001). Changes in copepod distributions associated with increased turbulence from wind stress. *Marine Ecology Progress Series*, 213:229–240.

Irigoien, X., Conway, D. V., and Harris, R. P. (2004). Flexible diel vertical migration behaviour of zooplankton in the Irish Sea. *Marine Ecology Progress Series*, 267:85–97.

Irigoien, X. and Harris, R. P. (2003). Interannual variability of Calanus helgolandicus in the English Channel. In *Fisheries Oceanography*, volume 12, pages 317–326.

Irigoien, X., Klevjer, T. A., Røstad, A., Martinez, U., Boyra, G., Acuña, J. L., Bode, A., Echevarria, F., Gonzalez-Gordillo, J. I., Hernandez-Leon, S., Agusti, S., Aksnes, D. L., Duarte, C. M., and Kaartvedt, S. (2014). Large mesopelagic fishes biomass and trophic efficiency in the open ocean. *Nature Communications*, 5(1):3271.

Isla, A., Scharek, R., and Latasa, M. (2015). Zooplankton diel vertical migration and contribution to deep active carbon flux in the NW Mediterranean. *Journal of Marine Systems*, 143:86–97.

Iversen, M. H. (2023). Carbon Export in the Ocean: A Biologist's Perspective. *Annual Review of Marine Science*, 15(1):1–25.

Janssen, J. (1982). Comparison of searching behavior for zooplankton in an obligate planktivore, blueback herring (Alosa aestivalis) and a facultative planktivore, bluegill (Lepomis machrochirus). *Canadian Journal of Fisheries and Aquatic Sciences*, 39(12):1649–1654.

Jech, J. M., Schaber, M., Cox, M., Escobar-Flores, P., Gastauer, S., Haris, K., Horne, J., Jarvis, T., Ladroit, Y., O'Driscoll, R., Pedersen, G., Peña, M., Ryan, T., Sakinan, S., Thomas, R., Viehman, H., Wall, C., Whitton, T. T., O'Driscoll, R., Pedersen, G., Pena, M., Ryan, T., Sakinan, S., Thomas, R., Viehman, H., and Whitton, T. T. (2021). Collecting Quality Echosounder Data in Inclement Weather. Technical report, ICES Cooperative Research Reports (CRR).

Jensen, H., Rindorf, A., Wright, P. J., and Mosegaard, H. (2011). Inferring the location and scale of mixing between habitat areas of lesser sandeel through information from the fishery. *ICES Journal of Marine Science*, 68(1):43–51.

Johnsen, S. (2001). Hidden in plain sight: The ecology and physiology of organismal transparency. *The Biological Bulletin*, 201(3):301–318.

Jónasdóttir, S. H. and Koski, M. (2011). Biological processes in the North Sea: Comparison of Calanus helgolandicus and Calanus finmarchicus vertical distribution and production. *Journal of Plankton Research*, 33(1):85–103.

Jones, S., Inall, M., Porter, M., Graham, J. A., and Cottier, F. (2020). Storm-driven across-shelf oceanic flows into coastal waters. *Ocean Science*, 16(2):389–403.

Kaartvedt, S., Klevjer, T. A., and Aksnes, D. L. (2012). Internal wave-mediated shading causes frequent vertical migrations in fishes. *Marine Ecology Progress Series*, 452:1–10.

Kaartvedt, S., Melle, W., Knutsen, T., and Skjoldal, H. R. (1996). Vertical distribution of fish and krill beneath water of varying optical properties. *Marine Ecology Progress Series*, 136(1-3):51–58.

Kaartvedt, S., Røstad, A., and Aksnes, D. L. (2017). Changing weather causes behavioral responses in the lower mesopelagic. *Marine Ecology Progress Series*, 574:259–263.

Kaartvedt, S., Røstad, A., Klevjer, T. A., and Staby, A. (2009). Use of bottom-mounted echo sounders in exploring behavior of mesopelagic fishes. *Marine Ecology Progress Series*, 395(Patel 2007):109–118.

Kaltenberg, A. M. and Benoit-Bird, K. J. (2009). Diel behavior of sardine and anchovy schools in the California Current System. *Marine Ecology Progress Series*, 394:247–262.

Kang, M., Furusawa, M., and Miyashita, K. (2002). Effective and accurate use of difference in mean volume backscattering strength to identify fish and plankton. *ICES Journal of Marine Science*, 59(4):794–804.

Kankaala, P. (1984). A quantitative comparison of two zooplankton sampling methods,

a plankton trap and a towed net, in the Baltic. *Internationale Revue der Gesamten Hydrobiologie und Hydrographie*, 69(1957).

Keerthi, M. G., Prend, C. J., Aumont, O., and Lévy, M. (2022). Annual variations in phytoplankton biomass driven by small-scale physical processes. *Nature Geoscience*, 15(12):1027–1033.

Kelley, D. and Richards, C. (2022). oce: Analysis of oceanographic data. R package version 1.7-3. https://CRAN.R-project.org/package=oce.

Kent, M. I., Lukeman, R., Lizier, J. T., and Ward, A. J. (2019). Speed-mediated properties of schooling. *Royal Society Open Science*, 6(2).

Kessel, R. (2019). How Sea-Wave Spectra Naturally Limit the Speed of Wave Gliders. *Seamount Analytics Technical Note*.

Killen, S. S., Marras, S., Steffensen, J. F., and Mckenzie, D. J. (2012). Aerobic capacity influences the spatial position of individuals within fish schools. *Proceedings of the Royal Society B: Biological Sciences*, 279(1727):357–364.

Kirby, R. R. and Beaugrand, G. (2009). Trophic amplification of climate warming. *Proceedings of the Royal Society B: Biological Sciences*, 276(1676):4095–4103.

Kirby, R. R., Beaugrand, G., and Lindley, J. A. (2008). Climate-induced effects on the meroplankton and the benthic-pelagic ecology of the North Sea. *Limnology and Oceanography*, 53(5):1805–1815.

Kirby, R. R., Beaugrand, G., and Lindley, J. A. (2009). Synergistic effects of climate and fishing in a marine ecosystem. *Ecosystems*, 12:548–561.

Klais, R., Lehtiniemi, M., Rubene, G., Semenova, A., Margonski, P., Ikauniece, A., Simm, M., Põllumaë, A., Grinienė, E., Mäkinen, K., and Ojaveer, H. (2016). Spatial and temporal variability of zooplankton in a temperate semi-enclosed sea: Implications for monitoring design and long-term studies. *Journal of Plankton Research*, 38(3):652–661.

Klevjer, T. A., Irigoien, X., Røstad, A., Fraile-Nuez, E., Benítez-Barrios, V. M., and

Kaartvedt., S. (2016). Large scale patterns in vertical distribution and behaviour of mesopelagic scattering layers. *Scientific Reports*, 6(1):19873.

Klevjer, T. A., Torres, D. J., and Kaartvedt, S. (2012). Distribution and diel vertical movements of mesopelagic scattering layers in the Red Sea. *Marine Biology*, 159(8):1833–1841.

Kloser, R. J. (1996). Improved precision of acoustic surveys of benthopelagic fish by means of a deep-towed transducer. *ICES Journal of Marine Science*, 53(2):407–413.

Kloser, R. J., Ryan, T., Sakov, P., Williams, A., and Koslow, J. A. (2002). Species identification in deep water using multiple acoustic frequencies. *Canadian Journal of Fisheries and Aquatic Sciences*, 59(6):1065–1077.

Kloser, R. J., Ryan, T. E., Keith, G., and Gershwin, L. (2016). Deep-scattering layer, gas-bladder density, and size estimates using a two-frequency acoustic and optical probe. *ICES Journal of Marine Science*, 73(8):2037–2048.

Knutsen, T., Hosia, A., Falkenhaug, T., Skern-Mauritzen, R., Wiebe, P. H., Larsen, R. B., Aglen, A., and Berg, E. (2018). Coincident mass occurrence of gelatinous zooplankton in Northern Norway. *Frontiers in Marine Science*, 5(MAY).

Kongsberg Maritime (2023). WBT mini. https://www.kongsberg.com/maritime/products/ocean-science/ocean-science/es_scientific/sci_es_transceivers/simrad-wbt-mini/.

Korneliussen, R. and Ona, E. (2002). An operational system for processing and visualizing multi-frequency acoustic data. *ICES Journal of Marine Science*, 59(2):293–313.

Korneliussen, R. and Ona, E. (2004). Verified acoustic identification of Atlantic mackerel. *Ices Cm2004*.

Korneliussen, R. J. (2018). Acoustic target classification. Technical report, ICES Cooperative Research Reports (CRR).

Korneliussen, R. J., Diner, N., Ona, E., Berger, L., and Fernandes, P. G. (2008). Proposals for the collection of multifrequency acoustic data. *ICES Journal of Marine Science*, 65(6):982–994.

Korneliussen, R. J., Heggelund, Y., Eliassen, I. K., and Johansen, G. O. (2009). Acoustic species identification of schooling fish. *ICES Journal of Marine Science*, 66(6):1111–1118.

Korneliussen, R. J., Heggelund, Y., Macaulay, G. J., Patel, D., Johnsen, E., and Eliassen, I. K. (2016). Acoustic identification of marine species using a feature library. *Methods in Oceanography*, 17(17):187–205.

Krause, J., Bumann, D., and Todt, D. (1992). Relationship between the position preference and nutritional state of individuals in schools of juvenile roach (Rutilus rutilus). *Behavioral Ecology and Sociobiology*, 30(3-4):177–180.

Krause, M., Dippner, J. W., and Beil, J. (1995). A review of hydrographic controls on the distribution of zooplankton biomass and species in the North Sea with particular reference to a survey conducted in January–March 1987. *Progress in Oceanography*, 35(2):81–152.

Kröncke, I., Dippner, J. W., Heyen, H., and Zeiss, B. (1998). Long-term changes in macrofaunal communities off Norderney (East Frisia, Germany) in relation to climate variability. *Marine Ecology Progress Series*, 167:25–36.

Kröncke, I. and Knust, R. (1995). The Dogger Bank: A special ecological region in the central North Sea. *Helgoländer Meeresuntersuchungen*, 49(1-4):335–353.

Kubilius, R., Macaulay, G. J., and Ona, E. (2020). Remote sizing of fish-like targets using broadband acoustics. *Fisheries Research*, 228:105568.

Kubilius, R. and Ona, E. (2012). Target strength and tilt-angle distribution of the lesser sandeel (Ammodytes marinus). *ICES Journal of Marine Science*, 69(6):1099–1107.

Kubilius, R. and Pedersen, G. (2016). Relative acoustic frequency response of induced methane, carbon dioxide and air gas bubble plumes, observed laterally. *The Journal of the Acoustical Society of America*, 140(4):2902–2912.

Lacoursière-Roussel, A., Côté, G., Leclerc, V., and Bernatchez, L. (2016). Quantifying relative fish abundance with eDNA: a promising tool for fisheries management. *Journal of Applied Ecology*, 53(4):1148–1157.

Lampert, W. (1989). The Adaptive Significance of Diel Vertical Migration of Zooplankton. *Functional Ecology*, 3(1):21.

Larsson, M. (2012). Why do fish school? *Current Zoology*, 58(1):116–128.

Lassen, J., Kortegård, M., Riisgård, H. U., Friedrichs, M., Graf, G., and Larsen, P. S. (2006). Down-mixing of phytoplankton above filter-feeding mussels - Interplay between water flow and biomixing. *Marine Ecology Progress Series*, 314:77–88.

Last, K. S., Hobbs, L., Berge, J., Brierley, A. S., and Cottier, F. (2016). Moonlight Drives Ocean-Scale Mass Vertical Migration of Zooplankton during the Arctic Winter. *Current Biology*, 26(2):244–251.

Laurel, B. J., Gregory, R. S., Brown, J. A., Hancock, J. K., and Schneider, D. C. (2004). Behavioural consequences of density-dependent habitat use in juvenile cod Gadus morhua and G. ogac: The role of movement and aggregation. *Marine Ecology Progress Series*, 272:257–270.

Lavery, A. C., Wiebe, P. H., Stanton, T. K., Lawson, G. L., Benfield, M. C., and Copley, N. (2007). Determining dominant scatterers of sound in mixed zooplankton populations. *The Journal of the Acoustical Society of America*, 122(6):3304–3326.

Lawson, G. L., Barange, M., and Fréon, P. (2001). Species identification of pelagic fish schools on the South African continental shelf using acoustic descriptors and ancillary information. *ICES Journal of Marine Science*, 58(1):275–287.

Lee, H. W., Ban, S., Ikeda, T., and Matsuishi, T. (2003). Effect of temperature on development, growth and reproduction in the marine copepod Pseudocalanus newmani at satiating food condition. *Journal of Plankton Research*, 25(3):261–271.

Levine, R. M., De Robertis, A., Grünbaum, D., Woodgate, R., Mordy, C. W., Mueter, F., Cokelet, E., Lawrence-Slavas, N., and Tabisola, H. (2021). Autonomous vehicle surveys indicate that flow reversals retain juvenile fishes in a highly advective high-latitude ecosystem. *Limnology and Oceanography*, 66(4):1139–1154.

Lezama-Ochoa, A., Irigoien, X., Chaigneau, A., Quiroz, Z., Lebourges-Dhaussy, A., and Bertrand, A. (2014). Acoustics reveals the presence of a macrozooplankton biocline in

the bay of Biscay in response to hydrological conditions and predator-prey relationships. *PLoS ONE*, 9(2).

Lindegren, M., Möllmann, C., Nielsen, A., and Stenseth, N. C. (2009). Preventing the collapse of the Baltic cod stock through an ecosystem-based management approach. *Proceedings of the National Academy of Sciences of the United States of America*, 106(34):14722–14727.

Lindegren, M., Thomas, M. K., Jónasdóttir, S. H., Nielsen, T. G., and Munk, P. (2020). Environmental niche separation promotes coexistence among ecologically similar zooplankton species—North Sea copepods as a case study. *Limnology and Oceanography*, 65(3):545–556.

Lindegren, M., Van Deurs, M., MacKenzie, B. R., Worsoe Clausen, L., Christensen, A., and Rindorf, A. (2018). Productivity and recovery of forage fish under climate change and fishing: North Sea sandeel as a case study. *Fisheries Oceanography*, 27(3):212–221.

Lindley, J. A. and Batten, S. D. (2010). Long-term variability in the diversity of North Sea zooplankton. *Journal of the Marine Biological Association of the United Kingdom*, 82(1):31–40.

Lindley, J. A., Beaugrand, G., Luczak, C., Dewarumez, J. M., and Kirby, R. R. (2010). Warm-water decapods and the trophic amplification of climate in the North Sea. *Biology Letters*, 6(6):773–776.

Liquid Robotics, Inc. (2015). Liquid Robotics Frequently Asked Questions (FAQs). https://nmssanctuaries.blob.core.windows.net/sanctuaries-prod/media/archive/news/press/hawaii-uas/liquid-robotics-faq-2015.pdf.

Liquid Robotics, Inc. (2018). The Wave Glider — How It Works. https://www.liquid-robotics.com/platform/how-it-works/.

Liquid Robotics, Inc. (2023). Flexible Design Supports Wide Range of Sensors and Payloads. https://www.liquid-robotics.com/wave-glider/supported-sensors/.

Liu, Y., Guo, J., Xue, Y., Sangmanee, C., Wang, H., Zhao, C., Khokiattiwong, S., and Yu, W. (2022). Seasonal variation in diel vertical migration of zooplankton and micronekton in the

Andaman Sea observed by a moored ADCP. *Deep-Sea Research Part I: Oceanographic Research Papers*, 179.

Longhurst, A. and Williams, R. (1979). Materials for plankton modelling: Vertical distribution of atlantic zooplankton in summer. *Journal of Plankton Research*, 1(1):1–28.

Løvik, A. and Hovem, J. M. (1979). An experimental investigation of swimbladder resonance in fishes. *The Journal of the Acoustical Society of America*, 66(3):850–854.

Ludvigsen, M., Berge, J., Geoffroy, M., Cohen, J. H., De La Torre, P. R., Nornes, S. M., Singh, H., Sørensen, A. J., Daase, M., and Johnsen, G. (2018). Use of an autonomous surface vehicle reveals small-scale diel vertical migrations of zooplankton and susceptibility to light pollution under low solar irradiance. *Science Advances*, 4(1).

Luo, J. Y., Grassian, B., Tang, D., Irisson, J. O., Greer, A. T., Guigand, C. M., McClatchie, S., and Cowen, R. K. (2014). Environmental drivers of the fine-scale distribution of a gelatinous zooplankton community across a mesoscale front. *Marine Ecology Progress Series*, 510:129–149.

Lynam, C. P., Attrill, M. J., and Skogen, M. D. (2010). Climatic and oceanic influences on the abundance of gelatinous zooplankton in the North Sea. *Journal of the Marine Biological Association of the United Kingdom*, 90(6):1153–1159.

Lynam, C. P., Hay, S. J., and Brierley, A. S. (2005). Jellyfish abundance and climatic variation: Contrasting responses in oceanographically distinct regions of the North Sea, and possible implications for fisheries. *Journal of the Marine Biological Association of the United Kingdom*, 85(3):435–450.

Maar, M., Visser, A. W., Nielsen, T. G., Stips, A., and Saito, H. (2006). Turbulence and feeding behaviour affect the vertical distributions of Oithona similis and Microsetella norwegica. *Marine Ecology Progress Series*, 313:157–172.

Machairopoulou, M., Lusseau, D., and Rasmussen, J. (2013). Acoustic detection of zooplankton during fishery surveys and sensitivity of acoustic backscatter prediction models to parameters estimates. In *ICES CM*.

Mackas, D. L., Greve, W., Edwards, M., Chiba, S., Tadokoro, K., Eloire, D., Mazzocchi, M. G., Batten, S., Richardson, A. J., Johnson, C., Head, E., Conversi, A., and Peluso, T. (2012). Changing zooplankton seasonality in a changing ocean: Comparing time series of zooplankton phenology. *Progress in Oceanography*, 97-100:31–62.

MacKenzie, B. R., Miller, T. J., Cyr, S., and Leggett, W. C. (1994). Evidence for a dome-shaped relationship between turbulence and larval fish ingestion rates. *Limnology and Oceanography*, 39(8):1790–1799.

Mackenzie, K. V. (1981). Nine-term equation for sound speed in the oceans. *The Journal of the Acoustical Society of America*, 70(3):807–812.

Mackinson, S. and Daskalov, G. (2007). An ecosystem model of the North Sea to support an ecosystem approach to fisheries management: description and parameterisation. Technical Report 142, Sci. Ser. Tech Rep. Cefas Lowestoft.

Maclennan, D. N., Fernandes, P. G., and Dalen, J. (2002). A consistent approach to definitions and symbols in fisheries acoustics. *ICES Journal of Marine Science*, 59(2):365–369.

Maclennan, D. N. and Holliday, D. V. (1996). Fisheries and plankton acoustics : past , present , and future. *ICES Journal of Marine Science*, 53:513–516.

Magurran, A. E. (1990). The adaptive significance of schooling as an anti-predator defence in fish. *Annales Zoologici Fennici*, 27(2):51–66.

Mahaffey, C., Palmer, M., Greenwood, N., and Sharples, J. (2020). Impacts of climate change on dissolved oxygen concentration relevant to the coastal and marine environment around the UK. *MCCIP Science Review*, 2020:31–53.

Mair, A. M., Fernandes, P. G., Brierley, A. S., and Examination, B. A. S. (2004). Examination of North Sea plankton samples in relation to multifrequency echograms . *Ices CM2004*.

Mair, A. M., Fernandes, P. G., Lebourges-Dhaussy, A., and Brierley, A. S. (2005). An investigation into the zooplankton composition of a prominent 38-kHz scattering layer in the North Sea. *Journal of Plankton Research*, 27(7):623–633.

Malde, K., Handegard, N. O., Eikvil, L., and Salberg, A. B. (2020). Machine intelligence and the data-driven future of marine science. *ICES Journal of Marine Science*, 77(4):1274–1285.

Maldonado-Aguilar, A., Ladah, L. B., Fernandez-Aldecoa, G., Solana, E., Lorda, J., Beas-Luna, R., Filonov, A., Leichter, J., and Zertuche-González, J. A. (2023). Small-scale spatiotemporal thermal regimes drive patterns of zooplankton abundance in a kelp forest. *Continental Shelf Research*, 257:104957.

Mallat, B., Germain, G., Gaurier, B., Druault, P., and Billard, J. Y. (2018). Experimental study of the bubble sweep-down phenomenon on three bow designs. *Ocean Engineering*, 148(November 2017):361–375.

Manjón, J. V., Carbonell-Caballero, J., Lull, J. J., García-Martí, G., Martí-Bonmatí, L., and Robles, M. (2008). MRI denoising using Non-Local Means. *Medical Image Analysis*, 12(4):514–523.

Manley, J. and Willcox, S. (2010). The wave glider: A new concept for deploying ocean instrumentation. *IEEE instrumentation & measurement magazine*, 13(6):8–13.

Mariotti, A. and Arkin, P. (2007). The North Atlantic Oscillation and oceanic precipitation variability. *Climate Dynamics*, 28(1):35–51.

Marques, J. C., Li, M., Schaak, D., Robson, D. N., and Li, J. M. (2020). Internal state dynamics shape brainwide activity and foraging behaviour. *Nature*, 577(7789):239–243.

Marras, S. and Domenici, P. (2013). Schooling Fish Under Attack Are Not All Equal: Some Lead, Others Follow. *PLoS ONE*, 8(6).

Marras, S., Killen, S. S., Lindström, J., McKenzie, D. J., Steffensen, J. F., and Domenici, P. (2015). Fish swimming in schools save energy regardless of their spatial position. *Behavioral Ecology and Sociobiology*, 69(2):19–226.

Marshall, N. J., Powell, S. B., Cronin, T. W., Caldwell, R. L., Johnsen, S., Gruev, V., Chiou, T. H., Roberts, N. W., and How, M. J. (2019). Polarisation signals: A new currency for communication. *Journal of Experimental Biology*, 222(3).

Martin, L. V., Stanton, T. K., Wiebe, P. H., and Lynch, J. F. (1996). Acoustic classification of zooplankton. *The Journal of the Acoustical Society of America*, 98(5):2881.

Martynova, D. M. and Gordeeva, A. V. (2010). Light-dependent behavior of abundant zooplankton species in the White Sea. *Journal of Plankton Research*, 32(4):441–456.

Massé, J., Koutsikopoulos, C., and Patty, W. (1996). The structure and spatial distribution of pelagic fish schools in multispecies clusters: An acoustic study. *ICES Journal of Marine Science*, 53(2):155–160.

Mathis, M., Elizalde, A., Mikolajewicz, U., and Pohlmann, T. (2015). Variability patterns of the general circulation and sea water temperature in the North Sea. *Progress in Oceanography*, 135:91–112.

Maud, J. L., Hirst, A. G., Atkinson, A., Lindeque, P. K., and McEvoy, A. J. (2018). Mortality of Calanus helgolandicus: Sources, differences between the sexes and consumptive and nonconsumptive processes. *Limnology and Oceanography*, 63(4):1741–1761.

McAllister, C. D. (1969). Aspects of estimating zooplankton production from phytoplankton production. *Journal of the Fisheries Board of Canada*, 26(2):199–220.

McClatchie, S., Thorne, R. E., Grimes, P., and Hanchet, S. (2000). Ground truth and target identification for fisheries acoustics. *Fisheries Research*, 47(2-3):173–191.

McGillicuddy, Jr, D. J. (2001). Small-scale patchiness, models of. *Encyclopedia of Ocean Sciences*, 5:2820–2833.

McLaren, I. A. (1963). Effects of Temperature on Growth of Zooplankton, and the Adaptive Value of Vertical Migration. *Journal of the Fisheries Research Board of Canada*, 20(3):685–727.

McLean, S., Persson, A., Norin, T., and Killen, S. S. (2018). Metabolic Costs of Feeding Predictively Alter the Spatial Distribution of Individuals in Fish Schools. *Current Biology*, 28(7):1144–1149.e4.

McManus, M., Cheriton, O., Drake, P., Holliday, D., Storlazzi, C., Donaghay, P., and

Greenlaw, C. (2005). Effects of physical processes on structure and transport of thin zooplankton layers in the coastal ocean. *Marine Ecology Progress Series*, 301:199–215.

McQuatters-Gollop, A., Guérin, L., Arroyo, N., Aubert, A., Artigas, L., Bedford, J., Corcoran, E., Dierschke, V., Elliott, S., Geelhoed, S., Gilles, A., González-Irusta, J., Haelters, J., Johansen, M., Le Loc'h, F., Lynam, C., Niquil, N., Meakins, B., Mitchell, I., Padegimas, B., Pesch, R., Preciado, I., Rombouts, I., Safi, G., Schmitt, P., Schückel, U., Serrano, A., Stebbing, P., De la Torriente, A., and Vina-Herbon, C. (2022). Assessing the state of marine biodiversity in the Northeast Atlantic. *Ecological Indicators*, 141:109148.

McQuinn, I. H. and Winger, P. D. (2003). Tilt angle and target strength: target tracking of Atlantic cod (Gadus morhua) during trawling. *ICES Journal of Marine Science*, 60(3):575–583.

Medwin, H. (1976). Acoustical probing for microbubbles at sea. *Saclant Undersea Research Centre La Spezia (Italy) La Spezia Italy*, pages 1–29.

Mehl, S. and Westgård, T. (1983). The diet and consumption of mackerel in the North Sea (a preliminary report).

Meinig, C., Lawrence-Slavas, N., Jenkins, R., and Tabisola, H. M. (2015). The use of Saildrones to examine spring conditions in the Bering Sea: Vehicle specification and mission performance. In *OCEANS 2015 - MTS/IEEE Washington*, number October, pages 1–6. IEEE.

Melle, W. and Skjoldal, H. R. (1998). Reproduction and development of Calanus finmarchicus, C. glacialis and C. hyperboreus in the Barents Sea. *Marine Ecology Progress Series*, 169:211–228.

Mello, L. G. and Rose, G. A. (2005). Using geostatistics to quantify seasonal distribution and aggregation patterns of fishes: An example of Atlantic cod (Gadus morhua). *Canadian Journal of Fisheries and Aquatic Sciences*, 62(3):659–670.

Met Office (2023). Beaufort wind force scale.

Meyer-Gutbrod, E., Greene, C. H., Packer, A., Dorn, H., and Griffith, J. (2012). Long term

autonomous fisheries survey utilizing active acoustics. In *2012 Oceans*, number October, pages 1–5. IEEE.

Miller, M. E. C. and Graham, W. M. (2012). Environmental evidence that seasonal hypoxia enhances survival and success of jellyfish polyps in the northern Gulf of Mexico. *Journal of Experimental Marine Biology and Ecology*, 432-433(November 2012):113–120.

Misund, O. (1993). Dynamics of moving masses: variability in packing density, shape, and size among herring, sprat, and saithe schools. *ICES Journal of Marine Science*, 50(2):145–160.

Misund, O. A. (1990). Sonar observations of schooling herring. *Analysis*, pages 135–146.

Misund, O. A. (1997). Underwater acoustics in marine fisheries and fisheries research. *Reviews in Fish Biology and Fisheries*, 7(1):1–34.

Misund, O. A. and Aglen, A. (1992). Swimming behaviour of fish schools in the north sea during acoustic surveying and pelagic trawl sampling. *ICES Journal of Marine Science*, 49(3):325–334.

Mitson, R. B. (1995). Underwater noise of research vessels: review and recommendations. Technical report, ICES Cooperative Research Reports (CRR).

Moline, M. and Benoit-Bird, K. (2016). Sensor Fusion and Autonomy as a Powerful Combination for Biological Assessment in the Marine Environment. *Robotics*, 5(1):4.

Moline, M. A., Benoit-Bird, K., O'Gorman, D., and Robbins, I. C. (2015). Integration of scientific echo sounders with an adaptable autonomous vehicle to extend our understanding of animals from the surface to the bathypelagic. *Journal of Atmospheric and Oceanic Technology*, 32(11):2173–2186.

Montero, J. T., Lima, M., Estay, S. A., and Rezende, E. L. (2021). Spatial and temporal shift in the factors affecting the population dynamics of Calanus copepods in the North Sea. *Global Change Biology*, 27(3):576–586.

Moore, M. V., Pierce, S. M., Walsh, H. M., Kvalvik, S. K., and Lim, J. D. (2000). Urban

light pollution alters the diel vertical migration of Daphnia. *SIL Proceedings, 1922-2010*, 27(2):779–782.

Moran, N. P., Sánchez-Tójar, A., Schielzeth, H., and Reinhold, K. (2021). Poor nutritional condition promotes high-risk behaviours: a systematic review and meta-analysis. *Biological Reviews*, 96(1):269–288.

Mordy, C., Cokelet, E., De Robertis, A., Jenkins, R., Kuhn, C., Lawrence-Slavas, N., Berchok, C., Crance, J., Sterling, J., Cross, J., Stabeno, P., Meinig, C., Tabisola, H., Burgess, W., and Wangen, I. (2017). Advances in Ecosystem Research: Saildrone Surveys of Oceanography, Fish, and Marine Mammals in the Bering Sea. *Oceanography*, 30(2):113–115.

Moriarty, M., Sethi, S. A., Pedreschi, D., Smeltz, T. S., McGonigle, C., Harris, B. P., Wolf, N., and Greenstreet, S. P. R. (2020). Combining fisheries surveys to inform marine species distribution modelling. *ICES Journal of Marine Science*, 77(2):539–552.

Motro, R., Ayalon, I., and Genin, A. (2005). Near-bottom depletion of zooplankton over coral reefs: III: Vertical gradient of predation pressure. *Coral Reefs*, 24(1):95–98.

Nakamura, I., Goto, Y., and Sato, K. (2015). Ocean sunfish rewarm at the surface after deep excursions to forage for siphonophores. *Journal of Animal Ecology*, 84(3):590–603.

Nayak, A. R., Malkiel, E., McFarland, M. N., Twardowski, M. S., and Sullivan, J. M. (2021). A Review of Holography in the Aquatic Sciences: In situ Characterization of Particles, Plankton, and Small Scale Biophysical Interactions. *Frontiers in Marine Science*, 7(January):1–16.

Nero, R. and Magnuson, J. (1989). Characterization of patches along transects using high-resolution 70-khz integrated acoustic data. *Canadian Journal of Fisheries and Aquatic Sciences*, 46(12):2056–2064.

Nero, R. W., Thompson, C. H., and Jech, J. M. (2004). In situ acoustic estimates of the swimbladder volume of Atlantic herring (Clupea harengus). *ICES Journal of Marine Science*, 61(3):323–337.

Nnanatu, C. C., Thompson, M. S. A., Spence, M. A., Couce, E., van der Kooij, J., and

Lynam, C. P. (2020). Bayesian hierarchical space-time models to improve multispecies assessment by combining observations from disparate fish surveys. pages 1–32.

NOC (2021). NZOC: Net Zero Oceanographic Capacity Summary Report. Technical report.

Novarini, J. C. and Bruno, D. R. (1982). Effects of the sub-surface bubble layer on sound propagation. *The Journal of the Acoustical Society of America*, 72(2):510–514.

Novarini, J. C., Keiffer, R. S., and Norton, G. V. (1998). A model for variations in the range and depth dependence of the sound speed and attenuation induced by bubble clouds under wind-driven sea surfaces. *IEEE Journal of Oceanic Engineering*, 23(4):423–438.

Offshore Sensing - Sailbuoy (2023). Offshore Sensing AS.

Ohman, M. D., Davis, R. E., Sherman, J. T., Grindley, K. R., Whitmore, B. M., Nickels, C. F., and Ellen, J. S. (2019). Zooglider: An autonomous vehicle for optical and acoustic sensing of zooplankton. *Limnology and Oceanography: Methods*, 17(1):69–86.

Ohman, M. D., Frost, B. W., and Cohen, E. B. (1983). Reverse diel vertical migration: An escape from invertebrate predators. *Science*, 220(4604):1404–1407.

Ohman, M. D. and Romagnan, J. B. (2016). Nonlinear effects of body size and optical attenuation on Diel Vertical Migration by zooplankton. *Limnology and Oceanography*, 61(2):765–770.

Omand, M. M., Steinberg, D. K., and Stamieszkin, K. (2021). Cloud shadows drive vertical migrations of deep-dwelling marine life. *Proceedings of the National Academy of Sciences of the United States of America*, 118(32).

Ona, E. (1990). Physiological factors causing natural variations in acoustic target strength of fish. *Journal of the Marine Biological Association of the United Kingdom*, 70(1):107–127.

Ona, E. and Traynor, J. (1990). Hull mounted, protruding transducer for improving echo integration in bad weather. *ICES CM*.

Opdal, A. F., Lindemann, C., and Aksnes, D. L. (2019). Centennial decline in North Sea water clarity causes strong delay in phytoplankton bloom timing. *Global Change Biology*, 25(11):3946–3953.

OSPAR (2017). Intermediate Assessment 2017. Technical report. Available at: https://oap.ospar.org/en/ospar-assessments/intermediate-assessment-2017.

Ottersen, G., Planque, B., Belgrano, A., Post, E., Reid, P. C., and Stenseth, N. C. (2001). Ecological effects of the North Atlantic Oscillation.

Otto, L., Zimmerman, J., Furnes, G., Mork, M., Saetre, R., and Becker, G. (1990). Review of the physical oceanography of the North Sea. *Netherlands Journal of Sea Research*, 26(2-4):161–238.

Otto, S. A., Diekmann, R., Flinkman, J., Kornilovs, G., and Möllmann, C. (2014). Habitat Heterogeneity Determines Climate Impact on Zooplankton Community Structure and Dynamics. *PLoS ONE*, 9(3):e90875.

Painting, S. J., Devlin, M. J., Rogers, S. I., Mills, D. K., Parker, E. R., and Rees, H. L. (2005). Assessing the suitability of OSPAR EcoQOs for eutrophication vs ICES criteria for England and Wales. *Marine Pollution Bulletin*, 50(12):1569–1584.

Paradis, E. and Schliep, K. (2019). Ape 5.0: An environment for modern phylogenetics and evolutionary analyses in R. *Bioinformatics*, 35(3):526–528.

Paramo, J., Gerlotto, F., and Oyarzun, C. (2010). Three dimensional structure and morphology of pelagic fish schools. *Journal of Applied Ichthyology*, 26(6):853–860.

Parker-Stretton, S. L., Rudstam, L. G., Sullivan, P. J., and Warner, D. M. (2009). Standard Operating Procedures for Fisheries Acoustic Surveys in the Great Lakes. Technical report.

Parra, S. M., Greer, A. T., Book, J. W., Deary, A. L., Soto, I. M., Culpepper, C., Hernandez, F. J., and Miles, T. N. (2019). Acoustic detection of zooplankton diel vertical migration behaviors on the northern Gulf of Mexico shelf. *Limnology and Oceanography*, 64(5):2092–2113.

Parsons, M. J. G., Parnum, I. M., and Mccauley, R. D. (2013). Quantifying the acoustic packing density of fish schools with a multi-beam sonar. *Acoustics Australia*, 41(1):107.

Pauli, N.-C., Flintrop, C. M., Konrad, C., Pakhomov, E. A., Swoboda, S., Koch, F., Wang, X.-L., Zhang, J.-C., Brierley, A. S., Bernasconi, M., Meyer, B., and Iversen, M. H. (2021).

Krill and salp faecal pellets contribute equally to the carbon flux at the Antarctic Peninsula. *Nature Communications*, 12(1):7168.

Pearre, S. (1979). Problems of detection and interpretation of vertical migration. *Journal of Plankton Research*, 1(1):29–44.

Pearre, S. (2003a). Eat and run? The hunger/satiation hypothesis in vertical migration: History, evidence and consequences. *Biological Reviews of the Cambridge Philosophical Society*, 78(1):1–79.

Pearre, S. (2003b). When lights are low: Comment on 'Midnight sinking behaviour in Calanus finmarchicus. A response to satiation or krill predation?' by Tarling et al. (2002). *Marine Ecology Progress Series*, 252:303–305.

Pedersen, G., Peddie, D., Falk-Petersen, S., Dunlop, K., Camus, L., Daase, M., Basedow, S. L., Bandara, K., Tverberg, V., and Pederick, J. (2019). Autonomous surface vehicles for persistent acoustic monitoring of zooplankton in a highly productive shelf area. In *OCEANS 2019 - Marseille*, pages 1–7. IEEE.

Peña, M. (2016). Incrementing data quality of multi-frequency echograms using the Adaptive Wiener Filter (AWF) denoising algorithm. *Deep-Sea Research Part I: Oceanographic Research Papers*, 116(August):14–21.

Peña, M. (2021). Full customization of color maps for fisheries acoustics: Visualizing every target. *Fisheries Research*, 240(March):105949.

Perry, M. J., Sackmann, B. S., Eriksen, C. C., and Lee, C. M. (2008). Seaglider observations of blooms and subsurface chlorophyll maxima off the Washington coast. *Limnology and Oceanography*, 53(5 PART 2):2169–2179.

Pershing, A. J., Head, E. H., Greene, C. H., and Jossi, J. W. (2010). Pattern and scale of variability among Northwest Atlantic Shelf plankton communities. *Journal of Plankton Research*, 32(12):1661–1674.

Petitgas, P. and Levenez, J. J. (1996). Spatial organization of pelagic fish: Echogram structure, spatio-temporal condition, and biomass in Senegalese waters. *ICES Journal of Marine Science*, 53(2):147–153.

Pickwell, G. V., Barham, E. G., and Wilton, J. W. (1964). Carbon monoxide production by a bathypelagic siphonophore. *Science*, 144(3620):860–862.

Pikitch, E. K., Rountos, K. J., Essington, T. E., Santora, C., Pauly, D., Watson, R., Sumaila, U. R., Boersma, P. D., Boyd, I. L., Conover, D. O., Cury, P., Heppell, S. S., Houde, E. D., Mangel, M., Plagányi, É., Sainsbury, K., Steneck, R. S., Geers, T. M., Gownaris, N., and Munch, S. B. (2014). The global contribution of forage fish to marine fisheries and ecosystems. *Fish and Fisheries*, 15(1):43–64.

Pinnegar, J. K., Engelhard, G. H., Jones, M. C., Cheung, W. W., Peck, M. A., Rijnsdorp, A. D., and Brander, K. M. (2016). Socio-economic impacts—fisheries. In *North sea region climate change assessment*, pages 375–395. Springer International Publishing.

Pischedda, L., Poggiale, J. C., Cuny, P., and Gilbert, F. (2008). Imaging oxygen distribution in marine sediments. The importance of bioturbation and sediment heterogeneity. *Acta Biotheoretica*, 56(1-2):123–135.

Pitcher, T. (1978). Heuristic definitions of fish shoaling behaviour. *Animal Behaviour*, pages 611–612.

Planque, B. and Fromentin, J. (1996). Calanus and environment in the eastern North Atlantic. I. Spatial and temporal patterns of C. finmarchicus and C. helgolandicus Benjamin. *Marine Ecology Progress Series*, 134:101–109.

Platt, T., Fuentes-Yaco, C., and Frank, K. T. (2003). Spring algal bloom and larval fish survival off Nova Scotia. *Nature*, 423(May):398–399.

Postel, L., da Silva, A. J., Mohrholz, V., and Lass, H. U. (2007). Zooplankton biomass variability off Angola and Namibia investigated by a lowered ADCP and net sampling. *Journal of Marine Systems*, 68(1-2):143–166.

Prairie, J. C., Sutherland, K. R., Nickols, K. J., and Kaltenberg, A. M. (2012). Biophysical interactions in the plankton: A cross-scale review. *Limnology and Oceanography: Fluids and Environments*, 2(1):121–145.

Proud, R., Handegard, N. O., Kloser, R. J., Cox, M. J., Brierley, A. S., and Demer, D. (2019).

From siphonophores to deep scattering layers: Uncertainty ranges for the estimation of global mesopelagic fish biomass. *ICES Journal of Marine Science*, 76(3):718–733.

Purcell, J. E. (1981). Dietary composition and diel feeding patterns of epipelagic siphonophores. *Marine Biology*, 65(1):83–90.

QGIS Development Team (2018). Qgis Geographic Information System, version 3.2.3-Bonn. Open Source Geospatial Foundation. http://qgis.org.

Quante, M. and Colijin, F. (2016). *North Sea Region Climate Assessment (NOSCCA)*. Number October.

Queste, B. Y., Fernand, L., Jickells, T. D., and Heywood, K. J. (2013). Spatial extent and historical context of North Sea oxygen depletion in August 2010. *Biogeochemistry*, 113(1-3):53–68.

Queste, B. Y., Fernand, L., Jickells, T. D., Heywood, K. J., and Hind, A. J. (2016). Drivers of summer oxygen depletion in the central North Sea. *Biogeosciences*, 13(4):1209–1222.

R Core Team (2022). R: A Language and Environment for Statistical Computing. *R Foundation for Statistical Computing*. Vienna, Austria, https://www.R-project.org/.

Raab, K., Nagelkerke, L. A., Boerée, C., Rijnsdorp, A. D., Temming, A., and Dickey-Collas, M. (2012). Dietary overlap between the potential competitors herring, sprat and anchovy in the North Sea. *Marine Ecology Progress Series*, 470:101–111.

Rabalais, N. N., Turner, R. E., Díaz, R. J., and Justić, D. (2009). Global change and eutrophication of coastal waters. *ICES Journal of Marine Science*, 66(7):1528–1537.

Ratnarajah, L., Abu-Alhaija, R., Atkinson, A., Batten, S., Bax, N. J., Bernard, K. S., Canonico, G., Cornils, A., Everett, J. D., Grigoratou, M., Ishak, N. H. A., Johns, D., Lombard, F., Muxagata, E., Ostle, C., Pitois, S., Richardson, A. J., Schmidt, K., Stemmann, L., Swadling, K. M., Yang, G., and Yebra, L. (2023). Monitoring and modelling marine zooplankton in a changing climate.

Reeve, M. R. (1981). Large cod-end reservoirs as an aid to the live collection of delicate zooplankton. *Limnology and Oceanography*, 26(3):577–580.

Reid, P. C., De Fatima Borges, M., and Svendsen, E. (2001). A regime shift in the north sea circa 1988 linked to changes in the north sea horse mackerel fishery. *Fisheries Research*, 50(1-2):163–171.

Reid, P. C., Edwards, M., Beaugrand, G., Skogen, M., and Stevens, D. (2003). Periodic changes in the zooplankton of the North Sea during the twentieth century linked to oceanic inflow. *Fisheries Oceanography*, 12(4-5):260–269.

Reid, P. C., Hari, R. E., Beaugrand, G., Livingstone, D. M., Marty, C., Straile, D., Barichivich, J., Goberville, E., Adrian, R., Aono, Y., Brown, R., Foster, J., Groisman, P., Hélaouët, P., Hsu, H. H., Kirby, R., Knight, J., Kraberg, A., Li, J., Lo, T. T., Myneni, R. B., North, R. P., Pounds, J. A., Sparks, T., Stübi, R., Tian, Y., Wiltshire, K. H., Xiao, D., and Zhu, Z. (2016). Global impacts of the 1980s regime shift. *Global Change Biology*, 22(2):682–703.

Reiss, C. S., Cossio, A. M., Walsh, J., Cutter, G. R., and Watters, G. M. (2021). Glider-Based Estimates of Meso-Zooplankton Biomass Density: A Fisheries Case Study on Antarctic Krill (Euphausia superba) Around the Northern Antarctic Peninsula. *Frontiers in Marine Science*, 8(March):1–18.

Ressler, P. H., De Robertis, A., Warren, J. D., Smith, J. N., and Kotwicki, S. (2012). Developing an acoustic survey of euphausiids to understand trophic interactions in the Bering Sea ecosystem. *Deep Sea Research Part II: Topical Studies in Oceanography*, 65-70:184–195.

Révelard, A., Tintoré, J., Verron, J., Bahurel, P., Barth, J. A., Belbéoch, M., Benveniste, J., Bonnefond, P., Chassignet, E. P., Cravatte, S., Davidson, F., DeYoung, B., Heupel, M., Heslop, E., Hörstmann, C., Karstensen, J., Le Traon, P. Y., Marques, M., McLean, C., Medina, R., Paluszkiewicz, T., Pascual, A., Pearlman, J., Petihakis, G., Pinardi, N., Pouliquen, S., Rayner, R., Shepherd, I., Sprintall, J., Tanhua, T., Testor, P., Seppälä, J., Siddorn, J., Thomsen, S., Valdés, L., Visbeck, M., Waite, A. M., Werner, F., Wilkin, J., and Williams, B. (2022). Ocean Integration: The Needs and Challenges of Effective Coordination Within the Ocean Observing System. *Frontiers in Marine Science*, 8(January):1–15.

Reygondeau, G. and Beaugrand, G. (2011). Water column stability and Calanus finmarchicus. *Journal of Plankton Research*, 33(1):119–136.

Richardson, A. J. (2008). In hot water: Zooplankton and climate change. *ICES Journal of Marine Science*, 65(3):279–295.

Richardson, A. J. and Schoeman, D. S. (2004). Climate impact on plankton ecosystems in the Northeast Atlantic. *Science*, 305(5690):1609–1612.

Rieucau, G., Fernö, A., Ioannou, C. C., and Handegard, N. O. (2015). Towards of a firmer explanation of large shoal formation, maintenance and collective reactions in marine fish. *Reviews in Fish Biology and Fisheries*, 25(1):21–37.

Robinson, H. E., Finelli, C. M., and Koehl, M. A. (2013). Interactions between benthic predators and zooplanktonic prey are affected by turbulent waves. *Integrative and Comparative Biology*, 53(5):810–820.

Robinson, K. L., Sponaugle, S., Luo, J. Y., Gleiber, M. R., and Cowen, R. K. (2021). Big or small, patchy all: Resolution of marine plankton patch structure at micro- To submesoscales for 36 taxa. *Science Advances*, 7(47):2904.

Romenskyy, M., Herbert-Read, J. E., Ioannou, C. C., Szorkovszky, A., Ward, A. J., and Sumpter, D. J. (2020). Quantifying the structure and dynamics of fish shoals under predation threat in three dimensions. *Behavioral Ecology*, 31(2):311–321.

Romey, W. L. (1996). Individual differences make a difference in the trajectories of simulated schools of fish. *Ecological Modelling*, 92(1):65–77.

Rousselle, F., Knaus, C., and Zwicker, M. (2012). Adaptive rendering with non-local means filtering. *ACM Transactions on Graphics*, 31(6):1–11.

RStudio Team (2022). Rstudio: Integrated Development Environment for R. *RStudio, PBC*, Boston, MA, http://www.rstudio.com/.

Ryan, T. E., Downie, R. A., Kloser, R. J., and Keith, G. (2015). Reducing bias due to noise and attenuation in open-ocean echo integration data. *ICES Journal of Marine Science*, 72(8):2482–2493.

Saavedra, A., Castillo, J., Niklitschek, E. J., and Saavedra-Nievas, J. C. (2012). Reducing uncertainty and bias in acoustic biomass estimations of southern blue whiting (Micromesistius australis) in the southeastern Pacific: transducer motion effects upon acoustic attenuation. *Latin American Journal of Aquatic Research*, 40(3):743–754.

Sabatés, A. (2004). Diel vertical distribution of fish larvae during the winter-mixing period in the Northwestern Mediterranean. *ICES Journal of Marine Science*, 61(8):1243–1252.

Sackmann, B. S., Perry, M. J., and Eriksen, C. C. (2008). Seaglider observations of variability in daytime fluorescence quenching of chlorophyll-a in Northeastern Pacific coastal waters. *Biogeosciences Discuss.*, 5(4):2839–2865.

Salt, L. A., Thomas, H., Prowe, A. E. F., Borges, A. V., Bozec, Y., and de Baar, H. J. W. (2013). Variability of North Sea pH and CO 2 in response to North Atlantic Oscillation forcing. *Journal of Geophysical Research: Biogeosciences*, 118(4):1584–1592.

Sarr, J.-M. A., Brochier, T., Brehmer, P., Perrot, Y., Bah, A., Sarré, A., Jeyid, M., Sidibeh, M., and El Ayoubi, S. (2021). Complex data labeling with deep learning methods: Lessons from fisheries acoustics. *ISA Transactions*, 109:113–125.

Sato, M., Horne, J. K., Parker-Stetter, S. L., and Keister, J. E. (2015). Acoustic classification of coexisting taxa in a coastal ecosystem. *Fisheries Research*, 172:130–136.

Scalabrin, C. and Massé, J. (1993). Acoustic detection of the spatial and temporal distribution of fish shoals in the Bay of Biscay. *Aquatic Living Resources*, 6(3):269–283.

Scott, J., Pitois, S., Close, H., Almeida, N., Culverhouse, P., Tilbury, J., and Malin, G. (2021). In situ automated imaging, using the Plankton Imager, captures temporal variations in mesozooplankton using the Celtic Sea as a case study. *Journal of Plankton Research*, 43(2):300–313.

Scott, J., Pitois, S., Creach, V., Malin, G., Culverhouse, P., and Tilbury, J. (2023). Resolution changes relationships: Optimizing sampling design using small scale zooplankton data. *Progress in Oceanography*, 210(May 2022):102946.

Scoulding, B., Chu, D., Ona, E., and Fernandes, P. G. (2015). Target strengths of two

abundant mesopelagic fish species. *The Journal of the Acoustical Society of America*, 137(2):989–1000.

Scoulding, B., Gastauer, S., MacLennan, D. N., Fässler, S. M. M., Copland, P., and Fernandes, P. G. (2017). Effects of variable mean target strength on estimates of abundance: the case of Atlantic mackerel (Scomber scombrus). *ICES Journal of Marine Science*, 74(3):822–831.

Sepp, E., Vetemaa, M., and Raid, T. (2022). Use of autonomous research vehicles in Baltic fisheries acoustic surveys: Potential benefits and pitfalls. In *Trends in Maritime Technology and Engineering Volume 2*, number May, pages 613–616. CRC Press, London.

Shabangu, F. W., Ona, E., and Yemane, D. (2014). Measurements of acoustic attenuation at 38kHz by wind-induced air bubbles with suggested correction factors for hull-mounted transducers. *Fisheries Research*, 151:47–56.

Sharples, J., Ross, O. N., Scott, B. E., Greenstreet, S. P., and Fraser, H. (2006). Inter-annual variability in the timing of stratification and the spring bloom in the North-western North Sea. *Continental Shelf Research*, 26(6):733–751.

Shashar, N., Sabbah, S., and Cronin, T. W. (2004). Transmission of linearly polarized light in seawater: Implications for polarization signaling. *Journal of Experimental Biology*, 207(20):3619–3628.

Sheehan, P. M., Berx, B., Gallego, A., Hall, R. A., Heywood, K. J., and Queste, B. Y. (2020). Weekly variability of hydrography and transport of northwestern inflows into the northern North Sea. *Journal of Marine Systems*, 204:103288.

Sheehan, P. M. F., Berx, B., Gallego, A., Hall, R. A., Heywood, K. J., Hughes, S. L., and Queste, B. Y. (2018). Shelf sea tidal currents and mixing fronts determined from ocean glider observations. *Ocean Science*, 14(2):225–236.

Shelton, A. O., Ramón-Laca, A., Wells, A., Clemons, J., Chu, D., Feist, B. E., Kelly, R. P., Parker-Stetter, S. L., Thomas, R., Nichols, K. M., and Park, L. (2022). Environmental DNA provides quantitative estimates of Pacific hake abundance and distribution in the open ocean. *Proceedings of the Royal Society B: Biological Sciences*, 289(1971).

Sherlock, R. E. and Robison, B. H. (2000). Effects of temperature on the development and survival of Nanomia bijuga (Hydrozoa, Siphonophora). *Invertebrate Biology*, 119(4):379–385.

Shreyamsha Kumar, B. K. (2013). Image denoising based on non-local means filter and its method noise thresholding. *Signal, Image and Video Processing*, 7(6):1211–1227.

Siddorn, J., Blair, G., Boot, D., Buck, J., Kingdon, A., Kloker, A., Kokkinaki, A., Moncoiffe, G., Blyth, E., Fry, M., Heaven, R., Lewis, E., Marchant, B., Napier, B. Pascoe, C., Passmore, J., Pepler, S., Townsend, P., and Watkins, J. (2022). An Information Management Framework for Environmental Digital Twins (IMFe). Technical report, National Oceanography Centre, Southampton.

Simard, Y. and Sourisseau, M. (2009). Diel changes in acoustic and catch estimates of krill biomass. *ICES Journal of Marine Science*, pages 1318–1325.

Simmonds, J. and MacLennan, D. (2005). *Fisheries Acoustics*. Wiley.

Skjoldal, H. R., Wiebe, P. H., Postel, L., Knutsen, T., Kaartvedt, S., and Sameoto, D. D. (2013). Intercomparison of zooplankton (net) sampling systems: Results from the ICES/GLOBEC sea-going workshop. *Progress in Oceanography*, 108:1–42.

Slater, W. L., Pierson, J. J., Decker, M. B., Houde, E. D., Lozano, C., and Seuberling, J. (2020). Jellyfish : How Does Hypoxia Impact the Chesapeake Bay Zooplankton Community? *Diversity*, 12(35):1–26.

Smith, R. N., Das, J., Hine, G., Anderson, W., and Sukhatme, G. S. (2011). Predicting Wave Glider speed from environmental measurements. In *OCEANS'11 MTS/IEEE KONA. IEEE*, number September, pages 1–8.

Sparholt, H., Larsen, L. I., Nielsen, J. R., Rasmus Nielsen Sparholt, J., Sparholt, H., and Larsen, L. I. (2002). Verification of multispecies interactions in the North Sea by trawl survey data on Norway pout (Trisopterus esmarkii). *ICES Journal of Marine Science*, 59(6):1270–1275.

Stanton, T., Chu, D., and Wiebe, P. H. (1996). Acoustic scattering characteristics of several zooplankton groups. *ICES Journal of Marine Science*, 53(2):289–295.

Stanton, T., Wiebe, P. H., Chu, D., Benfield, M. C., Scanlon, L., Martin, L., and Eastwood, R. L. (1994). On acoustic estimates of zooplankton biomass. *ICES Journal of Marine Science*, 51(4):505–512.

Stanton, T. K. (1982). Effects of transducer motion on echo-integration techniques. *Journal of the Acoustical Society of America*, 72(3):947–949.

Stanton, T. K., Sellers, C. J., and Jech, J. M. (2012). Resonance classification of mixed assemblages of fish with swimbladders using a modified commercial broadband acoustic echosounder at 1-6 kHz. *Canadian Journal of Fisheries and Aquatic Sciences*, 69(5):854–868.

Stanton, T. K., Wiebe, P. H., and Chu, D. (1998). Differences between sound scattering by weakly scattering spheres and finite-length cylinders with applications to sound scattering by zooplankton. *The Journal of the Acoustical Society of America*, 103(1):254–264.

Steinberg, D. K. and Landry, M. R. (2017). Zooplankton and the Ocean Carbon Cycle. *Annual Review of Marine Science*, 9(1):413–444.

Suberg, L., Wynn, R. B., Kooij, J. V. D., Fernand, L., Fielding, S., Guihen, D., Gillespie, D., Johnson, M., Gkikopoulou, K. C., Allan, I. J., Vrana, B., Miller, P. I., Smeed, D., and Jones, A. R. (2014). Assessing the potential of autonomous submarine gliders for ecosystem monitoring across multiple trophic levels (plankton to cetaceans) and pollutants in shallow shelf seas. *Methods in Oceanography*, 10:70–89.

Sutherland, K. R., Gemmell, B. J., Colin, S. P., and Costello, J. H. (2019). Maneuvering Performance in the Colonial Siphonophore, Nanomia bijuga. *Biomimetics*, 4(3):62.

Swart, S., Zietsman, J., Coetzee, J., Goslett, D., Hoek, A., Needham, D., and Monteiro, P. (2016). Ocean robotics in support of fisheries research and management. *African Journal of Marine Science*, 38(4):525–538.

Swartzman, G., Huang, C., and Kaluzny, S. (1992). Spatial analysis of Bering Sea groundfish survey data using generalized additive models. *Canadian Journal of Fisheries and Aquatic Sciences*, 49(7):1366–1378.

Swartzman, G., Stuetzle, W., Kulman, K., and Wen, N. (1994). Modeling the distribution of fish schools in the Bering Sea: morphological school identification. *Natural Resource Modeling*, 8(2):177–194.

Takahashi, K., Kuwata, A., Sugisaki, H., Uchikawa, K., and Saito, H. (2009). Downward carbon transport by diel vertical migration of the copepods Metridia pacifica and Metridia okhotensis in the Oyashio region of the western subarctic Pacific Ocean. *Deep-Sea Research Part I: Oceanographic Research Papers*, 56(10):1777–1791.

Tanaka, M. (2019). Changes in vertical distribution of zooplankton under wind-induced turbulence: A 36-year record. *Fluids*, 4(4).

Tang, Y., Nishimori, Y., and Furusawa, M. (2009). The average three-dimensional target strength of fish by spheroid model for sonar surveys. In *ICES Journal of Marine Science*, volume 66, pages 1176–1183.

Tarling, G. A., Jarvis, T., Emsley, S. M., and Matthews, J. B. (2002). Midnight sinking behaviour in Calanus finmarchicus: A response to satiation or krill predation? *Marine Ecology Progress Series*, 240:183–194.

Tarling, G. A., Klevjer, T., Fielding, S., Watkins, J., Atkinson, A., Murphy, E., Korb, R., Whitehouse, M., and Leaper, R. (2009). Variability and predictability of Antarctic krill swarm structure. *Deep-Sea Research Part I: Oceanographic Research Papers*, 56(11):1994–2012.

Tenningen, M., MacAulay, G. J., Rieucau, G., Peña, H., and Korneliussen, R. J. (2017). Behaviours of Atlantic herring and mackerel in a purse-seine net, observed using multibeam sonar. *ICES Journal of Marine Science*, 74(1):359–368.

Thorpe, S. A. (1992). Bubble clouds and the dynamics of the upper ocean. *Quarterly Journal of the Royal Meteorological Society*, 118(503):1–22.

Tiselius, P. (1998). An in situ video camera for plankton studies: design and preliminary observations. *Marine Ecology Progress Series*, 164:293–299.

Toffoli, A. and Bitner-Gregersen, E. M. (2017). Types of Ocean Surface Waves, Wave Classification. *Encyclopedia of Maritime and Offshore Engineering*, pages 1–8.

Toresen, R. (1991). Absorption of acoustic energy in dense herring schools studied by the attenuation in the bottom echo signal. *Fisheries Research*, 10(3-4):317–327.

Torgersen, T. (2001). Visual predation by the euphausiid Meganyctiphanes norvegica. *Marine Ecology Progress Series*, 209:295–299.

Torgersen, T. (2003). Proximate causes for anti-predatory feeding suppression by zooplankton during the day: Reduction of contrast or motion - Ingestion or clearance? *Journal of Plankton Research*, 25(5):565–571.

Trenkel, V., Ressler, P., Jech, M., Giannoulaki, M., and Taylor, C. (2011). Underwater acoustics for ecosystem-based management: state of the science and proposals for ecosystem indicators. *Marine Ecology Progress Series*, 442:285–301.

Trenkel, V. M. and Berger, L. (2013). Corrigendum to "A fisheries acoustic multi-frequency indicator to inform on large scale spatial patterns of aquatic pelagic ecosystems" [Ecol. Indic. 30 (2013) 72–79]. *Ecological Indicators*, 34:649.

Trevorrow, M. V. (2003). Measurements of near-surface bubble plumes in the open ocean with implications for high-frequency sonar performance. *The Journal of the Acoustical Society of America*, 114(5):2672.

Trevorrow, M. V., Mackas, D. L., and Benfield, M. C. (2005). Comparison of multifrequency acoustic and in situ measurements of zooplankton abundances in Knight Inlet, British Columbia. *The Journal of the Acoustical Society of America*, 117(6):3574.

Trifonova, N. I., Scott, B. E., De Dominicis, M., Waggitt, J. J., and Wolf, J. (2021). Bayesian network modelling provides spatial and temporal understanding of ecosystem dynamics within shallow shelf seas. *Ecological Indicators*, 129(April):107997.

Truelove, N. K., Patin, N. V., Min, M., Pitz, K. J., Preston, C. M., Yamahara, K. M., Zhang, Y., Raanan, B. Y., Kieft, B., Hobson, B., Thompson, L. R., Goodwin, K. D., and Chavez, F. P. (2022). Expanding the temporal and spatial scales of environmental DNA research with autonomous sampling. *Environmental DNA*, 4(4):972–984.

Tsagarakis, K., Giannoulaki, Pyrounaki, M. M., and Machias, A. (2015). Species

identification of small pelagic fish schools by means of hydroacoustics in the Eastern Mediterranean Sea. *Mediterranean Marine Science*, 16(1):151–161.

Tsagarakis, K., Machias, A., Somarakis, S., Giannoulaki, M., Palialexis, A., and Valavanis, V. D. (2008). Habitat discrimination of juvenile sardines in the Aegean Sea using remotely sensed environmental data. *Hydrobiologia*, 612(1):215–223.

Tsagarakis, K., Pyrounaki, M. M., Giannoulaki, M., Somarakis, S., and Machias, A. (2012). Ontogenetic shift in the schooling behaviour of sardines, Sardina pilchardus. *Animal Behaviour*, 84(2):437–443.

Turrell, W. R. (1992). New hypotheses concerning the circulation of the northern North Sea and its relation to North Sea fish stock recruitment. *ICES Journal of Marine Science*, 49(1):107–123.

Turrell, W. R. (2019). Marine science within a net-zero emission statutory framework. *ICES Journal of Marine Science*, 76(7):1983–1993.

UK Government (2009). UK Offshore Energy Strategic Environmental Assessment. Future Leasing for Offshore Wind Farms and Licensing for Offshore Oil & Gas and Gas Storage. Technical report, Department of Energy and Climate Change, Aberdeen.

Uribe-Palomino, J., López, R., Gibbons, M. J., Gusmão, F., and Richardson, A. J. (2019). Siphonophores from surface waters of the Colombian Pacific Ocean. *Journal of the Marine Biological Association of the United Kingdom*, 99(1):67–80.

Urmy, S. S. and Benoit-Bird, K. J. (2021). Fear dynamically structures the ocean's pelagic zone. *Current Biology*, 31(22):5086–5092.e3.

Urmy, S. S. and De Robertis, A. (2021). Scalable, probabilistic echo inversion for multifrequency and broadband acoustic surveys.

Urmy, S. S., Horne, J. K., and Barbee, D. H. (2012). Measuring the vertical distributional variability of pelagic fauna in Monterey Bay. *ICES Journal of Marine Science*, 69(2):184–196.

Urmy, S. S. and Warren, J. D. (2019). Seasonal changes in the biomass, distribution, and patchiness of zooplankton and fish in four lakes in the Sierra Nevada, California. *Freshwater Biology*, 64(10):1692–1709.

Urmy, S. S., Williamson, C. E., Leach, T. H., Schladow, S. G., Overholt, E. P., and Warren, J. D. (2016). Vertical redistribution of zooplankton in an oligotrophic lake associated with reduction in ultraviolet radiation by wildfire smoke. *Geophysical Research Letters*, 43(8):3746–3753.

Uumati, M. (2013). *Acoustic investigations on bearded goby and jellyfish in the northern Benguela ecosystem*. PhD thesis, School of Biology.

van der Kooij, J., Fässler, S. M., Stephens, D., Readdy, L., Scott, B. E., and Roel, B. A. (2016). Opportunistically recorded acoustic data support Northeast Atlantic mackerel expansion theory. *ICES Journal of Marine Science*, 73(4):1115–1126.

Van Der Kooij, J., Scott, B. E., and Mackinson, S. (2008). The effects of environmental factors on daytime sandeel distribution and abundance on the Dogger Bank. *Journal of Sea Research*, 60(3):201–209.

van der Molen, J. and Pätsch, J. (2022a). An overview of Atlantic forcing of the North Sea with focus on oceanography and biogeochemistry. *Journal of Sea Research*, 189(September):102281.

van der Molen, J. and Pätsch, J. (2022b). An overview of Atlantic forcing of the North Sea with focus on oceanography and biogeochemistry. *Journal of Sea Research*, 189(September):102281.

Van Leeuwen, S., Tett, P., Mills, D., and Van Der Molen, J. (2015). Stratified and nonstratified areas in the North Sea: Long-term variability and biological and policy implications. *Journal of Geophysical Research: Oceans*, 120(7):4670–4686.

Verfuss, U. K., Aniceto, A. S., Harris, D. V., Gillespie, D., Fielding, S., Jiménez, G., Johnston, P., Sinclair, R. R., Sivertsen, A., Solbø, S. A., Storvold, R., Biuw, M., and Wyatt, R. (2019). A review of unmanned vehicles for the detection and monitoring of marine fauna. *Marine Pollution Bulletin*, 140:17–29.

Vestheim, H. and Kaartvedt, S. (2006). Plasticity in coloration as an antipredator strategy among zooplankton. *Limnology and Oceanography*, 51(4):1931–1934.

Visser, A. W., Saito, H., Saiz, E., and Kiørboe, T. (2001). Observations of copepod feeding and vertical distribution under natural turbulent conditions in the North Sea. *Marine Biology*, 138(5):1011–1019.

Visser, A. W. and Stips, A. (2002). Turbulence and zooplankton production: Insights from PROVESS. *Journal of Sea Research*, 47(3-4):317–329.

Walday, M. and Kroglund, T. (2002). Europe's biodiversity. Technical report, European Environment Agency.

Wallace, M. I., Cottier, F. R., Berge, J., Tarling, G. A., Griffiths, C., and Brierley, A. S. (2010). Comparison of zooplankton vertical migration in an ice-free and a seasonally ice-covered Arctic fjord: An insight into the influence of sea ice cover on zooplankton behavior. *Limnology and Oceanography*, 55(2):831–845.

Wang, Y., Zhang, L., Ma, W., Wang, Y., Niu, W., Song, Y., and Wang, W. (2022). Ocean Plankton Biomass Estimation with a Digital Holographic Underwater Glider. *Journal of Marine Science and Engineering*, 10(9):1258.

Wanner, H., Brönnimann, S., Casty, C., Gyalistras, D., Luterbacher, J., Schmutz, C., Stephenson, D., , and Xoplaki, E. (2001). North Atlantic Oscillation – concepts and studies. *Surveys in Geophysics*, 22(4):321–382.

Ward, P. and Hirst, A. G. (2007). Oithona similis in a high latitude ecosystem: Abundance, distribution and temperature limitation of fecundity rates in a sac spawning copepod. *Marine Biology*, 151(3):1099–1110.

Warren, J. D., Stanton, T. K., Benfield, M. C., Wiebe, P. H., Chu, D., and Sutor, M. (2001). In situ measurements of acoustic target strengths of gas-bearing siphonophores. *ICES Journal of Marine Science*, 58(4):740–749.

Watkins, J. L. and Brierley, A. S. (2002). Verification of the acoustic techniques used to identify Antarctic krill. *ICES Journal of Marine Science*, 59(6):1326–1336.

Wehner, R. (2001). Polarization vision - A uniform sensory capacity? *Journal of Experimental Biology*, 204(14):2589–2596.

Weill, A., Scalabrin, C., and Diner, N. (1993). MOVIES-B: an acoustic detection description software. Application to shoal species' classification. *Aquatic Living Resources*, 6(3):255–267.

Wenz, G. M. (1962). Acoustic Ambient Noise in the Ocean: Spectra and Sources. *The Journal of the Acoustical Society of America*, 34(12):1936–1956.

Weston, K., Fernand, L., Mills, D. K., Delahunty, R., and Brown, J. (2005). Primary production in the deep chlorophyll maximum of the central North Sea. *Journal of Plankton Research*, 27(9):909–922.

Whitmore, B. M., Nickels, C. F., and Ohman, M. D. (2019). A comparison between Zooglider and shipboard net and acoustic mesozooplankton sensing systems. *Journal of Plankton Research*, 41(4):521–533.

Whitt, C., Pearlman, J., Polagye, B., Caimi, F., Muller-Karger, F., Copping, A., Spence, H., Madhusudhana, S., Kirkwood, W., Grosjean, L., Fiaz, B. M., Singh, S., Singh, S., Manalang, D., Gupta, A. S., Maguer, A., Buck, J. J., Marouchos, A., Atmanand, M. A., Venkatesan, R., Narayanaswamy, V., Testor, P., Douglas, E., de Halleux, S., and Khalsa, S. J. (2020). Future Vision for Autonomous Ocean Observations. *Frontiers in Marine Science*, 7(September).

Widmer, C. L., Fox, C. J., and Brierley, A. S. (2016). Effects of temperature and salinity on four species of northeastern Atlantic scyphistomae (Cnidaria: Scyphozoa). *Marine Ecology Progress Series*, 559:73–88.

Wiebe, P. H., Boyd, S. H., Davis, B. M., and Cox, J. L. (1982). Avoidance of towed nets by the euphausiid Nematoscelis megalops. *Fishery Bulletin*, 80(1):75–91.

Winther, N. G. and Johannessen, J. A. (2006). North Sea circulation: Atlantic inflow and its destination. *Journal of Geophysical Research: Oceans*, 111(12):1–12.

Wishner, K. F., Outram, D. M., Seibel, B. A., Daly, K. L., and Williams, R. L. (2013). Zooplankton in the eastern tropical north Pacific: Boundary effects of oxygen minimum

zone expansion. *Deep-Sea Research Part I: Oceanographic Research Papers*, 79(May 2022):122–140.

Wishner, K. F., Seibel, B. A., Roman, C., Deutsch, C., Outram, D., Shaw, C. T., Birk, M. A., Mislan, K. A., Adams, T. J., Moore, D., and Riley, S. (2018). Ocean deoxygenation and zooplankton: Very small oxygen differences matter. *Science Advances*, 4(12):1–9.

Wood, S. N. (2011). Fast stable restricted maximum likelihood and marginal likelihood estimation of semiparametric generalized linear models. *Journal of the Royal Statistical Society (B)*, 73(1):3–36.

Wood, S. N. (2017). *Generalized Additive Models An Introduction with R, Second Edition*. Chapman and Hall/CRC, New York, 2nd editio edition.

Yassir, A., Jai Andaloussi, S., Ouchetto, O., Mamza, K., and Serghini, M. (2023). Acoustic fish species identification using deep learning and machine learning algorithms: A systematic review. *Fisheries Research*, 266(July):106790.

Yin, M. C. and Blaxter, J. H. (1986). Morphological changes during growth and starvation of larval cod (Gadus morhua L.) and flounder (Platichthys flesus L.). *Journal of Experimental Marine Biology and Ecology*, 104(1-3):215–228.

Zhi, W., Shuli, Z., Jie, L., Yuefei, L., Yuguo, X., and Xinhui, L. (2021). Spatial autocorrelation and heterogeneity of fish resources in the Xijiang River, Pearl River Basin, China. *Indian Journal of Fisheries*, 68(3):38–43.

Zhou, G., Wang, J., Xu, W., Zhang, K., and Ma, Z. (2017). Polarization patterns of transmitted celestial light under wavy water surfaces. *Remote Sensing*, 9(4).

Zimmermann, F. and Werner, K. M. (2019). Improved management is the main driver behind recovery of Northeast Atlantic fish stocks. *Frontiers in Ecology and the Environment*, 17(2):93–99.

Zuur, A. F., Ieno, E. N., Walker, N. J., Saveliev, A. A., and Smith, G. M. (2009). *Mixed effects models and extensions in ecology with R*. Springer-Verlag, New York.

Zwolinski, J., Morais, A., Marques, V., Stratoudakis, Y., and Fernandes, P. G. (2007). Diel variation in the vertical distribution and schooling behaviour of sardine (Sardina pilchardus) off Portugal. *ICES Journal of Marine Science*, 64(5):963–972.

# A

# Effect of calibration temperature and salinity settings on range and TVG

## A.1 Purpose

It is common practice in fisheries acoustics to use constant temperature and salinity values to calibrate acoustic data, despite these variables typically varying in the ocean both horizontally and with depth. Acoustic surveys may span different oceanographic regimes both spatially, for example transects running from over the continental shelf to off-shelf oceanic regions or by sampling through different water masses with depth, and temporally, for example from times of year when the water column is well-mixed to periods of strong stratification.

Temperature and salinity values are required for calculating the speed of sound in water, $c$, and the absorption coefficient, $\alpha$, both relevant to the accuracy of acoustic data. The speed of sound impacts calculations of range, since range is defined as:

$$R = \frac{c\tau}{2} \tag{A.1.1}$$

where $R$ is the range (in $\mathrm{m}$) from the transducer, $c$ is the speed of sound (in $\mathrm{m\,s^{-1}}$), and $\tau$ is the pulse duration (in $\mathrm{s}$). Range accuracy subsequently impacts estimation of acoustic sampling volumes, including backscatter estimates ($S_v$), since volumes are scaled by the thickness (in range) of the region sampled. The absorption coefficient is used by the time-varied-gain (TVG) function which amplifies the signal with range. Temperature and salinity

therefore play an important role in the estimation of several key acoustic parameters.

This appendix investigates whether representative temperature and salinity depth profiles from representative periods at the start and end of the mission impact range estimation and gain required to compensate absorption as compared to constant values input in the calibration.

## A.2 Methods

Temperature and salinity depth profiles were obtained from the Seaglider 'Orca' SG510, which undertook the transect from two contrasting periods: $14^{th}$ to $15^{th}$ May 2018, shortly after the start of *Lyra's* mission; and $29^{th}$ to $30^{th}$ May 2018, towards the end of the mission. SG510 was equipped with an unpumped glider conductivity-temperature sail. Depth was calculated from pressure. Temperature and salinity depth sections were generated from approximately 80 profiles of the glider during each period (Figure A.2.1). Mean depth profiles were calculated for each variable for each period. Three cases were defined to test the effect of different temperature and salinity depth profiles on range offset and gain required to compensate absorption on the $200\,\mathrm{kHz}$ data. Since higher frequency sounds are absorbed more rapidly than lower frequencies, absorption coefficients were calculated for $200\,\mathrm{kHz}$ data only as this frequency would show greater variation, if any, than $70\,\mathrm{kHz}$. The three cases were:

- Case 1: Temperature of $8\,^{\circ}\mathrm{C}$ and salinity of 35 PSU, constant with depth, as per calibration of the ES70-18CD and ES200-7CD transducers
- Case 2: Mean temperature and salinity depth profiles obtained by SG510 from $14^{th}$ to $15^{th}$ May 2018
- Case 3: Mean temperature and salinity depth profiles obtained by SG510 from $29^{th}$ to $30^{th}$ May 2018

Sound speeds, $c$, and absorption coefficients, $\alpha$, were calculated for each case based on the formulae by Mackenzie (1981) and Francois and Garrison (1982) respectively, both

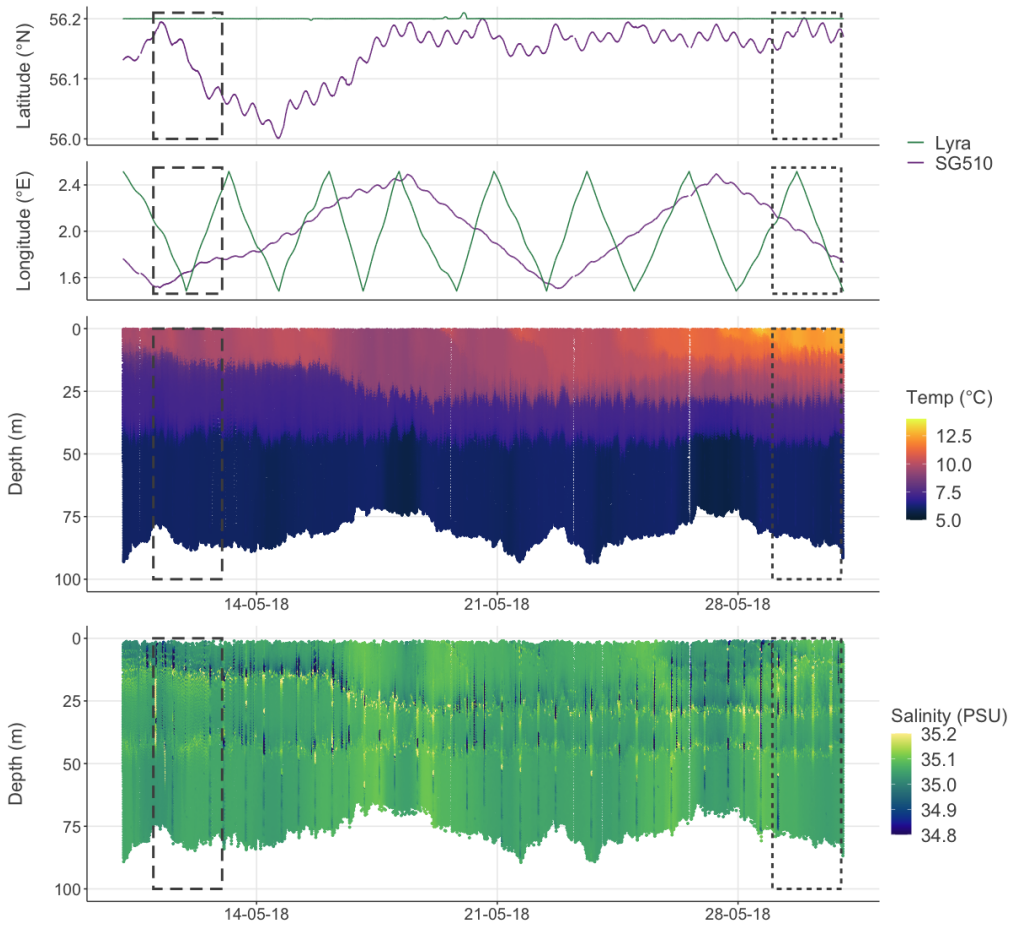


Figure A.2.1: **Position, temperature, and practical salinity measured by Seaglider SG510 together with Lyra's concurrent position.** Top plots a) and b) show proximity to *Lyra*, bottom plots c) and d) show temperature and salinity sections. Periods 1 and 2 are outlined by grey dashed and dotted boxes respectively.

implemented in *R* (R Core Team, 2022) using the *sonar* package (Gama, 2016). Effect on range was investigated by calculating range offset per metre of cases 2 and 3 as compared to case 1 along the propagation path to a maximum of $80\,\mathrm{m}$ range. Range per metre were calculated by taking the cumulative sum of the sound speed for each metre depth bin multiplied by the time taken to travel $1\,\mathrm{m}$ with a sound speed of $1482.41\,\mathrm{m\,s^{-1}}$ (i.e. $t = 6.75 \times 10^{-2}\,\mathrm{s}$) in order to compare with case 1. TVG curves were generated as per Subsection 1.3.3 using these absorption values, and gain offset (dB-difference) between the default case and cases 1 and 2 calculated in the logarithmic (i.e. decibel) domain.

## A.3 Results

### A.3.1 Temperature and salinity profiles

Mean temperature and salinity profiles for cases 2 and 3 both showed variation with depth, as well as variation between the two cases (Figure A.3.1). Cases 1 and 2 both suggest stratification in the upper $50\,\mathrm{m}$, the most salient features being two thermoclines. Surface temperatures rose and the thermocline deepened from approximately $18\,\mathrm{m}$ (case 2) to $30\,\mathrm{m}$ (case 3) over the course of the mission. The depth of the second thermocline appeared relatively constant throughout the mission, at approximately $40\,\mathrm{m}$, and water mean temperature below this feature appeared relatively stable with depth and time, remaining at $6\,^{\circ}\mathrm{C}$.

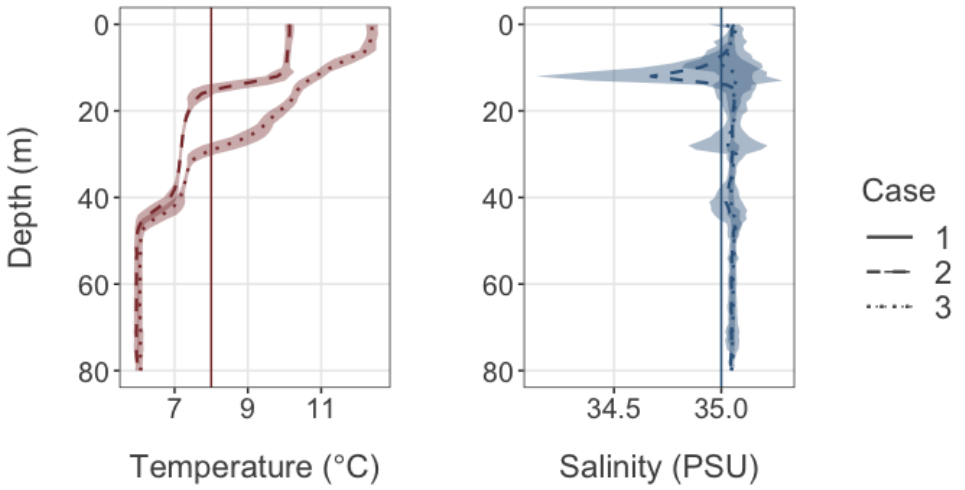


Figure A.3.1: **Mean temperature and salinity depth profiles from cases 1 (calibration constants, solid line), 2 (start of mission, dashed lines), and 3 (end of mission, dotted lines).** Shaded regions show mean $\pm$ standard deviation.

Temperature variability in the upper $50\,\mathrm{m}$ had a corresponding effect on sound speed profiles (Figure A.3.2). The echosounder was calibrated with a sound speed of $c = 1482.41\,\mathrm{m\,s^{-1}}$ (case 1), differing from minimum and maximum sound speeds from cases 2 and 3 by $-6.61\,\mathrm{m\,s^{-1}}$ at $51\,\mathrm{m}$ (case 3) and ($+15.79\,\mathrm{m\,s^{-1}}$) near the surface (case 3). In general, case 1 appeared to underestimate sound speeds near the surface and overestimate them below depths corresponding to the bottom of the first thermocline.

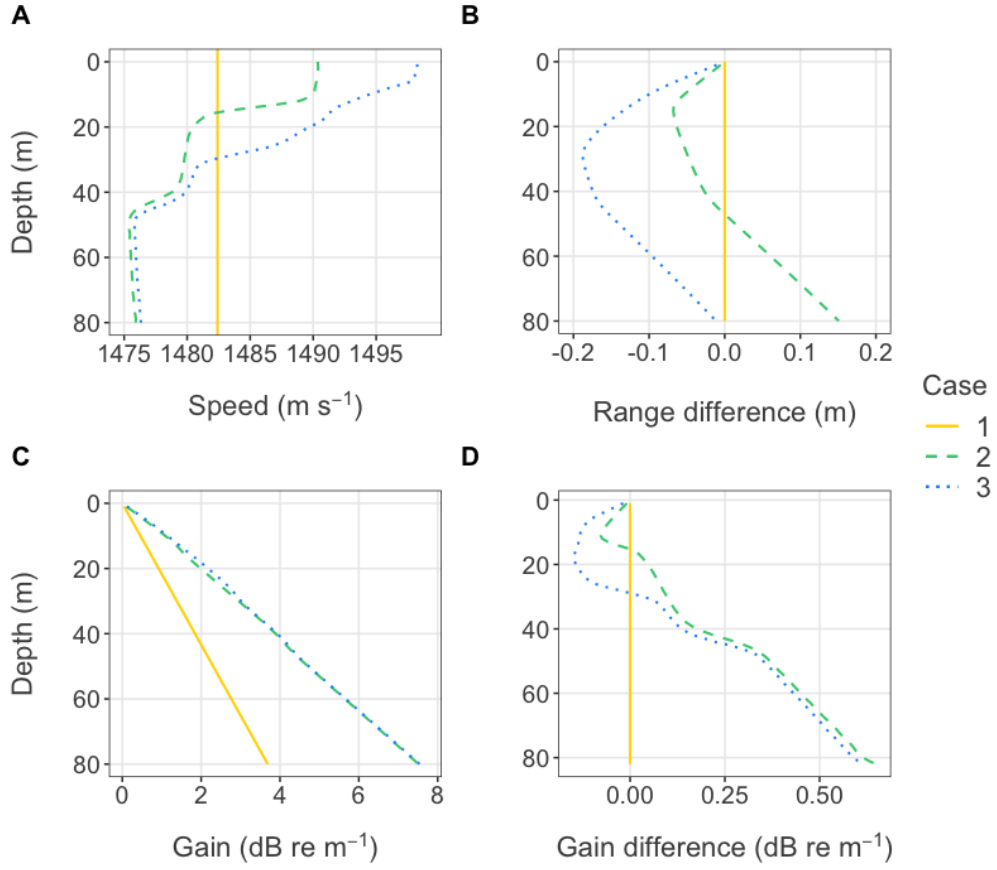


Figure A.3.2: **Depth profiles of acoustic-relevant parameters for cases 1 (calibration constants, dashed green line), 2 (start of mission, blue dot-dash line); and 3 (end of mission, solid yellow line).** A: Speed of sound in seawater, B: difference in range, as compared to case 1, C: gain (TVG) required to counteract absorption and spreading losses for 200 kHz, D: Difference in gain, as compared to case 1. Positive range difference indicates that cells extend further along the acoustic axis.

### A.3.2 Range offset

At the start of the mission, maximum range underestimation was less than 5 cm at the thermocline depth, with increasing overestimation below 40 m to a maximum offset of approximately 15 cm range offset by 80 m (Figure A.3.2). Range offset by the end of the mission led to a cumulative effect of underestimating range by 20 cm at approximately 30 m range (solid yellow line in B of Figure A.3.2). However, since range was overestimated at depths below the first thermocline, range calculations for cases 1) and 3) realigned at 80 m depth, the approximate maximum depth of the seabed whilst on transect. Therefore, although some distortion of range may have occurred in the water column, the bathymetry of the bottom obtained from the acoustics was likely accurate.

### A.3.3 Absorption and TVG

In general, absorption was increasingly overestimated with depth by case 1. These differences, together with the different sound speed profiles, had the impact of case 1 overestimating TVG at shallow depths (close range) and under-estimating TVG at depth (far ranges) when compared to both cases 2 and 3 (Figure A.3.2, C & D). TVG offset ranged between $-0.18\,\mathrm{dB}$ to $+0.6\,\mathrm{dB}$. Overestimation of TVG in the upper ocean was slightly more pronounced at the start of the mission than at the end. Maximum difference from case 1 occurred at the furthest range for both cases 2 and 3, with underestimation appearing not to vary temporally very much over the course of the mission.

## A.4 Discussion

During *Lyra's* mission, acoustic measurements were made over a period when the surface waters were undergoing stratification and deepening of the surface mixed layer. Temperature measurements taken by the seaglider indicated that the increase in surface temperatures changed gradually over the course of the mission, rising from below $8\,^{\circ}\mathrm{C}$ to over $12\,^{\circ}\mathrm{C}$ by the end of the mission. In contrast, temperatures below $40\,\mathrm{m}$ remained fairly constant over time, and salinity measurements varied over the course of the mission, however the coherence between salinity measurements at different depths and variability coinciding with changes in bathymetry and longitude suggest that salinity gradients occurred due to spatial heterogeneity, i.e. passage of the glider through different water masses.

Despite these changes in temperature and salinity, effects on range and TVG were minimal. Range offsets only reached a maximum of $\pm\ 0.2\,\mathrm{m}$. Discrepancies of this order might negatively impact the accuracy of fine-scale analyses of small single targets. However, for analyses where acoustic metrics are integrated over depth bins larger than range offsets (as presented in this thesis), the error is negligible. TVG offsets were within the range of $-0.6\,\mathrm{dB}$ to $0.2\,\mathrm{dB}$. These errors are small compared to the natural variability of target backscatter (e.g. zooplankton sound scattering layers). TVG offsets estimated here would largely only affect comparisons of backscatter at different depths, as the similarity of TVG curves for

cases 2 and 3 suggest little temporal or horizontal spatial difference. Depth- and time-varying temperature and salinity values had little impact on range and TVG. Therefore, constant values were deemed adequate for calibration during *Lyra's* mission. However, acoustic data which are collected over more diverse oceanographic conditions, higher frequencies, and larger ranges would be expected to show greater offsets. Such instances might therefore warrant use of variable temperature and salinity, particularly if the acoustic data are to be used for very fine-scale analyses.

Calibrating CTD sensors on gliders can be a complicated task. Cross-calibrations were conducted in the field, however they were infrequent. Glider temperature measurements often suffer from a thermal lag effect, thus inaccuracies may have been introduced into SG510's measurements. Furthermore, SG510 was not co-located with *Lyra*. The argument to keep nominal constants (case 1, $c = 1482.41\,\mathrm{m\,s^{-1}}$ and $\alpha = 0.023\,\mathrm{dB\,m^{-1}}$) therefore avoided introducing error from poorly calibrated or corrected CTD data.

# B

# Unfiltered 70 kHz backscatter echograms

Transect echograms of raw 70 kHz backscatter data from are shown in Figure B.0.1, Figure B.0.2 and Figure B.0.3. The first 2 m range have been excluded.

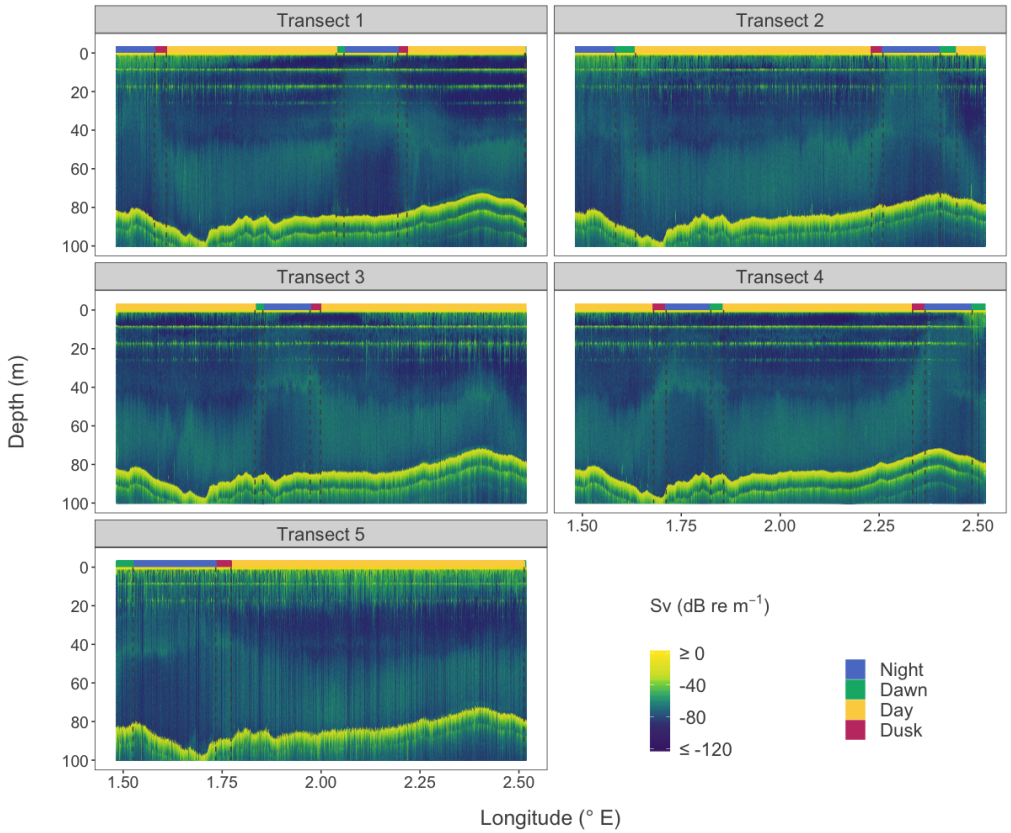


Figure B.0.1: **Raw 70 kHz volume backscatter echograms of Transects 1 to 5.** Time of day categorisation shown in the coloured strip at top, with transitions between each category demarcated with dashed grey lines across the echograms.

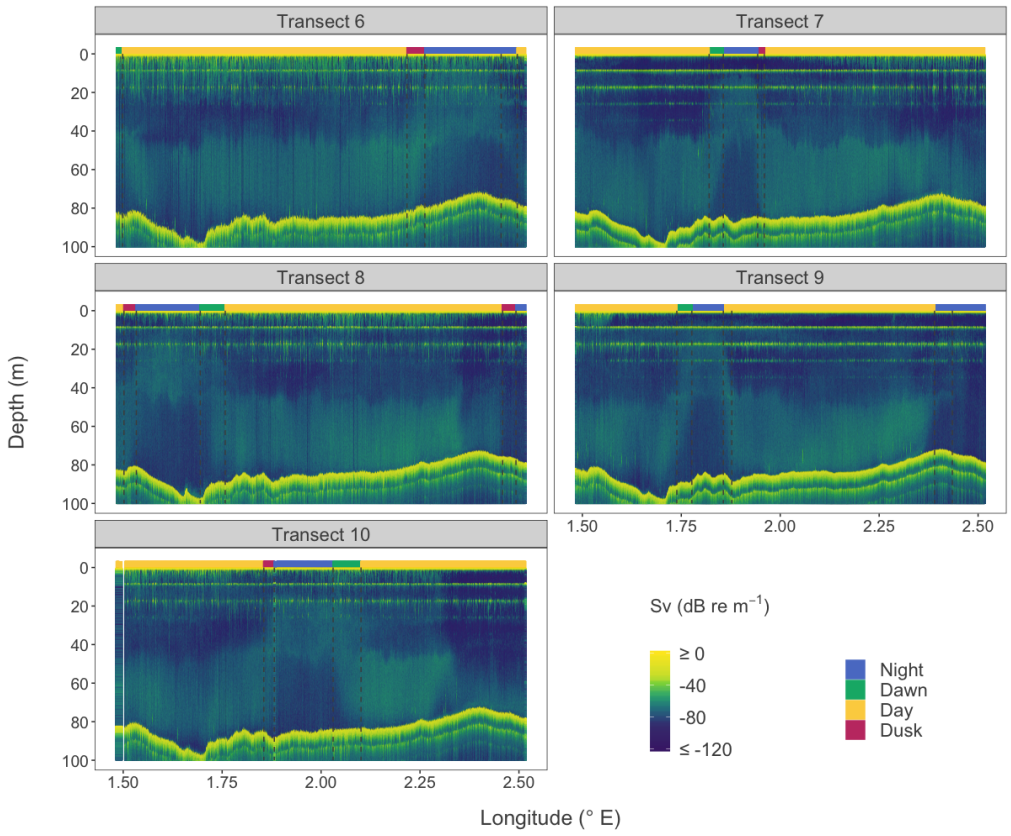


Figure B.0.2: **Raw 70 kHz volume backscatter echograms of Transects 6 to 10.** Time of day categorisation shown in the coloured strip at top, with transitions between each category demarcated with dashed grey lines across the echograms.

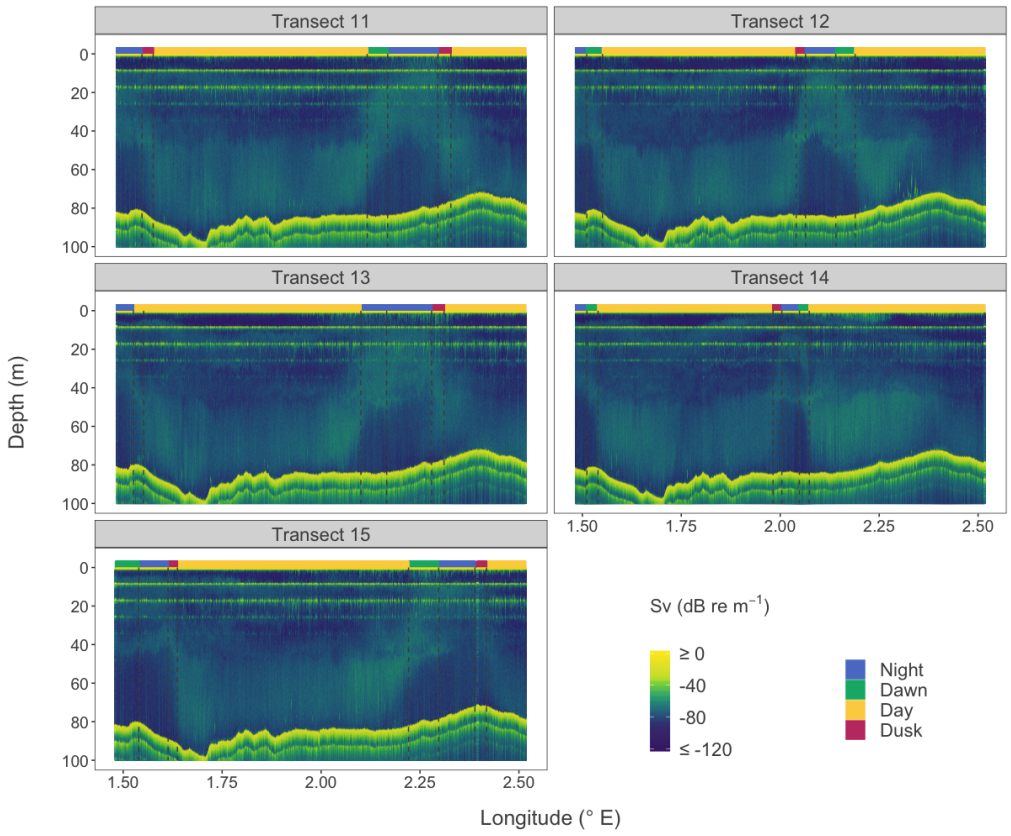


Figure B.0.3: **Raw 70 kHz volume backscatter echograms of Transects 11 to 15.** Time of day categorisation shown in the coloured strip at top, with transitions between each category demarcated with dashed grey lines across the echograms.

# C

# LCAS and LCTN sensitivity analyses

## C.1 Introduction

Data quality issues such as transient noise and attenuation are highly individual and idiosyncratic, with factors such as platform, environmental conditions, and the choice of target organism all affecting how acoustic data are best cleaned. There are complex and contrasting ways that filter design can bias results of data cleaning, warranting careful examination of each dataset to determine the characteristics of transient noise and attenuation if present, and sensitivity analyses to underpin parameter choices in order to optimise the filter for each application. Here I assess the sensitivity of results to the choice of convolution kernel widths and thresholds.

The local convolution filters, LCAS and LCTN, compare cell backscattering strengths to neighbouring values in order to detect sharp increases or decreases in backscattering strength that are indicative of short-lived attenuation and transient noise. The kernel is an $n$x1 matrix which is convolved with ping median backscatter values (cells) from the SB layer (seabed). Kernel weighting describes the degree to which neighbouring cell values affect the results of the convolution to which the central cell value is compared. Equally-weighted kernels, except for the central cell, were used in all cases (see Equation 2.2.1 for an example of a 9x1 kernel). The width, $n$, of the convolution kernel determines how many neighbouring pings each cell is compared to. Thresholds determine whether the difference between cells and the mean of neighbouring values (derived from the convolution process) is great enough to indicate that the ping was affected by either attenuation or transient noise and marked as AS

or TN respectively.

Efficient filters should minimise false positive and false negative detections. False positives are likely to increase with stricter (lower) thresholds, as more of the natural variability in the application layer (here, the seabed) can increase false detections. Any technique that relies on detecting a distinct change in power or its derivatives - whether by human eye or computer - is subject to two problems: 1) it is more difficult to detect true changes in backscatter amongst a patchy, or 'noisy' background, especially when changes in signal strength are smaller than background variance. This has implications for where filters are best applied. Application to water column data can result in mistaken detection of patchy target biology which could lower biomass and abundance estimates, and the patchiness (background contrast) of backscatter has the ability to impact filter efficacy. When the LCTN was applied to the water column layer I found that time of day affected detections; more detections were made during the daytime because biota in the main SSL migrated into the analysis layer used, increasing the background patchiness and thus reducing contrast. Using data from the seabed as the application layer reduced the likelihood of false positives biasing the filter detections, since the correlation between the seabed and water column layers was low during calm weather.

Filters with very narrow kernels can also be prone to increased rates of false positives, should the layer be particularly variable over a very fine scale, and cells within the kernel are not representative of the variability of unaffected cells. Very wide kernels can also be problematic, however, as cells are compared to values from distant neighbours where conditions might have changed (e.g. different seabed substrate, time of day). Wide kernels can therefore exacerbate the problem of false negatives. False negatives may also increase during periods marked by very frequent attenuation or transient noise, as representative values from neighbouring cells may be artificially low or high. The efficacy of filters using different kernel widths is sensitive to the temporal frequency of attenuation or transient noise itself, and visual assessment of echograms is recommended to find a reasonable set of kernel widths upon which to perform sensitivity analyses. Similarly, assessment of backscatter variability within the application layer is advised in order to get an approximate understanding of the range of values within which the underlying backscatter distribution might reside,

enabling the selection of an appropriate set of thresholds for sensitivity analyses based on this. Individual datasets (or even different backscattering regimes within the same dataset) warrant careful examination to 1) understand the characteristics of presenting transient noise and attenuation, 2) select an appropriate region of the data for filter application, and 3) conduct sensitivity analyses to select a suitable kernel and threshold.

## C.2 Methods

These sensitivity analyses tested a range of different kernel widths and thresholds used in the LCAS and LCTN filters, following the method outlined in Subsection 2.2.4. Filters were applied using thresholds $\delta \in \mathbb{N}, 1 \leq \delta \leq 8$, and $n$x1 kernels for $n \in$ 3, 5, 7, 9, 31, 61, 121, 361, 721, 1441 such that each kernel window compared the central ping to the median of $k = \frac{1}{2}(n-1)$ pings either side of it. Kernel windows spanned the equivalent of 30 seconds, 50 seconds, 70 seconds, 1.5 minutes, 5 minutes, 10 minutes, 20 minutes, 1 hour, 2 hours and 4 hours respectively. Cells with Sv-difference values that exceeded the thresholds, satisfying Equation C.2.2 or Equation C.2.3, were marked as 'AS' (attenuated signal) or 'TN' (affected by transient noise) respectively.

Sensitivity analyses were first undertaken for the LCAS, then the LCTN, as per the order of filter application used in Section 2.2. Local convolution filters for each kernel and threshold combination were applied to the subset of all resampled pings within each layer, except for the pings:

- designated as AS by the local seabed reference attenuation (SRAS) filter with a threshold of $\delta = -3\,\mathrm{dB}$, for the LCAS sensitivity analyses
- designated as AS by either the SRAS ($\delta = -3\,\mathrm{dB}$) or the LCAS ($\delta = -6\,\mathrm{dB}$, 9x1 kernel), for the LCTN sensitivity analyses

To evaluate the impact of each filter, the difference made to mean and median average backscatter across the entire mission was calculated by subtracting values in the linear

domain. The proportions of AS and TN pings for each wind category were also calculated.

$$K_{7\text{x}1} = \begin{bmatrix} 1 & 1 & 1 & 0 & 1 & 1 & 1 \end{bmatrix} \tag{C.2.1}$$

$$S_{vi} < 10log_{10} \left( \frac{\left( \sum_{j=-k}^{k} s_{vi+j} \right) - s_{vi}}{2k} \right) + \delta \tag{C.2.2}$$

$$S_{vi} > 10log_{10} \left( \frac{\left( \sum_{j=-k}^{k} s_{vi+j} \right) - s_{vi}}{2k} \right) + \delta \tag{C.2.3}$$

where $s_{vi} = 10^{\frac{S_{vi}}{10}}$ is the linear volume backscattering coefficient of cell $i$, $\delta$ is the threshold in $\mathrm{dB}$, and $k$ is such that $n = 2k + 1$ denotes a kernel of size $n$x1.

## C.3 Results

Almost all kernel and threshold combinations had the effect of increasing (LCAS) and decreasing (LCTN) mean and median $S_v$ across the whole mission in both the Seabed and Water Column layers (Figure C.3.1). Some small increases ($< 0.002\,\mathrm{dB}$) in mean and median $S_v$ were observed in the water column after application of the LCAS with thresholds $\geq 4\,\mathrm{dB}$ and small kernels. Similarly, small decreases in median $S_v$ in the water column were observed after application of the LCTN with mostly a selection of smaller kernels and all thresholds, save for $1\,\mathrm{dB}$.

Kernel size had only a small effect on mission-wide changes in mean and median Sv for LCAS and LCTN filters applied to the WC and SB layers (Figure C.3.1). This effect was amplified with stricter thresholds, where the difference between average $S_v$ after filtering with the smallest and largest kernels (3x1 30 second window and 1441 x 1 4 hour

window) was at most $2.2\,\mathrm{dB}$ (Table C.1). The pattern of larger kernels having a greater impact held for all filter-metric combinations, except for the impact of the LCTN on median $S_v$ which seemed largely insensitive to kernel size for all thresholds tested.

Table C.1: **Decibel span of impacts on mean and median backscatter in the SB and WC layers after appying the LCAS and LCTN filters with thresholds of** $1\,\mathrm{dB}$**.** The range provides a measure of the sensitivity of each metric to kernel size for the strictest threshold tested, where the greatest impact of kernel was observed. Entries in descending order of span.

| **Filter (layer)** | **Metric** | **Span (dB)** |
|---|---|---|
| LCAS (WC) | Median | 2.02 |
| LCAS (WC) | Mean | 1.34 |
| LCTN (WC) | Mean | 1.13 |
| LCTN (WC) | Median | 0.85 |
| LCAS (SB) | Median | 0.6 |
| LCAS (SB) | Mean | 0.41 |
| LCTN (SB) | Mean | 0.22 |
| LCTN (SB) | Median | 0.06 |

Decreasing the thresholds (i.e. making them stricter) had the effect of increasing and decreasing the mean and median backscatter over the mission for the LCTN and LCAS respectively, for all kernels tested. Changes were gradual, but mean and median statistics began to noticeably decrease at $4\,\mathrm{dB}$ for the LCTN, and increase at $6\,\mathrm{dB}$ for the LCAS.

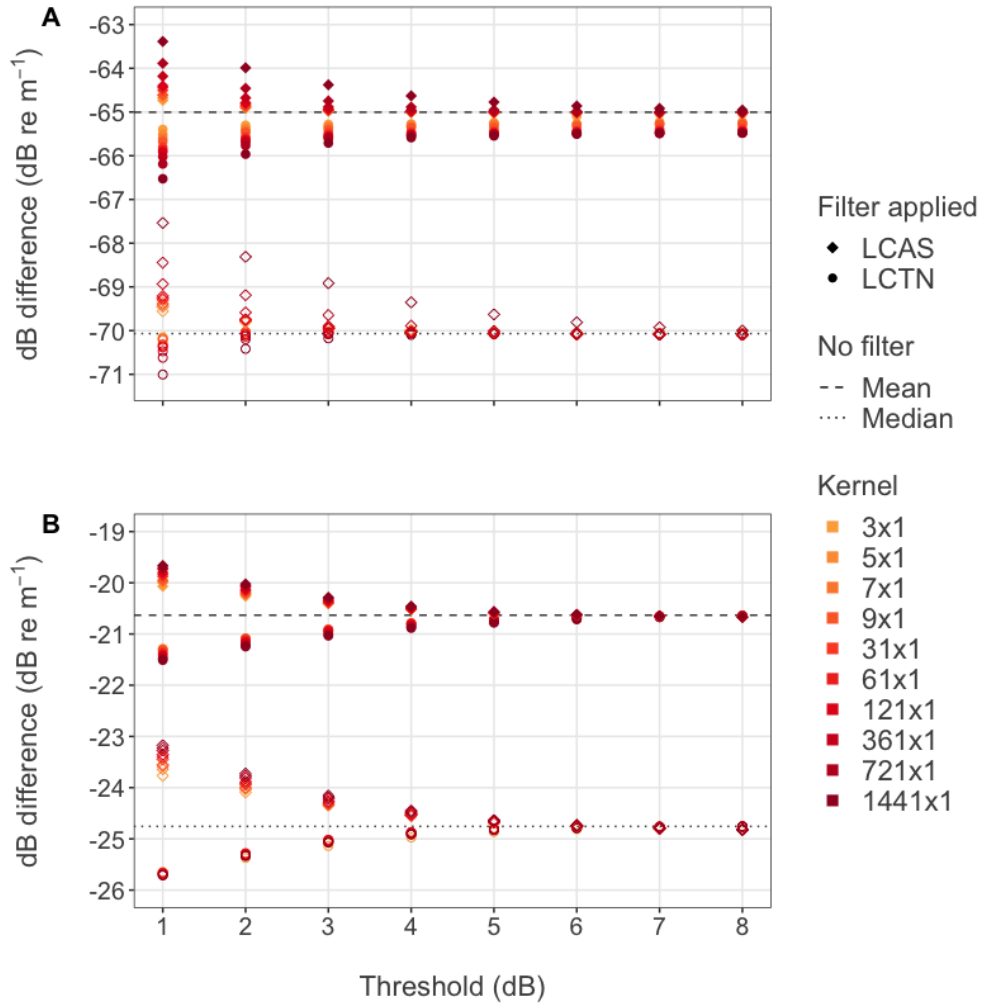


Figure C.3.1: **Effects of different kernel-threshold combinations on average backscatter across the mission**. Mean (filled shapes) and median (hollow shapes) average backscatter after applying the LCAS (circle) and LCTN (diamond) filters on the A) Water Column and B) Seabed layers. Mean and median backscattering strengths for each unfiltered layer are shown by dashed and dotted lines respectively.

## C.4 Discussion

Several candidate kernels performed similarly. The 9x1 kernel performed adequately with mid-range effects on average $S_v$ across M1. It was felt that comparing values within a 90-second window would provide enough pings for comparison (four each side) and those pings would not be so distant as to be potentially less representative of the underlying backscatter, and therefore the 9x1 kernel was selected for both LCAS and LCTN.

The SRAS filter had already been applied with a strict threshold of 3 dB to identify pings

with median $S_v$ outside the range during calm weather which were affected by attenuation. It was therefore felt that a less strict threshold of $6\,\mathrm{dB}$ was more appropriate for the LCAS, and this coincided with noticeable changes in mean and median backscatter across the mission. This relatively relaxed threshold potentially meant that fewer false positive detections were made, reducing the amount of good data excluded by the filter.

# D

# Seabed and Water Column layer Sv-difference correlations

---

Tables of correlation test statistics given below for unfiltered data (Table D.1) and following application of filters (SRAS, Table D.2; LCAS, Table D.3; SRAS and LCAS Table D.4; LCTN Table D.5; and SRAS, LCAS and LCTN Table D.6).

Table D.1: **Spearman's correlation coefficients for SB and WC Sv-differences of unfiltered data, per $1\ \mathrm{m\ s^{-1}}$ wind speed interval.**

| Wind speed ($\mathrm{m\,s^{-1}}$) | Spearman's $\rho$ | *P* value | S statistic |
|---|---|---|---|
| [0-1) | 0.04 | 0.17 | 426456690 |
| [1-2) | -0.03 | 0.05 | 35313105532 |
| [2-3) | -0.02 | 0.01 | 513627433356 |
| [3-4) | -0.01 | 0.03 | 1712729620104 |
| [4-5) | 0.01 | 0.05 | 3198955129868 |
| [5-6) | 0.04 | $< 0.001$ | 2568812096304 |
| [6-7) | 0.10 | $< 0.001$ | 2584875997980 |
| [7-8) | 0.17 | $< 0.001$ | 1191191233442 |
| [8-9) | 0.26 | $< 0.001$ | 346271359802 |
| [9-10) | 0.36 | $< 0.001$ | 85277486446 |
| [10-11) | 0.48 | $< 0.001$ | 13290858464 |
| [11-12) | 0.58 | $< 0.001$ | 3356444146 |
| [12-13) | 0.64 | $< 0.001$ | 544034480 |
| [13-14) | 0.71 | $< 0.001$ | 120162292 |
| [14-15) | 0.72 | $< 0.001$ | 20596832 |
| [15-16) | 0.74 | $< 0.001$ | 4347282 |
| [16-17) | 0.73 | $< 0.001$ | 419624 |
| [17-18) | 0.73 | $< 0.001$ | 58728 |
| [18-19) | 0.73 | $< 0.001$ | 2118 |
| [19-20) | 0.95 | $< 0.001$ | 12 |
| [20-21) | 1.00 | 0.02 | 2 |
| [21-22) | -1.00 | 1.00 | 2 |

Table D.2: **Spearman's correlation coefficients for SB and WC Sv-differences after application of the SRAS filter, per $1\ \mathrm{m\ s^{-1}}$ wind speed interval.**

| Wind speed ($\mathrm{m\,s^{-1}}$) | Spearman's $\rho$ | *P* value | S statistic |
|---|---|---|---|
| [0-1) | 0.04 | 0.17 | 426527516 |
| [1-2) | -0.03 | 0.05 | 35217753948 |
| [2-3) | -0.02 | 0.01 | 513264937220 |
| [3-4) | -0.02 | 0.03 | 1711217894888 |
| [4-5) | 0.01 | 0.05 | 3193914212060 |
| [5-6) | 0.04 | $< 0.001$ | 2567119074952 |
| [6-7) | 0.10 | $< 0.001$ | 2579593426880 |
| [7-8) | 0.15 | $< 0.001$ | 1191176537016 |
| [8-9) | 0.22 | $< 0.001$ | 347159723488 |
| [9-10) | 0.30 | $< 0.001$ | 86368988846 |
| [10-11) | 0.40 | $< 0.001$ | 13460197728 |
| [11-12) | 0.47 | $< 0.001$ | 3450983606 |
| [12-13) | 0.54 | $< 0.001$ | 540374258 |
| [13-14) | 0.58 | $< 0.001$ | 120271350 |
| [14-15) | 0.61 | $< 0.001$ | 19596370 |
| [15-16) | 0.60 | $< 0.001$ | 4288748 |
| [16-17) | 0.52 | $< 0.001$ | 390050 |
| [17-18) | 0.60 | $< 0.001$ | 55392 |
| [18-19) | 0.55 | $< 0.001$ | 2016 |
| [19-20) | 0.38 | 0.36 | 52 |
| [20-21) | 0.80 | 0.33 | 2 |
| [21-22) | -1.00 | 1.00 | 2 |

Table D.3: **Spearman's correlation coefficients for SB and WC Sv-differences after application of the LCAS filter, per 1 $\mathrm{m\,s^{-1}}$ wind speed interval.**

| Wind speed ($\mathrm{m\,s^{-1}}$) | Spearman's $\rho$ | *P* value | S statistic |
|---|---|---|---|
| [0-1) | 0.02 | 0.41 | 397351206 |
| [1-2) | -0.03 | 0.02 | 34598820964 |
| [2-3) | -0.02 | 0.01 | 504619347754 |
| [3-4) | -0.02 | 0.02 | 1688223721442 |
| [4-5) | 0.01 | 0.05 | 3140070761246 |
| [5-6) | 0.04 | $< 0.001$ | 2496798968392 |
| [6-7) | 0.09 | $< 0.001$ | 2493612008280 |
| [7-8) | 0.14 | $< 0.001$ | 1126887071218 |
| [8-9) | 0.21 | $< 0.001$ | 331272976408 |
| [9-10) | 0.30 | $< 0.001$ | 82687274588 |
| [10-11) | 0.43 | $< 0.001$ | 12743448742 |
| [11-12) | 0.51 | $< 0.001$ | 3292247662 |
| [12-13) | 0.59 | $< 0.001$ | 510905576 |
| [13-14) | 0.65 | $< 0.001$ | 113520648 |
| [14-15) | 0.69 | $< 0.001$ | 18566694 |
| [15-16) | 0.69 | $< 0.001$ | 4155452 |
| [16-17) | 0.71 | $< 0.001$ | 360606 |
| [17-18) | 0.73 | $< 0.001$ | 51348 |
| [18-19) | 0.71 | $< 0.001$ | 2044 |
| [19-20) | 0.85 | $< 0.01$ | 34 |
| [20-21) | 1.00 | 0.08 | 0 |
| [21-22) | -1.00 | 1.00 | 2 |

Table D.4: **Spearman's correlation coefficients of SB and WC Sv-differences after application of the SRAS and LCAS filters, per $1\ \mathrm{m\ s^{-1}}$ wind speed interval.**

| Wind speed ($\mathrm{m\,s^{-1}}$) | Spearman's $\rho$ | $P$ value | S statistic |
|---|---|---|---|
| [0-1) | 0.02 | 0.41 | 397381298 |
| [1-2) | -0.03 | 0.02 | 34495138352 |
| [2-3) | -0.02 | 0.01 | 504321629634 |
| [3-4) | -0.02 | 0.01 | 1686875120026 |
| [4-5) | 0.01 | 0.05 | 3135307377720 |
| [5-6) | 0.03 | $< 0.001$ | 2495550428046 |
| [6-7) | 0.08 | $< 0.001$ | 2488882276204 |
| [7-8) | 0.12 | $< 0.001$ | 1127168773384 |
| [8-9) | 0.18 | $< 0.001$ | 332276647416 |
| [9-10) | 0.24 | $< 0.001$ | 83814702942 |
| [10-11) | 0.32 | $< 0.001$ | 12998571530 |
| [11-12) | 0.37 | $< 0.001$ | 3397297018 |
| [12-13) | 0.46 | $< 0.001$ | 516428724 |
| [13-14) | 0.47 | $< 0.001$ | 118891858 |
| [14-15) | 0.54 | $< 0.001$ | 17998140 |
| [15-16) | 0.48 | $< 0.001$ | 4248742 |
| [16-17) | 0.43 | $< 0.001$ | 355728 |
| [17-18) | 0.54 | $< 0.001$ | 53508 |
| [18-19) | 0.57 | $< 0.01$ | 1740 |
| [19-20) | 0.21 | 0.62 | 66 |
| [20-21) | 0.50 | 1.00 | 2 |
| [21-22) | -1.00 | 1.00 | 2 |

Table D.5: **Spearman's correlation coefficients for SB and WC Sv-differences after application of the LCTN filter, per $1\ \mathrm{m\ s^{-1}}$ wind speed interval.**

| Wind speed ($\mathrm{m\,s^{-1}}$) | Spearman's $\rho$ | *P* value | S statistic |
|---|---|---|---|
| [0-1) | 0.02 | 0.45 | 387423872 |
| [1-2) | -0.03 | 0.05 | 33133590656 |
| [2-3) | -0.02 | 0.01 | 481171809240 |
| [3-4) | -0.01 | 0.07 | 1596532277692 |
| [4-5) | 0.01 | 0.32 | 3000641676586 |
| [5-6) | 0.04 | $< 0.001$ | 2376561059994 |
| [6-7) | 0.10 | $< 0.001$ | 2376466089730 |
| [7-8) | 0.17 | $< 0.001$ | 1093976443802 |
| [8-9) | 0.26 | $< 0.001$ | 310050216402 |
| [9-10) | 0.35 | $< 0.001$ | 78989837432 |
| [10-11) | 0.48 | $< 0.001$ | 12133171690 |
| [11-12) | 0.57 | $< 0.001$ | 3121407812 |
| [12-13) | 0.63 | $< 0.001$ | 510927716 |
| [13-14) | 0.71 | $< 0.001$ | 107921330 |
| [14-15) | 0.73 | $< 0.001$ | 17710244 |
| [15-16) | 0.74 | $< 0.001$ | 3775090 |
| [16-17) | 0.73 | $< 0.001$ | 372352 |
| [17-18) | 0.73 | $< 0.001$ | 54112 |
| [18-19) | 0.74 | $< 0.001$ | 1730 |
| [19-20) | 0.92 | $< 0.001$ | 18 |
| [20-21) | 0.90 | 0.08 | 2 |
| [21-22) | -1.00 | 1.00 | 2 |

Table D.6: **Spearman's correlation coefficients for SB and WC Sv-differences after application of the SRAS, LCAS, and LCTN filters, per 1 $\mathrm{m\,s^{-1}}$ wind speed interval.**

| Wind speed ($\mathrm{m\,s^{-1}}$) | Spearman's $\rho$ | *P* value | S statistic |
|---|---|---|---|
| [0-1) | 0.02 | 0.54 | 355775140 |
| [1-2) | -0.03 | 0.05 | 32254240392 |
| [2-3) | -0.02 | 0.01 | 472754047752 |
| [3-4) | -0.01 | 0.05 | 1569894565844 |
| [4-5) | 0.01 | 0.37 | 2940349119002 |
| [5-6) | 0.03 | $< 0.001$ | 2303574781266 |
| [6-7) | 0.07 | $< 0.001$ | 2287808103790 |
| [7-8) | 0.12 | $< 0.001$ | 1035156197128 |
| [8-9) | 0.17 | $< 0.001$ | 298176543712 |
| [9-10) | 0.22 | $< 0.001$ | 77792479954 |
| [10-11) | 0.31 | $< 0.001$ | 11971620186 |
| [11-12) | 0.35 | $< 0.001$ | 3133755942 |
| [12-13) | 0.43 | $< 0.001$ | 492062638 |
| [13-14) | 0.47 | $< 0.001$ | 106380014 |
| [14-15) | 0.53 | $< 0.001$ | 15599372 |
| [15-16) | 0.45 | $< 0.001$ | 3636840 |
| [16-17) | 0.41 | $< 0.001$ | 312906 |
| [17-18) | 0.52 | $< 0.001$ | 51062 |
| [18-19) | 0.54 | $< 0.01$ | 1502 |
| [19-20) | 0.45 | 0.27 | 46 |
| [20-21) | 0.50 | 1.00 | 2 |
| [21-22) | -1.00 | 1.00 | 2 |

# E

# Cleaning the 200 kHz data

---

The 200 kHz backscatter data did not appear to be affected badly by attenuation or transient noise, and no background or impulse noise was evident. Seabed and water column Sv-difference correlation values remained low, regardless of wind speed, and neither seabed nor water column backscatter showed any strong pattern with wind speed. Data cleaning procedures used for the 70 kHz data, outlined in Chapter 2, did not have any appreciable effect on correlation values even when strict thresholds were set and a relatively large proportion of pings was removed. Consequently, I decided not to apply data cleaning filters to the narrowband 200 kHz data, and instead countered any effects of short-lived attenuation or noise in the dataset by applying a median filter.

Visual inspection of the echograms corroborated the idea that the 200 kHz backscatter data was relatively clean. This was somewhat surprising, since the two transducers were co-located and subject to very similar conditions. Other factors that might have resulted in different impacts on data quality include TVG amplification, transducer design, and the distribution of bubble sizes and frequency spectra of crashing waves. Amplification by TVG would, all things being equal, result in more severe transient noise for the higher frequency transducer; however the opposite was observed. A more likely explanation is that differences in beam width and receiver size of the transducers affected their propensity to suffer from noise and attenuation. The 70 kHz had a much wider beam angle (18°) compared to the 70 kHz (7°); narrower acoustic beams are generally thought to have better signal-to-noise ratios and suffer less from side lobe interference.

# F

# Threshold sensitivity analysis for fish school detections

## F.1 Purpose

Fish schools are commonly detected in acoustic backscatter data using the SHAPES algorithm (Coetzee, 2000) and verified by targeted fishing. The SHAPES algorithm identifies contiguous regions of backscatter above a minimum threshold which meet specified morphological constraints. The threshold ideally screens out contiguous regions of background backscatter that could otherwise be erroneously identified as fish schools (Coetzee, 2000). However, when background or non-fish school backscattering strength is high, thresholding can result in a trade-off between excluding strong contiguous patches of backscatter from non-fish sources and retaining fish school backscatter. Dense aggregations of gas-filled zooplankton may scatter as strongly as some fish schools, rendering complete separation by thresholding alone impossible. To ensure accurate detections of fish schools, a threshold which optimises the trade-off between maximising detection of fish schools and minimising inclusion of backscatter from other sources must be established.

Mean volume backscattering strength (MVBS) of fish schools depends on many biological factors: school composition; fish packing density; behaviour (particularly orientation of fish); demography; and physiology (Fässler et al., 2007; Tsagarakis et al., 2012; Huse and Korneliussen, 2000). Therefore, optimal threshold selection can be species-, region- and timing-specific. Reasons for the choice of thresholds used in published studies are not

always provided, with the decision often being made subjectively following visual scrutiny of echograms (Brautaset et al., 2020).

Thresholds used to aid detection of swim-bladdered fish schools are most commonly applied to $38\,\mathrm{kHz}$ data. Values typically range from $-55\,\mathrm{dB}$ to $-70\,\mathrm{dB}$, although some are not explicitly stated (e.g. Haralabous and Georgakarakos, 1996). Korneliussen et al. (2009) used a threshold of $-60\,\mathrm{dB}$ to detect schools of capelin in the Barents Sea. Coetzee (2000) used a threshold equivalent to $-66\,\mathrm{dB}$ for detecting sardine schools. Schools of pollock in the Bering Sea were distinguished using a threshold of $-55\,\mathrm{dB}$ by Swartzman et al. (1994). Herring schools can reach backscattering strengths of over $-45\,\mathrm{dB}$ at $38\,\mathrm{kHz}$, though a threshold of $-60\,\mathrm{dB}$ has been suggested as sufficient for their detection (Beare et al., 2002b).

Multifrequency techniques such as dB-differencing can help to distinguish between taxonomical groups, for example between fish schools and zooplankton, and between schools of different fish species (Martin et al., 1996; Kang et al., 2002; Kloser et al., 2002). However, where co-occurring groups have similar acoustic properties, these techniques may be less effective. Multifrequency techniques alone were not capable of distinguishing between Atlantic herring (*Clupea harengus*) and Norwegian pout (*Trisopterus esmarkii*) in the North Sea (Fässler et al., 2007), or between horse mackerel, anchovy and sardine in the Central Mediterranean (D'Elia et al., 2014).

Thresholding and dB-differencing both consider the energetic properties of the signal, that is, the signal strength. Although by themselves energetic properties may have limited discriminatory power, reasonable success classifying schools to species level has been achieved by considering energetic properties in conjunction with other acoustic descriptors (Swartzman et al., 1994; Coetzee, 2000; Tsagarakis et al., 2015). Fish schools are dynamic in composition, structure, and dimension, in order to adapt to ever-changing predation, foraging, and environmental conditions (Massé et al., 1996; Tsagarakis et al., 2012). Despite this, morphometric descriptors of school size and shape have proven useful for species classifications in some regions (Korneliussen et al., 2009; Haralabous and Georgakarakos, 1996). Morphometric descriptors may include various aspects of fish school size (e.g. area, perimeter, length, height) and shape (e.g. elongation, the ratio between horizontal and vertical

lengths; fractal dimension, which evaluates the complexity of the boundary; rectangularity, ratio of the bounding box to the area; and circularity, a measure of roundness). Positional descriptors such as time, depth or height above the bottom, and geographic coordinates, can also aid discrimination for species with distinct habitat preferences and aggregation and movement behaviours (D'Elia et al., 2014; Lawson et al., 2001).

Energetic, morphological and positional descriptors derived from acoustic data have been used extensively to classify potential schools to various taxonomical levels. The set of descriptors which provide most discriminatory power varies from study to study. Korneliussen et al. (2009) found elongation useful to distinguish between monospecific schools of capelin and herring in Barents Sea, but other morphometric properties of schools (fractal dimension, rectangularity, circularity) did not improve discrimination, whereas Haralabous and Georgakarakos (1996) found rectangularity provided the most discriminatory power. In contrast, Campanella and Taylor (2016) and (Lawson et al., 2001) found morphometric descriptors contributed less than energetic descriptors. Other studies found bathymetric descriptors provided most discriminatory power (Tsagarakis et al., 2015; D'Elia et al., 2014; Lawson et al., 2001). Benoit-Bird and Waluk (2021) found energetic and morphometric descriptors crucial for distinguishing between fish schools and non-fish school aggregations, however time of day (a positional metric) was not. In general, the fewer species co-occur, the more likely classifications based on acoustic descriptors will perform reliably (Tsagarakis et al., 2015).

Morphological image processing filters are commonly applied prior to or after thresholding to enhance school boundaries, improving detection of fish schools and reducing the likelihood of detecting non-fish school aggregations. The use of morphological filters to delineate fish schools pre-dates the development of SHAPES and typically consists of an ordered process of erosion followed by dilation (Swartzman et al., 1994; Korneliussen et al., 2009; Brautaset et al., 2020). This process reduces diffuse scattering by erosion then fills small gaps by dilation, thus bolstering better connected clusters. These filters necessarily alter energetic properties of detected schools and distort morphometric features, thus affecting optimality of thresholds to some degree. In fact, various artefacts of data collection and processing can affect threshold optimality (Benoit-Bird and Waluk, 2021). Attenuation, noise, and

smoothing filters can artificially increase or decrease MVBS. Attenuation, noise, along-track resolution, and erosion and dilation filters can change the shape of schools as perceived in echograms. Since processing decisions can affect morphometric and energetic properties of fish schools, and relative target to background signal strengths are study- and region-dependent, thresholds stated in the literature cannot be applied *a priori*. Nevertheless, they offer a reasonable starting point for assessing a range of thresholds in sensitivity analyses.

Here, a suite of morphometric, energetic and bathymetric descriptors of clusters detected by SHAPES following application of thresholds ranging between $-55\,\mathrm{dB}$ and $-60\,\mathrm{dB}$ was examined. The aim was to identify a threshold which optimally distinguished clusters as being from fish school and non-fish school sources. Together with knowledge of behaviour of schooling fish in the North Sea and descriptions of the clusters, thresholds were assessed according to how well the clusters fitted the criteria set for the 'fish school' class: clusters of contiguous strong backscatter with well-defined boundaries that aligned with expected behavioural patterns of schooling fish in the North Sea.

## F.2 Methods

Table F.1: **Transects used for threshold analysis.** Transects were chosen to be representative of different weather conditions to represent the range of acoustic data quality collected, and were spread across the mission since attenuation and variation in the strength of the background SSL (expected to vary following the spring phytoplankton blooms) have the potential to affect sensitivity of fish school detections. Transects took 1.84, 1.46, 1.08, and 1.37 days respectively.

| **Transect** | **Period** | **Mean along-track speed (m/s)** | **Mean wind speed (m/s)** |
|---|---|---|---|
| 1 | 02:50 10-05-18 to 22:55 11-05-18 | 0.41 | 4.81 |
| 4 | 15:38 14-05-18 to 02:37 16-05-18 | 0.51 | 5.02 |
| 8 | 19:38 19-05-18 to 21:35 20-05-18 | 0.69 | 8.91 |
| 11 | 14:32 23-05-18 to 23:29 24-05-18 | 0.54 | 5.99 |

Water column $70\,\mathrm{kHz}$ backscatter data were extracted from a horizontal layer that ranged from between $1\,\mathrm{m}$ above the bottom to $36\,\mathrm{m}$ range across four transects (Table F.1). Different morphological filters and, in particular, their processing order can result in varying detection results (Swartzman et al., 1994; Fässler et al., 2007), necessarily affecting how different thresholds will perform. For this reason, a set order of implementation, developed by preliminary testing and subjective evaluation, was used. For all thresholds, a median 3x3 filter was first applied, then a minimum threshold $\delta \in [-55\,\mathrm{dB}, -60\,\mathrm{dB}\,]$, where $\delta \in \mathbb{Z}$, followed by the application of morphological filters in the following order: 3x3 erosion, 3x3 dilation and 5x5 dilation. Similarly, school detection parameters for the SHAPES algorithm were held constant throughout the analysis (Table F.2).

Table F.2: **Detection parameters used for SHAPES algorithm detection of potential fish school clusters**.

| **Parameter** | **Value (m)** |
|---|---|
| Minimum total school height | 1 |
| Minimum candidate school length | 12 |
| Minimum candidate height | 0.75 |
| Maximum vertical linking distance | 15 |
| Maximum horizontal linking distance | 36 |
| Minimum total school length | 12 |

SHAPES was run after filtering and average energetic, morphometric, and positional descriptors from resulting detections (here termed 'clusters') were exported from Echoview (Echoview Software Pty Ltd, 2021) for analysis in R (R Core Team, 2022). Energetic descriptors included dB-difference ($\Delta\mathrm{MVBS}_{200-70}$), calculated from 3x3 median filtered data at both frequencies. Two outlying positive dB-difference clusters ($> 10\,\mathrm{dB}$) were visually scrutinised and found to have been contaminated by accidental integration of bottom echo. Statistics from these clusters were retained for all metrics except energetic, where they were excluded from analysis. Positional descriptors included mean cluster depth ($\mathrm{m}$) and time of day. Morphometric descriptors of mean size included thickness (vertical extent, in $\mathrm{m}$), length ($\mathrm{m}$), perimeter ($\mathrm{m}$), and area ($\mathrm{m}^2$); all were uncorrected for beam width

effects. Clusters with perimeters that exceeded $10\,000\,\mathrm{m}$ were visually scrutinised. Cluster morphometric descriptors were derived from the exported dimensions. These included: fractal dimension - a measure of how convoluted the perimeter is in relation to the area (Equation F.2.1), sensu Nero and Magnuson (1989); elongation - the ratio between the length and thickness (Equation F.2.2), sensu Weill et al. (1993); and rectangularity - the ratio between the rectangle formed by maximum thickness by maximum length to area calculated from average dimensions (Equation F.2.3), sensu Scalabrin and Massé (1993).

$$\text{Fractal dimension (FD)} = \frac{2ln[\frac{P}{4}]}{ln[A]} \tag{F.2.1}$$

$$\text{Elongation (E)} = \frac{L}{H} \tag{F.2.2}$$

$$\text{Rectangularity (R)} = \frac{L\,H}{A} \tag{F.2.3}$$

where $P$ is perimeter in $\mathrm{m}$), $A$ is area in $\mathrm{m}^2$, $L$ is mean horizontal (along-track) length in $\mathrm{m}$, and $H$ is mean height in $\mathrm{m}$ (i.e. thickness or vertical extent) of each cluster. Fractal dimension values closer to $1$ indicate clusters have simple boundaries; fractal dimensions closer to $2$ indicate clusters have complex, convoluted boundaries. Rectangularity approaching $1$ indicates that mean lengths and thickness approach their maximum, i.e. the school appears very rectangular. At values greater than $1$, the length or thickness varies across the school such that mean length or thickness is less than maximum and the school is less rectangular.

## F.3 Results

Marked changes in number and morphological properties below $-57\,\mathrm{dB}$ could be explained by dominance of a different type of cluster as the threshold was lowered. At thresholds

between $-55\,\mathrm{dB}$ to $-57\,\mathrm{dB}$, clusters were compact and rarely exceeded lengths of $200\,\mathrm{m}$. These clusters had statistical properties that aligned with their attribution to schooling fish; subjective visual scrutiny supported this conclusion. These clusters were categorised as 'Type A' clusters. Type A clusters were present throughout the 24-hour period, although they were most commonly detected during daylight hours, with few observed during dawn and dusk. They were located at depths close to the bottom, as is common behaviour for schooling clupeids and gadoids during daytime to minimise their predation risk (ICES, 2005; Bailey, 1975). Their dimensions were similar to those observed for sardines, where mean school lengths can vary between $2\,\mathrm{m}$ to $250\,\mathrm{m}$, and North Sea herring schools (Coetzee, 2000; Misund, 1990). Clusters detected using lower thresholds ($< -57\,\mathrm{dB}$) included the Type A clusters, co-located in the echograms, and many more clusters; compare $n_{-55} = 23$ to $n_{-60} = 203$. These additional clusters are categorised as 'Type B' clusters: generally larger than Type A, with increasingly convoluted perimeters (higher fractal dimensions) and horizontal elongation. Like Type A, Type B clusters were predominantly detected during daylight hours. Unlike the consistent near-bottom depths of Type A clusters, which remained largely below $70\,\mathrm{m}$, Type B clusters were located shallower in the water column; mean depth of clusters detected at $-60\,\mathrm{dB}$ were $10\,\mathrm{m}$ shallower than those detected at $-55\,\mathrm{dB}$.

A natural grouping was evident in the bathymetric, morphometric and energetic properties whereby clusters detected at higher thresholds between $-55\,\mathrm{dB}$ to $-57\,\mathrm{dB}$ were more similar than those at lower thresholds between $-58\,\mathrm{dB}$ to $-60\,\mathrm{dB}$ (Figure F.3.1). This points to the idea that many of the clusters only detected at lower thresholds ($\delta \leq -58\,\mathrm{dB}$) had distinct properties from those detected at higher thresholds. It should be noted that sets of clusters detected at a particular threshold generally included the subsets of clusters detected at higher thresholds, albeit with modified boundaries. Most descriptors showed greater similarity at high thresholds ($\delta \geq -57\,\mathrm{dB}$) in both median values and spread, with an increasing propensity towards outlying values as the threshold reached $-60\,\mathrm{dB}$, the exception being dB-difference. Mean dB-difference, $\Delta\mathrm{MVBS}_{200-70}$, ranged from $-12\,\mathrm{dB}$ to $3\,\mathrm{dB}$, however a larger proportion of values close to the median (approximately $-5\,\mathrm{dB}$) occurred as the threshold decreased (Figure F.3.1, B). From here on the term 'low threshold only clusters' (LTOCs) refers to these distinct clusters only found at low thresholds, where

'high thresholds' refer to $\delta \geq -57\,\mathrm{dB}$ and 'low thresholds' to $\delta \leq -58\,\mathrm{dB}$.

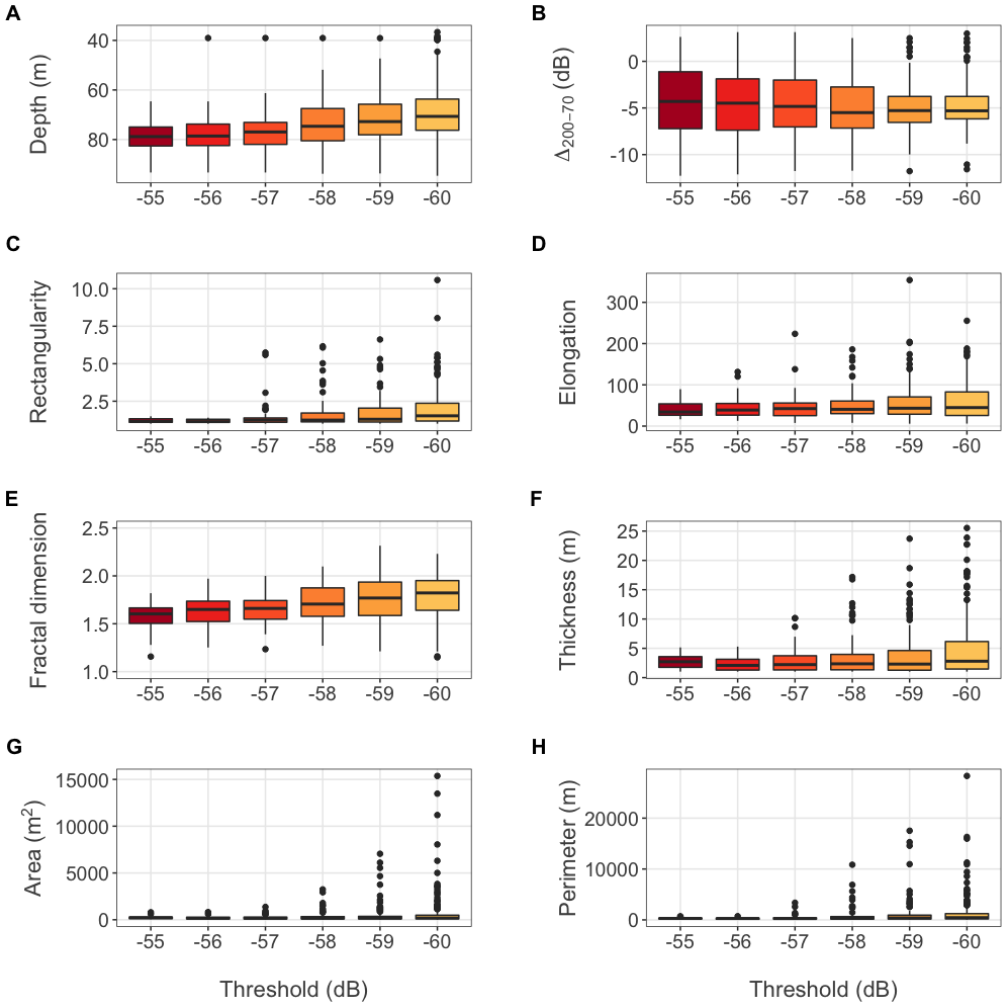


Figure F.3.1: **Boxplots of positional, energetic, and morphometric cluster descriptors, for thresholds coloured from red, -55 dB, to yellow, -60 dB.** Box plots depict median (central line), first and third quartiles (hinges), whiskers extending to no less/more than one and a half times the interquartile range from hinges, and outliers (points) for: A) mean depth of clusters; B) dB-difference (200 kHz minus 70 kHz); C) rectangularity; D) elongation (length to thickness ratio); E) fractal dimension (smoothness of outline); F) thickness (vertical extent); G) area; and H) perimeter of clusters detected using the SHAPES algorithm.

Median depths remained between $70\,\mathrm{m}$ and $80\,\mathrm{m}$ for all thresholds (Figure F.3.1, A). Depths spanned the full range possible within the analysis layer; the shallowest was detected at $37\,\mathrm{m}$, the deepest at $95\,\mathrm{m}$ (both at $\delta = -60\,\mathrm{dB}$). However, high threshold clusters remained close to the bottom, whereas low threshold clusters were found across a greater range of depths as LTOCs were typically detected in much shallower waters.

LTOCs were less rectangular (R $\gg$ 1) and elongated than high threshold clusters (Figure F.3.1, C & D). They also had more convoluted boundaries; fractal dimension, which measures complexity of the two-dimensional outline, increased as the threshold decreased. Although median morphometrics remained similar for all thresholds, some LTOC clusters were much larger than high threshold clusters in terms of area, thickness and perimeter (Figure F.3.1), F-H). Maximum perimeter lengths increased 40-fold from clusters detected at the highest to the lowest thresholds, and maximum thickness more than doubled. Increased thickness was associated with an increase in elongation, indicating that low threshold clusters also became more spread out horizontally. It is this horizontal elongation that primarily drives the rapid increase in cluster area as thresholds decreased.

The number of clusters detected rapidly increased as the threshold was lowered, detecting an order of magnitude more clusters at $-60\,\mathrm{dB}$ ($n = 203$) than at $-55\,\mathrm{dB}$ ($n = 23$) (Figure F.3.2, A). Regardless of threshold, more than 92% of clusters were detected during the daytime. A small increase in clusters detected during the dusk, dawn and nighttime occurred as the threshold lowered. Only seven of the total 552 clusters were detected during the night; these were only found with low thresholds ($n_{-59} = 1$ and $n_{-60} = 6$). Clusters outside of daytime hours were typically only detected using low thresholds, and appeared either very shallow in the water column between $50\,\mathrm{m}$ and $60\,\mathrm{m}$ following dusk or very close to the bottom at over $90\,\mathrm{m}$ near midnight (Figure F.3.2, C). Only one cluster shallower than $60\,\mathrm{m}$ was detected using a high threshold ($-56\,\mathrm{dB}$), observed during early daytime.

Visual inspection of clusters with perimeters exceeding $10\,000\,\mathrm{m}$ suggested that vast swathes of the sound-scattering layer (SSL) had been detected, rather than fish schools with well-defined, distinct boundaries. The cluster perimeters were highly convoluted and irregular in shape, see examples in Figure F.3.3. Lower thresholds resulted in a higher propensity for these outlying clusters to be detected; $n_{-60} = 5$, $n_{-59} = 4$, and $n_{-58} = 1$. The clusters detected at $-58\,\mathrm{dB}$ and $-59\,\mathrm{dB}$ were co-located to those detected by $-60\,\mathrm{dB}$ with almost identical descriptors, i.e. the clusters were centred around the same kernels. This confirms the supposition that the subsets of higher threshold clusters are included in the set of clusters detected using lower thresholds, but also points to the possibility that as thresholds are lowered clusters in close proximity (particularly those which may be the SSL) may

conglomerate, thus forming fewer but much larger clusters with similar properties.

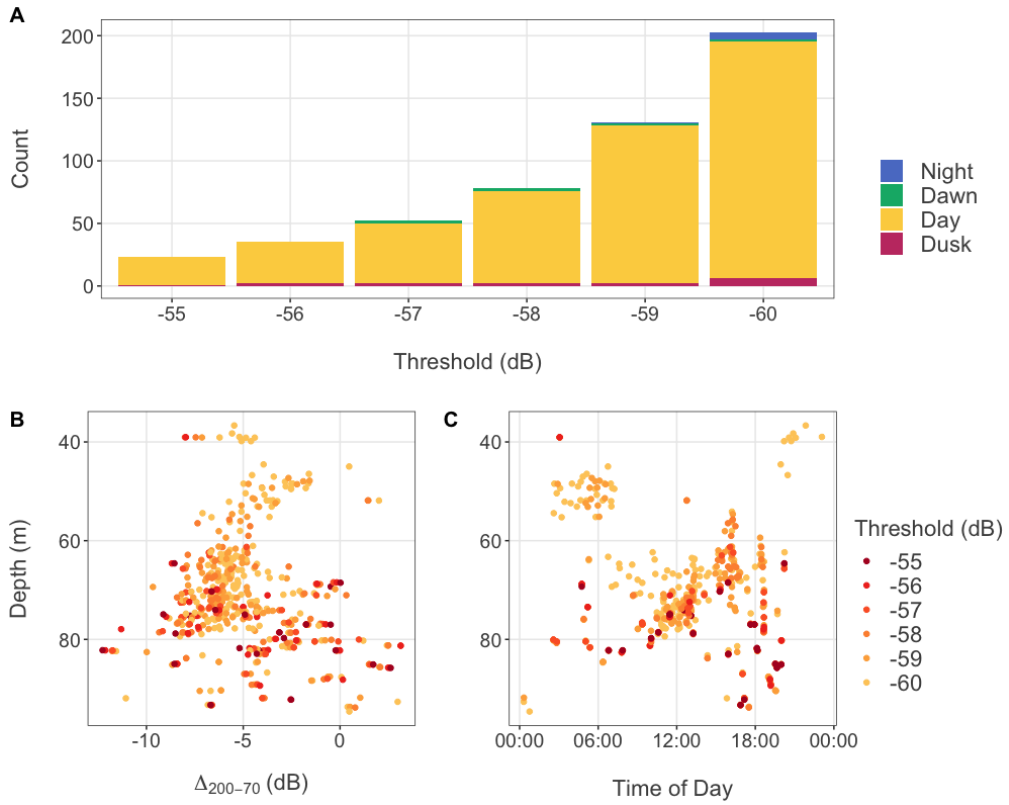


Figure F.3.2: **Number of clusters detected at each threshold (A) and relationships between cluster depth and: dB-difference (B); and time of day (C), coloured by threshold.** dB-difference of MVBS at 200 kHz minus MVBS at 70 kHz calculated in the decibel (logarithmic) domain.

Marked changes in number and morphological properties of clusters detected using thresholds below $-57\,\mathrm{dB}$ could be explained by increasing dominance of a different type of cluster from those detected at or above $-57\,\mathrm{dB}$. At high thresholds clusters were compact and rarely exceeded lengths of $200\,\mathrm{m}$. These clusters had statistical properties that aligned with their attribution to schooling fish; subjective visual scrutiny supported this conclusion. In contrast, LTOCs were often large, irregular and more elongated clusters that occurred shallower in the water column, further from the bottom, suggesting they were detections of dense regions of the SSL.

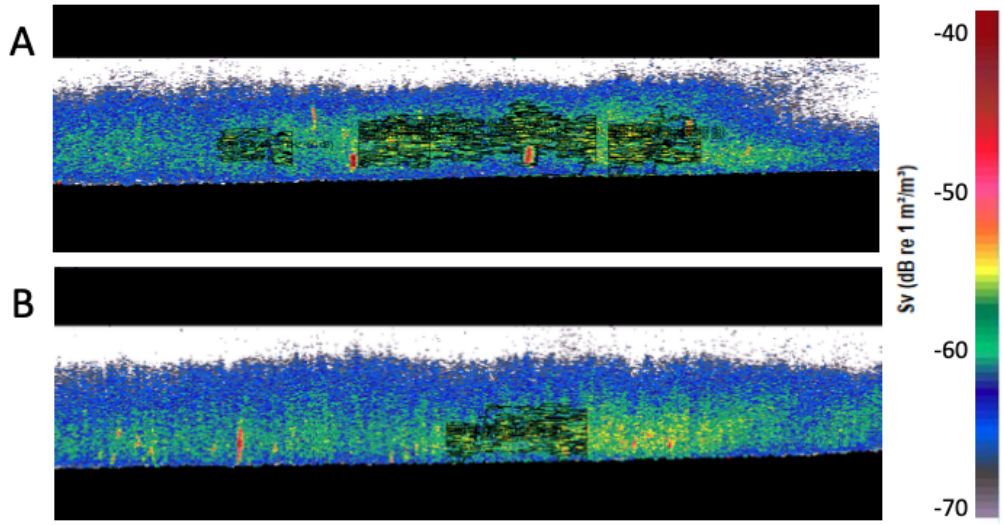


Figure F.3.3: **Examples of clusters with perimeters exceeding 10 km.** Black lines (excluding black label text) outline: A) a single cluster detected only by the $-60\,\mathrm{dB}$ threshold, at a depth of $71\,\mathrm{m}$ with a perimeter exceeding $16\,\mathrm{km}$; and B) several clusters detected by $-60$, $-59$, and $-58\,\mathrm{dB}$ thresholds at depths between $61$ to $65\,\mathrm{m}$ and perimeters of either between $10$ to $11\,\mathrm{km}$. Echograms show vertical range from $1$ to $100\,\mathrm{m}$, however horizontal resolution may vary. Regions above $36\,\mathrm{m}$ and below $1\,\mathrm{m}$ above the bottom are masked in black.

## F.4 Discussion

The aim of this study was to find a threshold that would best discriminate backscatter from fish schools and non-fish school sources based on acoustic descriptors alone since ground-truthing data were not available. Energetic, morphological and positional descriptors were used to assess the suitability of a range of thresholds applied to $70\,\mathrm{kHz}$ backscatter prior to SHAPES detection of potential fish schools. My assessment of statistical patterns was subjective, with interpretations based on ecological knowledge of schooling behaviour of swim-bladdered fish commonly encountered in the North Sea. Statistical techniques such as discriminant function analysis, principal components analysis, artificial neural networks, or supervised or unsupervised statistical cluster analysis may reduce the subjectivity of such assessments. These techniques have proven useful for the purpose of fish school discriminations in the past (Haralabous and Georgakarakos, 1996; Campanella and Taylor, 2016; Lawson et al., 2001; Paramo et al., 2010; Tsagarakis et al., 2015; Gastauer et al., 2017; Brautaset et al., 2020; Benoit-Bird and Waluk, 2021) and may improve upon the analysis

presented here. Nevertheless, simple comparison of average cluster properties using different thresholds revealed the presence of two distinct cluster groups, one of which likely comprised fish schools, and the other dense regions of the SSL, i.e. background backscatter. The rapid increase in detections of the latter cluster group with thresholds lower than $-57\,\mathrm{dB}$ suggests it is an optimal threshold to separate fish school from non-fish school backscatter within the range tested here.

Thresholds are ideally evaluated based on the trade-off between precision (minimising false negatives) and recall (maximising true positives) of correct fish school classification, validated with ground-truth samples. Although more clusters were detected at lower thresholds (higher recall), the likelihood of these including non-fish school scatterers is increased (reduced precision). Such an evaluation was not possible without independent validation of the classification by, for example, trawl or optical sampling. Nevertheless, lowering the threshold below $-58\,\mathrm{dB}$ had the effect of increasing detections of clusters with distinct properties. Clusters that were only detected at low thresholds (LTOCs) had a more consistent bi-frequency response but more variable positional and morphometric properties, suggesting the inclusion of a different type of scatterer. Examination of schools with particularly large perimeters, which had dB-difference and positional properties typical of the LTOCs, suggest that the rapid increase in clusters as the threshold decreased may be caused, in part, by numerous detections of the SSL. This would also explain the increase in depth with low thresholds: fish schools are thought to frequent depths close to the bottom in shallow regions of the North Sea, such as this study region, in order to reduce predation risk; whereas the densest part of the SSL occurred in its vertical centre which was typically located between $60\,\mathrm{m}$ and $70\,\mathrm{m}$. An alternative hypothesis is that variable positional and morphometric properties of the LTOCs could reflect different depth-preferences and sizes of schools for a different species, only detected at lower thresholds. Both hypotheses are consistent with the finding that LTOCs were primarily detected during the daytime: the main SSL exhibits diel vertical migration, sinking deeper in the water column and thus within the analysis region during the daytime but ascending above the analysis region during the night; and fish schools in the North Sea, regardless of species, are known to school primarily during the day and disperse at night. Therefore, detections during non-daytime hours are unlikely for either

scatterer and consistent with our results. Nevertheless, the possibility of LTOCs representing alternative fish school species does not change the outcome. The main goal was to identify a threshold that separated fish school from non-fish school detections, and evidence for SSL detections when using low thresholds was found. Inclusion of dense parts of the SSL in the fish school group might substantially impact patchiness and positional metrics for the fish school class. Conversely, exclusion of the densest regions of the SSL could substantially impact patchiness and positional metrics of the gas-filled, and possibly also fluid-like, groups. Therefore, a threshold of $-57\,\mathrm{dB}$ was chosen as suitable for the detection of fish schools.

Fish schools exhibit high plasticity; their shape, packing density, movement and formation/dissolution are influenced by various factors including environmental conditions, predation and feeding behaviour, physiology and ontogeny (Parsons et al., 2013; Tsagarakis et al., 2012). School shape and position, in particular, can respond very quickly to changes in the environment such as the presence of predators (Massé et al., 1996; Marras and Domenici, 2013). Nevertheless, there is generally lower intra-specific variability in morphometric, positional and energetic descriptors as compared to inter-specific variability in these properties, allowing schools to be discriminated to species level based on these properties. The argument put forward here rests on an analogous assumption that schools of swim-bladdered fish, regardless of their species, have more coherent morphometric, positional and energetic characteristics than scattering from other biotic sources. Furthermore, they are detected at the highest thresholds and non-fish school clusters generally backscatter at a lower intensity, thus allowing reasonable separation by thresholding. Benoit-Bird and Waluk (2021) found distinct statistical groupings that agreed with subjective classification of fish school and non-fish school aggregations by experts. The classifications, however, were not verified independently. Whilst they demonstrate an alignment between statistical features, which are quantifiable, and human judgement, which are qualitative but often proven reliable by ground-truthing in past instances, more work is needed before statistical analyses alone can be proven to accurately classify acoustic features.

As Swartzman et al. (1994) noted, it is not trivial to determine a suitable threshold for discriminating fish schools from background backscatter. Swim-bladdered fish schools

produce a characteristically strong scattering response at commonly used fisheries acoustics frequencies due to resonance of their gas inclusion. This characteristic may be sufficient to distinguish fish school backscatter in some ecosystems, however where other strong biological scatterers co-occur, separation by threshold alone may not be feasible.

Fish schools are usually detected using lower frequencies ($18\,\mathrm{kHz}$ or $38\,\mathrm{kHz}$) nearer to their resonance peaks; no reports of thresholds applied to $70\,\mathrm{kHz}$ data for the purpose of fish school detections were found in the literature. At these lower frequencies, dense aggregations of other scattering types, such as elastic-shelled and fluid-like scatterers, are unlikely to produce a strong response as scattering occurs within the Rayleigh region. Backscattering strength for these organisms is expected to increase with frequency until transition to the geometric scattering region, whereafter it fluctuates with gradually decreasing amplitude. In theory, therefore, threshold separation of fluid-like or elastic-shelled scatterers from swim-bladdered fish schools is best achieved at lower frequencies. At $70\,\mathrm{kHz}$, dense aggregations of organisms without gas inclusions may also produce a relatively strong response and there may be increased overlap of scattering strengths from these differing scatterer-types.

Multifrequency techniques, such as dB-differencing, often prove useful to separate different scattering types. In our study, the range of $\Delta\mathrm{MVBS}_{200-70}$ values did not differ with changing thresholds, however the proportion of extreme to central values (around $-5\,\mathrm{dB}$) decreased with lower thresholds. This suggests that overlap at $70\,\mathrm{kHz}$ is most likely to have occurred with non-backscattering sources with a similar frequency response to the fish schools and not with dense aggregations of fluid-like and elastic-shelled scatterers which are predicted to have a positive dB-difference at $\Delta\mathrm{MVBS}_{200-70}$. The frequency response pattern from dense aggregations of gas-filled zooplankton, such as siphonophores with pneumatophores, is expected to be similar to swim-bladdered fish schools since the majority of backscatter is reflected from the gas inclusions in both instances. Resonance frequency and backscattering strength primarily depend on the size of the gas inclusions and numerical density of scatterers, and may allow for some separation via thresholding where these factors are known a priori. In other cases, descriptors of cluster shape and position in the water column may prove particularly useful for separation. Benoit-Bird and Waluk (2021) found that applying statistical cluster analysis to higher frequency ($200\,\mathrm{kHz}$ data did not

substantially reduce successful discrimination of fish schools from other scattering sources as compared to using 38 kHz. Therefore detections using 70 kHz, whilst not standard, may still be reliable in certain circumstances, particularly when shape and positional characteristics are taken into account.

In areas where aggregations of strong scatterers besides swim-bladdered fish occur, such as the North Sea, complete separation between the two groups using a single, fixed absolute threshold may not be viable. One criterion for the fish school acoustic group was for clusters to have well-defined boundaries, however our methodology did not directly assess backscatter gradients at cluster boundaries. Benoit-Bird and Waluk (2021) demonstrated a technique to threshold dynamically according to the local backscatter regime. This technique identifies backscatter clusters that contrast against the background, for example a fish school within a dense sound-scattering layer, without the need to impose a high threshold that might preclude detection of fish schools in other areas of the echogram. Although fish schools may be found amongst high densities of their prey (Stanton et al., 2012), the likelihood of prey field backgrounds reaching scattering strengths similar to fish schools and thus not breaching the locally imposed threshold is low. Dynamical thresholding according to background scattering can result in both higher recall and, in theory, precision (Benoit-Bird and Waluk, 2021).

Fish schools are dynamic and many species exhibit diel patterns in movement and aggregation behaviour. Herring schools disperse horizontally at night, and move to shallower depths to forage on zooplankton which have migrated nearer the surface or to reduce energy expenditure associated with buoyancy (Toresen, 1991; Huse and Korneliussen, 2000). Whiting, cod, and sardine also exhibit daytime schooling and nighttime dispersal behaviour, with concurrent movement from near the bottom to higher in the water column. Schools of the same species exhibit great variability in size and shape. Herring, for example, appear spherical in midwater but more flattened when located nearer to the seabed or surface (Misund, 1990). Schools are more compact during the daytime, and more irregularly-shaped at night (Fréon et al., 1996), becoming elongated as fish disperse into layers during the night (Toresen, 1991). During transition periods, herring schools are often smaller and more numerous (Fréon et al., 1996; Beare et al., 2002b). Fréon et al. (1996) found that at dawn,

small herring schools merge to form fewer, but larger schools; however at dusk, schools disperse more slowly. Although the dispersed layers of fish can have similar biomass to schools, they nevertheless have lower average energy (Freon et al., 1996), and therefore may be excluded by high thresholds but retained by lower thresholds. It was considered whether morphometric changes associated with different thresholds were the result of such diel behavioural changes, however no association between time of day and changes in cluster dimensions was found.

Schooling is primarily a behavioural response to predation pressures, the need to find food, and remain in social contact with others of the same species. The balance of these drivers alters through different life stages. Smaller, slower-swimming fish may face increased predation pressure. Consequently many juvenile fish form large schools as these act to reduce their individual predation risk, although some, like sardines, form smaller schools as juveniles than when they are adult (Tsagarakis et al., 2012). As fish mature and grow in size, they often form less densely-packed schools and many, such as cod, tend towards solitary living. Habitat use may also change as they grow; nursery grounds provide favourable environmental conditions and refuge for juvenile fish, however they may not meet the foraging demands of larger fish (Tsagarakis et al., 2008; Hinrichsen et al., 2017; Huijbers et al., 2015; Dahlgren and Eggleston, 2000). Similarly, depth-location preferences may also change to reflect changing feeding requirements and energetic costs associated with buoyancy and metabolism. Tsagarakis et al. (2012) found that schools of juvenile sardines formed more elongated, irregularly-shaped schools located nearer to the surface and scattered more weakly than schools of adults. Ontogenetic shifts in schooling behaviour such as this could provide an explanation for the increase in number of clusters at lower thresholds and their differing properties.

Fish school MVBS and dB-difference is expected to vary somewhat within and amongst schools. Tenningen et al. (2017) observed reductions in target strength of 25 dB from peak volume backscatter in the centre of herring schools towards the edges, thought primarily to be due to variation in fish orientation at school boundaries. Other factors, such as variable packing density throughout schools, may also explain variability in target strength. However, since target strength of modelled broadside-on and end-to-end fish have been shown to vary

by up to $30\,\mathrm{dB}$ (Tang et al., 2009), orientation is likely the dominant factor. Fish in the centre of schools are primarily receptive to neighbouring fish, feeding conditions (food may become depleted) and environmental conditions (oxygen may become depleted and chemical concentrations from excretion may reach high levels). Peripheral fish must be alert and responsive to predation threats coming from several directions. Fish at frontal positions may be better located for foraging, at the expense of higher energetic swimming costs (Deblois and Rose, 1996). Such variation in factors affecting fish behaviour within schools may necessitate variation in intra-school orientation, despite an overall tendency towards polarisation during schooling. Lowering the threshold may expand school boundaries and thus change the average dB-difference of the school. However, changes in dB-difference did not fit the expected pattern of increasingly variable dB-difference as cluster boundaries expand, expected either due to changes in fish orientation or the effect of differential beam spreading at school boundaries. Instead cluster dB-difference ($\Delta\mathrm{MVBS}_{200-70}$) was less variable for low-threshold only clusters (LTOCs), providing further support for the idea that these clusters were not fish schools.

# G

# Zooplankton net samples

Time and locations of zooplankton net sampling at stations in the North Sea given in Table G.1. Percentages of fluid-like and gas-filled scatterers at each station, sampled by net given in Table G.2. Table G.2 gives the total count of each taxon identified. Taxonomic identification of mesozooplankton ($< 2\,\mathrm{mm}$) fraction of net subsamples is provided in Table G.4. Taxonomic identification of macrozooplankton ($\geq 2\,\mathrm{mm}$) fraction of net subsamples is provided in Table G.5. Both Table G.4 and Table G.4 also detail scattering and acoustic groups assigned to each zooplankton taxa.

Table G.1: **Net sample stations.** A single vertical haul of the 270 µm ring net was taken at each station to characterise the zooplankton community. Max net depth is the maximum depth recorded by the mini-CTD attached at the top of the net opening.

| Station | Time (UTC) | Latitude (°N) | Longitude (°E) | Max net depth (m) | Water column depth (m) |
|---|---|---|---|---|---|
| 18 | 08.05.2018 21:49 | 56.3 | 2.1 | 76 | 82 |
| 19 | 08.05.2018 22:36 | 56.3 | 2.2 | 74 | 81 |
| 20 | 08.05.2018 23:32 | 56.3 | 2.2 | 74 | 81 |
| 22 | 09.05.2018 00:30 | 56.3 | 2.2 | 73 | 81 |
| 23 | 09.05.2018 01:32 | 56.3 | 2.2 | 74 | 81 |
| 24 | 09.05.2018 02:32 | 56.4 | 2.2 | 73 | 79 |
| 26 | 09.05.2018 03:30 | 56.4 | 2.3 | 70 | 78 |
| 27 | 09.05.2018 04:35 | 56.3 | 2.3 | 70 | 78 |
| 28 | 09.05.2018 05:30 | 56.3 | 2.3 | 69 | 77 |
| 36 | 09.05.2018 17:27 | 56.3 | 2.5 | 64 | 73 |
| 37 | 09.05.2018 18:31 | 56.3 | 2.5 | 67 | 73 |
| 38 | 09.05.2018 19:31 | 56.3 | 2.5 | 65 | 73 |
| 40 | 09.05.2018 20:37 | 56.3 | 2.5 | 67 | 74 |
| 41 | 09.05.2018 21:33 | 56.3 | 2.5 | 67 | 75 |
| 42 | 10.05.2018 05:30 | 56.2 | 2.5 | 69 | 76 |
| 43 | 10.05.2018 06:15 | 56.2 | 2.5 | 69 | 76 |
| 45 | 10.05.2018 07:30 | 56.2 | 2.4 | 68 | 75 |
| 46 | 10.05.2018 08:30 | 56.2 | 2.4 | 67 | 74 |
| 47 | 10.05.2018 09:30 | 56.2 | 2.4 | 66 | 74 |
| 49 | 10.05.2018 10:20 | 56.2 | 2.4 | 67 | 74 |

Table G.2: **Number and proportion of fluid-like and gas-filled acoustic scattering organisms sampled by nets.**

| Station | Fluid-like scatterers | Gas-filled scatterers | Total number of individuals | % fluid-like | % gas-filled |
|---|---|---|---|---|---|
| 18 | 34264 | 0 | 34264 | 100.00 | 0.00 |
| 19 | 55952 | 0 | 55952 | 100.00 | 0.00 |
| 20 | 48254 | 0 | 48254 | 100.00 | 0.00 |
| 22 | 44904 | 0 | 44904 | 100.00 | 0.00 |
| 23 | 26887 | 0 | 26887 | 100.00 | 0.00 |
| 24 | 41779 | 1 | 41780 | 100.00 | 0.00 |
| 26 | 58099 | 2 | 58101 | 100.00 | 0.00 |
| 27 | 42503 | 0 | 42503 | 100.00 | 0.00 |
| 28 | 16930 | 1 | 16931 | 99.99 | 0.01 |
| 36 | 22692 | 0 | 22692 | 100.00 | 0.00 |
| 37 | 18145 | 1 | 18146 | 99.99 | 0.01 |
| 38 | 10511 | 0 | 10511 | 100.00 | 0.00 |
| 40 | 14356 | 2 | 14358 | 99.99 | 0.01 |
| 41 | 15261 | 1 | 15262 | 99.99 | 0.01 |
| 42 | 9444 | 0 | 9444 | 100.00 | 0.00 |
| 43 | 11587 | 0 | 11587 | 100.00 | 0.00 |
| 45 | 8768 | 0 | 8768 | 100.00 | 0.00 |
| 46 | 7547 | 32 | 7579 | 99.58 | 0.42 |
| 47 | 18070 | 1 | 18071 | 99.99 | 0.01 |
| 49 | 7320 | 0 | 7320 | 100.00 | 0.00 |

Table G.3: **Total count of each zooplankton taxon sampled by net.**

| Taxon | | | Total count |
|---|---|---|---|
| Annelida | Polychaeta | Polychaete | 3 |
| | | Polychaete larvae | 3200 |
| | | Tomopteris sp | 250 |
| Bryozoa | | Bryozoan cyphonautes larve | 180 |
| Chaetognatha | | Chaetognath sp | 9480 |
| Chordata | | Fish eggs unidentified | 413 |
| | | Fish larvae unidentified | 172 |
| Cnidaria | Hydrozoa | Aglantha sp | 12130 |
| | | Hydromedusae | 1 |
| | | Hydromedusae unidentified | 2400 |
| | | Laodicea sp | 1 |
| | | Nanomia nectophore | 360 |
| | | Siphonophore float | 30 |
| Crustacea | Amphipoda | Gammarid amphipod | 10 |
| | | Hyperiid amphipod | 553 |
| | Cirripedia | Cirripede cyprid | 280 |
| | | Cirripede nauplii | 1080 |
| | Cladocera | Podon sp | 60 |
| | Copepoda | Acartia clausi | 60 |
| | | Anomolocera | 11 |
| | | Calanus spp. 1-6 | 131480 |
| | | Candacia armata 1-6 | 360 |
| | | Candacia sp | 7 |
| | | Centropages typicus | 240 |
| | | Copepod nauplii | 520 |
| | | Euchaeta hebes 1-6 | 60 |
| | | Metridia sp 1-6 | 8010 |
| | | Oithona spp. unidentified | 3880 |
| | | Oncaea spp. unidentified | 160 |
| | | Para/Pseudo/Clauso/Ctenocalanus | 156710 |
| | | Temora sp | 9640 |
| | Cumacea | Cumacean | 13 |
| | Decapoda | Brachyuran larvae | 365 |
| | | Decapod larvae unidentified | 159 |
| | | Paguridae | 19 |
| | | Porcellanid larvae | 1 |
| | Euphausiacea | Euphausiid adult | 2 |
| | | Euphausiid calyptopis | 97 |
| | | Euphausiid furcilia | 176 |
| | Mysida | Mysid spp. unidentified | 51 |
| Echinodermata | Ophiuroidea | juvenile ophioroid | 60 |
| | | Echinoderm echinopluteus larvae | 11520 |
| Mollusca | Gastropoda | Limacina sp | 3600 |
| | | Prosobranch gastropod larvae | 120 |
| | | Bivalve | 420 |
| Tunicata | Appendicularia | Appendicularia unidentified | 155330 |

Table G.4: **Mesozooplankton $<$ 2 mm fraction of net subsamples.**

| Taxon | Count | Scattering group | Acoustic group |
|---|---|---|---|
| Bivalve | 420 | Elastic-shelled | FL |
| Limacina sp | 3600 | | |
| Prosobranch gastropod larvae | 120 | | |
| Acartia clausi | 60 | Fluid-like | |
| Aglantha sp | 12130 | | |
| Appendicularia unidentified | 155330 | | |
| Brachyuran larvae | 360 | | |
| Bryozoan cyphonautes larve | 180 | | |
| Calanus spp. 1-6 | 131480 | | |
| Candacia armata 1-6 | 360 | | |
| Centropages typicus | 240 | | |
| Chaetognath sp | 9480 | | |
| Cirripede cyprid | 280 | | |
| Cirripede nauplii | 1080 | | |
| Copepod nauplii | 520 | | |
| Decapod larvae unidentified | 60 | | |
| Echinoderm echinopluteus larvae | 11520 | | |
| Euchaeta hebes 1-6 | 60 | | |
| Euphausiid calyptopis | 90 | | |
| Euphausiid furcilia | 160 | | |
| Fish eggs unidentified | 410 | | |
| Fish larvae unidentified | 160 | | |
| Hydromedusae unidentified | 2400 | | |
| Hyperiid amphipod | 480 | | |
| juvenile ophioroid | 60 | | |
| Metridia sp 1-6 | 8010 | | |
| Mysid spp. unidentified | 30 | | |
| Oithona spp. unidentified | 3880 | | |
| Oncaea spp. unidentified | 160 | | |
| Para/Pseudo/Clauso/Ctenocalanus | 156710 | | |
| Podon sp | 60 | | |
| Polychaete larvae | 3200 | | |
| Temora sp | 9640 | | |
| Tomopteris sp | 240 | | |
| Siphonophore float | 30 | Gas-filled | GF |

Table G.5: **Macrozooplankton $\geq$ 2 mm fraction of net subsamples.**

| Taxon | Count | Size class | Scattering group | Acoustic group |
|---|---|---|---|---|
| Anomolocera | 11 | 2-6 mm | Fluid-like | FL |
| Brachyuran larvae | 5 | | | |
| Candacia sp | 7 | | | |
| Cumacean | 2 | | | |
| Decapod larvae unidentified | 42 | | | |
| Euphausiid adult | 1 | | | |
| Euphausiid calyptopis | 4 | | | |
| Euphausiid furcilia | 14 | | | |
| Fish larvae unidentified | 1 | | | |
| Gammarid amphipod | 4 | | | |
| Hyperiid amphipod | 57 | | | |
| Mysid spp. unidentified | 1 | | | |
| Paguridae | 19 | | | |
| Porcellanid larvae | 1 | | | |
| Cumacean | 11 | 6-10 mm | Fluid-like | FL |
| Decapod larvae unidentified | 55 | | | |
| Euphausiid calyptopis | 3 | | | |
| Euphausiid furcilia | 2 | | | |
| Fish eggs unidentified | 3 | | | |
| Gammarid amphipod | 3 | | | |
| Hydromedusae | 1 | | | |
| Hyperiid amphipod | 15 | | | |
| Laodicea sp | 1 | | | |
| Mysid spp. unidentified | 8 | | | |
| Polychaete | 2 | | | |
| Tomopteris sp | 2 | | | |
| Fish larvae unidentified | 8 | | Gas-filled | GF |
| Decapod larvae unidentified | 2 | 10-14 mm | Fluid-like | FL |
| Gammarid amphipod | 3 | | | |
| Hyperiid amphipod | 1 | | | |
| Mysid spp. unidentified | 12 | | | |
| Polychaete | 1 | | | |
| Tomopteris sp | 3 | | | |
| Fish larvae unidentified | 2 | | Gas-filled | GF |
| Euphausiid adult | 1 | >14 mm | Fluid-like | FL |
| Tomopteris sp | 5 | | | |
| Fish larvae unidentified | 1 | | Gas-filled | GF |

# H

# Variability in the vertical distribution of the gas-filled scattering layer

Figure H.0.1 demonstrates the variability in centre of mass and altitude over the course of six days, with daytime variability resulting from the competing pressures of the shallow, variable bathymetry and steep gradient of light from the surface. It was difficult on a day-by-day basis to demarcate a point in time where the layer began to ascend or descend due to DVM, rather than due to spatial heterogeneity whereby the centre of mass shallowed as *Lyra* travelled over shallower bathymetry.

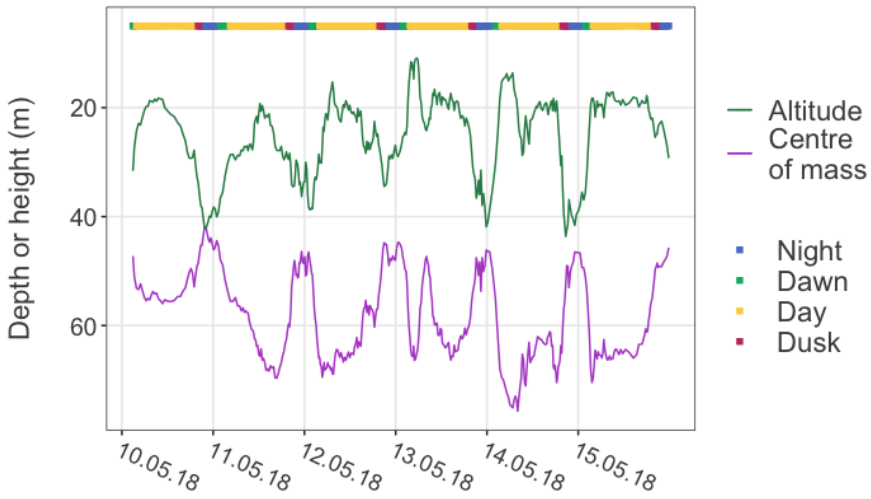


Figure H.0.1: **Variability in altitude and centre of mass of the GF layer.** Example provided for the first six days of the mission.

Figure H.0.2 further emphasises this point by highlighting that the time when the deepest centre of mass was observed during either the pre- or post-noon period each day was often markedly different from the times when the layer was closest to the bottom.

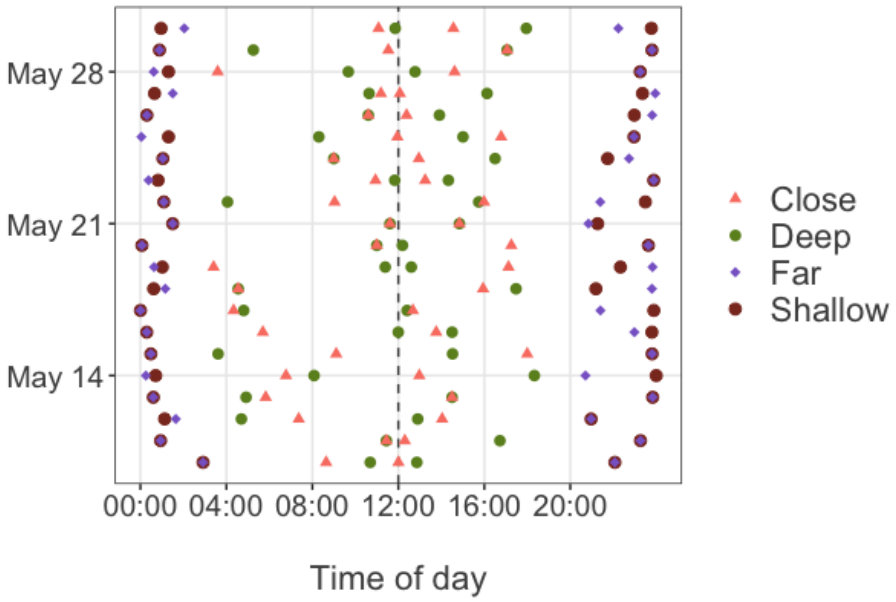


Figure H.0.2: **Pre- and post-noon observations of extremes in centre of mass and altitude.** Circles: deepest (green) and shallowest (brown) centre of mass. Closest (pink triangle) and farthest (purple diamond) from the bottom.